Underground Coal Gasification and Combustion

Edited by Michael S. Blinderman
and Alexander Y. Klimenko

Underground Coal Gasification and Combustion

Related titles

Coal Bed Methane, from Prospect to Pipeline
(ISBN 978-0-12-800880-5)

Coal and Coalbed Gas: Fuelling the Future
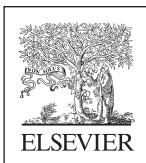(ISBN 978-0-12-396972-9)

The Coal Handbook, Vol 1
(ISBN 978-0-85709-422-3)

Underground Coal Gasification and Combustion

Edited by

Michael S. Blinderman
Alexander Y. Klimenko

For information on all Woodhead publications visit our
website at https://www.elsevier.com/books-and-journals

Working together
to grow libraries in
developing countries

www.elsevier.com • www.bookaid.org

Contents

List of contributors

M.S. Blinderman Ergo Exergy Technology Inc., Montreal, QC, Canada

A. Blinderman Ergo Exergy Technology Inc., Montreal, QC, Canada

H. Bockhorn Karlsruhe Institute of Technology, Engler-Bunte-Institute, Karlsruhe, Germany

D.W. Camp Lawrence Livermore National Laboratory, Livermore, CA, United States

E.V. Dvornikova Ergo Exergy Technology Inc., Montreal, QC, Canada

J.I. Gerhard University of Western Ontario, London, ON, Canada

G.P. Gruber Black & Veatch Corp., Kansas City, KS, United States

K. Kapusta Główny Instytut Górnictwa (Central Mining Institute), Katowice, Poland

L.L. Kinsman University of Western Ontario, London, ON, Canada

A.Y. Klimenko The University of Queensland, Brisbane, QLD, Australia

S. Lavis University of the West of England, Bristol, United Kingdom

S. Maev Laurus Energy Inc., Edmonton, AB, Canada

G.V. Orlov Ergo Exergy Technologies Inc., Montreal, QC, Canada

S. Pershad Eskom Research, Testing & Development, Johannesburg, South Africa

J. Pistorius Eskom Research, Testing & Development, Johannesburg, South Africa

B.V. Reddy University of Ontario Institute of Technology, Oshawa, ON, Canada

A. Reva Ergo Exergy Technology Inc., Montreal, QC, Canada

M.A. Rosen University of Ontario Institute of Technology, Oshawa, ON, Canada

Ivan M. Saptikov Ergo Exergy Technologies Inc., Montreal, QC, Canada

V. Sarhosis Newcastle University, Newcastle upon Tyne, United Kingdom

D. Saulov The University of Queensland, Brisbane, QLD, Australia

S.J. Self University of Ontario Institute of Technology, Oshawa, ON, Canada

A. Taskaev Ergo Exergy Technology Inc., Montreal, QC, Canada

J.L. Torero The University of Queensland, Brisbane, QLD, Australia

M. van der Riet Eskom Research, Testing & Development, Johannesburg, South Africa

A. Veeraragavan The University of Queensland, Brisbane, QLD, Australia

L. Walker Phoenix Energy Ltd., Melbourne, VIC, Australia

L. Yermán The University of Queensland, Brisbane, QLD, Australia

Introduction to underground coal gasification and combustion

M.S. Blinderman*, A.Y. Klimenko†
*Ergo Exergy Technology Inc., Montreal, QC, Canada, †The University of Queensland, Brisbane, QLD, Australia

1.1 Coal and future of energy consumption

Global consumption of energy and hydrocarbons shows steady growth. The trend is sustained and prominent, displaying no signs of slowing down. The reasons seem obvious—the same processes are driving growth in consumption of food, water, and other necessities of human existence:

−Growth of the Earth's population, most pronounced in developing countries
−Growing life standards, again, most prominent in developing countries

The graph in Fig. 1.1 shows world population growth according to projections published by the United Nations (UN DESA, 2017).

The graph in Fig. 1.2 presents a projection of the world primary energy consumption, respectively, for more developed and less developed regions (EIA, 2016). Comparison of the two charts in Figs. 1.1 and 1.2 supports a clear conclusion that increases in the world energy consumption are driven predominantly by growth of both population and life standards in developing countries.

These trends are playing out against the background of increasingly apparent climate change that, many argue, has its root causes in human activity, especially that
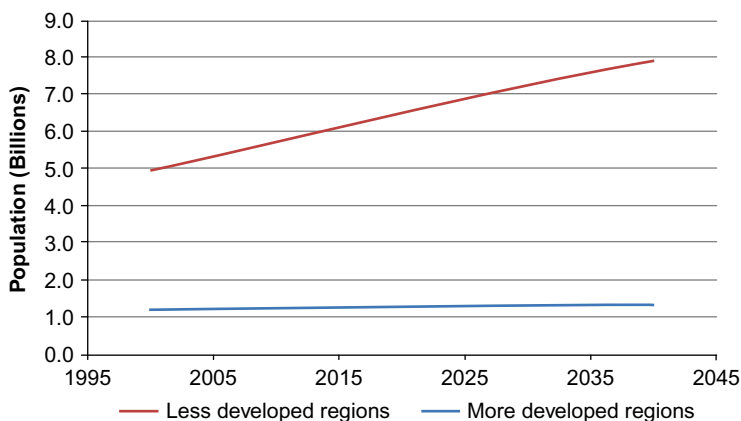
Fig. 1.1 Global population growth projections (UN DESA, 2017).
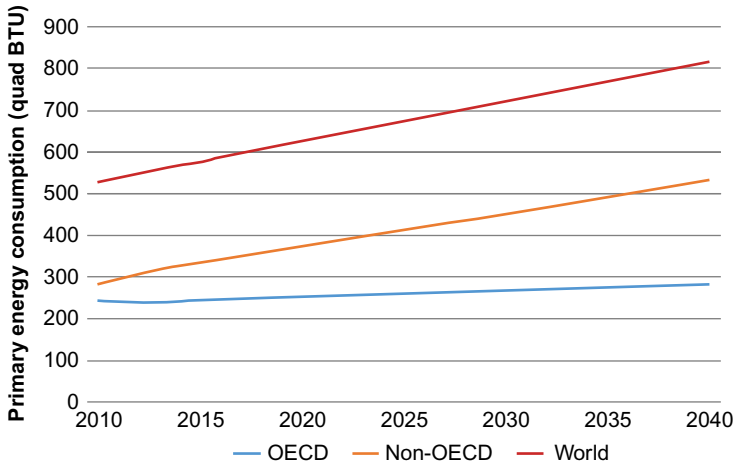
Fig. 1.2 Projections of the world primary energy consumption.

related to energy production and consumption. It is the reality of the day that no discussion of a proposed energy source may avoid the issue of global warming and greenhouse gas (GHG) emissions.

A widely discussed sustainability approach to the global energy supply proposes that agriculture grow energy crops that can be converted into primary energy and hydrocarbons, so that, ideally, an annual harvest cycle would cover the annual cycle of global consumption of energy and hydrocarbons, in addition to satisfying annual food and industrial needs. With rapidly growing population and practically exhausted availability of new agricultural land, it is hard to see how this strategy could be viable.

Given these long-term tendencies, what are the answers to the challenge of supplying affordable clean energy to meet the ever-growing demand? There seems to be a consensus among energy policy experts that renewable sources of energy will not be able to fully meet the growing global energy demand in the foreseeable future. Energy supply from these sources is intermittent by their very nature and requires supplementing by other energy sources, e.g., a fossil-fuel power plant that can produce electricity in a load-following mode (IEA CIAB, 2013). There is also a widespread concern with strains on transmission system that should accommodate variability of renewable sources and incorporate them in a modern power supply network. Discussion of specific issues inherent in renewable power generation is beyond our scope. However favorable they may seem for the environment, they appear to be insufficient in meeting growing global power demand. Besides, solar and wind plants do not produce hydrocarbons: these come primarily from fossil-fuel processing.

Few developing countries can claim oil and gas self-sufficiency; most are importing oil, gas, and petroleum products at a rising rate. Typical supply and demand trends show climbing hydrocarbon consumption increasingly fed by imported oil, gas, and petroleum products, draining hard currency reserves and increasing pressure on the finances of developing countries. The "shale revolution" appears unlikely to

change the dynamics of hydrocarbon markets in developing nations. In these circumstances, coal, the most ubiquitous and affordable of fossil fuels, seems set to continue playing the key role in power generation and, increasingly so, in chemical industries of the developing world (Butler, 2017). But isn't coal the most polluting source of energy, responsible for the highest GHG emissions, let alone emissions of particulates, mercury, SO_x, and NO_x? Aren't ash dams of coal-fired power plants a major source of water and soil contamination? What would be the consequences of its rising use for the environment, for global climate change, assuming that emissions produced in the developing world are to become more and more prevalent?

1.2 Underground coal gasification

The most effective technical solution for controlling pollution while using coal is offered by its gasification (Higman and Van der Burgt, 2008). The main deficiency of conventional coal gasification that converts mined, prepared (washed, milled, or sifted) coal to synthesis gas (syngas) in large steel chemical reactors is that it is expensive and mostly unaffordable in the developing nations. Besides, conventional gasification uses mined coal and thereby perpetuates its ills—mining health and safety problems, environmental issues of open-cut and underground mines, coal market fluctuations, limited and progressively depleted minable resources, etc. Conventional gasification plants continue to use large ash dams. In terms of GHG emissions, gasification facilitates CO_2 capture but does not have any advantages in terms of finding the sinks for GHG sequestration.

What would be the attributes of a coal-based energy and hydrocarbon-producing technology that could make it beneficial and acceptable in the environmentally concerned and carbon-restricted world?

It should be a coal gasification technology that could

1. make use of unminable coal resources;
2. be independent of the coal market price;
3. produce syngas at a low, competitive cost;
4. provide for efficient carbon capture;
5. offer accessible and affordable carbon sinks;
6. eliminate the health and safety hazards of conventional coal mining;
7. produce a fuel for clean, efficient power generation and a feedstock for petrochemical industry.

The listed features seem to fit an existing technology, underground coal gasification (UCG), which is the primary focus of this book. Given the unique and important role that it may play in the future, one could say, paraphrasing Voltaire, "si il n'existait pas, il faudrait l'inventer."

UCG provides the means to create and maintain a coal gasification process within an unmined coal seam that can be accessed by drilling wells from the surface (Ergo Exergy, 2017). This technology does not require the presence of human operators underground; the process is controlled from the surface. Following its invention in 1868, the technology underwent a long and tortuous development and now seems

to be on the verge of wide commercial deployment. As the following chapters of this book set out to demonstrate, modern UCG technology can meet the seven criteria of coal-based environmentally friendly and affordable energy and hydrocarbon technology outlined above.

Forty years have passed since the publication of the previous book on UCG (Lamb, 1977). These years have seen a great deal of research, development, field demonstrations, process modeling, and commercialization attempts that significantly changed UCG knowledge and understanding. Our book is intended to capture the main results achieved in recent stages of global UCG development and to provide a modern and multifaceted view of the technology. The authors of the book come from a variety of academic, industrial, and commercial backgrounds and represent a wide geographic and institutional UCG experience.

1.3   Multidisciplinary nature of UCG

The book is not restricted to presentation and analysis of mainstream UCG technology, but endeavors to cross the boundaries of conventional fields and disciplines to analyze applications where the accumulated knowledge and experience in UCG can be useful in offering viable alternatives to conventional technologies. While historically a few of these fields were seen as being a part of UCG technology, this is not necessarily the case at present. The authors, however, do not intend to bring forward methodological arguments about the right or wrong placement of disciplinary boundaries. Our approach is based on the productive tradition of practical interdisciplinary engineering: the book presents ideas and applications that are relevant to UCG technology, whether or not this implies crossing the boundaries of conventional branches of engineering and science.

It is important to stress that the development of UCG technology has always been a multidisciplinary endeavor, combining, applying, and enriching knowledge from many different fields. UCG lies at the intersection of practical engineering and fundamental science, involving chemistry and physics, fluid mechanics and solid mechanics, thermodynamics and kinetics, and geology and hydrology. Intensive interactions of numerous factors make underground gasification and combustion extremely complex. These underground processes have common features but always remain site-dependent. The complexity of the processes needs to be dealt with in conditions of limited underground access, restricting opportunities for monitoring and control. Despite these difficulties, "no men underground" has become the key principle of modern UCG, which perhaps should eventually be extended to all mining operations—only implementation of this principle can eliminate the inherent danger of underground mining to workers.

Historically, the state of the underground reactors in UCG operations and trials often had to be judged on the basis of secondary indicators, not direct measurements within the gasifier. Under these conditions, development of the technology was relatively slow, based on intuition and accumulated experience, often resorting to trial and error. Some of the techniques and physical effects were uncovered only by

chance. The accidental discovery of reverse combustion linking at the Soviet Tula (Podmoskovnaia) UCG station in 1941 may serve as a good example. At the end, a long series of trials (some of which involved posttrial excavations) brought about new understanding of the underground processes. This statement is primarily related to UCG—our knowledge of underground fires, their configurations, extents, and evolutions to this day remains very limited and often based on guessing rather than knowing.

Modern conditions, however, have brought new tools of measurements and simulations into UCG technology. Stringent environmental monitoring has become an inseparable part of good UCG practice. These tools, combined with nearly a century of accumulated UCG experience, form the basis of the modern UCG technology. It must be noted that proper operational conditions for UCG have not always been followed in the past. For example, prolonged periods of keeping excessively high pressures in the underground reactor may result in a short-lived improvement in product gas quality but lead to environmental contamination and trial failure. This book advocates environmentally responsible application of UCG technology based on best practices and solid and comprehensive scientific approach supported by sound and transparent regulatory framework. In fact, as discussed in this book, UCG-related technologies can be used to remedy environmental impact of some natural disasters or technological mistakes.

1.4 Gasification and combustion

We note that the separation between underground gasification and underground combustion of coal seams is rather nominal. Both processes, gasification and combustion, involve the same reactants and the same kinetics (see Chapter 7). Ineffective operational conditions during gasification (such as oxygen bypass) may lead to burning of syngas before it has a chance to be delivered to the surface, that is, to combustion replacing gasification. In the same way, underground coal fires usually produce a mixture of gases involving CO_2, H_2, and CO, and combustion is rarely complete under these conditions. The main difference between UCG and underground coal fires is in localization, depth, pressure, and, most importantly, in the level of control over these processes.

The first ideas of UCG were formulated as a means of controlling underground fires. Further advancements in UCG technology have brought a much better understanding of underground processes of gasification and combustion of coals, at least because underground gasification is conducted in purposely designed conditions involving accurate measurements and analysis. It seems, however, that in the past, this acquired understanding has not been used for the purpose of controlling and extinguishing underground fires. In many cases, extinction of underground fires remains extremely difficult or impossible with the use of conventional techniques. Extinguishing attempts based on poor understanding of underground combustion may lead to apparent success in the short run and exacerbation of the problem in the long run. Under such conditions, establishing full or partial control over fire by UCG-originated

techniques seems to be a logical choice. Since this would allow to mitigate and reduce the environmental damage caused by the fires, it would be important to find a cost-effective way to trial and implement these techniques in practice.

1.5   The scope of the book

The book deals with the history of UCG, UCG technology and applications, and possible extensions of the technology. As described in the first chapters of this book, the development of UCG in the world has been uneven, which may seem surprising given reasonable conceptual understanding achieved during the earliest stages of the technology life, which is covered in the chapter describing the early history of UCG (Chapter 2). The following chapters consider the history of UCG development with a focus on the main geographic centers that attained the highest technical and commercial advancement—the former USSR (Chapter 3), the United States (Chapter 4), Europe (Chapter 5), and, most recently, Australia (Chapter 6). The editors had hoped to include in the book an account of UCG projects in China, where the government-sponsored UCG program spanned some 30 years starting from the late 20th century, but it proved impossible within the necessary time frame due to logistic reasons.

The technical aspects of UCG implementation are covered in Chapters 7–11. This part involves chapters on gasification kinetics (Chapter 7) and the role of groundwater in the gasification process (Chapter 8). Chapter 9 reviews the rock mechanics issues of UCG in terms of understanding surrounding rock deformation as a cause of potential environmental impacts and a key factor affecting processes in the gasification system. Another chapter provides a summary of the efforts to create a mathematical model of the UCG process (Chapter 10). Finally, there is a chapter concerned with environmental performance of UCG plants, concentrating on protection of groundwater with examples, primarily, from the former Soviet UCG program (Chapter 11).

A special emphasis of the book has been placed on potential commercialization of UCG technology. A chapter is dedicated to considering the features of the technology that make it suitable for large-scale energy and petrochemical applications (Chapter 12). Processes, equipment, efficiencies, and costs of utilizing syngas for production of electricity, synthetic methane, fertilizers, synthetic automotive fuels, methanol, and other value-added commodities are discussed in another chapter of this book (Chapter 13). Two chapters are dedicated to consideration of commercialization issues using examples of two recent UCG projects—in South Africa and Australia (Chapters 14 and 15).

A great deal of interest in recent years has been attracted to oil shale deposits, predominantly focusing on the shale gas and shale oil fracking revolution that took place in the United States in the last decade. The fracking is used to facilitate release and production of gaseous and liquid hydrocarbons from the shale matrix, while the organic matter of the matrix itself remains largely untouched. However, UCG experience offers an alternative, which is based on establishing a gasification process within the underground shale seam in situ and converting the shale organic mass into

gaseous and liquid hydrocarbons, which would result in *underground gasification* of the shale. Our book includes a full chapter (Chapter 16) dedicated exclusively to the description of underground shale gasification research and development efforts and outcomes.

As any industrial activity, UCG operation has an impact on the environment, which is minimized provided that proper operational procedures are followed. This book gives due emphasis to potential environmental impacts of UCG (see Chapter 11), which need to be compared with the environmental impacts of alternative technologies. Proper application of underground gasification and combustion technologies should reduce this impact. The closing chapters of the book deal with possible extensions of UCG technologies, especially when knowledge of underground processes accumulated in UCG operations can be useful in mitigation or reduction of environmental damage caused by various factors not related to UCG.

Chapter 17 is dedicated to analysis of underground fires from the perspective of UCG technology. We must note, however, that comprehensive treatment of underground fires or discussion of even more remote topics such as fire safety in mines is not within the scope of this book. Extensive treatment of underground fires can be found in other publications (see Stracher et al., 2010). Environmental remediation of contaminated soils can be achieved very effectively through a specifically designed underground combustion process. One of the chapters in this book (Chapter 18) reports on a positive experience of such remediation.

Both successful UCG operations and successful control and extinction of underground fires can be achieved only with appropriate monitoring and analysis. A spectrum of monitoring techniques is now standard in the best UCG operations. Chapter 19 of this book reviews measurement techniques that are commonly used in UCG operations and can be used in monitoring underground fires. The section also examines physical principles that may form a basis for advanced measurements and monitoring of underground gasification and combustion in the future. Once developed, these technologies may be suitable for monitoring a broad range of underground processes.

In general, this book is addressed to an educated reader with some experience in the area; to people who have interest in commercial, technical, and scientific aspects of UCG; to research students; and to experienced researches who have a limited access to UCG-related information. The recent developments of the theory of key UCG processes (e.g., the theory of reverse and forward combustion linking, the theory of the flame position in the channel, and the theory of stability of evaporation fronts), which are highly mathematical and hardly suitable for general readers, are not included in the book. Readers interested in theoretical aspects of underground gasification and combustion are referred to relevant publications (Blinderman and Klimenko, 2007; Blinderman et al., 2008a,b; Saulov et al., 2010; Plumb and Klimenko, 2010).

Acknowledgments

References

Blinderman, M.S., Klimenko, A.Y., 2007. Theory of reverse combustion linking. Combust. Flame 150 (3), 232–245.

Blinderman, M.S., Saulov, D.N., Klimenko, A.Y., 2008a. Forward and reverse combustion linking in underground coal gasification. Energy 33 (3), 446–454.

Blinderman, M.S., Saulov, D.N., Klimenko, A.Y., 2008b. Optimal regimes of reverse combustion linking in underground coal gasification. J. Energy Inst. 81 (1), 7–12.

Butler, Nick, 2017. Alternative truths and some hard facts about coal. Financial Times. April 3.

Ergo Exergy, 2017. Welcome to Underground Coal Gasification. http://www.ergoexergy.com (accessed 22.07.17).

Higman, C., Van der Burgt, M., 2008. Gasification, second ed. Elsevier, Amsterdam.

IEA Coal Industry Advisory Board, 2013. 21st Century Coal: Advanced Technology and Global Energy Solution. OECD/IEA, Paris.

Lamb, G.H., 1977. Underground Coal Gasification. Energy Technology Review No. 14, Noyes Data Corp.

Plumb, O.A., Klimenko, A.Y., 2010. The stability of evaporating fronts in porous media. J. Porous Media 13 (2), 145–155.

Saulov, D.N., Plumb, O.A., Klimenko, A.Y., 2010. Flame propagation in a gasification channel. Energy 35 (3), 1264–1273.

Stracher, G., Prakash, A., Sokol, E., 2010. Coal and Peat Fires: A Global Perspective. In: Coal-Geology and Combustion, vol. 1. Elsevier Science, Amsterdam/London.

U.S. Energy Information Administration, 2016. International Energy Outlook 2016. Report DOE/EIA-0484(2016), DOE, Washington, DC.

Unite Nations, Department of Economic and Social Affairs, Population Division, 2017. World Population Prospects: The 2017 Revision. custom data acquired via website.

Part One

Historical development of underground coal gasification (UCG)

This page intentionally left blank

Early developments and inventions in underground coal gasification

2

A.Y. Klimenko
The University of Queensland, Brisbane, QLD, Australia

2.1   Introduction

Great ideas need great men to introduce them. The history of the invention of underground coal gasification (UCG) confirms this statement and involves four people of outstanding qualities and intellect: William Siemens, Dmitri Mendeleev, Anson Betts, and William Ramsay. The history of UCG invention and development is at the intersection of science and industry, discovery and progress, individual contribution, and large-scale research efforts. This article examines technical issues as they were understood by the four "founding fathers" of UCG, but the story has also a political dimension. For many years, the pivotal role of Betts, which perhaps eclipsed the roles of the other three great men in invention of UCG, was either not known or not sufficiently understood and appreciated. The purpose of this chapter is to describe the historical scene for the further development of UCG and associated technologies, which are presented in other chapters of this book and, maybe, to correct the historical injustice mentioned above.

The pattern of many prominent inventions resembles a relay—the idea is passed from inventor to inventor, and at every step, it is reinterpreted and developed further up until it starts to work. At this point, the idea is rapidly replicated by many; its implementations become more and more diverse. This chapter, however, focuses only on the first stage of invention of UCG, which was terminated with the beginning of the WW1.

2.2   William Siemens: The first mention

Sir William Siemens was a German-born prominent engineer, scientist, and businessman. After studying both engineering and science in Magdeburg and Goettingen, Siemens moved to Britain, where his numerous talents received wide recognition. Siemens was a member of the Royal Society, president of the British Association for the Advancement of Science, president of the Institution of Mechanical Engineers, and president of Society of Telegraph Engineers, as well as a co-owner and director of successful industrial companies. He advocated the modern understanding of heat as a form of energy, developed industrial gasifiers, constructed an improved steam engine, invented a regenerative furnace, and stretched telegraph cables across the continents. The professional and personal qualities of William Siemens—a talented engineer who was also well-grounded in science—were widely known and highly respected in the society (Thurston, 1884) (Fig. 2.1).

Fig. 2.1 Sir William Siemens.
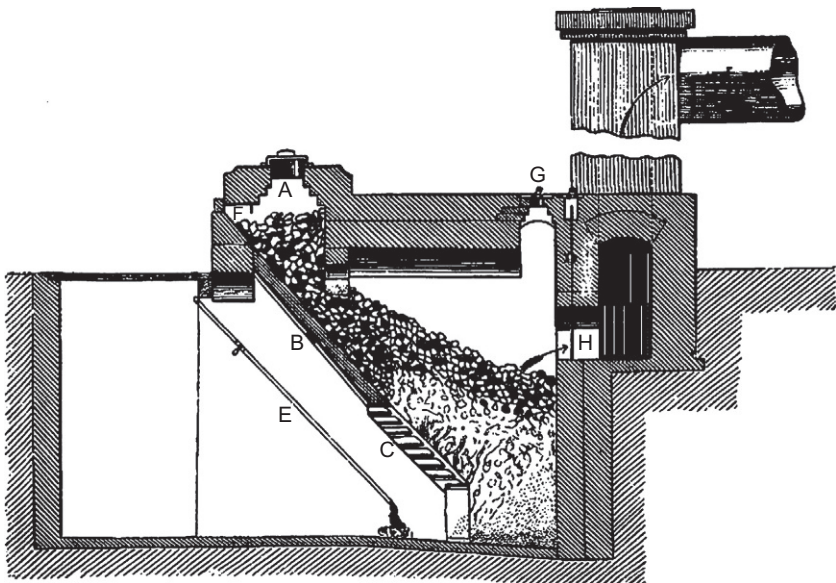
Fig. 2.2 Siemens gasifier (gas producer) as shown by Siemens (1868).

In his lecture delivered to the fellows of the chemical society, Siemens (1868) made a reference that suggested a possibility of gasifying coal in situ. The large part of his lecture was dedicated to the benefits of using coal gasifiers (gas producers in the terms of the time—see Fig. 2.2) in steelmaking. In the middle of the lecture, he made a remark that instead of delivering coal to gas producers located in proximity of the steel furnaces, these producers can be placed in the coal mines to burn slack coal, while the produced gas is to be delivered to the furnace through a system of pipes.

Was this suggestion practical? The answer is obviously negative. Gas produces placed into a mine would represent an extreme fire danger and a problem for mine ventilation and maintenance and make the working conditions of the personnel servicing the mine and the producers unbearable. While this suggestion of William Siemens was not viable and not parallel to modern understanding of UCG, this was the first known mention of the possibility of industrial gasification of coal conducted in situ.

2.3 Dmitri Mendeleev: Vision into the future

Dmitri Mendeleev was a famous Russian scientist best known for his invention of the modern periodic table of elements, which not only corrected inaccurately known atomic masses of several elements but also predicted existence of several unknown elements. Mendeleev was a foreign member of the British Royal Society and Royal Swedish Academy of Sciences. He was repeatedly nominated for the Nobel Prize but missed it, reportedly, due to objections of Svante Arrhenius (Fig. 2.3).

It is less known that he also made numerous contributions not only to chemistry and physics but also to the diverse fields of engineering, economics, industrial technology, and state governance. Mendeleev helped with establishing first oil refineries in Russia
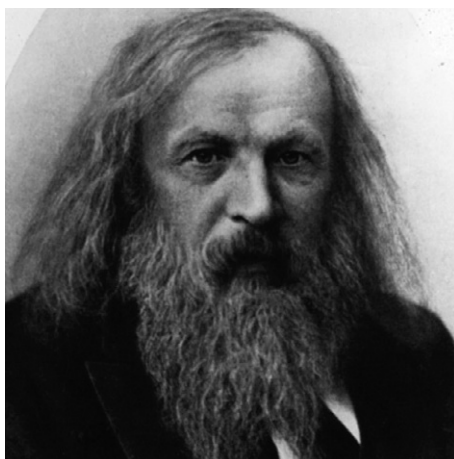
Fig. 2.3 Dmitri Mendeleev.

and introduced metric system to the country. Mendeleev was less recognized in Russian academic circles, but his talents were valued by the government of Imperial Russia and especially by Sergei Witte—a prominent statesman and intellectual. After Mendeleev resigned from his professorship at St. Petersburg University, he was appointed to the prestigious position of head of the State Archive of Weights and Measures. Both Witte and Mendeleev played key roles in establishing St. Petersburg Polytechnic Institute. Mendeleev was repeatedly asked to advise on technological and socioeconomic aspects of industry development in the empire. He traveled as far as Ukraine and Ural, wrote notes, and reported to the government after his return. His notes provide an accurate historical account of the state of industry at the turn of the century. These notes impress with sharpness and versatility of Mendeleev's mind, combining wide knowledge and practical sense and his ability to understand complex problems and point to effective solutions.

Mendeleev's (1888) first remark mentions the possibility of gasifying coal underground without mining it and delivering the produced gas through a network of pipes. He predicted that wide-pipe networks will be built in the future to deliver natural and coal gases to leading consumers. This first remark is more or less similar to Siemens's suggestion, but Mendeleev's thought progressed further in the coming years. In his book *Industry Foundations*, Mendeleev (1897) added an important detail suggesting to conduct gasification of coals of lower grades without breaking them up—this corresponds to modern understanding of UCG, and is the most interesting observation Mendeleev made during his trip to the Ural region (Mendeleev, 1900). While visiting the Kizil plant and mine in 1899, he observed an underground fire and discussed incidents of underground fires with Chief Engineer Mr. Pivinsky and other educated people at the mine. The main extinguishing technique accepted at that time was sealing the fire area to prevent consumption of oxygen. This was not always effective, and some of these fires could last for years. During these discussions, Mendeleev suggested the possibility of establishing control over underground fires and using them for producing syngas. Air is to be supplied in controlled quantities to the fire through a single pipe, while the produced syngas is drawn through a system of pipes that are different from the air injection pipe. The principal points of the scheme are illustrated in Fig. 2.4.
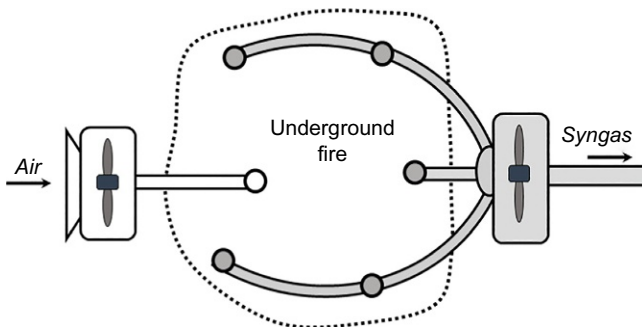
Fig. 2.4 The gasification scheme illustrating the description of the underground fire experiment suggested by Mendeleev (1900).

Mr. Pivinsky was keen to conduct experiments, but this needed agreement of the plant owners. As far as it is possible to judge from the text, the fire was extinguished, and the experiments were not conducted, but if they were, could these experiments be successful? Most likely not. Without an accurate information on location of the fire and understanding hydraulic connectivity in the area, it would be difficult to establish any form of control. The most likely outcome of these experiments, if they were conducted more than a hundred years ago, would be a gas of a very low or inconsistent quality.

The other question is if Mendeleev had seen the Siemens remark on gasification in situ. This is possible and, in my view, likely. Mendeleev was interested in gasifiers and positively characterized the Siemens gasifiers in his works (Mendeleev, 1897). At the same time, Mendeleev clearly had his own thoughts about the matter; his suggestions were not only different from that of Siemens but also very practical. Mining coal through a system of pipes without underground access corresponds to modern understanding of UCG. Another important suggestion of Mendeleev was possibility and even necessity of exercising control over underground fires.

2.4 Anson Betts: Inventing UCG

Anson Gardner Betts, a notable American engineer and chemist, was born in 1876 in a suburb of town of Troy, New York State, in a prominent family derived from America's first settlers. His father Edgar was a successful businessman. His grandfather Henry was noted for introducing many inventions, including improvements of printing and papermaking. Anson Betts graduated from Sheffield Scientific School of Yale University in 1897 with a bachelor degree and, the next year, from Columbia University with a master's degree. The following 15 years of his life were especially productive; Betts made many significant inventions and obtained a long list of patents registered in the United States, the United Kingdom, Canada, Australia, Spain, Belgium, etc. He introduced a new process for refining lead—the Betts process— and in 1908 published a book on this matter (Betts, 1908). This book has been recently reprinted (Fig. 2.5).

In the years between the wars, Betts became an entrepreneur, lived in different states, and owned a business in North Carolina. In 1925, he purchased Betts Manganese Mines in Massachusetts, returned to his birthplace, and operated the mines with the help of his son, Anson K. Betts. Even at his old age, Anson G. Betts always displayed strength of his mind and character. His last invention was filed for patent in 1970 (Betts, 1972) when he was 94 years old. Anson G. Betts died in 1976.

In 1906–10, Anson Betts filed and obtained three patents from the patent offices of the United States, the United Kingdom, and Canada (Betts, 1910). While technical details of the Betts invention are considered later in this section, we stress the outstanding value of these patents for the further development of UCG. Neither before nor after this invention, was Betts overly interested in gasification, and his other patents are not related to this area. It seems quite possible that Mendeleev's remarks ignited interest in Betts' inventive mind to produce a workable method for UCG. In any case, Betts has made an outstanding contribution to UCG; unlike his

LEAD REFINING BY ELECTROLYSIS

BY

ANSON GARDNER BETTS

FIRST EDITION
FIRST THOUSAND

LIBRARY
OF THE
UNIVERSITY
OF
CALIFORNIA

NEW YORK
JOHN WILEY & SONS
London: CHAPMAN & HALL, Limited
1908
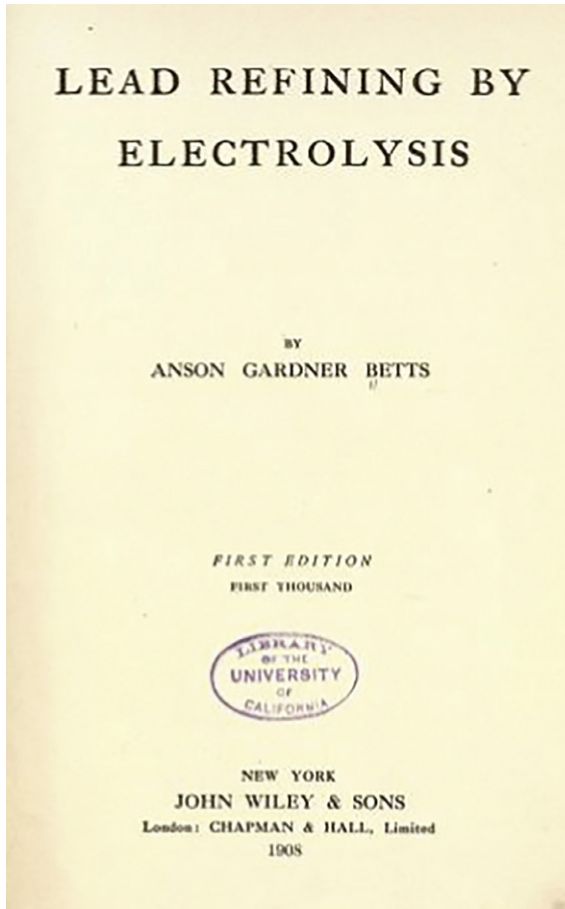
Fig. 2.5 The original title page of the book by Anson G. Betts published in 1908.

predecessors, he not only nominated the idea but also stipulated specific methods that this idea can be achieved with. These methods form the basis of subsequent development of industrial UCG. Filing these three patents (Betts, 1910) marks the point of invention of UCG.

The three Betts UCG patents are very similar. However, unlike the other two patents, the UK patent distinguishes the current invention from previously discovered extraction and utilization of coal methane. Betts suggested several schemes, four of which are most interesting. Fig. 2.6 illustrates the basic principles of UCG: existence of at least two wells (injection well 3 and the production well 8) and a hydraulic connection between the wells through drift 7. This can be practically achieved by using two shafts or a shaft and a borehole. The coal is then gasified by a stream of oxidizing agent (air and steam) in its original location, without being broken or mined.

Betts does not stop at this point and discusses many details of the scheme in a remarkably insightful manner. He notes that gasification can cause subsidence and
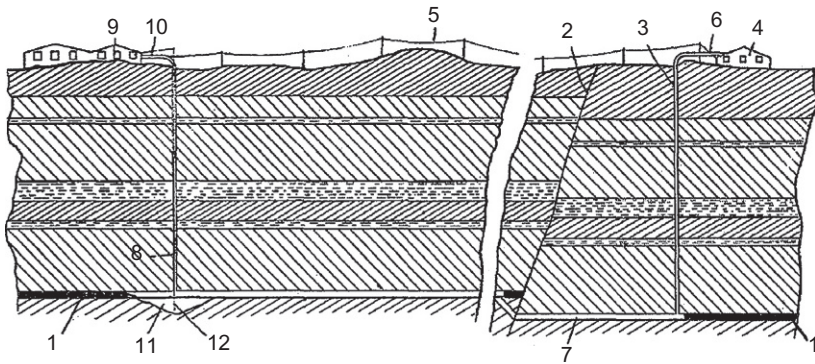
Fig. 2.6 Stream gasification by Betts (1910).

cracks in the overburden that can cause gas leakages. This can be tackled by introducing a slight suction at point 10 creating a controlled inflow of air into the gasifier. The subsidence is nevertheless useful as it allows to fill the gasified space while keeping the free passage close to the coal surface. Betts discusses the problem of oxygen bypass to the production well but correctly managed subsidence, good separation of the injection and production wells and curved passages should improve contact of the agent with the coal surface and, consequentially, the quality of the produced syngas. Betts mentions the problem of gas cleaning, tar removal, and other problems that are practically important in UCG.

Betts considers the benefits of having several injection and production wells, which however, need to be carefully controlled to ensure the best quality of the syngas while using several fires at different stages of completion. He illustrates this point with Fig. 2.7 that has valves 21 and 22 controlling injection wells 13 and 14 and valves 24 and 25 controlling production wells 15 and 16. Fig. 2.8, which is perhaps less informative than the other figures, illustrates Betts's suggestion of gasifying residual coal in a worked-out mine using two shafts 26 and 27 for injection and production.

Betts also suggests the possibility of using a single borehole 31 for both injection and production by installing two concentric pipes 32 and 33. The purpose of this suggestion, which can be referred to as the blind borehole method, is often misunderstood. It was clear to Betts that the quality of the gas will decrease after the size of the cavity increases. The goal of this scheme is to create a hydraulic link between wells 31 and 37 without men working underground to stretch a drift from one shaft to another. This resembles the latter invention of combustion linking, which was discovered by pure chance much later, in 1941 at the Soviet Tula UCG station. We also note another invention—directional injection of air improving contact with the coal surface. This method was proved useful much later, in the Soviet UCG program.

Overall, Betts's patent introduced the following gasification schemes:

1. Stream gasification using two shafts (or a shaft and a borehole)—Fig. 2.6
2. Stream gasification with multiple injection and production points and multiple passages—Fig. 2.7
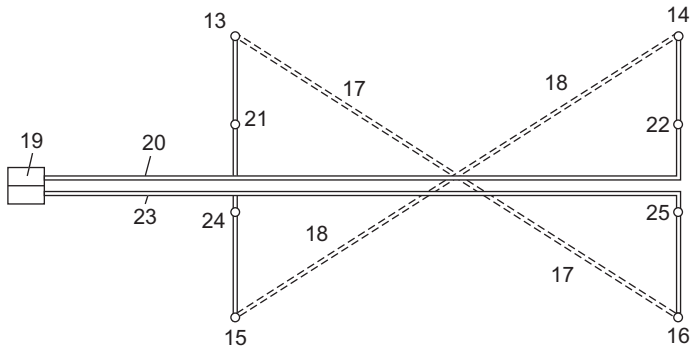
Fig. 2.7 Stream gasification with multiple injection and production points by Betts (1910).

Fig. 2.8 Gasification of coal in worked-out mine (Betts, 1910).
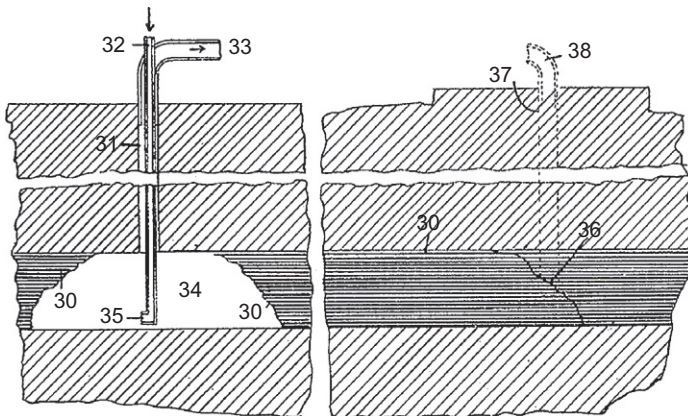
Fig. 2.9 The blind borehole method (left) and well linking (left-right) according to Betts (1910).

3. Stream gasification in work-out mines—Fig. 2.8
4. Blind borehole method (with the possibility of combustion linking)—Fig. 2.9
5. Gasification with drift located under the coal seam (not discussed here)

2.5   William Ramsay: Preparing first trail

Sir William Ramsay was one of the most prominent figures in British science, who was awarded the Noble Prize in chemistry for discovery of the noble gases, was elected the president of the Chemical Society and the president of the British Association for the Advancement of Science, and, of course, was a member of the Royal Society (Fig. 2.10). Ramsay has a long list of prestigious academic awards including honorary doctorates and academic medals and prizes. His persistent pursuit and one-by-one discovery of the noble gases earned Ramsay an eminent reputation in scientific circles (Tilden, 1918). Ramsay was also interested in practical and commercial aspects of science and in inventions and patents. Although this side of his interests is generally less known, it was thoroughly investigated by Watson (1995).

There is, however, one fact—Ramsay's interest in UCG—which is widely known due his two brief remarks on UCG that attracted attention of the media. The first remark took place when Ramsay proposed success of the Smoke Abatement Exhibition at the opening luncheon in March 1912; the second was a response to the opening toast at a dinner of the Institution of Mining Engineers in June 1912. Both of these remarks were lighthearted yet related to the occasion. Ramsay mentioned the possibility of converting coal to syngas in the "bowels of Earth" and then to electricity, which is to be delivered to consumers. He saw ecological and economic benefits in UCG and predicted that it is gas and not coal that is the future of energy supply. Using
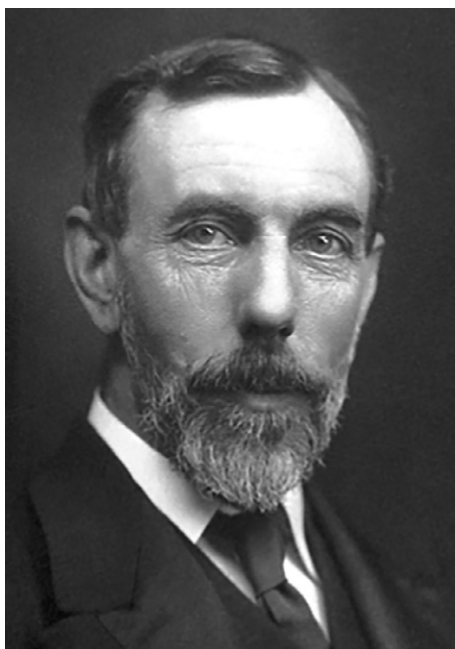
Fig. 2.10 Sir William Ramsay.

this perspective, Ramsay also warned mining workers, who went on strike, against excessive demands.

The media bombarded Ramsay with questions, and later in March, he agreed to give an interview to the Daily Express, which was also reported in Gas World (1912). During this interview, Ramsay clearly described the principles the fourth Betts UCG scheme (the blind borehole), with only a minor difference of having three concentric pipes instead of two. Whatever subsequent interpretations of the media could be, on all of these occasions, Ramsay did not claim to be the inventor of the method. He never published anything on the topic, and all that we know is the media interpretations of his remarks, which can be inaccurate. It seems that Ramsay admitted in his interview some exaggerations and played down the novelty of his remarks—"there is nothing new in that." At the dinner in June, Ramsay mentioned America, where the idea "is going to be tried" along with the United Kingdom, which perhaps was an indirect reference to the source of the idea.

In September of 1912, Ramsay traveled to the United States and stayed there till November. He had a few trips across the country and within the New York State (Travers, 1956), the home state of Betts. We may assume that Ramsay and Betts met and agreed to cooperate, although there is no direct evidence that this meeting ever took place (other than this cooperation would be beneficial for both of them). Travers (1956) noted that many documents, which were not related to Ramsay's fundamental research, were destroyed after his death—this may explain the absence of such evidence. When Ramsay returned to the United Kingdom, he convinced an industrialist and engineer Sir Hugh Bell to support the trial, which was to be conducted at Hett Hill near Tursdale Colliery in Durham. Two important testimonies came from Hugh Bell (1916) and his son Maurice Bell (Jolley and Booth, 1945).

It is clear from Bell's (jnr) recollection, who mentioned concrete-lined shaft of 6 ft in diameter and a drift stretching into the coal seam, that Ramsay was implementing the first Betts scheme (and not the fourth scheme as assumed in many publications). Ramsay's planned experiment is illustrated in Fig. 2.11 and corresponds very well to
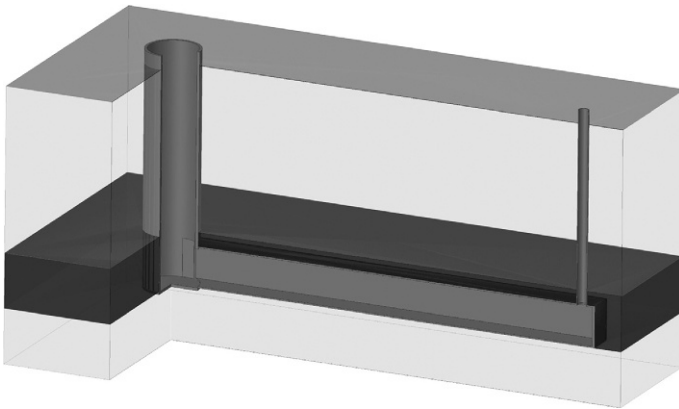
Fig. 2.11 Reconstruction of the Ramsay-Bell experiment prepared at Hett Hill near the Tursdale Colliery in Durham, as described by Sir Maurice Bell.

the description given by Betts. The borehole was not mentioned by Bell (jnr), but it was probably the last and the easiest element to be completed. The preparations were nearly completed, but Ramsay was not able to start his experiment due to the outbreak of World War I in 1914, which was soon followed by Ramsay's death. Bell (snr) was looking for an individual to continue but could not find anyone who would even remotely be as knowledgeable and enthusiastic as Ramsay. However, as it is possible to judge from available information, this experiment (if conducted) had good chances to be successful, assuming that Ramsay—one of the most distinguished scientists of his time—would have made correct choices and, during the experiment, reached the temperatures required for effective gasification.

2.6 The invention of UCG and its impact

While Ramsay's remarks received plenty of public attention, V.I. Lenin, who at that time lived in exile in Europe, eventually responded with an article praising Ramsay "for his invention" and used this occasion to make a political point about advantages of socialism (Lenin, 1913). During the first years of the Soviet UCG program (Sov1 in Fig. 2.12), Lenin's biased assessment of Ramsay's role became indoctrinated into the Soviet ideology. The first series of Soviet trials followed Siemens's paradigm of breaking coal and constructing a surface-like gasifier underground (the chamber method). While some of these experiments were conducted at a high technical level and with good preparations, all of them were unsuccessful.

Another approach named the stream method was suggested by the Donetsk Institute of Coal Chemistry (DICCh) that formed the basis of the Sov2 program (Fig. 2.12)
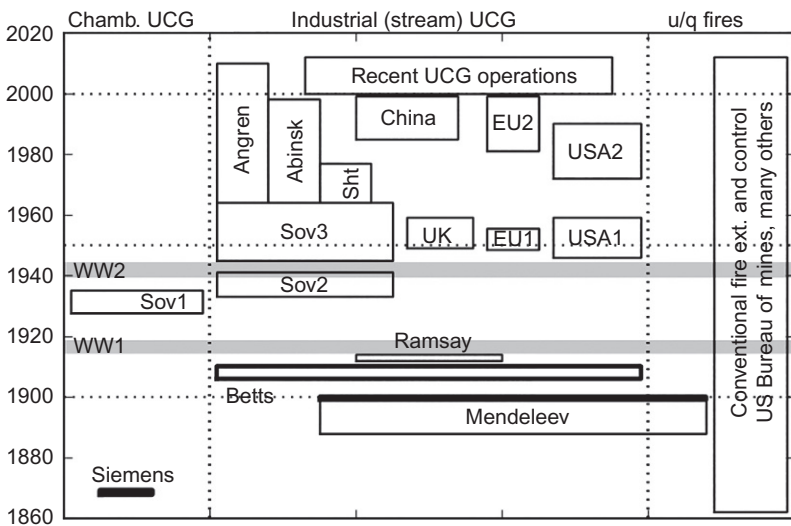
Fig. 2.12 The timeline of major UCG programs around the world. Further details can be found in Olness and Gregg (1977) and Klimenko (2009).

Table 2.1 Main periods in the UCG research and operations shown in Fig. 2.12

No	Period		Start	End	Countries
1	Invention		1868	WW1	The United Kingdom, the United States, Russia
2	First success		WW1	WW2	USSR
3	No men underground	Early	WW2	1964	USSR, the United Kingdom, the United States, Europe, China
		Late	1964	1999	
4	The recent surge		2000	Present	Canada, Australia, South Africa, China, the United Kingdom, NZ, the United States, EU

and proved to be a notable success. It is this approach (with numerous modifications and improvements, of course) that was later used in the USSR and in successful UCG programs in the United States, Europe, and China and in recent trails and operations. It is clear that this approach followed conceptual ideas of Dmitri Mendeleev and, even more so, the invention of Anson Betts. While Mendeleev has received regular, almost ceremonial praise in many Soviet UCG publications, the Soviet-style wording and unnecessary exaggerations would make any unbiased reader unsure about Mendeleev's genuine contribution to the area (which, in fact, was significant) (Table 2.1).

At the same time, the role of Betts in inventing UCG was ignored in the Soviet literature. It appears, however, that the contents of Betts's patent were known in the USSR, although the patent was incorrectly dated in year 1930 (Kirichenko, 1936; Chekin et al., 1936). The filing date—September 22—is nevertheless correct. Substitution of 1930 for 1910 was not a typographic mistake; Kirichenko (1936) showed the sketch of the blind borehole method by Betts, the same as displayed in Fig. 2.9, and described it as a variation that followed "the Ramsay method." It seems that this interpretation was common in the USSR. Since this mistake did not advantage Soviet researchers (as they made their inventions after 1930), one can only speculate about its nature. The Soviet patent obtained by DICCh (Korobchanskij et al., 1938) is granted not for a general formulation of the stream method but for a specific implementation of the method in steeply inclined coal seams.

As the Soviet UCG programs accumulated the highest expertise and used to set the agenda around the world, Betts's role was not recognized in the other countries including even the United States. In their historical review, Olness and Gregg (1977) discussed the role of Betts in inventing UCG, but this happened only after Betts death in 1976. As it can be seen from Fig. 2.12, all successful UCG operations are based on the stream method invented by Betts and on the conceptual understanding of UCG introduced by Mendeleev.

There is another aspect of Mendeleev's thoughts that, it seems, was completely overlooked in 20th century. Mendeleev envisaged the possibility of controlling, using

and extinguishing underground fires by UCG-like methods. Despite a long and generally not so successful worldwide history of fighting underground fires by conventional methods, the approach originated by Mendeleev has not received any attention. The volume of knowledge accumulated in UCG operations may change this and open opportunities for research and experiments.

2.7   Conclusions

The pattern of a successful invention often stretches from person to person and from place to place. The first idea may not be viable or productive at all, but it triggers someone's intuition and a more rational and practical version appears. However, even a productive idea is just an idea that needs to be attached to the real world and be expressed in terms of real devices and mechanisms. At this point, the idea becomes an invention. Finally, an invention needs someone with enthusiasm and leadership who can make it happen and ensure its commercial success. This general pattern is clearly visible in the chain Siemens→Mendeleev→Betts→Ramsay (although the first success was achieved only in the Soviet UCG program).

While Siemens and Ramsay have contributed to UCG, the main credit should go to Mendeleev, who envisaged the concept, and especially to Betts, who is the undisputable inventor of the process. Siemens had the first mention. Ramsay attempted to implement Betts invention and approached this with good understanding and leadership but was not able to finish this work and start the experiment due to the outbreak of WW1 and his premature death.

The family of ideas considered here involves the chamber method, the stream method, and the underground fire control. The chamber method has been intensively investigated and proved unviable. The stream method is the main method in industrial UCG. The ideas of Mendeleev on dynamic fire control have been overlooked.

References

Bell, H.B., 1916. Memorial to the late Sir William Ramsay. Nature 98, 197.

Betts, A.G., 1908. Lead Refining by Electrolysis. Wiley, New York.

Betts, A G., 1910, Method of utilizing buried coal, U.S. Patent No. 947608, filed 1906, issued 1910; Process of gasifying unmined coal, Canadian Patent No. 123068, filed 1909, issued 1910; An improved process for utilizing unmined coal, UK Patent No. 21674, filed 1909, issued 1910.

Betts, A.G., 1972, Recovery of sulphur dioxide (SO_2) from gas streams and precipitation of aluminum fluorine product, US patent No 3697248, filed 1970, issued 1972.

Chekin, P.A., Semenov, A.I., Galinker, J.S., 1936. Underground gasification of coals. Colliery Guardian 152, 1193–1196.

Gas World, 1912. How Sir William Ramsay would dispense with the coal miners. March, pp. 422–432.

Jolley, L.J., Booth, N., 1945. The underground gasification of coal. Survey of the literature. Fuel 24 (31–37), 73–79.

Kirichenko, I.P., 1936. Results and prospects for underground coal gasification. Ugol 124, 7–15.

Klimenko, A.Y., 2009. Early ideas in underground coal gasification and their evolution. Energies 2, 456–476.

Korobchanskij, I.E., Skafa, P.V., Matveev, V.A., Filipov, D.I., et al., 1938. Method of underground gasification of hard fuels, USSR Patent No. 947,608, filed 1934.

Lenin, V.I., 1913. A great technical achievement. Pravda, 91.

Mendeleev, D.I., 1888. The strength resting on the shores of Donetz river. Northern Digest, December, Collected works XI. Akademiya Nauk SSSR, 1949.

Mendeleev, D.I., 1897. Industry foundations, Denakov Printing House, St. Petesburg; in Collected works XI. Akademiya Nauk SSSR, 1949.

Mendeleev, D.I., 1900. Metallurgical industry of Ural region. Denakov Printing House, St.Petesburg Collected works XII. Akademiya Nauk SSSR, 1949.

Olness, D. U., Gregg, D.W., 1977. The historical development of underground coal gasification. Technical Report UCRL-52283, California Univ., Livermore (USA). Lawrence Livermore Lab.

Siemens, C.W., 1868. On the regenerative gas furnace as applied to the manufacture of cast steel. In: Meeting of the Chemical Society, May 7th.

Thurston, R.H., 1884. Sir Charles William Siemens. Science 3 (49), 34–36.

Tilden, W.A., 1918. Sir William Ramsay; Memorials of his Life and Work. Macmillian and Co., London.

Travers, M.W., 1956. A Life of Sir William Ramsay. Edward Arnold, London.

Watson, K.D., 1995. The chemist as expert: the consulting career of Sir William Ramsay. AMBIX 42, 143–159.

Further reading

Ignatieff, A., 1949. Underground gasification of coal: Review of progress. Trans. Can. Inst. Min. Metall. Min. Soc. Nova Scotia LII, 265–271.

The Times, 1912. (a) Coal smoke abatement March 25; (b) Sir G. Askwith on the industrial outlook, June 7.

History of UCG development in the USSR

3

Ivan M. Saptikov
Ergo Exergy Technologies Inc., Montreal, QC, Canada

3.1 Introduction

Underground coal gasification (UCG) is the process of in-situ conversion of coal to fuel or synthesis gas. The idea of converting coal in situ to an artificially produced fuel gas was first put forward in 1888 by Dmitri Mendeleev.

"Perhaps there will come a time when coal will not be mined and brought to the surface, but rather converted in the bed in its natural state of deposition to fuel gas which will be transported via a pipeline to be distributed over great distances," the great scientist wrote.

Sometime thereafter, he postulated the main mechanism of UCG: "After drilling several boreholes into the coal seam, use one of them to inject air; the other to produce—even suction out—fuel gas mixtures, they can then be easily delivered over long distances to furnaces."

In 1913, the world-renowned English chemist Sir William Ramsay was first to design an experiment in UCG producing fuel gas using the *well-gasifier* method. It was Sir William Ramsay's never implemented proposal for pilot application of the technology that received special recognition by the founder of the Soviet Union, Vladimir Lenin, in a Pravda newspaper article (Issue 91) that ran under the headline "One of the *Great Victories of Technology*," published on May 4, 1913. Thus, two great scientists, the Russian Dmitri Mendeleev and the Englishman Sir William Ramsay, are rightfully considered to be the founding fathers of UCG.

The practical implementation of the bold idea proposed by these great men meant the possibility of using the thermal energy of coal without bringing it up to the surface, in the hope of freeing mankind from the arduous and dangerous job of underground mining. However, up until the 1930s, no significant practical applications in the field of UCG were produced in either the USSR or abroad. Sir William Ramsay died in 1916 before commencing the pilot trial; World War I and revolutions in Europe delayed advance of the new technology. This was also due to the fact that UCG presented a complex technological challenge requiring a high level of technology development across many industries and science disciplines.

© 2018 Elsevier Ltd. All rights reserved.

3.2   Initiation of UCG technology development

3.2.1   Government's focus on UCG technology, bringing industry and science together

Initial UCG activities were commenced in the USSR in 1933. The work to achieve the technological outcomes was organized at the central government level. Later on, in 1939, a special government department responsible for UCG was set up, the Uprpodzemgaz, which included the scientific research institute VNIIPODZEMGAZ. A design team that was initially part of this R&D organization was later assigned to the independent design institute GIPROPODZEMGAZ located in the city of Donetsk (formerly Stalino). On July 11, 1939, on orders of the government of the USSR, the Presidium of the Academy of Sciences of the USSR heard a report presented by the task force of the USSR Academy of Sciences consisting of Academician A.M. Terpigorev and corresponding members of the USSR Academy of Sciences A.B. Chernyshev and Z.F. Chukhanov, who studied the UCG trials at the Gorlovskaya UCG plant noting that the first successful experiments achieved in the implementation of UCG required a wide deployment of research and development effort in this field. It was agreed to deem UCG the leading R&D effort of the Academy of Sciences. On June 4, 1940, the Presidium of the USSR Academy of Sciences established a permanent commission on UCG, chaired by Academician G.M. Krzhizhanovsky. The commission was charged with the specific task of coordinating scientific research carried out at the institutes of the Academy of Sciences of the USSR and industry research centers.

A number of research institutes of the Academy of Sciences of the USSR were involved in the work on UCG: the Krzhizhanovsky Power Engineering Institute, the Mining Institute, the Institute of Automation and Remote Control, the Institute of Mechanics, and the Underground Gasification Laboratory of the Ministry of Oil Industry and other scientific organizations. The research work, which was launched under the general guidance of the Commission, laid the groundwork of the systematic study of the most important issues of UCG problem and the training of scientific personnel. During the World War II, all work on UCG was temporarily suspended.

3.2.2   Variety of engineering approaches to UCG

First proposals with regard to UCG were based on technological principles developed for gasification of coal in surface producer gasifiers, an absolute prerequisite for which is the use of graded coal that is arranged into a layer of a specific height. A total of nine trials were conducted in 1933–35 in the Donbass and the Podmoskovny coal basin to test UCG methods based on the principles of gasification of crushed coal. These methods differed only in the approaches to loosening the coal seam and creating a working layer of coal. Some methodologies encompassed the placement of explosive charges in the coal seam with the subsequent command detonation (manual firing) of these charges from the surface (the Fedorov method), while other techniques

relied on self-detonation of charges as coal was gasified and the high-temperature front advanced in the seam (engineer Kirichenko's method). Lastly, the third group of proposals entailed mining coal from the coal seam, crushing, grading, and sizing it underground, followed by storing it in the mined-out workings or so-called underground magazines and, finally, its gasification (method of underground magazining developed by the engineer Kuznetsov).

All of these methods turned out to be unsuccessful in their application, primarily because of the nonuniform composition of the coal layer that led to the combustible gas components burning up even as they formed in narrow gasification channels between the coal particles, given the presence of free oxygen from the injected air which did not yet have time to react with coal in wider gasification channels.

The technological processes underlying these methods did not result in reliable gasification of coal underground and still required a great deal of labor-intensive work underground, as coal that was attempted to be gasified had already been removed from the seam and decompacted. These methods proved to be overly complicated. They could not support long-term, consistent quality gas production and, therefore, could not form the technological foundation for the new coal extraction method.

3.2.3 Workable UCG technology

At the end of 1933, a group of scientists and engineers of the Donetsk Institute of Coal Chemistry (Korobchansky et al.) developed and patented the UCG method that was based on the new technological principles of gasification of coal without preparation of coal, in a virgin coal seam. This method was termed the "stream gasification" method, otherwise known as the Donetsk Institute of Coal Chemistry method. The stream gasification method involves gasification taking place inside a gasification channel whose three walls are the coal seam floor, roof, and rubble consisting of collapsed rock, while the fourth wall is the coal seam (the extraction face moves orthogonally to the injected air and gas flow path).

In embodying this method, the underground gasifier can have a great many layouts. The simplest is the U-shaped gasifier layout that consists of three in-seam channels. Two shafts are tunneled from the surface to the coal seam in the downdip direction and serve to supply injection agent (air) and to produce gas, while the third one is cut in-seam along the strike and connects the first two excavations. Using shaft mining to expose coal for recovery by gasification, these channels were driven by hand. Initially, all trials were run using manual tunneling.

The gasification of coal takes place in the updip direction in steeply dipping coal seams and in the direction of the fresh coal yet to be gasified in subhorizontal coal seams. If two U-shaped gasifiers are connected, with one excavation left in the middle, we get a trident-shaped gasifier. This connection can be repeated any number of times to get new gasifiers with fundamentally similar layouts. The diagrams (Figs. 3.1 and 3.2) show the main underground gasifier layouts using precrushing of coal and stream gasification method.
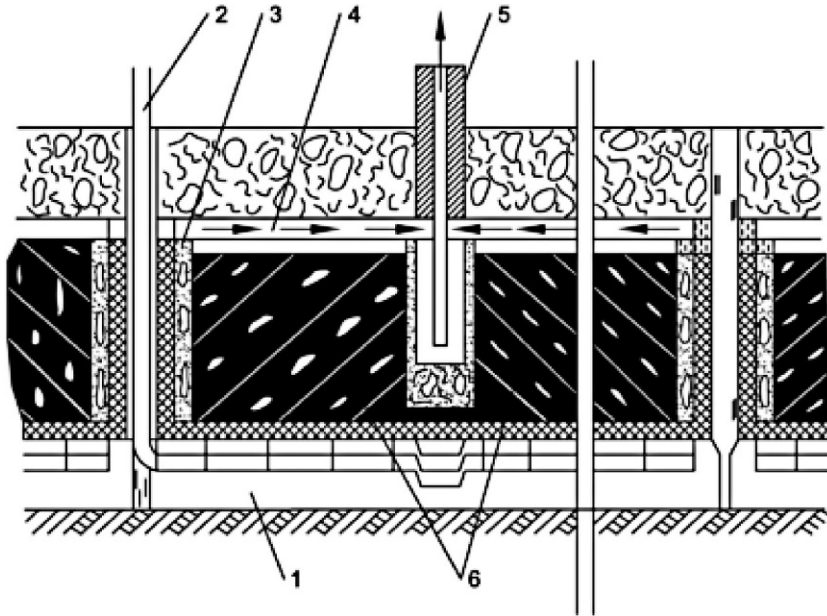
Fig. 3.1 Conceptual design of underground generator with crushed coal seam (1, lower channel; 2, injection well; 3, initial ignition workout; 4, upper syngas removal channel; 5, syngas production well; 6, wells with blast charges).
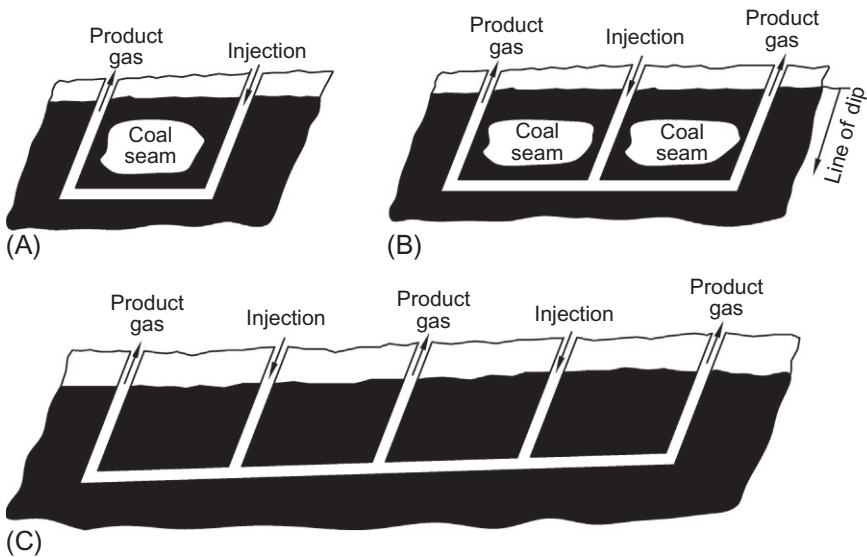
Fig. 3.2 Conceptual design of "stream method" of underground coal gasification. (A) A two-well stream method design; (B) A three-well stream method design; (C) A multiple-well stream method design.

3.3   Pilot UCG technology deployment in the USSR prior to WWII

3.3.1   Overview of experimental trials using coal prepared for gasification

3.3.1.1   Field trials at the Krutovskoe pilot site (Podmoskovny coal basin)

Panel 1

Trials ran from April 4 to April 17, 1933. The amount of coal exposed and prepared for gasification was 200 t. The panel consisted of a 10×10 m panel of coal to be gasified occurring at the depth of 15 m (Fig. 3.3). The air flow rate from the injection compressor and that of the exhaust blower was 6000 m^3/h, with the actual flow rate of the injected air being 1500 m^3/h. By the time when the prestart-up, commissioning, and construction activities were completed, the entire panel of coal to be gasified was crushed. An attempt to crush the coal even more by using explosives did not succeed due to difficulty of drilling blast holes. As a result of the experiment, an exhaust flue gas was produced containing excess oxygen. Subsequent opencasting of the trial panel revealed that of the 200 t of exposed coal, no more than 10 t was gasified.

Panel 2

Trials ran from August 13 to December 1, 1934. The amount of coal exposed and prepared for gasification was ~1000 t. The panel consisted of a 25×16 m coal block slated for gasification, bordered by mine workings and a brick wall.

A channel was tunneled through the center of the panel dividing it into two equal parts. Eleven wells were drilled in each and loaded with explosive material. It was believed that as the combustion zone advanced, the detonating charges would loosen
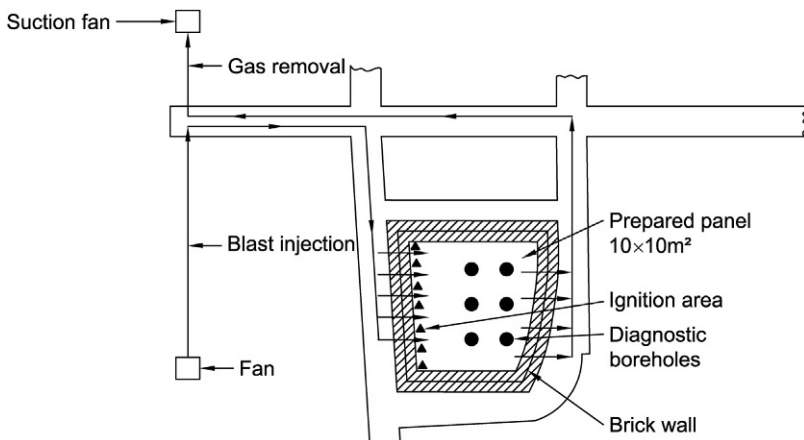
Fig. 3.3 Krutovskoe pilot site, experimental panel no. 1.

the coal creating favorable conditions for gasification. The injection agent (air) and production of gas were done using compressors (injection flow 1000–1500 m^3/h). The experiment yielded only poor combustion performance.

The gas contained CO_2 2.5%–7.5%, O_2 12%–18%, and CO 0.1%–1%. During selected periods, however, fuel gas was also produced. No postgasification opencasting was done at this panel. The amount of coal gasified was estimated at about 500 t (Fig. 3.4).

3.3.1.2   Field trials at the Shakhtinskaya pilot UCG plant

Experimental UCG runs were conducted in a thin seam of anthracite. The precommissioning activities on the panels included breaking up the coal block using explosives and manual crushing (*method of storing coal in an underground magazine*). The panel design and layout remained essentially the same; there were some variations in the size, location, and specific features. The trials involving precrushing of coal started in November 1933 and lasted 2 months, yielding no product fuel gas.

Experiments using the underground coal magazining method were conducted during the period from 1934 to 1936. Gasification would initially yield fuel gas. Burnouts ensued, the product gas had too much of incombustible constituents, resulting in disruption of the process and effectively stopping the trial. Further work at the Shakhtinskaya UCG plant was discontinued and the plant shut down (Fig. 3.5).

3.3.1.3   Field trials at the Lisichanskaya pilot UCG plant (Donbass)

Panel 1
Field trial activities were conducted from February 16 to July 29, 1934. The amount of coal exposed and prepared for gasification was 1600 t. Diagonal boreholes were drilled in the working section of the coal seam (Fig. 3.6). The wells were loaded with explosives. A grate assembly was installed in the lower portion of the panel
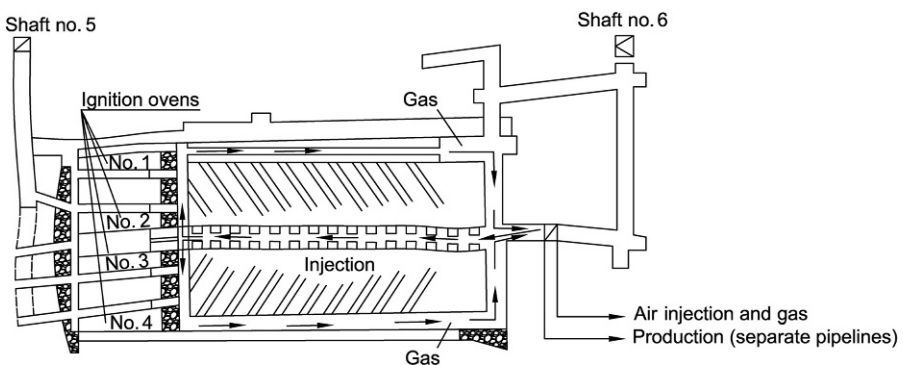
Fig. 3.4 Krutovskoe pilot site, experimental panel no. 2.
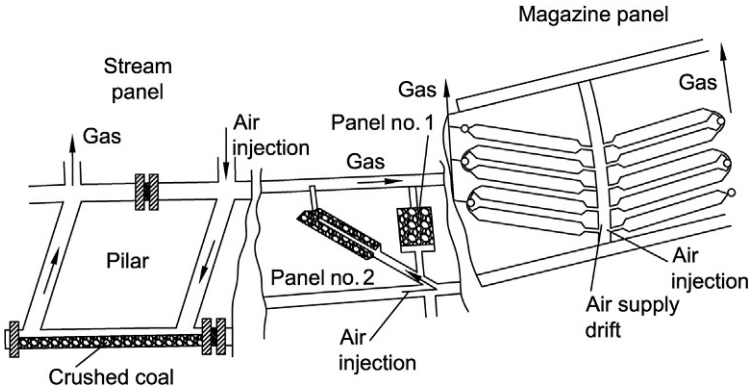
Fig. 3.5 Shakhtinskaya pilot UCG plant, experimental panels.
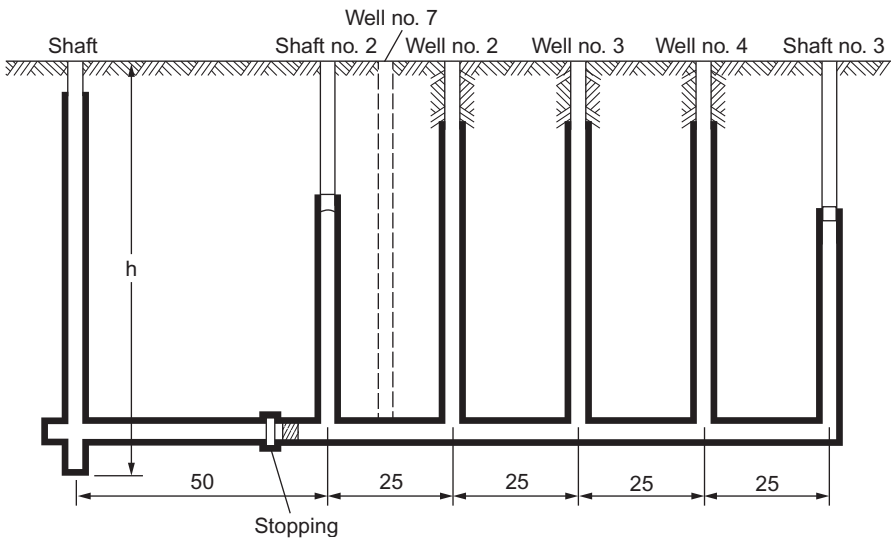
Fig. 3.6 Gorlovskaya pilot UCG plant, experimental panel 1.

and served as the air injection point. However, the loosening of coal was not uniform and led to an unfavorable resistance to gas flow, resulting in poor outcomes with no product fuel gas.

Panel 2

Trials ran from November 26 to December 16, 1934. The amount of coal exposed and prepared for gasification was ~200 t. The underground gasifier design incorporated an underground magazine bordering a section of the coal seam 12.5 m along the strike

and 25 m in the updip direction. All coal at the panel was manually precrushed and left in place.

Trials conducted at this panel initially did produce a fuel gas with the following composition: CO_2 10%–12%, O_2 1%–2%, CO 12%–15%, H_2 18%–14%, CH_4 1%–3%, and a calorific value of 757–1080 kcal/m^3. Subsequently, however, burnouts caused the gas to deteriorate, with only flue gas produced by the end of the trial.

3.3.2   An overview of trials using the "stream gasification" method

Practical field trials that would put the "stream gasification" method to the test in a solid block of coal commenced in 1935. A total of nine trials were conducted during the period from 1935 to 1941:

– Three trials at the Gorlovskaya UCG plant
– One trial at the Podmoskovnaya UCG plant
– Two trials at the Lisichanskaya UCG plant
– One trial at the Shakhtinskaya pilot UCG plant Shakhty
– Two trials at the Leninsk-Kuznetsk UCG plant in the Kuzbass region

At the very outset, the first experiments using the stream gasification method resulted in positive outcomes. The trials were conducted both in steeply dipping coal seams (in the Donbass at the Gorlovskaya and Lisichanskaya UCG plants and in the Kuzbass at the Leninsk-Kuznetsk UCG plant) and in subhorizontal lignite seams (Podmoskovnaya UCG plant).

3.3.2.1   Experimental work at the Gorlovskaya pilot UCG plant

Panel 1
Trials ran from February 5 to May 1, 1935. Experimental work at the Gorlovskaya UCG plant involved the largest-scale trials, and the results proved to be compelling. The experiments were carried out using continuous and intermittent injection for air-blown, oxygen-blown, and steam-/oxygen-/air-blown UCG process. During this period, about 12 million m^3 of product gas was produced with a calorific value of 900 kcal/m^3 using injected air and a calorific value of 2500 kcal/m^3 with a steam-oxygen injection agent.

Various modes of operation were trialed: Oxygen concentration varied from 21% to 80%; the intermittent flow and continuous injection modes were tested. Different modes of operation produced different quality product gas, from usable fuel gas to process gas suitable for further chemical processing.

The product gas composition results (Table 3.1) fell into the following ranges.

Production totals for the period trial activities at the panel were 9 million m^3 of product fuel gas with a calorific value of about 1000 kcal/m^3 and about 3 million m^3 of process gas with a calorific value in excess of 2000 kcal/m^3.

The practical field experience at Gorlovskaya panel 1 demonstrated the feasibility of UCG in a solid block of coal, laid the core foundation for operating the coal gasification process, and served as the launching pad for further development of the UCG

Table 3.1 **Gorlovskaya UCG plant, syngas composition**

	CO_2 (%)	O_2 (%)	CO (%)	H_2 (%)	CH_4 (%)	Q (kcal/ m^3)
Using injected air as the oxidant	8–10	0.2	13–16	11–15	2–5	900–1000
With $O_2 = 23\%$	12–17	0.2	17–19	19–20	2–5	1300–1400
During the interrupted flow mode (air injection temporarily stopped)	14–20	0.2	16–17	45–55	4–5	2000–2100

technology in the USSR. The schematic diagram (Fig. 3.6) shows the design and layout of Gorlovskaya UCG panel 1.

Further applications of the "stream gasification" method at the Gorlovskaya UCG plant were carried out during the period from December 1, 1937 to October 10, 1939 on panels 5 and 6. The process utilized injected air as the oxidant, which ensured steady operation of the plant and yielded product gas with the following composition: CO_2 9%–11%, O_2 0.2%, CO 15%–19%, H_2 14%–17%, CH_4 1.4%–1.5%, and $Q = 900$–1000 kcal/m^3. During this period, 59.5 million m^3 of gas was produced, of which 18 million m^3 was delivered to and used by the ultimate consumer through a system of distribution piping for the first time in the world (the Gorlovka coke processing plant).

The next stage of trials began on gasifier 8 in April 1941. The process of the UCG plant was based on an air-blown gasifier with the high-pressure air injection flow rate of 5–10 m^3/h. The calorific value of the gas was 850–950 kcal/m^3. Gas was delivered in the minimum specified quantities to the gas turbine designed by Prof. Makovsky, which was set up and tested at the Gorlovskaya UCG plant.

Following the invasion of the Nazi forces during World War II, UCG trials at the Gorlovka plant were stopped, the plant itself closed, and the underground gasifiers flooded. Since the Nazi Germans undermined the barrier pillar separating the underground gasifier from neighboring coal mines, restoration of the UCG plant after the war was deemed inadvisable. Successful trials at the Gorlovskaya UCG plant in a solid block of coal put an end to any further attempts to pursue other methods involving precrushing coal or breaking up the coal seam. The practical field experience at Gorlovskaya panel 1 demonstrated the feasibility of UCG in a solid block of coal, laid the core foundation for operating the coal gasification process, and served as the launching pad for further development of the UCG technology in the USSR.

3.3.2.2   Field trials at the Lisichanskaya UCG plant

During the period from January 1936 to December 1940, UCG trials were conducted using the "stream gasification" method at several panels in Lisichansk (the Donbass).

The pilot UCG panel design was similar to the gasifiers at the Gorlovskaya UCG plant, with the exception of the use of boreholes ancillary design elements. During the trials, air-blown and water-vapor-blown modes of operation were attempted. When using injected air as the oxidant at the flow rate of about 2000 m^3/h, the following gas quality was obtained: CO_2 15.5%, CO 12%, H_2 14%, CH_4 2.5%, and calorific value $= 930$ kcal/m^3.

With water vapor injection, the following gas quality was obtained: CO_2 21%, CO 15%, H_2 51%, CH_4 5%, and calorific value $= 2200$ kcal/m^3. Positive outcomes obtained during UCG trials led to the decision to commission the commercial Lisichansk UCG plant. Construction and commissioning of three commercial gasifiers were completed in December 1940. The schematic diagram below (Fig. 3.7) shows the gasifier design and layout.

These gasifiers operated from December 18, 1940 to November 10, 1941. The amount of coal exposed and prepared for gasification was 186,000 t. The objective was to achieve commercial levels of gas production and to supply gas to the Donsoda plant. All three UCG gasifiers were trident-shaped in design, with prestart-up construction completed using shaft mining methods. An ignition crosscut was driven in the lower part of the gasifier at a depth of 120 m from the ground surface, which delimited the gasifier boundaries. Three in-seam upraises in the updip direction were put through to each gasifier. Upraises were connected to the surface via shafts. The distance between the shafts was 115–130 m.

Over the first 5 months of operation (from December 1940 to June 1, 1941), product gas had a calorific value of 900–1800 kcal/m^3, about 10 million m^3, of which 6 million m^3 was delivered to the consumer and used in commercial manufacturing processes. Faced with the invading Nazi troops, the Lisichanskaya UCG plant was shut down by flooding the gasifiers.
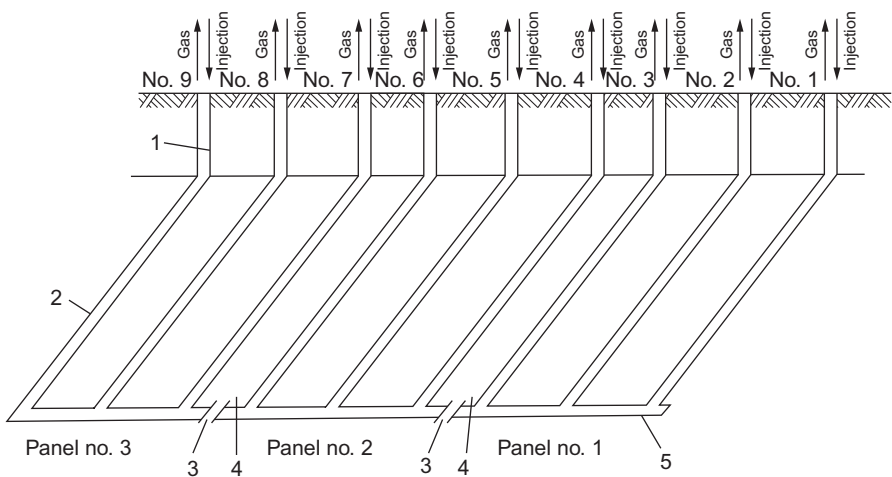
Fig. 3.7 Lisichanskaya UCG plant, commercial panels nos. 1, 2, and 3 in seam K_8.

3.3.2.3 Field trials in Leninsk-Kuznetsk (Kuzbass)

Panel 1

Field trial activities were conducted from June 1 to November 17, 1934. The amount of coal exposed and prepared for gasification was 1500 t. The target coal block was accessed with two shafts (shafts A and B) and was delineated by a bypass crosscut. Air injection flow rate was 150–200 m^3/h and supplied through a pipeline that passed through shaft A and a brick bulkhead. Gas was drawn off by an exhaust blower through a pipeline passing through shaft B. The trial did produce fuel gas. By the end of the experiment, the bulkhead had burned causing a loss of an airtight seal of the panel, and the panel was shut down (Fig. 3.8).

Panel 2

Field trial activities were conducted from April 27, 1935 to February 25, 1936. The amount of coal exposed and prepared for gasification was 18,000 t. The panel consisted of a 50 × 60 m section of the coal seam. The coal was exposed by shafts 3 and 4. A 12 m cross channel was put through from shaft 3, perpendicular to which, along the strike of the coal seam, a 50 m fire channel was made in both directions. From the fire channel, five furnaces were put through, 60 m long each, 10–12 m from each other. At the end of the furnaces, they were connected by a collector channel that ran parallel to the fire channel. Furnaces 1, 3, and 5 were intended for gas production while furnaces 2 and 4 for air injection to the fire face.

After a long period of ignition and heat-through, fuel gas was in fact produced with the following average composition: CO_2 12%, O_2 0,2%, CO 12%, H_2 16%, CH_4 4%, and calorific value = 1100 kcal/m^3. The flow rate of the injected air was about
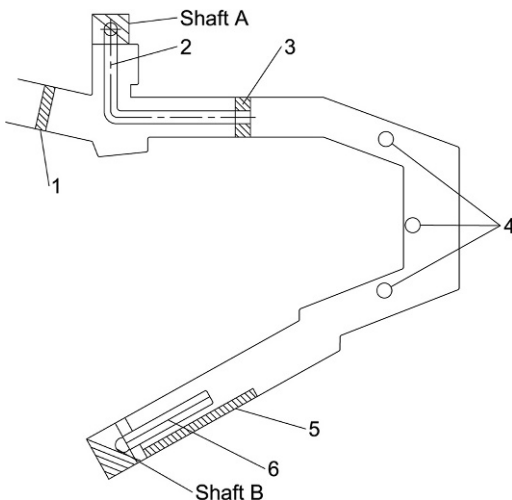
Fig. 3.8 Leninsk-Kuznetsk pilot UCG plant, experimental panel 1 (1, clay wall; 2, air pipeline; 3, brick wall; 4, ignition devices; 5, clay wall; 6, syngas pipeline).
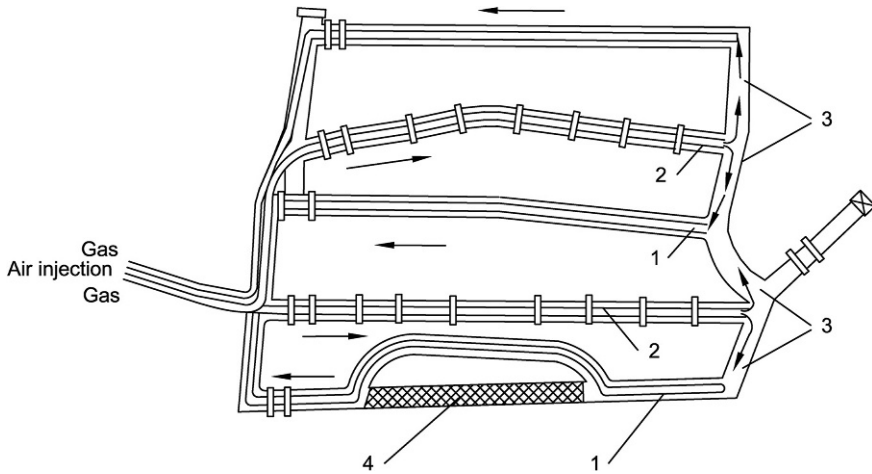
Fig. 3.9 Leninsk-Kuznetsk pilot UCG plant, experimental panel (1, syngas pipelines; 2, air pipelines; 3, ignition channel; 4, old collapsed channel).

2000 m^3/h, with approximately the same amount of fuel gas produced. The gas was burned in the boilers of the neighboring Lenin mine. During the trial, about 4000 t of coal was gasified.

The schematic diagram above (Fig. 3.9) shows the design and layout of the UCG panel.

3.3.2.4 Field trials at the Podmoskovnaya UCG plant

Panel 1
Field trial activities were conducted from November 7, 1940 to October 15, 1941. The amount of coal exposed and prepared for gasification was 35,000 t. The objectives included the following:

– To organize a UCG trial in the solid block of coal at the Podmoskovny coal basin using the "stream gasification" method
– To discover experimentally a system suitable for UCG in the Podmoskovny coal basin
– To initiate major development of UCG in the Podmoskovny coal basin

The panel was constructed using shaft mining and a trident-shaped stream gasification layout and consisted of three cased pitholes and channels and an uncased connecting channel that was 100 m long at a distance of 70 m from the vertical pitholes. Each pithole could be used for air injection or gas production. The direction of the process could be reversed. Compressors were capable of providing a flow rate of 12,000 m^3/h. The capacity of the oxygen plant was about 1000 m^3/h.

Gas produced by the UCG plant was used to power its own heating boilers and boiler plants at commercial enterprises in the city of Tula, which was the largest

Table 3.2 **Podmoskovnaya UCG plant, performance indicators**

	1940	1941
Total amount of gas (million m^3)	8.950	26.360
Amount of gas used in boilers (million m^3)	0.36	12.60
CV (kcal/m^3)	827	890

consumer, specifically the Tula armament plant. The UCG plant remained operational up until the time when the occupying Nazi troops advanced, which necessitated the shutdown of the plant and evacuation of equipment. The main performance indicators of the Podmoskovnaya UCG plant are summarized in Table 3.2.

Prior to World War II, in the course of all UCG trials, coal was exposed in the coal block and prepared for gasification using shaft mining methods. During experimental work at the Gorlovka UCG plant between 1935 and 1936 and then at the Podmoskovnaya UCG plant in 1940, a high gas permeability of coal seams was established. This phenomenon was first utilized at the Podmoskovnaya UCG plant in 1941 for purposes of performing precommissioning preparation activities without the use of shaft mining methods, but rather drilling vertical wells from the surface to the coal seam, linking the wells to the active fire face by means of burning an in-seam channel, followed by stream gasification, and discontinuing the use of coal precrushing. The experimental work carried out in the USSR prior to WWII demonstrated that stream gasification in the solid block of coal in situ, without precrushing or breaking up the coal, may provide a strong foundation for commercial applications of UCG as an alternative coal mining method.

3.4 UCG production recommencement and commercial deployment post WWII

3.4.1 Introduction

As early as in 1942, further development effort in UCG recommenced in the USSR. The Council of Ministers of the USSR tapped 11 research centers of the Academy of Sciences of the USSR and 9 industry research centers to conduct further research in UCG.

Field research centers from the VNIIPODZEMGAZ research institute were set up at all UCG plants under construction and in operation. In 1942, before the end of the war, work began on the restoration of the Podmoskovnaya UCG plant and scaling up production to commercial levels.

By 1948, the Lisichanskaya UCG plant was commissioned in Donbass where an experimental directional drilling task force was appointed. The Yuzhno-Abinskaya UCG plant was designed and put into commercial operation in 1955 in the city of Kiselevsk in Kuzbass. Plant designs were completed by 1952, and construction was finished by 1957 at the following sites:

- Shatskaya UCG plant in the Moscow region, some 30 km from the city of Tula.
- Kamenskaya UCG plant in Kamensk-Shakhtinsky.
- Angren UCG plant in Angren, Uzbekistan.
- In Gorlovka, on the basis of the tool engineering and precision machining shop of the Gorlovskaya UCG plant, a machine engineering plant was set up to manufacture specialized drilling equipment and other types of equipment and components for the rest of the UCG plants.

In 1956, the VNIIPODZEMGAZ team in Donetsk was reorganized into an independent design facility GIPROPODZEMGAZ. A new program for training UCG engineers was established at the Donetsk Industrial Institute under the auspices of the Ministry of Higher Education of the USSR. The new department (known as the UCG group) produced over 500 leading UCG process engineers prior to its closure in 1962. Dozens of manufacturing and metalworking plants throughout the USSR churned out machinery and equipment for the construction of UCG plants, including pipework and machines that were cutting edge for their time, such as the GT12 gas turbine for the Shatskaya UCG plant or the 2 m diameter pipes custom rolled and welded for the Angren UCG plant's main gas pipeline. This large-scale work was organized and carried out by Glavpodzemgaz at the Ministry of Coal Industry of the USSR under the leadership of outstanding engineers and industry leaders V.A. Matveev and P.V. Skafa.

Since 1957, UCG, as a countrywide industry branch, was transferred from the jurisdiction of the Ministry of Coal Industry to the administration of the Glavgaz of the USSR by decision of the Council of Ministers of the USSR. The three previously commissioned UCG plants continued to operate (the Podmoskovnaya, Lisichanskaya, and Yuzhno-Abinskaya), while construction of three new commercial plants—the Shatskaya, Angrenskaya, and Kamenskaya—was completed followed by their commissioning and start-up.

During this period, the technology and volumes of commercial production of UCG gas in the USSR reached their highest levels. Active research was ongoing at the research institutes on fundamentals of in situ gasification processes, the science and engineering of UCG. The results of this work were widely applied at the commercial UCG plants in an effort to develop and improve the large-scale plant operation. New methods and operational techniques were developed, trialed, and implemented at all the commercial UCG plants of the VNIIPODZEMGAZ Research Institute, with new types of drilling rigs, more advanced compressors, and other process equipment being introduced.

3.4.2 Commercial UCG plants operating in steeply dipping coal seams

3.4.2.1 Lisichanskaya UCG plant

The commercial UCG plant was commissioned just before the breakout of WWII. After the end of WWII, the UCG plant was rebuilt and put into operation in 1948 using injected air and steam-enriched air injection. The product gas was delivered to the

Sevdon hydroelectric power plant. Gas deliveries to the ultimate consumer amounted to 150–200 million m^3/year by the beginning of the 1960s. Coal gasification at the UCG plant was conducted in steeply dipping coal seams ranging 0.5–1.2 m in thickness. The parameters of Lisichansk coal are presented in Table 3.3.

The average composition of the gas produced by the Lisichanskaya UCG plant is presented in Table 3.4.

The first gasifiers soon after the UCG plant was rebuilt were constructed and operated with the preparation of coal for gasification using shaft mining methods. Despite good outcomes in terms of technological and economic efficiency, innovation efforts at the UCG plant continued with a view to preparing coal for gasification without the use of conventional mining methods. The next line of underground gasifiers was constructed using the so-called combined scheme, where the fire channel was driven, with directional wells drilled into it in the downdip direction, followed by coal ignition in the fire channel and gasification, and was operated inside this structure. Gasifiers of this series functioned with adequate efficiency.

The next stage of work was aimed at developing gasification process completely excluding any underground mining work associated with gasifier preparation for the gasification process. The challenge was to develop methods for preparing gasifiers and operating the gasification process using the natural permeability of the coal seam and developing horizontal and directional drilling methods. An experimental directional drilling task force was formed at the Lisichanskaya UCG plant charged with the responsibility of developing and implementing the technology of drilling directional and horizontal wells within the coal seam. The technology of drilling such wells developed by this task force was applied at all the UCG plants, both in steeply dipping and subhorizontal coal seams. Fig. 3.10 shows the schematic diagram of a basic design of a gasifier that does not require underground mining works to prepare coal in steeply dipping coal seams as used in Lisichansk.

Three types of wells drilled into the coal seam were employed to prepare coal for UCG:

- Vertical injection/ignition wells completed into the coal seam to the depth of the lower boundary of the gasification chamber
- Directional injection wells drilled in the footwall and installed into the coal seam at the depth level of the fire front
- Directional production wells drilled and cased through rock strata to the point of intersection with the coal seam and further along the strike to the initial gasification interval or to the boundary of the advancing fire front

This design was termed the continuous gasification system where the fire front advances in the updip direction. The simplicity of the gasifier design, the flexibility in maneuvering the injection and gas production points, and the ability to vary the distance and direction of production wells relative to the injection/gas streams made for a stable gasification with consistent gas quality and high coal recovery. In addition to the UCG gas, production of inert gases (argon and krypton) was started utilizing the existing oxygen plant. The UCG plant was completed distributing the on-spec fue gas to the consumers, but starting in 1963, the construction

Table 3.3 **Lisichanskaya UCG plant, coal parameters**

Proximate analysis (%)				Ultimate analysis (%)						
FC	Ash	VM	IM	C	H	O	N	S	LHV (kcal/kg)	HHV (kcal/kg)
47.5	25.1	13.8	13.6	54.4	3.8	11.0	1.2	2.2	5031	5318

Table 3.4 Lisichanskaya UCG plant, syngas composition

Gas composition (vol%)							
CO_2	O_2	CO	H_2	H_2S	CH_4	N_2	CV (kcal/m^3)
19.0	0.1	4.0	19.1	1.1	3.2	53.5	896
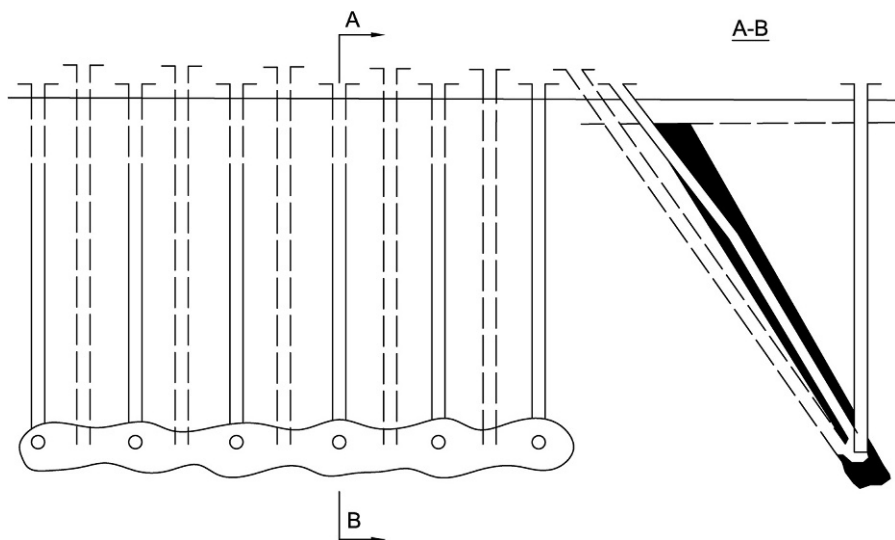
Fig. 3.10 Lisichanskaya UCG plant, conceptual design with directional wells.

and commissioning of new gasifiers were stopped due to lack of new investment. By the mid-1970s, it became impossible to produce syngas at the plant, and this UCG facility ceased to exist.

3.4.2.2 Yuzhno-Abinskaya UCG plant

The UCG plant was designed, built, and put into operation in May 1955 as a commercial UCG plant located in the South Abinsk area in Kuzbass. As in Lisichansk, the initial gasifier was constructed with the use of mining excavation of the gasification channel, while subsequent gasifiers no longer involved any underground mining work. The gasifier design employed was largely the same as in Lisichansk.

The UCG plant operated in steeply dipping coal seams of various thicknesses, 2, 4, and 9 m. By 1958, the plant reached its design production capacity. As a commercial UCG plant, its design capacity was not set at a very high level. The product gas had a calorific value of 1000–1200 kcal/m^3 and was supplied to the heating boilers of the nearby coal mines and other enterprises. The plant was contemplated for future expansion with higher gas production output. After 1965, all new development work slowed

down due to lack of investment. The commercial UCG plant operated at reduced capacity and served its customers for many years until it gradually exhausted all previously constructed gasifiers. By the mid-1990s, commercial production of gas ceased. The coal composition of the Yuzhno-Abinskaya was characterized as shown in Table 3.5.

The average gas composition of the Yuzhno-Abinskaya UCG plant is presented in Table 3.6.

3.4.2.3   Kamenskaya UCG plant

This UCG plant was designed to operate in steeply dipping coal seams of the so-called "lean" coal, which is close in composition to anthracite. By 1961, the main production facilities were built there, a pilot gasifier was commissioned, and several ignition and linking trials were conducted. However, the UCG plant was never put into commercial operation due to the government's decision to stop UCG development work in the country.

3.4.3   Commercial UCG plants operating in subhorizontal coal seams

3.4.3.1   Podmoskovnaya UCG plant

In 1942, after partial restoration of the Podmoskovnaya UCG plant, new semicommercial panel no. 2 was introduced into operation. Panel no. 2 was developed by expanding the fire source that had remained in the no. 1 pilot panel, with new wells drilled and introduced into the gasification process using reverse combustion linking (RCL). Gasification activities were conducted at the no. 2 panel from July 1942 to the end of 1946.

The objectives of this trial were as follows:

- Master gasification without the use of supplementary underground mining works, using the natural permeability of coal.
- Perfect the ignition and fire control management system.
- Gain the experience necessary for commercial scale-up.

During the period from 1943 to 1946, the directional combustion linking technique was developed and implemented, with a certain system of combustion work applied, which made it possible to scale up the Podmoskovnaya UCG plant to a large commercial enterprise. Table 3.7 summarizes the main performance indicators of the no. 2 Podmoskovnaya semicommercial panel.

The first commercial UCG panel (no. 3) was introduced in 1947. Panel no. 3 was in operation from March 1947 to early 1949.

Objectives were as follows:

- Start commercial production of UCG gas.
- Gain experience of commercial UCG application to lignites.
- Conduct further studies of the UCG in a commercial production setting.

Table 3.5 **Yuzhno-Abinskaya UCG plant, coal composition**

Proximate analysis (%)				Ultimate analysis (%)						
FC	Ash	VM	IM	C	H	O	N	S	LHV (kcal/kg)	HHV (kcal/kg)
66.9	3.7	25.0	6.4	75.0	4.4	10.2	2.3	0.0	6854	7130

Table 3.6 Yuzhno-Abinskaya UCG plant, syngas composition

Gas composition (vol%)							
CO_2	O_2	CO	H_2	H_2S	CH_4	N_2	CV (kcal/m^3)
15.4	0.2	11.9	15.2	0.0	3.2	53.4	1037

Table 3.7 Podmoskovnaya UCG plant, panel no. 2 performance indicators

Year	Gas production, total million m^3	Supplied to outside end user and own boiler (million m^3)	Average CV (kcal/m^3)
1942	10	7.3	876
1943	14.5	7.4	714
1944	21.7	18.5	835
1945	31.8	17.1	765
1946	32.5	21.2	840
Total	**121**	**72**	
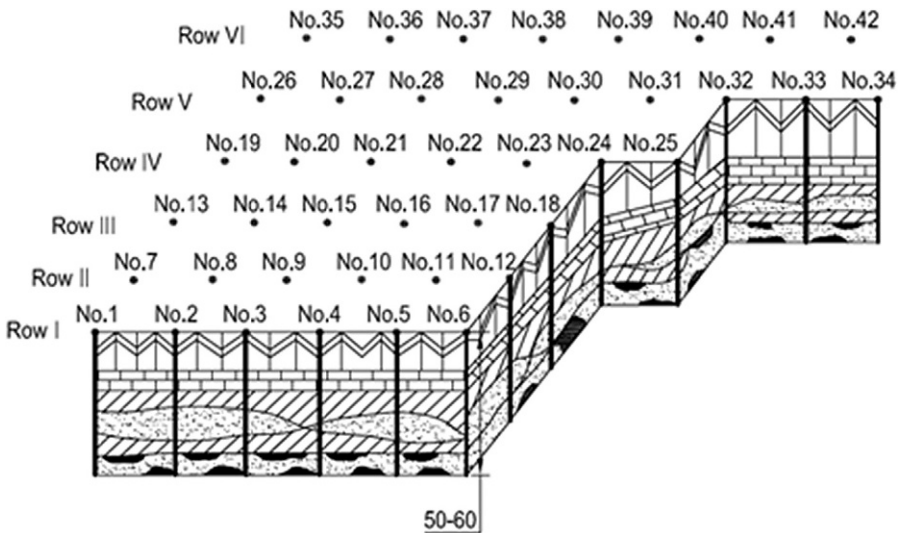
Fig. 3.11 Podmoskovnaya UCG plant, panel no. 3 design.

The panel was constructed as a system of vertical injection and production wells drilled from the surface and completed into the coal seam. Wells were connected with each other by combustion linking, which is based on the permeability of coal and the fire front moving in direction opposite to direction of injected air. Fig. 3.11 shows the panel no. 3 design.

The construction of the panel and ignition was done without mining. After the initial ignition and heating of the coal resulting in sufficient increase of reactive surface area of the coal, in October 1947, the panel no. 3 reached its design capacity. By 1949, the production capacity of the Podmoskovnaya UCG plant was expanded to 450 million m^3/year. The UCG plant operated in the coal seam at an average depth of 45 m. The composition of coal at the Podmoskovnaya is presented in Table 3.8.

The average composition of gas produced by the Podmoskovnaya UCG plant is summarized in Table 3.9.

The UCG plant operated at this production level until the beginning of the 1970s, supplying syngas for boilers of several industrial enterprises and institutions of the city of Tula. Concurrently with the production activities, the engineering and technical service of the UCG plant and the research division of VNIIPODZEMGAZ continued work on the development and improvement of operational regimes, increasing the efficiency of gasification and well linking, investigating the causes and repeating patterns of the geomechanical response of the rock strata during UCG and the effects of the hydrogeologic factors, and studying the impact on the environment and the development of measures to prevent contamination of the environment. A hydrogen sulfide removal unit was operating at the plant, generating not only processed hyposulfite but also pure hyposulfite employed as a fixing agent in photography.

The production costs at the Podmoskovnaya UCG plant in terms of solid fuel equivalent were one and a half times lower than at the Tulaugol coal mines. The outcomes obtained at this UCG plant formed the basis for UCG plant design for operation at shallow depth of occurrence of coal seams. In particular, the gasifier design used at the Shatskaya and Angren UCG plants was patterned after that of the Podmoskovnaya UCG plant. In the course of over 20 years of uninterrupted commercial production, the Podmoskovnaya UCG plant delivered to its customers about 10 billion m^3 of syngas. Starting in 1963, further development of the UCG technology at this UCG plant was halted. By the 1970s, the plant closed having recovered all previously delineated reserves.

3.4.3.2   Shatskaya UCG plant

The UCG plant was built at the Shatskoye coalfield in the Mosbass (the Podmoskovny coalfield), some 30 km from the Podmoskovnaya UCG plant. UCG operations were conducted in the lignite coal seam occurring at a depth of 40–45 m. The coal quality and the properties of the coal seam were the same as those at the Podmoskovnaya UCG plant; hence, the gasifier design, linking modes, and gasification modes of operation were the same that had been successfully used at the Podmoskovnaya UCG plant. Fig. 3.12 shows the basic gasifier design at the Shatskaya UCG plant.

The coal composition at the Shatskaya is presented in Table 3.10.

The average composition of gas produced by the Shatskaya UCG plant is summarized in Table 3.11.

The UCG plant was designed as an industrial complex consisting of the UCG plant and a power plant with two gas-fired turbine generators. Construction was started in 1952. Meanwhile, design and manufacture of the GT-12 UCG gas-fired turbine

Table 3.8 Podmoskovnaya UCG plant, coal composition

Proximate analysis (%)				Ultimate analysis (%)					LHV (kcal/kg)	HHV (kcal/kg)
FC	Ash	VM	IM	C	H	O	N	S		
28.2	21.2	20.6	28.9	32.4	2.6	10.2	0.7	3.5	2916	3230

Table 3.9 **Podmoskovnaya UCG plant, syngas composition**

Gas composition (vol%)							
CO$_2$	O$_2$	CO	H$_2$	H$_2$S	CH$_4$	N$_2$	Q (kcal/m^3)
21.2	0.2	5.6	17.0	1.5	2.1	52.4	828
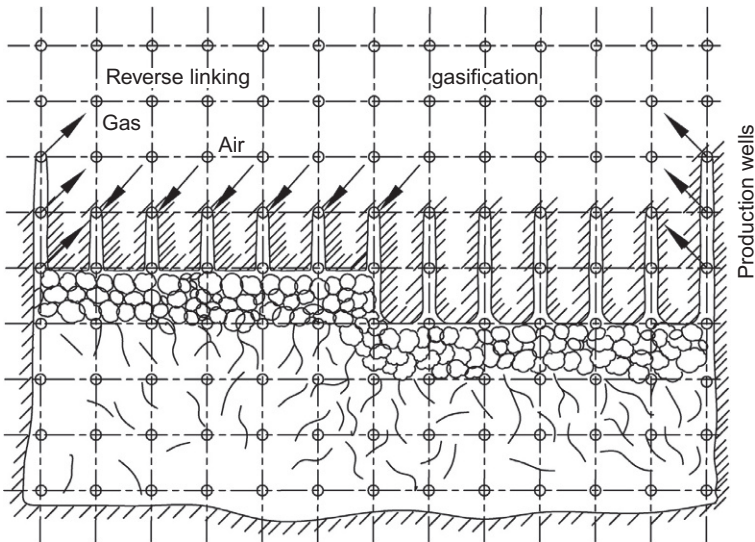
Fig. 3.12 Shatskaya UCG plant, conceptual gasifier design.

generator began at the Leningrad Metalworking Plant (LMZ). By 1957, construction of all the gas production facilities was completed. Miscellaneous electric work was completed during the period from 1955 to 1957. Installation of the gas turbine commenced in May 1956 and was completed in early 1958. In May 1958, the unit was tested in the no-load condition. The gas turbine was synchronized with the electric grid for the first time and was running at working load starting from June 4, 1958. By August 1958, the unit was running at maximum load conditions of 12,000 kW. In 1958, the gas turbine produced and exported to the Mosenergo grid about 8 million kWh, having run about 860 h. During the months of January and February 1959, the turbine produced and fed to the Mosenergo grid about 11 million kWh, with a total running time of 11,260 h. In February, the unit was operated at full load without interruption. The challenges in the design of the gas turbine that were revealed during these trials were reported back to LMZ for redesign and modification and fabrication of some parts and units. This work progressed very slowly for a whole host of reasons, and in 1963, pursuant to the order of Mingazprom mentioned above, it was stopped altogether.

Table 3.10 **Shatskaya UCG plant, coal composition**

Proximate analysis (%)				Ultimate analysis (%)						
FC	Ash	VM	IM	C	H	O	N	S	LHV (kcal/kg)	HHV (kcal/kg)
29.2	21.2	21.6	22.6	33.4	2.6	10.2	0.7	2.0	3216	3230

Table 3.11 **Shatskaya UCG plant, syngas composition**

Gas composition (vol%)							
CO_2	O_2	CO	H_2	H_2S	CH_4	N_2	Q (kcal/m³)
19.7	0.2	6.9	20.5	0.5	2.1	50.1	896

Thus, a remarkable project that would allow power generation to tap into immense reserves of low-quality coals at a high-technological level was frozen halfway. The Shatskaya UCG plant continued to produce UCG gas that was delivered to the Podmoskovnaya UCG plant via a 35-km-long pipeline and then to the ultimate consumer. Since the decision of Mingazprom to stop the development of UCG was taken in 1963, the Shatskaya UCG plant gradually reduced gas production and by the mid-1970s permanently ceased operation.

3.4.3.3   Angren UCG plant

Design of the Angren UCG plant was completed in 1952, and starting in 1953, construction began. The project entailed gasification of 25 million t of coal reserves and a coal seam thickness of 2–28 m. The initial design brief called for a UCG plant as a commercial UCG plant consisting of a UCG plant and a thermal power plant with high-pressure steam turbines, with power generation capacity of 200 MW.

During the design stage, the proposal of the Ministry of Energy of the USSR to supply gas from the UCG plant to the regional coal-fired power station, which at the time was under construction in Angren, was considered. Based on the review of this proposal, the design brief for the Angren UCG plant was amended. A gas pipeline from the UCG plant to the Angren power station was constructed, which was 4.5 km long and 2 m in diameter. Six-meter pipe sections for this pipeline were manufactured at the Chelyabinsk Metallurgical plant, which also produced pipes for the main trunk pipelines and panel pipelines from the surface UCG plant to underground gasifiers. The total length of these pipelines was over 35 km. The design production capacity of the UCG plant was estimated at 2.3 billion m³/year (300,000 m³/h), which in terms of heating equivalent equals 500,000 t/year of the Angren coal. The Angren power station was equipped with boilers for burning solid fuels, but they were refitted for cofiring of coal and UCG gas. The challenging task of refitting the boilers for cofiring was carried out by the Rostov YUVENERGOMETALLURG-PROM Institute, with a boiler combustion efficiency of 87%–88%, compared with 84%–85% when fired on solid fuel alone. Fig. 3.13 shows the design and layout of the Angren UCG plant.

The first underground gasifiers were built similar to the Podmoskovnaya UCG plant, that is, using the natural permeability of the coal seam without supplementary underground mining. During the pilot operations at the pilot VNIIPODZEMGAZ gasifier, which were conducted in 1956–57, it was found that the effective lignite seam permeability of the Angren coal is much lower than that of the Podmoskovnaya, where
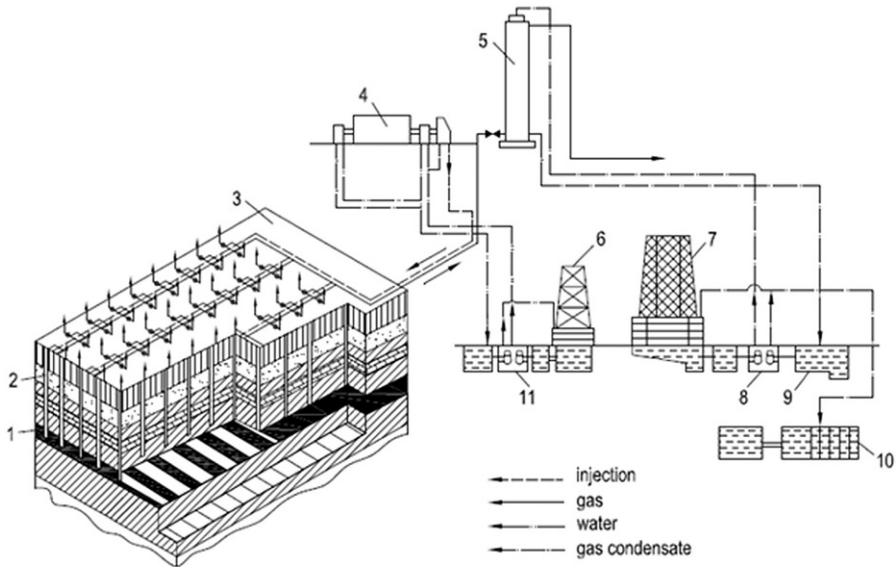
Schematic of Angren Underground Coal Gasification Plant:

1- coal seam; 2 - opening well; 3 - underground gasifier; 4 - air blowing compressor; 5- Initial gas cleaning;
6 - secondary cleaning and cooling of gas; 7 - cooling of technical water; 8, 9 - pump; 10 - settling tank;
11- cooling of gas condensate.

Fig. 3.13 Angren UCG plant, design and layout.

RCL was carried out at a pressure of 4–6 bar. Combustion linking in Angren plant was conducted using mobile high-pressure UKP80 compressors, with a wellhead pressure of 35–40 bar. Fig. 3.14 shows a schematic diagram of the first gasifiers at the Angren UCG plant.

During the commissioning of gasifiers, it was established that the combustion linking of wells at Angren proceeded successfully, with the exception of some limitations: the rate of linking was below 0.5 running meters per day, with the distance between the wells being below 25 running meters, with a highspecific air injection
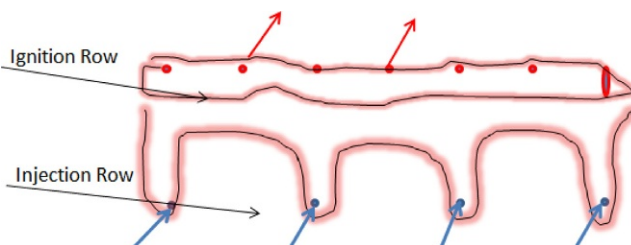
Fig. 3.14 Angren UCG plant, conceptual design of the first gasifiers—nos. 1–6.

rate that required the utilization of a large number of high-pressure compressors and, consequently, increased capital costs and electric power consumption, as a result slowing the gasifier commissioning rate and decreasing production output.

It was decided that horizontal in-seam drilling should be attempted. The Lisichansk drilling team was dispatched to Angren. A pilot horizontal well was drilled using a proprietary methodology, which was done in an efficient and cost-effective manner. Drilling horizontal wells was conducted along the coal to an active fire front, which had been created by the ignition row; thus, a new 250–300 m channel was introduced into the gasification process. All subsequent gasifiers, starting with gasifier no. 6, were constructed and introduced into the gasification process with the help of a combination of vertical wells, which were introduced into the process by combustion linking, and horizontal directional wells. Fig. 3.15 shows a schematic diagram of such a gasifier at the Angren UCG plant.

By the beginning of 1961, initial construction was completed at the UCG plant. On September 15, 1961, first quantities of gas were supplied to the Angren power station. The introduction of horizontal directional drilling made it possible by the beginning of 1962 to complete construction of gasifiers nos. 4, 5, 6, and 7, in that order. The production output was rapidly increasing. By the end of 1964, the hourly output of syngas was 300,000 m^3/h, that is, the UCG plant reached its design capacity of 2.3 billion m^3/year. In 1963, the second stage of construction and commissioning was completed, including installation of all systems and equipment. Selected pieces of equipment and facilities are shown in Pictures 3.1–3.4.

The coal quality at the Angren UCG plant is presented in Table 3.12.

The gas composition at the UCG plant (by gasifier) is presented in Table 3.13.

The gas composition was averaged to on-spec level of 800–950 kcal/m^3 by connecting other gasifiers to the gas pipeline. These gasifiers were operating at various stages of development (newly commissioned, with less than 50% of the reserves
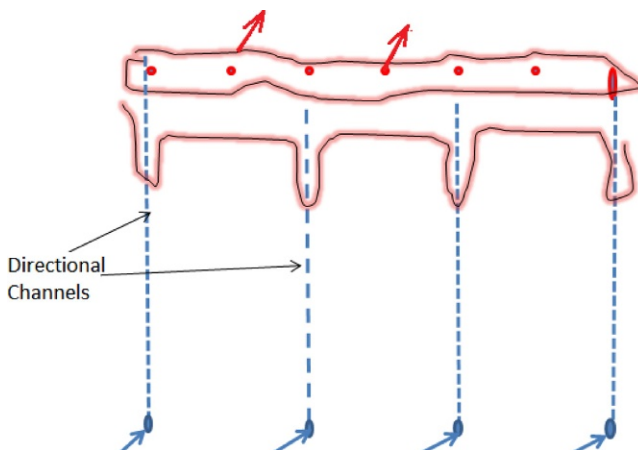
Fig. 3.15 Angren UCG plant, conceptual design of gasifier no. 6.

Picture 3.1 Drilling rig NBU ZIF1200.
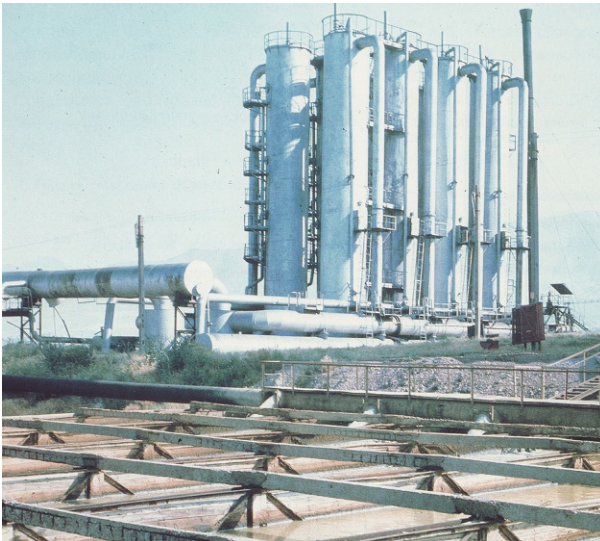
Picture 3.2 Gas scrubbers.

Picture 3.3 Main trunk gas pipeline to power station.

Picture 3.4 Engine room of the compressor plant.

Table 3.12 Angren UCG plant, coal composition

Proximate analysis (%)				Ultimate analysis (%)					LHV (kcal/kg)	HHV (kcal/kg)
FC	Ash	VM	IM	C	H	O	N	S		
39.8	9.2	21.0	30.0	44.9	2.8	9.5	0.9	2.8	3972	4303

Table 3.13 **Angren UCG plant, syngas composition**

	Gas Composition (vol%)							CV (kcal/ m^3)
	CO$_2$	O$_2$	CO	H$_2$	H$_2$S	CH$_4$	N$_2$	
Gasifier 10	13.2	0.2	14.2	22.8	0.5	3.6	45.5	1293
Pilot gasifier	17.7	0.1	10.5	20.5	0.5	3.2	47.5	1093
Gasifier 5	19.5	0.3	6.0	19.7	0.4	2.5	51.6	876
Gasifier 15	20.1	0.1	7.7	20.1	0.7	2.0	50.3	903

gasified, and gasifier where more than 50% of the reserves were gasified, gasifiers constructed in thin coal seams, operating in thick coal seams, etc.). At Angren lignite deposit, the same coal seam was concurrently mined by the Angren open-pit mine and underground mine no. 9.

For comparison, characteristics and performance parameters for these enterprises are listed in Table 3.14 using comparable units.

Starting in 1964, on orders of Mingazprom, new construction of gasifiers to maintain the design capacity was terminated. The syngas production volumes were steadily decreasing. In the 1970s, new gasifiers were still being commissioned, such as gasifier nos. 10, 11, and 12. In the meantime, Mingazprom intensively refocused the UCG plant to production of parts for various machineries. In 1973, an official order was issued by the minister of the gas industry, S.A. Orudzhev, to shut down all gas production at the UCG plant at Angren. Only after intervention of Mr. Tikhonov, deputy chairman of the Council of Ministers of the USSR, the order was rescinded. However, no new funding for the construction of gasifiers was appropriated.

Gas production continued to decline, reaching less than 160 million m^3/year by 1985. The syngas delivered to the UCG power station at Angren over time is presented in Table 3.15.

Table 3.14 **Angren UCG plant, open-pit mine and underground mine performance**

	Angren open-pit mine	No. 9 coal mine	Angren UCG plant
Depth of occurrence (m)	75	150	220
Production (1000 t/year)	1000	500	500
Cost (ruble/ton)	6.1	14.8	5.23
Capital cost per unit of output (ruble/ton)	34.8	30.8	19.0
Specific materials (ruble/ton)	3.4	4.0	2.5

Table 3.15 Angren UCG plant, syngas deliveries 1962–85

Year	1962	1963	1964	1965	1970	1975	1980	1985
Million m^3	489	893	1063	1410	996	514	299	157

In 1983, Mr. Bratchenko, Minister of the Coal Industry of the USSR, proposed to return UCG back under the administration of the Ministry of Coal Industry. Upon approval, a resolution of the Council of Ministers of the USSR was adopted, and as of January 1, 1985, the Angren UCG plant was transferred to the Ministry of Coal Industry and became part of Sredazugol Industrial Group, which was an independent company operating on a commercial basis. This was a turning point in the revival of the Angren UCG plant.

Production at the Angren UCG plant was carefully reviewed by the Ministry of Coal Industry. It was decided that the plant will be restructured to achieve an annual production of 1 billion m^3/year by 1990. It was also decided to prepare a feasibility study for the construction of five new UCG plants at Angren with a total capacity of 20 billion m^3/year. The Institute of Dongiproshaht was allocated 100 thousand rubles for FY1985 to develop a design for the reconstruction of the first stage of the Angren UCG plant. The capital investments into Angren Podzemgaz were allocated for the replacement of obsolete equipment and reconstruction of the pipeline network. A total of about 15 km of pipeline networks was repaired during that year; four new drilling rigs, three new high-pressure compressors, and other pieces of equipment were acquired; and gasifier no. 15 was built and commissioned. By the end of 1985, gasifier no. 15 was producing about 60,000 m^3/h of UCG gas with a calorific value of more than 900 kcal/m^3. Gas production for the period from 1986 to 1990 is shown in Table 3.16.

Since 1991, due to the collapse of the USSR, the Angren UCG plant has become state property of the Republic of Uzbekistan. Uzbekistan did not have the resources to implement the reconstruction projects of the existing Angren UCG plant, not to mention construction of new plants. The Angren UCG plant continued production of UCG gas at 500–600 million m^3/year. In 1995, the UCG plant was reorganized into an open joint-stock company, with a controlling stake of 51% owned by the state and 25% sold to members of the workforce using the remaining net profit balance while 24% was listed on the stock exchange. Gas production for the period 1991–2000 is presented in Table 3.17.

In 2000, the state-owned stock (51%) was sold off to various private companies and individual owners. The author does not have information on the operations of the Angren UCG plant after 2000.

Table 3.16 Angren UCG plant, syngas deliveries 1986–90

Year	1986	1987	1988	1989	1990
Million m^3	198	325	540	493	480

Table 3.17 Angren UCG plant, syngas deliveries 1991–99

Year	1991	1992	1993	1994	1995	1996	1997	1998	1999
Million m^3	578	583	540	510	520	482	504	480	512

3.5 The demise of UCG industry in USSR

By the beginning of the 1960s, the UCG was a full-scale industry employing thousands of people, with a number of commercial plants operating in various regions of USSR and scientific and research institutions conducting advance research into materials, equipments, and processes in the field of UCG and university programs for UCG professionals.

However, given the rapid development of natural gas production, the leaders at the newly formed Ministry of the Gas Industry of the USSR deemed UCG too complicated to develop. In 1964, a resolution of the Council of Ministers of the USSR was passed to cease further work on the development of UCG in the USSR. All scientific research work was terminated; training of new UCG process engineers at the Donetsk Polytechnic Institute was discontinued. The VNIIPODZEMGAZ and GIPROPODZEMGAZ research institutes were reorganized to meet new Gazprom's natural gas-related objectives. Design and construction of new UCG plants were stopped. The existing commercial UCG plants gradually ceased to function as the coal reserves were exhausted and because of gradual wear and tear of equipment and impairment of obsolete or damaged equipment. By 1990, the time of the Soviet Union disintegration, there were only two UCG plants still in operation—in the city of Angren, Uzbekistan, and in Kiselevsk, Siberia, while a research team continued its work at the VNIIPODZEMGAZ Research Center, which was later converted to VNIIPROMGAZ.

Thus, at the stroke of a pen of incompetent, short-sighted bureaucrats, enormous scientific and technological achievement of Soviet scientists and engineers was rendered all but null and void. Even upon a cursory review of the results and outcomes of then operational UCG plants, it is clear that those momentous decisions were not justified.

Underground coal gasification research and development in the United States*

4

D.W. Camp
Lawrence Livermore National Laboratory, Livermore, CA, United States

4.1 Introduction and scope

An intense and productive period of research and development on underground coal gasification (UCG) took place in the United States from the mid-1970s to the late 1980s. This period began with little domestic understanding of UCG. Early steps included the translation and review of Soviet literature, proposals of large-scale UCG schemes, and some early calculations and modeling that were often not well informed by experimental observations. Field tests became the marquis activities around which an integrated multifaceted program was built. Efforts included extensive monitoring and measurements of field tests, scientific analyses, mathematical modeling, and laboratory experimentation. The period ended with an accurate observation-based conceptual understanding of how UCG works and a corresponding predictive multiphysics mathematical model of the process. Innovative methods and technologies were invented and developed that form the basis of many UCG projects around the world today.

This chapter also covers recent US activities and accomplishments during the period 2004–15 and touches briefly on preceding work between 1948 and 1963.

The goals of this chapter are to summarize what has been done on UCG in the US and, more importantly, what has been learned about UCG from these activities. This chapter is largely a condensed version of a recent comprehensive review by this author of US UCG work that is broader in scope and much longer and more detailed than space allows here (Camp, 2017).

4.2   Major contributing institutions and field-test locations

4.2.1   *Bureau of Mines, AEC, ERDA, DOE*

Several federal organizations in the United States had an important role in UCG's development. Management and funding of much of the UCG program and some of its main technical contributors resided at various times in the Bureau of Mines (within the Department of the Interior), Atomic Energy Commission (AEC), and Energy Research and Development Agency (ERDA) and finally centralized in the Department of Energy (DOE) into which many of the functions of the other institutions were rolled in 1977.

4.2.2   *Bureau of Mines station in Tuscaloosa, Alabama*

The Bureau of Mines office in Tuscaloosa, Alabama, had a technology division and experimental station that conducted the Gorgas, Alabama UCG tests in the late 1940s to 1950s.

4.2.3   *MERC, METC, NETL*

A government research center with expertise in coal gasification in Morgantown, West Virginia, became the Bureau of Mines' Morgantown Energy Research Center (MERC) and then the Morgantown Energy Technology Center (METC) under DOE and, more recently, merged with its Pittsburgh, Pennsylvania counterpart to form the National Energy Technology Laboratory (NETL). METC looked at UCG scale-up and economics, operated the Pricetown field test, and helped DOE manage the UCG program.

4.2.4   *LERC, LETC, WRI, Universities of Wyoming and Colorado*

The Bureau of Mines Laramie Energy Research Center (LERC), in Laramie, Wyoming, conducted the first and successive UCG tests at the nearby Hanna site. This was renamed to the Laramie Energy Technology Center (LETC) under DOE and then privatized in 1983 into the Western Research Institute (WRI), which remained an important part of the UCG program through the Rocky Mountain 1 test and related follow-on work.

4.2.5   *LLL, LLNL*

Lawrence Livermore Laboratory (LLL), renamed to Lawrence Livermore National Laboratory (LLNL) in 1982, is in Livermore, California, and is named after its founder, Earnest Lawrence. It is a very large multidisciplinary science and engineering research institution whose core mission since it began in 1952 has been in nuclear security. Livermore's original charter and its continuing nature has been innovation—pioneering new and better ways to do things. That can be seen in its series of UCG activities. Every one of Livermore's field tests was different and pioneered something new.

4.2.6 Universities of Wyoming and Colorado

Researchers at the University of Wyoming (Laramie) and the University of Colorado (Boulder) collaborated with LETC and other institutions, analyzing UCG field data and developing UCG models (c.f. Krantz and Gunn, 1983c).

4.2.7 Texas institutions

A modest amount of UCG work was aimed at lignite fields in the state of Texas. This has mostly been funded by private industry with some state support. Organizations involved include a company named Basic Resources, which operated the Tennessee Colony field test, Texas A&M University in partnership with a consortium of companies, and the University of Texas at Austin.

4.2.8 Gulf Research and Development and Energy International

Gulf Research and Development Company, the R&D arm of the major oil company Gulf, had the most active and longest-running UCG program in American private industry. On a cost-shared basis with the DOE, Gulf ran the two Rawlins field tests and had a key role in the Rocky Mountain 1 test. Some of Gulf's UCG principals later joined Energy International, which aimed at larger UCG projects.

4.2.9 ARCO

The major oil company ARCO had a subsidiary coal company that conducted the Rocky Hill field test and made plans for larger scale operations. Some of its UCG staff had been principals in LETC's UCG program.

4.2.10 Gas Research Institute

The Gas Research Institute (GRI) was an independent research institute in Chicago, Illinois, with expertise that includes coal gasification (mainly surface) that operated on a mix of industrial and government grant funding. GRI funded some of the efforts and was a leader in the DOE-assembled consortium that ran the Rocky Mountain 1 test. More recently, it merged with the Institute of Gas Technology to form the Gas Technology Institute (GTI).

4.2.11 Other institutions

Many other research and engineering institutions participated and made contributions to the UCG program. Many researchers at universities and research institutions conducted laboratory experiments and developed models related to UCG. Many engineering and geologic service providers did much of the support work under contracts, including United Engineers for the Rocky Mountain 1 field test and Williams Engineering for some of the earlier field tests.

Fig. 4.1 Location of US UCG institutions and field tests (Map by LLNL and Ergo Exergy).

4.2.12   Locations

Fig. 4.1 shows the locations of many of the field tests and institutions involved with UCG.

4.3   Periods of UCG activities

4.3.1   Pre-1970 work

The only significant work before 1970 seems to be by the US Bureau of Mines at Gorgas, Alabama. This began in the late 1940s, included field tests, and ended with summary reports in the early 1960s (c.f. Capp et al., 1963). Unfortunately, little from this project appeared to become part of the 1970s program consciousness.

4.3.2   The main 1970–80s program and activities

US government institutions (see Section 4.2) initiated UCG research in the early 1970s and grew it into a well-funded, sustained, and technically vibrant program. The primary motivation was to advance the domestic energy security of the United States. Oil and gas supplies were appearing limited, the OPEC oil embargo was to hit soon, and US coal resources were and still are enormous. Throughout its course, the long-term program objective was large-scale commercial operations that would have a significant impact on US energy supplies.

The program began with paper studies and the creation of large-scale conceptual design schemes. An important early activity in the program was the translation and

study of Soviet reports on UCG, thus taking advantage of the greatest previous efforts in UCG technology development. This guided early program thinking and approaches.

The US approach was a multifaceted program that included well-instrumented and monitored field tests of modest scale (100–10,000 Mg), large-scale conceptual designs and economic estimates, scientific analyses and modeling, some focused laboratory experiments, and technology innovation. Concepts began by emulating Soviet technical approaches and evolved into US-developed methods and technologies. Great progress was made in understanding and modeling the process and development of designs and operations that held promise for improved efficiency, operations, cleanliness, and scale-up. A sizable workforce grew in numbers and experience with UCG research, development, and operations. The capstone field test was Rocky Mountain 1, conducted by a DOE- and GRI-led consortium of public and private organizations. In addition to being by far the largest US field test, this provided a second and convincing demonstration of the new controlled retractable injection point (CRIP) technology (described later) for efficient operation and growth of the process and the "Clean Cavern" approach for minimizing groundwater contamination (also described later).

By the late 1980s and early 1990s, American UCG activities tailed off to only a bit of Rocky Mountain 1 technical follow-up and report writing and some groundwater remediation activities. Oil and gas prices had stabilized, and the US government philosophy of energy technology development had shifted toward the private sector. Over the next two and three decades, nearly all the individuals who developed UCG expertise moved to other work, retired, and/or passed on.

4.3.3 A small revival in 2005–15

Growing UCG interest and activities around the world in the early 2000s, largely motivated by increasing and more variable gas prices, rekindled US activities from the mid-2000s to the mid-2010s. In addition to commercial project planning activities, some federal and state government agencies, universities, and nongovernmental organizations took an interest in and studied UCG to various degrees during this period. Wyoming supported a UCG review and detailed study of a notional large project and its costs (GasTech, 2007). The Indiana Geological Survey and Purdue University evaluated the suitability of Indiana coal resources for UCG (Shafirovich et al., 2009). The US Department of Interior, Office of Surface Mining, Restoration, and Enforcement organized regulators from several states and Native American nations to become better versed in UCG.

LLNL revived a modest UCG program at the beginning of this period and motivated largely by the goal of coupling carbon capture and sequestration (CCS) with UCG to affordably reduce the carbon footprint of energy produced from coal (c.f. Friedmann, 2005). This seemed especially relevant for locations with plentiful coal, scarce oil and gas, high energy prices and energy security issues, and anticipated time when economic incentives to minimize CO_2 emissions would be in place. The program's UCG technical work emphasized mathematical models, evaluation of resources for UCG suitability, technical education and training, geophysical monitoring, and groundwater contamination.

Interest and activities in UCG and coal diminished in the latter years of this period with plentiful oil and gas production from fracturing operations and greater weighting of the challenge of groundwater cleanliness and the impacts from greenhouse gas emissions.

4.4   Recommended references

The following references are recommended for the "top shelf" of both the serious newcomer to UCG and the working professional.

An exceptionally complete chronicle of US UCG activities in the 1970s and 1980s is provided in the Proceedings of the Annual Underground Coal Gasification/Conversion Symposia that ran from 1976 to 1989 (Proceedings, 1976, 1977, 1978, 1979, 1980, 1981, 1982, 1983, 1984, 1985, 1986, 1987, 1988, 1989). LLNL's final program report (Thorsness and Britten, 1989b) contains a concise summary of 18 years of UCG work by Livermore that emphasizes what was learned. Britten and Thorsness (1989b) describe LLNL's conceptual understanding of UCG and its important phenomena. In the mid-1980s, UCG overviews are found in Dockter (1986), Stephens et al. (1985), Stephens et al. (1982), and Krantz and Gunn's "State-of-the Art" collection (1983a).

LERC and LETC's Hanna series of field tests were summarized by Bartke and Gunn (1983) and detailed by Bartke et al. (1985). LLL's Hoe Creek series of field tests and their results were described in detail by Stephens (1981) and more briefly by Thorsness and Creighton (1983). ARCO's Rocky Hill test is described by Bell et al. (1983), the Pricetown test is summarized by Schrider and Wasson (1981), and the tests in Texas are reviewed by Edgar (1983). Both of Gulf's Rawlins tests are covered in detail by Bartke (1985). LLL's Large Block tests at Centralia were summarized by Hill and Thorsness (1983), and their Centralia Partial Seam CRIP test was summarized by Cena et al. (1984). Cena and Thorsness (1981) give, for each DOE-funded UCG field test through 1979, a general description, well layout, simplified chronology, summary tables of flows, compositions, etc. for each major time period and time-history plots of interesting parameters.

The Rocky Mountain 1 test is described very briefly by Dennis (2006). Contemporary descriptions of many specific aspects of Rocky Mountain 1 appear in the Proceedings of the 14th Annual UCG Symposium (1988), including a chronology and description of results (Bloomstran et al., 1988). Reviews and analyses of results are found in Cena et al. (1988a,b) and Thorsness et al. (1988), cross sections of the cavities are found in Oliver et al. (1991), and the Clean Cavern operations and groundwater contamination results and overviews are found in Boysen et al. (1988, 1990) and Lindblom and Smith (1993).

Modern-era reviews include Camp (2017), which provides more detail than this chapter in several areas including narrations for most field tests, covers a few additional topics, and provides more references. Shafirovich et al. (2011) is a convenient reference for factual information from DOE-sponsored UCG field tests. Couch (2009) is an excellent wide-scope review of UCG that includes a generous portion devoted to US contributions. LLNL's recent program began with the critical review of UCG

titled "Best Practices in Underground Coal Gasification" (Burton et al., 2006). GasTech (2007) reviewed UCG with emphasis on a modern commercial project. Groundwater contamination phenomena are reviewed in Camp and White (2015), geophysical monitoring in Mellors et al. (2016). Modeling references are in Section 4.6.

4.5   Field tests

4.5.1   Summary

Table 4.1 provides summary information for all of the UCG field tests conducted in the United States between 1948 and 1995.

In the first several field tests, several US institutions developed competency in the Soviet-developed approach in which reverse burns are used to link vertical wells, with the main "forward-burn" phase of gasification taking place by injecting air into one of those wells or a sequence of them. Subbituminous and nonagglomerating bituminous coals were gasified successfully. An agglomerating swelling bituminous coal proved very problematic. Lignite beds were gasified, but their low heating value, thin seams, and high water influx produced poor gas.

Oxygen-steam injection was tried successfully and over time became the preferred injectant. The later tests in the series began to take advantage of the newly emerging and improving technology of directional drilling to create in-seam links between injection and production points. The Soviet scheme for gasifying steeply dipping beds was tried successfully, using directionally drilled boreholes for links. Further innovation led to the invention of the CRIP process. By the last field test, US practice and preferences had swung solidly toward using directionally drilled in-seam borehole links and CRIP.

McVey and Camp (2012) calculated the average dry product gas composition, weighted by mass of coal, for all the air-blown periods of US field tests and for all the oxygen-steam-blown periods of US tests. All field tests listed in Table 4.2 were included, from Hanna I to Rocky Mountain 1, with the exceptions of Rocky Hill, the Texas lignite tests, and the Centralia Small Block tests.

Throughout the series, the R&D nature of the program advanced the understanding of the UCG process and its interactions with the environment. This included a growing awareness of problems with groundwater contamination and improved understanding of how to minimize it, including the Clean Cavern concept of operation demonstrated successfully at Rocky Mountain 1. It became expected that deeper projects would be favored because of better isolation of contamination risks from the surface.

4.5.2   Gorgas (USBM)

Initial UCG activities in the United States were carried out by the US Bureau of Mines in 1947–60 near Gorgas, Alabama. The program included multiple field tests, used or explored combustion in mine tunnels, grouted boreholes, hydraulic fracturing and

Table 4.1 Summary of UCG field tests in the United States (parameter definitions appear at the end)

	Early Hanna					
Test name	Hanna I hydr.frac	Hanna I main phase	Hanna II Phase 1A	Hanna II Phase 1B	Hanna II Phase 2	Hanna II Phase 3
Dates	3/73–5/73	5/73–3/74	5/75–7/75	7/75–8/75	12/75–5/76	5/76–7/76
Operator	LERC	LERC	LERC	LERC	LERC	LERC
Location	Hanna, WY	Hanna, WY	Hanna, WY	Hanna, WY	Hanna, WY	Hanna, WY
Basin	Hanna	Hanna	Hanna	Hanna	Hanna	Hanna
Coal						
Consumed (Mg)	818	4347	1650	769+RB	4311	4641
Rank	HV Bit. C	HV Bit. C	HV Bit. C	HV Bit. C	HV Bit. C	HV Bit. C
	Not swell/agglom	Not swell/agglom	Not swell/agglom	Not swell/agglom	Not swell/agglom	Not swell/agglom
Htg. value (kJ/kg)	20,000	20,000	20,000	20,000	20,000	20,000
Thickness (m)	8.8	Top ~5 of 8.8	9.1	9.1	9.1	9.1
Depth (m)	114	114	84	84	84	84
Dip (degrees)	7	7	7	7	7	7
Process						
Injectant	Air	Air	Air	Air	Air	Air
Link method	Hydraulic fracturing	Reverse burn	Reverse burn	Reverse burn	Reverse burn	Reverse burn
Inj-prod spacing (m)	9 and 18	18	18	18	18	18

Design and operations	Ignition and injection into a central well. Production from multiple surrounding wells	5 vertical inj/prod wells. RB links between many pairs of these. Forward burns between combinations of wells	Simple two vertical wells linked by reverse burn, followed by forward burn	RB linked from the HII-1A cavity to a new third vert. well. Forward burn injecting into the new well	Simple two vertical wells linked by reverse burn, followed by forward burn	Tried to create a broad link between one link and a parallel burn cavity (failed). Did simple two-well forward burn
Results						
Days of Ign. and R.B.	1	128	14	11	45	16
Days fwd (air/ox-st)	60	168	37	37	27	45
Consumed fwd. (Mg)	818	3304	1620	769	3680	4258
Gas HV fwd (MJ/Nm^3)	4.2	5.0	5.5	5.7	6.8	5.5
Gas recov fwd (%)	14	103	78	129	99	100
Highlights, accomplishments, observations, comments, problems, conclusions	Hydraulic fracturing with sand proppant is not an adequate link. High gas leakage through open boreholes and casing failures	First UCG test of this era was successful. RB linking between many wells and burn cavities showed scale-up potential	Did simple two-well test that worked well	Repeated scale-up technique of linking from a mature cavity to a new well, and injecting into the new well	Did another similar test that worked pretty well	Attempted broad front advancement between links and cavities in both reverse and forward modes. Both failed

Table 4.1 **Continued**

Later Hanna, Rocky Hill, and Pricetown				
Test name	**Hanna III**	**Hanna IV-A**	**Hanna IV-B**	**Rocky Hill**	**Pricetown I**
Dates	6/77–7/77	12/77–6/78	4/79–9/79	9/78–11/78	6/79–10/79
Operator	LERC	LERC	LETC	ARCO (LETC heritage)	METC
Location	Hanna, WY	Hanna, WY	Hanna, WY	Reno Junction, WY	Pricetown, WV
Basin	Hanna	Hanna	Hanna	Powder River	Pittsburg seam
Coal					
Consumed (Mg)	4771	5036	2042	3270+RB	885
Rank	HV Bit. C	HV Bit. C	HV Bit. C	Subbit. C	HV Bit. A
	Not swell/ agglom	Not swell/agglom	Not swell/agglom		Swelling and agglomerating
Htg. value (kJ/kg)	20,000	20,000	20,000	20,800	High
Thickness (m)	9.7	8.5	8.5	Top 20 of 30	1.8
Depth (m)	50	98	98	190	270
Dip (degrees)	7	7	7	Low	Low
Process					
Injectant	Air	Air	Air	Air	Air
Link method	Reverse burn	Reverse burn	Reverse burn	Reverse burn	Reverse burn
Inj-prod spacing (m)	18	31	23	23	18
Design and operations	Simple two vertical wells linked by reverse burn, followed by forward burn	Multiple vert. inj/ prod wells attempted to link by RB. Forward burns attempted between various well combinations	Multiple vert. inj/ prod wells attempted to link by RB. Forward burns attempted between various well combinations	3 vert. inj/prod wells in a line linked by RB. Forward burn injected into an end well and produced from the middle well	3 vert. inj/prod wells in a line linked by RB and cycled to open links. Fwd burn injected into an end well and produced from the middle well

Results

Days of Ign. and R.B.	16	107	83	10	106
Days fwd (air/ox-st)	38	58	23	60	12
Consumed fwd. (Mg)	4734	4550	1334	3270	450
Gas HV fwd (MJ/Nm^3)	5.5	4.1	5.4	7.4	6.9
Gas recov fwd (%)	92	80	92		114
Highlights, accomplishments, observations, comments, problems, conclusions	Extensive groundwater monitoring, but no results reported	Seemed like another similar test, but there were many problems	Seemed like another similar test, but there were many problems	Replicated Hanna-METC methods in a thicker deeper seam of different coal. Monitored overburden subsidence and hydrology effects	Only US test attempted in a swelling agglomerating coal. RB links were eventually created, but had high resistance. Persistent plugging in rev. and fwd. modes

Hoe Creek and Rawlins

Test name	Hoe Creek I	Hoe Creek II	Hoe Creek III	Rawlins I	Rawlins II
Dates	10/76–10/76	10/77–12/77	8/79–10/79	10/79–12/79	8/81–11/81
Operator	LLL	LLL	LLL	Gulf R&D	Gulf R&D
Location	Gillette, WY	Gillette, WY	Gillette, WY	Rawlins, WY	Rawlins, WY
Basin	Powder River	Powder River	Powder River	Hanna	Hanna

Coal

Consumed (Mg)	190	2658	4036	1513	7770+RB
Rank	Subbit.	Subbit.	Subbit.	Subbit. B	Subbit. B
Htg. value (kJ/kg)	18,960	18,960	18,960	23,550	23,550
Thickness (m)	7.6\(5)\3.4	7.6\(4.6)\3.4	7.6\(5.4)\3.0	11.4	11.4

Continued

Table 4.1 **Continued**

Hoe Creek and Rawlins				
Test name	**Hoe Creek I**	**Hoe Creek II**	**Hoe Creek III**	**Rawlins I**	**Rawlins II**
Depth (m) Dip (degrees)	~40 m to lower Low	38 to lower Low	54 to lower Low	113 63	155 63
Process					
Injectant Link method	Air/- Explosive fracturing	Air/oxy-stm Reverse burn	Air/oxy-stm Borehole+RB expansion	Air/oxy-stm Borehole	-/Oxy-stm Borehole+RB links
Inj-prod spacing (m)	10	18	30.5 and 41	16	60
Design and operations	High explosive fractured between two vertical process wells. Forward burn between them	Simple two vertical wells linked by reverse burn, followed by forward burn	Horizontal borehole link between three vertical wells. Expanded by RB. Fwd burn at 30 m space, then extended out to 41 m	Steeply dipping bed. Directionally drilled injection and production wells and link. Injection point ~16 m downdip from production point	One vertical production borehole between two injection wells w RB links between them. Injected into each well separately and into both together
Results					
Days of Ign. and R.B.	1	14	3	7	~30
Days fwd (air/ ox-st)	11/-	56/2	7/47	28/5	-/65
Consumed fwd. (Mg)	190/-	2470/55	334/3655	1225/228	-/7767
Gas HV fwd (MJ/ Nm^3)	4.0/-	4.3/10.5	4.5/8.4	6.0/8.4	-/12.8
Gas recov fwd (%)	93	78	83	97	

Highlights, accomplishments, observations, comments, problems, conclusions	First explosively fractured rubble bed trial in program. Successful but suboptimal; hard to control pattern	First oxygen-steam UCG in program. Inj. well broke near top causing heat loss to wet roof rock	First horizontal borehole link and borehole ELW in program. UCG "burns" through a 5-m interburden to reach the next seam	First successful US test in steeply dipping bed. Used directionally drilled boreholes	Many challenges. RB links between boreholes and cavities don't go where expected. Gasified lots of coal but not easy
Centralia and Rocky Mountain 1					
Test name	**Centralia LBK5,2,3,4**	**Centralia LBK1**	**Centralia PSC (CRIP)**	**Rocky Mountain 1 ELW module**	**Rocky Mountain 1 CRIP module**
Dates	11/81–1/82	1/82	10/83–11/83	11/87–1/88	11/87–2/88
Operator	LLL	LLL	LLNL	GRI consortium	GRI consortium
Location	Centralia, WA	Centralia, WA	Centralia, WA	Hanna, WY	Hanna, WY
Basin	Tono	Tono	Tono	Hanna	Hanna
Coal					
Consumed (Mg)	25 each (4)	30	2400	4000	10,200
Rank	Subbit.	Subbit.	Subbit.	HV Bit. C	HV Bit. C
Htg. value (kJ/kg)	11,770	11,770	11,770	20,000	20,000
Thickness (m)	Top 8 of 11	Top 2 of 11	Top 6 of 11	Top 5 of 9	Top 7 of 9
Depth (m)	16	16	52	112	108
Dip (degrees)	15	15	14	7	7
Process					
Injectant	-/Oxy-stm	-/Oxy-stm	-/Oxy-stm	Air/oxy-stm	Air/oxy-stm
Link method	Borehole	Borehole	Borehole	Borehole	Borehole
Inj-prod spacing (m)	18	11 then 18	22, 22, 15	90	90

Continued

Table 4.1 **Continued**

	Centralia and Rocky Mountain 1				
Test name	**Centralia LBK5,2,3,4**	**Centralia LBK1**	**Centralia PSC (CRIP)**	**Rocky Mountain 1 ELW module**	**Rocky Mountain 1 CRIP module**
Design and operations	One vertical production well. One horizontal injection well and borehole link	One vertical production well. One horizontal injection well and borehole link. Linear CRIP	Parallel CRIP w vertical initial production well (1H Inj well and borehole link. 1H Prod well and borehole link. 1 V initial prod well)	Horizontal production well and borehole link to two vertical inj. wells. Fwd burn fr distal well. ELW switch to second well failed	Parallel CRIP w vertical initial production well (1H Inj well and borehole link. 1H Prod well and borehole link. 1 V initial prodn well)
Results					
Days of Ign. and R.B.	1	1	1	4	4
Days fwd (air/ox-st)	-/3–6 ea	-/4	-/30	7/40	3/90
Consumed fwd. (Mg)	-/~25 ea	-/30	-/2400	4000 total	10,200 total
Gas HV fwd (MJ/Nm^3)	-/10.7	-/10.8	-/9.2	-/10.3	-/11.3
Gas Recov fwd (%)	21–61	85	83	91	89
Highlights, accomplishments, observations, comments, problems, conclusions	Excavation showed cavities filled with rubble, even in early all-coal stages	First CRIP maneuver tried in the field was successful. First linear CRIP! Postburn excavation of young cavity	First CRIP system at full field-test scale. First parallel CRIP field test. Postburn excavation of full-sized cavity	Clean Cavern concept minimized groundwater contamination Injection well completion at top of seam gave poor performance	Parallel CRIPdemonstrated successfully again. Three CRIP maneuvers created three fresh cavities. CRIP repeatedly rejuvenated burn Clean Cavern minimized contamination

Other field tests					
Test name	**Gorgas series**	**Fairfield or Big Brown**	**Tennessee Colony**	**Alcoa**	**Carbon County**
Dates	1948–59	1976	1978–79	1980	1995
Operator	US Bureau of Mines	Basic Resources	Basic Resources	Texas A&M Consortium	Williams
Location	Gorgas, AL	Fairfield, TX	Tennessee Colony, TX	Alcoa, TX	Rawlins, WY
Basin					Hanna
Coal					
Consumed (Mg)	215 in first test		4100	Small	Subbit.
Rank	HV Bit. A	Lignite	Lignite	Lignite	~=Rawlins
Htg. value (kJ/kg)					~=Rawlins
Thickness (m)	1		2.2	4.5	>Rawlins
Depth (m)	9				Steep
Dip (degrees)	Flat				
Process					
Injectant	Air, maybe oxy-stm	air	Air/oxy-stm	Air	
Link method	R. Brn, hyd.frac?			Reverse burn	
Inj-prod spacing (m)				9	
Design and operations	"Soviet methods." Incl. mine addits, RB links, possibly hydraulic fracturing	"Soviet"	"Soviet"		
Results					
Days of Ign. & R.B.				All the days	
Days fwd (air/ox-st)		26	197 total	0	

Continued

Table 4.1 **Continued**

Other field tests					
Test name	**Gorgas series**	**Fairfield or Big Brown**	**Tennessee Colony**	**Alcoa**	**Carbon County**
Consumed fwd. (Mg) Gas HV fwd (MJ/Nm^3) Gas recov fwd (%) Highlights, accomplishments, observations, comments, problems, conclusions	$2^+/5^-$ first test Low First US field tests! High gas losses. Roof collapse	4.7 26-day trial	4100 total 3.0/8.6 Heat loss to overburden, high water intrusion rates	0 1.3–5.6 when linking 21 days of unsuccessful RB linking. Mech failure of well casings	Unsuccessful short operation. Groundwater contamination from high operating pressures

Table definitions	
Parameter	**Parameter definitions**
Dates Operator Location Basin	Date range from first ignition to termination of oxidant injection Institution in charge of the test City, state in United States Geologic basin
Coal	
Consumed (Mg) Rank Htg. value (kJ/kg)	Total coal consumed (Mg) for all phases of the entire field test (gas loss corrected and including char) Coal rank Coal heating value, as received (kJ/kg). (Reports rarely specified whether they were giving the higher heating value or the lower heating value. More likely it was the higher.)

Thickness (m)	True seam thickness. "Top x of y" used the upper x m of the y m-thick seam, leaving the bottom (y-x) m untouched. For two seams separated by a rock interburden, thicknesses are bottom\(interburden)\top
Depth (m)	Vertical depth from the surface to the top of the seam at the main cavity or injection point (m)
Dip (degrees)	Seam dip, degrees (horizontal is 0 degrees)

Process

Injectant	Injection gas composition: air or mixtures of oxygen and steam (oxy-stm). Tests with separate periods of each are shown as: Air/oxy-stm
Link method	Main method of creating a permeable path(s) between injection and production well(s)
Inj-prod spacing (m)	Distance between cased injection points and cased production points
Design and operations	Description of design and operations, including process wells, linking, forward-burn injection and production wells, switching injection points

Results

Days of Ign. and R.B.	Number of days for ignition, reverse burn linking, connecting, and link enhancement operations
Days fwd (air/ox-st)	Number of days of main forward-burn operation (while injecting air/while injecting oxy-st)
Consumed fwd. (Mg)	Coal consumed during the main forward-burn periods (gas loss corrected and including char) (air/oxy-st)
Gas HV fwd (MJ/Nm^3)	Average higher heating value of dry product gas during forward-burn phases (air/oxy-st)
Gas recov fwd (%)	Estimated percent of gas that is recovered through the production well during forward burns (1 minus loss)
Highlights, accomplishments, observations, comments, problems, conclusions	Highlights, accomplishments, observations, comments, problems, conclusions

Table 4.2 Tonnage-weighted average dry product gas composition (mol%) of US field tests done on bituminous or subbituminous coal

Species	Air blown (mole %)	Oxygen-steam blown (mole %)
$N_2 + Ar$	53.86	2.29
O_2	0.19	0.01
H_2	13.53	33.26
CH_4	4.51	9.83
CO	10.65	9.78
CO_2	16.01	42.06
C_{2+} HCs	0.45	1.20
NH_3	0.64	1.26
H_2S	0.16	0.31

electrolinking to prepare the seam, and tried oxygen-enriched air. The small amount of data available conveniently from secondary sources appears in Table 4.1. There are very few references to these tests in the US literature of the 1970s, and it appears that the Gorgas program did not play a significant role in informing that generation of US UCG researchers.

4.5.3   Hanna series (LETC)

From 1973 to 1979, LERC and its successor LETC operated a series of UCG field tests south of the town of Hanna, Wyoming. The site was favorable, with a single, low-dip-angle seam of high-quality coal overlain by reasonably competent rock of low moisture content. Counting the various defined phases and subphases, there were at least nine identifiable tests that are summarized in Table 4.1. Each of the tests used air as the injectant and reverse burns to link between multiple vertical process wells laid out in various patterns.

The first UCG test of this generation, Hanna I, was a remarkable success. Through perseverance, the LERC team got UCG to work well. They accomplished multiple reverse-burn links, some between wells and some from forward-burn cavities to wells. They operated effectively in forward gasification mode for five and a half months and showed that forward burn was robust, tolerating changes in flows, pressures, and even changes in the injection location. They also showed the feasibility of scale-up by successfully extending the process laterally from the initial well pair out to additional process wells. Three important negative results were learned: neither sand-propped hydraulic fracturing nor pneumatic fracturing created sufficient connectivity between wells to sustain a forward burn; ungrouted process and instrument wells and uncemented boreholes result in large gas losses; and, for a given injection-production well pair, product quality tended to decrease with time. Given all the challenges involved in all the subsequent US field tests, getting the first test of this generation to work well was an impressive accomplishment. Technical failure or a severe safety incident could have derailed the entire US program. The success of Hanna I paved the way for the major US program that followed.

The subsequent Hanna tests were remarkably similar to each other in their main aspects. The well patterns and intended link paths seemed to be the main design/preparation variable, and the sequence of injection and production wells during the main forward gasification phases seemed to be the main operations variable. Many difficulties were encountered, and most test histories ended up being very different than their test plans.

The overriding objective appeared to be to test well and link patterns for their scale-up potential, looking for high production rates, high resource utilization, and extension of the process to large and larger areas. Hanna II Phase 2 and Hanna II Phase 3 were notable for having two adjacent two-well cavities merge into each other to essentially create a larger combined cavity, again showing lateral scale-up potential.

Hanna III had the objective of investigating groundwater contamination, but it was dry and didn't recharge as expected, so little useful data were collected. Hanna IV had a seemingly endless series of problems and revisions.

4.5.4   Rocky Hill (ARCO)

ARCO's Rocky Hill field test was conducted in 1979 in the very thick subbituminous Wyodak seam of Wyoming's Powder River Basin. The design and operations were similar to the simpler Hanna tests, with a vertical injection and production well linked by reverse burn. The gas quality was very good, probably because of a low ratio of heat loss to the roof per volume of coal consumed in the very thick seam. Evidence suggests that the cavity grew upward faster than sideward and that there was a significant degree of sagging and/or fractures extending some distance up into the overburden, although no surface subsidence had occurred 3 years later.

4.5.5   Pricetown (METC)

METC, with operations support from Monsanto's Mound facility, conducted in 1979 the Pricetown field test in northern West Virginia. They targeted a seam of swelling agglomerating bituminous coal that was 2-m thick and 270-m deep. Three vertical process wells were drilled and completed into the lower third of the seam. They were in a line, with 18 m between wells. With great effort, perseverance, and high injection pressures, reverse-burn links were eventually completed between the wells, using reverse-forward alternation with limited success to expand the links. Finally, a proper gasification phase was started, but it only lasted 12 days. A series of flow resistances were encountered underground and/or in production wells. Injection locations were moved around, with mixed success, followed by more flow resistance. The test was stopped after a rupture in the casing of a production well occurred, pressurizing the aquifer at a depth of 62 m with product gas.

The clear conclusion is that trying to do UCG in swelling agglomerating coals is problematic. UCG capabilities must improve considerably before trying to tackle these difficult coals again. Large-diameter drilled boreholes may work better than reverse burns for creating links.

4.5.6   Hoe Creek series (LLNL)

LLL conducted three UCG field tests from 1976 to 1979 at the Hoe Creek site in north-eastern Wyoming. Initially intending to use the 30-m-thick Wyodak seam at a depth of 300 m, plans were changed to target a much shallower seam for the first experiment to reduce its drilling costs. As it turned out, all three tests were done there. The shallow depth allowed more tests with more downhole instrumentation for a given amount of R&D funding but contributed to unexpected and unacceptable environmental impacts. A horizontal 8-m subbituminous seam was targeted. Above it were 5 m of weak interburden and a second coal seam that was 3-m thick.

These tests were sponsored by the US DOE and its predecessors, with the GRI cosponsoring the third of these tests. Each test pioneered something new.

The Hoe Creek I was intended to be a first small pilot test of a large-scale explo-sively fractured packed bed reactor concept that LLL had developed. Two simul-taneous 340-kg chemical explosive charges at the bottom of the lower seam, spaced about 7 m apart, were used to create a packed bed of coal rubble and suf-ficient permeability to gasify coal between two vertical process wells. It worked, producing gas of good but declining quality. Most of the permeability was in the top of the seam resulting in heat loss to the roof, poor resource recovery, and pre-mature air bypass. In part because of the difficulty of creating a uniform perme-ability field, explosive fracturing was abandoned as a linking/preparation step for UCG.

The Hoe Creek II test retreated to the simple two-vertical-well, reverse-burn linked process, similar to LERC's previous Hanna II-1A and II-2 tests, but in different geo-logy than Hanna. It also fielded intensive instrumentation to define the temperature field and cavity location. Linking went well, but forward burn suffered from a break in the injection well early in the test that caused poor gas quality because of roof heat loss and override. An important lesson was learned when they switched injection to a surviving smaller pipe that reached the bottom of the seam—the gas quality rose directly. Hoe Creek II also included the first period of oxygen-steam injection for the first time in this era and made a medium-quality product gas. Another important observation, also observed in nearly all field tests of the era, is that the cavity grew up faster than sideways, extended far up into the overburden, and was filled with rubble. Process instrumentation and postburn drill backs produced the cavity cross sections shown in Fig. 4.2.

Experience at both Hanna and Hoe Creek II had shown that the paths of reverse-burn links could not be controlled; they were often multiple and often included a link along the top of the seam. In addition, Hanna had repeatedly been unable to link wells at spacings greater than 23 m, suggesting that scale-up of a reverse-burn linked process would require a large number of vertical process wells. Directional drilling technology was improving, and Livermore decided to use it to control the placement of a long link near the bottom of the Felix 2 seam for the Hoe Creek III test. This had the potential of scaling up with fewer wells and helped the process stay low in the seam for good thermal efficiency.
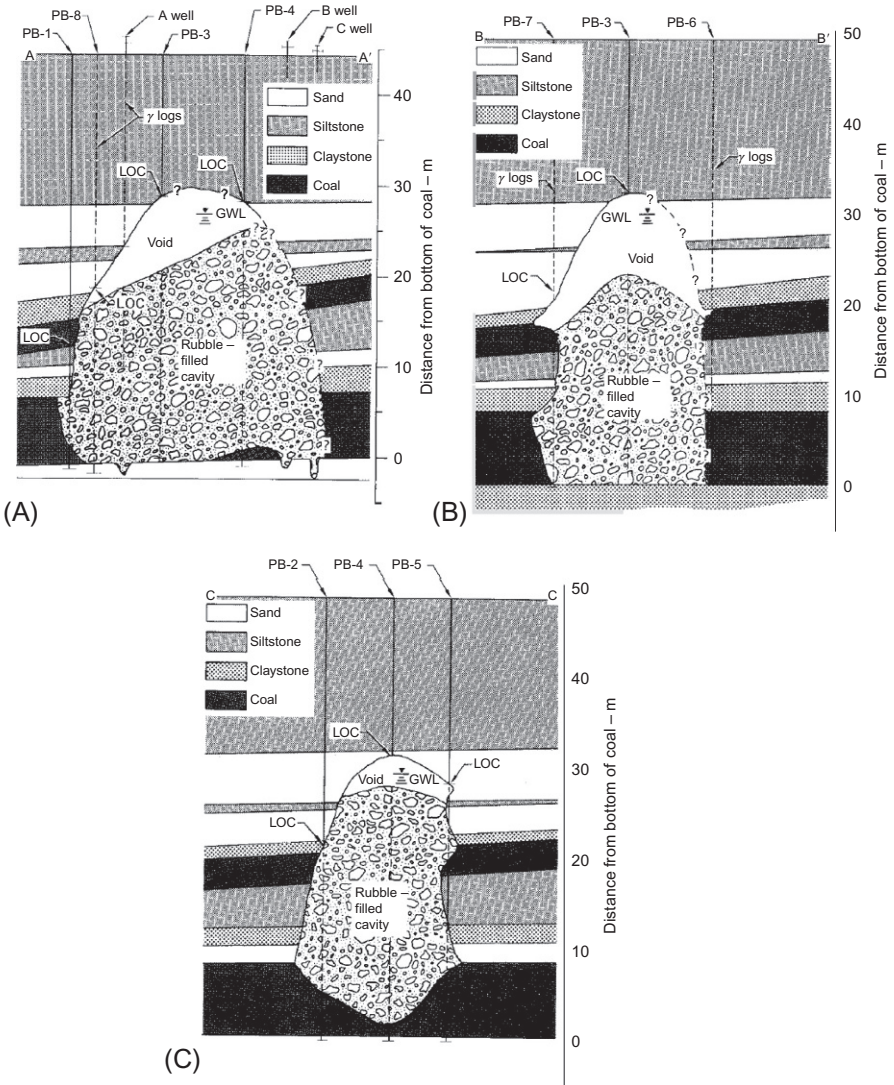
Fig. 4.2 Hoe Creek II postburn cross sections. Left: in the plane of the injection well (A) and production well (B). Middle and right: orthogonal cross sections near the injection well (middle) and production well (right). Scale in meters. Figure credit: Stephens (1981).

The Hoe Creek III test pioneered three things. It demonstrated extended operation with oxygen-steam injection to make a medium-quality gas that would be suitable for conversion to transportation fuels; it made use of the emerging technology of directional drilling to create a single link along the bottom of the seam with controlled location; and it pioneered and demonstrated the Extended Linked Well method (the method chosen for one of Rocky Mountain 1's modules 8 years later), in which

new UCG cavities could be ignited and burned at the bottom of different vertical injection wells that intersect a directionally drilled horizontal borehole link. The oxygen-steam injection was successfully implemented. Plugging of the injection well, probably from molten slag covering the injection point, forced impromptu switching of injection to a different well, resulting in an increase in gas quality. These experiences were on the evolutionary path toward the invention of the CRIP process.

In general, the process efficiency and gas quality of all the tests at the Hoe Creek site were relatively poor compared with most other sites. In addition to the override problems that all sites wrestle with, the Hoe Creek coal seams that were gasified had a thick interburden layer and a weaker wetter overburden, as well as higher seam and overburden permeability for water influx, all leading to more heat loss per energy content of the consumed coal. Problems with subsidence and groundwater contamination were experienced, especially at Hoe Creek III; these are discussed in Section 4.8.

All the Hoe Creek tests, consistent with Hanna test observations, showed the benefits of having a low-seam injection placement and the rejuvenation of efficiency when the injection point is moved to a new low location. "Based on the experience of the Hoe Creek experiments two things were done. First, a new, more favorable site was sought [with low coal and overburden permeabilities] and a drier and more competent overburden. Secondly, a new method of performing the gasification process, the CRIP process, was conceived" (Thorsness and Britten, 1989b).

4.5.7   Rawlins series (Gulf)

Gulf Research and Development Company operated the two Rawlins tests under shared funding with the DOE. These were done in a 7-m-thick steeply dipping (63°) subbituminous seam west of Hanna.

Rawlins I was an air-blown test with a smaller oxygen-steam phase at the end. As with Hoe Creek III, Gulf used a directionally drilled borehole for the in-seam link. As shown in Fig. 4.3, the injection well, AIW, was directionally drilled to enter the seam from below (to protect it from heat and collapse events) and completed near the bottom of the seam. The production borehole and link, PGW, was directionally drilled along the bottom of the seam to below the injection well and completed and cased to a point about 15 m updip from the injection point. The process ran well and demonstrated the feasibility of gasifying a steeply dipping seam using a directionally borehole link and process wells. The reactor apparently grows via periodic dropping of large chunks of coal and roof rock into the base of the reactor. A rubble bed was established over the base of the injection well, serving as a fire pit. The cavity expanded significantly up into the roof rock that was vertically above the gasified coal cavity.

Rawlins II was a larger and more complicated version of Rawlins I that mainly injected oxygen-steam. It used directional drilling to complete two injection wells roughly across dip from each other and a production well and borehole running downdip to the midpoint of the injection points. Reverse burns linked the injection wells to the production borehole. The sequence of events was very complicated and did not go according to plan. Ultimately, with considerable improvisation, various

Gulf Res. & Dev. Co.
Test 1 Section View
S 64.5°W
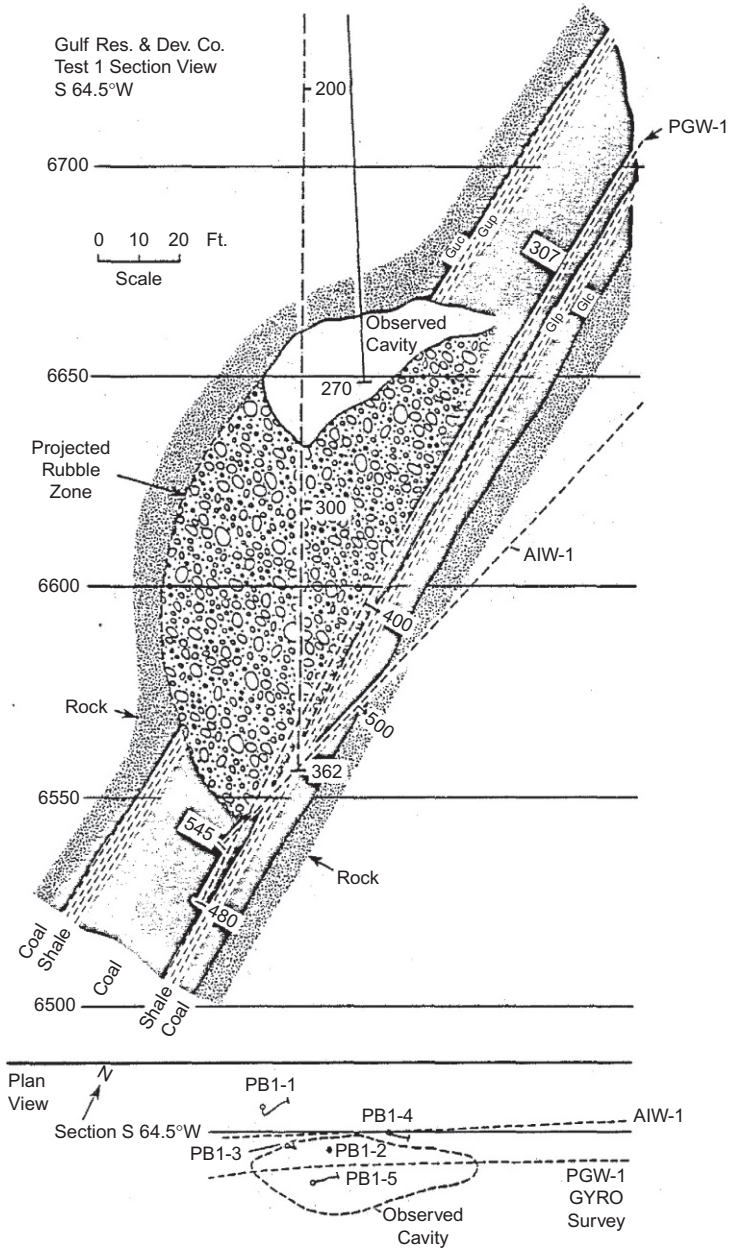
Fig. 4.3 Cross section of Rawlins I test after gasification. The injection well, AIW-1, was cased to about the 6550' elevation. The production well, PGW-1, was cased to about the 6600' elevation and continued down as a borehole in the seam past the injection point. Figure credit: Bartke (1985).

combinations of injection wells were used, and the gasification was successful. As at Rawlins I, with both spalling and collapse events grew the cavity upward through the coal and the overburden, feeding rubble beds at the bottom. Excellent quality gas was produced, largely because the steep dip keeps the upward-growing cavity within the coal seam, minimizing the ratio of roof heat loss to coal consumed.

The Rawlins I and II tests showed that once linked, a steeply dipping bed process can be run with a low injection point and a borehole and/or reverse link extending from it upward to a production well. Steeply dipping bed UCG can produce excellent quality product gas, because of the thermal efficiency of the "fire pit" packed bed nature of the process and the low ratio of roof heat loss to coal consumption. The burn cavity tends strongly to go more up than sideways. Although material balances showed little gas loss, it was observed at an updip surface outcrop of the seam and at the surface from the exterior surface of an imperfectly grouted well.

4.5.8   Centralia series (LLNL)

The Large Block tests (LBK) and the Partial Seam CRIP (PSC) test were conducted in 1981–83 by LLNL near Centralia in southwestern Washington. They were done in cooperation with the Washington Irrigation and Development Company (WIDCO), under the sponsorship of DOE and GRI. These tests are notable for the first field demonstrations of the Controlled Retracting Injection Point (CRIP) system (described in Section 4.8.9) and for being excavated afterward.

These tests were unique in that they were conducted at an exposed face or "high wall" of a subbituminous coal seam at a mine on the side of a hill. This allowed postburn excavation of the cavities. Fig. 4.4 is a cutaway sketch of the site, showing the configuration of the Partial Seam CRIP test. The Large Block tests were done first on
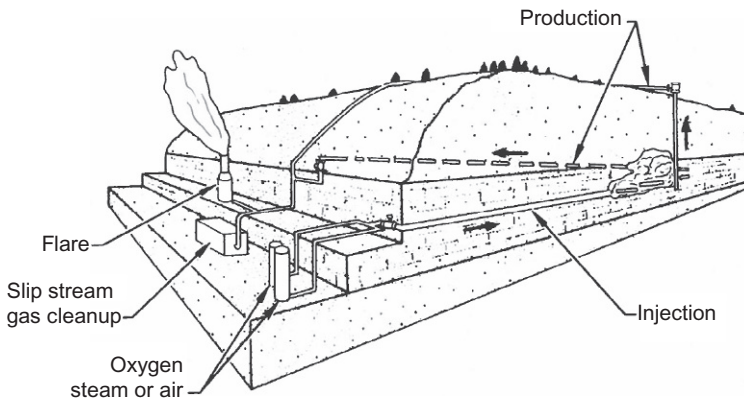
Fig. 4.4 Sketch of the WIDCO mine site at Centralia showing the configuration of the Partial Seam CRIP test. The terraces on the left are real. The right face of the figure is a cutaway cross section. Figure credit: Hill et al. (1984).

Fig. 4.5 All five of the Centralia Large Block tests were excavated, inspected, described, and documented. This advanced an understanding of the rubble-filled nature of UCG cavities. Photo courtesy of LLNL photo.

an adjacent area of the same exposed coal face. (The name "Large Block" came from an earlier plan for experiments in large isolated blocks of coal from which the actual test evolved.)

The Large Block tests were five similar small-scale oxygen-steam tests constructed with a vertical production well and a horizontal injection borehole drilled from the face and cased only part way in. Each of the tests lasted 3–5 days and consumed about 20 t of coal.

The first test in the field of LLNL's CRIP process was the fifth of the Large Block tests, LBK-1 (the test numbers did not reflect their sequence), proving CRIP's feasibility to relocate the injection point to a new location upstream in the injection well in unburned coal and ignite the burn there.

After the tests, the cavities were excavated and inspected (Fig. 4.5). The height-to-width ratio was typically 1.3–1.7 to 1. Most of the cavity volume was filled with rubble consisting of dried coal, char, ash, and some slag. Ash and slag are confined to the bottom. Toward the production well, the volume is entirely dried coal and char rubble extending upward from the original borehole. During one of the Large Block tests, an injection point had plugged during a period of high injected oxygen concentration. The excavation inspection revealed this to be plugged with mineral slag. This is another failure mechanism that CRIP can help with.

The Partial Seam CRIP test was a full-scale oxygen-steam field test, of similar magnitude to most of the others in the past decade. Fig. 4.6 shows the well and borehole configurations. After 12 days of forward burn using the initial injection point, a successful CRIP maneuver was performed, burning a hole in the injection well liner and igniting the coal there and starting a new burn cavity. Forward burn continued
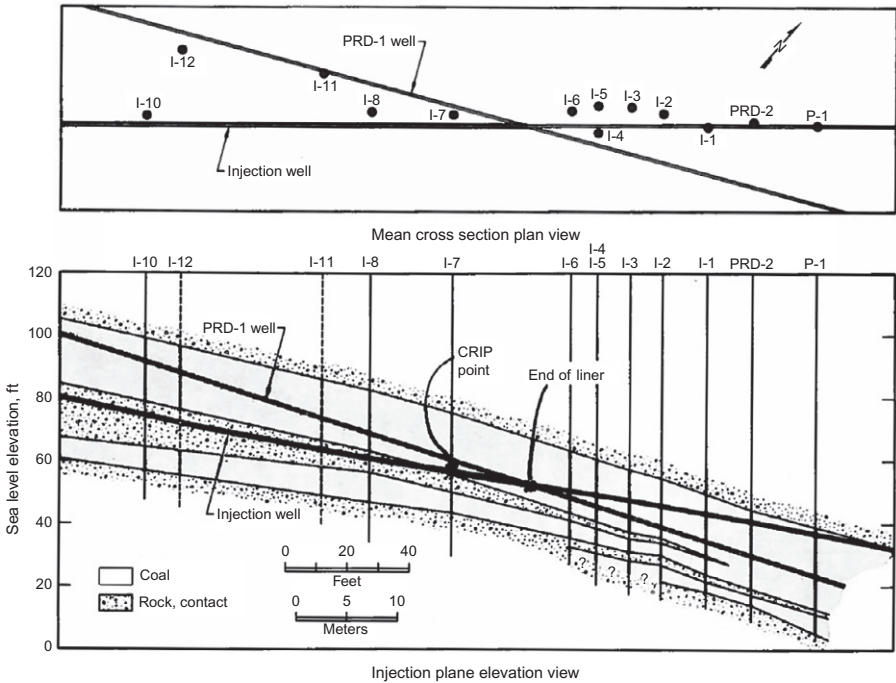
Fig. 4.6 Plan (top) and elevation (bottom) views of the Partial Seam CRIP process and instrument wells. The burn was started at the end of the injection-well liner near I-6 and that was the injection point until the CRIP maneuver burned a hole in the liner at the CRIP point near I-7, igniting and injecting there. Initial production was out of vertical well PRD-2 and later through the slant production well, PRD-1. Figure credit: Hill et al. (1984).

from this new injection point for an additional 18 days. In addition to the usual small-scale spalling and fracture growth of the cavity, a major roof collapse even occurred after a total of 20 days of gasification, with the top of the collapse block at 5.5 m above the coal seam. This major addition of wet inert roof rock into the process reduced the gas quality for the rest of the test.

Postburn coring was done to delineate and characterize the cavity. Later, the mine operators began to actively mine coal there, allowing excavation of the two (pre- and post-CRIP) burn cavities and the outflow channel at and above the in-seam production borehole. Fig. 4.7 shows the exposed coal face where the cavity was relatively large and a sketch of the cavity based on observations and characterization of thermally modified minerals. The sidewalls of the ~20-m-wide cavity were bowl-shaped (concave up) near the bottom, becoming largely vertical and extending far up into the overburden, higher than wide. Any remaining notion that UCG could be pictured as an open cavity and a rock ceiling was dispelled by the excavation of the Partial Seam CRIP test. The excavation found the "cavity" to be full of ash, slag, char, dried coal, and rubblized overburden, with a few gaps. The outflow channel had an upward V shape and was filled with char and dried coal rubble.
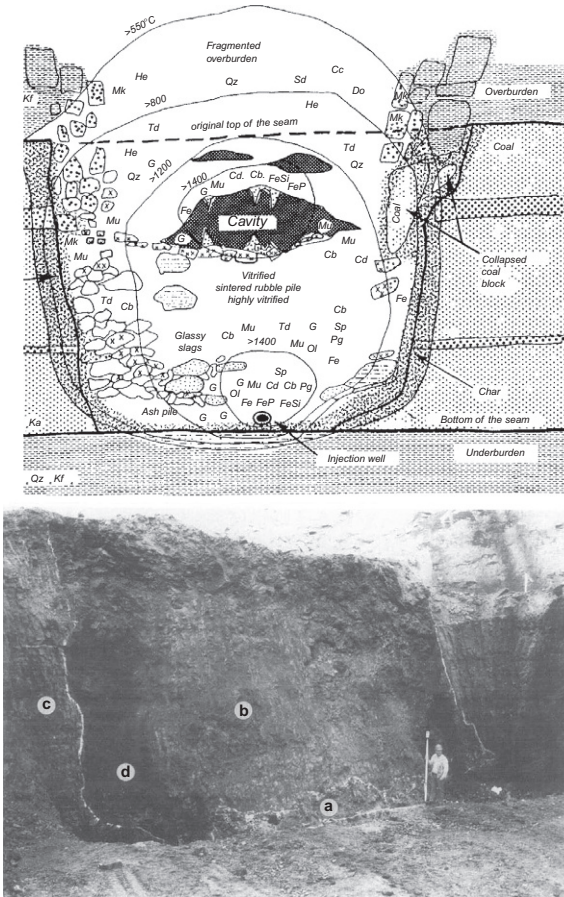
Fig. 4.7 The Partial Seam CRIP field test, done at the exposed face of a coal seam, was excavated, inspected, sampled, and analyzed to learn the nature of the rubble-filled cavity; (c) is virgin coal, (d) is char, (a) is ash slag, and (b) is thermally affected overburden rubble. Figure credit: Kühnel et al. (1993).

4.5.9 Rocky Mountain 1 (DOE-industry consortium)

4.5.9.1 Overview

Rocky Mountain 1 (Fig. 4.8) was the largest, most successful, and final test of the US UCG program. It was organized by the DOE and cost-shared 50/50 with industry. Major participants included GRI, Stearns-Rogers Engineering (United Engineers), Gulf (later Energy International), LLNL, and WRI. The test was conducted several hundred meters southeast of the Hanna tests in the same low-dip nonswelling bituminous coal seam at a depth of about 110 m.

Fig. 4.8 The Rocky Mountain 1 test took place near the old Hanna Wyoming site from November 1987 to February 1988.
Photo courtesy of LLNL photo.

There were two adjacent but separate modules, CRIP (which used the Controlled Retracting Injection Point system - see Section 4.8.9) and ELW (which used the Extended Linked Well system). Both used horizontal boreholes for linking. The well configuration of the two modules is shown in Fig. 4.9. ELW was thought to have the best economic potential for relatively shallow seams in which many vertical wells could be afforded. The newly invented CRIP method was thought to have the best economic potential for relatively deep seams for which having fewer longer wells may be more cost-effective. The descriptions below emphasize the CRIP module because it was much more successful than the ELW module and because it appears to be more relevant to modern UCG practice.

The modules were ignited, started up, stabilized, and switched to the main phase of oxygen-steam gasification in late November 1987 and run continuously until being shut down in mid-January (ELW) and late February 1988 (CRIP). Perhaps to remind the US team of its Russian predecessors, the weather provided blizzards and wind-chills to $-36°C$ and challenges with frozen equipment (Fig. 4.10). The CRIP module ran very well and is described further below. The ELW module ran but was handicapped because its injection wells were completed at the top of the seam by mistake. Groundwater contamination received serious attention and the Clean Cavern approach was used to minimize it. This is discussed more in Section 4.7.1. A postburn drilling, coring, and logging program was done in the years after the test. This was used, along with downhole thermocouple data and material balance information obtained during the test, to delineate the cavity boundaries and extent of thermal alteration of surroundings and describe the cavity contents.
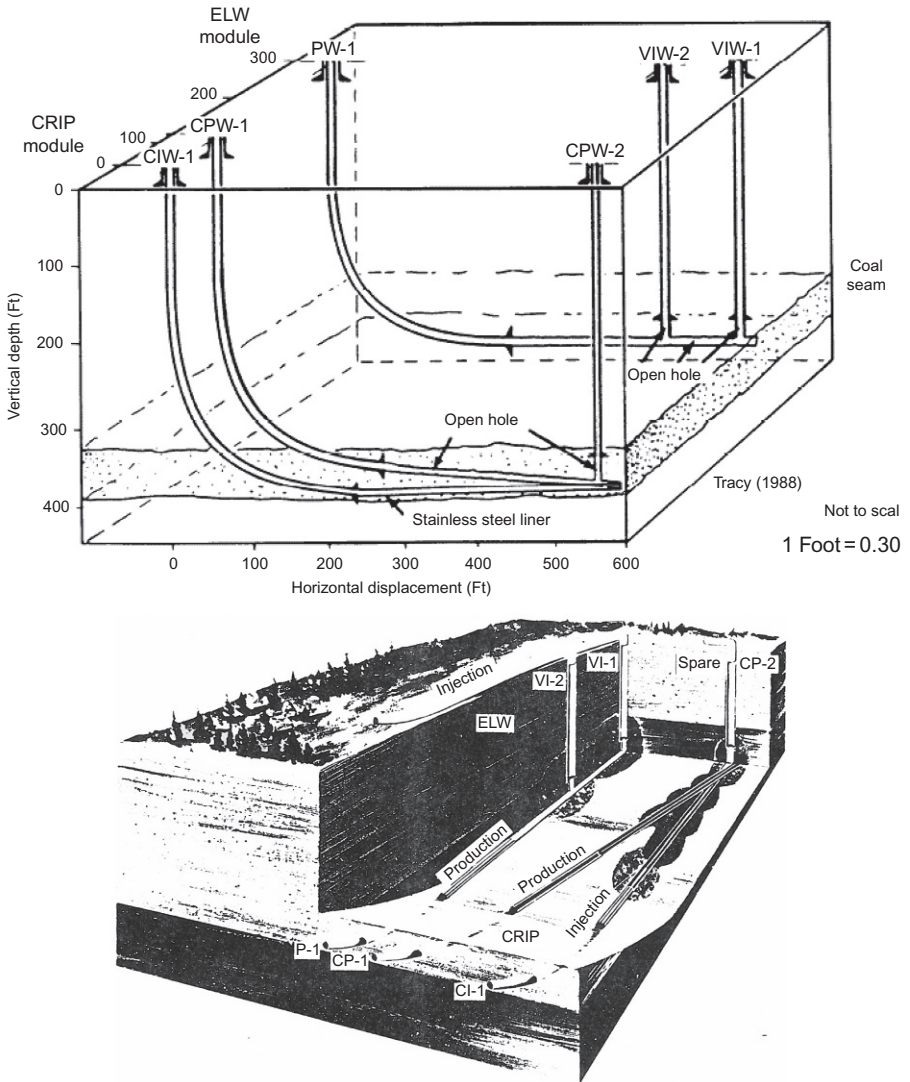
Fig. 4.9 Rocky Mountain 1's process well layout for its side-by-side ELW and CRIP modules. The artist's cutaway shows the planned cavity sequences; both modules stopped one cavity short of what is shown, and the cavities in both modules extended up higher into the overburden than shown. Figure credit: Thorsness and Britten (1989a).

Fig. 4.10 Wyoming's winter weather repeatedly challenged US UCG field-test operations, including this final Rocky Mountain 1 test.
Photo courtesy of LLNL photo.

4.5.9.2   CRIP module

Fig. 4.11 is a plan view of the CRIP module. The casing endpoint of the vertical production well (CPW-2) was near the bottom of the coal seam. The horizontal injection and production boreholes were in the bottom half of the seam. The injection well was cased to 4 m from CPW-2. The horizontal production well's casing started about 90 m downstream of CPW-2. Injection was always into the horizontal well CIW-1. The injection point was initially at the end of the well casing within about 4 m of CPW-2 but was periodically moved upstream about 18 m at a time by a CRIP maneuver. The burn was initiated using vertical well CPW-2 for production but then was soon switched to the CPW-1 production well that was cased to about 90 m from CPW-2 and open borehole the rest of the way to its intersection with CIW-1 and CPW-2.

The CRIP module ran very well and had no serious problems over 93 days of forward-burn gasification when it was shut down because of schedule and budget. It produced high-quality gas, with efficiency parameters comparable with surface gasifiers. Four successive cavities were operated, using three CRIP maneuvers to create new ones, with each new injection point located about 18 m upstream of the previous one. For each injection point and cavity, the process efficiency and product gas quality followed the usual decline with time but improved again with each CRIP maneuver (Fig. 4.12). There was a long-term decline in product quality and efficiency, possibly because of the growing ratios of exposed roof area (and corresponding heat loss) and cavity perimeter (and corresponding water influx) to rate of coal consumption. Table 4.3 shows summary performance data for the CRIP module and the ELW module. Table 4.4 shows the energy balance for the steam-oxygen periods of the first CRIP cavity and the entire ELW module.
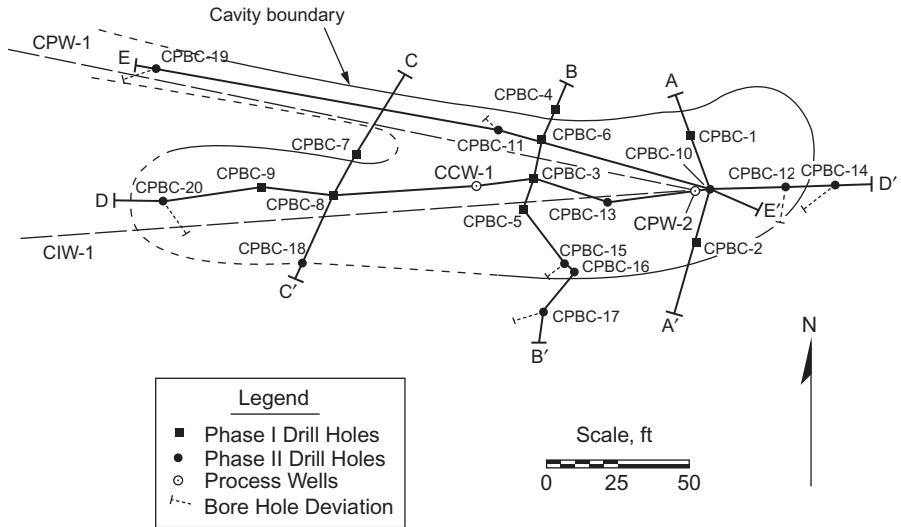
Fig. 4.11 Plan view of Rocky Mountain 1's CRIP module, including the horizontal production borehole (CPW-1), horizontal injection well (CIW-1), vertical initiation and initial production well (CPW-2), and final cavity boundary (solid and short-dashed perimeter). The initial injection point (end of the CIW-1 casing/liner) was 4 m in unknown direction from CPW-2. The production well (CPW-1) casing ends about 25 m west of this figure. Figure credit: Oliver et al. (1991).
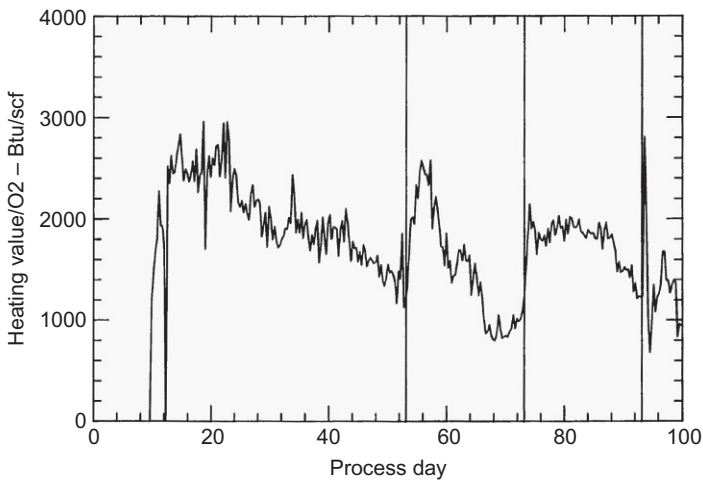
Fig. 4.12 Process efficiency parameter (product heating value divided by injected oxygen rate) as a function of process day for Rocky Mountain 1's CRIP module. Oxygen-steam injection started on day 12. Vertical lines show the times of CRIP maneuvers. Figure credit: Cena et al. (1988b).

Table 4.3 Summary data for the CRIP module, the individual CRIP cavities (the initial one plus the three that followed each CRIP maneuver), and the ELW module

Module	CRIP	CRIP first	CRIP second	CRIP third	CRIP fourth	ELW
Duration (days)	93.0	43.8	19.9	20.0	9.3	57.4
Coal gasified (Mg)	10,184	3719	2159	2277	798	4030
Gas HHV (MJ/Nm^3)	11.3	11.7	10.8	11.6	9.7	10.3
H$_2$ (dry mol%)	38.0	38.0	38.0	39.0	40.0	31.0
CH$_4$ (dry mol%)	9.4	10.5	8.6	9.5	6.7	10.1
CO (dry mol%)	11.9	11.6	10.8	14.3	9.9	9.0
CO$_2$ (dry mol%)	38.0	37.0	40.0	35.0	42.0	44.0
O$_2$/C (mol/mol)	0.27					0.35

The first two rows (days and Mg) include the air injection forward-burn stabilization phases of the ELW and the first CRIP cavity. All other rows of intensive properties are for oxygen-steam periods only (Cena et al., 1988a,b)

Table 4.4 Computed energy distribution as a percent of the consumed coal heat of combustion for the ELW module and the first CRIP cavity during their steam-oxygen period

	CRIP	ELW
Heating value of combustible gas product	62.4	52.1
Heating value of combustible tar product	6.1	5.9
Sensible heat of gas product	2.7	3.2
Sensible and vaporization heat of in situ water influx converted to product steam ($\sim$30% from rock drying, $\sim$70% from permeation inflow)	0.7	3.4
Sensible and vaporization heat of added cooling water converted to product steam	0.0	0.6
Heating value of char left underground	20.1	21.6
Sensible heat of char and ash left underground	0.6	0.7
Sensible heat of overburden rock left underground	7.0	12.3

The basis is the heat of combustion of all the coal that was thermally converted (pyrolyzed or more) (Thorsness and Britten, 1989a).

Fig. 4.13 shows the movement of the injection points with time and an early estimate of the cavity progression (Cena et al., 1988b). The actual injection points are further west (left) than the intended CRIP points because of thermal attack recession. Figs. 4.14 and 4.15 show the lengthwise cross sections of the final cavity, D-D' along the line of injection points and E-E' along the production borehole. Figs. 4.16–4.18 show the three cross sections perpendicular to the injection and production boreholes,
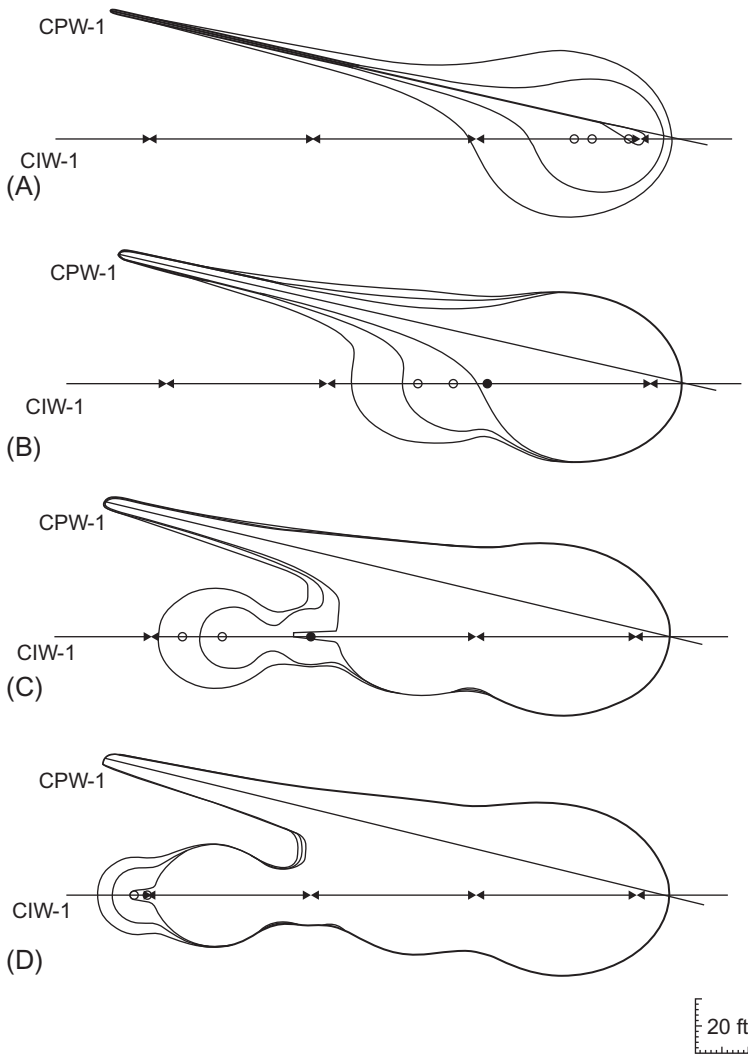
Fig. 4.13 Early estimates of the cavity evolution with time, based on mass balance, downhole thermocouples, and knowledge of the injection point. Each figure represents one of the CRIP periods, with maneuvers in between. Each period shows contours near the period's beginning, middle, and end. The locations of the actual injection points at those three times are shown with open circles. X marks the intended CRIP injection locations at the beginning of each period. Figure credit: Cena et al. (1988b).
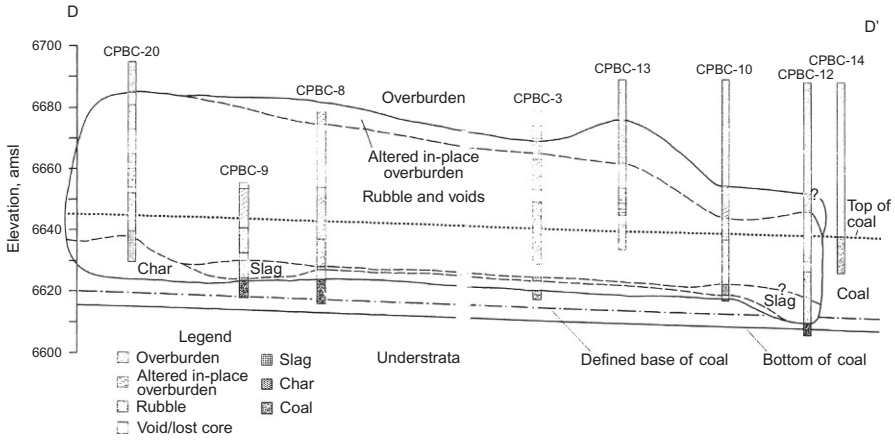
Fig. 4.14 Rocky Mountain 1's CRIP module final cavity geometry looking north, cross section D-D'. Fig. 4.11 shows the corresponding plan view with a scale. Figure credit: Oliver et al. (1991).
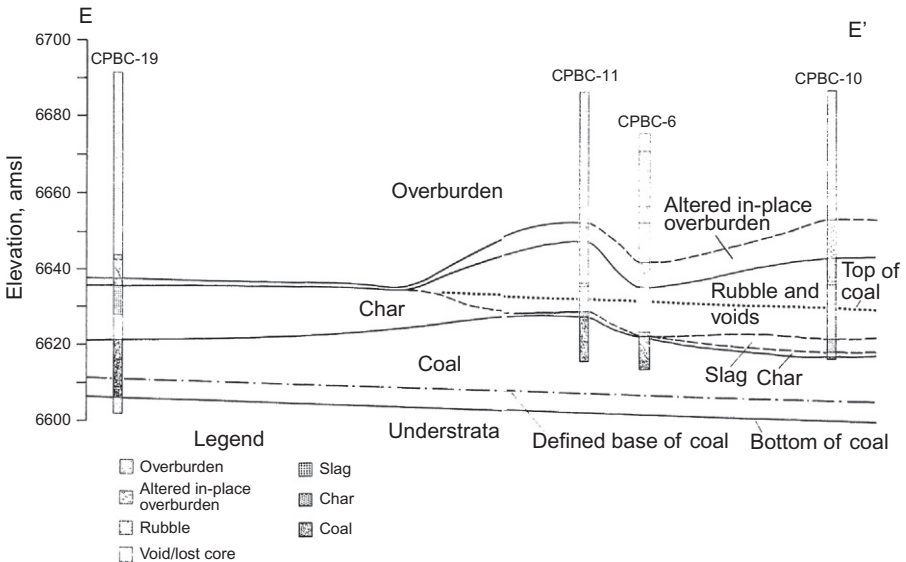
Fig. 4.15 Rocky Mountain 1's CRIP module final cavity geometry looking north, cross section E-E'. Fig. 4.11 shows the corresponding plan view with a scale. Figure credit: Oliver et al. (1991).

all looking west (Oliver et al., 1991). These cross sections show that the thickness of the part of the seam that was utilized was about 6 m, probably because that was the elevation of the imperfectly placed injection well and production borehole. Where adequate time for growth had been allowed, the cavity width was roughly 18 m or about 3 times the thickness of the gasified coal. The height of roof rock that fell into
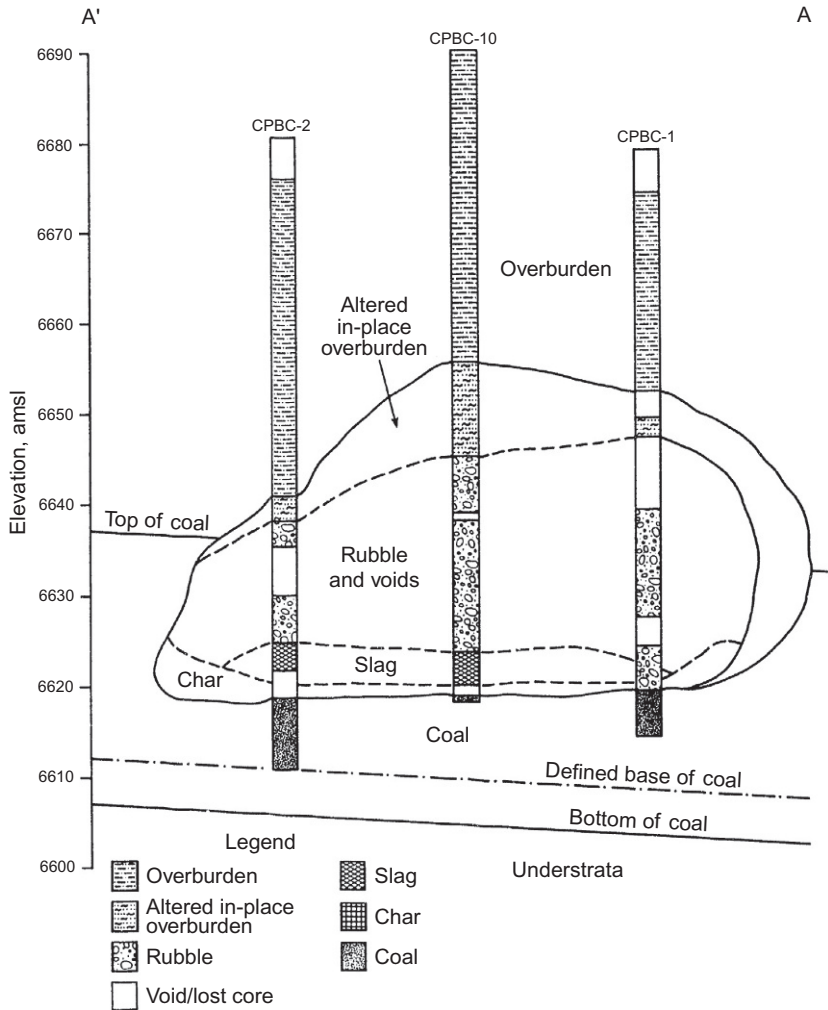
Fig. 4.16 Rocky Mountain 1's CRIP module final cavity geometry looking west, cross section A'-A. Figure credit: Oliver et al. (1991).

the cavity or was thermally altered was typically 1.5–2.0 times the height of the coal below it that was converted.

4.5.9.3 ELW module

For the ELW module, the initial injection well was VI-1 with VI-2 being the planned second injection well. The ELW production well P-1 was cased to about 90 m from VI-1 and open borehole the rest of the way. Produced gas was intended to flow through the open production borehole, thought to be in the bottom half of the seam, and into the
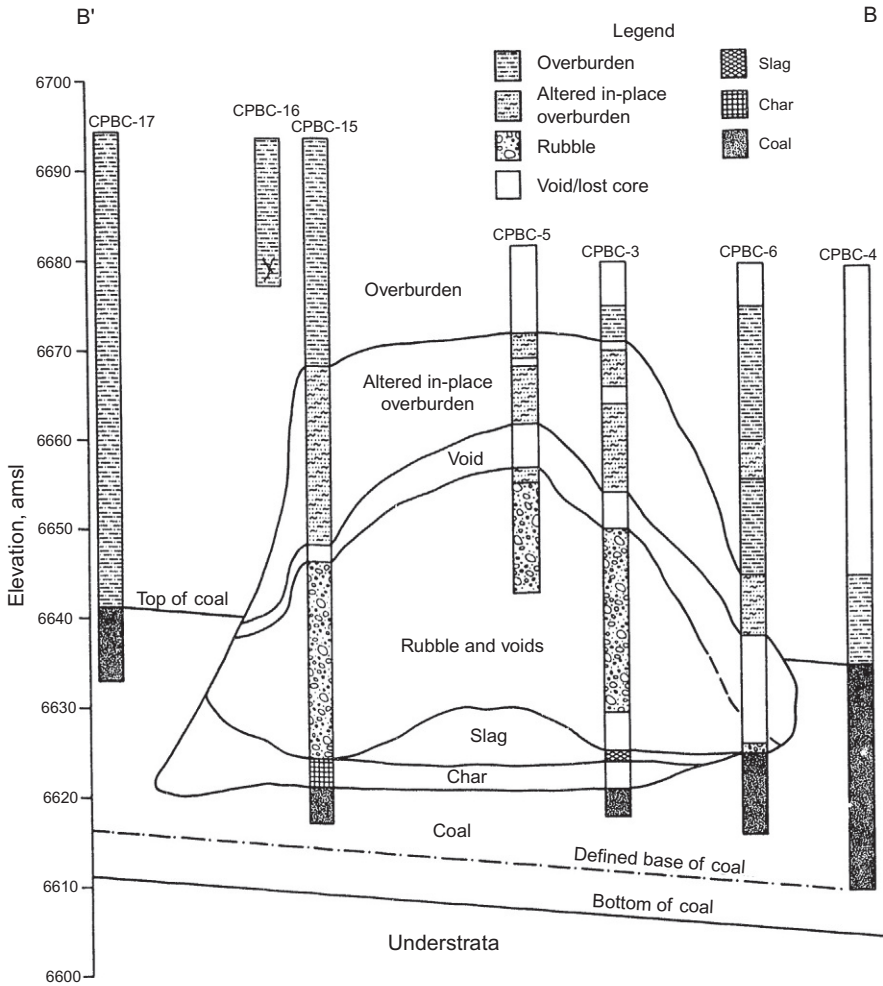
Fig. 4.17 Rocky Mountain 1's CRIP module final cavity geometry looking west, cross section B'-B. Figure credit: Oliver et al. (1991).

cased portion of production well P-1. The casing endpoints of the two vertical injection wells were in the top 2 m of the coal seam instead of the bottom as planned. This handicapped the ELW module from the beginning.

The ELW module ran fairly well initially, but it struggled with override and oxygen bypass that hurt its performance and duration. It was not able to successfully switch injection to the second injection well, VI-2. Unacceptably, high oxygen levels in the product gas began to be seen that could not be remedied, and the module was shut down for safety considerations after 46 days of forward burn. Process results were given in Tables 4.3 and 4.4.
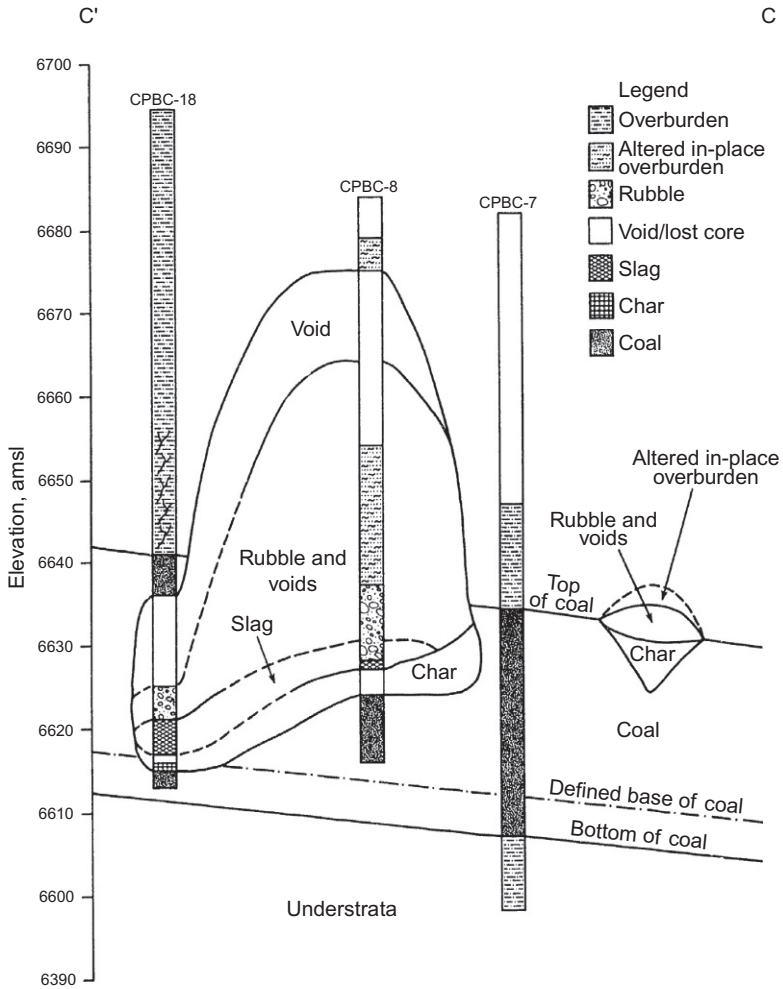
Fig. 4.18 Rocky Mountain 1's CRIP module final cavity geometry looking west, cross section C'-C. Figure credit: Oliver et al. (1991).

The cavity width that was in the vicinity of the injection well was roughly 15 m or about 3 times the thickness of the gasified coal. The height of roof rock that fell into the cavity or was thermally altered was typically 2–3 times the height of the coal below it that was converted.

4.5.9.4 General observations

The Rocky Mountain 1 test demonstrated: the importance of a bottom-seam injection point; the feasibility of the CRIP process for establishing a series of at least four new injection points and cavities at field-test scale; and the production of a gas with quality

and efficiency metrics that are comparable with surface gasification processes (Thorsness and Britten, 1989b).

The ratio of product heating value to injected oxygen, a common efficiency metric, was 50% higher for the CRIP module than the ELW module. The CRIP module's superior performance is directly traceable to differences in geometry. The CRIP method assured that the injection point was always low in the seam, and CRIP maneuvers were able to generate new cavities whenever the cavity grew big enough to involve much overburden. The ELW module suffered from a high injection point, making the burn primarily near the top of the seam, thus involving a proportionally large amount of overburden and correspondingly high heat loss.

The extent of upward roof heating and rubblization was less in the CRIP module than the ELW module, despite having a slightly larger thickness of consumed coal, slightly wider cavity, and much greater duration of operation and quantity of coal processed. This is probably because the CRIP process frequently moved the injection point, reducing the duration of time that any one roof area is exposed to the hottest conditions.

There was more hydrologic connectivity and fluid/pressure interaction between the two modules than had been anticipated based on preburn characterization. This is an important finding that relates to scale-up in a nonhorizontal bed.

Reverse-burn connections were problematic. Drilling technology of the time resulted in boreholes missing their intended intersections by a few meters. Reverse burns were used to make these short connections in both the ELW and CRIP modules. Speaking of the CRIP module but applicable to both modules, Cena et al. (1988a) said that "the linking phase of the test was of short duration but was by far the most taxing phase in terms of the physical plant and personnel. Also, high pressures used for air acceptance tests and linking phases may have produced local, unwanted increases in permeability… Startup and subsequent operation would have been much easier had mechanical connection of the wells existed… ."

In addition to the inconvenience, the high air pressures (4–7 bar over hydrostatic) used to reverse burn the short connections drove product gas outward more than 200 m, mainly in the southwest direction as shown in Fig. 4.19 (Beaver et al., 1988). Contaminants were found updip in excess of permit requirements, but the regulators allowed the test to continue because of prompt discovery, understanding of the cause, and assurances of no more high pressures (Dennis, 2006).

The high pressures used during air acceptance testing that preceded reverse-burn operations caused some of the monitoring wellhead flanges to mechanically fail. The pressure pathway for this is from the injection well into and through the formation to the open/screened bottom of the monitoring well and up the monitoring well.

Drilling navigation has improved greatly since 1987. Now, intersections are likely to be very precise, requiring less effort, pressure, hassle, and time to connect them, hopefully by water-jet erosion.

Minimization of groundwater contamination using the Clean Cavern concept was a high priority for Rocky Mountain 1. This is described in Section 4.7.1.
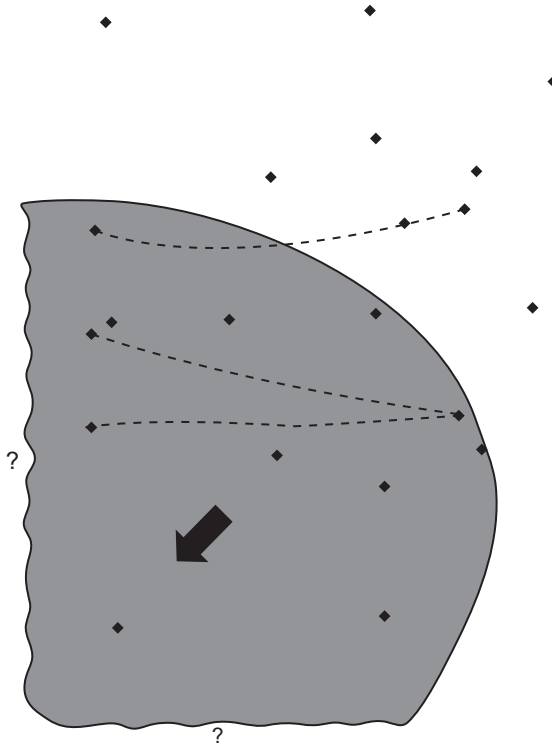
Fig. 4.19 High injection gas pressures that occurred during the brief reverse-burn connection-making operations at Rocky Mountain 1 drove gas including pyrolysis and gasification products out and updip more than 200 m. Figure credit: Beaver et al. (1988).

4.5.10   Other field tests

These commercial field tests were not well reported and had little impact on the main US UCG program.

4.5.10.1   Texas lignite field tests (Basic Resources and the Texas A&M Consortium)

Basic Resources, a subsidiary of Texas Utilities, purchased the US rights of the Soviet UCG technology in 1975. They operated a 26-day air-blown test in 1976 near Fairfield, Texas. In 1978–79, Basic Resources operated a 197-day test near Tennessee Colony in Anderson County, Texas. Table 4.1 contains information about this test. The product has had high CO_2 concentrations. Efficiency suffered from heat losses to the overburden and water influx from adjacent sand formations.

A corporate consortium led by Texas A&M University carried out three short and small tests in Texas lignite, all air-blown. Operations and results were poor. The first

two lasted 1 and 2 days. Problems included sand control, excessive water production, heat loss due to the thin seam, casing problems, and air/gas bypass. The third test, in 1980, spent 21 days at the Alcoa site trying to achieve reverse-burn linkage at well spacing as small as 9 m. Problems included mechanical failure of well casings due to thermal expansion.

4.5.10.2   Carbon County (Williams Energy)

"In 1995, Williams Energy conducted a UCG pilot project in Carbon County near Rawlins, WY. This test was located adjacent to the Rawlins UCG trials… however, it was performed at deeper levels…. The test was unsuccessful and resulted in ground-water contamination due to poor well linkage and operation of the UCG reactor above hydrostatic pressures" (GasTech, 2007). Organic compounds including benzene increased in concentration after the burn in groundwater within the coal seam and in overlying and underlying sandstone units.

4.6   Modeling

4.6.1   Introduction

Much effort in the United States has been devoted to mathematical modeling of UCG. The best of these have been well informed by field-test observations of the cavity and its nature of growth and an accurate understanding and conceptual model of the UCG process. Two excellent high-fidelity, multiphysics, integrated models, CAVSIM and UCG-SIM3D, were developed that capture the most important phenomena of the full multidimensional dynamic UCG process in its main forward gasification mode. Some much-simplified lumped-parameter engineering models, EQSC, UCG-MEEE, and UCG-ZEEE, were developed that are useful for rough estimates, trade-off studies, or screening of resource suitability.

4.6.2   High-fidelity, multiphysics models of the UCG process and cavity growth

The model of the 1970s and 1980s that most accurately and completely captured the important aspects and phenomena of UCG was LLNL's CAVSIM model (Britten and Thorsness, 1988, 1989). As illustrated in Fig. 4.20 (top), CAVSIM modeled a single cavity in a horizontal seam. The cavity was constrained to be 2D axisymmetric (i.e., varying only in vertical and radial directions), with a fixed injection point on the symmetry axis low in the coal seam. It included the essential chemistry, heat transfer, gas transport, water permeation influx with both a saturated and unsaturated zone in the surroundings, upward and outward cavity growth by spalling of coal and over-burden, accumulation of coal, char, ash, and roof rock rubble in the lower fraction of the cavity, pyrolysis, gasification, and combustion of coal at the wall and in the packed bed of rubble. It also had an added module to represent the heat transfer and chemistry in the link between the main cavity and the production well entrance. It accurately
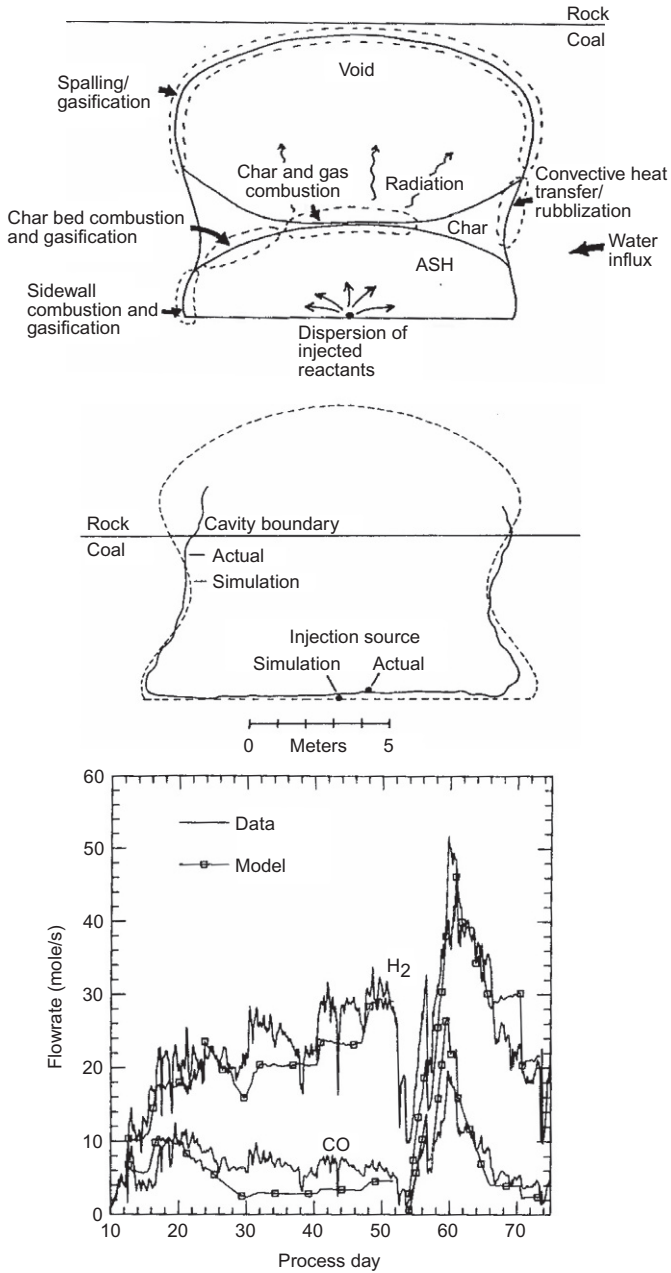
Fig. 4.20 Top: schematic of CAVSIM model, showing phenomena occurring in zones treated by various submodels. Middle: predicted and measured shape of the Centralia Partial Seam CRIP field test. Bottom: predicted and measured production rates of H_2 and CO for the first two cavities of Rocky Mountain 1's CRIP module. Figure credit: Britten and Thorsness (1989).

reproduced the approximate cavity shape, water influx, and product gas compositions for the Centralia Partial Seam CRIP test and the first two cavities of Rocky Mountain 1's CRIP module (Fig. 4.20, middle and bottom).

More recently, a different LLNL team developed a modern high-fidelity multiphysics integrated model of UCG called UCG-SIM3D (Nitao et al., 2011; Camp et al., 2013). It models essentially the same phenomena as CAVSIM but takes advantage of modern computational capabilities, algorithms, and software elements of other state-of-art codes. Important advances over CAVSIM include flexible three-dimensional (3D) geometry that allows for arbitrary spatial variations of geologic properties such as multiple coal seams of different compositions, dip, and varying permeabilities; flexibility to move one or more injection points and production points to locations that can change with time; a sophisticated algorithm that tracks 3D growth of the cavity and rubble boundaries and rubble composition; an improved 3D model of flow, reactions, and heat transfer within the rubble bed and in the open void region; and a 3D nonisothermal unsaturated water and gas flow model for both the near- and far-field surroundings. As with CAVSIM, sideward and upward growth of the cavity in coal and overburden rock is by spalling, with user-specified rate coefficients in a temperature-dependent model. The code structure would allow for interface with a geomechanics code that could predict cavity growth by structural roof collapse, but this was not implemented. After fitting some parameters, UCG-SIM3D accurately calculated for both the Hoe Creek III and Rocky Mountain 1-CRIP field tests: the 3D development of the cavities and their rubble contents; the 3D time histories of the temperature, pressure, and composition fields within the cavities and in their surroundings; and the product gas composition histories (Figs. 4.21–4.23). UCG-SIM3D development ended before being matured into an engineering tool for use by nonexperts.

4.6.3   Simplified engineering models

Simpler engineering models were developed that are easier to use by a competent UCG engineer and are useful for obtaining rough estimates, dependencies/sensitivities, and screening resources. These are typically lumped-parameter models with no spatial or temporal resolution.

LLNL developed EQSC (Upadhye, 1986) to calculate energy and material balances (by species) based on a simple multizone model of UCG, chemical equilibrium, and a set of required inputs. In addition to the coal analysis, inputs included the water influx and the fraction of this that enters the process before and after the water-gas shift equilibrium is set, the methane ratio (since methane is governed more by pyrolysis than equilibrium), the effective temperature for calculating water-gas-shift equilibrium (different than the process temperature), heat loss, and product exit temperature. EQSC was extended in recent years by LLNL to a spreadsheet-based model called UCG-MEEE (material, energy, and economics estimator) (Upadhye et al., 2013). Its core is the EQSC model for a single (but reproducible) UCG module. UCG-MEEE provides side calculations to help estimate some of the required input parameters. It envisions many UCG modules operating in parallel on industrial scale
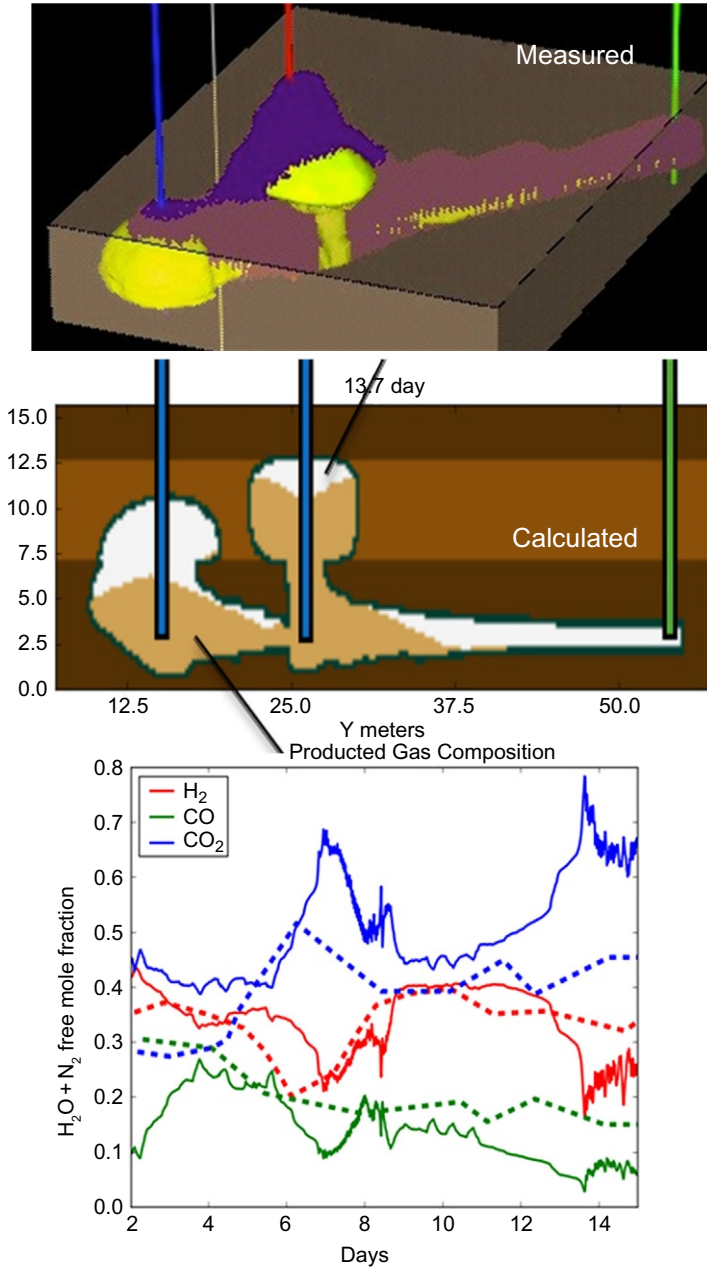
Fig. 4.21 UCG-SIM3D calculations of cavity and rubble geometry and product composition, compared with measurements for the first 15 days of the Hoe Creek III field test. Figure credit: Camp et al. (2013).
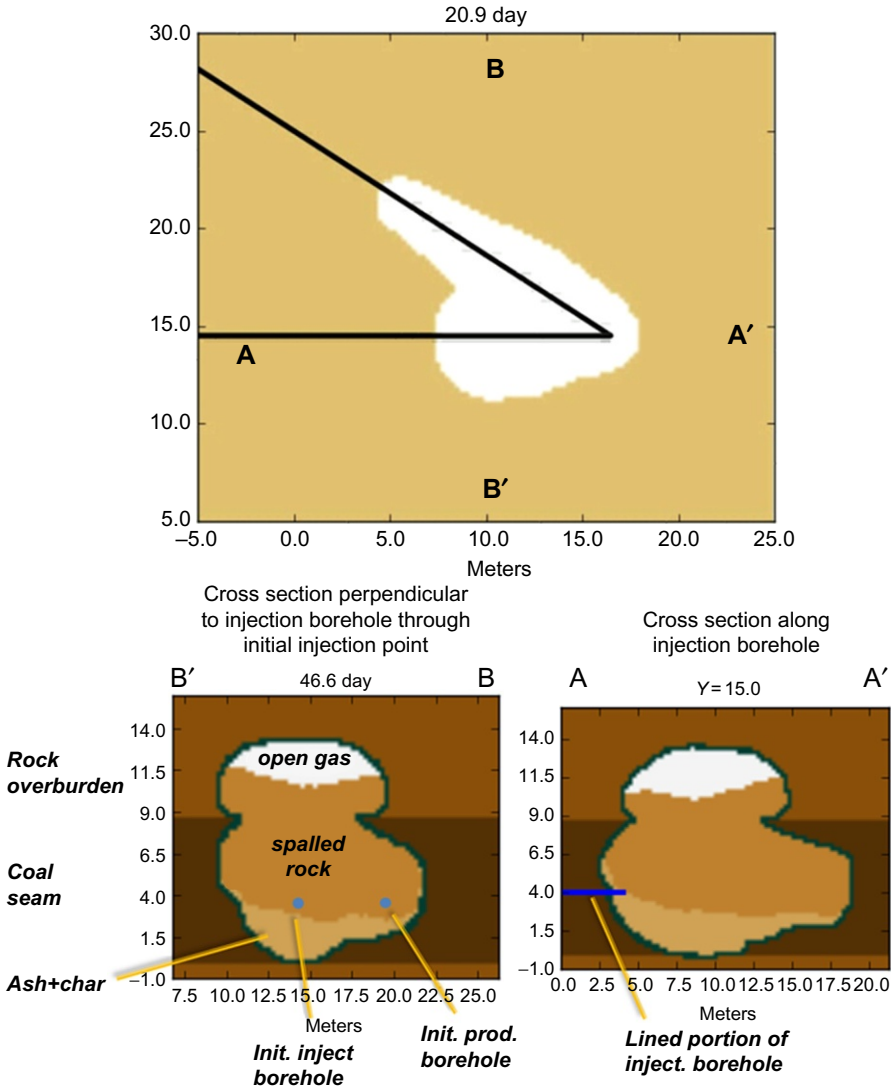
Fig. 4.22 UCG-SIM3D calculations of cavity and rubble geometry for the Rocky Mountain 1 CRIP module. Top: plan view at 21 days, bottom: cross sections after 47 days. Figure credit: Camp et al. (2013).

for a long project duration, and so, it requires and calculates industrially relevant engineering parameters. In addition to a full material (by species) and energy balance and large-scale flow and resource parameters, UCG-MEEE estimates a selling price for the product gas to achieve a desired rate of return. The economics are based on the GasTech (2007) study and standard scaling factors. UCG-MEEE's utility for determining parameter sensitivities and trade-offs was illustrated in Burton et al. (2012).
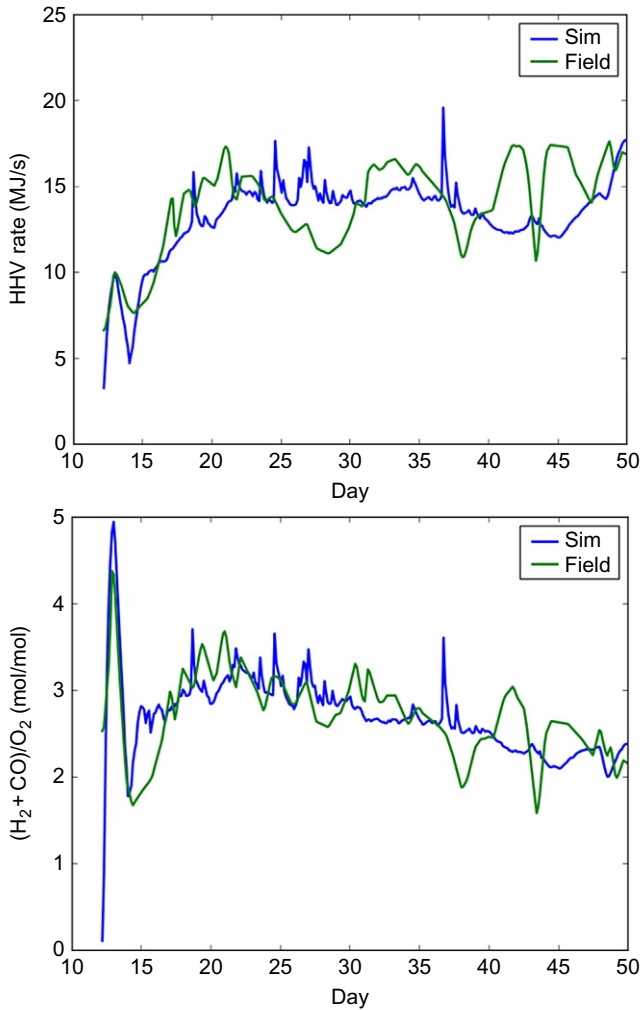
Fig. 4.23 UCG-SIM3D calculations of product gas history compared with measurements for the Rocky Mountain 1 CRIP module. Top: heating value rate, bottom: (H_2+CO) per injected O_2. Figure credit: Camp et al. (2013).

4.6.4 *Models of narrower scope*

Krantz and Gunn (1983b) and Dobbs and Krantz (1988) review US models of the reverse-burn mode of UCG. Models that describe narrower set(s) of phenomena have been developed or applied to UCG, such as detailed chemical reaction models, multiphase hydrologic reactive flow and transport models, or state-of-art geomechanical codes. These are not reviewed here.

4.7   Environmental aspects

4.7.1   Groundwater contamination

US field tests demonstrated repeatedly that the risk of groundwater contamination from UCG is real. The Hanna tests resulted in small amounts of contamination. Relatively minor remediation was needed at two of the four Hanna test areas. The Hoe Creek tests, especially Hoe Creek III, seriously contaminated the site, requiring an extensive expensive remediation. The reported gas escape, large upward extent of cavity growth, fracturing, subsurface subsidence, and overlying aquifer at Rocky Hill are all indirect indications of the spread of contaminants although ARCO's paper on this test did not say so. There was upward transport of product gas to the surface in the steeply dipping coal seam and in the periphery of a well at Rawlins. The rupture of a production well at Pricetown pressurized an overlying aquifer and required shutdown. The extent of research on UCG-produced contaminant species by Texas-based workers of the time (c.f. Humenick and Mattox, 1978, 1982) suggests that it was a concern in the Texas lignite tests. Rocky Mountain 1 lost about 10% of its gas overall, and early in the test, it spread product gas hundreds of yards updip, exceeding contamination limits, during their high-pressure reverse-burn connecting operations. Williams' short-lived Carbon County testing at greater depths in the steeply dipping G seam near Rawlins operated at pressures higher than surroundings and contaminated groundwater in the seam and overlying and underlying sandstone units with benzene and other organic compounds, requiring remediation. There were significant differences in observed groundwater contamination between tests, with only minor changes in groundwater over limited areas found and reported after some tests and serious contamination over broader areas following other tests, with imperfect correlation to operating practices and estimated gas losses.

Gas escape is the major mechanism for transporting contaminants away from the immediate process area. Material balances, tracer tests, and other observations (c.f. Cena and Thorsness, 1981; Cena et al., 1988a; Bell et al., 1983; Davis, 2011) indicate that losing 10%–20% of the produced gas was common throughout the entire field-test program all the way through Rocky Mountain 1.

Factors that contribute to groundwater contamination were generally known at the beginning and early phases of the main US field-test program, but they appear to have been given lower priority over technical success, process efficiency, and project costs. Ironically, the early environmental failures motivated significant efforts that resulted in improved approaches for operating more cleanly. As the reality and importance of minimizing groundwater contamination impacts became more apparent, more attention was devoted to this, resulting in a greater understanding of the processes and the development of mitigating practices. WRI was perhaps the largest contributor in this area; additional contributors included LLNL, GRI, and researchers from Texas.

By the time of Rocky Mountain 1, this understanding and a growing body of research led to a set of recommendations called the Clean Cavern concept. Mainly advanced by WRI researchers, these made sense, were adopted by Rocky Mountain 1's management, and facilitated successful permitting (Covell et al., 1988;

Boysen et al., 1990). Clean Cavern recommendations included maintaining cavity pressures below the hydrologic confining pressures, actively monitoring surrounding hydrologic pressures to inform the control of cavity pressures, postburn venting and steam flushing of cavities to evacuate pyrolysis vapors, cooling of the cavity to minimize further pyrolysis, and assuring subsequent inflow and production of groundwater from the cavity. Except for the pressure excursions of reverse-burn connections and their associated small contamination levels, Rocky Mountain 1 operations followed these rules and the resulting magnitudes and spatial extents of contamination were low.

Groundwater contamination was a major area of emphasis in LLNL's recent (2005–15) UCG program. Burton et al. (2006) summarize the Hoe Creek investigation and made general recommendations for cleaner practices. Camp and White (2015) describe the phenomena involved with groundwater contamination, contaminant transport scenarios and pathways, and practices to minimize the magnitude and spatial extent of contamination and its impacts. Fig. 4.24 summarizes some of the phenomena, pathways for transport, and opportunities for early detection of potential contaminant transport. Fig. 4.25 shows a semiquantitative estimate of the relative propagation rates of temperature, condensation, and dissolution that would be expected if gas escaped from a UCG cavity along a pathway of fixed diameter.

An understanding of groundwater contamination mechanisms and scenarios includes the following:

- Pyrolysis occurs in UCG. It produces many toxic organics. Unlike many surface gasification processes, a large fraction of these organics is not completely converted to simple gases. They remain in the gas product in the cavity, link, and production well.
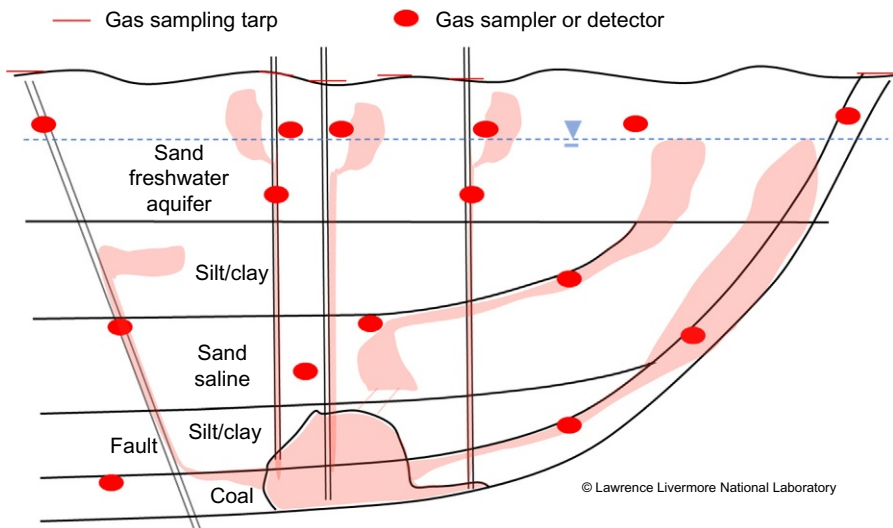
Fig. 4.24 Possible UCG contaminant transport pathways and opportunities for using gas detection or sampling to discover them early. Figure credit: Camp and White (2015).
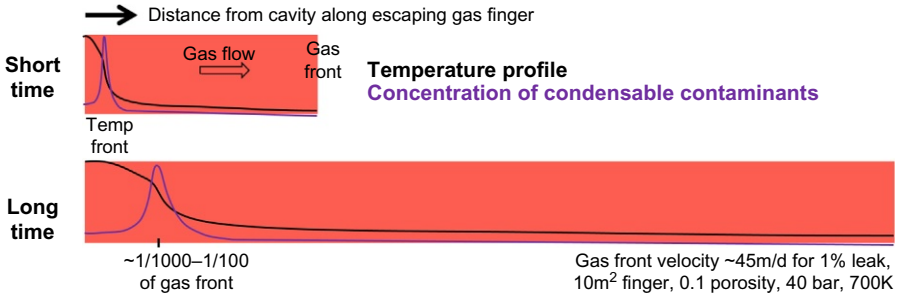
Fig. 4.25 Qualitative profiles of temperature and condensable species concentration after UCG gas has leaked out along a permeable channel of fixed cross section for a short and a long period of time. For typical UCG situations, the thermal front will travel outward only 1/1000th or 1/100th as far as the gas front. The rock heat capacity will cool the gas, and the condensable species will be deposited onto cool rock after flowing past the thermal front. Figure credit: Camp and White (2015).

- Inorganic contaminants can result from secondary processes driven by higher temperatures and/or geochemical changes such as pH change from increased CO_2, NH_3, or SO_x concentrations.
- Gas escape from the process is the primary vector for transporting these contaminants away from the process, although the lower-volatility and higher-solubility contaminants will condense into their liquid or solid phase or dissolve into less-mobile groundwater along the way and go out much more slowly than the uncondensable and insoluble components of the gas.
- Transport of low-solubility contaminants by groundwater flow is slow and retarded by adsorption. Char, coal, and carbonaceous species in sedimentary strata tend to adsorb organic contaminants, which can greatly retard their transport by both gas and aqueous flow.
- Gas will tend to escape if the cavity gas pressure exceeds the pressure of its water-saturated surroundings. In a permeable dipping coal seam with impermeable roof rock, gas may escape updip unless inward permeation gradients overwhelm the dip. The magnitude of gas escape will be greater if the seam and surroundings have high permeabilities or high-permeability paths.
- UCG cavities can grow upward a long distance into the overburden, with fractures extending above those, and these will bring contaminant-laden UCG process gas to these higher elevations where the surrounding hydrostatic water pressure may be lower than the cavity pressure.
- Drawdown (cone of depression) from water flowing from the surroundings into the process cavity can reduce the water pressure of the surroundings, and, if the cavity pressure is not correspondingly reduced with time, the cavity pressure will exceed that of the changed surroundings.
- Gas can escape to shallower surroundings by flowing up uncemented boreholes, the outside of poorly grouted boreholes, natural faults, and permeable pathways such as dipping permeable strata or coarsely filled stream beds. Gas can escape to shallower (and therefore lower-pressure) surroundings by leaking at joints or failure points from wells that are open to the cavity (at its pressure) but closed or restricted at the surface, including the main production wells and instrument wells.

The following activities and choices will reduce the risk of unacceptable groundwater contamination. These are consistent with the Clean Cavern procedures but are broader in scope and stated more generally:

- A site should minimize exposure to sensitive environmental receptors. This means minimizing nearby, downgradient, and updip uses of groundwater and surface water; proximity to potentially usable aquifers; and proximity to residences, businesses, and recreational activities of people and of valued animal habitats.
- A site should be chosen that has barriers to transport of contaminants from the immediate and contaminated UCG process area to overlying or nearby sensitive environmental receptors. UCG should be deep and in horizontal or very low-dip strata. Thick and wide-extending continuous strata of low permeability should exist between the sensitive receptors and the highest possible zone of fracturing or subsidence-induced permeability above the UCG cavity. There should be no faults that could provide a transport path through the low-permeability barrier strata.
- Operations should not create or increase transport pathways, such as with uncemented or poorly cemented boreholes, hydraulic, or pneumatic fracturing that extends up or out of the immediate future cavity or leaky process or instrumentation wells. The design and construction of production wells and their external grouting must be of the highest quality to withstand severe temperature changes and gradients, erosive and corrosive particulate-laden gas flows, and mechanical stresses from ground movement. These wells are the barrier between high-pressure, contaminant-laden product gas and shallower, low-pressure aquifers.
- Operations must assure that the cavity pressure (and therefore the pressure in all gas-connected volumes) is lower than the pore water pressure in the surroundings of those gas-connected volumes that include the highest connected fractures above the cavity. The hydrologic pressure field must be actively monitored (by a combination of measurements and modeling) to assure that potential gradients are always and everywhere inward toward the cavity. The operator must be vigilant in accounting for upward growth of the cavity and its gas-connected fractures and drawdown of surrounding aquifer pressures.
- Methods should be deployed to detect gas escape from the cavity. Early detection of gas escape allows process adjustments to be made quickly to and reduce the distance and extent that contaminants are transported.
- The quantity of contaminants left underground in and near the cavity and product exit pathway should be minimized. It will help to continue the gasification until the downstream link areas, in which tars accumulate early in the process, have been consumed. The Clean Cavern shutdown protocol or an evolved version of it should be followed.
- Groundwater and pore gas in the immediate process area and the surroundings, especially in and near aquifers and sensitive receptors, must be characterized before operations begin, during, and afterward for several years.

4.7.2 Subsidence and changes to the overburden permeability field

Roof collapse and subsidence were analyzed in the main era of UCG research and in LLNL's recent (2005–15) UCG program. As with removing coal from the underground by mining, UCG can cause overburden to collapse, rubblize, fracture, and strain. One unwanted outcome of this is surface subsidence. But long before there

is much surface subsidence, collapse, movement, fractures, and strains underground are likely to change the permeability field. In large-scale UCG operations, it is more likely that higher permeabilities would be created far above the seam.

This can make groundwater contamination worse. To isolate the UCG operation environmentally from shallower sensitive contaminant receptors, the zone of enhanced permeability must stay below the impermeable barriers that are counted on to protect shallower aquifers.

Modern geotechnical modeling and engineering must be used to help assure that UCG operations don't affect the subsurface above them in unacceptable ways. Model calibration/validation must be consistent with the tall cavities observed in US UCG field tests. A large degree of conservatism is needed for UCG because of thermally accelerated drying/fracturing/spalling of the roof rock and lesser control over and knowledge of cavity geometry.

4.7.3   UCG and greenhouse gases

LLNL's recent UCG program in the 2000s was motivated in large part by a perceived opportunity to reduce emissions of carbon dioxide (Section 4.3.3). Effort was devoted effort to understanding UCG's advantages and disadvantages with respect to greenhouse gas emissions.

Gasification is technically amenable to efficient separation and capture of carbon dioxide that could then be sequestered. This has been advanced for surface gasifiers in recent developments and demonstrations. UCG could work similarly, although the methane in UCG's product gas cannot easily be water-gas shifted, limiting the extent of carbon capture that can be achieved. The utility of carbon capture and sequestration (CCS) at a scale that is large enough to matter assumes that sequestration technology matures and becomes accepted. CCS consumes significant additional energy and adds significant cost. If carbon "utilization" is substituted for sequestration, the specifics must be analyzed to assure that the carbon is kept out of the atmosphere for the long term.

In the early 2000s, the notion was advanced of using UCG cavities for sequestering captured carbon dioxide from UCG-produced gas. Considered analysis shows this to be a poor idea for several reasons, and it should be dropped for the foreseeable future.

Methane comprises a significant fraction of UCG product gas. Methane is a much more potent greenhouse gas than carbon dioxide. Potential leaks of methane-containing product gas from UCG operations need to be included in analyses.

As with other coal energy technologies, UCG will produce more greenhouse gases per unit of useful energy than many other energy sources. If UCG tilts the energy mix toward more coal and less other sources, then this creates more greenhouse gases that will enter the atmosphere or need to be captured and sequestered.

But if the same amount of coal will be used anyway because of local circumstances, UCG, like surface gasification, may have carbon capture advantages over combustion. Coupled with CCS, it could approach the carbon footprint of natural gas (without CCS). Doing so economically at large scale would require incentives for reducing

greenhouse gas emissions and development, maturation, and acceptance of both UCG and CCS technologies.

4.8 Process technology, characteristics, and performance

4.8.1 Ignition

Several methods of igniting the coal downhole were used successfully. Sometimes ignition went easily on the first try. Other times, it took many tries over many days with many modifications. No test was canceled because the coal could not be ignited, but sometimes, failure to ignite when and where desired required changing the operation plans.

Two general types of methods were used to ignite exposed coal in a borehole, generally after pumping out free water. In the first type, which only works at the bottom of vertical wells, crushed coal and/or charcoal was placed (dropped) to cover an electric igniter, and air (sometimes enriched with oxygen and/or methane or propane, staying outside of explosion limits) is fed to the location. In the second type, a fluid that autoignites in air (e.g., tetraethyl borane or silane in argon) is fed to the ignition point where it contacts injected air (sometimes with oxygen and/or methane/propane enrichment) to get the initial flame, followed by flow of easy-burning hydrocarbon fuel (ranging from methane to liquid diesel fuel) and more air (or oxygen-enriched air).

Ignition proved challenging as late in the program as the final Rocky Mountain 1 field test, which took several tries and modifications in both modules to succeed. This is detailed by Thorsness et al. (1988). They used a silane-argon mixture, air, methane, a special ignitor tool, and special nozzles. Laboratory testing before and after the Rocky Mountain 1 field test found that qualitative differences in ignition behavior and the ease of successful ignition depended on the relative directions of flow of the fluids in the borehole or well and nozzle jets, and the orientation of the borehole/well (vertical or horizontal) depended on the relative directions of flow of the gases in the well and nozzle jets, and the orientation of the borehole or well (vertical or horizontal) and whether the borehole was vertical or horizontal.

4.8.2 Forward gasification requires a link, not coal permeability

Forward-burn gasification requires an open or highly permeable link or pathway from the burn area to the production well. Repeated tries, during several of the Hanna phases, to get a forward burn to proceed out from a well-ignited injection well into either a virgin coal seam or a hydraulically or pneumatically fracked coal seam were never successful.

UCG forward burn does not operate in unlinked or unrubblized coal according to some of the early conceptual and mathematical 1D "permeation" models of UCG. These erroneous conceptual models contributed to the incorrect general assertion that high permeability was desirable for a UCG coal seam. Except for reverse-burn linking,

high coal permeability is generally bad for UCG because of water influx, gas escape, and groundwater contamination.

Sufficient links were shown to include the following and combinations thereof: an open borehole; a char-filled reverse-burn channel; an initial borehole or reverse-burn channel that has become full of char and dried coal rubble and surrounded by fissured dried coal; an open burn cavity volume; a burn cavity volume that is filled with rubble of ash, char, dried coal, and rock pieces; and an explosively fractured bed of rubblized coal.

4.8.3 Reverse-burn links

Most US field tests through 1978 and some in 1979 used reverse burns to link process wells and boreholes. Details of field-test experiences and technical practices are documented in most of the field-test reports. An excellent simple sketch (Fig. 4.26) and description of reverse-burn linking appeared in Bell et al. (1983). "After igniting the coal at the base of well P, air injection is then introduced to well I that causes reverse combustion links (RCLs) to propagate from well P toward well I. These link channels are not open conduits, but are very permeable regions of char, approximately 1 m in diameter, which form along the paths of greatest oxygen supply. More than one RCL may form, and they may propagate at different rates. Eventually, one of the links breaks through to injection well I. In practice, the idealized case does not usually occur. RCLs may follow irregular paths from one well to another. The flow path may rise to the top of the seam."

Even with the drilled borehole links used in most tests from 1979 on, reverse burns were often used to make short connections between wells/boreholes that missed each other by a few meters.

The US field-test experience with reverse-burn linking was mixed. Sometimes, it worked smoothly, and a link could be accomplished in days. Sometimes, it did not go smoothly and required a great deal of fussing and trials, even in the hands of experienced operators. Hanna IV and Rawlins II had the worst experiences. Even with all
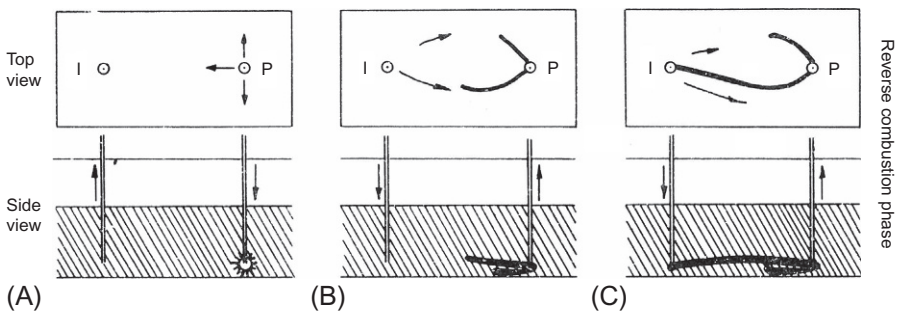
Fig. 4.26 Sketch of ignition and reverse-burn linking, showing two wells completed into the lower zone of a coal seam. I and P are the injection and production wells for the reverse burn (and often but not always for the subsequent forward burn). (A) Ignition—start burn, (B) reverse combustion, and (C) link established. Figure credit: Bell et al. (1983).

the experienced personnel present at Rocky Mountain 1, using reverse burn to make short connections between boreholes "was by far the most taxing phase in terms of the physical plant and personnel. … Startup and subsequent operation would have been much easier had mechanical connection of the wells existed" (Cena et al., 1988a).

Links were preceded by pumping/blowing water out of wells and followed by air acceptance testing between candidate well combinations. When connectivity was inadequate, pneumatic or hydraulic fracturing was tried (sometimes producing unwanted permeability pathways), and even then, closer-spaced wells had to be drilled. The linking process itself always used air injection pressures that exceeded surrounding hydrostatic pressure. Sometimes, product gas was observed to move out a long distance during this operation. Links up to 23 m in length were usually successful, although some required fracturing. Links 30 m and longer were never successful, even with fracturing. Reverse links were sometimes enhanced by alternating forward periods by switching injection and production back and forth.

Reverse burns were successfully drawn from a large active burn cavity through the coal seam to a linking injection well. When the source burn was broad and the injection air source was also broad and parallel to it across the seam, only one or a few narrow links will be made—a reverse burn will not advance as a broad front.

Reverse-burn linking accomplished, with great difficulty, in a swelling agglomerating bituminous coal seam in the Pricetown field test, but the link(s) permeability was very low and repeatedly plugged up.

4.8.4   Directionally-drilled links

LLL's Hoe Creek III field test in 1979 was the first of the US program to replace reverse-burn links with a directionally drilled horizontal borehole. (To improve the conductivity of the small-diameter borehole that was drilled in this first experiment, it was expanded by a reverse burn along its length, a practice not done in future tests using larger-diameter boreholes.) Gulf's Rawlins 1 test 2 months later also used a directionally drilled in-seam borehole for its link. With the exception of the failed Alcoa test, all US field tests from 1980 on used directionally drilled boreholes for links.

Drilled links facilitate keeping both the injection points and product gas pathway low in the seam. They provide tight spatial control that will be beneficial for scale-up to multiple modules. Directionally drilled boreholes allow for a variety of completion designs such as the location and details of casing, liners, tubes, devices, and instruments. This makes scalable and efficient process schemes such as CRIP and ELW possible, as making possible other schemes not yet invented.

4.8.5   Characteristics of the main forward-burn phase of gasification

Given the preparation of a link between the main injection well and a production well, either by reverse burn or a drilled borehole (or even by explosive rubblizing), forward-burn operations could always be established easily and reliably. In field tests, the forward-burn period was almost always easier than ignition and linking.

Forward-burn operations repeatedly proved to be very robust. It operated well over a wide turndown range in injection rate. Operations could be stopped for days or weeks and resume quite easily. UCG operations in forward-burn mode responded quickly, stably, smoothly, and predictably to changes in injection gas pressure and composition, such as switching back and forth between air and oxygen-steam mixtures. They even tolerated major events such as collapsing volumes of roof coal and/or rock with only modest and conceptually reasonable changes in behavior.

Given suitable links and a mature forward burn associated with one injection point, a new forward burn can be initiated and grown at a different injection point by stopping injection to the first location and starting it at the second location. Sometimes, this happened unintentionally, as when an injection well failed and the injection point moved from the bottom of the seam to a break near the top of the seam. Moving the injection point intentionally, either by plan or improvisation, was common and successful.

This ability to switch locations of injection point was found to be useful in at least two ways. If there is a mechanical problem with one injection well, another can be substituted to "rescue" an operation. Moving to a new injection point at the bottom of the seam in new coal will improve gasification efficiency and performance.

The natural tendency of a forward burn is to ride up and consume coal near the top of the seam or in the upper half of the seam. Not only is this bad for resource utilization, but also it hurts thermal efficiency and gas quality (see Section 4.8.7). The best way to keep the burn from overriding into the top of the seam is to assure that the injection point is at the bottom of the seam and that it is moved to a new location at the bottom in new coal when heat losses to the roof significantly erode efficiency, such as when it is predominantly consuming coal near the roof. In field tests where the performance was declining due to override or excessive heat loss to the roof, moving the injection point to a new place at the bottom of the seam in ungasified coal usually restored performance. This understanding motivated the invention of CRIP.

4.8.6   A conceptual model for the UCG process and cavity growth

Most reports on field tests contain sketches of the best estimate of the final cavity geometry (c.f. Singer et al., 2012). These are based on a combination of postburn drill backs, in situ temperature measurements, geophysical monitoring, and material balances.

The field-test observations and model calculations evolved into a conceptual model and scientific understanding of the UCG process. This is described well in the phenomenology sections of Stephens et al. (1982), Thorsness and Britten (1989b), and Britten and Thorsness (1989) and formed the basis for the CAVSIM model.

To a first approximation, cavities are symmetrical with respect to a vertical axis through the injection point. They are rubble-filled and have nearly vertical walls. More precisely, they grow about twice as fast in the direction of the product gas exit as in the backward direction and they are perhaps more elliptical than cylindrical in a vertical cross section through the middle of the cavity taken perpendicular to the injection-production line.

In cross section, perpendicular to the flow path, cavities are usually taller than wide, both in early stages when the cavity is still within the coal and late stages when the cavity extends into the overburden. Every US field test of significant duration and coal consumption showed time and again that the cavity extended far up into the overburden, often by many or tens of meters.

The "cavity" was consistently found to be filled with rubble, often with a small void volume near the top. This rubble consists of slag, ash, char, dried coal, and thermally altered overburden rubble. This was seen clearly and conclusively during postburn excavations at Centralia following the very short-duration Large Block tests and the full-duration Partial Seam CRIP test.

Cavity growth can be complicated but seems to always involve thermal spalling and sometimes involve structural collapse events and intermediate-scale fracturing and block falling. Spalling grows the cavity in the coal seam and in the overburden, both sideward and upward. Nonswelling coals and sedimentary rocks overlying all the US tests tended to spall upon heating and drying. Large collapse events were occasionally observed and inferred.

The rubble bed covers the injection point, dispersing injected oxidant and evolving gases through the bed and out to the side walls and small voids near the ceiling. Gas reactions with the coal, char, and pyrolysis gases in this bed define much of the activity in the system.

The spalling of coal and char pieces into a rubble bed is likely very good for UCG efficiency as it increases surface area. But spalling of roof rock is bad because it increases the rate at which roof rock becomes heated, causing heat loss and water influx. An ideal site would have coal that spalls easily and roof rock that does not.

Exit channels that began as horizontal boreholes were discovered to evolve into a steep-sided upward "V" shape containing thermally affected dried coal and char rubble filling the V. The permeability to gas flow was greater near the top of the V channel. This presumably applies also to exit channels that began as reverse-burn channels of permeable char. When coal above was dried and pyrolyzed, it apparently shrunk in volume, fractured, spalled, and fell, opening void and fractures above and outward. Downward growth of this exit channel was limited by thermal conduction.

4.8.7   Energy balance determines process efficiency and gas quality

For a given coal, the process efficiency and the product gas quality are largely determined by an energy balance. (c.f. Thorsness and Creighton, 1983). Four losses are usually considered: sensible heat of overburden (and interburden) rock that remains underground, sensible heat of the gas product, vaporization and sensible heat of water that flows into the process underground, and vaporization and sensible heat of the pore water that had been in overburden (and interburden) rock that was heated. Only the first of these is a true loss (stays underground), but it is impractical to recover useful energy from the other product streams—one wants the energy to be in the chemical heating value of the product gas.

In virtually every field test, for a given injection point, thermal efficiency and gas quality started high and tapered down as the burn progress. The decrease was associated with the gasification cavity reaching the roof. The ratio of coal consumption to the amount of roof rock that is heated and dried (and falls into the cavity by spalling) decreases. If the roof rock stayed in place, the slow conduction of heat through the rock would not progress far, and only a small volume of rock would become heated. But spalling keeps exposing new surface and enhances the overall rate at which rock is dried and heated (Camp et al., 1980).

The best way to minimize heat loss to overburden rock and its pore water is to choose a site whose overburden does not readily spall, is resistant to structural collapse, and has a low water content. But in all the US tests, the cavity extended far up into the overburden and that volume of rock ended up as hot rubble in the cavity. Stephens et al. (1985) put it this way, "Site selection plays a major role in gasification quality. Sites with relatively dry, strong overburden, and at least moderately thick coal produce favorable results. Sites with thin coal or containing wet, weak overburden produce less favorable results."

For a given geology, these overburden losses can be minimized by moving the injection point into an adjacent volume of new coal (e.g., by doing a CRIP maneuver) as soon as the roof rock is exposed in the currently burning cavity. Many field tests, including Rocky Mountain 1's CRIP module, demonstrated that moving the injection point to a new location "rejuvenates" the process efficiency and product quality.

Gas (and produced water) sensible heat can be minimized by having the hot gas leaving the cavity flow through a long channel in coal that will be preheated now and consumed later. Long links made by in-seam boreholes will help accomplish this.

Experience has shown that for a given geology, reducing the cavity pressure far below the water pressure in the surroundings so that the gradients in potential are more strongly inward tends to increase water influx. However, increasing the cavity pressure so that the gradients in potential are outward does not reduce water influx by much and results in gas losses that are detrimental to both process efficiency and groundwater contamination. The best practice is to operate the cavity pressure just low enough to assure that the hydraulic gradients are everywhere inward. Therefore, for a given geology (and its permeability field) and a requirement of no gas loss, the only way to minimize permeation influx is to minimize the vertical extent of the gas-connected cavity. This could be done by moving the injection point to new coal before the overburden roof spalls or collapses much (e.g., by doing a CRIP maneuver).

The best way to minimize water influx by permeation is to choose a site with low-permeability underburden, coal, and overburden, with that priority order set by the relative magnitude of the inward gradient in potential.

These energy-balance considerations provided much of the motivation for LLNL to use in-seam drilling to put a long borehole link at the bottom of the seam (Hoe Creek III) and for inventing CRIP to assure bottom-seam injection and conveniently move the injection point into new coal (Centralia).

4.8.8 Prediction of gas composition

Product gas compositions from different UCG field tests vary quite widely, even from tests at the same site and often between different periods of the same test. Much effort was put into finding simple ways to predict the composition of the product gas from a UCG operation. Simple equilibrium and kinetic models were ineffective. Correlations were repeatedly looked for with little success. There is no simple "UCG assay" that can be done on a coal to predict a UCG product gas composition. This is because the composition of the product gas exiting from a UCG operation results from its entire detailed spatial and temporal history of chemical species and energy concentrations and fluxes. The best simple predictive methods, described in Section 4.6.3, involve several physically based but adjustable/fitted parameters. Unless enough process information is available to justify using such a model, the average gas compositions of Table 4.2 are reasonable first approximations.

4.8.9 CRIP—the Controlled Retracting Injection Point system

Arguably, the most outstanding, useful, and enduring product of the entire US UCG effort was the invention of the Controlled Retracting Injection Point (CRIP) system. CRIP provides positive control of the gasification process—a means to extend the process spatially into successive volumes of new coal while keeping the injection point low in the coal seam, roof involvement low, and efficiency high. The CRIP system consists of compatible well design and completions, CRIP-specific down-hole hardware, and operating technique.

The first publication describing CRIP was in the 7th UCG Symposium (Hill and Shannon, 1981). Its abstract reads as follows. "The underground coal gasification process, in practice, is subject to various problems that make it difficult to maintain and control an efficient long-term operation. One of the major problems is the need to move the injection point to new areas of unburned coal as the burn progresses. To achieve better control of the gasification process, we recommend the controlled retracting injection point or CRIP system. With this technique, the operator can choose the optimum time and distance to move the injection point and consequently the burn zone, to get the best possible performance from the gasification process." The essence of CRIP was illustrated in Hill and Shannon (1981), shown here in Fig. 4.27.

CRIP was conceived and developed by the LLL team after the Hanna and Hoe Creek field tests showed the importance of keeping the injection point low in the seam, the viability of a directionally drilled borehole to be a link, and the benefit of being able to inject at different points along such a borehole into new coal to create successive "young" cavities.

CRIP requires the construction of a long cased or lined injection well in a coal seam, and it requires a specialized downhole tool fed by a gas line that can be moved inwards and outwards. CRIP provides a way to ignite the coal at the end of the lined portion, inject at that point, start and continue a burn cavity at that point, and then later melt a hole in the liner at an upstream location, ignite the coal there, inject there, burn a
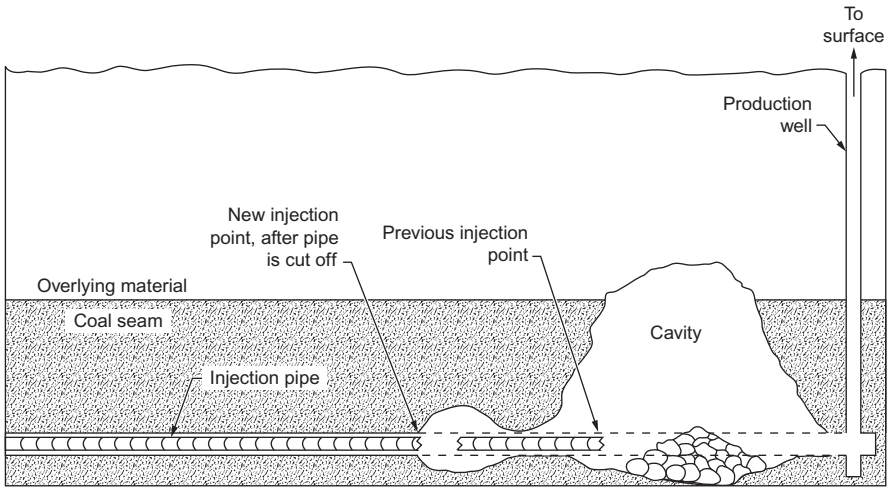
Fig. 4.27 Hill and Shannon's original sketch of CRIP. Their caption read: *"Basic design of the controlled retracting injection point (CRIP) system. As the cavity burns toward the left, the injection point is moved to the left also, step by step, by cutting off or perforating the injection pipe, which can be done remotely from the surface. Thus the injectant gas is always being fed to a zone of the coal seam where unburned coal remains to be gasified."*
Figure credit: Hill and Shannon (1981).

cavity there, and continue repeating this process. The injection well would be drilled along the bottom of the seam to always assure the injection point would be low in the seam.

Fig. 4.27 shows exactly how CRIP was first demonstrated in the field in LLL's Centralia Large Block test number LBK-1. Comparing this figure to a cross section of LLL's Hoe Creek III test shows that Hoe Creek III was a stepping stone in the evolution of CRIP. The borehole and production well are the same, but Hoe Creek III used two vertical wells to reach the two injection points.

While Fig. 4.27 shows CRIP in what has now become known as the "linear CRIP" configuration, the CRIP system has never been wed to this geometry; from the beginning, CRIP was intended to be usable in a variety of configurations. "There are several possible geometries for the gas production well (as shown in Fig. 4.1.), or one can use another horizontal hole in the seam, parallel to the injection hole. A third possibility, with particular application to thick seams, is a horizontal (production) hole at the top of the coal seam, vertically above the horizontal injection hole (well)" (Hill and Shannon, 1981). Original sketches of these, with captions, are shown in Fig. 4.28. Hill and Shannon describe how these can be scaled up to long injection well lengths and arranged parallel to each other with the spacing set by trading off resource recovery against subsidence.

LLL's Partial Seam CRIP field test in Centralia, Washington, provided the first full-size field-test demonstration of CRIP. This was deployed in what is now known as "parallel CRIP" configuration, similar to Fig. 4.28 (top) but with only one
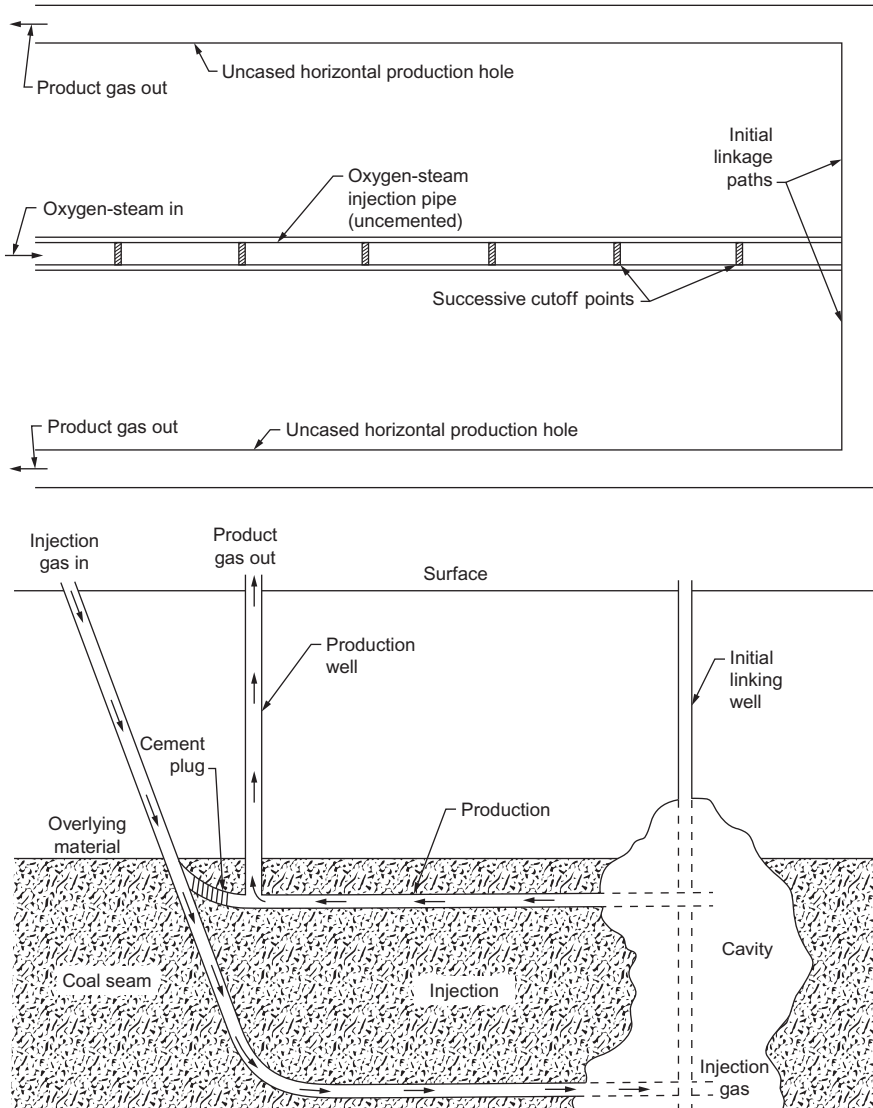
Fig. 4.28 Hill and Shannon's original illustrations of two possible CRIP configurations. Top: what now would be called double parallel CRIP. Their caption read: "*Plan view of stream method adaptation of the CRIP system, with both injection and production holes drilled at the bottom of the coal seam. This version would be advantageous for dipping seams where slag accumulation in the bottom of the cavity might plug a down-dip production well*." Bottom: vertically-stacked parallel CRIP. Their caption read: "*Vertical cross-sectional view of a module of a commercial CRIP system, in which the injection hole is at the bottom of the seam, while the production hole is at the top of the seam*." Figure credit: Hill and Shannon (1981).

production borehole, angled slightly differently. Rocky Mountain 1's CRIP module also used CRIP in the parallel configuration. While not needed in theory, the practice at that time for parallel CRIP used a vertical production well to get the process initiated, and the first cavity begun in the linear configuration.

Thorsness et al. (1988) describe in detail the tool and procedure used in the Rocky Mountain 1 field test to perform a CRIP maneuver. This uses a silane torch to melt the steel liner and ignite the coal at a new location. When not in use, it is retracted a distance back upstream in the injection well, out of harm's way. When a CRIP maneuver is needed, it is pushed out to the desired position, operated, and retracted again.

4.8.10   Steeply dipping beds and thick seams are efficient but risk gas loss

UCG in steeply dipping beds will tend to be thermally more efficient than in flat beds. Burns and cavity growth tend to go upward, largely because overlying spalled material falls from its location down into the burned cavity. In a steeply dipping bed, such a cavity will have a higher ratio of coal consumption to thermal loss to roof rock. The high heating values obtained in the steeply dipping Rawlins I-air and Rawlins II tests and the very thick-seam Rocky Hill test demonstrate this.

Steeply dipping beds make it more challenging, if not impossible to avoid updip gas loss and its associated transport of contaminants toward the surface where pollutant receptors are more sensitive. Product gas escaped up the seam to the surface at Rawlins, as evidenced by carbon monoxide readings. Even the $7°$ dip at Rocky Hill enabled a few days of high-pressure operation to push gas many hundreds of meters up dip. Vertically tall cavities, operated at pressures below the water pressure of the surroundings at the top, will have a large inward gradient at the bottom, resulting in high inward permeation of water there.

UCG in thick seams will tend to be thermally more efficient than in medium or thin seams because of the ratio of roof rock involvement to coal consumed. Water permeation influx at the bottom or gas escape at the top may be a problem because of the large vertical extent of the cavity. Gasification of thick seams may result in a greater vertical extent of roof collapse (goafing). This can open up gas connectivity far up into the fractures of a sagging overburden, making it more likely for product gas to escape up into shallow strata. Even though it consumed a modest 3300 Mg of coal, the thick-seam Rocky Hill field test produced a high vertical extent of roof collapse and fracturing.

4.8.11   Monitoring of UCG operations and cavity evolution

The philosophy of the government-funded UCG program recognized that for UCG to be effectively developed into an efficient large-scale industrial process, it had to be understood. Understanding requires detailed knowledge of conventional chemical process parameters such as flow rate, composition, pressure, and temperature. Understanding also requires knowledge of what the process is like underground—how the

cavity grows and what is it like, where the fluids flow, how the temperature field evolves, etc. A great deal of effort was spent on this, and it was valuable in understanding the process. These monitoring and postburn characterization efforts helped to evolve a better conceptual model of how UCG proceeds and consequentially guided mathematical model development. Monitoring details are in the technical reports of the time, found mainly in the Annual UCG Symposia proceedings.

4.8.12   Technical maturity and scale-up

The US program demonstrated UCG's feasibility many times at the single- or few-cavity scale-up to about 10,000 Mg. But even after dozens of tests at this scale, UCG design, construction, and operation had not become routine. As late as Rocky Mountain 1, experienced operators were not able to have the project, and operations go smoothly. UCG was still young in its maturation.

Many sketches were produced that envisioned how UCG techniques or systems might be scaled up by adding multiple modules, but none of these were tested. Nor were the sketches subjected to a detailed geotechnical design analysis that would look quantitatively at geomechanical aspects such as roof collapse, goafing, room-and-pillar resource recovery, and subsidence (not only at the surface but also of the strata that provide environmental isolation) or hydrologic aspects such as groundwater depletion, multimodule interactions, and gas escape.

Technologies and approaches that would facilitate scale-up were conceived and tested. Directionally drilled boreholes and wells for linking and gas injection/production were tried successfully. CRIP was invented and has excellent potential for helping scale-up. Use of successive reverse burns to extend the process laterally by linking many closely spaced vertical wells was demonstrated successfully.

One of the biggest problems needing more development is the design and construction of well completions. There were many failures from heat, structural failure, leaks, poor grouting between the well and the formation, and plugging by slag accumulation. A number of factors in different tests caused the air or oxygen-steam to be injected high in the seam instead of at the bottom as intended. Mundane process engineering technologies, such as particulate erosion of pipes, were also still a challenge and needed maturation.

At the end of the US field-test program, UCG remained low on the curve of technology development toward routine operations at large scale.

4.9   Conclusions

4.9.1   Technical accomplishments

Successful field tests at scales up to 10,000 Mg of consumed coal were conducted on several different subbituminous and nonswelling bituminous coals. Successful tests were done with both air and with oxygen-steam mixtures as the injectant, producing gas with heating values of 4.3–7.4 and 8.4–12.5 MJ/Nm^3, respectively. The tests in lignite appeared to struggle operationally and/or produce low-quality gas, but other

than its heating value, there is nothing to suggest that UCG could not work well with lignite. One test in an agglomerating swelling bituminous coal went poorly, with struggles to establish and maintain a sufficiently permeable link; expectations are low for such coals.

Successful tests were run in flat, slightly dipping, and steeply dipping seams; in seams with thicknesses between 6 and 30 m; and at depths between 40 and 190 m. Steeply dipping and very thick seams show good efficiency and gas quality, but they are more prone to gas escape and contaminant transport. One cause of poor gas quality from the lignite field test was its thin (2 m) seam. Deeper seams provide better environmental isolation from valuable and sensitive near-surface receptors, but wells must be engineered to contain the higher-pressure gas.

Several methods of ignition were used successfully, although ignition was sometimes challenging. Directional drilling of in-seam boreholes, reverse burns, and even high-explosive fracturing produced adequate initial links to initiate and grow the main forward-burn process. Unfractured, pneumatically fractured, and hydraulically fractured coal seams did not provide sufficient communication to get a successful forward burn going.

Once started, forward gasification was found to be robust and easy to manage. It responds in a stable and predictable manner to changes in operating parameters and the underground environment. It tolerated high turndown ratios and even stopping of injection for days or weeks. As long as a link existed to a production well, a new injection point could readily be ignited and started.

The UCG "cavity" was found to be full of rubble, not void. The rubble consisted of ash (and sometimes slag for hot-burning oxygen-steam-fired tests), char, dry coal, and rock. These enter the cavity largely by small-scale spalling of dry and fractured coal and rock from the sidewalls and ceiling. The cavity is usually taller than wide and grows toward the production well about twice as fast as backward, with sideward being in between. Downstream links, even simple boreholes, evolve into an upward "V-shape" cross section of rubblized char and dried coal.

An improved conceptual model of UCG evolved, along with scientific understanding of its important phenomena. Mathematical models of UCG and its phenomena were developed that allow accurate calculation of cavity growth, temperature and composition fields, and product gas composition. Simpler models were also developed to assist with engineering estimates.

For a given coal, the process efficiency and product gas quality are largely determined by an energy balance, with two of the main losses going to the drying and heating of roof rock (that ends as hot rubble), and the vaporization of water flowing into the process by permeation. Strong, spalling-resistant, low-water-content roof rock, and low coal and rock permeabilities are desirable.

It was demonstrated repeatedly that the highest quality gas is produced when the injection point is low in the seam, the burn is low in the seam, and the injection point is surrounded by coal and char and their rubble, and there is little involvement of roof rock.

The CRIP system was invented to assure that the injection point is always low in the seam and can be easily moved into a new volume of coal. It was demonstrated successfully, in both linear and parallel configurations, in two of the last three field tests, showing great promise for efficiently and cost-effectively scaling up the process.

While most UCG tests ended up being successful, they did not always go smoothly as planned. Hardware issues and operational challenges, even as late as Rocky Mountain 1, were a frequent reminder that UCG remained low on the technological development curve toward mature industrial practice. A high degree of watchfulness and creative ingenuity were needed for most field tests.

Some field tests resulted in unacceptable groundwater contamination, and some of these proved very difficult and expensive to remediate. It became apparent that the hazard of groundwater contamination from UCG operations was real and serious. After groundwater contamination became a priority, research led to a better understanding of this problem and approaches to minimize it. Rocky Mountain 1's "Clean Cavern" approach resulted in only minor and local contamination that was reduced to de minimis levels after a period of pumping. It remains to be seen if subsequent UCG operations, especially ones at larger scale, can be operated with acceptably low environmental impacts. It will take great care and commitment to reduce this risk to an acceptable level.

4.9.2   Programmatic aspects

The advances during the 1970s and 1980s resulted from intense activity by a critical mass of participants that produced a fast pace of development and learning. Some of the keys to its technical success were the continuity of institutions working on it, government funding, sharing of results in public conferences and reports, and determination to understand UCG and continuously make innovative improvements.

While the many field tests formed the centerpiece of the program, they were not isolated activities. There was iteration between field-test observations, scientific understanding of phenomena, modeling, and lab experiments, with each informing and improving the other. Field tests were first and foremost experimental trials and innovation test beds; they were highly instrumented and monitored, and drill backs were common. Learning, understanding, and technical innovation were emphasized.

Program participation was well rounded. Government research institutions led much of the field test and modeling work. Large energy companies and small UCG-niche companies also had programs that typically included field tests, sometimes with government support and sometimes not. University researchers were involved with laboratory experiments and model development.

One of the outstanding aspects of the US program of the 1970s and 1980s was the extent to which results were communicated and documented. The Annual UCG Symposia were especially effective at fostering communication among researchers, and their written proceedings left a rich legacy.

4.9.3   Closing

Beginning with very little domestic knowledge or experience in UCG, the United States caught up and made its own important contributions. The technical feasibility of UCG was demonstrated convincingly in many configurations in several coal seams. UCG field tests were designed, constructed, started, operated, and shut down safely with no significant accidents. Researchers from multiple organizations working at different sites developed a breadth and depth of competence and understanding of UCG and used this expertise to experiment and innovate. Approaches and technologies were developed that allow UCG to be done better and more easily than ever before. The reader is encouraged to immerse themselves in the references below, as this summary can only scratch the surface in describing all that has been done.

Auspices and disclaimer statements

This work was performed under the auspices of the U.S. Department of Energy by Lawrence Livermore National Laboratory under Contract DE-AC52-07NA27344.

This document was prepared as an account of work sponsored by an agency of the United States government. Neither the United States government nor Lawrence Livermore National Security, LLC, nor any of their employees makes any warranty, expressed or implied, or assumes any legal liability or responsibility for the accuracy, completeness, or usefulness of any information, apparatus, product, or process disclosed, or represents that its use would not infringe privately owned rights. Reference herein to any specific commercial product, process, or service by trade name, trademark, manufacturer, or otherwise does not necessarily constitute or imply its endorsement, recommendation, or favoring by the United States government or Lawrence Livermore National Security, LLC. The views and opinions of authors expressed herein do not necessarily state or reflect those of the United States government or Lawrence Livermore National Security, LLC, and shall not be used for advertising or product endorsement purposes.

Reference Sources

Most UCG literature is in the form of topical reports and papers in conference proceedings. The following suggestions may make it easier to find and acquire references.

Reports by government organizations, reports on government-funded work, and conference proceedings organized by government organizations that have been approved for public release may be obtained from the US Department of Commerce's National Technical Information Service (NTIS, https://ntrl.ntis.gov/NTRL/) and/or (for documents funded or authored by DOE or its institutions, especially more recent documents) DOE's Office of Scientific and Technical Information (OSTI, https://

www.osti.gov/scitech/). These are the first places to look, as they should have whatever LLNL and NETL have.

If not available from NTIS or OSTI, LLNL's library (https://library-ext.llnl.gov/) may have a copy of LLL/LLNL reports that have been approved for public release. NETL's library (https://www.netl.doe.gov/library) may have a copy of reports by MERC/METC or METC-managed contracts and proceedings of conferences they organized, including some of the annual symposia.

Acknowledgments

I thank professors Bill Krantz and Bob Gunn, my MS thesis advisor at the University of Colorado and coadvisor at the University of Wyoming, for introducing me to the fascinating technology of UCG. Lawrence Livermore Lab's UCG team of the 1970s and 1980s deserves special recognition, including Chuck Thorsness, my first UCG summer-job mentor, Doug Stevens, who hired me into LLNL, Bob Cena, Dick Hill, Jerry Britten, and George Metzger, the team's instrumentation hardware guy. More recently, Julio Friedmann championed UCG, grew LLNL's 2005–15 program, and gave me the chance to join it. I thank the many people who contributed to this and especially wish to recognize Jeff Wagoner, John Nitao, Josh White, Ravi Upadhye, Xianjin Yang, Steve Hunter, and visiting professor Evgeny Shafirovich. Finally, I thank Burl Davis, technical director of the Rawlins and Rocky Mountain 1 tests, for sharing his UCG knowledge and stories with me and the community.

References

Bartke, T.C., 1985. Underground coal gasification for steeply dipping coal beds. Research Report, DOE/METC-85/2006 (DE85008558).

Bartke, T.C., Gunn, R.D., 1983. The Hanna, wyoming underground coal gasification field test series. In: Krantz and Gunn (1983a), pp. 4–14.

Bartke, T.C., Fischer, D.D., King, S.B., Boyd, R.M., Humphrey, A.E., 1985. METC Report Series: Hanna, Wyoming Underground Coal Gasification Data Base, vol. 1–7. DOE/METC 85/2015, DE85013695- DE85013701.

Beaver, F.W., Groenewold, G.H., Schmit, C.R., Daly, D.J., Evans, J.M., Boysen, J.R., 1988. The role of hydrogeology in the Rocky Mountain 1 underground coal gasification test, Carbon County, Wyoming. In: Proc. 14th An. UCG Symp., pp. 162–174.

Bell, G.J., Brandenburg, C.F., Bailey, D.W., 1983. ARCO's research and development efforts in underground coal gasification. In: Krantz and Gunn (1983a), pp. 44–56.

Bloomstran, M.A., Galyon, G., Davis, B.E., 1988. Rocky Mountain I UCG operations. In: Proc. 14th An. UCG Symp. (1988), pp. 182–191.

Boysen, J.E., Sullivan, S., Covell, J.R., 1988. Venting, flushing, and cooling of the RM1 UCG cavities. In: Proc. 14th An. UCG Symp., pp. 284–292.

Boysen, J.E., Covell, J.R., Sullivan, S., 1990. Results from venting, flushing, and cooling of the Rocky Mountain 1 UCG cavities. Topical report GRI-90/0156 and WRI-90-R026.

Britten, J.A., Thorsness, C.B., 1988. The Rocky Mountain 1 CRIP experiment: comparison of model predictions with field data. LLNL-UCRL-98642, or In: Proc. 14th An. UCG Symp., pp. 138–145.

Britten, J.A., Thorsness, C.B., 1989. A model for cavity growth and resource recovery during underground coal gasification. In Situ 13 (1&2), 1–53.

Burton, E., Friedmann, J., Upadhye, R., 2006. Best practices in underground coal gasification. LLNL-TR-225331.

Burton, G., Camp, D., Friedmann, J., Goldstein, N., Nitao, J., Reid, C., Wagoner, J., White, J., 2012. How wide should our UCG cavity be?—Relationships, dependencies, and trade-offs. LLNL-PRES-553131, and In: Proc. 7th UCGA Conf. & Workshop on UCG, May 2-3, 2012, London.

Camp, D.W., 2017. A review of underground coal gasification research and development in the United States. LLNL-TR-733952.

Camp, D.W., White, J.A., 2015. Underground coal gasification: an overview of groundwater contamination hazards and mitigation strategies. LLNL-TR-668633; or online at: http://www.osmre.gov/programs/TDT/appliedScience/2012LLNL-JWhiteUndergroundCoal GasificationFR.pdf.

Camp, D.W., Krantz, W.B., Gunn, R.D., 1980. A water influx model for UCG with spalling-enhanced drying. In: Proc. 15th Intersociety Energy Conversion Engr. Conf. Seattle, August 18-22, Amer. Inst. Aero. & Astronautics, paper 809256, pp. 1304–1310.

Camp, D.W., Nitao, J.J., White, J.A., Burton, G.C., Buscheck, T.A., Reid, C.M., Ezzedine, S.M., Chen, M., Friedmann, S.J., [2013] 2017. A 3-D integrated multi-physics UCG simulator applied to UCG field tests. LLNL-TR-738118.

Capp, J.P., Lowe, R.W., Simon, D.W., 1963. Underground gasification of coal, 1945-1960; a bibliography. BuMines Info. Circ. 8193.

Cena, R.J., Thorsness, C.B., 1981. Lawrence Livermore National Laboratory underground coal gasification data base. LLNL-UCID-19161.

Cena, R.J., Hill, R.W., Stephens, D.R., Thorsness, C.B., 1984. The Centralia Partial Seam CRIP underground coal gasification experiment. AIChE National Meeting Nov. LLNL UCRL-91252 and LLNL UCRL-91786.

Cena, R.J., Britten, J.A., Thorsness, C.B., 1988a. Resource recovery and cavity growth during the Rocky Mountain 1 field test. LLNL-UCRL-98643. In: Proc. 14th An. UCG Symp., pp. 200–212.

Cena, R.J., Thorsness, C.B., Britten, J.A., 1988b. Assessment of the CRIP process for underground coal gasification: the Rocky Mountain I test. AIChE Summer Meeting, Denver, Aug. LLNL UCRL-98929.

Couch, G.R., 2009. Underground coal gasification. IEA Clean Coal Centre report CCC-151.

Covell, J.R., Dennis, D.S., Barone, S.P., 1988. Preliminary results of the environmental program and permitting at the Rocky Mountain 1 underground coal gasification project. In: Proc. 14th An. UCG Symp., pp. 152–161.

Davis, B., 2011. Personal Communication. .

Dennis, D.S., 2006. Rocky Mountain 1 UCG test project Hanna, Wyoming—final technical report for the period 1986 to 2006. Washington Group International, for DOE-NETL, Contract DE-FC21-86LC11063.

Dockter, L., 1986. Underground coal gasification in the United States—an overview. In: Proc. 12th An. UCG Symp., pp. 2–13.

Dobbs II, R.L., Krantz, W.B., 1988. A transient model of reverse combustion channel propagation. In: Proc. 14th An. UCG Symp. pp. 102–106.

Edgar, T.F., 1983. Research and development on underground gasification of Texas Lignite. In: Krantz and Gunn (1983a), pp. 66–76.

Friedmann, S.J., 2005. Underground coal gasification in the USA and abroad. congressional hearing on climate change, US Senate Foreign Relations Committee, November 14.

GasTech, Inc., 2007. Viability of underground coal gasification in the "deep coals" of the powder river basin, wyoming. Prepared for the Wyoming Business Council Business and Industry Division, State Energy Office.

Hill, R.W., Thorsness, C.B., Cena, R.J., Stephens, D.R., 1984. Results of the centralia underground coal gasification field test. LLNL UCRL-90680, and in: Proc. 10th An. UCG Symp. (1984).

Hill, R.W., Shannon, M.J., 1981. The Controlled Retracting Injection Point (CRIP) system: a modified stream method for in-situ coal gasification. LLNL UCRL-85852, and In: Proc. 7th An. UCG Symp., pp. 730–737.

Hill, R.W., Thorsness, C.B., 1983. The large block experiments in underground coal gasification. In: Krantz and Gunn (1983a), pp. 57–65.

Humenick, M.J., Mattox, C.F., 1978. Groundwater pollutants from underground coal gasification. Water Res. 12, 463–469.

Humenick, M.J., Mattox, C.F., 1982. Characterization of condensates produced during UCG. In Situ 6 (1), 1–27.

Krantz, W.B., Gunn, R.D. (Eds.), 1983a. Underground Coal Gasification, The State of the Art. In: AIChE Symposium Series, vol. 79(226). American Institute of Chemical Engineers, New York, NY.

Krantz, W.B., Gunn, R.D., 1983b. Modeling the underground coal gasification process: part I—reverse combustion linking. In: Krantz and Gunn (1983a), pp. 89–97.

Krantz, W.B., Gunn, R.D., 1983c. Modeling the underground coal gasification process: part II—water influx. In: Krantz and Gunn (1983a), pp. 121–128.

Kühnel, R.A., Schmit, C.R., Eylands, K.E., McCarthy, G.J., 1993. Comparison of the pyrometamorphism of clayey rocks during underground coal gasification and firing of structural ceramics. Appl. Clay Sci. 8, 129–146.

Lindblom, S.R., Smith, V.E., 1993. Final report Rocky Mountain 1 underground coal gasification test Hanna Wyoming, groundwater evaluation volume I. GRI-93/0269.1, WRI-93-R020.

McVey, T.F., Camp, D.W., 2012. Internal LLNL Spreadsheet and Memo.

Mellors, R., Yang, X., White, J.A., Ramirez, A., Wagoner, J., Camp, D.W., 2016. Advanced geophysical underground coal gasification monitoring. Mitig. Adapt. Strateg. Glob. Change 21, 487–500.

Nitao, J.J., Camp, D.W., Buscheck, T.A., White, J.A., Burton, G.C., Wagoner, J.L., Chen, M., 2011. Progress on a new integrated 3-D UCG simulator and its initial application. LLNL-CONF-50055. In: Proc. Int. Pittsburgh Coal Conf., Pittsburgh, September.

Oliver, R.L., Lindblom, S.R., Covell, J.R., 1991. Results of phase II postburn drilling, coring and logging: Rocky Mountain 1 underground coal gasification test, Hanna, Wyoming. DOE/MC/11076-3061, or similar WRI-90-R054.

Proceedings of the Second Annual Underground Coal Gasification Symposium. (1976). Morgantown Energy Technology Center, Morgantown, WV, August 10–12, 1976. MERCSP-763 or -76/3.

Proceedings of the Third Annual Underground Coal Conversion Symposium. (1977). U.S. DOE and LLNL, Fallen Leaf Lake, CA, June 6–9, 1977.

Proceedings of the 4th Underground Coal Conversion Symposium. (1978). U.S. DOE and Sandia Laboratories, Steamboat Springs, CO, July 17–20, 1978. SAND 78-0941.

Proceedings of the 5th Annual Underground Coal Conversion Symposium. (1979). U.S. DOE, Alexandria, VA, June 18-21, 1979. CONF. NO: 790630.

Proceedings of the Sixth Underground Coal Conversion Symposium. (1980). LETC and Williams Brothers Engineering Company, Shangri-La/Afton, OK, July 13–17, 1980. DE81-027669, CONF NO. 800716.

Proceedings of the Seventh Annual Underground Coal Conversion Symposium. (1981). U.S. DOE and LLNL, Fallen Leaf Lake, CA, September 8–11, 1981. DE82 004729, CONF-810923.

Proceedings of the Eighth Annual Underground Coal Conversion Symposium. (1982). U.S. DOE and Sandia National Laboratories, Keystone, CO, August 15–19, 1982. SAND82-2355.

Proceedings of the Ninth Annual Underground Coal Gasification Symposium. (1983). U.S. DOE and METC, Bloomingdale, IL, August 7–10, 1983. DOE/METC/84-7, CONF-830827, DE84003052.

Proceedings of the Tenth Annual Underground Coal Gasification Symposium. (1984). U.S. DOE and METC, Williamsburg, VA, August 12–15, 1984. DOE/METC-85/5, DE85001956, CONF-840835.

Proceedings of the Eleventh Annual Underground Coal Gasification Symposium. (1985). U.S. DOE and WRI, Denver, CO, August 11–14, 1985. DOE/METC-85/6028, DE85013720, CONF-8508101.

Proceedings of the Twelfth Annual Underground Coal Gasification Symposium. (1986). U.S. DOE and Forschung und Technologie, Republik of Germany. Europe, August 24–28, 1986. DOE/FE/60922-H1.

Proceedings of the Thirteenth Annual Underground Coal Gasification Symposium. (1987). (details unavailable).

Proceedings of the Fourteenth Annual Underground Coal Gasification Symposium. (1988). U.S. DOE and GRI, Chicago, IL, August 15–18, 1988. DOE/METC-88/6097, CONF-880874, DE88001093.

Proceedings of the International UCG Symposium. (1989). Delft, Netherlands, October 9–10, 1989.

Schrider, L.A., Wasson, J.A., 1981. Eastern in situ coal gasification field trial. J. Energy 5 (4), 244–248.

Shafirovich, E., Varma, A., Mastalerz, M., Drobniak, A., Rupp, J., 2009. The potential for underground coal gasification in Indiana. Final Report to the Indiana Center for Coal Technology Research.

Shafirovich, E., Jones, B., Machado, M., Mena, J., Rodriguez, D., Hunter, S., Camp, D., [2011] 2017. A review of underground coal gasification field tests sponsored by the US Department of Energy. LLNL-TR-738162.

Singer, S.L., Wagoner, J.L., Hunter, S.L., Yang, X., Camp, D.W., [2012] 2017. Final geometry and dimensions of UCG field test cavities. LLNL-TR-738163.

Stephens, D.R., 1981. The Hoe Creek experiments: LLNL's underground coal gasification project in Wyoming. LLNL-UCRL-53211.

Stephens, D.R., Thorsness, C. B., Hill, R.W., Thompson, D.S., 1982. Technical underground coal gasification summation: 1982 status. LLNL-UCRL-87689.

Stephens, D.R., Hill, R.W., Borg, I.Y., 1985. Underground coal gasification review. In: Proc. 18th An. Oil Shale Symp. and Western Synfuels Symp., Grand Junction, CO, April. LLNL-UCRL-92068.

Thorsness, C.B., Britten, J.A., 1989a. Analysis of Material and Energy Balances for the RM1 UCG Field Test. In: Proc. Int. UCG Symp, Delft, Netherlands, October 9–10, 1989. LLNL-UCRL-101619.

Thorsness, C.B., Britten, J.A., 1989b. Lawrence Livermore National Laboratory underground coal gasification project: final report. LLNL UCID-21853.

Thorsness, C.B., Creighton, J.R., 1983. Review of underground coal gasification field experiments at Hoe Creek. LLNL-UCRL-87662Rev.1, and In: Krantz and Gunn (1983a), pp. 15–43.

Thorsness, C.B., Hill, R.W., Britten, J.A., 1988. Execution and performance of the CRIP process during the Rocky Mountain 1 UCG Field Test. LLNL UCRL-98641, and In: Proc. 14th An. UCG Symp., pp. 192–199.

Upadhye, R.S., 1986. User documentation for EQSC. LLNL UCID-20900.

Upadhye, R.S., Camp, D.W., Friedmann, S.J., 2013. A material, energy, and economics estimator for underground coal gasification (UCG-MEEE)—Model Description and User Guide. LLNL-SM-422270.

This page intentionally left blank

Underground coal gasification (UCG) in Europe: Field trials, laboratory experiments, and EU-funded projects

5

V. Sarhosis*, K. Kapusta[†], S. Lavis[‡]

*Newcastle University, Newcastle upon Tyne, United Kingdom, [†]Główny Instytut Górnictwa (Central Mining Institute), Katowice, Poland, [‡]University of the West of England, Bristol, United Kingdom

5.1 Introduction

The European Union (EU) is currently highly dependent on energy from abroad, importing 53% of all the energy it consumes at a cost of more than a billion euros per day (Commission to the European Parliament, 2014). Many EU member states are also heavily reliant on a single supplier, including six that are entirely dependent on Russian's natural gas, which increases susceptibility to energy supply shortages and instability, as was highlighted by the winter gas shortages of 2006 and 2009 and the recent political crisis in Ukraine in 2013. Also, the need for a diversified, resilient, and low-carbon domestic energy industry was one of the main points highlighted during the recent G7 Rome Energy Initiative Ministerial meeting (European Commission, 2014) and the follow-up 40th G7 summit 2014 held in Brussels (G7 Summit, 2014). Furthermore, the need for the EU to put in place emergency response systems, including reserves and fuel substitution, to better manage major energy disruptions has been agreed on The Brussels G7 Summit Declaration (2014).

Although there is currently a shift toward using more renewable energy, fossil fuels (and in particular coal use) in the EU have not decreased substantially in the last 10 years. For example, in the decade leading up to 2014, there has been no obvious decreasing trend in coal use for the EU's top five largest economies (Fig. 5.1) and will likely continue to be a major source of energy for the foreseeable future. According to the IEA World Energy Outlook (IEA, 2014), the global coal demand will increase by 25% for the decades between 2015 and 2035. The EU does not have sufficient oil and gas resources to effectively manage a supply shock, but it does have substantial coal resources that could be used to reduce the impact of such shock. At the same time, approximately 80% of Europe's coal resources are greater than 500 m deep (EURACOAL, 2013), which is too deep to be mined economically. Even if it could be mined economically, a further restriction on the use of coal in the EU is that all
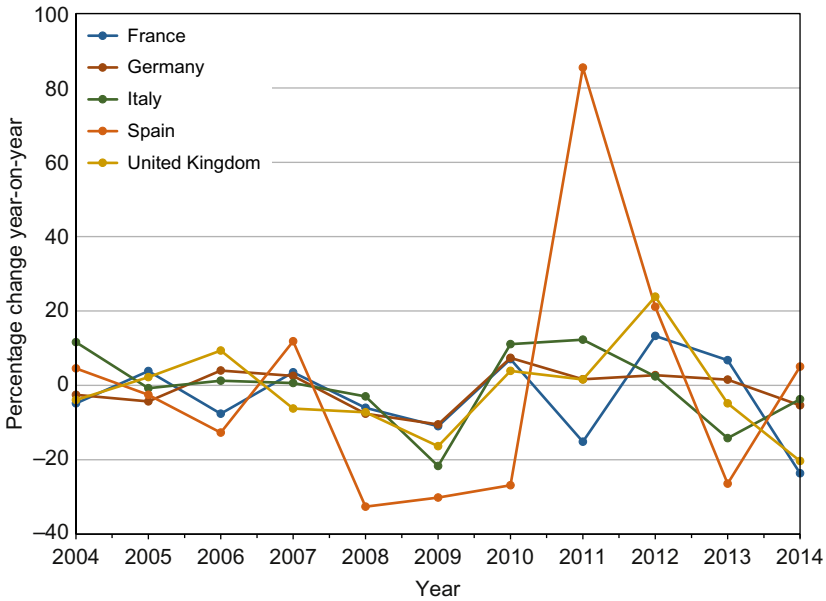
Fig. 5.1 Percentage change (year-on-year) of coal use from 2004 to 2014 of the largest five economies in the EU (BP, 2015).

fossil-fuel-burning power plants will have to incorporate carbon capture and storage (CCS) to meet EU targets on greenhouse gas emissions by 2020. There is therefore a discord between the need to use coal on one hand and the increasing demand for environmental protection on the other (Blinderman and Jones, 2002). The key to manage this discord is to develop clean coal technologies (CCT), such as underground coal gasification (UCG). UCG is a technology that could contribute to future energy needs by exploiting deep (i.e., >500 m deep) coal seams with relatively minor environmental impacts compared with conventional coal technologies (Kempka et al., 2011; Creedy et al., 2004; Couch, 2009; Bhutto et al., 2013; Roddy and Younger, 2010). Importantly, for European countries and after the conception of the UCG by the British scientist Sir William Ramsay (Klimenko, 2009; Bailey et al., 1989), Europe has been at the forefront of developing UCG and has undertaken some of the most important and innovative research and development (R&D) to date.

UCG in Europe (or undertaken by European organizations) has undergone three phases of major R&D, including

(a) Phase 1—field trials between 1940 and 1960
(b) Phase 2—field and laboratory-based trials during 1980 to 2000
(c) Phase 3—field and laboratory-based trials from 2010 to the present (2016)

This chapter reviews the various field and laboratory-based trials undertaken in Europe to date and summarizes the key lessons learned from this R&D.

5.2 Phase 1: Field trials between 1940 and 1960

The first significant UCG field trial undertaken by a European organization was the 1947 French-led trial in Morocco, which was followed by the trials at Bois-la-Dame, Belgium, from 1948 to 1950 and the trials at Newman Spinney and Bayton, the United Kingdom between 1949 and 1959. All of these trials were operated in shallow, thin coal seams using air as the primary oxidant. The amount of inclination for the target coal seams ranged from nearly horizontal to steeply dipping, and module configurations were strongly influenced by the series of trials operated in the former USSR; that is, they comprised vertical (or nearly vertical) wells that were linked in-seam via either reverse combustion, electrolinking, or slanted in-seam boreholes (for steeply dipping seams). Although large volumes of coal were gasified, the trials were all abandoned due to environmental and economic reasons because the process was inefficient and the product gas was generally of low quality.

5.2.1 Djerada, Morocco (1947–50)

The field trial at Jerada, northeastern Morocco, was initially operated in 1947 by the resident-general of Morocco and continued after 1950 by the Research and Experimental Centre of the Charbonnages de France. The trial was undertaken in a mine using the "streaming process," where coal was continuously gasified across a retreating coal face exposed by in a gallery that links two process wells, which were about 100 m apart (Fig. 5.2). The first attempt at gasification was in 1949 but was quickly abandoned. The second attempt took place in 1950 and ran for 5 months.

The coal seam dipped at 77° (i.e., almost vertical) and had thickness ranging from 1 to 1.1 m. The coal was anthracite with 5.8% volatile matter and 5% ash.

C: Chimneys
R: Regenerators
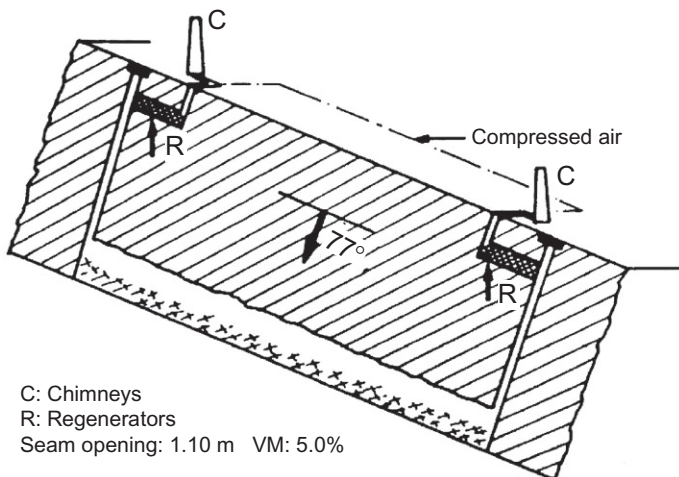Seam opening: 1.10 m   VM: 5.0%

Fig. 5.2 Schematic of the georeactor configuration at the Jerada trial, Morocco (Ledent, 1989).

During gasification, the direction of gas flow was periodically reversed so that the oxidant could be preheated prior to participating in gasification, thereby improving the thermal efficiency of the process and converting the coal evenly across the retreating face. The trial was abandoned because of considerable leakage to the mine workings. The experiment was able to produce syngas with a calorific value (CV) ranging from 1.3 to 2.5 MJ/Nm^3, which, when water injected, was produced at a rate comparable with that of surface gas gasifiers of the time. The trial also showed that the water-gas reaction played a dominant role in the production of hydrogen and carbon dioxide in the syngas. Examination of the workings after the experiment showed that the cavity behind the fresh coal face was bound by a pillar of fused ash and spalled and collapsed roof rock that acted to keep the injected airstream in close contact with the virgin coal during the gasification process (Ledent, 1984).

5.2.2   Bois-la-Dame, Belgium (1948–50)

A Belgian research consortium setup in 1944 sponsored three small-scale UCG experiments in shallow brown coal deposits in northern Italy. At the end of 1947, the consortium was reorganized into the "Socogaz," a cooperative company founded with the support of Belgium and, later, with the French and Polish governments. Socogaz operated the two Bois-la-Dame field tests in a coal mine situated a few kilometers north of Liège, Belgium.

The coal seam was thin, steeply dipping, and semianthracitic, with volatile matter (VM) of 12.3 wt%. Both trials accessed the coal by drilling two in-seam boreholes to intersect a mine shaft/gallery that was orientated at an angle to the dip of the coal seam (Fig. 5.3). The coal was gasified between the two boreholes, creating an inclined longwall that retreated up-dip as the coal was gasified (Ledent, 1989). The product
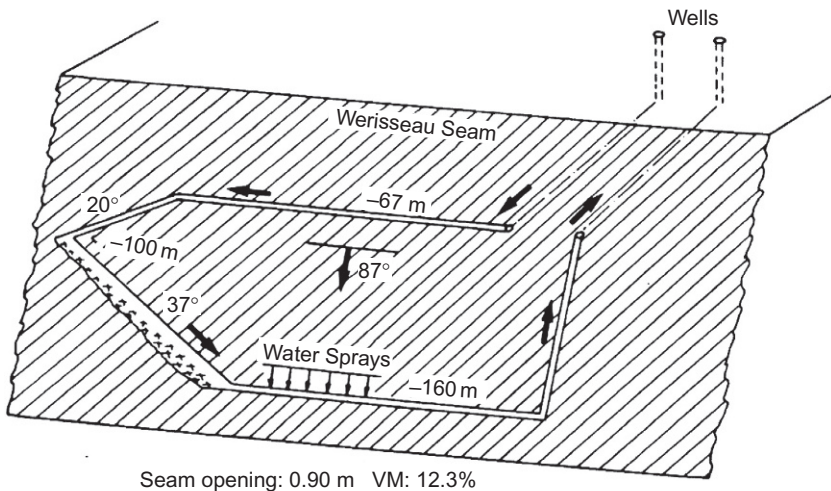

Fig. 5.3 Schematic view of the Bois-la-Dame field test configuration (Ledent, 1989).

gas flow was reversed periodically in an effort to keep coal consumption even across the retreating coal face. As the coal was converted, fresh/partially gasified coal fell into the void beneath, creating a pile of rubblized coal in the combustion zone (Gregg et al., 1976), which improved gasification efficiency in much the same way as observed in the steeply dipping bed module configuration.

The first test started in 1948 and lasted for 35 days. The coal was ignited by setting fire to wooden piles introduced in the upper part of the coal face, and the resulting syngas was cooled by water at the base of the module. About 400 t of coal was gasified yielding a product gas with a CV of 1.5–2.5 MJ/Nm^3 and occasional peaks of 3–4 MJ/Nm^3, equating to a thermal power output in the order of 1–6 MW.

Despite it producing syngas of relatively poor quality, the trial highlighted a flaw in the module design. The gasification front migrated down-dip following the predominant syngas flow direction and leaving the coal up-dip unaffected with no possibility of reigniting the coal again. Furthermore, the gasification front migrated into the zone containing the water sprays and destroying the equipment.

Lessons learned from the first module at Bois-la-Dame were used to redesign the module for the second experiment. Air and syngas were carried through 600 mm diameter boreholes that were drilled into the coal face. Fans for injecting the oxidants were upgraded, a gasoil burner was installed to enable reignition of the coal, and oxygen and steam injection facilities were provided. The active periods of the test totaled 45 days, between November 1949 and September 1950. The flow varied from 0 to 12,000 Nm^3/h, but there were significant issues with obstructions and gas leakages. No combustible syngas was obtained when blowing with air. A gas with a CV of 4 MJ/Nm^3 was obtained when using enriched air (30% O_2), and peaks at 5.6 MJ/Nm^3 were reached when gasifying with an oxygen and steam mixture.

5.2.3   Newman Spinney and Bayton trials, UK (1949–59)

Research into UCG in the United Kingdom began in 1949 under the direction of the Ministry of Fuel and Power, which remained in control until 1956, when the National Coal Board (NCB) overtook the responsibility (Thompson, 1978). According to Thompson (1978), the trials aimed at making UCG a working reality by focusing on linking between processes wells and testing several linking technologies. The first UCG trials were undertaken near Sheffield at the Newman Spinney opencast mine. The second trial was undertaken at Bayton, Worcestershire, and a third trial was undertaken back at Newman Spinney.

5.2.3.1   Initial Newman Spinney trials

The first Newman Spinney trial was undertaken down-dip of a coal seam that was exposed by an opencast mine working (Fig. 5.4). To create the module, a borehole was drilled into the quarry face initially above the coal seam (which was known as the Fox Earth Coal) and allowed to "fall through" the Fox Earth coal seam approximately 70 m down-dip from the quarry face. The borehole remained within the seam for about 15 m before passing through the floor (Thompson, 1978; Beath et al., 2004).
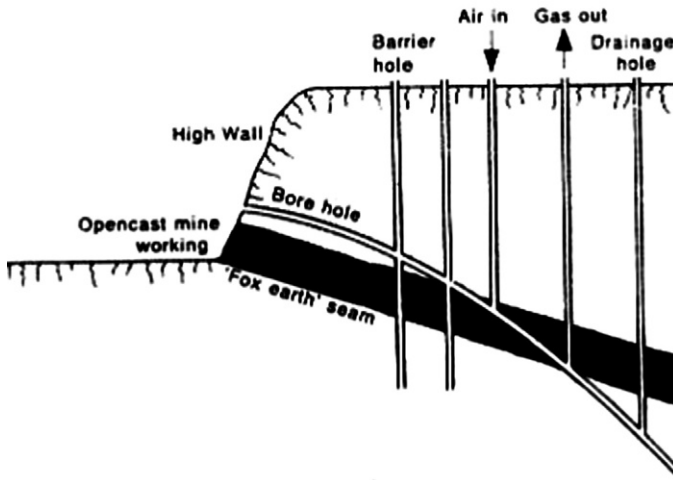
**Fig. 5.4** The module configuration used at the Newman Spinney trial (Thompson, 1978).

Several boreholes were drilled from the surface to intersect the in-seam borehole including an injection well ("air in"), a production well ("gas out"), a drainage hole (presumably to collect water and pyrolysis products), and at least one "barrier hole" (Fig. 5.4). A total of 180 t of coal was gasified, and some of the knowledge gained from drilling proved to be invaluable for the subsequent European trials.

5.2.3.2   The Bayton trials

The Bayton trials were undertaken in buried coal, and several linking methods were tested. The first trial involved linking between vertical process wells using compressed air (i.e., the pneumatic method). The process was slow, but it was found that it could be speeded up by increasing the proportion of oxygen in the compressed airstream, although that produced relatively narrower channels that required high air pressures during gasification (Thompson, 1978). The second attempt used electrolinking, where electrodes were placed at the base of the injection and production wells and high voltages were used to pyrolyze the coal between them. It was found that the current would often track in the wrong direction and the path could not be corrected. Consequently, after several attempts, the method was abandoned in favor of using drilling from undergrounds galleries.

At first, two galleries were created within the coal seam and linked together in-seam by horizontal drilling, but as expertise improved, a single gallery was used. The modules were completed by drilling vertically from the surface and creating multiple module arrays (Fig. 5.5).

During gasification, it was found that the reaction would migrate rapidly away from the injection point down the in-seam borehole, leaving much coal in place.
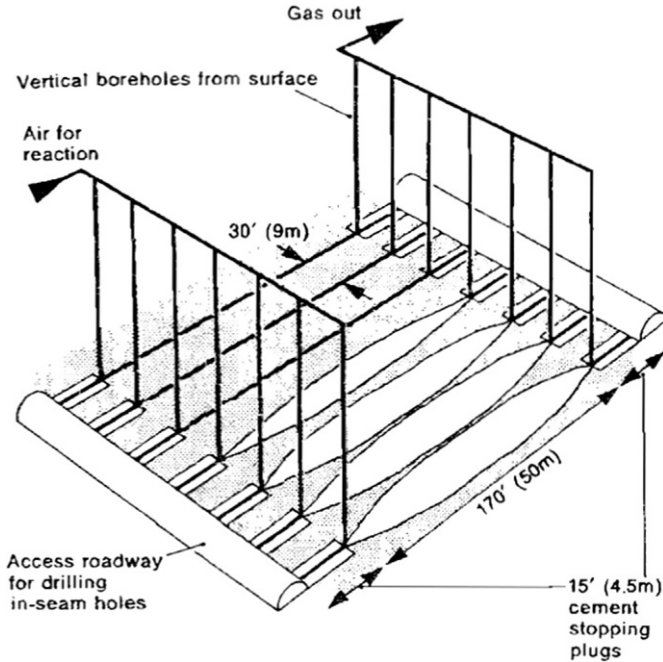
Fig. 5.5 The first module array created at Bayton, England (c.1955) (Thompson, 1978).

This necessitated frequent reversals of the air injection direction to move the reaction front back up the borehole. This consequently led to poor conversion efficiency, and it appears that this issue together with loss of control of the reaction when adjacent modules connected led to the development of a different approach to UCG: the "blind borehole method" (Thompson, 1978). The blind borehole technique involved drilling a single 0.2 m diameter borehole into a coal face and inserting a steel pipe to almost the full length of the hole to enable oxidant to be introduced to the exposed coal (Fig. 5.6). Although, the coal was able to be gasified, it was observed that steel quickly corroded in the georeactor. More advanced steels were used, but at this time, the NCB took over control of the trials and moved them back to Newman Spinney.
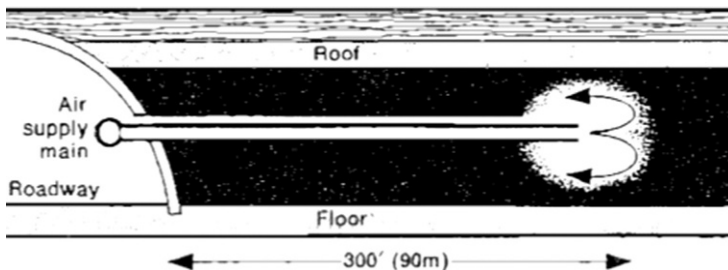
Fig. 5.6 The blind borehole technique (Thompson, 1978).

5.2.3.3   Second phase of trials at Newman Spinney

In 1956, the second phase of research at Newman Spinney focused on the potential of a commercial-scale UCG facility capable of supplying a small power generation unit of approximately 4–5 MWe. The "P5 trial" was the last of a long series of trials, which developed on the sites of Bayton and Newman Spinney. The P5 trial took place in the Sough seam, a thin seam of high-volatile bituminous (VM > 35%) coal with a gentle dip angle. The blind borehole technique was at first further developed at Newman Spinney. An array was created comprising several blind borehole drilled horizontally in-seam from a central gallery (Fig. 5.7).

Gasification was achieved, with over 1050 t of coal gasified at an efficiency of 42%, producing syngas with a CV of 2.8 MJ/Nm^3. However, difficulties in controlling the reactions occurred, especially when adjacent georeactors came into contact. In parallel with the blind borehole method, another set of trials using an alternative method of UCG were able to produce syngas without the control issues of the former. The blind borehole method was abandoned, and a new array of modules was created based on a new technique: UCG was initiated in a large georeactor (e.g., a mine gallery), and gases were drawn through an in-seam borehole where CO_2 was reduced to CO. The layout of the final trial at Newman Spinney, the "P5 trial," is shown in Fig. 5.8.
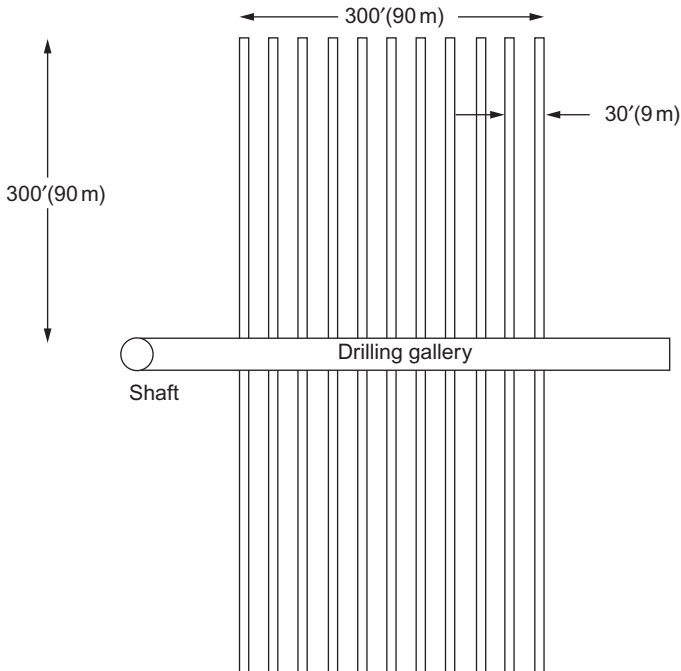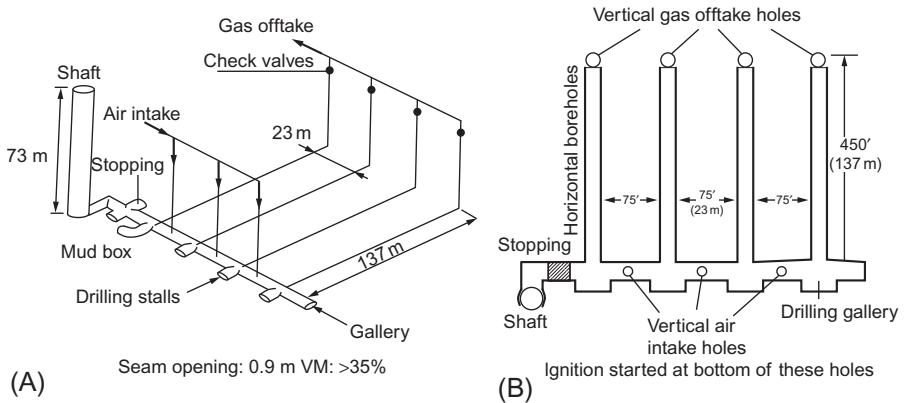

Fig 5.7 The blind borehole array, Newman Spinney c.1958 (Thompson, 1978).

Fig. 5.8 Layout of the P5 field trial at Newman Spinney: (A) 3-D sketch and (B) cross section. Figure not to scale (Thompson, 1978).

To construct the modules, a shaft and an in-seam gallery were created at 73 m depth. Three vertical boreholes of 30 cm diameter were sunk from ground level to the gallery to provide air intake. From the gallery, four 35.6 cm diameter gasification boreholes were drilled laterally through the coal seam at 23 m intervals. Four production boreholes of 30 cm diameter were then drilled from ground level to intersect the end of the four gasification boreholes. During gasification, a several smaller diameter monitoring wells were also sunk to the seam to enable gas analysis and to check the progress of the reaction zone.

Gasification began on 22 April 1959 and ended 118 days later on August 17. About 9150 t of coal was gasified, out of a total of 11,000 t in place (i.e., an 84% sweeping efficiency), at a rate of up to 23,000 m^3/h producing syngas with a CV ranging from 1.5 to 3.4 MJ/Nm^3, which was to lean to power the power plant without the addition of oil to the burner. According the Thompson (1978), the poor quality syngas probably resulted from the inherent limited efficiency when undertaking UCG in thin coal seams.

At the time the P5 trial concluded, conventional energy supplies were plentiful and relatively inexpensive, and so further trials on experimental technologies such as UCG were abandoned on economic grounds.

5.2.4 Phase 2: Field and laboratory-based trials during 1980 to 2000

5.2.4.1 France (1979–86)

The Groupe d'Etude de la Gazéification Souterraine (GEGS) group was founded in 1976 by associating the research teams of Charbonnages de France (CdF), Gaz de France (GdF), Bureau de Recherche Géologique et Minière (BRGM), and Institut Français du Pétrole (IFP).

Three phases of trials took place in the coalfields of France at Bruay-en-Artois, Echaux, and Haute-Deule between 1979 and 1986, with the aims of developing a better understanding of the reactivity of hard coal at great depth (i.e., >800 m) and investigating different linking techniques. The trials experimented with hydraulic fracturing, reverse combustion, and electrolinking to link the boreholes drilled either from underground mine works or vertically from surface.

The first phase of trials was carried out from 1979 to 1981 at Bruay-en-Artois in a coal mine in process of closure (Nord and Pas-de-Calais coalfield). Boreholes, spaced at 65 m apart, were drilled from old mine workings 170 m deep down to a lower coal seam, which was 1000 m deep, bituminous, and 1.2–1.5 m thick (Fig. 5.9). Linkage between injection and production wells was achieved by hydrofracking the coal seam over a period of several months.

In August 1979, water was first injected into one of the process wells at 300 bar to determine the degree of hydraulic continuity, but only 10% of the injected water was recovered at the second process well. In subsequent phases of the trial (from February 1980), a water and sand mixture was used to ensure that the fractures remained open during the operation, but during injection, the pressure reached 750 bar, causing the injection fluid to flow back up the injection well. Later examination found that the injection well was filled with a coal-sand slurry that was later removed. Finally, water alone was injected, and the recoverable flow at the outlet well was found to have increased to 30% of the injected volume.

The first ignition of the coal was produced in June 1980 (Bruay 1 test), around the well II, by injecting hot air, at a flow varying between 100 and 200 m^3/h. The ignition phase lasted 20 h, the air being heated at a temperature of 250–450°C by means of an electric igniter. At the end of the ignition period, air injection was transferred from well II to well I, in order to begin the reverse combustion operations.

During the following days, the injectivity of the circuit declined very quickly, sign of a spontaneous ignition of the coal, around the well I. Attempts to extinguish the fire by water injections were unsuccessful, and during the following weeks, the air injection was transferred a first time from well I to well II, and a second time again from well II to well I, but the injectivity of the circuit remained very low, and it became evident that two combustion zones had been produced, the first at bottom of the well II, created by electric igniter and the second around well I, created by self-ignition of the coal.

During the following months, new tests (Bruay 2 test) were organized, the injected air being replaced by air/nitrogen mixtures. With 10% of oxygen in the mixture, it was still impossible to prevent the self-ignition of the coal. The experiment ended in June 1981, when the mine at Bruay-en-Artois was definitively closed.

At Echaux, near St Etienne in central France, experiments with electrolinking were undertaken in a seam, which was 30 m deep. During the first experiment, the method carbonized the coal between the electrodes, but very high temperatures (~1500°C) destroyed the equipment in less than 24 h (Couch, 2009). A later experiment used a cooling system, but it appears little information remains on the success of the experiment other than less electric power was required to produce coke channel between the electrodes.
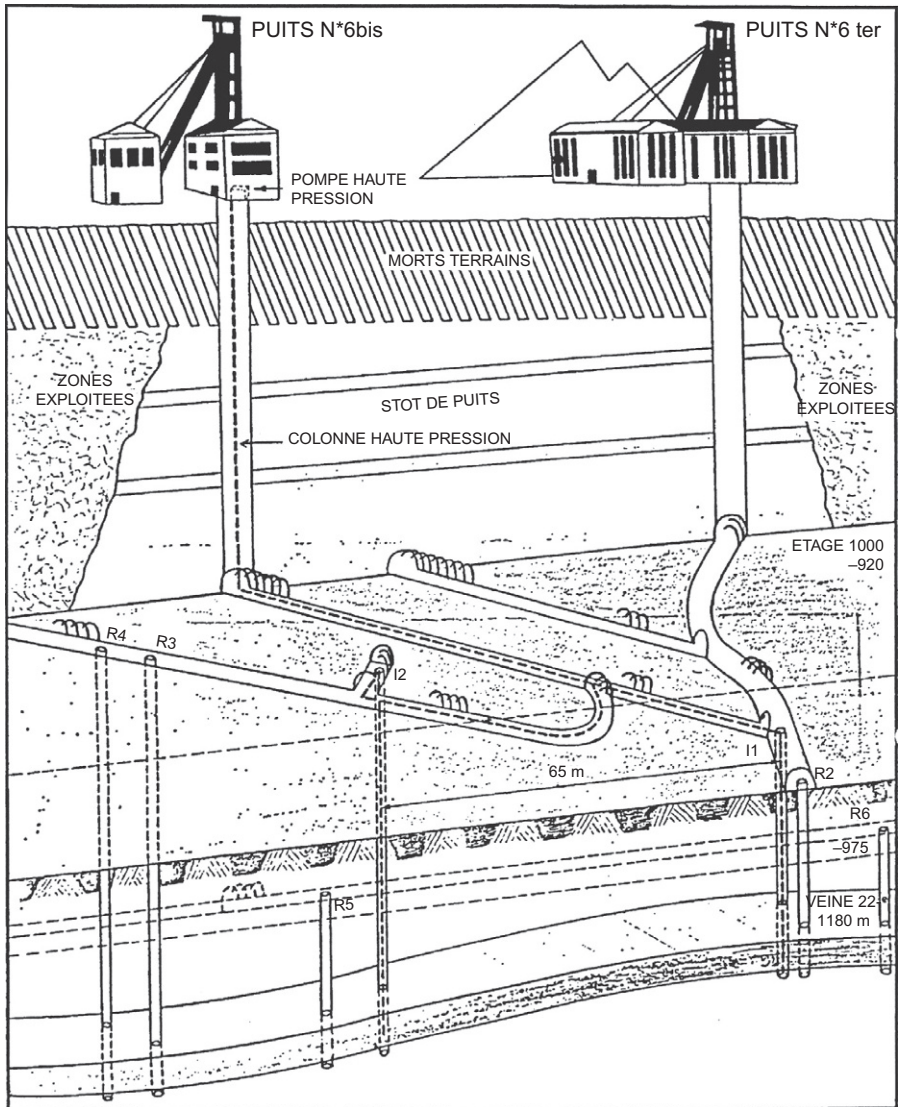
Fig. 5.9 Schematic representation of Bruay-en-Artois experiments (Leplat, 1995).

The third phase of trials was undertaken at Haute-Deule (Fig. 5.10); process wells were drilled from the surface to a semianthracite seam 880 m deep and 2 m thick (Gadelle et al., 1985, 1986). To link the wells, water was injected through the boreholes at a low flow rate and pressure for approximately 3 months. This was followed by hydraulic fracturing using nitrogen foam, which resulted in a superior linkage compared with the Bruay-en-Artois trial (Couch, 2009). Although the coal was ignited by an electric ignition system, the ignition equipment became quickly corroded. Forward
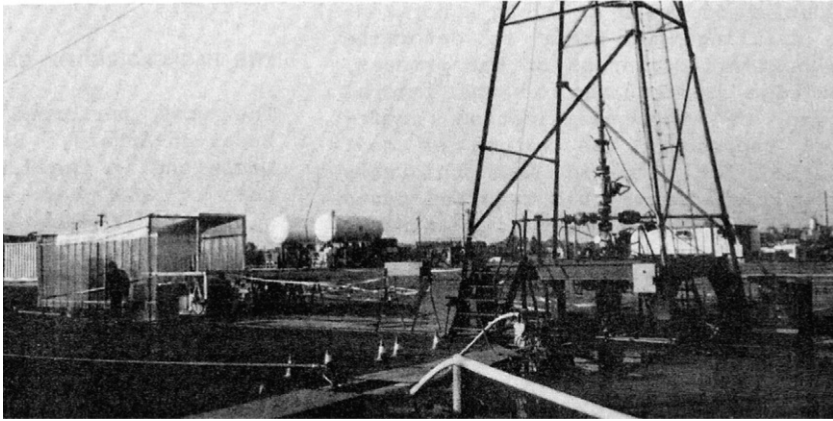
Fig. 5.10 General view of the Haute-Deule site.

combustion began during November 1984 using an oxidant mixture comprising N_2, O_2, CO_2, and C_3H_8. Forward combustion did not last long, however, because the production well became blocked by formation of tars, oxidation products, and coal particles.

Overall, the results of the French trials were mixed; hydraulic fracturing did not lead to a satisfactory link between the process wells and attempts to gasify at great depth failed because the coal self-ignited close the injection well. Electrolinking also proved problematic because of design issues (i.e., the electrodes were not designed to withstand the corrosive environment of UCG). Additionally, the semianthracite seam at Haute-Deule was not suitable for reverse combustion because of its very low volatile matter content and low in situ permeability.

In addition to the French field trials, significant laboratory work and research was carried out in the laboratories of GEGS group. This body of research was invaluable to the second and third phases of UCG trials in Europe.

5.2.4.2 Thulin, Belgium (1978–88)

The Belgo-German trial at Thulin began on April 1, 1979 and ended on March 31, 1988. The Thulin trial was conducted following an agreement between the governments of Belgium and Germany in October 1976, which was later supported by the European Commission (EC) and the costs shared between the EC (40%), Germany (29.4%), and Belgium (30.6%). The Institution pour le Développement de la Gazéification Souterraine (IDGS) was created by Belgium to safeguard and support the project's implementation in the host country (Mostade, 2014a).

The trial at Thulin was undertaken in a coal deposit in the Western Hainaut Coalfield of the South Belgian Coal belt. The target seam was the Léopold-Charles, a semianthracite, nonswelling coal seam approximately 860 m deep comprising multiple leaves reaching a maximum combined thickness of 6.9 m (ref. Table 5.1 for the

Table 5.1 **Analysis of the Léopold-Charles series coal**

Proximate analysis	
Moisture	0.83 wt%
Ash	9.25 wt%
Volatile matter	12.20 wt%
Fixed carbon	77.72 wt%
Elemental analysis (wt%)	
C—Carbon	91.44 wt%
H—Hydrogen	4.25 wt%
O—Oxygen	2.15 wt%
N—Nitrogen	1.29 wt%
S—Sulfur	0.87 wt%
High heating value (dry-ash-free basis):	32.1 GJ/t
Coal rank	semianthracite
Swelling index	0.5
Ash fusion temperature	1450–1580°C
In situ temperature	31°C
Autoinflammation temperature	245°C at atm. pressure; 195°C at 100 bar

coal characteristics), with a maximum net "pure coal" thickness of 4.2 m. The main objectives of Thulin trial were as follows:

- Demonstrate that UCG can be operated at great depth (> 800 m) with a gasification agent mixture of air and steam.
- Select a trial site in the southern coalfield of Belgium.
- Drill four vertical process wells (named from Thulin 1 to Thulin 4), approximately 35 m apart and up to a depth of 1100 m.
- Realize the engineering, procurement, and construction (EPC) of the required surface plant.
- Demonstrate that the LVW configuration can work at >800 m deep.

Initially, four exploration boreholes arranged in a star-shaped pattern (Fig. 5.11) were drilled, with three wells surrounding a central well (Thulin 2) at an angle and distance of 120° and 35 m, respectively (Chandelle et al., 1988). Thulin 1, 2, and 3 were later converted for use in reverse combustion tests. It was found that the seam encountered in Thulin 4 and Thulin 3 was tectonically disturbed but that the seam between Thulin 1 and Thulin 2 was relatively undisturbed. Across the four boreholes, total net pure coal thickness was highly variable, ranging from 1.4 to 4.7 m thick.

At the beginning of the trial, hydrogeologic testing showed that the coal seam permeability was low and highly variable at between 0.003 and 0.1 mD. It was also found that the effective permeability of the seam was increased when the injection pressure was increased. A combination of hydrogeologic testing and gas acceptance testing (i.e., injection of nitrogen) showed that hydraulic communication was best achieved between Thulin 1 and Thulin 2.

Fig. 5.11 The process
well arrangement used at
Thulin (Chandelle et al., 1988).
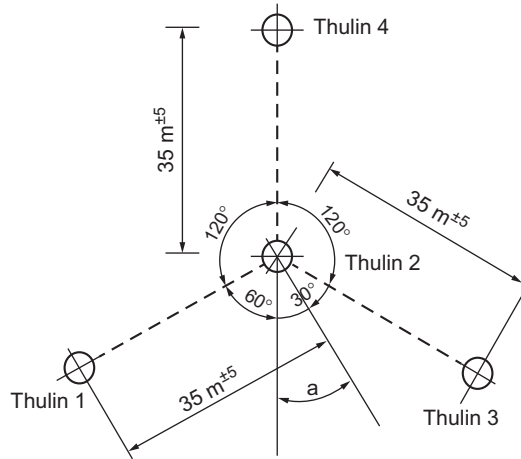
Reverse combustion was used in two separate trials over the period 1982–84 to link the process wells. The first trial used an electric ignition system and the second used an ignition torch. However, neither technique was successful as they did not create a sufficient flow channel between Thulin 1 and Thulin 2. Furthermore, the operations were hampered by complications arising from spontaneous combustion at the base of the process well and repeated tubing/casing ruptures and subsequent process well reengineering.

To explain the lack of channel formation, Chandelle et al. (1988) considered the role of high lithostatic pressure on the behavior of coal at great depth. Firstly, high lithostatic stresses across a linkage between both process wells reduce the permeability and reactivity of the coal (i.e., lower permeabilities reduce the surface area available for gasification reactions) and in order to produce significant gas flow it is necessary to inject at pressures greater than the mechanical strength of the coal. Secondly, high lithostatic stresses around the injection wells creates a limited "creep zone" surrounding the injection point, where the reactivity of the coal is enhanced such that it is very difficult to stop self-ignition of the coal. It was found that the combustion front did not further propagate the creep zone during oxidant injection because the pressure of the infiltrating gases counterbalanced the radial stress acting on the virgin coal. Also, the high-temperature combustion in the creep zone transitioned to lower-temperature oxidation when gases infiltrated into the low-permeability virgin coal at the creep zone/virgin coal boundary.

The coal in the creep zone around the production well can also combust/pyrolyze when (if oxygen levels are sufficiently high) oxidant injected at the injection well flows into the production well creep zone. The combustion front will only propagate, however, if the water produced by the oxidation reactions can be removed from the system (presumably because free water present in the virgin coal reduces the effective permeability). If these conditions are satisfied, a reverse combustion front can develop, and large volumes of coal may be pyrolyzed around the injection well. As the pressure of the infiltrating gas is relatively low compared with the lithostatic stress
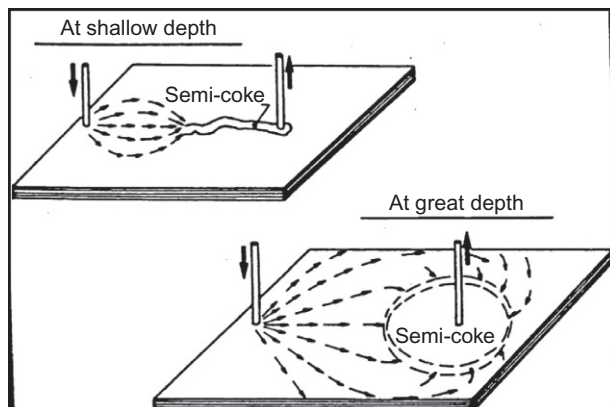
Fig. 5.12 Comparison between reverse combustion linking at shallow depth and great depth.

around the production well, the creep zone expands (Fig. 5.12). In contrast to reverse combustion in low-pressure conditions (i.e., shallow coal seams), however, the development of flow channels between two process wells does not occur at high pressure. Rather, the virgin coal at the boundary of the creep zone around the injection well acts like a gas diffuser, resulting in a uniform gas flow across a wide arc emanating from the injection point. Under high-pressure conditions at the production well side, pyrolysis and relatively low air pressures resulted in an expanding creep zone. On the basis of these findings, Chandelle et al. (1988) concluded that reverse combustion cannot be used as linking method at great depth.

After consideration of the existing advanced drilling techniques and the geologic conditions at the site, it was decided to use short-radius directional drilling techniques to drill from Thulin 1 in-seam toward Thulin 2. It was anticipated that the in-seam borehole would miss Thulin 2 by an order of a few meters, and so it was decided to use sidetrack drilling from Thulin 2 to intercept the in-seam borehole and complete the final linkage using hydraulic fracking. Hydraulic communication was achieved between the two process wells, resulting in expulsion of drilling mud frim Thulin 2, and the module was further purged of coal and rock prior to completion. In addition to the adaption of the process wells using directional drilling, the surface plant was upgraded to allow injection of oxygen, carbon dioxide, and foamy water into the injection well (the original plan was to use air and water).

Gasification tests were undertaken between October 1, 1986 and May 16, 1987. The operations were divided into 18 separate gasification phases based on varying the oxidizer mixture and on the reactor pressure variation (Table 5.2). As can be expected, given the different gasification conditions and oxidizer composition, the syngas composition varied significantly across the 18 tests, with $CV = 12–10,250$ kJ/Nm^3 (mean $= 4500$ kJ/Nm^3), coal consumption $= 216–1761$ kg/day (mean $= 800$ kg/day), gasification efficiency $= 18–59\%$ (mean $= 44\%$), and thermal power $= 0.1–0.4$ MW (mean $= 0.2$ MW).

Table 5.2 Average main process data per gasification phase (Chandelle et al., 1988)

Period	①	②	③ a	③ b	③ c	③ d	④ a	④ b	⑤ a	⑤ b	⑤ c	⑥
Gasification agents												Inject in both wells
O_2 (m_N^3/h)	9	30	66	70	99	89	49	66	66	38	55	(59)
N_2 (m_N^3/h)	22	62	251	262	372	335	110	78	13	12	14	(256)
H_2O (ℓ/h)	0	0	0	0	0	0	0	15	36	22	26	(10)
Pressure												
Wall I (bar)	106	146	193	193	200	202	179	177	186	194	193	221
Wall II (bar)	104	101	144	129	101	127	123	100	100	147	43	218
Reactor outlet												
- Flow (dry gas)												
H_2 (m_N^3/h)	0	2.73	1.69	4.97	6.67	1.14	2.10	3.12	5.20	4.31	7.53	—
O_2 (m_N^3/h)	8.48	2.29	6.12	4.50	2.95	2.02	0.49	0.71	0.07	0	0	—
CO (m_N^3/h)	0	1.23	0.59	2.36	3.17	1.55	0.59	0.91	0.83	0.22	1.05	—
CO_2 (m_N^3/h)	0	10.82	8.93	29.28	37.97	35.04	34.31	45.76	43.77	21.08	54.23	—
CH_4 (m_N^3/h)	0	6.14	5.09	18.30	20.45	11.10	13.42	18.90	23.30	14.29	30.59	—
N_2 (m_N^3/h)	22.02	13.80	33.66	110.59	151.29	132.36	82.59	62.98	23.27	8.61	22.78	—
Total	30.50	37.01	56.08	170.00	222.50	183.21	133.50	132.38	96.44	48.51	116.18	—
- H_2O (ℓ/h)	2	5	4	24	21	12	10	7	48	24	51	—
- Composition (dry gas)												
H_2 (%)	0	7.4	3.0	2.9	3.0	0.6	1.6	2.4	5.4	8.9	6.5	—
O_2 (%)	27.8	6.2	10.9	2.6	1.3	1.1	0.4	0.5	0.1	0	0	—
CO (%)	0	3.3	1.1	1.4	1.4	0.8	0.4	0.7	0.9	0.5	0.9	—
CO_2 (%)	0	29.2	15.9	17.2	17.1	19.1	25.7	34.6	45.4	43.5	46.7	—
CH_4 (%)	0	16.6	9.1	10.8	9.2	6.1	10.1	14.3	24.2	29.5	26.3	—
N_2 (%)	72.2	37.3	60	65.1	68	72.3	61.8	47.5	24	17.6	19.6	—
Low heating value (kJ/m_N^3)	0	7168	3726	4363	3802	2353	3848	5476	9378	11.606	10249	—
Thermal power (Mw)	0	0.07	0.06	0.21	0.23	0.12	0.14	0.20	0.25	0.16	0.33	—
Coal consumption (kg/day)	0	288	216	816	960	696	720	1008	1080	600	1368	—
Coal affected (kg/day)	0	768	600	2112	2424	1176	1464	2088	2640	1680	3504	—
Recovery rate (%)	0	47.1	23.0	49. 4	44.3	45.6	70.7	70.8	66.1	52.6	31.1	—
Gasification efficiency (%)		56	59	56	54	40	45	45	52	57	53	—

⑦	⑧ a	⑧ b	⑨	⑩	12	13 a	13 b	14	15	16	17	18
58 14 29	62 247 0	73 287 0	63 8 21	0 28 0	204 313 25	210 59 105	127 25 68	33 146 40	184 38 92	91 345 0	193 44 99	0 310 0
192 109	217 100	234 41	199 40	163 40	189 41	273 41	283 100	253 97	258 40	248 40	262 41	249 45
2.74 0.46 0.05 41.32 14.45 67.65 126.67 38	2.85 0 0.27 45.93 4.59 134.86 188.50 38	3.23 0 0.40 39.76 9.39 178.14 230.92 30	2.24 0 0.19 45.68 15.68 28.44 92.23 36	2.20 0 0.03 24.76 15.01 35.11 77.11 25	4.39 3.96 2.35 44.95 11.83 122.43 189.91 14	15.5 3.2 15.4 68.0 32.3 44.0 178.4 39	5.45 0.30 2.44 71.22 20.51 30.43 130.35 45	5.26 0 0.37 55.72 29.12 22.79 111.26 68	3.55 0.93 3.67 48.08 8.74 28.54 91.51 61	6.99 5.79 3.58 39.43 5.75 82.46 144 42	5.12 10.45 4.40 58.31 3.71 46.67 128.66 41	1.40 3.39 0.43 28.50 4.10 98.86 136.68 36
2.2 0.4 0 32.6 11.4 53.4 4329	1.5 0 0.1 24.4 2.4 71.6 1034	1.4 0 0.2 17.2 4.1 77.1 1645	2.4 0 0.2 49.5 17.0 30.9 6385	2.9 0 0 32.1 19.5 45.5 7310	2.3 2.1 1.2 23.7 6.2 64.5 2625	8.7 1.8 8.5 38.2 18.2 24.0 8553	4.2 0.2 1.9 54.6 15.7 23.4 6326	4.6 0 0.1 49.2 18.2 20.2 9755	3.8 1.0 3.9 51.4 9.3 30.6 4237	4.9 4.0 2.5 27.4 4.0 57.2 2278	4.0 8.1 3.4 45.3 2.9 36.3 1901	1.0 2.5 0.3 20.9 3.0 72.3 1227
0.15	0.05	0.11	0.16	0.16	0.14	0.42	0.23	0.31	0.11	0.09	0.07	0.05
840	696	720	914	624	862	1781	1385	1334	858	700	450	270
1776	1176	2160	1705	1630	1421	4065	2362	3227	1085	994	639	488
41.4 41	73.9 18	49.0 32	72.7 41	— 53	22.6 37	40.4 53	54. 1 33	13. 7 51	27.7 30	52. 7 31	39.6 35	— 40

During test 12, significant volumes of oxygen were measured in the syngas at the production well, indicating that oxygen bypass had occurred. The problem persisted intermittently throughout the remaining tests, and the reactor was extinguished during test 18, during which there was continued production of pyrolysis gases. From the mass balance, it was found that 157 t of coal had completely converted into syngas, and 183 t of semicoke was left underground in the georeactor.

The Thulin trial demonstrated that UCG is technically feasible at great depths and contributed significantly to future UCG research and development in Europe. The main phases of the Thulin project are summarized in Table 5.3.

After the termination of the Thulin project, IDGS became involved in "the new future development of UCG in Europe," which involved (i) a comprehensive report to the EC, Brussels, Belgium (April 1989) and (ii) the "El Tremedal" UCG trial (see below), Alcorisa. Following dissolution of IDGS in 2001, the "Underground Energy Recovery Belgium (UNERBEL)," a nonprofit association, was created to receive all IDGS data (from the Thulin trial, European Working Group works, El Tremedal trial, and former mining activities in south of Belgium). The archives of IDGS data are now located at the Earth Science Library of the University of Liège, Belgium.

Table 5.3 Summary of the main phases of the Thulin trials between 1978 and 1987

Date/year	Phase
1978	Drilling and completion Thulin 1 with works managed and financed by the Belgian Institut National des Industries Extractives
1979	Project definition and front-end engineering design (FEED)
1979–1980	Drilling and completion of Thulin 2, Thulin 3, and Thulin 4. Geologic assessment of the site and measurement of coal characteristics
1980–1982	Surface plant procurement and construction
February 1981–January 1982	Permeability testing between wells
February 1982–September 1984	Linking attempts using reverse combustion
November 1984–September 1986	Engineering, drilling, and completion of directionally drilled boreholes to link Thulin 1 and Thulin 2. Engineering, procurement, and construction (EPC) to modify the surface plant
October 1986–April 1987	Gasification operations from Thulin 1 (injection well) to Thulin 2 (production well)
May 1987–October 1987	Additional communication testing, removal of downhole equipment, and well abandonment

5.2.4.3   European Working Group on UCG (1988–90)

In 1987, it was realized that the future of UCG in Europe would be secured when states interested in the technology came together. In April 1988, Belgium, the Federal Republic of Germany, France, the Netherlands, Spain, and the United Kingdom came together to form the European Working Group (EWG) on UCG, which received financial support from the Commission of European Communities (CEC). In a comprehensive report (CR) submitted to the CEC in April 1989, the EWG showed that UCG is feasible in the thin, deep seams typical of European coal resources. The CR also included an economic assessment that demonstrated the considerable economic potential of the technology and that UCG syngas could be used in combined cycle power plants to produce electricity cost-effectively. On the back of this, the EWG conducted a feasibility study and made proposals for future EC-sponsored UCG projects in Europe.

Following this, a program to implement commercial-scale UCG in Europe was undertaken over a 15-year period. The first phase of this program comprised planning two field trials (and supporting R&D) using directional and in-seam drilling to construct CRIP modules. The first trial was planned to be at a depth of about 600 m, which at the time was significantly deeper than UCG trials using CRIP in the United States. This trial was seen as an important step in developing the technologies necessary to access coal at even greater depth (i.e., > 900 m) in the subsequent trial (Mostade, 2014b).

Potential sites in Spain and France were identified for the first test and sites in the United Kingdom and Belgium for the second (although it was deemed that further evaluation was necessary for the latter). It was finally agreed that the first trial at intermediate depth should be undertaken in Spain, and work to complete detailed project proposals was completed in 1990.

5.2.4.4   El Tremedal field trial (1991–99)

The El Tremedal project was jointly sponsored by Spanish, Belgian, and UK organizations, with support of the CEC as part of the "THERMIE" framework program. The main objective of the project was to demonstrate the technical feasibility of UCG using CRIP at an intermediate depth of about 600 m. The trial had several technical objectives, chief of which was demonstrating that long in-seam boreholes could be drilled and linked at this depth.

The trial was located at a site near to the town of Alcorisa in Teruel, Spain. The area selected for the trial, known as "El Tremedal," contains subbituminous coal of the Teruel coal basin. The Teruel coal basin was formed at the end of the Lower Cretaceous epoch (Chappell and Mostade, 1998). The coal-bearing zones targeted for UCG occurred within the Escucha Formation, which was renamed as the Val de la Piedra Formation at El Tremedal. This formation unconformably overlays Jurassic sediments. In general, two coal seams are present in the Val de la Piedra Formation, separated by several meters of fossiliferous clay and/or limestone. The upper coal seam is discontinuous, having been eroded during deposition of an overlying sandstone layer

(i.e., coal "washouts" were common), whereas the lower coal seam is continuous across the whole site area. The Utrillas Formation, which lies above the Val de la Piedra Formation, reaches a thickness of about 100 m and is composed of clay stone and sandstone. Jurassic tectonism caused faulting, and the development of subbasins into which the Cretaceous sediments were deposited.

The potential of the El Tremedal area was previously examined for conventional deep mining by a local mining company, which undertook seismic investigations and exploratory drilling. The El Tremedal area was selected on the basis of the following:

- No nearby mining operations
- No nearby groundwater abstractions
- A well-characterized coal seam with properties suitable for UCG
- Low incidence of faulting
- Topography suitable for access and site preparation
- A small number of landowners involved for site access

Two exploratory boreholes were initially planned, but a third was added later to better characterize variations in dip, seam thickness faults, washouts, and splits prior to directional drilling in the lower coal seam. The exploration phase showed that both coal seams dipped at about 30° and were fairly continuous between the three exploration wells. There were no significant faults in the area, although there was evidence of incomplete coal washouts near the third exploration well, which resulted in a mean true thickness of the upper coal seam of being reduced to 2.6 m. Furthermore, the lower coal seam near the third exploration well was of low quality, being a carbonaceous mudstone-siltstone, rather than coal.

Based on the results of the exploration phase, the upper coal seam offered the best conditions for in-seam drilling and gasification and was selected as the target seam. The thickness of the seam ranged from 2 to 5 m, with a dip angle of about 30° at a depth of 530–580 m. The coal was subbituminous with 22.2% moisture, 36.0% fixed carbon, 27.5% volatiles, 14.3% ash, and very high sulfur contents of 7.6%. The permeability of the coal was measured at 2 mD. The higher heating value of the coal in place was estimated to be 18 MJ/kg. The overburden consisted of clay and sand with the permeability of the latter permeability measured at 17.6 mD. The conditions of the coal seam and the quality of the coal are summarized in Table 5.4.

The main objectives of the El Tremedal trial were to carry out UCG using the L-CRIP method and to undertake multiple CRIP maneuvers and reignitions. The module was designed to incorporate three process wells: (i) a deviated injection well with an in-seam distance of about 100 m, (ii) a directionally drilled production well steered to intersect the end of the in-seam section of the injection well, and (iii) a transverse injection well terminated in the coal seam 30 m off the long axis of the in-seam section of the injection well.

The drilling and well completion operations for the deviated injection well were successfully completed as planned in October 1993. There were, however, difficulties in maintaining the in-seam section within the coal seam and the drill passed through the seam and into limestone underburden for a 50 m section of the well before returning into the coal seam (Fig. 5.13). Given that the drilling technology was in its infancy at the time, the difficulties in maintaining the borehole in-seam are perhaps unsurprising.

Table 5.4 Main characteristics of the upper coal seam (Fiévez et al., 1997)

Depth (bottom)	530–580 m
Hydrostatic head	48–52 bar
Seam thickness	2–5 m
Dip angle	+/− 29°
As received data	
Total moisture	22.2 wt%
Volatile matter	27.5 wt%
Fixed carbon	36.0 wt%
Ash	14.3 wt%
Total sulfur	7.6 wt%
High heating value	18,125 kJ/kg
Rank	Subbituminous class C
Moisture/ash flee data	
C	71.4 wt%
H	3.9 wt%
N	0.6 wt%
S	6.4 wt%
O	17.7 wt%
High heating value	28,453 kJ/kg
Permeability	2.0 mD
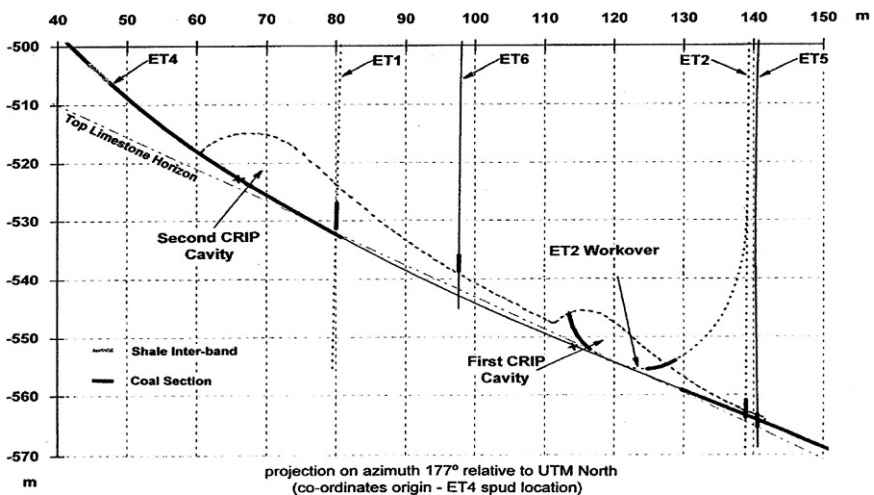
Fig. 5.13 Cross section showing the trajectory of the injection well (and other boreholes) and sections of the in-seam well that were drilled within the coal seam or the underlying limestone (Fiévez et al., 1997).

The directional drilling and completion operations for the vertical production well were successfully completed in December 1994. The directional control for the production well was intrinsically simpler than for the injection well (i.e., it was not necessary to drill horizontally within a thin horizon), and the production well was placed within 0.5 m from the target at the end of the injection well. The production well was fully completed with UCG-specific tubing and equipment in less than 13 days.

The transverse injection well, the smallest and simplest of the three process wells, was drilled and completed by December 1994. Again, directional drilling was successful in accurately positioning the well, and borehole completion operations were completed in 7 days.

Gasification operations involved creating two CRIP georeactors along the in-seam section of the injection well. The first georeactor was designed to be about 20 m in length and the second about 80 m. The main gasification agents were oxygen and water.

The first gasification phase ran from 21 July to July 29, 1997, but due to surface and well equipment problems, operations were stopped halfway through the planned trial phase. After minor alterations to the equipment, the second gasification phase began on 1 October and lasted until October 5, 1997 and was stopped because of damage to the injection well equipment. As there was a period of sustained gasification during which significant data were collected and given that the costs to fix the injection well equipment were high, it was decided to cease gasification and concentrate efforts on investigating the georeactors using an additional drilling program.

During the active gasification phases, which lasted in total 12 days, an estimated 237 t of coal (on a moisture-ash-free basis) was gasified, and 90 t of oxygen was injected. The thermal power output reached a maximum of 6 MW, with an average of 2.6 MW. The average syngas composition (on a dry, N_2-free basis) was $H_2 = 25\%$, $CO = 11\%$, $CH_4 = 14\%$, $CO_2 = 42\%$, and $H_2S = 8\%$. The raw syngas contained approximately 46 vol% water, and the average CV of the syngas (LHV) on dry-basis was 11 MJ/m_N^3. Postburn drilling identified a caved zone extending to approximately five times the coal seam thickness above the volume of the seam that was gasified.

The El Tremedal trial was able to gasify coal at intermediate depth and producing a high-quality syngas at a relatively high rate (up to 6 $MW_{thermal}$) using the L-CRIP method. Although there were some issues with the downhole equipment, which were adapted to during the test, it was the choice of site that perhaps caused the greatest problems during the test. The high permeability and low strength of the sandstone overburden resulted in large quantities of water flowing into the georeactor, reducing the efficiency of gasification and creating large volumes of steam/water. Furthermore, the high gasification pressure and high permeability of the overburden allowed approximately 17% of the product gases to escape into the surrounding strata. As no significant contamination was detected at the site, it is likely that any condensates from the syngas were flushed back into the georeactor with the infiltrating syngas.

The El Tremedal trial provided a number of essential lessons for future UCG trials regarding directional drilling, detailed engineering design of the underground components, and the selection of trial sites. The problems identified during the Spanish trial

are relatively easy to solve, especially given advances in drilling and exploration technologies. For example, the maximum in-seam length that could be achieved at the time was about 100 m, whereas technologies developed for coal-bed methane and shale gas are now capable of drilling several kilometers within a coal seam. Furthermore, the geologic and hydrogeologic conditions necessary for the safe operations of UCG are well characterized and can be identified using modern exploration techniques. The El Tremedal trial was therefore seen as laying the foundations for subsequent CRIP-based UCG trials in Europe; for example, the UK Department of Trade and Industry (DTI) identified UCG as one of the potential future technologies for the development of the United Kingdom's large coal reserves and completed a comprehensive assessment of the geoenvironmental, regulatory, and technology issues required for commercial UCG in the United Kingdom (DTI references to add).

5.3   Phase 3: Field and laboratory-based trials from 2010 to the present (2016)

The study of hydrogen-oriented from underground gasification (HUGE) was a €3 million EU-sponsored project undertaken by the Polish Central Mining Institute and 10 other European institutions. Its aim was to optimize hydrogen production from European lignite and hard coals and to simultaneously consider capturing and sequestration of CO_2 in an all embracing georeactor. The project focused on the critical evaluation of process parameters and geologic conditions required for the successful and safe conversion of coal resources to hydrogen and their subsequent matching to suitable European coal deposits. A wide range of gasification tests were undertaken, including experiments in blocks of coal in situ and ex situ in high-pressure reactors. Two types of test were undertaken, one to vary the operating dynamics of UCG and the other to examine the effects of introducing calcium oxide into the gasification reactions. The experiments were supported by small-scale laboratory work, environmental studies, and computer modeling. The research was then continued by the HUGE2 project (a €2.5 million EU-sponsored project), which mostly focused on the environmental and safety aspects of UCG. These research projects included two in-seam gasification trials at the Experimental Mine Barbara in southern Poland. The UCG reactors were prepared using a system of existing underground galleries and utilized two different process well configurations (Fig. 5.14).

5.3.1   The first UCG trial in Poland (2010)

The first underground reactor was constructed in coal seam no. 310, which was 30 m below ground level in the northeastern part of the Barbara mining area (Wiatowski et al., 2012, 2015). The selected part of the coal seam was made available using an existing system of mine shafts and galleries. The results of proximate and ultimate analyses of coal sampled from the seam at the test site are presented in Table 5.5.

A horizontal borehole (a "fire channel") with a diameter of 0.14 m was drilled through the coal seam to a length of 15 m. The channel was fitted with steel pipes with
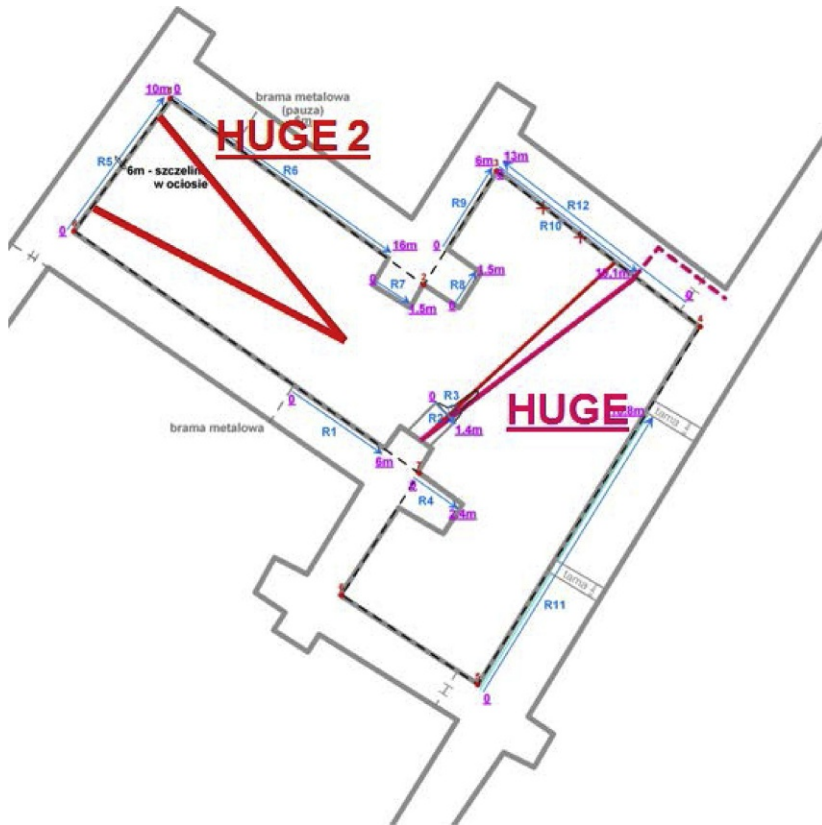
Fig. 5.14 Configurations of HUGE and HUGE2 gasifiers at the Experimental Mine Barbara.

Table 5.5 Proximate and ultimate characteristics of coal at the test site

Parameter	Value
As received	
Total moisture (wt%)	11.81
Ash (wt%)	15.56
Total sulfur (wt%)	0.51
Calorific value (KJ/kg)	21,708
Analytic	
Moisture (wt%)	6.39
Ash (wt%)	16.52
Volatiles (wt%)	29.84
Calorific value (kJ/kg)	23,019
Total sulfur (wt%)	0.54
Carbon (wt%)	57.95
Hydrogen (wt%)	3.70
Nitrogen (wt%)	0.87
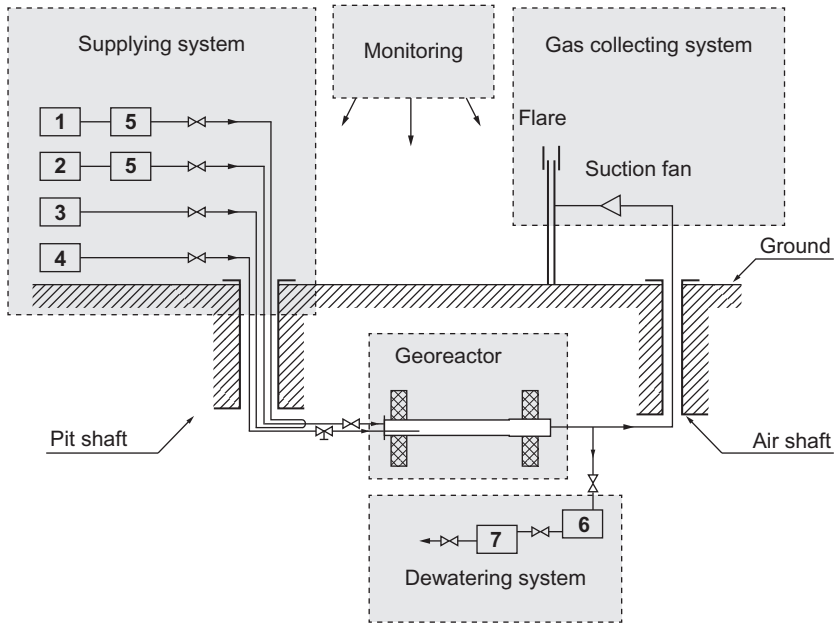
Fig. 5.15 Scheme of the UCG installation constructed for the first trial at Barbara Mine (Wiatowski et al., 2015).

diameters of 0.15 and 0.20 m on the inlet and outlet, respectively. Four pipelines fed oxygen, air, nitrogen, and water into the reactor. A gaseous product pipeline with a diameter of 0.20 m and a length of approximately 150 m was routed from the end of the georeactor through the air heading and up the mine's ventilation shaft. The general scheme of the installation and details of the underground reactor are presented in Figs. 5.15 and 5.16, respectively.

The first in situ experiment ran from 7 to April 22, 2010 (a total of 355 h), and it was divided into three stages:

1. 0–190 h: coal seam ignition and stabilization of operating conditions
2. 190–355 h (total of 165 h): stable operation of the georeactor
3. 355 h and for the next 40 days: safe shutdown of the georeactor and termination of the experiment

During the first phase of the experiment, oxygen was injected at a rate of 20–40 Nm^3/h. During the course of the experiment, oxygen injection was periodically changed into air or oxygen-enriched air (OEA) injection to verify predictions made from laboratory and modeling work. Stable operation of the underground gasifier was achieved after approximately 190 h after initiation, and it continued for the next 165 h. After process termination (at 355 h) and for the next 40 days, the reaction site was cooled with nitrogen gas. The change in product gas composition over time is presented in Fig. 5.17.
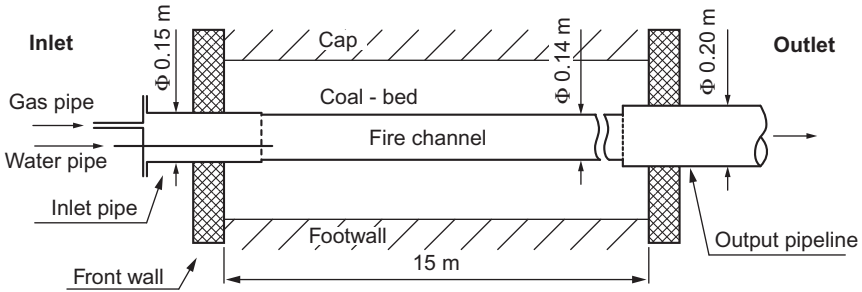
Fig. 5.16 Construction of the first UCG reactor at Barbara Mine (Wiatowski et al., 2012).
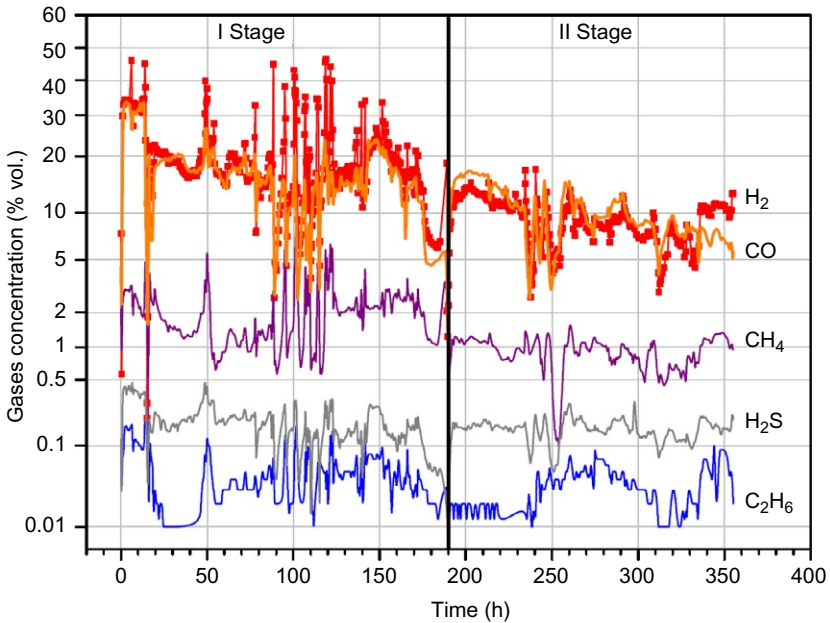
Fig. 5.17 Changes in the gas composition over the course of the first UCG trial at Barbara Mine (Wiatowski et al., 2012).

The maximum concentrations of H_2 (45 vol%), CO (35 vol%), and CH_4 (8 vol%) were recorded during the first phase of the experiment, after which the concentration of these gases gradually declined. The average concentrations of the components are presented in Table 5.6. The CO_2 content of the syngas increased from initially 13 to 30 vol% and averaged at 16.4 vol%. The nitrogen content also increased from an average of 47.8 vol% in stage 1 to over 57 vol% in stage 2.

The first Barbara experiment revealed that UCG in shallow, thin coal seams in mines is feasible but that it can be operationally problematic. Under mine conditions,

Table 5.6 **Average concentrations of gas components in the first Barbara trial**

Gasification stage	Average concentration (vol%)							
	H_2	CO	CH_4	C_2H_6	H_2S	CO_2	N_2	O_2
(1) 0–190 h	18.5	15.7	2.0	0.05	0.18	13.2	47.8	2.6
(2) 90–355 h	9.2	10.7	0.0	0.03	0.16	20.2	57.6	1.2
Average	14.2	13.4	1.5	0.04	0.17	16.4	52.4	1.9

the georeactor, which is initially a "closed system," becomes progressively open to the surroundings, enabling an inflow of excess air to the gasification zone and adversely affecting the product gas quality. The thin seam also resulted in high thermal losses (as a proportion of the energy produced during gasification) to the surrounding rock, which reduced the overall energy efficiency of the process to about 56%.

5.3.2 The second Polish UCG trial

The second UCG georeactor in the Barbara Mine was located in the same coal seam as the first trial. A horizontal V-shaped fire channel, consisting of two boreholes of 0.14 m in diameter and 17.3 m in length, was drilled into the coal seam (Wiatowski et al., 2015). The general scheme of the installation and geometry of the reactor are presented in Figs. 5.18 and 5.19, respectively.

The second in situ experiment took place between 1 and August 7, 2013 (for a total of 142 h) and was divided into the three stages:

1. 0–101 h: coal seam ignition and stable operation of the georeactor
2. 101–142 h (41 h): continued operation of the georeactor unsteady conditions
3. 142 h and during the following 4 weeks: safe shutdown of the georeactor and termination of the experiment

The changes in production gas composition over the course of the experiment are presents in Fig. 5.20.

During the 6-day oxygen-blown gasification trial, 5364 kg of coal was gasified with an efficiency of 70%. The average heating value of the produced gas and the thermal power of the gases supplied to the combustor were 8.91 MJ/Nm^3 and 192.5 kW, respectively. The maximum concentrations of hydrogen and carbon monoxide in the product gas were 47.8% and 40.5%, respectively. Average gas composition is presented in Table 5.7.

The second gasification trial proved again that it is feasible to undertake UCG in mine conditions but that it is very important to ensure that the georeactor remains a closed system. At 101 h, large volumes of N_2 appeared in the product gas stream, and the quality of the gas decreased, indicating that the georeactor was in continuity with its surroundings. This also resulted in losses of UCG product gas to the surroundings.
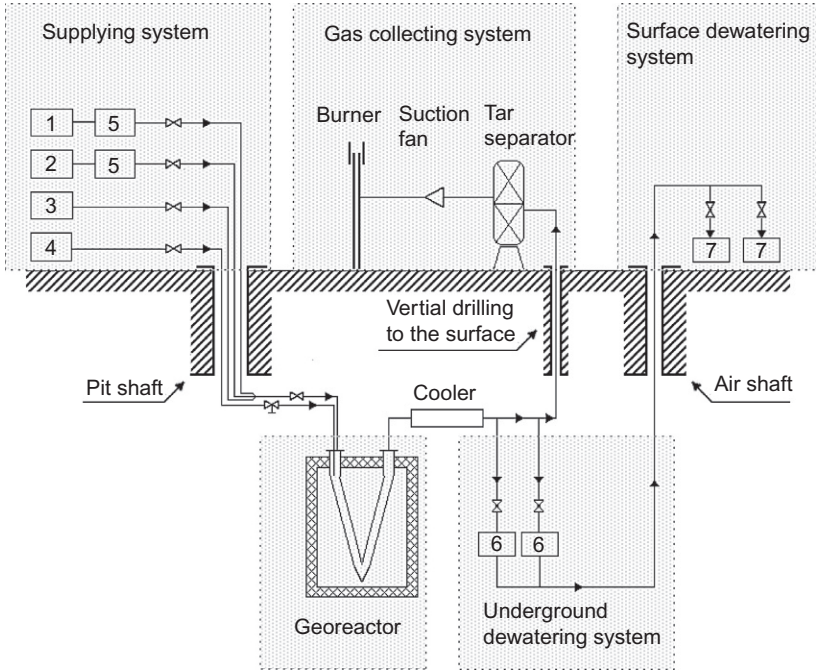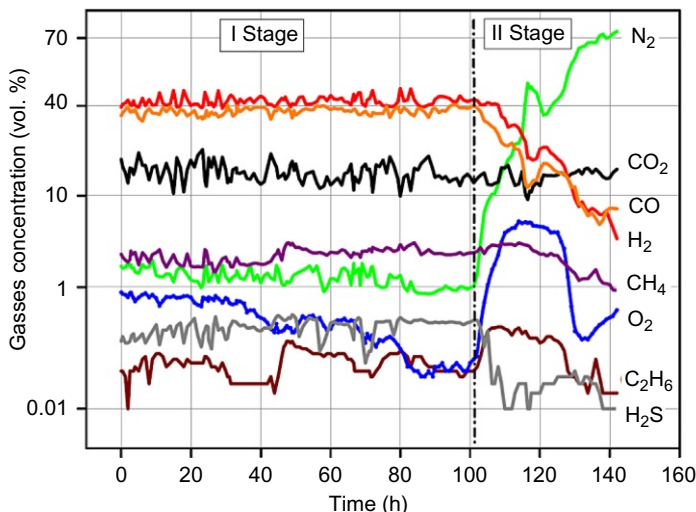
Fig. 5.18 Scheme of the UCG installation used for the second trial at Barbara Mine (Wiatowski et al., 2015).
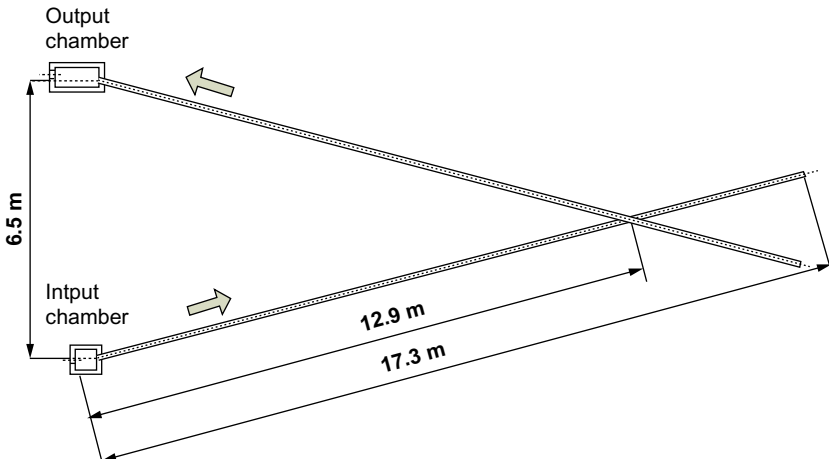
Fig. 5.19 Geometry of the georeactor for the second Barbara Mine experiment (Wiatowski et al., 2015).

Fig. 5.20 Changes in the production gas composition over the course of the second UCG trial at Barbara Mine (Wiatowski et al., 2015).

Table 5.7 Average concentrations of gas components in the second trial in Barbara mine

Gasification stage	Average concentration, vol%							
	H_2	CO	CH_4	C_2H_6	H_2S	CO_2	N_2	O_2
(1) 0–101 h	42.2	37.7	2.5	0.07	0.27	15.5	1.3	0.4
(2) 101–142 h	21.9	17.4	2.3	0.14	0.05	14.4	41.3	2.5
Total	32.1	27.56	2.4	0.11	0.16	14.9	21.3	1.5

5.3.3 Pilot-scale UCG operations at the Wieczorek Mine, Poland (2014)

A V-shaped UCG reactor was constructed in coal seam no. 510, in the Wieczorek Mine, located in the Upper Silesian Coal Basin, Poland (Mocek et al., 2016). The coal was bituminous; the coal seam was about horizontal with a thickness of 5–6 m. The geometry of the reactor is presented in Fig. 5.21. The average depth of the coal seam was approximately 465 m, and the overlying strata were predominantly low-permeability shale and sandstone.

The gasification trial was divided into six stages (Table 5.8). Changes in the gas composition over the course of the experiment are presents in Fig. 5.22. During the 60-day gasification trial, approximately 230 t of coal was affected. The process yielded syngas at around 600–800 Nm^3/h, and the gas calorific value ranged from 3.0 to 4.5 MJ/Nm^3. The experiment demonstrated that through the appropriate
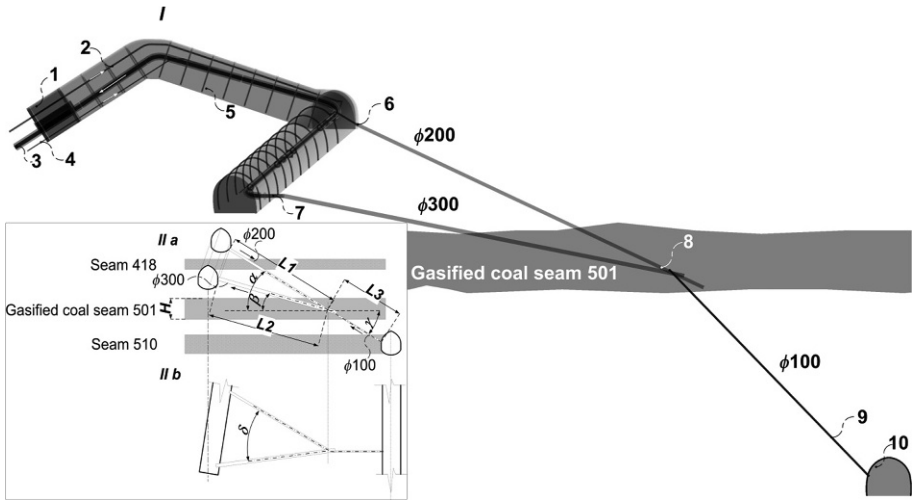
Fig. 5.21 Geometry of the UCG reactor used for the Wieczorek Mine experiment: (I) front view of the UCG reactor and experimental gallery; (II) reactor's dimensions: (a) longitudinal section, (b) horizontal section. Symbols: 1, sand backfill dam; 2, oxidants supply pipeline; 3, raw gas pipeline; 4, nitrogen pipe to safety dam; 5, part of experimental gallery behind the backfill dam; 6, oxidants supply drill hole; 7, gas recovery drill hole; 8, ignition point; 9, measurement drill hole; 10, gallery behind the target coal seam (Mocek et al., 2016).

Table 5.8 Stages of UCG trial in Wieczorek Mine

Stage no.	Gasification reagent	Period, h
I	Air + oxygen	0–193
II	Air	193–888
III	Air + carbon dioxide	888–1008
IV	Air	1008–1181
V	Air + nitrogen	1181–1343
VI	Nitrogen	Cooling

selection of the test site and by applying all safety standards essential for the coal mining industry, UCG in an active mine can be conducted safely and efficiently.

5.3.4 Laboratory tests in Poland

In recent years, studies on UCG using large-scale experimental simulations on artificially created coal seams were conducted by research groups including the Central Mining Institute (GIG) in Poland [38-44], the China University of Mining and Technology in Beijing (Liu, 2006a,b), and the Technical University of Kosice, Slovakia
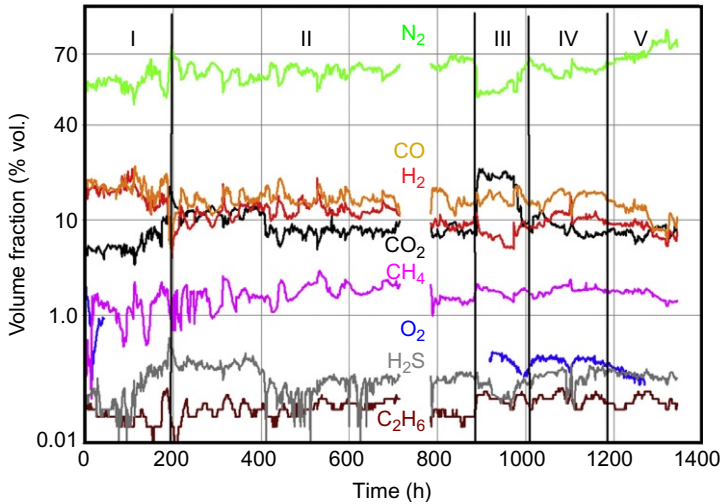
Fig. 5.22 Changes in the gas composition over the course of pilot-scale UCG trail in Wieczorek Mine (Mocek 2016).

(Kostur and Blistanova, 2009). The most intensive experimental program in this field was conducted by the UCG group from GIG. The first experiments for surface UCG simulations at GIG were designed and developed within the RFCS-funded project HUGE1 (2007–10). A schematic of the ex situ experimental apparatus is shown in Fig. 5.23.

The central part of the apparatus was a rectangular gasification chamber with dimensions of $2.6 \times 1.0 \times 1.1$ m. An artificial coal seam sandwiched between rock overburden and underburden was created in the gasification chamber. UCG simulations were carried out under near ambient pressures and at temperatures up to 1600°C using air, oxygen, and steam injected individually or as mixtures in different proportions. The product gas was purified in a gas treatment module, and part of the gas
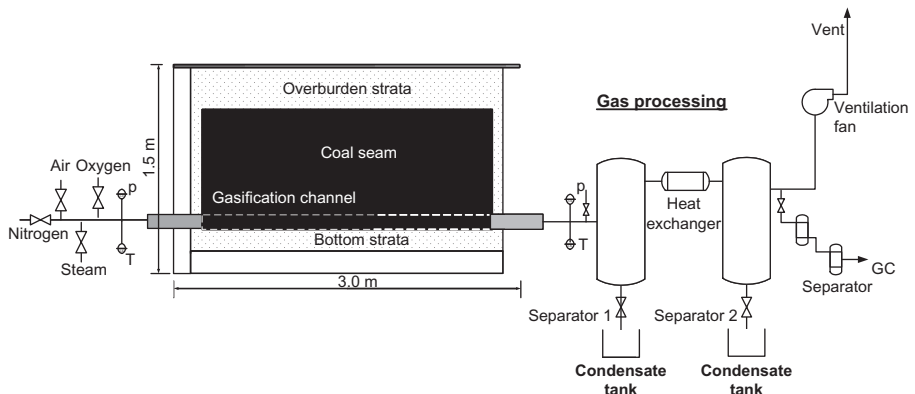
Fig. 5.23 Schematic of the experimental apparatus developed at GIG as part of HUGE1.

stream was directed to a chemical analysis line, where, after dehumidification and filtering, the main syngas components (H_2, CO, CO_2, and CH_4) were determined using gas chromatography (GC). The temperatures inside the reactor were recorded by a set of 25 thermocouples installed in various parts of the simulated coal seam and surrounding strata. Examples of typical temperature profiles during UCG experiments using Polish ortholignite are presented in Fig. 5.24.

During 2008–13, GIG carried out 12 UCG experiments using coal varying in rank from bituminous hard coals to ortholignites and applying three different gasification reagents, that is, oxygen, air, and oxygen-enriched air (OEA). It was found that oxygen was necessary to sustain the gasification process of both lignite and hard coal. Optimal oxygen/air ratios for both types of coal were identified, although the ratio was strongly related to the reactor geometry. Later, a two-stage gasification approach was applied to increase hydrogen production, which also provided invaluable information on the temperature profile of a georeactor for future thermodynamics analysis.

Using ground-penetrating radar technology, the shape of the gasification cavity was also observed. The results were described in detail in a series of articles published in FUEL (Kapusta et al., 2013; Mocek et al., 2016; Kapusta and Stańczyk, 2011; Stańczyk et al., 2010, 2011, 2012; Smoliński et al., 2012; Kapusta et al., 2016).

More advanced ex situ experimental units for UCG simulations were designed and constructed within GIG's Clean Coal Technology Centre. Two large-scale installations are currently in use there: an atmospheric pressure unit and a high-pressure (5 MPa) unit. The atmospheric pressure installation is shown in Fig. 5.25.

The maximum length of the artificial coal seam was 7 m. Oxygen, air, and steam can be used as gasification reagents, supplied individually or as a mixture. Nitrogen is used as a safety agent for inertizing and cooling down the reactor after gasification. The raw UCG-derived gas is subject to scrubbing with water to reduce its temperature, remove particulate matter, and condense high-boiling tar components. The subsequent gas treatment step involves separation of aerosols. The produced gas is finally burnt in a natural gas-fueled thermal combustor. The distributions of temperature fields during the experiments are recorded by thermocouples (Pt10Rh-Pt) installed directly in the various zones of the reaction chamber. The inlet and outlet gas temperatures (T) and pressures (p) are also monitored as the crucial operational parameters. Results of the recent experimental studies on the suitability of high moisture ortholignite for underground coal gasification process were presented in this paper (Kapusta et al., 2016).

The second, high-pressure unit (Figs. 5.26 and 5.27), allowed gasification tests to be conducted in an artificial coal seam at a maximum pressure of 5.0 MPa and at temperatures of up to 1600°C using oxygen, air, steam, and hydrogen.

5.4 Summary of recent research projects on UCG funded by the European Union

In parallel to the UCG trials in Poland, the EU-based Research Fund for Coal and Steel (RFCS) program has provided significant funding to support further UCG research in Europe.
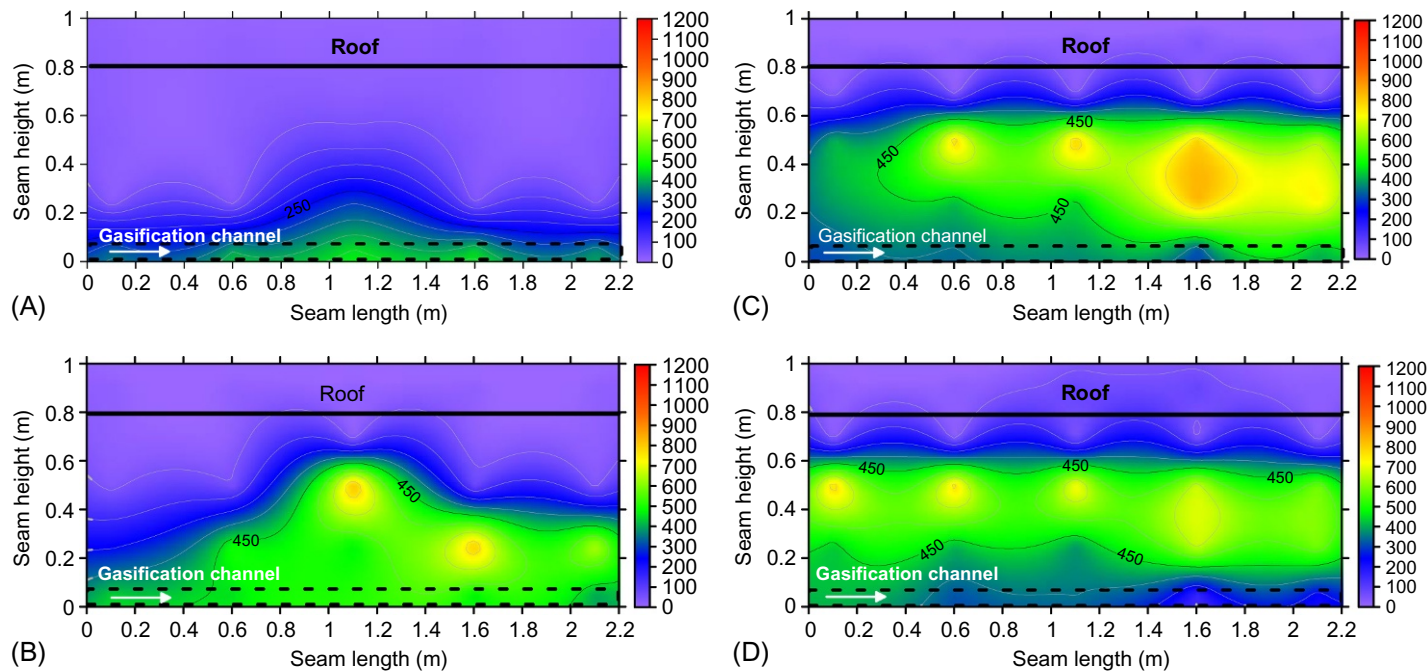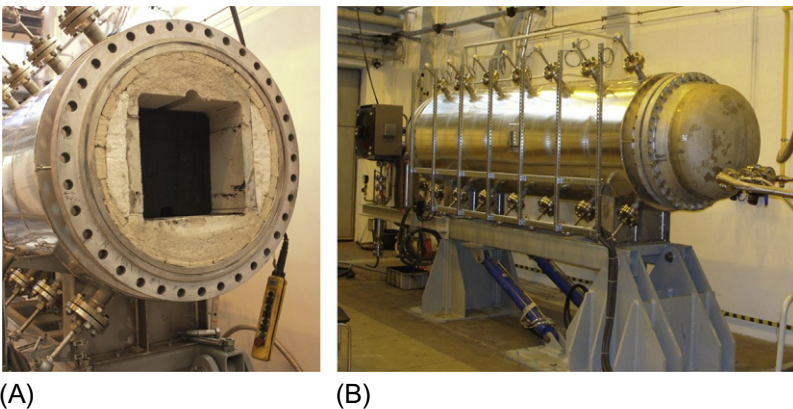
Fig. 5.24 Distribution of temperatures during experimental simulation of UCG with Polish ortholigniteat time (hours): (A) 5, (B) 15, (C) 35, and (D) 50 from the process initiation.
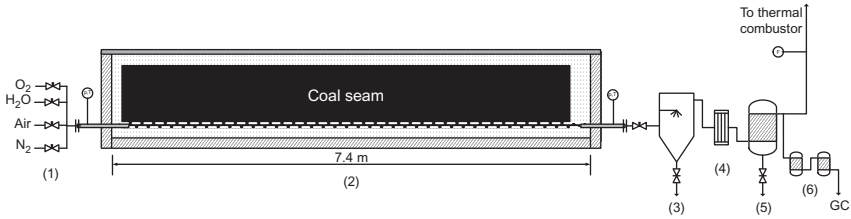
Fig. 5.25 Schematic view of the laboratory UCG installation: (1) reagents supply system and (2) gasification.
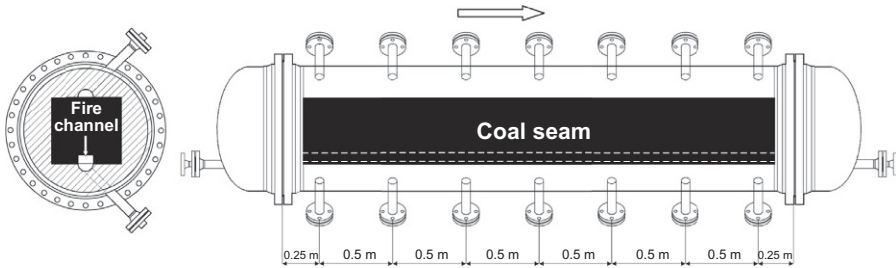
Fig. 5.26 Sections of the high-pressure reactor: (A) cross section and (B) longitudinal section.

Fig. 5.27 Experimental stand for the high-pressure simulations of UCG: (A) the reaction chamber partially loaded with coal and (B) the reactor ready for gasification.

5.4.1 Technology options for coupled underground coal gasification and CO$_2$ capture and storage (TOPS)

Technology options for coupled underground coal gasification and CO$_2$ capture and storage (TOPS) commenced in November 2013 and will complete in November 2016. The main objectives of the project are to develop a generic UCG-CCS site characterization workflow identifying the necessary technologies and to assess the potential of using a spent UCG georeactor to store CO$_2$. The project integrates research across cavity progression and geomechanics, groundwater contamination, and subsurface and surface subsidence.

5.4.2 Underground coal gasification in operating mine and areas of high vulnerability (COGAR)

The project commenced in 2013–16 and focuses on risk assessment of UCG in operating mines and in areas of high vulnerability. This project brings together a large number of underground and laboratory measurements and monitoring data collected during two underground trials (RFCS-funded project HUGE2 and a second project funded by the Polish government). The most important aspects of COGAR relate to the impact of UCG on the environment (i.e., parameters of rock strata, water and air, underground workings, and surface) and the development of a UCG-specific risk assessment methodology.

5.4.3 COAL2GAS

COAL2GAS is a research project that ran from 2015 to 2017 and addressed underground gasification of lignite in previously active conventional mining areas. The project is focusing on preparing a fully monitored, low-cost field trial at a decommissioned mine in Romania's major lignite producing area.

5.4.4 UCG&CO2STORAGE

UCG&CO2STORAGE ran from 2009 to 2010 and studied deep UCG (1200 m) and the permanent storage of CO$_2$ in the affected areas. The project began by developing site characterization strategies, hydrogeologic and geomechanical models, well panel designs, and economic assessments. The project also successfully demonstrated that CO$_2$ could be injected down the boreholes used for UCG following their modification.

5.5 Lessons learned on the way to commercialization and future trends of UCG in Europe

Research and development (R&D) of UCG in Europe has a history of over 60 years and includes significant laboratory studies, numerical modeling, and field trials at shallow and at great (i.e., >600 m) depth. Together with UCG R&D carried out in

other regions (e.g., the United States, Canada, USSR, New Zealand, South Africa, and Australia), this body of research has enabled the industry to reach a point of nascent commercialization in Europe by learning several lessons, including

  i. site selection,
 ii. public perception and the role of governments,
iii. UCG technologies—drilling, well completion, linking, reactor operations, and decommissioning

5.5.1   Site selection

Site selection is perhaps the most important factor to consider for environmental risk management (Burton et al., 2006; Mastalerz, 2011; Lavis et al., 2013; Sheng et al., 2015; Sarhosis et al., 2016a; Yang et al., 2014). The essential role of site selection is to identify a coal resource that can be gasified with minimal impact to the natural environment (i.e., the products and by-products of UCG remain in the reactor, the production well and surface facilities, and the physical changes to the geology surrounding the coal seam are minimized).

Given that UCG takes place in the natural environment, a large number of factors must be taken into consideration, including coal rank and quality, coal seam depth, hydrogeology, and the nature of the overburden. Several quantitative and semiquantitative site selection criteria have been published (e.g., Mastalerz, 2011), which are broadly in agreement, in that

- the coal seam should be deep (> 300 m) and overlain by consolidated rock with high mechanical strength, low permeability, and minimal faulting;
- the target coal seam should be saturated with water and surrounded by low-permeability rocks that are also saturated with water;
- the target coal seam should be located a significant distance from any groundwater resources or potential groundwater resources and be a confined aquifer that isolates any contaminated water from the surrounding environment.

European UCG research has mainly considered deep coal seams (>300 m deep), which is in contrast to some more recent field trials in the United States and in Australia, where thick, shallow coal seams are relatively more frequent. While the decision to concentrate on deep coals in Europe is clearly related to the fact that much of Europe's coal seams occur at greater than 300 m deep, it has been recognized for decades that, all things being equal, UCG in deep coal seams present a lower environmental risk than shallow coal seams (e.g., Burton et al., 2006). That being said, the importance of selecting a site with the appropriate hydrogeology and geology, irrespective of the depth of the coal seam, was demonstrated by the El Tremedal project, which suffered excessive water infiltration following collapse of the (relatively weak) overburden.

In addition to minimizing environmental risks, site selection plays a key role in ensuring that a commercial UCG project is profitable (Lavis et al., 2013; Nakaten et al., 2014a). Ignoring the effects of gasification efficiency and coal quality, the greater the volume of coal converted per module, the more economic the project is.

The volume of coal converted per module depends on the coal seam thickness, the in-seam length (i.e., the distance between injection and production wells), and the volume of the in situ reactor. While coal seam thickness is clearly an intrinsic property of a coal seam that cannot be changed, the other two factors are limited by site conditions and must be optimized in order to maximize the project's profitability (Nakaten et al., 2014b,c).

5.5.2   Public perception and the role of governments

Understanding public attitudes and the ways in which energy and technologies are themselves understood and used is vital for a technology to progress to commercialization (e.g., Whitmarsh et al., 2011). Before a UCG project can be undertaken, it will clearly be essential to gain approval from the public. Perhaps the clearest example of the importance of public perception to UCG was the reaction to a planned UCG trial at Silverdale in the United Kingdom (Shackley et al., 2006). Despite the project being located on a recently closed coal mine, the project was abandoned at the planning stage before a borehole had been drilled, largely as a result of objections by the local population and following a legal challenge. Following the closure, Shakely et al. analyzed the social, cultural, and institutional factors relating to the project and formed a "discussion group," where members of the public were invited to discuss issues relating to UCG. This, together with information held by the local planning authority, identified concerns relating to uncontrollable coal fires underground, waste from the UCG contaminating aquifers, danger from underground explosions, and carbon dioxide emissions. To improve public perceptions, Shackley et al. recommend the following:

1. Building trust between the developer, the regulator, and the local community
2. Ensuring greater transparency in regulatory and assessment processes, responsibilities, and liabilities
3. Providing more proactive community participation in site selection and monitoring
4. Facilitating independent reviews of the submitted case for development and regulatory data
5. Establishing a site liaison committee with membership from the local community, regulators, and site operators

Carbon dioxide emissions will remain an important factor for UCG in EU continues and any future UCG projects will have to limit CO_2 emissions to gain public acceptance and regulatory approval. The UCG industry is currently adapting to this by investigating the potential for combined UCG, carbon capture and sequestration/utilization (CCS/U), and reuse of CO_2 via processes such as enhanced oil recovery.

As UCG syngas is similar to other gases produced by industries, the technologies for capturing CO_2 from UCG syngas are in existence, well understood and widely available. Relatively little adaption of these technologies to UCG syngas will be required. The principal barrier to combined UCG-CCS is sequestration. Efforts continue around the EU to develop sequestration sites, but the progress is slow, and this, above all others, is probably the most difficult obstacle to overcome for UCG to commercialize in the EU.

The importance of clear government support is inevitable. A recent example of the importance of a clear energy strategy is the decision by Five-Quarter Energy, a UK UCG company, to cease trading despite it being prequalified for a government infrastructure guarantee worth over £1 bn. At the time of prequalification, the project was deemed to be nationally strategically important. Five-Quarter Energy, however, states that they recently ceased trading because "…global market conditions have changed, North Sea activities are in rapid decline, *and there is considerable uncertainty about the direction of government strategy for energy* (emphasis added). Five-Quarter has been unable to persuade the British government to provide supporting statements to allow it to proceed with negotiations for FDI" (source— http://www.five-quarter.com/).

Government support of UCG field trials is needed to grow our knowledge base, to gain more environmental data, and to attract more private investment. Although it is recognized that investors have confidence in the long-term future of the UCG as an option for low-carbon electricity production (e.g., Nakaten et al., 2014a; Sarhosis et al., 2016a), the technology needs to "derisked" from both economic and environmental perspectives in the near-medium term.

5.5.3   UCG technologies

There are essentially two different ways of connecting the injection and production wells: by enhancing natural permeability or by drilling and maintaining a borehole between them. The European trials undertaken in the 1980s demonstrated clearly that enhancing natural permeability using techniques, such as reverse combustion or hydrofracking, were not suitable for deep coals because high lithostatic pressure acted to reduce permeability (e.g., Patigny et al., 1989). The trials also showed, however, that it is possible to successfully link the wells using directional drilling and that the use of oxygen+water (or CO_2) are preferable to using air as the primary oxidant. As deeper coal offers both improvements in gasification efficiency and environmental risk management, future UCG projects in Europe will probably focus on using directional drilling and advanced borehole completion technologies to complete UCG modules and gasifying coal using the CRIP method (Depouhon and Kurth, 1986; EWG, 1989; Patigny et al., 1989; Henquet et al., 1985, 1998; Lavis et al., 2013). A summary of the some of the key outcomes from European R&D is shown in Fig. 5.28.

The correct operation of UCG modules is essential for protecting the environment and ensuring efficient gasification. If the pressure of a UCG reactor exceeds the hydrostatic pressure, gas loss via leakage through the reactor walls will take place. To avoid this, UCG should only take place at a pressure below hydrostatic pressure, which in addition to being surrounded by low permeability, coal and rocks that are water-saturated will ensure the reactor remains a "closed system."

UCG operators have to carefully decommission UCG modules after use because the reactors can remain hot for time periods in the order of months and years (EWG, 1989; Sarhosis et al., 2014). Left unmanaged, high reactor temperatures

Fixed injection	⟶	Controlled retractable injection point
Enhancing natural permeability for linking	⟶	In-seam drilling
Air/steam	⟶	Oxygen/water or CO_2
Shallow depths	⟶	Intermediate/great depth
Simple borehole completion technologies	⟶	High-grade corrosion-resistant steel alloys and advanced borehole completion technologies
Simple monitoring technologies (e.g., thermocouples)	⟶	Advanced monitoring techniques, mass balance calculations, and tracer gas tests

Fig. 5.28 Summary of some of the key advancements made during European UCG trials and R&D over the last 50 years.
M. Green, Presentation UCG COAL AUTHORITY LEEDS 2015.

can allow coal to continue to pyrolyze and water to vaporize, which could raise the reactor pressure above hydrostatic pressure and elevate the risk of environmental impact. To prevent this, the "clean cavern" technique was developed (Boysen et al., 1990), which involves quenching the reactor with water and nitrogen to quickly stop coal pyrolysis. The reactor is allowed to vent continuously during quenching to avoid the pressure exceeding hydrostatic pressure.

5.5.4 Future trends in UCG in Europe

The UCG industry in Europe has limited experience of operating multiple UCG modules simultaneously, which would be required for a commercial UCG project. There is also no experience of underground coal gasification (UCG) combined with carbon capture storage/utilization (CCS/U) or coal-bed methane (Sarhosis et al., 2016b). It is recognized that future commercial projects would require time to demonstrate to investors, regulators, and general public that economic, environmental, and financial risks from the technology can be managed. The UCG industry in Europe is at a very exciting time in its development; the technologies, materials, know-how, and experience necessary for UCG to commercialize in Europe have all developed and are ready for deployment. To improve investor and stakeholder confidence, it will be necessary to deploy these technologies progressively, from the initial one or two modules ("early-commercial") to perhaps from six to seven ("semicommercial") to 10 or more modules ("full-commercial") operating simultaneously. Eventually, this will be able to provide confidence and long-term commercial guarantees for the environmental impact, gas quality, and specification and help to provide Europe with a safe, economic, and domestic energy source.

5.6   Conclusions

Many countries in the EU (and worldwide) struggle to meet their energy needs despite containing very large reserves of coal, which cannot be exploited conventionally because of its depth. Application of modern UCG techniques, state-of-the-art drilling and monitoring technologies offer the opportunity to extract the energy from deep coal resources economically and with limited environmental impacts; however, several hurdles, such as public opinion and CO_2 emission limits, must be overcome before UCG can commercialize in the EU. The EU has a long history of supporting UCG projects (from the French-led trial in Morocco in the 1940s to the recent trials in Poland) and has funded some of the most important research undertaken to date. The United Kingdom, Poland, Slovenia, and Slovakia are some of the counties showing active interest in UCG. Continued support by member states will attract more private investment, enable more field trials, and allow Europe's world-class UCG experts to demonstrate that the technology is ready to provide cleaner energy from coal for the EU in the 21st century.

References

Bailey, A.C., et al., 1989. The Future Development of UCG in Europe. A Comprehensive Report to CEC, April 1989, Brussels, Belgium.

Beath, A., Craig, S., Littleboy, A., Mark, R., Mallett, C., 2004. Underground coal gasification: evaluating environmental barriers. CSIRO Exploration and Mining report P2004/5, Kenmore, Queensland, Australia, CSIRO, 125 pp.

Bhutto, A.W., Bazmi, A.A., Zahedi, G., 2013. UCG: from fundamentals to applications. Prog. Energy Combust. Sci. 38, 189–214.

Blinderman, M.S., Jones, R.M., 2002. The chinchilla IGCC project to date: underground coal gasification and environment. In: Paper to Gasification Technologies Conference, San Francisco, USA, 27–30 October 2002.

Boysen, J.E., Covell, J.R., Sullivan, S., 1990. Rocky Mountain 1 Underground Coal Gasification Test, Hanna, Wyoming, results from venting, flooding and cooling of the Rocky Mountain 1 UCG cavities. Research report, US Department of Energy contract No. DE-FG21-88MC25038, Western Research Inst, Laramie.

BP Statistical Review of World Energy, June 2015. Available at: bp.com/statisticalreview.

Burton, E., Friedmann, J., Upadhye, R., 2006. Best practices in underground coal gasification. Draft. US DOE contract no. W-7405-Eng-48. Livermore, CA, USA, Lawrence Livermore National Laboratory, 119 pp.

Chandelle, V., Li, T.K., Mostade, M., 1988. The Thulin Belgian-German field test and its outlooks. In: Fourteenth Annual UCG Symposium, 15–18 August 1988, Chicago, Illinois, USA.

Chappell, R., Mostade, M., Chappell, R., Mostade, M., 1998. The El Tremedal UCG field test in Spain – first trial at great depth and high pressure. In: Fifteenth Annual International Pittsburgh Coal Conference, 14–18 September 1998, Pittsburgh, USA.

Commission to the European Parliament and the Council European Energy Security Strategy, 2014. Available online at http://ec.europa.eu/energy/security_of_supply_en.htm.

Couch, G.R., 2009. Underground Coal Gasification. IEA Clean Coal Centre.

Creedy, D.P., Garner, K., Oajkey, J.E., Abbott, D., Edwards, J.S., Ren, T.X., Liang, J., Liu, S., 2004. Clean energy from UCG in China. Report No. COAL R250, DTI/Pub URN 03/1611, DTI Cleaner Fossil Fuels Programme, Oxfordshire, UK.

Depouhon, F., Kurth, M., 1986. UCG deep well completion with corrosion resistant alloys. In: Twelfth Annual UCG Symposium, 24–28 August 1986, Saarbrucken, Germany.

EURACOAL, 2013. Available at: https://euracoal.eu.

European Commission—IP/14/530, 2014. G7 Rome Energy Ministerial Meeting, Energy Initiative for Energy Security Joint Statement.

Fiévez, P., González Lago, J.M., Goode, A., Green, M., Mostade, M., Obis, A., 1997. Drilling, well completion and engineering activities in preparation of the first UCG trial in the framework of a European Community Collaboration, Alcorisa, Spain. In: Fourteenth Annual International Pittsburgh Coal Conference, 23–27 September 1997, Taiyuan, Shanxi, People's Republic of China.

G7 Summit—Brussels G7 Summit 2014, 2014. Available at http://www.european-council. europa.eu/g7brussels.

Gadelle, C., et al., 1985. Status of French UCG field test at La Haute Deule. In: Eleventh Annual UCG Symposium, DOE/METC-85/6028 (DE85013720).

Gadelle, C., et al., 1986. An attractive pilot test site for UCG. In: Twelfth Annual UCG Symposium, August 24–28, Saarbrucken, Germany.

Gregg, D.W., Hill, R.W., Olness, D.U., 1976. An Overview of the Soviet Effort in Underground Gasification of Coal. Lawrence Livermore National Laboratory, UCRL-52004.

Henquet, H., et al., 1985. Studies of CRIP application in deep lying coal. Eleventh Annual UCG Symposium, August 15–19, Denver, CO, USA.

Henquet, H., et al., 1998. Using Stainless steel coiled tubing in a novel application. SPE 46054, Coiled Tubing Roundtable, SPE/ICoTA, April 15, Houston, TX, USA.

International Energy Agency, 2014. World Energy Investment Outlook, Fossil Fuels.

Kapusta, K., Stańczyk, K., 2011. Pollution of water during underground coal gasification of hard coal and lignite. Fuel 90, 1927–1934.

Kapusta, K., Stańczyk, K., Wiatowski, M., Chećko, J., 2013. Environmental aspects of a field-scale underground coal gasification trial in a shallow coal seam at the Experimental Mine Barbara in Poland. Fuel 113, 196–208.

Kapusta, K., Wiatowski, M., Stańczyk, K., 2016. An experimental ex-situ study of the suitability of a high moisture ortho-lignite for underground coal gasification (UCG) process. Fuel 179, 150–155.

Kempka, T., Plötz, M.-L., Schlüter, R., Hamann, J., Deowan, S.A., Azzam, R., 2011. Carbon dioxide utilisation for carbamide production by application of the coupled UCG-urea process. Energy Procedia 4, 2200–2205.

Klimenko, A.Y., 2009. Early ideas in underground coal gasification and their evolution. Energies 2, 456–476.

Kostur, K., Blistanova, M., 2009. The research of underground coal gasification in laboratory conditions. Petrol. Coal 51 (1), 1–7.

Lavis, S., Courtney, R., Mostade, M., 2013. Underground coal gasification. In: Osborne, D. (Ed.), The Coal Handbook: Towards Cleaner Production. Woodhead Publishing Series in Energy, Vol. 1. Woodhead Publishing, ISBN: 9780857094223, pp. 226–239 (Chapter 8).

Ledent, P., 1984. What can be learned from linking tests at great depth? In: Tenth Annual UCG Symposium 1984.

Ledent, P., 1989. Retrospect of UCG Research in Western Europe. In: International UCG Symposium 9–11 October 1989. Deft University of Technology, The Netherlands.

Leplat, J., 1995. Gazéification Souterraine Profonde des Charbonds. Synthèse des recherches et experimentations françaises et étrangères. BRGM Report R 38, 266.

Liu, S., Wang, Y., Yu, L., Oakey, J., 2006a. Thermodynamic equilibrium study of trace element transformation during underground coal gasification. Fuel Process. Technol. 87, 209–215.

Liu, S., Wang, Y., Yu, L., Oakey, J., 2006b. Volatilization of mercury, arsenic and selenium during underground coal gasification. Fuel 85, 1550–1558.

Mastalerz, M.E., 2011. Site Evaluation of Subsidence Risk, Hydrology, and Characterization of Indiana Coals for Underground Coal Gasification (UCG). Center for Coal Technology Research, West Lafayette.

Mocek, P., Pieszczek, M., Świądrowski, J., Kapusta, K., Wiatowski, M., Stańczyk, K., 2016. Pilot-scale underground coal gasification (UCG) experiment in an operating mine "Wieczorek" in Poland. Fuel 111, 313–321.

Mostade, M., 2014a. Underground coal gasification: the path to commercialisation. J. Coal Prep. Soc. India. .

Mostade, M., 2014b. The Thulin UCG Field Test in Belgium – Summary of Resource and Gasification Data. UNERBEL Archives. University of Liège, Belgium.

Nakaten, N.C., Azzam, R., Kempka, T., 2014a. Sensitivity analysis on UCG–CCS economics. Int. J. Greenh. Gas Control 26, 51–60.

Nakaten, N.C., Schlüter, R., Azzam, R., Kempka, T., 2014c. Development of a techno-economic model for dynamic calculation of cost of electricity, energy demand and CO_2 emissions of an integrated UCG–CCS process. Energy 66, 779–790.

Nakaten, N.C., Islam, R., Kempka, T., 2014b. Underground coal gasification with extended CO_2 utilization—an economic and carbon neutral approach to tackle energy and fertilizer supply shortages in Bangladesh. Energy Procedia 63, 8036–8043.

Patigny, J., Li, T.K., Ledent, P., Chandelle, V., Depouhon, F., Mostade, M., 1989. Belgian-German field test Thulin – results of gasification. In: Thirteenth Annual UCG Symposium, 24–26 August 1987, Laramie, Wyoming, USA.

Roddy, D.J., Younger, P.L., 2010. Underground coal gasification with CCS: a pathway to decarbonising industry. Energy Environ. Sci. 3 (4), 400–407.

Sarhosis, V., Lavis, S., Mostade, M., Thomas, H.R., 2016a. Towards commercialising underground coal gasification in the EU. Environ. Geotechnics. Epub ahead of print.

Sarhosis, V., Jaya, A.A., Thomas, H.R., 2016b. Economic modelling for coal bed methane production and electricity generation from deep virgin coal seams. Energy 107, 580–594.

Sarhosis, V., Yang, D., Sheng, Y., 2014. Thermo-mechanical modelling around the UCG reactor. J. Energy Inst. (in Press).

Shackley, S., Mander, S., Reiche, A., 2006. Public perceptions of underground coal gasification in the United Kingdom. Energy Policy 34 (18), 3423–3433.

Sheng, S., Benderev, A., Bukolska, D., Eshiet, K., Gama, C., Gorka, T., et al., 2015. Interdisciplinary studies on the technical and economic feasibility of deep underground coal gasification with CO_2 storage in bulgaria. Mitig. Adapt. Strategies Glob. Chang. 2015, 1–33.

Smoliński, A., Stańczyk, K., Kapusta, K., Howaniec, N., 2012. Chemometric study of the ex situ underground coal gasification wastewater experimental data. Water Air Soil Pollut. 223, 5745–5758.

Stańczyk, K., Smoliński, A., Kapusta, K., Wiatowski, M., Świądrowski, J., Kotyrba, A., 2010. Dynamic experimental simulation of hydrogen oriented underground coal gasification of lignite. Fuel 89, 3307–3314.

Stańczyk, K., Howaniec, N., Smoliński, A., Świądrowski, J., Kapusta, K., Wiatowski, M., Grabowski, J., Rogut, J., 2011. Gasification of lignite and hard coal with air and oxygen enriched air in a pilot scale ex situ reactor for underground gasification. Fuel 90, 1953–1962.

Stańczyk, K., Kapusta, K., Wiatowski, M., Świądrowski, J., Smoliński, A., Rogut, J., Kotyrba, A., 2012. Experimental simulation of hard coal underground gasification for hydrogen production. Fuel 91, 40–50.

The Brussels G7 Summit Declaration. Available at http://www.consilium.europa.eu/uedocs/cms_data/docs/pressdata/en/ec/143078.pdf.

Thompson, P.N., 1978. Gasifying coal underground. Endeavour 2 (2), 93–97.

Wiatowski, M., Stańczyk, K., Świądrowski, J., Kapusta, K., Cybulski, K., Krause, E., Grabowski, J., Rogut, J., Howaniec, N., Smoliński, A., 2012. Semi-technical underground coal gasification (UCG) using the shaft method in experimental mine "Barbara." Fuel 99, 170–179.

Whitmarsh, L., Upham, P., Poortinga, W., 2011. Public Attitudes to Low-Carbon Energy—Research Synthesis. Research Councils UK, London, UK.

Wiatowski, M., Kapusta, K., Świądrowski, J., Cybulski, K., Ludwik-Pardała, M., Grabowski, J., Stańczyk, K., 2015. Technological aspects of underground coal gasification in the Experimental "Barbara" mine. Fuel 159, 454–462.

Yang, D., Sarhosis, V., Sheng, Y., 2014. Thermal–mechanical modelling around the cavities of underground coal gasification. J. Energy Inst. 87 (4), 321–329.

Further reading

Chandelle, V., Fabry, R., Kurth, M., Li, T.K., Patigny, J., Sonntag, C., 1986. Overview about Thulin field test. In: Twelfth Annual UCG Symposium. 24–28 August 1986, Saarbrucken, Germany.

Kurth, M., Li, T.K., Patigny, J., Sonntag, C., 1986. Linking and gasification in Thulin – a new endeavor. In: Twelfth Annual UCG Symposium. 24–28 August 1986, Saarbrucken, Germany.

This page intentionally left blank

Part Two

Underground coal gasification (UCG) technology development

This page intentionally left blank

The development of UCG in Australia

6

L. Walker

Phoenix Energy Ltd., Melbourne, VIC, Australia

6.1 UCG origins (1970s to mid-1980s)

The origins for the development of UCG technology in Australia can be firmly attributed to Ian Stewart, professor of chemical engineering at the University of Newcastle in New South Wales. Over the period from 1974 to 1982, Professor Stewart, with the support of a series of government research grants, undertook a detailed review of the state-of-the-art of the technology, its potential application to Australian coals, and the benefits likely to accrue from its adoption nationally.

The work undertaken over this period is described in a report (Stewart, 1984). It consisted of a number of elements:

- Visits and inspections to a number of locations in the United States, Europe, and the former Soviet Union (FSU) in 1976.
- Attendance and presentation of papers to underground coal gasification conferences in the United States (1976, 1979, and 1981) and in Europe (1979).
- Laboratory experimentation to improve the operation of borehole injection systems (Stewart et al., 1981).
- A brief review of the potential for application of UCG technology to coals in a number of states in Australia.

The report concluded that "in situ gasification of deep seams of hard coal should be commenced now to provide for future power and syngas requirements." It recommended that field development work be undertaken using known techniques, with a recommendation that this work be done either at the existing Leigh Creek coal mine site in South Australia or in the lower Hunter Valley region of New South Wales.

Late in 1981, Ian Shedden, founder of Shedden Pacific Pty Ltd, a consulting engineering company based in Melbourne, was requested by CSR Ltd to undertake a prefeasibility study for in situ gasification of the Anna lignite coal deposit in South Australia, with a review of the then-current aboveground coal gasification technologies as an alternative option (Shedden Pacific, 1981). Professor Stewart was commissioned to review the basic data for the deposit and provide a preliminary design for the UCG process and the suitability of the technology for the process. The coal analysis indicated a moisture content of 54%, an ash content of 10.9%, and a specific energy of 9.9 MJ/kg. No detail of the site geology was included, although Stewart's evaluation assumed a coal seam thickness of 4 m at a depth of 75 m and drew heavily on information gained from a review of the UCG programs in the FSU and the United States.

Shedden Pacific used this work to complete an engineering and economic study for use of the gas to generate 250 MW of power or as an alternative 2000–2500 tonnes/year of methanol (Shedden Pacific, 1983). The study concluded that "in situ gasification of the Anna deposit appears feasible and warrants further investigation." No further work on this project was reported.

Perhaps, as a follow-on from this work and in response to the developing recommendations ultimately published in Stewart's, 1984 report (Stewart, 1984), Shedden Pacific was requested by the Department of Mines and Energy (DME) and the Electricity Trust of South Australia (ETSA) to undertake a prefeasibility study of the application of UCG technology to the Leigh Creek coal deposit. The study was undertaken with the assistance of Professor Stewart (UCG process design) and Dr. Len Walker, a geotechnical engineer with consulting engineering firm Golder Associates Pty Ltd (geology, rock mechanics, and groundwater evaluation).

Lobe B in the Leigh Creek coal deposit was estimated to contain a reserve of some 120 million tonnes of coal, with seams ranging in thickness from 8 to 13 m at depths projected to 400 m and with the coal analysis indicating a moisture content of around 26%, an ash content of 20%, and a specific energy of 14–15 MJ/kg.

The project report (Shedden Pacific, 1983) describes the UCG process design, the gas and wastewater treatment, and the design of 2×35 MW gas turbines for power generation, with provision for expansion to 250 MW. Indicative levelized power costs were estimated to be around 3 c/kWh for the larger plant, significantly below the cost of alternative energy sources. The report recommended a project development program involving field geotechnical work, gas turbine evaluation for combustion of low calorific fuels, and initial demonstration of gas production prior to design and construction of the 70 MW plant.

Although a further field investigation program was undertaken (Dames and Moore, 1996) to assess in more detail the impacts of the geotechnical properties of the rocks and the permeability of the coal seam, the project was not developed further due to the lack of financial support. Despite significant efforts by the various parties, no further funding for the project was obtained, and it was shelved.

By the middle of the 1980s, the oil price had dropped from a high in April 1980 of US$40/bbl to a low of US$10.25 in March 1986, thus reducing the incentive to develop alternative energy sources, causing severe cuts in government funding for research programs, and limiting any immediate further interest in the technology in Australia. However, the work undertaken had a clear focus on commercial project development using existing knowledge rather than the undertaking of new research activities. This approach was to be taken up in later years, supported by commercial rather than government funding, as detailed in following sections.

## 6.2   The quiet period (mid-1980s to 1999)

The lack of funding for the Leigh Creek project effectively ended the prospect for further development of the UCG work initiated by Professor Stewart. However, the authors of the report (Stewart, Shedden, and Walker) maintained their interest in

the technology and, over the following years, reviewed potential opportunities for applying it in Australia.

By 1988, Walker had assessed the prospects for developing UCG projects in both Queensland (Surat coal basin) and New South Wales (Gunnedah coal basin) due to the abundance of coal available and the lack of any interest in underground mining of deep coal deposits in these basins. The focus eventually turned to Queensland as a result of greater interest from the relevant government department. As a result, in 1988, he applied for coal exploration licenses in the Ipswich and Chinchilla areas. The former was a coal-mining area some 50 km from Brisbane, with an old power station nearby (Swanbank) being considered for shutdown. The Chinchilla area was selected because of the likely large size of a prospective underground coal deposit, sufficient for a major, long-term project. The location of Chinchilla is shown in Fig. 6.1.

Late that year, Walker commissioned a preliminary study into the potential for supplying UCG syngas to the Swanbank station and adapting the existing coal burner system to receive the gas (Kinhill Engineers, 1989). The study was undertaken with the support of CS Energy, the owner of the power station, and concluded that electricity could be generated and supplied to the existing grid at a competitive price. Despite these efforts, no funding could be raised for developing the project, and the coal applications were dropped.

The lack of interest in financial support for UCG development continued for the rest of the decade, although by the end of 1990 the oil price had increased back above US$20, with a peak of US$40. These fluctuations, and the previous work undertaken
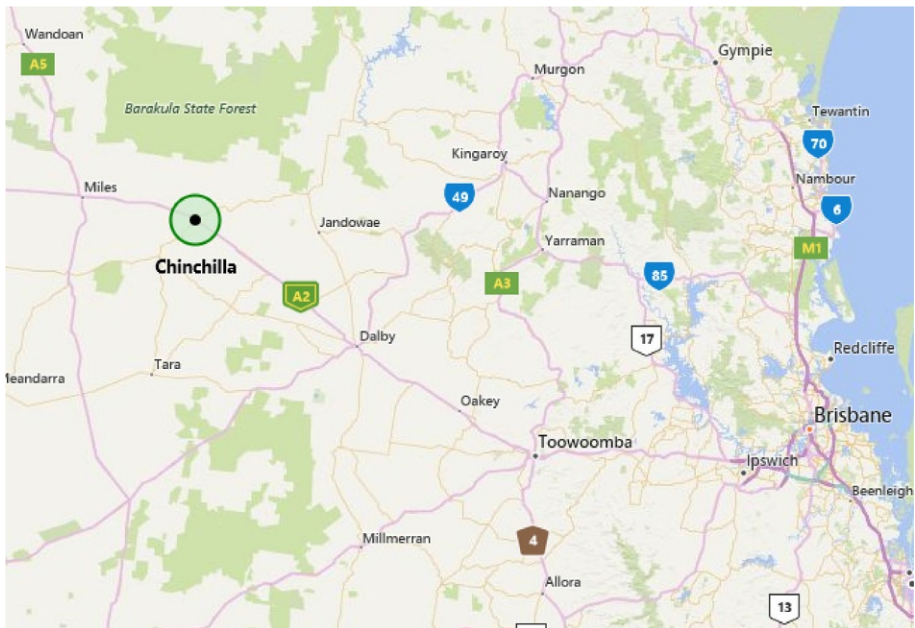
Fig. 6.1 Surat Basin coalfield—Queensland.

on the commercial prospects for UCG in Australia, helped to maintain an underlying interest in the technology (Walker et al., 1993). During this time, Walker had a number of meetings with US companies involved in the successful Rocky Mountain 1 test in Wyoming. As a result of this continuing interest, he founded Linc Energy Ltd in October 1996 with the purpose of acquiring rights to coal in Queensland (following his initial efforts in 1988) and commercializing the technology in that state. Linc Energy lodged applications for three exploration permits for coal (EPCs) in Queensland, one each near Chinchilla and Ipswich west of Brisbane and one in the Galilee basin 300 km south of Townsville (Walker, 1999).

At the time that Linc Energy was founded, the international activity in UCG technology involved the effective closure of the development effort in the United States and the undertaking of a demonstration pilot project in Spain (the El Tremedal project). Both these activities had adopted the so-called CRIP technology involving the use of long deviated horizontal wells in the coal seam for both oxidant injection and for product gas recovery, which was proposed as the "way of the future" for the technology.

This situation changed in February 1997, when contact was made between Walker and Dr. Michael Blinderman, a UCG technologist from the FSU program. Dr. Blinderman had been at the center of the Soviet National UCG program and worked at the Angren (Uzbekistan) UCG plant and at the Yuzhno-Abinsk UCG plant in Siberia. It turned out that in 1994, Dr. Blinderman and his colleagues established a UCG technology company, Ergo Exergy Technologies (Ergo Exergy), which by 1997 was providing UCG expertise to several projects then under development in the United States, India, and New Zealand. Walker and Blinderman reached an agreement to develop a commercial UCG project in Australia, with Walker selecting a suitable coal deposit and organizing the commercial structure for the venture and Blinderman with Ergo Exergy providing the UCG technology based on their previous practical experience.

As a result of his review of historical UCG experience in the FSU, summarized in a US research report (Gregg et al., 1976), Walker was convinced of clear predominance of the FSU experience over work done in other countries and saw great value in visiting an FSU UCG plant and witnessing its performance. On Walker's request, Walker and Blinderman visited the Angren (Uzbekistan) UCG facility in May 1997—the first of three such trips to cement ongoing relationships between the parties. As a result of this visit and a review of past literature, it was agreed that the use of the Ergo Exergy technology, stemming from the vast R&D efforts in the FSU and the experiences of commercial-scale operations at the Angren plant, was the most effective means of developing a commercial UCG operation in Australia.

With the support of Ergo Exergy, Linc Energy in 1997 undertook a joint preliminary feasibility study with Austa Energy for a power station near Ipswich in Queensland fueled by UCG gas (Austa Energy and Linc Energy, 1997). Austa Energy was at the time a Queensland Government-owned company providing engineering services and creating business development opportunities for the state government. The report concluded that "power can be produced from this gas at least 25% cheaper than from a coal-fired power station costed on a comparable basis" and that the cost of the gas

production was "less than half the expected cost of natural gas." In preparation of the report and after reviewing the geology data and visiting Linc Energy coal tenements in Ipswitch and Surat basin, Ergo Exergy experts recommended the site near Chinchilla for initial UCG development in Australia in clear preference to the Ipswitch location.

With this report as confirmation of the commercial viability of the UCG process for power generation, Linc Energy sought a listing on the Australian Stock Exchange (ASX) and on 30 June 1998 lodged with the Australian Securities Commission a prospectus for the raising of A$4 million to undertake "a pilot burn on EPC(A)-635 (at Chinchilla) as phase 1 of a power generation project on the site" (Linc Energy, 1998). The Linc Energy directors at the time were Walker, Blinderman, and Mike Ahern, expremier of Queensland appointed as chairman. In August 1998, the prospectus was withdrawn as a result of the poor investment climate at the time. As a result, Linc Energy commenced negotiations with a number of companies with an existing commercial interest in power generation, ultimately signing a joint venture agreement in June 1999 with CS Energy, one of the Queensland Government-owned power-generating companies (Walker, 1999). The joint venture proposed an initial pilot burn at the Chinchilla site, to be followed by installation of a small-scale power plant of about 40 MW.

At about this time, CSIRO was developing an interest in UCG and in March 1999 held a workshop to discuss its potential in Australia. The workshop was led by Burl Davis, experienced in the UCG demonstration projects undertaken in the United States that were funded by the US Department of Energy. Following this workshop, a 6-year UCG research program was initiated by CSIRO focused on various aspects of the technology and site selection (Beath et al., 2000, 2003). It was during this time that Linc Energy initiated the first Australian demonstration of UCG technology at Chinchilla.

6.3   Initial success—Linc Energy at Chinchilla (1999–2004)

The joint venture between Linc Energy and CS Energy commenced in June 1999 and focused on the production of syngas as the first phase in the development of a 67 MWe IGCC project (Walker et al., 2001). The project was funded by CS Energy with the assistance of a research grant from the Australian government.

The project site involved the development of the MacAlister coal seam 10 m thick at a depth of 120 m. A site characterization program was initiated in June 1999 and concluded with UCG-specific in situ testing in September 1999. Properties of the coal are set out in Table 6.1.

Construction, commissioning, operations, controlled shutdown, and post-gasification monitoring of gasification panel at Chinchilla were based on the Ergo Exergy UCG technology and effected under direct supervision of Ergo Exergy UCG experts led by Dr. Blinderman. The UCG facility used air injection and reverse combustion linking to connect nine process wells to the gasifier over the period of operation (Blinderman and Fidler, 2003). First gas production was achieved on 26 December 1999, and the plant (Fig. 6.2) operated continuously until April 2002,

Table 6.1 **Chinchilla coal properties**

|	
Moisture %	6.8
Ash %	19.3
Volatile %	40.0
Fixed carbon %	33.9
Total %	100.0
Total moisture	10.1
Relative density	1.50
SE MJ/kg	23.0

Fig. 6.2 Chinchilla UCG production site.

with the gas being flared over this period. The process produced syngas at a calorific value of about 5 MJ/Nm^3, at a pressure of 10 barg and temperature up to 300°C.

Continuous gas production was achieved over the period of operations (Fig. 6.3), with some 35,000 tonnes of coal being gasified and with no evidence of environmental impact (Blinderman and Fidler, 2003). However, a controlled shutdown of operations was initiated in April 2002 (Blinderman and Jones, 2002), largely as a result of limited project finance being available following the terrorist attacks in the United States in September 2011.

As part of the project operation and ultimate shutdown, considerable attention was paid to the interaction between site geology and hydrogeology, described in detail by Blinderman and Fidler (2003). The factors most relevant to the UCG operations included the following:

- Overlying alluvium 10–20 m deep, generally dry over the UCG operating site, with a groundwater level 30–35 m belowground level.
- A known aquifer system in the Hutton Sandstone, at a depth of approximately 600–650 m.

Cumulative gas production
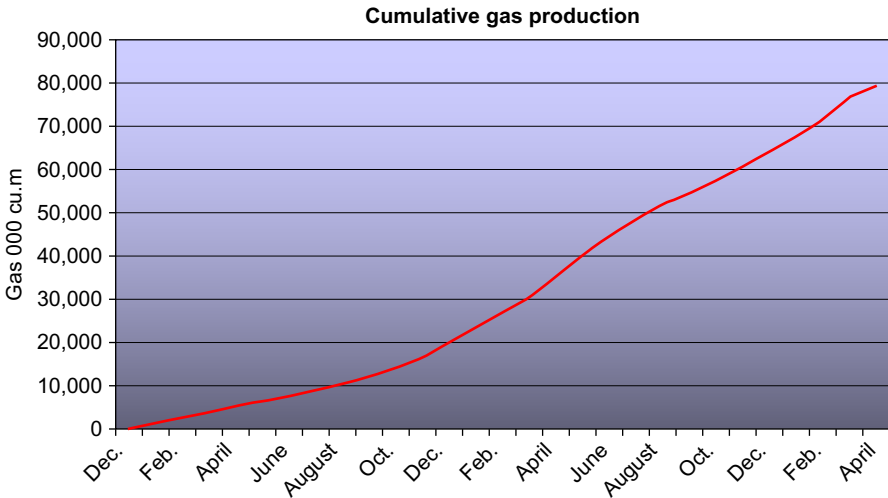
Fig. 6.3 UCG oroduction at Chinchilla—from December 1999 to April 2002.

- A significant fault some 300 m to the northwest of the operating area, with a throw estimated at 40 m, disrupting the hydraulic continuity of the coal seam in that direction.
- Coal seam thickness of 10 m at a depth of 120 m, dipping at $1°$–$5°$ to the south-southeast.
- Methane present in the coal seam, requiring monitoring bores to be sealed at the surface.
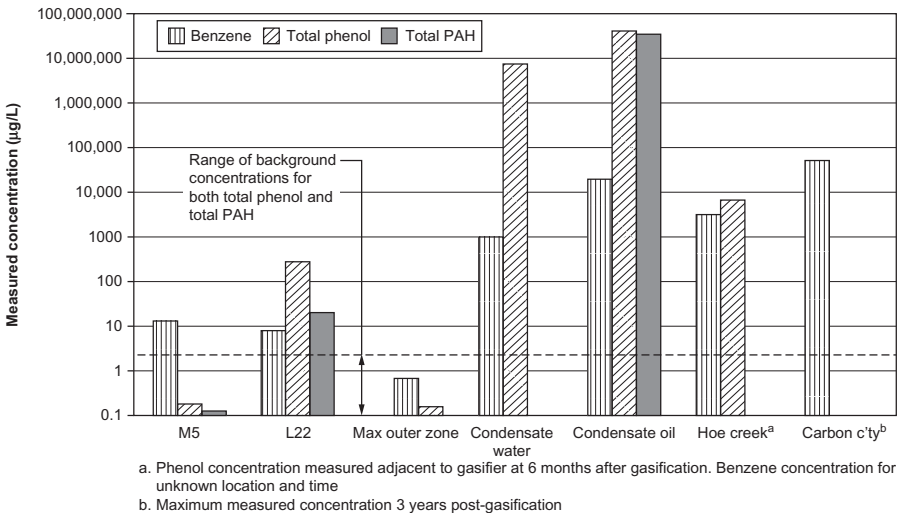
The general site layout is shown in Fig. 6.4.

Groundwater measurements indicated a hydraulic gradient of 0.0015 toward the southwest, i.e., subparallel to the fault shown in Fig. 6.4. Groundwater quality was generally poor, with total dissolved solids in the range of 1400–3900 mg/L. Pump testing to determine the permeability of the coal seam was not possible because of the impact of methane gas, with packer testing giving a wide range from 4×10^{-5} to 2×10^{-9} m/s, with a significant anisotropy being evident, and maximum permeability along the northeast/southwest axis. Testing showed high gas conductivity in the coal seam ranging between 0.3 and 1.5 darcy.

As indicated in Fig. 6.4, five vibrating wire piezometers (VWPs) and seven groundwater monitoring bores were located within an inner zone of about 300 m radius, and seven monitoring bores were outside this zone, three of which were installed prior to the cessation of air injection in the shutdown process. Blinderman and Fidler (2003) noted that a hydraulic connection existed between the process well area and monitoring bore M5 some 200 m away, confirming the high permeability in this direction and the effective extent of the gasifier area.

Groundwater samples were taking during the shutdown period from monitoring bore M5 and from the process well L22 located in Fig. 6.4 to assess the impact of the shutdown process. The results from these measurements are shown in Fig. 6.5 and were compared by Blinderman and Fidler (2003) with results from measurements
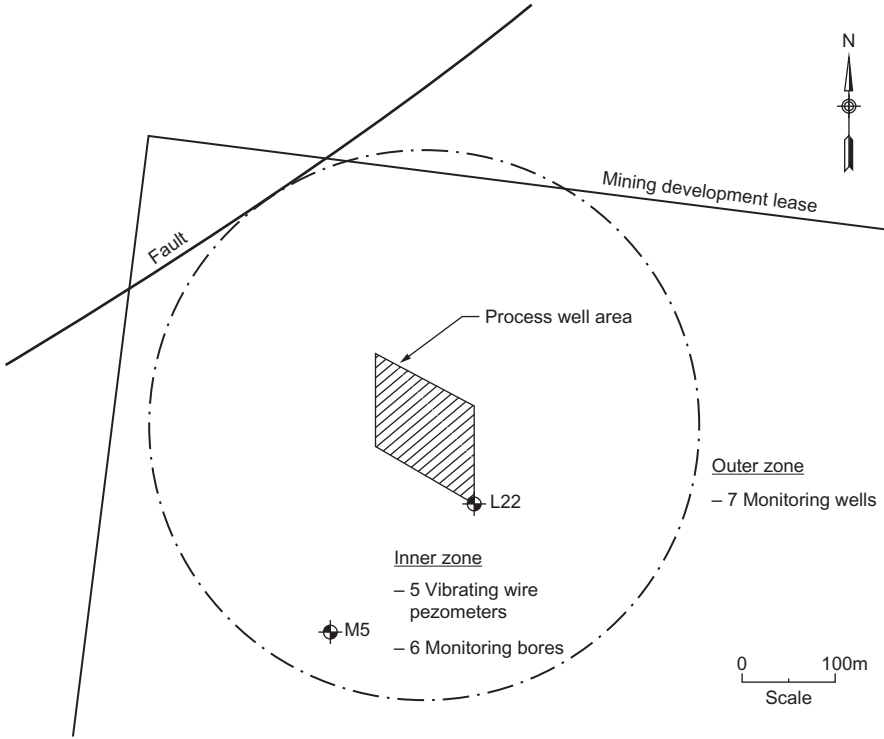
Fig. 6.4 Chinchilla site layout and monitoring system.
From Linc Energy UCG trial, Queensland Government.

a. Phenol concentration measured adjacent to gasifier at 6 months after gasification. Benzene concentration for unknown location and time
b. Maximum measured concentration 3 years post-gasification

Fig. 6.5 Results of groundwater quality monitoring (Blinderman and Fidler, 2003).

of the condensate water and from two other projects in the United States (Hoe Creek and Carbon County). The levels detected at the end of shutdown were below the advisory levels published by the USEPA and well below the levels at the US sites. The authors emphasized the need for proper operation of the cavity to ensure potential groundwater contaminants are removed in the condensate water.

As a result of its financing of the Chinchilla project, CS Energy had effective ownership and financial control of Linc Energy and the Chinchilla project. Late in 2001, CS Energy requested a review of the technical and economic viability of UCG technology for power generation, which was completed in April 2002 (Blinderman and Spero, 2002). Although the report resulted in positive recommendations for the Chinchilla project, CS Energy chose to withdraw from the joint venture in the absence of alternative project funding. It elected in May 2002 to close down the existing project, which led to the controlled shutdown process described above, and to offer its interest in the company for sale. Despite expressions of interest from a number of parties, a sale was not achieved until early 2004. The CS Energy shares were purchased by Peter Bond, a coal-mining entrepreneur, the Linc Energy board was restructured, and discussions about reestablishing the Chinchilla project followed.

In March 2006, the company issued a prospectus for raising A\$22 million and listing on the ASX (Linc Energy, 2006a). The funds were raised, and the company commenced trading on 8 May 2006. The prospectus described the company's business plan to use the UCG process to "deliver on its business to turn coal deposits into commercial quantities of diesel and jet fuels." In November 2006, with Ergo Exergy's termination of involvement with the Linc Energy as its technology provider, Linc Energy announced the signing of a UCG technology agreement with the Skochinsky Institute in Moscow (Linc Energy, 2006b).

Following the initial success of the Linc Energy project at Chinchilla (1999–2004), its successful listing of on the ASX, and its proposal to produce commercial quantities of liquid fuels, interest in UCG technology in Australia expanded. Over this period, the oil price accelerated past US\$40/bbl toward \$100/bbl, reinforcing the potential for commercial production of syngas using the UCG process, with its economic advantages over the alternative of surface gasification.

As a result of these factors, corporate interest in adopting UCG technology to develop commercial projects widened, with ASX listings as a focus for funding, and a range of potential end products being promoted. However, available information on these activities has been generally restricted to corporate presentations and ASX announcements rather than formal reviewed publications in professional journals. The reviews that follow below draw largely on this material that, by its nature, presents a preferred corporate perspective rather than a critical and technically substantial appreciation of project activity.

6.4   Rapid progress—Three active projects and many followers (2006–11)

6.4.1   The three active projects

6.4.1.1   Linc Energy

In September 2007, Linc Energy announced (Linc Energy, 2007a) that it had commenced producing UCG gas from a new field (subsequently referred to as gasifier 2) and in October that year (Linc Energy, 2007b) announced its purchase of a controlling interest in Yerostigas, the owner and operator of the UCG gas project at Angren in Uzbekistan, the largest of the UCG projects developed in the FSU. It also announced (Linc Energy, 2007c) the fabrication at Chinchilla of a demonstration gas-to-liquid (GTL) plant designed to convert the UCG syngas produced into liquid fuels.

Over the following 4 years, Linc Energy undertook the development of a succession of gasifiers represented as providing progressive improvements to the design of the UCG process. In July 2008, the company announced (Linc Energy, 2008a) it had completed the development of gasifier 3 and was finalizing testing of the GTL demonstration plant (Fig. 6.6). Subsequently, in October that year, the company announced its first production of liquid fuels from UCG syngas (Linc Energy, 2008b).

In March 2009, Linc announced the design of gasifier 4 to produce UCG syngas at a commercial rate of 5 PJ/annum (Linc Energy, 2009a). In November 2009, the company announced that this gasifier was to be commissioned by the year's end and that the design of gasifier 5 was also in progress (Linc Energy, 2009b). Gasifier 4 was reported to be in operation in February 2010, with gasifier 5 being planned to be

Fig. 6.6 Linc Energy GTL plant at Chinchilla.

developed on the company's new project in the Arckaringa Basin in South Australia (Linc Energy, 2010a). In May 2010, Linc announced the use of oxygen injection for the first time, being applied to gasifier 4 (Linc Energy, 2010b). Gasifier 5 was ultimately ignited at the Chinchilla site in 2011 and according to Linc Energy operated for 2 years over 2012/2013, testing both air and oxygen injection (Linc Energy, 2013a).

A summary of the sequence of Linc Energy's gasifier construction and operation as provided by the company (Linc Energy, 2013a) is shown in Table 6.2, and the location of the five gasifiers developed on the Chinchilla site are shown in Fig. 6.7 (Linc Energy, 2013a).

Linc Energy presented gasifier 5 as containing the design and implementation procedures that it would use to advance to commercial development. The design involved connecting one deviated in-seam injection well, installed using a coil tube rig, with a vertical production well 880 m away, as indicated in Fig. 6.8. Commercial production was to be achieved by replicating this system.

The performance of this gasifier was summarized (Linc Energy, 2013a) as follows:

- Start-up on 22 October 2011.
- Shutdown on 4 November 2013.
- 730 days on stream.

Table 6.2 **Linc Energy gasifier operating sequence**

Linc Energy's UCG Gasifier development and operation

Gasifier Design	Operated	Well Configuration	Oxidant	Comments
1	1999–2001	Linked Vertical Wells	Air	Designed for power generation
2	2007	Linked Vertical Wells	Air	
3	2008–2009	Linked Vertical Wells with Horizontally Drilled Linked	Air	Syngas first used in GTL plant Employed at Yerostigaz
4	2010–2012	2 parallel directionally drilled horizontal wells	Air, Enriched Air	Coiled tubing used for oxygen injection and well work-over
5	2011-2014	1 directionally drilled horizontal well and 1 vertical well	Air, Enriched Air, Pure Oxygen	Coiled tubing used for ignition and continuous oxygen injection

10
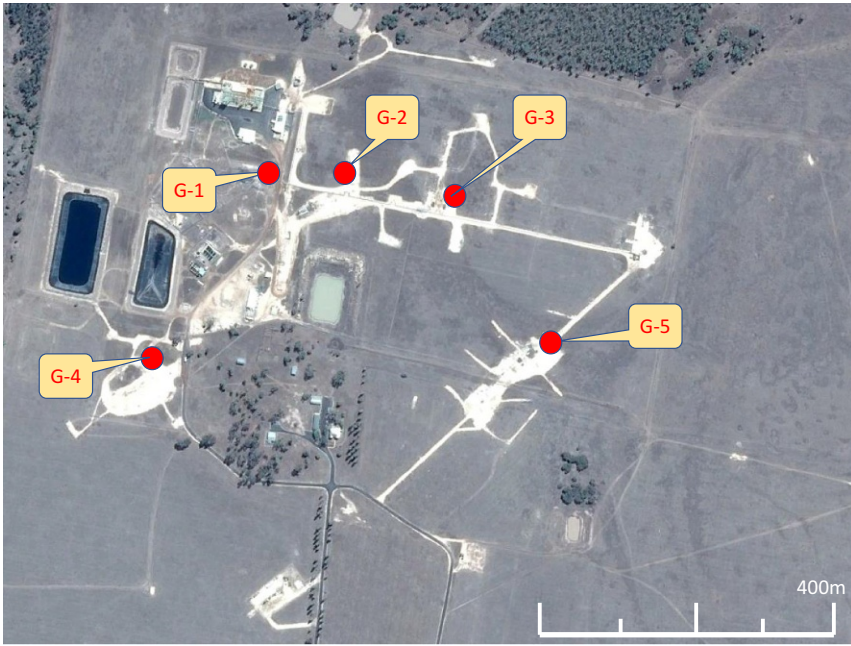
Fig. 6.7 Location of gasifiers 1–5 on the Linc Energy Chinchilla UCG site.

Fig. 6.8 Linc Energy gasifier 5 construction.

Twelve successive retractions of the injection well were completed, using both air blown and oxygen blown injection, with enrichment levels varying from 21 (air) to 100% (oxygen). Calorific values for the product gas up to 6.2 MJ/Nm^3 were achieved for air injection and up to 10.2 MJ/Nm^3 for oxygen injection. During operations, cavity growth models were constructed, and validation using field instrumentation was claimed, although no detailed presentation of these data has been published.

During the period of operation of the gasifier sequence described above, Linc Energy also developed a wide range of interests in the broader oil and gas industry, and further progress of the proposed GTL plant at Chinchilla stalled after shutdown of gasifier 5. This lack of further progress was also accentuated by the declining confidence in support for UCG technology exhibited by the Queensland Government.

It is difficult to assess the actual progress of Linc Energy's development of gasifiers 2–5 from their published information. However, in 2014, Linc Energy was charged under Queensland's Environmental Protection Act with five counts of wilfully and unlawfully causing serious environmental harm. The charges were subjected to a hearing in the Magistrates Court of Queensland in October/November 2015, and the decision to commit the company to trial was handed down on 11 March 2016 (Queensland Government, 2016a,b).

From the evidence presented at the hearing, it is clear that

- Pressures of between 28 and 48 bar were used in gasifier 2.
- Gases escaped "directly to the surface" from gasifier 2.
- Pockets of syngas were intersected in the overburden during drilling for gasifier 3.
- Gasifier 4 exhibited gas escapes from monitoring bores and bubbling of gas at the surface.
- Gas escapes from monitoring bores over the operational period of gasifier 5.
- Gasification pressure in gasifiers 2–5 consistently exceeded hydrostatic groundwater pressure.

From the above, it is evident that Linc Energy had technical difficulties in managing process operations at the Chinchilla site throughout the operation of gasifiers 2–5, which may at least partly explain the number of gasifiers developed. The apparent communication of gas across the site would appear to be consistent with the high horizontal permeabilities reported by Blinderman and Fidler (2003).

6.4.1.2 Carbon Energy

The program of research work undertaken by CSIRO early in the 2000s was led by Dr. Cliff Mallett and culminated in the formation of a wholly owned company (Coal Gas Corporation Pty Ltd-CGC) and its acquisition of three coal leases in the Surat Basin covering an area of 2375 km^2. In July 2006, a company listed on the ASX (Metex Pty Ltd) announced (Carbon Energy, 2006) that it had taken a 50% interest in CGC and provided $2.5 million for the company to progress "identifying and developing a suitable underground coal deposit for demonstration and development of the UCG process" and that "the initial trial would target coal seams at greater than 400 m depth."

Exploration drilling on the leases commenced in January 2007, and in May that year, the company announced (Carbon Energy, 2007a) that it was completing the

design of its demonstration plant, due for construction from September and had secured an exclusive alliance with Burl Davis (the United States) "to assist in the detailed design and operation of UCG." Davis had led the workshop on UCG organized by CSIRO in March 1999. By this time, CGC had been renamed Carbon Energy Ltd, and in November 2007, Metex purchased the remaining shares in the company, and Mallett joined the Carbon Energy board (Carbon Energy, 2007b). In July 2008, Metex changed its name to Carbon Energy Ltd (Carbon Energy, 2008a).

Carbon Energy had chosen a site at Bloodwood Creek in the Surat Basin containing a coal deposit in the same geological sequence and with similar properties to that utilized by Linc Energy in Chinchilla, with an operating depth of 200 m. The company elected to use the basic concept of the CRIP system, involving two parallel in-seam boreholes 850 m long and 30 m apart, with a vertical well for ignition as was developed in the United States in the 1980s. However, a modification to the injection well retraction system was incorporated into the design, referred to as the "key seam" technology.

Completion of the installation of the first panel was announced in August 2008 (Carbon Energy, 2008b), and ignition and initial gas production followed on October 8. However, several months later, the company reported a blockage in the injection well that required a "reconfiguration of the well layout" (Carbon Energy, 2008c). It is understood that with the horizontal injection well blocked, this involved the use of supplementary vertical wells for injection. The first 100 days of the trial was completed in February 2009 (Carbon Energy, 2009), and planning commenced for a commercial-scale UCG panel (panel 2) to be constructed with the installation of a small power plant (5 MW) to be later expanded to 20 MW (Carbon Energy, 2010a). Ultimately, the first panel was abandoned (Carbon Energy, 2010b), as it was considered "not cost-effective" to continue with its remediation. A delay in construction of the new panel occurred when the government in July 2010 required an environmental evaluation report from the company on the discharge of surface water from the test site (Carbon Energy, 2010c). This issue was resolved early in 2011, and panel 2 was ultimately installed and commissioned in March 2011 (Carbon Energy, 2011a).

The location of the two panels on the site is shown in Fig. 6.9 (Carbon Energy, 2013), with a horizontal separation of about 60 m. Published test data on gas composition from the second panel are shown in Table 6.3 for both air and oxygen injection. Subsequently, Carbon Energy advised in October 2011 of its first production of electricity from gas engines using the UCG syngas as a fuel (Carbon Energy, 2011b), but that further expansion to 5 MW and export of power to the grid system needed a modification to their existing environmental approvals. Panel 2 operated for 577 days and gasified 12,745 tonnes of coal, which corresponds to less than 2500 Nm^3/h average gas production flow rate.

Fig. 6.10 presents the calorific value (higher heating value) for a continuous 12-month operating period of panel 2 using air injection.

As part of the operation of panel 2, Carbon Energy undertook a survey of the extent of the gasification cavity using thermal and electroseismic techniques. The results from this survey are presented in Fig. 6.11, with the scale indicated by the 5 m spacing
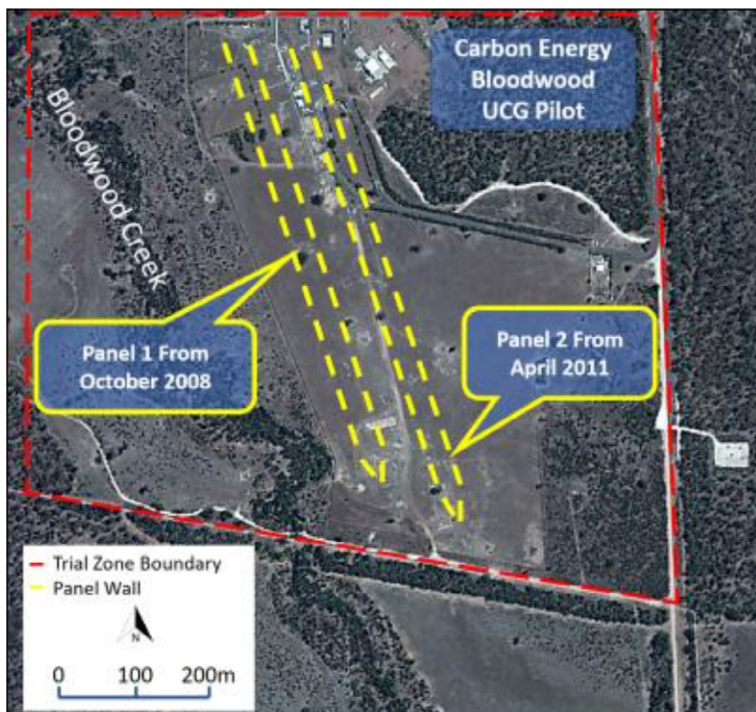
Fig. 6.9 UCG panel locations at Carbon Energy's Bloodwood Creek UCG site.

Table 6.3 Carbon Energy panel 2 gas composition—air and oxygen/steam blown

Primary constituents—dry gas basis	Average—mole % oxygen/steam blown	Average—mole % air blown
Hydrogen (H_2)	26.66	20.94
Methane (CH_4)	19.06	8.60
Carbon monoxide (CO)	7.13	2.56
Ethane (C_2H_6)	1.42	0.54
Carbon dioxide (CO_2)	45.21	21.63
Nitrogen (N_2)	0.28	44.67
Average calorific value—LHV (MJ/Sm^3)	10.94	5.71
Average calorific value—HHV (MJ/Sm^3)	12.24	6.46
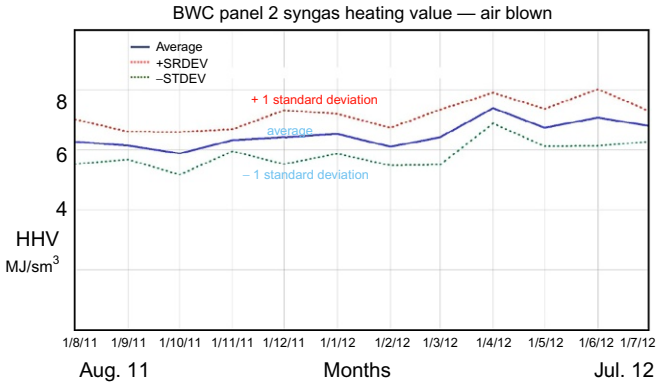
Fig. 6.10 Carbon Energy panel 2—syngas production.
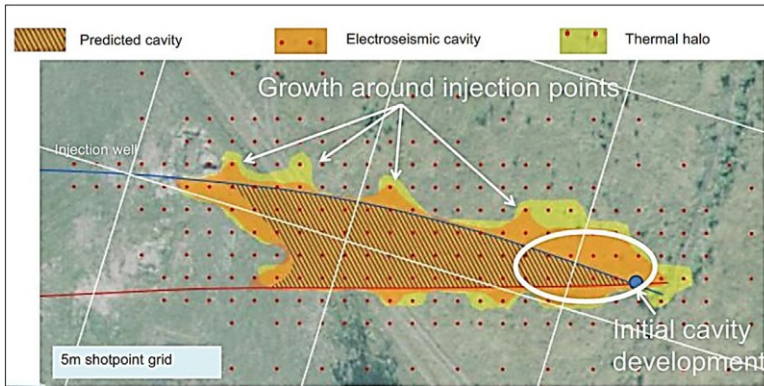
Fig. 6.11 Carbon Energy panel 2 gasification cavity.

of the electroseismic shot points. The data showed the capability of surface measurement techniques to define the extent of the underground cavity created, although the results have not been verified by extensive postgasification drilling into the cavity.

Further development of panel 2 and Carbon Energy's Bloodwood Creek project overall were delayed pending a review of UCG technology commissioned by the Queensland Government (refer to Section 6.7.3). Regardless of the findings of this report, the government placed a ban on further UCG development in April 2016 and ordered Carbon Energy to decommission UCG operations and rehabilitate the site.

The Carbon Energy test at Bloodwood Creek was undertaken on the same Surat Basin coal seam as that undertaken by Linc Energy at Chinchilla. It is of interest to compare the published data from these two tests, gasifier 1 at Chinchilla (using vertical wells and shutdown in 2002) with panel 2 at Bloodwood Creek (using the modified CRIP system). The results are shown in Table 6.4.

Table 6.4 **Test data comparison**

Item	Chinchilla (gasifier 1)	Bloodwood Creek (panel 2)
Total coal gasified	35,000 tonnes	12,750 tonnes
Operating period	850 days	577 days
	Air injection	Air injection
CV of product gas (LHV)	5.7 MJ/m^3	5.6 MJ/m^3
Max. coal usage	49 t/day	21 t/day
Max. energy prodn. rate[a]	750 GJ/day	325 GJ/day
Gas production rate	5470 m^3/h	2420 m^3/h
Energy produced/tonne coal	15.0 GJ/t	14.7 GJ/t
Panel area tested	2300 m^2	850 m^2

[a]Note that a 30 MW power plant will require syngas at a rate of about 6600 GJ/day.

Data in the table confirm that the Chinchilla test, when compared with the Bloodwood Creek test:

• Operated for 50% longer.
• Gasified nearly three times as much coal, with an effective panel area three times the size.
• Showed twice the average daily coal usage rate and more than twice the maximum gas production rate.

The average daily gas production rate in 1965 at the Angren plant in the FSU is reported (Gregg et al., 1976) at 12,900 GJ/day, approximately 17 times the rate for the Chinchilla test and 40 times the rate at the Bloodwood Creek test.

The above data confirm the continuing relevance of the large-scale UCG process procedures developed in the FSU while also illustrating the considerable expansion in gas production rates required to achieve a scale suitable for commercial development.

6.4.1.3 Cougar Energy

Cougar Energy was formed by Dr. Len Walker as an ASX listed company in October 2006, some 4 years after closure of the first successful Linc Energy demonstration at Chinchilla. The company acquired the rights to develop a UCG project on a coal deposit near Kingaroy, 150 km northeast of Brisbane in Queensland, and on additional potential deep coal deposits in the Surat and Bowen basins. The UCG technology was provided under a license agreement by Ergo Exergy. The coal seam selected for development at the Kingaroy site was the Kunioon seam, which ranged in thickness from 7 to 17 m, at depths from 60 to 206 m. The coal properties are summarized in Table 6.5.

Following resource definition and site characterization work, development of the Kingaroy project was planned in the following stages:

• Ignition and syngas production, gas cleaning, and flaring for a period of 6–12 months.
• Power generation by gas engines or gas turbine up to 30 MW.
• Expansion of power generation to 200 MW and then 400 MW.

Table 6.5 **Kunioon coal seam properties**

Coal properties (as received—% by weight)	
Relative density	1.59
Inherent moisture	4.85%
Ash	35.1%
Volatile matter	25.2%
Fixed carbon	32.6%
Total sulfur	0.25%
Specific energy	19.1 MJ/kg

This phased program was not greatly different from that contemplated for the Chinchilla site; however, it was more clearly defined at an early stage in Cougar Energy's life, and with the technical experience gained from the past demonstration and the availability of progressive funding from the ASX listing, it was considered to be realistic. Significant emphasis was also placed on the design of a pilot gas-cleaning plant, sufficient to provide an output gas composition suitable for direct combustion in existing commercial gas turbines.

The site layout plan for the project is shown in Fig. 6.12, and the gas treatment plant is shown in Fig. 6.13.

A detailed discussion of the company's progress at Kingaroy is contained elsewhere in another chapter; however, the time line of activity can be summarized as follows (Walker, 2014):

- Resource drilling completed—June 2008.
- Ignition and first gas production—15 March 2010.
- Air injection halted due to casing blockage—20 March 2010.
- Evidence of 2 ppb benzene in one monitoring bore—21 May 2010.
- Discussion of results with government officials—30 June 2010.
- New production wells drilled—early July 2010.
- False benzene test result of 82 ppb submitted to government—13 July 2010.
- Confirmation of false result submitted to government—14 July 2010.
- Shutdown notice received—17 July 2010.
- Environmental Evaluation reports prepared—from August to December 2010.
- Permanent shutdown and rehabilitation notice received—July 2011.

In total, the Kingaroy UCG facility effectively operated for only 5 days and gasified approximately 20 tonnes of coal. Even so, Kingaroy project has produced technically and environmentally valuable results discussed in a separate chapter of this book.

6.4.2   The followers

Over the period from 2006 to 2011, there was considerable UCG activity with demonstration pilot burns being undertaken by Linc Energy, Carbon Energy, and Cougar Energy. These three companies raised funds as a result of being listed on the ASX,
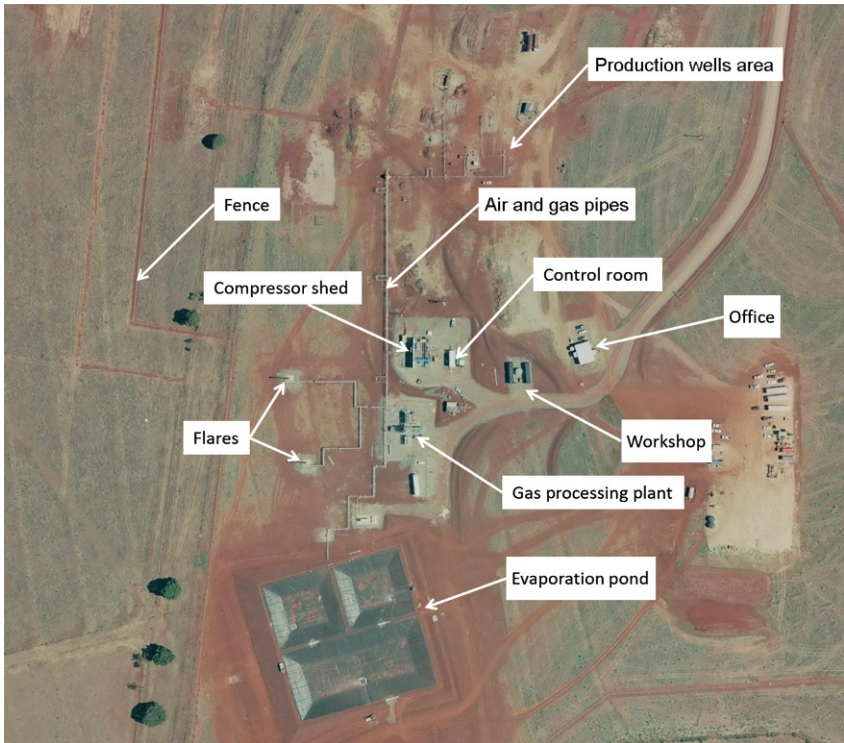
Fig. 6.12 Cougar Energy Kingaroy UCG site layout.

Fig. 6.13 Cougar Energy gas treatment plant at Kingaroy site.

and each had specific plans for developing significant commercial projects involving the production of diesel and jet fuels (Linc Energy), ammonia and methanol (Carbon Energy), and power (Cougar Energy). These project plans were underpinned by an oil price consistently around US$100/bbl.

Although the Queensland Government early in 2009 had approved only the three companies to demonstrate UCG technology (refer to Section 6.6), a number of other companies listed on the ASX saw the opportunity to promote their interest in UCG technology with a view to following on from the expected likely successful adoption of the technology in that state. The activities of these companies are summarized below, some of which included proposals that would have stretched the existing state of knowledge of the technology. However, they illustrate the wide spread of interest in UCG technology at the time, particularly over the period from 2008 to 2011 and the potential that existed for this to be translated into a national commercial industry in Australia. The information presented is again obtained from company presentations and from announcements made to the ASX.

6.4.2.1 Liberty Resources (ASX Code:LBY, now CNW)

In September 2008, Liberty Resources (LBY), an existing ASX listed company, announced (Liberty Resources, 2008a) that it had signed an option agreement to purchase companies holding for exploration permits for coal applications (EPCAs) in Queensland covering a total area of 64,000 km^2 "potentially suitable for underground coal gasification." On 11 December 2008, the company announced (Liberty Resources, 2008b) an inferred resource on its Galilee basin coal permit of 338 million tonnes of coal to "fast track UCG investigations and site selections." The option was exercised, and the purchase completed in April 2009 (Liberty Resources, 2009a).

In July 2009, LBY entered into a heads of agreement (HOA) with Carbon Energy to form a joint venture to develop a UCG project on its Galilee basin permit (Liberty Resources, 2009b) and a separate HOA with Clean Global Energy to undertake a similar project on its Surat Basin permits. It also announced "an exploration potential target of from 280 to 350 Bt (billion tonnes) of coal" on its coal permits based on a review of historic oil and gas well data. The company cemented its declared interest in UCG by joining the UCG partnership based in the United Kingdom in September 2009 (Liberty Resources, 2009c).

In June 2010, LBY reported (Liberty Resources, 2010a) the results of a scoping study into the economics of syngas production on one of its Queensland permits. The company also confirmed that it was unable to commence a pilot trial of the technology due to the limitations imposed by the Queensland Government's UCG policy. The company continued to focus on potential project analysis and, in October 2010, declared (Liberty Resources, 2010b) a focus on using UCG syngas for developing large-scale urea and fertilizer production. This project work continued through 2011–13, with no apparent progress on the development of a UCG gas production trial and an increasing interest by the company in conventional coal opportunities. In October 2014, LBY announced (Liberty Resources, 2014) a change of business

for the company, with confirmation of disposal of all its mining interests in April 2015 (Liberty Resources, 2015).

6.4.2.2   Clean Global Energy (ASX Code:CGV, now CTR)

Clean Global Energy (CGV) was formed initially as a private company to develop UCG on its coal leases in Queensland, using experience gained from the Spanish UCG trial in 1997. In April 2009 (Clean Global Energy, 2009a), it entered into a HOA to be taken over by a listed company and so acquire an ASX listing. A formal share sale agreement was signed in June 2009, and the transaction was completed in October 2009 (Clean Global Energy, 2009b). At that time, the company announced HOAs with Carbon Energy in Queensland and companies in Victoria and China as part of its plan to develop commercial projects in these areas as well as on its own coal leases in Queensland. By the end of 2010, the company had also identified UCG project prospects in the United States and India and established an initial resource for UCG development on its Queensland permits (Clean Global Energy, 2010).

However, following board changes in May 2011, CGV relinquished its UCG interests in China and the United States and in November announced (Clean Global Energy, 2011) the complete withdrawal of its interest in UCG, to focus on conventional coal mining and other energy activities.

6.4.2.3   Eneabba Gas (ASX Code:ENB)

In October 2008, Eneabba Gas (ENB), an ASX listed company, announced (Eneabba Gas, 2008) that it was in discussion with several providers of UCG technology in relation to applying the process to its coal leases near Geraldton in the Perth basin in Western Australia. The company was involved in gas supply contracts and had proposed a 168 MW power station near its leases to meet demand from nearby iron ore mines. In May 2009, ENB signed an HOA with Carbon Energy by which Carbon would acquire certain coal leases, apply its UCG technology and produce syngas for supply to ENB's proposed power station (Eneabba Gas, 2009). Following work by both parties during the year, the HOA expired in December 2009.

ENB's focus on UCG was confirmed in March 2010 when it joined the UCG Association based in London. Subsequently, in April 2010 (Eneabba Gas, 2010), it entered into an MOU with Cougar Energy for development of a UCG project on its permits, to be followed by the signing of a binding term sheet in early June that year. Cougar Energy's progress on the project was however greatly hampered by the events at its Kingaroy plant in Queensland, and the agreement was terminated in February 2011 (Eneabba Gas, 2011).

ENB maintained a declared interest in applying UCG to its coal leases until July 2015, when it advised (Eneabba Gas, 2015) that this activity would be discontinued and that the company would focus on conventional gas exploration.

6.4.2.4   Metrocoal (ASX Code:MTE, now MMI)

In May 2006, Metallica Minerals (MLM—ASX Code, MLM) announced an agreement with Cougar Energy (prior to its listing on the ASX) to investigate the feasibility of applying UCG to its coal tenements in Queensland, including one at Kingaroy that became the site of Cougar Energy's UCG project (Metallica Minerals, 2006). Cougar commenced drilling at Kingaroy early in 2007 and completed acquisition of the coal tenement in November 2008.

In May 2008, MLM announced (Metallica Minerals, 2008) that it would commence drilling to assess UCG potential on its other coal tenements to enable it "to join the emerging Australian UCG sector." By January 2009, MLM was aggressively pursuing a drilling campaign in the Surat Basin to establish a potential UCG project, with a proposal to obtain a separate listing for its subsidiary coal company (Metrocoal). This ASX listing for MTE was completed in December 2009 (Metallica Minerals, 2009).

During 2010/2011, MTE maintained an expressed interest in UCG but by the end of 2011 was confirming its preferred interest in conventional underground mining as a result of the declining support for UCG from the Queensland Government and also subsequently an added interest in bauxite mining.

6.4.2.5   Central Petroleum (ASX Code:CTP)

In June 2011, Central Petroleum (CTP) announced (Central Petroleum, 2011) a plan to develop its coal leases in the Pedirka basin in the Northern Territory using UCG technology. It provided a consultant's report concluding that a total "exploration target potential" of between 730 and 890 billion tonnes of coal existed on CTP's petroleum and mineral leases, above a depth of 1000 m. The shallowest intersection shown from existing drilling logs was at about 400 m depth. CTP proposed to call for expressions of interest in developing an integrated UCG facility to initially produce 60,000 bpd of liquid fuels.

This proposal was still being pursued when a change in board control occurred in April 2012 (Central Petroleum, 2012), and the emphasis of the company turned back to conventional oil and gas exploration. The UCG proposal was not pursued subsequently.

6.4.2.6   Wildhorse Energy (ASX Code:WHE, now SO4)

In September 2009, Wildhorse Energy (WHE), an Australian company listed on the ASX and active in uranium exploration in Poland, announced (Wildhorse Energy, 2009) the acquisition of Peak Coal, a company with significant coal permits in Hungary and a plan to develop those assets using the UCG process. This acquisition was ultimately completed in February 2010, and the company engaged the services of a number of former employees of the Sasol group of companies to undertake the UCG development program.

Over the following years, the company undertook a range of studies for a UCG project on its licenses in Hungary, with no active field work being undertaken. In February 2014, it announced (Wildhorse Energy, 2014a) an agreement to sell its UCG assets

to Linc Energy. In August 2014, Linc Energy withdrew from this agreement, and as a consequence, WHE relinquished all its interests in UCG as part of a company restructure announced in October 2014 (Wildhorse Energy, 2014b).

Although Australian-based, at no stage did WHE acquire any assets or express any interest in developing UCG technology in Australia.

6.4.3   Academic research

During the period of development of UCG projects in Australia, academic research efforts were undertaken in several Australian universities. A number of research projects in the University of Queensland were conducted in close cooperation with Ergo Exergy in support of the projects applying the εUCG technology, in particular, the Chinchilla UCG project (gasifier 1, 1999–2006) and the Majuba UCG project in South Africa.

A study of ash formation effects on ash leaching in the postgasification cavity focused on variation of residual ash leachability with changing physical condition of the ash sample (Jak, 2009). The combustion group at the University of Queensland led by Dr. A. Klimenko, working in close cooperation with Ergo Exergy and Dr. M. Blinderman, developed the theories for reverse and forward combustion linking, for flame propagation within the gasification zone in a channel and performed simulations of the gasification process (Blinderman and Klimenko, 2007; Blinderman et al., 2008a,b; Saulov et al., 2010; Chodankar et al., 2009). Exergy optimization of the linking process was considered as a part of this research, and theoretical results were compared with the data from field linking conducted under supervision of the Ergo Exergy technologists working at the Chinchilla UCG project (gasifier 1, 1999–2006).

A number of computational models for underground coal gasification were developed by Greg Perkins at the University of New South Wealth (Perkins, 2007, 2008). These models considered the heat and mass transport and incorporated evaluation of the cavity growth. The results of simulations were compared with the UCG trial in Centralia (the United States).

6.4.4   Summary of progress

By the end of 2009, there were six ASX listed companies actively pursuing UCG activities in Queensland and two others active in Western Australia and Hungary, respectively. The three main companies were also actively undertaking UCG gas production operations in the field in Queensland. This spread of activity at the time was probably unique in the recent history of the technology and gave considerable confidence to the belief that commercialization of the technology in Australia was imminent.

The essential contribution to this goal at the time can be summarized as follows:

- A number of active companies with a variety of objectives in adopting the technology.
- The use of private capital to pursue development, compared with previous international development almost exclusively relying on government research funding.

- The use of stock exchange listing to raise capital, spreading the investment risk among many individuals and investment funds, and taking advantage of market "excitement" for the technology to assist funding efforts.

The fact that the commercial objectives of none of these participants were achieved, despite the industry momentum at the time, requires careful analysis if a new generation of active UCG participants is not to suffer the same fate. The following analysis endeavors to highlight those factors impacting on successful commercial development, drawing on the experience obtained from UCG activities in Australia.

6.5   UCG and coal seam gas (CSG) interaction

To understand the factors involved in UCG development in Queensland, especially political ones, it is essential to review the competing interests of companies in that state involved in the coal seam gas (CSG) industry and those companies endeavoring to develop a commercial UCG industry.

A number of commercial facts are relevant to this understanding:

- The CSG industry in Queensland was led by a combination of large existing national oil and gas companies (Santos, Origin Energy) and a number of developing start-up companies (e.g., Arrow Energy, founded 1997, and Queensland Gas, founded 2000).
- The UCG industry in Queensland effectively commenced with the start-up of Linc Energy in 1996, and the successful Chinchilla demonstration from 1999 to 2002 that was shut down for lack of finance. A gap in activity of 4 years occurred before the follow-up stage led by the ASX listing of Linc Energy in 2006 and the formation of Carbon Energy and Cougar Energy in the same year.
- In the period from 2000 to 2006, major advances were being made in development of CSG production in the Surat Basin, using the same Walloon Coal measures as were being developed for UCG by Linc Energy during this time.

CSG exploration in the Surat Basin accelerated early in the 2000s, with Queensland Gas commencing in 2000 and Arrow Energy in 2001. Successful gas production was reported in July 2001 (Arrow Energy, 2001) from CSG wells in the Walloon Coal measures at 140 m (and shallower), that is, the same coal seams and depths being developed by Linc Energy at Chinchilla. Contracts for the supply of CSG to CS Energy (Linc Energy's JV partner) were signed with Santos in 2000, with Arrow Energy in 2001, and with Queensland Gas in 2002, as commercial quantities of gas were being developed.

The significance of these CSG developments at the time can be appreciated by reviewing a number of current proposals to recover CSG and pipe it to the eastern seaboard of Queensland for conversion to LNG for export. The proposals are very large in concept and cost and require very large supplies of gas. Company reports describe the large drilling campaigns necessary to meet the gas supply targets. For example, Arrow Energy announced (Arrow Energy, 2009) a Surat Basin Gas Project to supply gas to an LNG project on the east coast and gas for local power generation. The project was proposed to involve 1500 new CSG wells and gas

pipelines estimated to cost $1.5 billion to transport the gas to central gas processing and water treatment facilities. Also, Queensland Gas reported (Queensland Gas, 2017) that the first phase of its Surat Basin project up to June 2015 had drilled 2520 wells and was currently drilling at a rate of 25 wells per month to develop a similar coal seam gas to LNG project. Santos and Origin Energy are involved in similar large-scale projects.

This progressive acceleration of exploration and production of CSG in the Surat Basin reinforced the potential conflict of interest between CSG developers, whose permits were granted under the Queensland Government Petroleum and Gas Act, and UCG developers, whose production permits, when granted, were to be granted under the Mines Act. By 2008/2009, when the Queensland Government introduced its UCG policy (discussed in the following section), the impact of the permit overlap issue at the time was clearly evident as shown in Fig. 6.14, which illustrates the permits granted in the Surat Basin at that time.

Fig. 6.14 shows that virtually the whole basin is covered by exploration permits for petroleum/gas, and most of the shallow coal (depth less than 400 m) is covered by petroleum production licenses (cross-hatched). The coal deposits dip to the southwest beyond 400 m depth, where they are less attractive for UCG development. The two granted mineral development licenses (MDL) for Linc Energy and Cougar Energy are shown in blue. These were confirmed by the government as solely for the purpose of UCG pilot trials, but not for commercial development, pending its consideration of the future of the technology in the state.

This unbalanced access to coal in the Surat Basin in favor of the coal seam gas industry is exacerbated by the area required for a fixed-energy output by the two technologies. CSG recovers any free or extractable methane gas from the coal, while UCG converts 70%–80% of the energy in the coal into gas and recovers any free methane from the oxygen depleted process cavity. It has been estimated (Carbon Energy, 2013) that from a defined area of coal, the UCG process will recover 20 times the energy from the coal deposit when compared with the CSG process.

A consequence of this comparison is that for a fixed-energy supply requirement, a CSG operator will require access to 20 times the area of land below which the coal seam exists. This requirement explains the large allocation of petroleum permit areas shown in Fig. 6.14 that are necessary to achieve an energy output that could be achieved from a much smaller UCG permit. It is also an indicator of the vast energy source potentially recoverable from the Surat Basin if the UCG technology were to be developed on a commercial basis.

Several technical operating factors also impact on the interaction between UCG and CSG interests. Of these, the most significant is the impact on the groundwater table. Because of its method of operation, the CSG process removes large volumes of water resulting in a significant, possibly long-term reduction in the groundwater table, and hence lowers the groundwater pressure in the coal seam at depth below the surface. It is this pressure reduction that allows the recovery of the methane. By contrast, the UCG process requires the maintenance of a significant water pressure head in the coal seam to balance (and exceed) the injected air or oxygen pressure in the cavity.
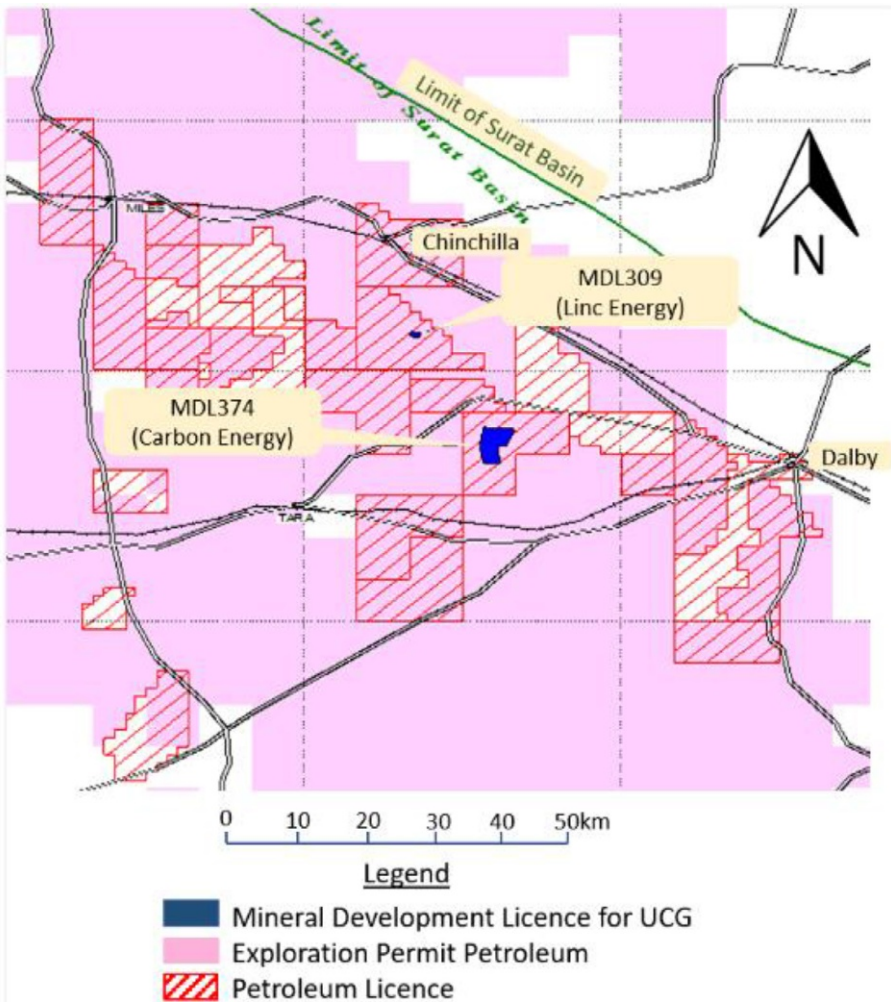
Fig. 6.14 Petroleum and CSG permits—Surat Basin 2008/2009.

Side by side operations of the two technologies would therefore not be possible unless reliable predictions of CSG groundwater drawdown could be made with respect to pressure, to lateral extent and to fluctuations with time. This would be a difficult exercise given the variability of in situ permeability and its difficulty of prediction in advance of operational start-up or during CSG operations, which could place an adjacent UCG operation at environmental risk.

There would also be concern about undertaking UCG operations in an area where coal seams have been fully developed for CSG. The impact of CSG operations on the structure and permeability of both coal seams and overburden would cause

considerable uncertainty for UCG operations, as would the risk of gas seepage paths being created around CSG well installations.

While it was not so evident in the late 2000s, it is clear with the advantage of hindsight that the aggressive development plans of a number of CSG companies and their effective control over the coal deposits through the permit system made any short-term development of the fledgling UCG industry in Queensland a doubtful proposition.

6.6 The Queensland Government UCG Policy

In the period from 1999 to 2008, the development of the UCG and CSG industries can be briefly summarized as follows:

- The Chinchilla test from 1999 to 2002 by Linc Energy provided evidence of successful production of UCG gas, followed by successful decommissioning.
- From 2000 onward, Linc Energy's partner CS Energy entered into a number of agreements to take CSG gas from existing development companies, withdrew from UCG development in 2002, and progressed its direct interest in developing CSG production.
- A strong interest in UCG was activated from 2006 with the renewed development plans of Linc Energy and the active development plans of Carbon Energy and Cougar Energy.
- The intervening period from 2002 to 2006 saw a rapid expansion in CSG exploration in the Surat Basin by a range of large and small companies.

Thus, by 2008, when commercial gas production from the three key UCG projects was imminent, the conflict between the technologies described in Section 6.5 was inevitably brought to a head.

The first indication of government action occurred in a press report responded to by Linc Energy (2008c), which quoted an unnamed source in the Department of Mines and Energy that "the government had no intention of granting production tenures for UCG for at least 3 years." The minister subsequently issued a statement that the government would not grant production tenure for any technology that was untried and untested in Australian conditions, without specifically referring to a potential moratorium on UCG development.

On 18 February 2009, the Queensland Government released an underground coal gasification policy paper (Queensland Government, 2009), which stated that "the intention is to provide the UCG pilot projects with the opportunity to demonstrate the technical, environmental, and commercial viability of the technology." No reference was made to the successful demonstration by Linc Energy from 1999 to 2002; hence, the UCG proponents were effectively asked to start again in satisfying the government as to the technology's potential.

The policy also included a number of other features:

- The appointment of an "independent scientific panel" (ISP) to assist in the preparation of a government report to enable it to "decide upon the future viability of the UCG industry in Queensland."

- The formation of an industry consultative committee (ICC) comprising representatives from both the UCG and CSG industries, "responsible for considering and providing options to the government for the resolution of resource and technology conflicts."
- No further UCG tenures were to be granted until the government decision on the future of the technology was made.
- "The findings of the government report on UCG will be presented to Cabinet in 2011/2012 and should the government report produce adverse findings on the UCG technology; ongoing constraint or even prohibition of UCG activities may be recommended."
- In discussing overlapping UCG and CSG tenure, "the Minister for Natural Resources, Mines, and Energy, if asked to determine a coordination or preference decision between the developer of a CSG resource and the developer of a UCG resource, the decision will be made in favour of the CSG tenure holder under the P&G Act, so as to allow the CSG tenure to progress to production stage."

This policy placed an effective moratorium on the issuing of UCG production tenures and achieved the objectives referred to in the press articles of August the previous year.

This UCG policy also had a number of implications for the small public listed companies proposing to develop UCG projects as their main objective:

- The future of the technology in Queensland was now in the hands of a political decision rather than determined by commercial development.
- The preference for CSG in any overlapping tenure dispute was compounded by the existing granted tenure positions shown in Fig. 6.14.
- The uncertainty generated by the policy was to have ongoing impacts on the financial resources of all UCG companies and their future capacity to raise funds from the public.

Despite these uncertainties, the three active companies received sufficient comfort from discussions with the government at the time to continue with their projects and to engage with both the ISP and with the ICC.

6.7 UCG development decay (2011–16)

6.7.1 Background

Progress of the three UCG companies actively developing projects in Queensland received a considerable setback with the announcement by the Queensland Government of its UCG policy. As a consequence of the policy, the plans of each company to rapidly progress from pilot plant to commercial operation were put on hold, with an uncertainty as to whether any project approvals would eventually be given.

With the passage of time and the events surrounding the decision to permanently shut down the Cougar Energy project in July 2011, the confidence that approval of commercial UCG projects in the state would be achieved progressively diminished.

The ISP (Queensland Government, 2013) released its report on the remaining two UCG pilot trials in June 2013 and concluded the following:

- *Underground coal gasification could,* in principle*, be conducted in a manner that is acceptable socially and environmentally safe when compared to a wide range of other existing resource-using activities.*

- *… for commercial UCG operations in Queensland* in practice *first decommissioning must be demonstrated and then acceptable design for commercial operations must be achieved within an integrated risk-based framework.*

While the first of these conclusions was welcomed as supporting commercial development, the second made it evident that the ISP was placing significant additional requirements on the companies to fully rehabilitate their existing pilots (i.e. they could not be continuously expanded into commercial operations), while requiring detailed design requirements for expansion to commercial size. The uncertainty of approval for commercial development therefore continued.

Eventually, all three operations in the state were terminated for reasons summarized below, with a flow-on effect for the rest of the embryonic UCG industry.

6.7.2 Linc Energy

In July 2013, Linc Energy announced (Linc Energy, 2013b) a positive response to the ISP report as an indication that the technology would be allowed to continue in Queensland, subject to successful evidence of cavity rehabilitation. In September 2013, the company confirmed (Linc Energy, 2013c) that it would be fully rehabilitating gasifier 3 to meet this part of the requirement of the ISP for commercial operations to be approved.

However, on 5 November 2013, the company announced (Linc Energy, 2010c) that it would be ceasing its operations at Chinchilla, decommissioning the site, and moving its operations offshore. The company gave its reason as "to date, the state has not provided the UCG industry with any material certainty or confidence capable of supporting commercial investment in UCG in Queensland." The company concluded that it "must continue to progress its UCG business offshore to ensure the future deployment of UCG into regions such as Asia." The company estimated the expenditure on its UCG program at A\$300 million.

In the previous month, the company indicated it would be seeking to move its stock exchange listing from Australia to Singapore, and this move was successfully completed in mid-December 2013.

Subsequent to these events, the Queensland Government laid criminal charges against the company for wilfully and unlawfully causing serious environmental harm—four charges were laid in April 2014 and one in June 2014 (refer to Section 6.4.1.1). These charges were subject to a magistrate hearing in October/November 2015, and in March 2016, the company was formally committed for trial on all charges.

6.7.3 Carbon Energy

Carbon Energy operated its second UCG panel until late 2012, at which time it entered into the decommissioning phase as required by the Queensland Government as a condition for receiving approval for development of its commercial project. The company completed this procedure and provided a report to the government on 1 October 2014 (Carbon Energy, 2014).

The company announced in December 2014 that the review of this report by an independent consultant to the government had been completed and that the company anticipated receiving approval to proceed early in 2015. On a number of occasions through 2015, the company expressed the view that it had met all of the government's requirements in relation to rehabilitation of the UCG panels, had satisfied the requirements of the ISP, and in December 2015 (Carbon Energy, 2015) had its mineral development license renewed so that it could continue its UCG activities on the site. It was also in the process of discussion with the government about submitting an environmental impact statement for the construction of its commercial project.

On 16 April, 2016, without prior consultation with the company, the Queensland Government announced (Queensland Government, 2016a,b) a complete ban on UCG development in the state. Carbon Energy responded with an expression of surprise at the decision (Carbon Energy, 2016a), having satisfied all of the government's requirements and confirming that it would now take its technology offshore for development—specifically to China. The company estimated its UCG expenditure in Australia to have been A$150 million.

6.7.4   Cougar Energy

As summarized in Section 6.4.1.3 above, the Queensland Government had issued a shutdown notice on the company's operations in July 2010 and requested the company's response to a series of technical questions arising from the short-lived measurement of small concentrations of benzene in one monitoring bore. These queries were answered in a series of environmental evaluation reports submitted between August and December 2010. In October/November 2010, the company announced the progress of proposed project developments in China and Mongolia and opened an office in Beijing in May 2011.

Ultimately, the government issued a notice for permanent shutdown and rehabilitation of the Kingaroy site in July 2011. The company unsuccessfully endeavored to have this notice overturned and continued with its objective of developing UCG projects in the Asian region. This plan was eventually shelved following changes in the company board and management early in 2013, and the company removed UCG development from its corporate strategy. The investment in the technology was estimated to be A$30 million.

6.7.5   Other companies

The Queensland Government's decision to slow its decision-making on the future of UCG in that state also impacted on the attitude of other state governments, who were deferring their approaches to the technology pending the outcome of the activities in Queensland. Effectively, this created an uncertainty about the technology nationally in Australia.

At the peak of activity in Australia in 2010/2011, in addition to the three government-approved UCG companies, six other ASX listed companies were proposing similar projects—three in Queensland—one each in Western Australia and the

Table 6.6 UCG companies—withdrawal from Australian activity

Company	Date commenced	Proposed activity	Date terminated	Reason
Linc Energy	Oct. 1996	Gas to liquids	Nov. 2013	Offshore due to govt. policy uncertainty
Carbon Energy	July 2006	Gas to ammonia	April 2016	Offshore due to govt. ban on UCG
Cougar Energy	Oct. 2006	Gas to electricity	July 2011	Offshore due to govt. shutdown
Liberty Resources	Sept. 2008	Gas to urea	Oct. 2014	Change of business. Coal assets sold
Clean Global Coal	Oct. 2009		Nov. 2011	Board change. UCG dropped
Metrocoal	May 2008		Dec. 2011	Preference for conventional underground mining
Eneabba Gas (WA)	Oct. 2008		July 2015	Preference for conventional oil and gas exploration
Central Petroleum (NT)	June 2011	Gas to liquids	April 2012	Board change. Return to oil and gas business
Wildhorse Energy	Sept. 2009		Oct. 2014	No Aust. Interests

Northern Territory and one offshore in Europe. Each of these companies independently reviewed their involvement with the technology and withdrew their UCG plans as summarized in Table 6.6, by either taking its UCG development interest offshore or dropping its interest completely.

6.8 Governmental decision making

In the development of the commercial operations planned by Linc Energy, Carbon Energy, and Cougar Energy in Queensland, where each company relied on rapid progress to efficiently use funds raised from the public, delayed government decisions, especially those made without consultation, had a significant impact on company development.

Within the environment of uncertainty existing late in the 2000s, the following examples of the timeliness of Queensland Government responses can be documented:

- The UCG Policy announced the formation of an expert panel in February 2009. The membership of the panel was announced in October 2009 (8-month delay).

- Carbon Energy released a limited amount of wastewater into a creek bed in August 2009. It was requested to submit a report on the incident to the government, which it did in October 2010. In July 2011, it was issued with criminal charges for breaching environmental law (9-month delay). The charges were settled with payment of a fine with confirmation of no environmental harm.
- Carbon Energy submitted the required decommissioning report on its Bloodwood Creek pilot project in October 2014. It received no decision until a complete ban on UCG technology in Queensland was announced without consultation with the UCG industry in April 2016 (18-month delay).
- Cougar Energy applied for its mineral development license at Kingaroy in December 2007. It was eventually granted in February 2009, 14 days after the announcement of the UCG policy (14-month delay).
- Cougar Energy submitted a number of environmental evaluation reports to the government following a temporary shutdown notice received without prior consultation in July 2010. The last of these reports was submitted in December 2010, and a permanent shutdown notice was issued, again without prior consultation, on 11 July 2011 (6-month delay).
- On 1 July 2011, Cougar Energy was charged with breaching environmental law relating to the failure of one of its injection wells in March 2010 (16-month delay). As with Carbon Energy, the matter was settled by payment of a fine with confirmation of no environmental harm.

In announcing the permanent ban on UCG in April 2016, the Queensland Government stated that "we have looked at the evidence from the pilot operation of UCG and we've considered the compatibility of the current technologies with Queensland's environment and our economic needs. The potential risks to Queensland's environment and our valuable agricultural industries far outweigh any potential economic benefits."

In its response to this announcement, Carbon Energy, as the only remaining UCG proponent active in Australia, issued several statements, including one (Carbon Energy, 2016b) reiterating the ISP's positive conclusions about the technology and also the following:

> The unexpected announcement was delivered without consultation despite recent meetings being held with company and the government's acknowledgement that Carbon Energy had worked openly and transparently with government.

While the detail of the environmental charges against Linc Energy appear to be serious and have some evidentiary backing, the charges against Carbon Energy and Cougar Energy were minor issues related to the normal course of business, confined to the immediate project operating zone, resolved speedily by the companies, and no different from similar operating issues occurring at mining or gas production facilities. The fact that they were treated with such severity, and with attached publicity despite acceptance that no environmental harm was caused, is confirmation of the significance of political factors operating at the time.

6.9   Conclusions and the future

Australia has made a significant contribution to the development of underground coal gasification technology over the last 40 years. The key features of this contribution can be summarized as follows:

- A focus since the 1970s on taking existing UCG technology through to commercialization.
- The introduction of private capital, through stock exchange listing, to provide substantial investment funding.
- The production of syngas from three UCG development sites since 1999 as the first stage in development of commercial projects. Only two other sites internationally (in South Africa and New Zealand, respectively) have reliably produced syngas over this period.
- The development of project plans from these three companies to produce a range of end products—liquid fuels, ammonia and methanol, and power generation.
- A total combined expenditure on the UCG effort in Australia estimated at A\$500 million.

The ultimate collapse of this extensive UCG effort can be attributed largely to political decision-making in Queensland resulting from the conflict between the technologies of CSG and UCG developing over the same period of time and utilizing the same coal deposits. Efforts to find common ground between the proponents of each technology were not successful, and the size and established permit position of the CSG industry effectively led to the government decision to ban UCG technology in that state.

This decision has effectively made the progress of UCG technology in other states of Australia difficult, particularly given the mounting environmental campaigns against any technologies that *may* create groundwater impacts. The complexities in presenting and utilizing UCG technology mean that creating a technical understanding in response to these concerns is difficult, especially as critics are apt to fall back on the so-called precautionary principle as a justification for not supporting development of the technology.

In considering the lessons that come from the UCG program in Australia, the overriding issue involves the interaction between government and UCG proponent in relation to the monitoring and setting of acceptable limits for potential groundwater contaminants such as benzene and phenols. This process is no different from the processes used in many other operations such as waste disposal or chemical manufacture. These issues are discussed in detail elsewhere (Walker, 2014), and it is essential that they be confronted and agreed prior to any significant project investment.

The role of governments in the cycles of UCG development over many years has largely been the provision of funding for R&D programs, which have led to intense efforts in the FSU (from the 1930s to 1960s) and the United States (from the 1970s to 1980s). The past progress in Australia confirms that alternative funding from private sources can be attracted on the back of using established technologies applied to commercial project plans that meet local energy needs. However, it has also shown the power of government to selectively use environmental law and community perceptions of the technology to support alternative energy options where it chooses.

It is essential if future commercial development of UCG technology is to occur that it be undertaken where it can satisfy projected energy shortfalls, where long-standing technologies do not have the same resource control as existed in Queensland, and where full government support exists in the execution of practical environmental permitting that protects the community and allows controlled project development to occur.

Unfortunately, it appears that these conditions will not be met in Australia for the foreseeable future as a result of the technology perceptions created by the events that took place in Queensland. A change of approach may only happen if a commercial project is clearly demonstrated outside the country. Given the evidence available from companies previously active in Australia, this demonstration is most likely to occur in the Asian region.

References

Arrow Energy, 2001. See www.asx.com.au/asx/statistics/announcements. ASX Code AOE (delisted in 2010), 9 July.

Arrow Energy, 2009. See www.asx.com.au/asx/statistics/announcements. ASX Code AOE (delisted in 2010), 14 October.

Austa Energy and Linc Energy N.L., 1997. Preliminary Feasibility Study, Underground Coal Gasification Fired Power Station near Ipswich, Queensland, November.

Beath, A.C., Wendt, M., Mallett, C.W., 2000. Optimisation of underground coal gasification for improved performance and reduced environmental impact. In: Ninth Australian Coal Science Conference, Brisbane, 26-29 November.

Beath, A.C., Mark, M.R., Mallett, C.W., 2003. An evaluation of the application of underground coal gasification technologies to electricity generation and production of synthesis gas. In: 12th International Conference on Soil Science, Cairns, Queensland, 2-6 November.

Blinderman, M.S., Fidler, S., 2003. Groundwater at the underground coal gasification site at Chinchilla, Australia. In: Proceedings of the Water in Mining Conference, Brisbane, October.

Blinderman, M.S., Jones, R.M., 2002. The Chinchilla IGCC project to date: underground coal gasification and environment. In: Gasification Technologies Conference, San Francisco, October.

Blinderman, M.S., Klimenko, A.Y., 2007. Theory of reverse combustion linking. Combust. Flame 150 (3), 232–245.

Blinderman, M.S., Spero, C., 2002. UCG in Australia: development to date and future options. Report by Ergo Exergy Technologies Inc., Linc Energy Ltd., and CS Energy Ltd., Brisbane, April.

Blinderman, M.S., Saulov, D.N., Klimenko, A.Y., 2008a. Forward and reverse combustion linking in underground coal gasification. Energy 33 (3), 446–454.

Blinderman, M.S., Saulov, D.N., Klimenko, A.Y., 2008b. Exergy optimisation of reverse combustion linking in underground coal gasification. J. Energy Inst. 81 (1), 7–13.

Carbon Energy, 2006. See www.asx.com.au/asx/statistics/announcements. ASX Code CNX, 11 July.

Carbon Energy, 2007a. See www.asx.com.au/asx/statistics/announcements. ASX Code CNX, 24 May.

Carbon Energy, 2007b. See www.asx.com.au/asx/statistics/announcements. ASX Code CNX, 7 November.

Carbon Energy, 2008a. See www.asx.com.au/asx/statistics/announcements. ASX Code CNX, 15 July.

Carbon Energy, 2008b. See www.asx.com.au/asx/statistics/announcements. ASX Code CNX, 29 August.

Carbon Energy, 2008c. See www.asx.com.au/asx/statistics/announcements. ASX Code CNX, 17 December.

Carbon Energy, 2009. See www.asx.com.au/asx/statistics/announcements. ASX Code CNX, 3 February.

Carbon Energy, 2010a. See www.asx.com.au/asx/statistics/announcements. ASX Code CNX, 25 January.

Carbon Energy, 2010b. See www.asx.com.au/asx/statistics/announcements. ASX Code CNX, 30 April.

Carbon Energy, 2010c. See www.asx.com.au/asx/statistics/announcements. ASX Code CNX, 22 July.

Carbon Energy, 2011a. See www.asx.com.au/asx/statistics/announcements. ASX Code CNX, 28 March.

Carbon Energy, 2011b. See www.asx.com.au/asx/statistics/announcements. ASX Code CNX, 18 October.

Carbon Energy, 2013. UCG keyseam proof of concept. In: IEA Workshop—UCG Technology, Brisbane, November.

Carbon Energy, 2014. See www.asx.com.au/asx/statistics/announcements. ASX Code CNX, 1 October.

Carbon Energy, 2015. See www.asx.com.au/asx/statistics/announcements. ASX Code CNX, 10 December.

Carbon Energy, 2016a. See www.asx.com.au/asx/statistics/announcements. ASX Code CNX, 18 April.

Carbon Energy, 2016b. See www.asx.com.au/asx/statistics/announcements. ASX Code CNX, 19 April.

Central Petroleum, 2011. See www.asx.com.au/asx/statistics/announcements. ASX Code CTP, 27 June.

Central Petroleum, 2012. See www.asx.com.au/asx/statistics/announcements. ASX Code CTP, 18 April.

Chodankar, C.R., Feng, B., Klimenko, A.Y., 2009. Numerical modelling of underground coal gasification process for estimation of product gas composition. In: Proceeding of 26th International Pittsburgh Coal Conference, Pittsburgh, USA, September 20-24.

Clean Global Energy, 2009a. See www.asx.com.au/asx/statistics/announcements. ASX Code CGV (now CTR) 30 September.

Clean Global Energy, 2009b. See www.asx.com.au/asx/statistics/announcements. ASX Code CGV (now CTR) 27 October.

Clean Global Energy, 2010. See www.asx.com.au/asx/statistics/announcements. ASX Code CGV (now CTR) 7 October.

Clean Global Energy, 2011. See www.asx.com.au/asx/statistics/announcements. ASX Code CGV (now CTR) 24 November.

Dames and Moore, 1996. Leigh Creek coalfield: lobe B. Geotechnical and hydrogeological investigations—phase 2. Report to Electricity Trust of South Australia, March.

Eneabba Gas, 2008. See www.asx.com.au/asx/statistics/announcements. ASX Code ENB, 3 October.

Eneabba Gas, 2009. See www.asx.com.au/asx/statistics/announcements. ASX Code ENB, 1 April.

Eneabba Gas, 2010. See www.asx.com.au/asx/statistics/announcements. ASX Code ENB, 15 April.

Eneabba Gas, 2011. See www.asx.com.au/asx/statistics/announcements. ASX Code ENB, 1 February.

Eneabba Gas, 2015. See www.asx.com.au/asx/statistics/announcements. ASX Code ENB, 29 July.

Gregg, D.W., Hill, R.H., Olness, D.U., 1976. An overview of the Soviet effort in underground gasification of coal. Lawrence Livermore Laboratory, University of California. Prepared for US Energy Research & Development Administration under Contract No. W-7405-Eng-48.

Jak, E., 2009. Gasification Ash Melting Effect on Leachability. Pyrometallurgy Research Centre, University of Queensland, Brisbane, p. 167.

Kinhill Engineers, 1989. Underground coal gasification—preliminary feasibility study. Report to WGN Ventures on Power Generation at Swanbank Power Station, January.

Liberty Resources, 2008a. See www.asx.com.au/asx/statistics/announcements. ASX Code LBY (now CNW), 24 September.

Liberty Resources, 2008b. See www.asx.com.au/asx/statistics/announcements. ASX Code LBY (now CNW), 11 December.

Liberty Resources, 2009a. See www.asx.com.au/asx/statistics/announcements. ASX Code LBY (now CNW), 22 May.

Liberty Resources, 2009b. See www.asx.com.au/asx/statistics/announcements. ASX Code LBY (now CNW), 27 July.

Liberty Resources, 2009c. See www.asx.com.au/asx/statistics/announcements. ASX Code LBY (now CNW), 15 September.

Liberty Resources, 2010a. See www.asx.com.au/asx/statistics/announcements. ASX Code LBY (now CNW), 29 June.

Liberty Resources, 2010b. See www.asx.com.au/asx/statistics/announcements. ASX Code LBY (now CNW), 4 October.

Liberty Resources, 2014. See www.asx.com.au/asx/statistics/announcements. ASX Code LBY (now CNW), 28 October.

Liberty Resources, 2015. See www.asx.com.au/asx/statistics/announcements. ASX Code LBY (now CNW), 28 April.

Linc Energy N.L., 1998. Prospectus lodged with Australian Securities Commission, June.

Linc Energy, 2006a. Prospectus lodged with Australian Securities and Investment Commission, March.

Linc Energy, 2006b. See www.asx.com.au/asx/statistics/announcements. ASX Code LNC, 4 December.

Linc Energy, 2007a. See www.asx.com.au/asx/statistics/announcements. ASX Code LNC, 3 September.

Linc Energy, 2007b. See www.asx.com.au/asx/statistics/announcements. ASX Code LNC, 11 October.

Linc Energy, 2007c. See www.asx.com.au/asx/statistics/announcements. ASX Code LNC, 28 November.

Linc Energy, 2008a. See www.asx.com.au/asx/statistics/announcements. ASX Code LNC, 28 July.

Linc Energy, 2008b. See www.asx.com.au/asx/statistics/announcements. ASX Code LNC, 14 October.

Linc Energy, 2008c. See www.asx.com.au/asx/statistics/announcements. ASX Code LNC, 7 August.

Linc Energy, 2009a. See www.asx.com.au/asx/statistics/announcements. ASX Code LNC, 10 March.

Linc Energy, 2009b. See www.asx.com.au/asx/statistics/announcements. ASX Code LNC, 27 November.

Linc Energy, 2010a. See www.asx.com.au/asx/statistics/announcements. ASX Code LNC, 4 February.

Linc Energy, 2010b. See www.asx.com.au/asx/statistics/announcements. ASX Code LNC, 19 May.

Linc Energy, 2010c. See www.asx.com.au/asx/statistics/announcements. ASX Code LNC, 5 November, 2013.

Linc Energy, 2013a. IEA Workshop—UCG Technology, Brisbane, November.

Linc Energy, 2013b. See www.asx.com.au/asx/statistics/announcements. ASX Code LNC, 8 July.

Linc Energy, 2013c. See www.asx.com.au/asx/statistics/announcements. ASX Code LNC, 3 September.

Metallica Minerals, 2006. See www.asx.com.au/asx/statistics/announcements. ASX Code MLM, 18 May.

Metallica Minerals, 2008. See www.asx.com.au/asx/statistics/announcements. ASX Code MLM, 22 May.

Metallica Minerals, 2009. See www.asx.com.au/asx/statistics/announcements. ASX Code MLM, 4 December.

Perkins, G., 2007. Modelling of heat and mass transport phenomena and chemical reaction in underground coal gasification. Chem. Eng. Res. Des. 85 (3), 329–343.

Perkins, G., 2008. Steady-state model for estimating gas production from underground coal gasification. Energy Fuel. 22(6).

Queensland Gas, 2017. See www.bg-group.com/713/qgc.

Queensland Government, 2009. See http://services.dip.gov.au/opendata/RTI/dsdip/rtip1415-086/Documentsforrelease-RTIP1415-086.PDF.

Queensland Government, 2013. See www.dnrm.qld.gov.au/_data/assets/pdf/0006/990555/isp-underground-coalgas-pilot-trials.pdf.

Queensland Government, 2016a. See http://archive.sclqld.org.au/qjudgement/2016/QMC16-004.

Queensland Government, 2016b. See http://statements.qld.gov.au/Statement/2016/4/18/underground-coal-gasification-banned-in-queensland.

Saulov, D.N., Plumb, O.A., Klimenko, A.Y., 2010. Flame propagation in a gasification channel. Energy 35 (3), 1264–1273.

Shedden Pacific Pty Ltd, 1981. Pre-feasibility study of the in-situ gasification of the Anna lignite deposit, South Australia. Draft Copy to CSR Limited, December.

Shedden Pacific Pty Ltd., 1983. Feasibility study. Underground coal gasification, Leigh Creek, South Australia. Report to Department of Mines and Energy, South Australia, August.

Stewart, I.McC., 1984. In-situ gasification of coal for Australia. Report Number 297, NERDD Program, Dept. of Resources and Energy, May.

Stewart, I.McC, Wibberley, L.J., Gupta, R., Mai Viet, T., 1981. Towards a high-output borehole system for hard coals. In: 7th Underground Coal Symposium, ERDA, USA.

Walker, L.K., 1999. Underground coal gasification: a clean coal technology ready for development. Aust. Coal Rev. 8, 19–21.

Walker, L.K., 2014. Underground coal gasification—issues in commercialisation. Proc. Inst. Civ. Eng. Energy (November), 188–195.

Walker, L.K., Walker, A.L., Beaver, F.W., Schmit, C.R., Young, B.C., Groenewold, G.H., Boysen, J.E., McKeough, W.R., Kuhnel, R.A., 1993. The future role of underground coal gasification in the Asia-Pacific Region. In: Proceedings of CHEMECA Conference, Melbourne, Australia, pp. 417–422.

Walker, L.K., Blinderman, M.S., Brun, K., 2001. An IGCC project at Chinchilla, Australia, based on underground coal gasification (UCG). In: Gasification Technologies Conference, San Francisco, October.

Wildhorse Energy, 2009. See www.asx.com.au/asx/statistics/announcements. ASX Code WHE (now SO4), 3 September.

Wildhorse Energy, 2014a. See www.asx.com.au/asx/statistics/announcements. ASX Code WHE (now SO4), 24 February.

Wildhorse Energy, 2014b. See www.asx.com.au/asx/statistics/announcements. ASX Code WHE (now SO4), 28 October.

Gasification kinetics

H. Bockhorn
Karlsruhe Institute of Technology, Engler-Bunte-Institute, Karlsruhe, Germany

7

7.1 Introduction

7.1.1 An attempt to a molecular view

Considering a chemical reaction of the type

$$\nu_A A + \nu_B B + \cdots \rightarrow \nu_C C + \nu_D D + \cdots \tag{7.1}$$

in a closed vessel, the chemical reaction rate R_{abs} is defined as the time change of the molar amounts dn_i/dt of the species i divided by its stoichiometric coefficients

$$R_{abs} = \frac{1}{\nu_i} \cdot \frac{dn_i}{dt}. \tag{7.2}$$

The advantage of this definition is that we have a unique reaction rate for any species. Expressing the change of the molar amounts with the help of a conversion variable $dn_i = \nu_i d\xi$, we can write

$$R_{abs} = \frac{d\xi}{dt}. \tag{7.3}$$

For chemical reactions in a homogeneous phase R_{abs} usually is expressed as a volume-specific quantity, therefore

$$r_{abs} = \frac{1}{V} \cdot \frac{d\xi}{dt}. \tag{7.4}$$

The volume-specific chemical reaction rate r_{abs} depends on the molar concentrations c_i of the involved species, temperature T, and pressure p. These dependencies can be expressed generally in a separable form like

$$r_{abs} = \frac{1}{V} \cdot \frac{d\xi}{dt} = k(T,p) \cdot c_A^{\mu_A} \cdot c_B^{\mu_B} \cdots \quad (\text{mol/m}^3 \text{ s}), \tag{7.5}$$

where the temperature dependency is contained in the rate coefficient $k(T, p)$ and the dependency on species concentrations is reflected by $c_A^{\mu_A} \cdot c_B^{\mu_B} \cdots$. The rate coefficient can also be dependent on pressure and the chemical reaction rate is inherently dependent on pressure through the pressure dependency of species concentrations.

The μ_i are the reaction orders with respect to the species i and $\sum_i \mu_i$ is the overall reaction order of the chemical reaction. If the chemical reaction written as in Eq. (7.1) is an elementary reaction, that is, the reaction equation represents the mechanism of the reaction and the reaction proceeds on a molecular level as written, the reaction orders μ_i equal the stoichiometric coefficients ν_i. However, this is not the case for most reactions and particularly—as we will see later on—in the case of coal gasification. Experimental reaction rates r_{exp} mostly are evaluated in the form

$$\frac{r_{exp}}{c_A^{\mu_A} \cdot c_B^{\mu_B} \cdots} = k_{exp}. \tag{7.6}$$

For temperature ranges not too large the temperature dependency of k_{exp} mostly is represented by an Arrhenius approximation

$$k_{exp} = k_0 \cdot \exp\left(-\frac{E_{A\ app}}{R \cdot T}\right), \tag{7.7}$$

where $E_{A\ app}$ denotes the apparent activation energy.

Experimental rate coefficients may be interpreted with the help of appropriate reaction rate theories. The simplest approach to the interpretation of k_{exp} for a bimolecular reaction

$$A + B \xrightarrow{k_{exp}} C + D \tag{7.8}$$

is collision theory, which gives for the hard sphere molecule model the intrinsic reaction rate coefficients $k(T)$ as

$$k(T) = \left(\frac{8 \cdot k_B \cdot T}{\pi \cdot \mu}\right)^{1/2} \cdot \pi \cdot d_{AB}^2 \cdot \left(1 + \frac{E_0}{k_B \cdot T}\right) \cdot \exp\left(-\frac{E_0}{k_B \cdot T}\right), \tag{7.9}$$

where k_B is the Boltzmann constant, d_{AB} the intermolecular distance, μ the reduced mass, and E_o a threshold energy, which must be exceeded by the kinetic energy of the colliding molecules for successful reaction. Without going too much into detail we see that the approach to the temperature dependency as given in Eq. (7.7) is only an approximation useful for parameterizing experimental reaction rates.

The more sophisticated approach of transition state theory of chemical reaction rates gives the rate of the bimolecular reaction Eq. (7.8) as translational flux of the involved molecules along the reaction trajectory and the intrinsic reaction rate coefficient is given by

$$k(T) = \kappa \cdot \frac{k_B \cdot T}{h} \cdot \frac{Q'_{AB^{\#}}}{Q'_A \cdot Q'_B} \cdot \exp\left(-\frac{E_0}{k_B \cdot T}\right). \tag{7.10}$$

In Eq. (7.10) h is Planck's constant, E_0 is the energy difference between the rovibrational ground states of the transition state $AB^{\#}$ and the reactants A and B,

and $Q_i' = Q_i/V$ with Q_i the partition function of educts A and B and the transition state $AB^\#$, respectively, the latter one without the vibrational degree of freedom along the reaction trajectory. κ represents a transmission coefficient describing the probability of forward decomposition of the transition state. It is beyond the scope of this chapter to discuss in detail the recent developments of transition state theory (for details see e.g., Battin-Leclerc et al., 2013; Steinfeld et al., 1989; Wright, 2005); however, it should be noticed that again the simple Arrhenius temperature dependency of the rate coefficient is an approximation valid only for a limited range of experimental conditions. Prerequisites of the transition state approach are the potential energy surfaces of the involved molecules in dependency on the atomic distances and directions of mutual approach.

The explanation of the pressure dependency of the reaction rate coefficients for thermal monomolecular dissociation reactions

$$A \xrightarrow{k_{exp}} C + D \tag{7.11}$$

via the bimolecular activation mechanism of Lindemann

$$A + A \underset{}{\overset{k_{act}}{\rightleftharpoons}} A* \xrightarrow{k_{react}} C + D \tag{7.12}$$

in principal reproduces the fall-off behavior of the rate coefficients with increasing pressure

$$\frac{1}{k_{exp}} = \frac{1}{k_\infty} + \frac{1}{k_{act} c_A}. \tag{7.13}$$

Here c_A is the concentration of A which acts also as a collision partner, k_{act} the rate coefficient of the activation step, and k_∞ the high-pressure limit $k_\infty = k_{act} \cdot k_{react}/k_{deact}$ of the rate coefficient. Extending the activation mechanism by introducing of energy-specific rate coefficients leads to

$$k_{exp} = N_c \cdot c_M \cdot \int_{E_0}^{\infty} \frac{k_{react}(E) \cdot f(E)}{N_c \cdot c_M + k_{react}(E)} dE, \tag{7.14}$$

where N_c is the gas kinetic collision number for the hard sphere molecule model (see Eq. 7.9),

$$N_c = \left(\frac{8 \cdot k_B \cdot T}{\pi \cdot \mu_{AM}} \right)^{1/2} \cdot \pi \cdot d_{AM}^2 \tag{7.15}$$

and c_M the concentration of a collision partner. This extension introduces the energy-specific rate coefficient $k_{react}(E)$ and the distribution function $f(E)$ of the reactant molecule over the possible energy states. In the recent past this approach has been expanded with the help of statistical reaction rate theory (see e.g., Olzmann, 2013).

The approach employs master equations with energy-specific rate coefficients $k_{react}(E)$ for every possible energy state from Rice-Ramsperger-Kassel-Marcus (RRKM) statistical theory and the simplified statistical adiabatic channel model and can be used for reactions over potential energy barriers and potential energy wells. The macroscopic rate coefficient $k(T, p)$ of a unimolecular reaction under steady-state conditions is then obtained by averaging its energy-specific rate coefficients over the normalized energy distribution of the reactant. The method is also based on the knowledge of the detailed respective potential energy surfaces.

This is the—often hard to access—idyllic world of reaction kinetics for homogeneous systems and the question arises whether—and if not why—kinetics of underground gasification of coal fits into this world.

Coal originates over million of years from large amounts of biomasses through biochemical and geochemical processes. The extent of coalification determines the degree of conversion of the original biomass to carbon. The degree of conversion is attributed to a number of properties, summarized as the rank of the coal, and Table 7.1 exhibits a wide variation of the elemental composition connected with the content of volatile matter (VM), content of water, and calorific value (CV) consolidated as the rank of coal.

The complexity of the chemical structure of coal, documented by the variation in elemental composition, is reflected by model molecules for coal. One model molecule for bituminous coal is depicted in Fig. 7.1. The coal molecule is characterized by a variety of organic functional groups containing the chemical elements C, H, O, N, and S. The fundamental carbon structures are the polynuclear aromatic, the hydroaromatic, and the aliphatic ones accounting for the largest part of carbon and hydrogen. Furthermore, oxygen-containing functional groups like carboxyl, carbonyl, and ether groups or OH groups are present as well as heterocyclic oxygen, nitrogen, or sulfur-containing groups. Thus coal is a complex structured "molecule" and we cannot expect that gasification of coal can be resolved into simple sequences of reactions between well-defined molecules as written in Eq. (7.1) or (7.11). Moreover, the

Table 7.1 **Variation of coal properties with rank** (Laurendeau, 1978; van Krevelen, 1961)

Rank	% C	% H	% O	% VM	CV (MJ/kg)	% H_2O
Lignite	65–72	4.5	30	40–50	<19.4	>15
Subbituminous (A, B, C)	72–76	5.0	18	35–50	19.4–25.6	10–15
Bituminous (C)	76–78	5.5	13	35–45	25.6–30.2	5–10
Bituminous (B)	78–80	5.5	10	31–45	30.2–32.6	3–5
Bituminous (A)	80–87	5.5	4–10	31–40	33.8	1–2
Bituminous (MV)	89	4.5	3–4	22–31	34.9	<1
Bituminous (LV)	90	3.5	3	14–22	36.8	<1
Anthracite	93	2.5	2	<14	35.4	<1

Note: Composition is given in percentage (mass) of dry mineral matter free coal.
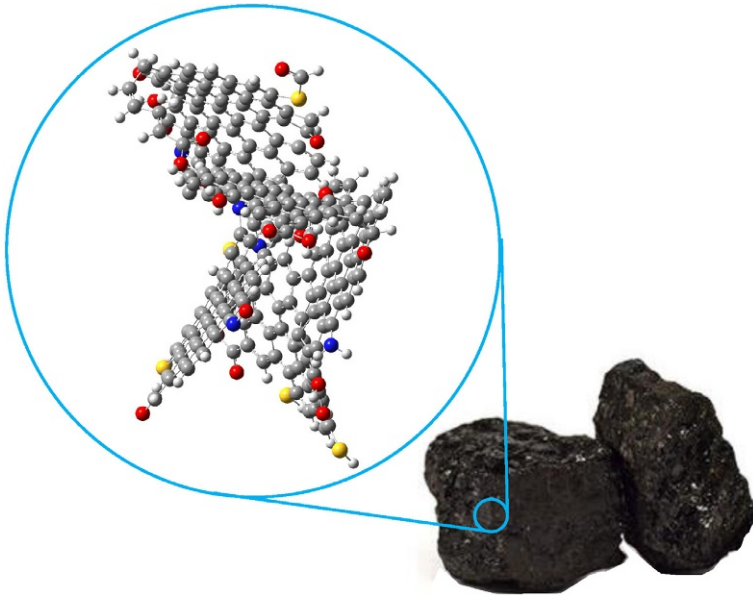
Fig. 7.1 Molecular representation of bituminous coal, see Mathews and Chaffee (2012) and Solomon et al. (1988). *Black*: carbon, *white*: hydrogen, *red*: oxygen, *yellow*: sulfur, *blue*: nitrogen.

different types of chemical bonds exhibit different bond energies, so that during gasification of coal the structure and reactivity of coal will change because functional groups with the weakest bonds will be eliminated first. As a consequence the mechanism and type of reactions will change during the progress of gasification.

The brief view upon that model molecule for coal, therefore, provides some obvious answers to the previous question:

- For the kinetics of coal gasification we will not expect a unique chemical reaction mechanism and unique rate expressions derived from the earlier briefly sketched (and advanced for application) theories.
- Furthermore, the "coal molecules" are assembled irregularly to a solid that exhibits a porous structure with pore sizes d_p ranging from micropores/nanopores with $d_p < 2$ nm, mesopores with 2 nm $< d_p < 50$ nm to macropores with $d_p < 50$ nm. The largest part of solid coal surface where the gasification reactions occur is presented by the internal surface of this porous structure so that gasification reactions are coupled with transport processes through this porous structure to the internal surface.
- Depending on the ratio between transport rates and chemical reaction rates, the apparent reaction kinetics are superposed intrinsic reaction kinetics and transport rates.

7.1.2 Gasification on the technical scale

Underground coal gasification as performed in coal seams is a zonal process. This is the consequence of the gas-solid heterogeneous character of coal gasification and the

fact that in underground coal gasification no feeding of coal through a gasification reactor is possible. In contrary, the "gasification reactor" migrates through the coal seam and only the gaseous reaction components are fed into and withdrawn from the moving reactor. Therefore, only a limited number of operating conditions are free to handle and the overall process is to a large extent autonomous, meaning that, for example, the necessary heat of reaction for the gasification of coal has to be provided by utilization of a part of the coal or that the amount of water expended for gasification is defined by the water content of the coal. The "coal molecule" then undergoes necessarily completely different types of reactions to keep the overall gasification process running. From this view we receive a further answer to the initial question:

- Apparent kinetics of underground gasification is intrinsic kinetics coupled with energy and mass balances of the zonal process.

Fig. 7.2 presents a scheme of underground coal gasification employing the controlled, retractable injection point (CRIP) process. This technique provides a more controllable operating of underground gasification by varying the distance between the production well and the injection well according to the progress of coal consumption. Looking at the enlarged section of the boundary between the gas phase and the solid, five layers in the simplified exposure can be observed with different processes occurring within those layers. At the cold end in the wet zone the original coal of the seam is present which contains water according to the hydrogeological conditions and history of the seam. Depending on these conditions a more or less influx of water into the adjacent zone can occur. The problem for the overall process of underground coal gasification is that this boundary condition can vary with time and often is ill defined or unknown.
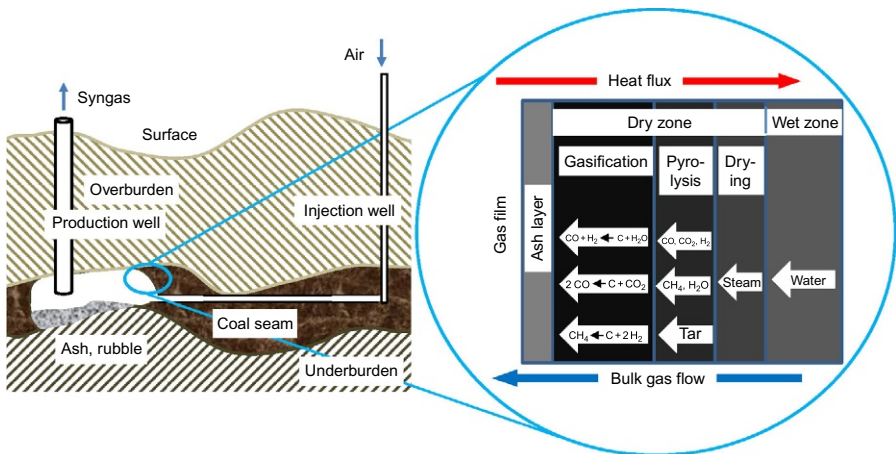
Fig. 7.2 Schematic of underground coal gasification using controlled, retractable injection point (CRIP) technology and qualitative description of processes occurring at the cavity wall, compare also Bell et al. (2011).

Subsequent in the direction to the solid-gas phase boundary the drying zone follows where solely water is vaporized and the resulting steam is possibly overheated under the prevailing conditions. The necessary vaporization energy is provided by heat conduction from the hot pyrolysis zone and the "kinetics" of vaporization are determined by the energy and mass balances for heat transfer and vaporization. Again the problem arises that the boundary conditions for these processes are not well-defined and time-dependent and, furthermore, for example, heat conductivities for the coal are uncertain due to the content of included rock and material properties may not be homogeneous and isotropic.

As can be seen from Table 7.1 bituminous coal contains up to 45% by mass volatiles which are released at higher temperatures in the pyrolysis zone according to the overall endothermic global reaction

$$\text{Coal} \rightarrow \text{Char}_s\ (C) + \text{Volatiles (VM)}. \tag{7.16}$$

Evolution of volatiles from coal is a result of complex chemical reactions, which eliminate the less stable functional groups contained in the coal molecule. According to the single building blocks of the coal molecule the gaseous products of this kind of reactions mainly are higher hydrocarbons, denoted as tar, smaller hydrocarbons, CH_4, H_2, CO, CO_2, and H_2O. The solid product of devolatilization and pyrolysis is char—denoted as C in Eq. (7.16)—with a high C/O- and C/H-ratio, compare Table 7.1. Together with the steam from the drying zone the pyrolysis products flow into the char gasification zone where they undergo further heterogeneous and homogeneous secondary reactions.

Finally, gasification of char occurs in the char gasification zone primarily by the two highly endothermic gasification reactions

$$C + H_2O \rightarrow CO + H_2 \tag{7.17}$$

and

$$C + CO_2 \rightarrow 2CO \tag{7.18}$$

and to a less extent by the slightly exothermic reaction

$$C + 2H_2 \rightarrow CH_4. \tag{7.19}$$

The overall gasification process is endothermic and the necessary reaction energy as well as the necessary energy for vaporization and devolatilization has to be provided and balanced by combustion of a part of the char

$$C + O_2 \rightarrow CO_2. \tag{7.20}$$

Combustion according to Eq. (7.20) is performed with air being fed through the injection well and proceeds near the phase boundary char-gas. The energy released by combustion is transported by heat conduction from that region converse to the bulk gas flow into the gasification zone, the pyrolysis zone and the drying zone to keep the process running.

The content of anorganics in the char from included or embedded minerals remains as ash layer covering the char. The products of gasification and the reactants must be transported through that ash layer and the rate of mass transfer may under circumstances determine the kinetics of the process.

In the gas phase secondary homogeneous reactions between the products of gasification and devolatilization and oxygen may occur.

In summary from the simplified schematic in Fig. 7.2 for underground coal gasification different classes of chemical reactions can be identified, namely

- drying of wet coal (vaporization of water);
- devolatilization and pyrolysis of coal;
- heterogeneous gasification of char;
- heterogeneous oxidation of char; and
- homogeneous (and heterogeneous) secondary reactions of gasification and pyrolysis products.

The kinetic aspects of which in connection with transport processes and mass and energy balances will be discussed in the following sections.

7.2 Kinetic aspects of the different classes of reactions during gasification

As discussed in Section 7.1.2 underground coal gasification consists of chemical reactions interacting with mass and energy transport. The chemical reactions are to the largest part heterogeneous with consumption of the solid phase. In contrast to Eq. (7.5), therefore, different methodology for the formulation of apparent reaction rates has to be used encompassing intrinsic reaction kinetics superposed with mass and energy transfer rates. The different types of transport processes and chemical reactions are distributed over different layers of the coal seam with different physical and chemical properties, leading to unknown or not well-defined and time-dependent operating and boundary conditions, complicating additionally the considerations.

7.2.1 "Kinetics" of drying

In the drying zone water is heated from the conditions in the wet zone to the boiling point under the prevailing conditions and the steam is overheated to the conditions of the adjacent boundary of the pyrolysis zone, compare Fig. 7.2. The necessary energy for drying and overheating is provided by heat conduction from the pyrolysis zone and occurs in counter flow to the transport of water/steam. For the surface of vaporization at temperature T_{vap} in the drying zone an energy balance can be drafted, which equalizes the most prominent heat fluxes (i.e., the heat flux by conduction, the heat of vaporization of the inflowing and contained water, and the heating of the solid)[1]

---

[1] For simplicity the formulation of balance equations will be one dimensional which may be appropriate for the discussion in this chapter.

$$\lambda_{\text{coal}} \cdot A_{\text{vap}} \cdot \left(\frac{dT}{dx}\right)_{x_{\text{vap}}} = \left(\dot{m}_{\text{H}_2\text{O}1} + \dot{m}_{\text{H}_2\text{O contained}}\right) \cdot h_{\text{vap}} + \dot{H}_{\text{heat}} \tag{7.21}$$

with

$$\dot{m}_{\text{H}_2\text{O contained}} = y_{\text{H}_2\text{O}1} \cdot \rho_{\text{coal}} \cdot \left(A_{\text{vap}} \cdot \frac{dx}{dt}\right) \tag{7.22}$$

and

$$\dot{H}_{\text{heat}} = \rho_{\text{coal}} \cdot c_{p\text{ coal}} \cdot T_{\text{vap}} \cdot \left(A_{\text{vap}} \cdot \frac{dx}{dt}\right). \tag{7.23}$$

Eqs. (7.22), (7.23) reflect that the surface of vaporization migrates toward the wet zone inducing a time change of the vaporization volume ($A_{\text{vap}} \cdot dx/dt$). In Eqs. (7.21)–(7.23) $\dot{m}_{\text{H}_2\text{O}1}$ is the mass flux of water into the drying zone, h_{vap} is the mass-specific heat of vaporization under the prevailing conditions, $y_{\text{H}_2\text{O}1}$ is the mass fraction of water in the coal, and A_{vap} is the area of the surface of vaporization. Material properties of the coal, namely heat conductivity λ_{coal}, specific heat capacity $c_{p\text{ coal}}$, and density ρ_{coal}, are averaged values. This formulation assumes that the contained water is in thermal equilibrium with the solid. Eq. (7.21) can be transformed to give the migration rate of the surface of vaporization dx/dt

$$u_{\text{migr}} = \frac{\lambda_{\text{coal}}}{y_{\text{H}_2\text{O}1} \cdot \rho_{\text{coal}} \cdot h_{\text{vap}} + \rho_{\text{coal}} \cdot c_{p\text{ coal}} \cdot T_{\text{vap}}} \cdot \left(\frac{dT}{dx}\right)_{x_{\text{vap}}}$$
$$- \frac{\dot{m}_{\text{H}_2\text{O}1} \cdot h_{\text{vap}}}{\left(y_{\text{H}_2\text{O}1} \cdot \rho_{\text{coal}} \cdot h_{\text{vap}} + \rho_{\text{coal}} \cdot c_{p\text{ coal}} \cdot T_{\text{vap}}\right) \cdot A_{\text{vap}}}. \tag{7.24}$$

Eq. (7.24) reveals that the surface of vaporization migrates toward the wet zone if there is no influx of water from the wet zone and the migration rate increases with increasing heat conductivity λ_{coal} and temperature gradient $(dT/dx)_{x_{\text{vap}}}$ and decreasing water content $y_{\text{H}_2\text{O}1}$ of the coal. Increasing influx of water reduces the migration rate and effects a stationary situation for the two terms on the right-hand side of Eq. (7.24) being balanced. If the last term on the right-hand side overtops the first term, the migration rate changes its direction and the surface of vaporization moves toward the pyrolysis zone.

The heat conductivity λ_{coal} of coal enters the balance equations discussed earlier. The variation of the thermal conductivity of a solid with temperature depends on the type of material. The conductivities of most metals decrease with temperature, whereas the conductivities of nonmetals increase and the variations in thermal conductivity usually parallel those of electrical conductivity. Experiments on heat conductivities of coals show a rise with increasing temperature, which has been attributed to radiant heat transfer across pores and cracks, changes in the conductivity of the coal due to pyrolysis and changes in the intrinsic conductivity with temperature.

Coal can be regarded as nonmetal and the rise in thermal conductivity observed at temperatures below 600°C is likely to be due to the latter effect. To account also for the elemental composition relations for the thermal conductivity of coals such as

$$\frac{1}{\lambda_{\text{coal}}} = \left(\frac{y_{\text{C}}}{1.47} + \frac{y_{\text{H}}}{0.0118}\right) \cdot \left(\frac{273}{T}\right)^{0.5} \quad (\text{m K}/W) \tag{7.25}$$

have been proposed (Merrick, 1987). In Eq. (7.25) T is the absolute temperature and y_{C} and y_{H} are the mass fractions of carbon and hydrogen, respectively, assuming that the contributions for each element are additive. To be applicable to coals in coal seams relations of the earlier kind have to be extended to reflect inclusions of minerals and the porous structure of the coals. The effective heat conductivity then is lower compared with the heat conductivities according to Eq. (7.25), which lie in the order of magnitude of 3 W/(m K) at 600°C.

Rearranging the energy balance Eq. (7.21) into

$$(\dot{m}_{\text{H}_2\text{O g}})_{\text{influx}} + (\dot{m}_{\text{H}_2\text{O l}})_{\text{contained}} = \frac{\lambda_{\text{coal}} \cdot A_{\text{vap}}}{h_{\text{vap}}} \cdot \left(\frac{dT}{dx}\right)_{x_{\text{vap}}} - \frac{\dot{H}_{\text{heat}}}{h_{\text{vap}}} \tag{7.26}$$

demonstrates that the flux of the generated steam is linearly correlated with the temperature gradient $(dT/dx)_{x_{\text{vap}}}$ at the vaporization surface the formation of steam, hence, being of "first order" in temperature. Variations in the inflowing or contained water lead to variations in the temperature gradient and migration rates.

Vaporization also is affected by mass transport of the inflowing water and/or generated steam. As mentioned in Section 7.1.1 coal offers a porous structure with different sized pores, see Fig. 7.3. Pore sizes range from smaller than 2 nm diameter for micropores to larger than 50 nm for macropores. Depending on the geohistoric situation also cracks with macroscopic dimensions and closed pores or cavities are present. Water contained in this porous structure or entering from the wet zone and steam generated during drying have to be transported in counterflow to the heat flux versus the pyrolysis zone. Depending on the pore sizes this transport can occur by viscous flow or diffusion.

For viscous flow the volumetric flow rate is given by Darcy's law and proportional to the pressure gradient with

$$\dot{m}_{\text{H}_2\text{O}} = -\rho_{\text{H}_2\text{O}} \cdot \frac{\kappa_{\text{coal}}}{\mu_{\text{H}_2\text{O}}} \cdot A_{\text{vap}} \cdot \frac{dp}{dx}, \tag{7.27}$$

where $\mu_{\text{H}_2\text{O}}$ is the viscosity of water and κ_{coal} the permeability of the coal. Similar to the heat conductivity of the coal the latter properties are dependent on the prevailing conditions and ill defined and may change during the drying process.

Diffusional transport of species through the porous structure from a macroscopic point of view is described by an empirically derived effective diffusivity D_{eff} and the mass fluxes are expressed with the help of Fick's diffusion law
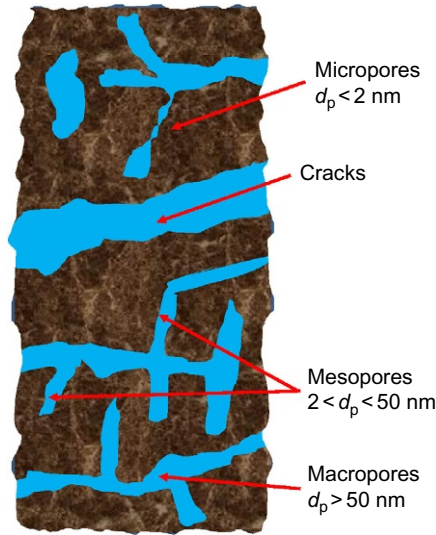
Fig. 7.3 Pore structure of coal (schematic).

$$\dot{m}_i = -D_{i\,\text{eff}} \cdot A \cdot M_i \cdot \frac{dc_i}{dx}. \tag{7.28}$$

The effective diffusivity $D_{i\,\text{eff}}$ represents the reciprocal of a diffusional resistance throughout the coal layer. From a microscopic approach, diffusion through a single pore rather than the entire porous particle is considered. The overall particle is depicted by an appropriate combination of single pores. Diffusion through an individual pore is described using capillary diffusion theory and according to that isobaric flow through a pore may involve molecular diffusion or Knudsen diffusion. Molecular diffusion becomes the predominant mode of transport whenever the pore size is large compared to the mean free path of the diffusing species $d_p/\lambda_i > 10$. The molecular diffusion coefficient is a function of temperature and pressure and can be expressed according to the kinetic theory of gases by

$$D_i(T,p) = D_{i\,0}(T_0,p_0) \cdot \left(\frac{T}{T_0}\right)^{7/4} \cdot \left(\frac{p_0}{p}\right), \tag{7.29}$$

where the index 0 refers to a reference state.

Knudsen diffusion is molecular transport via collisions with the walls of the pores and occurs primarily when the pore size is small with respect to the mean free path of the molecules $d_p/\lambda_i < 0.1$. For smooth pores, the Knudsen diffusion coefficient can be expressed as

$$D_{i\,\text{Kn}} = \frac{d_p}{3} \cdot \left(\frac{8 \cdot R \cdot T}{\pi \cdot M_i}\right)^{1/2}, \tag{7.30}$$

where M_i is the molar mass of the species i. From Eq. (7.30) it can be seen that the Knudsen diffusion coefficient $D_{i\,\mathrm{Kn}}$ in contrast to the molecular diffusion coefficient is independent of pressure and linearly proportional to pore diameter. Diffusion coefficients can be interpreted as reciprocal normalized diffusion resistances. Therefore, the combined effects of both Knudsen and molecular diffusion can be modeled as the addition of the respective resistances

$$\frac{1}{D_{i\,\mathrm{eff}}} = \frac{1}{D_{i\,\mathrm{Kn}}} + \frac{1}{D_i(T,p)}. \tag{7.31}$$

Fig. 7.3 exhibits that the material properties of coal due to the inclusion of pores and minerals are nonisotropic and heat conduction, for example, in the solid coal occurs with a different conductivity than in the water filled pores or in the rock leading necessarily to a three-dimensional heat conduction/heat transfer problem.

Despite the simplifications used here, the earlier discussion clearly documents that heat flux, extension, and location of the drying zone as well as migration rate adjust interdependently to variations of the flux and content of water. The flux of steam from the drying zone and the temperature gradient at the surface of vaporization in the drying zone are linearly related. The time change of the molar amount of water in the drying zone volume which represents a reaction rate for the "drying reaction" according to Eq. (7.2) or (7.5) then is of first order in temperature.

7.2.2   Devolatilization kinetics

As noted in Section 7.1.2 devolatilization of coal according to the overall endothermic formal reaction

$$\mathrm{Coal} \rightarrow \mathrm{Char_s}\ (\mathrm{C}) + \mathrm{Volatiles}\ (\mathrm{VM}) \tag{7.32}$$

occurs via a complex reaction mechanism with numerous single chemical reactions in the solid phase eliminating the less stable functional groups contained in the coal molecule outlined in Fig. 7.1. The reaction is of heterogeneous type with depletion of the solid phase and formation of gaseous and liquid phases. A general qualitative scheme (Solomon et al., 1988, 1992) for the chemical reactions occurring during devolatilization of coal derived from the coal molecule is depicted in Fig. 7.4. This coal molecule represents the chemical compositions and functional groups for a bituminous coal (Solomon et al., 1988). It consists of aromatic and hydroaromatic clusters including heterocycles linked by aliphatic bridges and is the point of origin of devolatilization reactions. Starting from the coal molecule in the raw coal the figure exhibits the formation of tar and light hydrocarbons during primary pyrolysis, and the formation of char through condensation and cross-linking during secondary pyrolysis.

During primary pyrolysis the weakest bridges indicated by red lines in the structure break producing mean sized molecular fragments. The fragments abstract hydrogen from the hydroaromatics or aliphatics, increasing the aromatic character of the residue. The formed fragments are released as tar if they are small enough to vaporize.
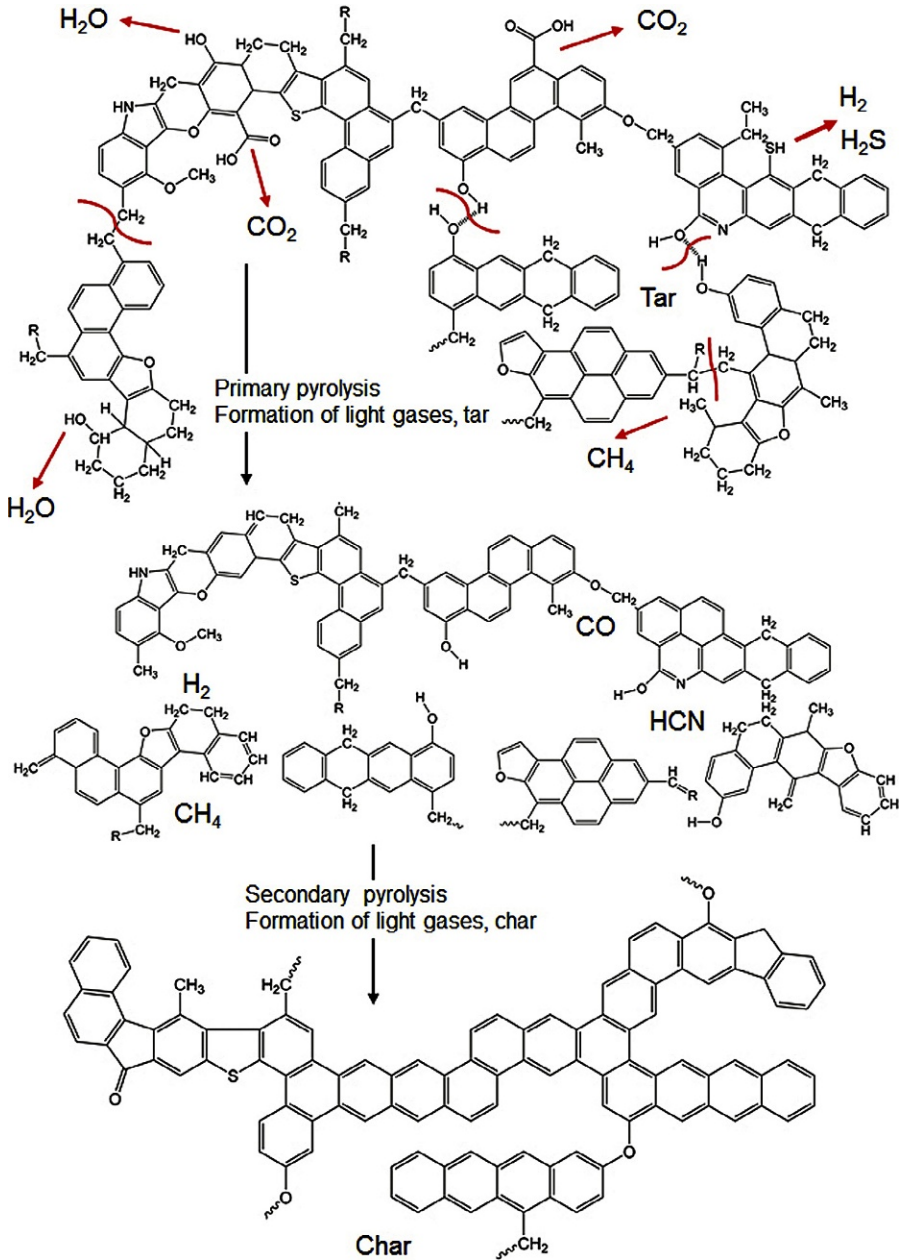
Fig. 7.4 Outline of the chemical reactions of devolatilization of coal (Solomon et al., 1988, 1992; Veras et al., 2002).

At the prevailing temperatures in the pyrolysis zone growth reactions appear to be slower than bond-breaking reactions. Therefore, the smaller fragments are transported out of the pyrolysis zone under typical pyrolysis conditions and do not undergo pyrolytic growth reactions before escaping from the pyrolysis zone. Growth reactions are connected to formation of CH_4 and lead to higher molecular weight components which are too large to vaporize and result in the formation of a type of tar which contributes to char formation.

The other processes during primary pyrolysis are the decomposition of functional groups to release gases, mainly CO_2, light aliphatic hydrocarbons, and some CH_4 and H_2O. The release of CH_4, CO_2, and H_2O is followed by growth reactions via cross-linking. Cross-linking reactions are induced via CH_4 by a substitution reaction in which the attachment of a larger molecule releases the methyl group. CO_2 induces cross-linking by condensation after a radical is formed on the ring when a carboxyl is removed. Cross-linking via H_2O occurs by condensation of two OH groups or an OH group and a COOH group. The competition between growth reactions and bond-breaking reactions determines the tar content of the char. The drift off of primary pyrolysis is connected with the depletion of disposable hydrogen from hydroaromatic or aliphatic portion of the coal.

During secondary pyrolysis there is additional formation of light gaseous molecules, CH_4 from methyl groups, HCN from heterocyclic nitrogen compounds, CO from ether links, and H_2 from ring condensation.

7.2.2.1 Kinetic description

The kinetic description of the devolatilization of coal obviously possesses two principal difficulties: first, devolatilization of coal is a very complex process between heterogeneous phases consisting of numerous bond-breaking elementary steps occurring for a wide variety of chemical bonds between divers reaction centers located at vastly different molecular (polymeric) structures. Rate equations for the devolatilization of solids can be derived from molecular mechanisms, for example, the thermal decomposition of single monomer polymers (Bockhorn et al., 1999, 2000); however, there is no hope to find an analogous way for the devolatilization of coal. Therefore, the formation reactions of the different pyrolysis products are mostly lumped together in single global reactions. Due to the predominating bond-breaking reactions the supposition of first-order reaction kinetics often seems to be justified. Second, the reaction products are partially gaseous, liquid, and solid, and for an appropriate kinetic description an adequate conversion variable has to be defined. For the products evolving from the solid coal structure during devolatilization the conversion variable can be given as

$$\xi_i = \frac{m_i(t)}{m_{i\,0}} \quad d\xi_i = \frac{1}{m_{i\,0}} \cdot dm_i, \tag{7.33}$$

where $m_i(t)$ is the amount of species i formed until time t and $m_{i\,0}$ is the ultimate amount which is a priori unknown and a function of the rank of coal (see Table 7.1). The conversion variable in terms of masses seems to be appropriate in this case because

molecular structures and molar masses of the volatiles (e.g., tars) are unknown. As evolution of volatiles diminishes with reaction progress, kinetic rate equations unlike Eq. (7.5) are written in the form

$$\frac{d\xi_i}{dt} = k_i(T,p) \cdot (1 - \xi_i)^{\mu_i} \quad (1/\text{s}). \tag{7.34}$$

In Eq. (7.34) $k_i(T, p)$ is the respective rate coefficient and μ_i the reaction order with respect to species i. Evaluating experimental conversion rates to obtain

$$k_{i\,\text{exp}} = \frac{\dfrac{d\xi_i}{dt}}{(1 - \xi_i)^{\mu_i}} \tag{7.35}$$

yields then an apparent rate coefficient $k_{i\,\text{exp}}$ and its temperature dependency may be expressed with the help of Eq. (7.7) and an apparent activation energy. If a first-order reaction $\mu_i \approx 1$ is utilized, this formulation gives the rate as proportional to the instantaneous source of species i. Kinetic rate equations for the devolatilization of coal, therefore, are mostly written in the form of Eq. (7.34) and pool all reactions for the formation of single species or groups of species.

For a constant heating rate $dT/dt = \beta$ which may prevail in underground gasification at a fixed location in the pyrolysis zone, temperature linearly increases with time $T = T_0 + \beta \cdot t$ and Eq. (7.34) can be rewritten

$$\frac{d\xi_i}{dt} = k_{0\,i} \cdot \exp\left[-\frac{E_{A\,i\,\text{app}}}{R(T_o + \beta t)}\right] (1 - \xi_i)^{\mu_i}. \tag{7.36}$$

Typical reaction rates $d\xi/dt$ and reaction progress ξ from the numerical integration of Eq. (7.36) for a reaction order $\mu_i = 1$ in dependence on time t and temperature T are given in Fig. 7.5. The diagram exhibits the trace of the reaction rate from low values at low temperatures passing through a maximum and then approaching zero when the source of species i is depleted and the devolatilization is complete. Accordingly, the reaction progress ξ asymptotically approaches 1. Increasing the heating rate dT/dt shifts the maximum of the reaction rate to smaller times, however, due to the nonlinear dependence of the reaction rates on temperature to higher temperatures. The increasing branch of the reaction rate trace is due to the exponential dependency of reaction rate on temperature whereas the decreasing branch reflects the limitation of the source of the species. As the pyrolysis zone migrates through the coal seam reaction progress and reaction rates as given in Fig. 7.5 apply for a fixed location in the pyrolysis zone. However, migration of the pyrolysis zone produces a continuous formation of devolatilization products.

7.2.2.2 SRFOM approach

Rate coefficients k_{exp} for the formation of pyrolysis products according to Eq. (7.34) are given in Table 7.2 (Serio et al., 1987; Solomon et al., 1992). The reaction model underlying these rate coefficients is a "single reaction first-order model" (SRFOM)
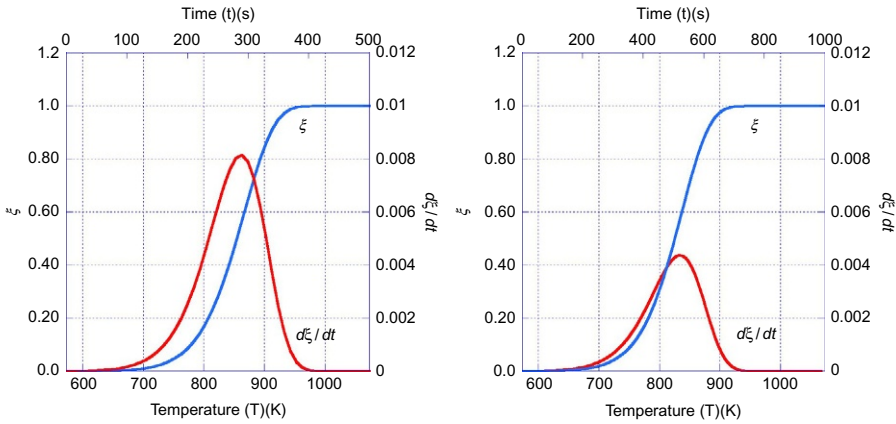
Fig. 7.5 Reaction progress ξ and reaction rate $d\xi/dt$ versus temperature and time according to Eq. (7.34) for parameters typically for the evolution of CH_4 from bituminous coal (Serio et al., 1984), see Table 7.2. *Left*: heating rate 1.0 K/s, *right*: heating rate 0.5 K/s.

Table 7.2 **Rate parameters k_{exp} according to Eq. (7.7) for the formation of pyrolysis products according to Eq. (7.34) and the SRFOM approach (Serio et al., 1987; Solomon et al., 1992)**

Species	Coal type	$k_{0\,i}$ (per s)	$E_{A\,i\,app}$ (kJ/mol)	k(773 K) (per s)
CH_4	Bituminous	7.5×10^5	125.6	2.44×10^{-3}
C_2H_6	Bituminous	3.0×10^6	134.0	2.64×10^{-3}
CO	Bituminous	1.0×10^{13}	230.3	2.74×10^{-3}
CO_2	Bituminous	1.0×10^{13}	167.5	4.80×10^{1}
H_2O	Bituminous	7.9×10^{13}	213.5	2.95×10^{-1}
H_2	Bituminous	1.0×10^{17}	376.8	3.45×10^{-9}
HCN	Bituminous	6.9×10^{12}	353.4	9.09×10^{-12}
NH_3	Bituminous	1.2×10^{12}	227.0	5.49×10^{-4}
Tar	Bituminous	4.1×10^5	117.3	4.86×10^{-3}

and the parameters of the model are evaluated by fitting the model to experimental data. It should be noted that the results from this procedure may be affected by the kinetic compensation effect (Zsakó, 1976). The kinetic compensation effect is an apparent effect, which is due to the form of the Arrhenius equation. This effect consists of a correlation between the kinetic parameters of the decomposition reactions, so that the increase of the apparent activation energy is accompanied by an equivalent increase of the pre-exponential factor. Table 7.2 contains also the rate coefficients for the formation of different pyrolysis products at a temperature of 500°C. According to this data the by far fastest reactions are the formation reactions of CO_2 and H_2O and the rates of the formation reactions of CH_4, C_2H_6, CO, and tar are by some orders of magnitude slower.

7.2.2.3   DAEM or DRM approach

To consider the multiplicity of reactions for the formation of a single species from the variety of functional groups in the coal molecule the approach according to Eq. (7.34) is extended by introducing a distribution of activation energies E_A and possibly frequency factors k_o (distributed activation energy model [DAEM] or distributed rate model [DRM]). This model assumes that the ultimate amount $m_{i\,0}$ giving to the same pyrolysis product is somewhat inhomogeneous due to the different functional groups in the coal molecule. Instead of a single activation energy E_A, the ultimate amount contains components having a distribution of activation energies about a mean $\langle E_A \rangle$. As distribution function often the Gaussian distribution function is used

$$m_i(E) = \frac{m_{i\,0}}{\sigma_i \cdot \sqrt{2 \cdot \pi}} \cdot \exp\left[-\frac{(E_{A\,i} - \langle E_{A\,i} \rangle)^2}{2 \cdot \sigma_i^2} \right], \tag{7.37}$$

where $m_i(E)$ is the part of the ultimate amount with activation energy $E_{A\,i}$, $\langle E_{A\,i} \rangle$ is the mean activation energy, and σ_i is the width of the distribution. The integral of $m_i(E)$ over $E_{A\,i}$ is the ultimate amount of the species i. Some models also use both distributed activation energies and frequency factors. Rate coefficients for the distributed activation energy model are given in Table 7.3. The ratio of the rate coefficients for the formation of the single components at a constant temperature for SRFOM and DAEM is comparable. This approach often results in better fits of experimental data, however, does not resolve the principal problems connected with this method.

7.2.2.4   Reaction networks

The literature about coal devolatilization offers numerous approaches to resolve the complex chemical reaction mechanism into a more or less complex network of single chemical reactions. A first step into that direction is the description of devolatilization by two competing reactions

Table 7.3 Rate parameters k_{exp} for the formation of pyrolysis products according to the distributed activation energy model Eq. (7.37) (Serio et al., 1984, 1987; Solomon et al., 1992)

Species	Coal type	$k_{0\,i}$ (per s)	$\langle E_{A\,i} \rangle$ (kJ/mol)	σ_i (kJ/mol)	$k(713\ K)$ (per s)
CH_4	Bituminous	4.7×10^{11}	209.4	2.5	2.08×10^{-4}
Light aliphatic	Bituminous	8.4×10^{14}	247.4	3.0	5.97×10^{-4}
CO	Bituminous	1.4×10^{18}	330.7	11.8	7.70×10^{-7}
CO_2	Bituminous	5.6×10^{17}	247.0	4.0	4.30×10^{-1}
H_2O	Bituminous	2.2×10^{18}	251.2	3.0	8.30×10^{-1}
H_2	Bituminous	1.0×10^{14}	334.9	12.5	3.80×10^{-11}
Tar	Bituminous	8.6×10^{14}	228.6	3.0	1.00×10^{-2}

$$\text{Coal} \xrightarrow{k_1} (1 - \alpha_1) \, \text{Char}_{s\,1} + \alpha_1 \, \text{Volatiles}_1 \tag{7.38}$$

and

$$\text{Coal} \xrightarrow{k_2} (1 - \alpha_2) \, \text{Char}_{s\,2} + \alpha_2 \, \text{Volatiles}_2, \tag{7.39}$$
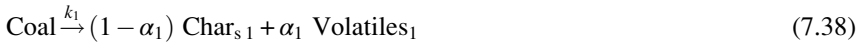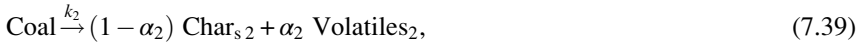
where the first reaction with a lower apparent activation energy predominates at low temperatures and the second one with high apparent activation energy at higher temperatures. With

$$k_{0\,1} = 2.0 \times 10^5 / \text{s} \quad E_{A\,1} = 100.5 \, \text{kJ/mol} \quad \alpha_1 = 0.3$$
$$k_{0\,2} = 1.3 \times 10^7 / \text{s} \quad E_{A\,1} = 167.5 \, \text{kJ/mol} \quad \alpha_1 = 1.0$$

a better fit for the experimental data for lignite and bituminous coal is obtained than with a single reaction approach (Kobayashi et al., 1977). This approach is extended to higher level of complexity by generalized devolatilization models such as tar formation models, species evolution/functional group models, and chemical network models that consider the evolution of single gas species. These models are based on the descriptions of the coal structure and on the processes that the coal experiences during devolatilization. One example of the tar formation models is the chemical percolation devolatilization (CPD) model (Jupudi et al., 2009). An example of the chemical network model is the functional group-devolatilization vaporization cross-linking (FG-DVC) model (Solomon et al., 1988). Predictions utilizing these models seem to be applicable over a wide range of coal types and process conditions as these models are based on fundamental processes occurring during devolatilization.

The FG-DVC model includes individual rate equations for various light gas species that evolve during devolatilization. The basis of this approach is that coal is viewed as an ensemble of functional groups that are organized into tightly bound aromatic ring clusters and are connected by bridges, see Fig. 7.4. Tar and light gas species are released by the thermal decomposition of these individual functional groups and the kinetics are expected to depend on the functional group or the nature of bond breaking (Solomon et al., 1988). One drawback of this approach is that the necessary structural data are not a priori available.

The CPD model considers the physical features of FG-DVC models and relates them to coal structural properties as inputs without any adjustable constants (Grant et al., 1989; Jupudi et al., 2009). The model employs percolation statistics to describe the generation of light gas/tar precursors of finite size based on the number of cleaved labile bonds in the infinite coal lattice. Coal-dependent chemical structure coefficients are taken directly from experiments, for example, by ^{13}C NMR measurements, or by using correlations developed from experiments with several coals. In addition, coal-independent kinetic parameters are employed for the formation of the different components of the reaction network. Fig. 7.6 shows the simple reaction scheme in the original CPD model (Grant et al., 1989). The reaction starts with the cleaving of a chemical bond in a labile bridge (Br) to form a highly reactive bridge intermediate
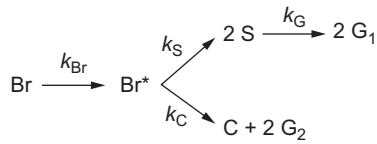
Fig. 7.6 Reaction scheme of the CDP model (Jupudi et al., 2009; Grant et al., 1989).

(Br*). The reactive bridge intermediate may either be released as a light gas (G_2) with the concurrent relinking of the two associated sites within the reaction cage to give a stable or charred bridge (C). Or the bridge material may be stabilized to produce side chains (S) that may convert into light gas (G_1) fragments through a subsequent slower reaction. Parameters of the CPD model are listed in Table 7.4 (Grant et al., 1989).

The parameters given in Table 7.4 can be used to simulate the evolution of the gaseous components G_1 and G_2 and formation of char C. The apparent activation energies used in the model are distributed to correspond with the changing distributions of bond strengths as the species evolve. A normal distribution of the activation energies with the width σ is used for calculations. The coal structure-dependent parameters entering the model and determined from experiments with the respective coals are on the basis of normalized site populations. ($\alpha + 1$) is the coordination number of a site in the coal lattice and determined from NMR data and is used for calculating m_{Br}/m_{site}.

7.2.2.5 Coupling to heat transport

Heat flux into the pyrolysis zone, extension and location of the pyrolysis zone, evolution rate of volatiles as well as migration rate of the pyrolysis zone adjust interdependently to variations of the content and evolution of volatiles in the coal. Detailed calculations need the solution of the nonstationary energy and mass balances in the pyrolysis zone. However, an energy balance for a surface of reaction in the pyrolysis zone can be drafted, which relates the most prominent heat fluxes, namely, the entire

Table 7.4 Coal type independent rate parameters (upper part) and coal type dependent parameters (lower part) for the CPD model (Grant et al., 1989)

	$k_{0\,i}$ (per s)	$E_{A\,i}$ (kJ/mol)	σ_i (kJ/mol)
k_{Br}	2.6×10^{15}	231.9	7.5
k_G	3.0×10^{15}	288.9	33.9
k_S/k_C		0.9	

	($\alpha + 1$)	m_{Br}/m_{site}	Br_0	C_0
Zap lignite	4.5	0.82	0.3	0.31
Rosebud subbituminous	5.8	0.35	0.12	0.44
High-volatile bituminous	4.6	0.35	0.11	0.48

heat of reaction $\sum_i \dot{m}_i \Delta_R h_i$ for the endothermic pyrolysis reactions, the heating of the solid and the energy provided by heat conduction into the surface of reaction in the pyrolysis zone

$$\lambda_{char} \cdot A_{pyr} \cdot \left(\frac{dT}{dx}\right)_{x_{pyr}} = \sum_i \dot{m}_i \Delta_R h_i + \dot{H}_{heat} \tag{7.40}$$

with

$$\dot{H}_{heat} = \rho_{coal} \cdot c_{p\,coal} \cdot T_{pyr} \cdot \left(A_{pyr} \cdot \frac{dx}{dt}\right), \tag{7.41}$$

where $\sum_i \dot{m}_i \Delta_R h_i$ is the overall heat of reactions of the devolatilization for the single components i and $(dT/dx)_{x_{pyr}}$ is the temperature gradient at the surface of reaction. Replacing $\dot{m}_i$ by the rate expressions from Eq. (7.34) we obtain an estimate for the migration rate of the surface of reaction

$$u_{migr} = \frac{\lambda_{coal}}{\rho_{coal} \cdot \sum_i (y_{i\,0} \cdot \Delta_R h_i \cdot d\xi_i/dt) + \rho_{coal} \cdot c_{p\,coal} \cdot T_{pyr}} \cdot \left(\frac{dT}{dx}\right)_{x_{pyr}}, \tag{7.42}$$

where $y_{i\,0}$ is the ultimate mass fraction of the volatile i in the coal, see Table 7.5. The migration rate increases with increasing temperature gradient and heat conductivity of the coal and decreases with increasing energy requirements from the devolatilization reactions. For depleting sources for the volatiles, the migration rate is determined by the heating rate of the solid.

Table 7.5 **Ultimate mass fractions $y_{i\,0}$ of different pyrolysis products from different coal types (Solomon et al., 1992)**

Species	Coal type					
$y_{i\,0}$	N. Dakota lignite	Gillette subbit.	Mont. rosebud bit.	Illinois no. 6 bit.	Kentucky no. 9 bit.	Pittsburgh no. 8 bit.
CH_4	0.025	0.043	0.034	0.044	0.050	0.050
CH_x	0.095	0.158	0.127	0.081	0.183	0.190
CO	0.194	0.154	0.068	0.123	0.096	0.092
CO_2	0.100	0.099	0.100	0.074	0.011	0.011
H_2O	0.094	0.062	0.102	0.045	0.022	0.022
$H_{arom.}$	0.017	0.012	0.013	0.016	0.012	0.012
HCN	0.018	0.022	0.020	0.026	0.035	0.031
NH_3	0.001	0.000	0.001	0.000	0.000	0.000

Due to the temperature gradient in the pyrolysis zone the pyrolysis reactions occur at higher temperatures at the hot end of the pyrolysis zone and at lower temperatures at the cold end of the pyrolysis zone. The different temperature dependency of the formation reactions of the single gaseous and liquid pyrolysis products (see Fig. 7.5 and Table 7.2) and the different ultimate amounts $m_{i\,0}$ of the single components cause a varying product distributions in the pyrolysis zone with time and from the hot side to the cold side.

The time change of the molar amounts of volatiles per volume of the pyrolysis zone which represents a reaction rate for the pyrolysis reactions follows rate expressions as given in Eq. (7.34) and is coupled to the temperature gradient at the surface of reaction in the pyrolysis zone. If $\dot{m}_i$ is controlled by diffusion of the components in the porous structure of the coal, compare Eq. (7.28), the migration rate is adapted accordingly, see discussion in Section 7.2.1.

7.2.3 Gasification kinetics

Pyrolysis products formed in the pyrolysis zone as well as water from the wet and drying zones enter conversely to the heat flux into the gasification zone. The large differences in the rate coefficients for the formation of the single components, compare Tables 7.2 and 7.3, spread the evolution of the single pyrolysis products over temperature and time. At temperatures of about 500°C the rate coefficient for the first-order reaction of formation of CO_2 is three orders of magnitude larger than that of formation of water, and about five orders of magnitude larger than those of formation of CH_4, C_2H_6, NH_3, and tar. The rate coefficients for formation of H_2 and HCN are even lower. Therefore, the formation of CO_2 and H_2O occurs at comparatively low temperatures and at high reaction rates compared with the formation of the other pyrolysis products. However, the increase of temperature in the gasification zone and the large time scale of the overall process finally cause the evolution of the pyrolysis products according to the ultimate amount of the component $m_{i\,0}$ in the coal. This source of the different pyrolysis products in terms of the ultimate mass fractions of the volatiles in the coal $y_{i\,0}$ is given in Table 7.5 for different types of coal (Solomon et al., 1992).

Table 7.5 exhibits vast variations in the ultimate mass fractions of the different pyrolysis products depending on the coal type. However, the most abundant components from pyrolysis of coal are H_2O, CH_4, CO, CO_2, and aliphatic hydrocarbons. The chemical reactions of these components with char (C) are solid/gaseous heterogeneous reactions with the depletion of the solid phase. Coincidentally, the solid phase offers a highly porous structure with changing morphology. Therefore, the gasification reactions may interfere with transport processes to the reacting surface of the solid and the kinetics of gasification are dependent on the morphology of the char. Furthermore, the solid phase can be consumed via different char particle conversion mechanisms.

Generally, a heterogeneous reaction occurs via a sequence of steps as depicted in Fig. 7.7:

1. The reactant gases move to the solid surface due to fluid flow and diffusion.
2. The reactant gases adsorb on the solid surface.
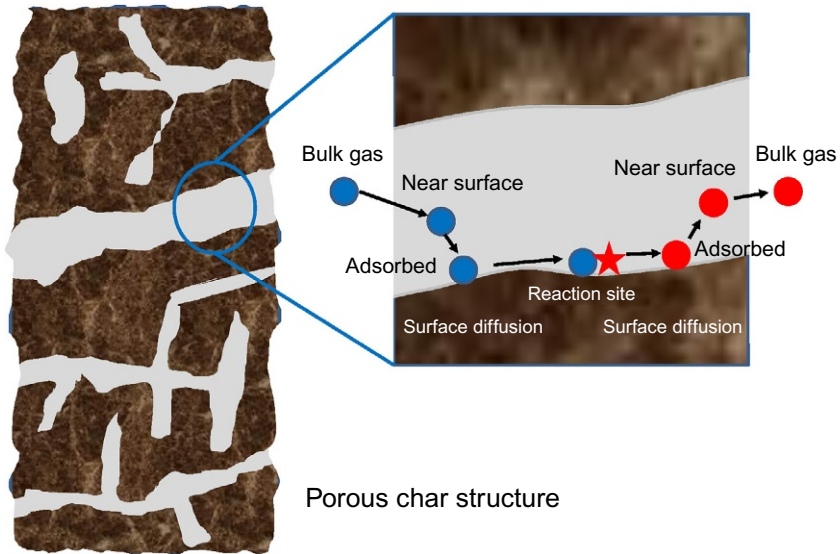
Fig. 7.7 Sequential steps of heterogeneous reactions.

3. The reactant gases surface diffuse from the adsorption site to the reaction site depending on the reaction mechanism.
4. The adsorbed gases and the solid react at the reaction sites.
5. The product gases surface diffuse from the reaction site to the desorption site depending on the reaction mechanism.
6. The product gases desorb from the solid surface.
7. The product gases move into the bulk gas due to fluid flow and diffusion.

Possibly, one of these steps is substantially slower than the other steps becoming the rate-limiting step that controls the overall reaction rate and the remaining steps then being nearly at equilibrium. While steps 1 to 3 and 5 to 7 of the earlier scheme are driven by transport processes rather than revealing differences due to the chemical nature, step 4 includes all the chemistry of the reactions of the most abundant species with char. These reactions are discussed in the following in more detail before discussing the transport-driven processes.

7.2.3.1 Kinetic description

A kinetic description of the char-gas reactions requires the detailed consideration of the interactions between gas and solid. The gasification of char formed in pyrolysis is characterized by the porous structure of the char and by variations in time and space of the local gas composition. The local heterogeneous reaction rate at any surface within the char is determined by the local concentration of the gaseous components and the different steps in the reaction sequence sketched in Fig. 7.7. Reaction rate expressions such as Eq. (7.5) have to be extended according to the appropriate occurring elementary mechanisms. The reaction site concept is employed for this.

The concept of reaction sites assumes the reactions occurring at favored sites on the surface. The nature of such sites may be carbon edges or dislocations, carbon atoms in vicinity to oxygen, hydrogen, and other functional groups, radicalic sites or inorganic components contained in the coal (see Fig. 7.4). These surface irregularities result in comparatively strong interaction forces, which induce electron transfer causing gas-solid bonding or chemisorption. At each reaction site, adsorption (chemisorption) of reactants, migration of intermediates, reaction, and product desorption may take place via single site or dual site mechanism.

For the formulation of rate expressions few more assumptions are necessary (Hayward and Trapnell, 1964; Frank-Kamenetzkii, 1969). The surface is supposed to be homogeneous with a uniform distribution of reaction sites, that is, a uniform average activity can be defined for the entire surface. Adsorption occurs localized via collisions with vacant reaction sites. There is only one adsorbed molecule or atom per site due to strong valence bonds. The surface coverage may not exceed a complete monomolecular layer and the mechanism of chemisorption/migration/desorption is not changing. No interaction occurs among adsorbed species, that is, the amount of adsorbed species has no effect on the adsorption rate per site. Chemisorption arises from gas molecules striking the surface at locations not covered by previously adsorbed species. If θ is the fraction of reaction sites covered by adsorbed species N_{ads}/N_{react}, the intrinsic rate of adsorption of a species i is

$$r_{ads} = k_{ads} \cdot p_i \cdot (1-\theta)^s, \quad s = 1,2. \tag{7.43}$$

Here s denotes single and dual site adsorption. From kinetic theory of gases

$$k_{ads} = k_{0\,ads} \cdot \exp\left(-\frac{E_{A\,ads}}{R \cdot T}\right) = \frac{\epsilon \cdot \nu_i}{(2 \cdot \pi \cdot R \cdot T \cdot M_i)^{1/2}} \cdot \exp\left(-\frac{E_{A\,ads}}{R \cdot T}\right) \tag{7.44}$$

is obtained, with ϵ the collision effectivity and ν_i a stoichiometric factor. Similarly, for desorption

$$r_{des} = k_{des} \cdot \theta^s, \quad s = 1,2, \tag{7.45}$$

with

$$k_{des} = k_{0\,des} \cdot \exp\left(-\frac{E_{A\,des}}{R \cdot T}\right) \tag{7.46}$$

can be written. Assuming steady-state and locally isothermal conditions, $r_{ads} = r_{des}$ resulting in

$$\left(\frac{\theta}{1-\theta}\right)^s = \frac{k_{ads}}{k_{des}} \cdot p_i. \tag{7.47}$$

Under the earlier assumptions $k_{ads}/k_{des} = a$ is solely a function of temperature T and independent of surface coverage θ. From Eq. (7.47) the surface coverage can be deduced:

$$\theta = \frac{(a \cdot p_i)^{1/s}}{1 + (a \cdot p_i)^{1/s}}. \tag{7.48}$$

Setting now $s = 1$ and assuming the rate determining step will be adsorption or desorption, the intrinsic surface reaction rate becomes (Langmuir-Hinshelwood kinetics)

$$r = r_{ads} = r_{des} = k_{ads} \cdot \frac{p_i}{1 + a \cdot p_i} \quad (mol/m^2 s). \tag{7.49}$$

Eq. (7.49) exhibits the general characteristics of heterogeneous reaction rates based on the reaction site approach. For $a \cdot p_i \leq 1$ the apparent order of the reaction is 1 and the reaction rate is linearly dependent on the partial pressure p_i. For increasing p_i the order of reaction decreases until for $a \cdot p_i \gg 1$, at complete coverage of the reaction sites, a reaction order of 0 with a constant reaction rate is attained. This holds also for $s = 2$. Eq. (7.49) also exhibits that the reaction rate for heterogeneous reactions in contrast to Eq. (7.4) is given as time change of the molar amounts per unit surface area of the solid, mol/(m^2 s). Considering multicomponent adsorption, which is most probable taking into account the composition of the gaseous mixture evolving from the pyrolysis zone, the balance $r_{ads} = r_{des}$ for multicomponent adsorption

$$k_{i\,ads} \cdot p_i \cdot \left(1 - \sum_{j=1}^{n} \theta_j \right) - k_{i\,des} \cdot \theta_i = 0 \tag{7.50}$$

for the example of a binary system and single site reactions leads to

$$\theta_i = \frac{(a_i \cdot p_i)}{1 + (a_1 \cdot p_1) + (a_2 \cdot p_2)}, \quad i = 1, 2. \tag{7.51}$$

The Langmuir-Hinshelwood kinetics for species 1 then is given by

$$r_1 = k_{1\,des} \cdot \theta_1 = \frac{k_{1\,ads} \cdot p_1}{1 + (a_1 \cdot p_1) + (a_2 \cdot p_2)}. \tag{7.52}$$

Accordingly, an analogous rate expression holds for species 2. Eq. (7.52) reveals that the reaction is inhibited by the adsorption of species 1 and, if or if not species 2 is a reactant, by the adsorption of this species. This is another characteristic of heterogeneous reactions.

For surface reactions or surface migration being the rate determining steps a variety of kinetic expressions arise. For the conversion of an adsorbed species we obtain

$$r = k_{chem} \cdot \theta = k_{chem} \cdot \frac{(a \cdot p)}{1 + (a \cdot p)}, \; s = 1, \quad r = k_{chem} \cdot \frac{(a \cdot p)^{1/2}}{1 + (a \cdot p)^{1/2}}, \; s = 2, \tag{7.53}$$

where k_{chem} means the rate coefficient for the chemical reaction or surface migration. If reactant species 2 from the gas phase reacts with adsorbed species 1 in a one site reaction, the reaction rate is given by

$$r = k_{chem} \cdot \theta_1 \cdot p_2 = k_{chem} \cdot \frac{(a_1 \cdot p_1) \cdot p_2}{1 + (a_1 \cdot p_1) + (a_2 \cdot p_2)}. \tag{7.54}$$

We see from Eqs. (7.52)–(7.54) that different molecular mechanisms of the heterogeneous reaction—chemisorption, surface migration, surface reaction—lead to similar rate expressions. However, they all are characterized by a change in reaction order with increasing reactant partial pressure and inhibition by inert components, reactants, and even products. This provides a further answer to the question raised in Section 7.1.1 and points out that for the kinetics of coal gasification no unique chemical reaction mechanisms and unique rate expressions comparable to homogeneous chemical reactions are to be derived.

For the Langmuir isotherms a homogeneous noninteracting surface has been assumed resulting in constant activation energies. However, the surface of char is non-homogeneous and due to the nature of the sites, they exhibit different activity for adsorption and different reactivity. The most active sites are covered first and for an interacting surface covering of adjacent sites creates repulsion forces inhibiting adsorption and promoting desorption of following molecules. Consequently, the activation energy for adsorption increases and the one for desorption decreases with increasing surface coverage θ. An expression for the activation energy reflecting the interactions would be

$$E_{A\,ads} = E_{A\,0\,ads} + \omega_{ads} \cdot \theta, \tag{7.55}$$

where $E_{A\,0\,ads}$ means the activation energy at $\theta \rightarrow 0$ and ω_{ads} a surface energy constant. The adsorption rate exhibits an exponential decrease according to

$$r_{ads} = r_{ads\,0} \cdot \exp\left(-\frac{\omega_{ads} \cdot \theta}{R \cdot T}\right). \tag{7.56}$$

The different nature of the sites with respect to reactivity can also be considered by using a distribution of the activation energies, see Section 7.2.2.3.

7.2.3.2 Surface reactions of water with char

Water formed in the pyrolysis zone and entering from the wet and drying zone reacts with char according to the formal reaction

$$C + H_2O \rightarrow CO + H_2, \quad \Delta_R h_{500^\circ C} \approx +135\,\text{kJ/mol C}, \tag{7.57}$$
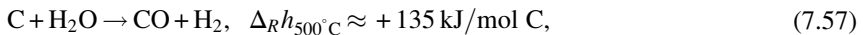
which is endothermic at 500°C by about 135 kJ/mol C. Following the reaction site approach the reaction is supposed to proceed on a molecular level via a single-site reaction mechanism according to (see Laurendeau, 1978; Roberts and Harris, 2006)

$$C^* + H_2O_g \xrightarrow{k_1} H_{2_g} + C(O)_s, \tag{7.58}$$

$$C(O)_s + H_{2_g} \xrightarrow{k_2} H_2O_g + C^*, \tag{7.59}$$

$$C(O)_s \xrightarrow{k_3} CO_g + C^*. \tag{7.60}$$

Here C^* means a free carbon site in the char structure accessible for reaction and $C(O)_s$ means a carbon site filled with atomic oxygen. The gasification is initiated by the attack of H_2O from the gas phase at a reaction carbon site C^* releasing H_2 into the gas phase and leaving an O in the carbon site. The reaction occurs also in the opposite direction. Mass loss of char is given by the transport of carbon atoms from the solid into the gas phase occurring through the elimination of CO from the $C(O)_s$ sites recovering free reaction sites C^*. The rate of molar loss of carbon from char is given by

$$r_C = k_3 \cdot N_{react} \cdot \theta_{C(O)_s}, \tag{7.61}$$

where N_{react} the total number of reaction sites. For the net formation rate of the $C(O)_s$ sites the assumption of quasisteady state is introduced, hence

$$\frac{d\theta_{C(O)_s}}{dt} = k_1 \cdot \theta_{C^*} \cdot p_{H_2O} - k_2 \cdot \theta_{C(O)_s} \cdot p_{H_2} - k_3 \cdot \theta_{C(O)_s} = 0. \tag{7.62}$$

Using $\theta_{C^*} + \theta_{C(O)_s} = 1$ we obtain

$$\theta_{C(O)_s} = \frac{k_1 \cdot p_{H_2O}}{k_1 \cdot p_{H_2O} + k_2 \cdot p_{H_2} + k_3} \tag{7.63}$$

and

$$r_C = \frac{k \cdot p_{H_2O}}{1 + a \cdot p_{H_2O} + b \cdot p_{H_2}}, \tag{7.64}$$

where $k = N_{react} \cdot k_1$, $a = k_1/k_3$, and $b = k_2/k_3$. The rate of molar carbon loss from the solid phase, Eq. (7.64), exhibits the typical characteristics for heterogeneous reactions, namely change of the reaction order with increasing partial pressure of H_2O and inhibition by the educt and product through oxygen exchange.

For high partial pressures of CO and particularly at temperatures above about 1200°C, CO_2 appears as a secondary product via the reaction (von Fredersdorf and Elliott, 1963; Ergun, 1961)

$$C(O)_s + CO_g \xrightarrow{k_4} CO_{2_g} + C^* \tag{7.65}$$

which proceeds also in the reverse direction

$$C^* + CO_{2g} \xrightarrow{k_5} CO_g + C(O)_s. \tag{7.66}$$

Together with the steam gasification reactions water-gas equilibrium may be attained at temperatures high enough. If as earlier steady-state approximations are introduced for $C(O)_s$, the reaction rate for the molar loss of carbon from char can be written as

$$r_C = \frac{N_{react} \cdot (k_5 \cdot p_{CO_2} + k_1 \cdot p_{H_2O})}{1 + \dfrac{1}{k_3} \cdot (k_5 \cdot p_{CO_2} + k_1 \cdot p_{H_2O} + k_4 \cdot p_{CO} + k_2 \cdot p_{H_2})}. \tag{7.67}$$

Eq. (7.67) illustrates the inhibition of the rate of carbon loss from char by CO, H_2, and CO_2 in addition to the educt H_2O.

7.2.3.3   Surface reactions of carbon dioxide with char

Carbon dioxide formed to a large extent during devolatilization reacts with char according to the formal reaction

$$C + CO_2 \rightarrow 2\,CO, \quad \Delta_R h_{500°C} \approx +172\,kJ/mol\,C, \tag{7.68}$$
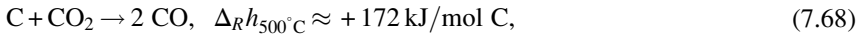
which is endothermic at 500°C by about 172 kJ/mol C. Adopting the reaction site approach the reaction on a molecular scale proceeds via (Ergun, 1961; Mentser and Ergun, 1973; Strange and Walker, 1976)

$$C^* + CO_{2g} \xrightarrow{k_5} CO_g + C(O)_s, \tag{7.69}$$

$$C(O)_s + CO_g \xrightarrow{k_4} CO_{2g} + C^*, \tag{7.70}$$

and finally

$$C(O)_s \xrightarrow{k_3} CO_g + C^*. \tag{7.71}$$

As for gasification with H_2O the gasification is initiated by the attack of CO_2 from the gas phase at a reaction carbon site C^* releasing CO into the gas phase and leaving an O in the carbon site. This reaction occurs also in the opposite direction. Finally, CO evolves from the $C(O)_s$ sites recovering free reaction sites C^*. The two first reactions have been introduced as side reactions occurring during the gasification by H_2O and the last reaction presents also the final step in the gasification by H_2O. For the formation of gaseous CO two sources exist in that reaction scheme; however, the rate of molar loss of carbon from char is the same as in the gasification by H_2O, see Eq. (7.61). The net formation rate of $C(O)_s$ sites applying quasisteady-state assumptions in this case is given by (see Eqs. 7.69–7.71)

$$\frac{d\theta_{C(O)_s}}{dt} = k_5 \cdot \theta_{C^*} \cdot p_{CO_2} - k_4 \cdot \theta_{C(O)_s} \cdot p_{CO} - k_3 \cdot \theta_{C(O)_s} = 0, \tag{7.72}$$

which gives introducing $\theta_{C^*} + \theta_{C(O)_s} = 1$

$$\theta_{C(O)_s} = \frac{k_5 \cdot p_{CO_2}}{k_5 \cdot p_{CO_2} + k_4 \cdot p_{CO} + k_3}. \tag{7.73}$$

For the rate of molar carbon loss from the char we obtain

$$r_C = \frac{k' \cdot p_{CO_2}}{1 + a' \cdot p_{CO_2} + b' \cdot p_{CO}} \tag{7.74}$$

where $k' = N_{react} \cdot k_5$, $a' = k_5/k_3$, and $b' = k_4/k_3$. The rate for molar carbon loss from the solid phase, Eq. (7.74), again exhibits the typical characteristics for heterogeneous reactions: change of the reaction order with increasing partial pressure of CO_2 and inhibition by the educt and product. It should be noted that the inhibition of the gasification reaction is not by adsorption as in the pure Langmuir-Hinshelwood approach, but rather via oxygen exchange at oxygen-filled reaction sites. It should also be noted that the gasification rate in presence of CO_2 and H_2O is not just the sum of the reaction rates Eq. (7.74) plus Eq. (7.64), but CO_2 and H_2O compete for the same reaction sites. Adsorption of H_2O is blocked by preadsorbed CO_2. Therefore, the rate of gasification by H_2O is reduced in presence of CO_2. Because the gasification rate by H_2O is much faster than the gasification rate by CO_2, the reverse is not the case. The rate equation for gasification by H_2O/CO_2 mixtures is given by (Roberts and Harris, 2007)

$$r_C = \frac{k' \cdot p_{CO_2}}{1 + a' \cdot p_{CO_2} + b' \cdot p_{CO}} + \frac{k \cdot p_{H_2O}}{1 + a \cdot p_{H_2O} + b \cdot p_{H_2}} \cdot \left(1 - \frac{a' \cdot p_{CO_2}}{1 + a' \cdot p_{CO_2}}\right). \tag{7.75}$$

According to Eqs. (7.64), (7.74) the rate of molar carbon loss from char is proportional to the total number of reaction sites N_{react}. The total number of reaction sites varies extremely among the chars from the different kinds of coal. Therefore, the prediction of the rate of carbon loss is impossible without the knowledge of that number even if reliable values for the different rate coefficients are available. If, however, the total number of reaction sites is responsible for the variations in the gasification rate, the temperature dependency of the individual steps can be obtained independently of the coal type so that the activation energies of the different reactions can be measured independently of the coal type.

7.2.3.4 Surface reactions of hydrogen with char

Hydrogen is formed during devolatilization of coal at very low reaction rates, see Table 7.2 and to little extent, see Table 7.5. Therefore, gasification of char via the global reaction

$$C + 2H_2 \rightarrow CH_4, \quad \Delta_R h_{500°C} \approx -86 \, \text{kJ/mol C}, \tag{7.76}$$
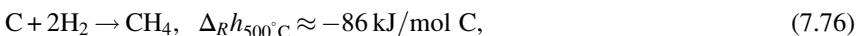
which is exothermic at 500°C by about 86 kJ/mol C contributes only little to the gasification of coal by formation of CH_4. The major part of CH_4 is formed during devolatilization. The surface mechanism seems to be complex because the product with five atoms appears not to be formed in single site reactions as in the case of gasification with H_2O or CO_2. A reaction scheme (Blackwood, 1962) starts with the adsorption of molecular H_2

$$C^* + H_{2g} \rightleftharpoons C(H_2)_s \tag{7.77}$$

followed by the dissociation of adsorbed H_2

$$C(H_2)_s + C^* \rightleftharpoons 2C(H)_s. \tag{7.78}$$

The sites filled with H-atoms incorporate further H-atoms from H_2 in the gas phase

$$2C(H)_s + H_{2g} \rightleftharpoons 2C(H_2)_s \tag{7.79}$$

and are finally converted with further H_2 from the gas phase to CH_4

$$C(H_2)_s + H_{2g} \rightleftharpoons CH_{4g} + C^*. \tag{7.80}$$

From this reaction scheme with reversible single reactions a typical heterogeneous rate expression for the gasification to CH_4 can be deduced:

$$r_C = \frac{c \cdot p_{H_2}^2 - d \cdot p_{CH_4}}{1 + e \cdot p_{H_2} + f \cdot p_{H_2}^2 + g \cdot p_{CH_4}}, \tag{7.81}$$

which collapses for low CH_4 partial pressures to

$$r_C = \frac{c \cdot p_{H_2}^2}{1 + e \cdot p_{H_2}} \tag{7.82}$$

and for high hydrogen partial pressures present in the final state of gasification to a reaction being of first order in hydrogen partial pressure

$$r_C = k \cdot p_{H_2}. \tag{7.83}$$

Eqs. (7.81)–(7.83) and likewise Eqs. (7.64), (7.74) provide gasification rates for a well-defined state in terms of temperature, pressure, and partial pressures of reactants and products. However, the rate equations also emphasize the particular problems of reaction kinetics in underground coal gasification: underground coal gasification is a zonal process with changes of state in time and space. Therefore, also reaction kinetics and mechanisms change in time and space and the rates for gasification reactions vary in magnitude and order and, therefore, product composition.

7.2.3.5   Surface reactions of oxygen with char

The necessary reaction energy for the overall endothermic gasification of coal as well as the necessary energy for vaporization and devolatilization has to be provided and balanced by combustion of a part of the char according to

$$C + O_2 \rightarrow CO_2, \quad \Delta_R h_{800°C} \approx -395 \, kJ/mol \, C. \tag{7.84}$$
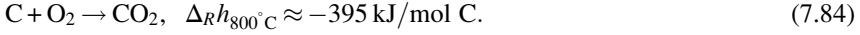
The reaction is exothermic at 800°C by about 395 kJ/mol C and apparently very fast compared with the gasification reactions discussed earlier. For typical combustion temperatures reaction schemes based on the reaction site concept involving the dissociative adsorption of O_2 (Nagle and Strickland-Constable, 1962; von Fredersdorf and Elliott, 1963; Spokes and Benson, 1967) end in the formation of CO and attribute the formation of CO_2 to the homogeneous reaction $CO + O \rightarrow CO_2 + h \cdot \nu$:

$$C* + O_{2g} \xrightarrow{k_6} O_g + C(O)_s \tag{7.85}$$

$$C* + O_g \xrightarrow{k_7} C(O)_s \tag{7.86}$$

$$C(O)_s \xrightarrow{k_3} CO_g + C* \tag{7.87}$$

and thermal annealing of reaction sites to inactive sites occurring at high temperatures

$$C* \xrightarrow{k_8} C_s. \tag{7.88}$$
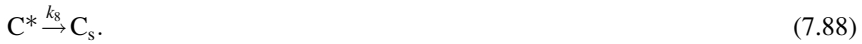
The dissociative adsorption of O_2 in contrast to the oxygen exchange by H_2O and CO_2 is supposed to be nonreversible. Omitting reaction (7.88) and applying steady-state assumptions for $C(O)_s$ a rate expression for the gasification is obtained

$$r_C = \frac{k \cdot p_{O_2}}{1 + a \cdot p_{O_2}} \tag{7.89}$$

where $k = N_{react} \cdot k_6$, $a = k_6/k_3$, which exhibits apparent reaction orders between 0 and 1 depending on the partial pressure of O_2 typical for heterogeneous reaction rates. Though the rate expression describes observed reaction rates well the rapid formation of CO_2 even at low temperatures cannot be reproduced. An extension of this reaction scheme introducing two-site adsorption of oxygen (Laurendeau, 1978) accounts also for the formation of CO_2 in a heterogeneous step:

$$2C* + O_{2g} \xrightarrow{k_8} 2C'(O)_s, \tag{7.90}$$

$$C'(O)_s \xrightarrow{k_9} C(O)_s, \tag{7.91}$$

$$C(O)_s \xrightarrow{k_3} CO_g + C^*, \tag{7.92}$$

$$C'(O)_s \xrightarrow{k_{10}} CO_g + C^*, \tag{7.93}$$

$$C(O)_s + C'(O)_s \xrightarrow{k_{11}} CO_2 + C^*. \tag{7.94}$$

Here $C'(O)_s$ represents a mobile site. Applying steady-state assumptions for the two kinds of sites $C(O)_s$ and $C'(O)_s$ and introducing estimations for the relative rates at the different temperature ranges and ranges of partial pressures of O_2 (Laurendeau, 1978), rate expressions of different apparent reaction order can be developed. For low temperatures

$$r_C = N_{react} \cdot k_{10}/2 \tag{7.95}$$

with an apparent reaction order $\mu_{app} = 0$ results, where the desorption from the mobile sites is rate determining. For intermediate temperatures

$$r_C = N_{react} \cdot k_9 \cdot \left(\frac{k_8}{k_{11}}\right) \cdot p_{O_2}^{1/2} \tag{7.96}$$

is obtained, where the apparent reaction order $\mu_{app} = 1/2$ and site migration is rate determining. Finally, for high temperatures a reaction order $\mu_{app} = 1$ is attained and the dissociative adsorption of O_2 is rate determining

$$r_C = 2 \cdot N_{react}^2 \cdot k_8 \cdot p_{O2}. \tag{7.97}$$

7.2.3.6   Reaction rate coefficients

As pointed out earlier the rate laws given in Eqs. (7.64), (7.67), (7.74), (7.81)–(7.83), or (7.95)–(7.97) all contain the number of reaction sites N_{react} of the char which may be different by orders of magnitudes for chars of different origin. Therefore, any compilation or comparison of kinetic data for coal gasification should refer to comparable N_{react} or at least to char with comparable specific surface area (see e.g., Laurendeau, 1978 for a detailed discussion). For the same reason rate coefficients for global reaction rates may be applied only for the same reaction conditions and char types that have been investigated for the evaluation of the rate coefficients. The coal-type independent parts of some rate coefficients for the gasification reactions discussed earlier are collected in Table 7.6. More data and ample discussion is given in Laurendeau (1978), Müllen et al. (1985), Roberts and Harris (2000), Kajitani et al. (2006), and Bell et al. (2011).

Table 7.6 Reaction rate parameters for gasification reactions of char

Overall reaction	Char type	Rate expression	E_A (kJ/mol)		
$C + CO_2 \rightarrow 2CO$	Graphite	$\dfrac{k' \cdot p_{CO_2}}{1 + a' \cdot p_{CO_2} + b' \cdot p_{CO}}$	$E_{A\,3}$	$E_{A\,4}$	$E_{A\,5}$
			364	322	415
$C + H_2O \rightarrow 2C + H_2$	Graphite	$\dfrac{k \cdot p_{H_2O}}{1 + a \cdot p_{H_2O} + b \cdot p_{H_2}}$	$E_{A\,1}$	$E_{A\,2}$	$E_{A\,3}$
			55–140	113–213	343–468

Reaction	Coal type	Rate expression	R.O. (μ)	E_A (kJ/mol)
$C + 2H_2 \rightarrow CH_4$	Coconut char	$k \cdot p_{H_2}^{\mu}$	1.0	150–160
$C + O_2 \rightarrow CO_2$	Graphite	$k \cdot p_{O_2}^{\mu}$	0.0	63–83
			1/2	125–210
			1	290–335

7.2.3.7 Coupling to mass transport

Table 7.6 illustrates that the rate coefficients for the gasification reactions exhibit different and comparably strong dependencies on temperature. Furthermore, the discussion of the different rate expressions clarified that the mechanism of the heterogeneous gasification reactions may change due to the changing composition and temperature of the gas phase. Altogether, this can cause a change in the rate determining steps illustrated in Fig. 7.7. A schematic of the effect of a variation in the rate determining steps is given in Fig. 7.8 (see also Emig and Dittmeyer, 1997).

Considering a porous char layer covered by an ash layer, compare Fig. 7.2, the reactant partial pressure within and outside the porous solid phase depends on the intrinsic reaction rate. At low temperatures where the intrinsic reaction rate is low mass transfer and diffusion rates are sufficient large producing an essentially constant reactant partial pressure profile throughout the solid phase and the adjacent fluid boundary layer. In this case the overall reactivity will be controlled by the intrinsic heterogeneous reaction rate (range 1 in Fig. 7.8). With increasing intrinsic reaction rate, the diffusion rate within the porous structure and at higher reaction rates even through the ash layer and the fluid boundary layer cannot keep up with the chemical reaction rate. Hence, the partial pressure profiles develop as indicated by range 2 and range 3. As can be seen from the schematic diagram in Fig. 7.8 less and less of the solid porous char phase volume becomes accessible to high gas concentrations. For range 4 the chemical reaction within the pore structure is so rapid compared with diffusion that the reactant gas concentration approaches zero both within and at the surface of the porous solid. In this case the overall reaction rate is controlled solely by diffusion across the ash layer and fluid boundary layer. The physical reason for this pattern is the different temperature dependency of diffusional transport (see Eqs. 7.29, 7.30) and chemical reaction rates (see Eq. 7.7).
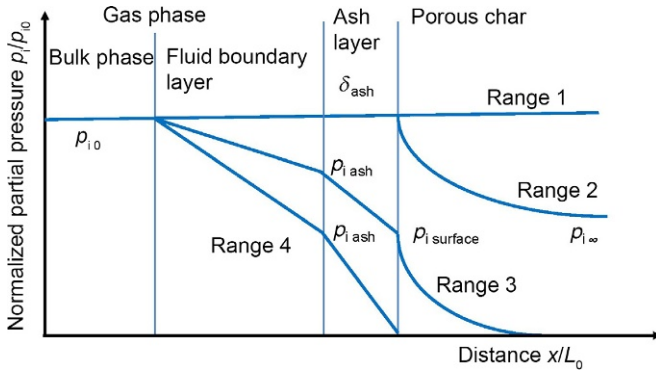
Fig. 7.8 Reactant profiles within and outside the porous char for different rate determining steps (schematically).

To provide a closer look into the kinetics under these circumstances the overall reaction rates for the different ranges depicted in Fig. 7.8 may be discussed. For range 1, the intrinsic kinetics is rate limiting, so that the overall reaction rate is given by one of the rate expressions from Eqs. (7.64), (7.67), (7.74), (7.81)–(7.83), or (7.95)–(7.97). This approach is assigned volume reaction models or modified volume reaction models (Zogala, 2014). For utilizing this kind of models correlations for the number of reaction sites with the total volume/total external surface must be available.

For the other ranges indicated in Fig. 7.8 the overall reaction rate is determined by the molar fluxes of the reactants into the porous solid caused by mass transfer and diffusion. For the fluid boundary layer we obtain with this using the integrated form of Fick's law

$$\dot{m}_C = \nu_i \cdot A_{geo} \cdot h_g \cdot (p_{i\,0} - p_{i\,ash}), \tag{7.98}$$

where ν_i represents a stoichiometric factor for the gasification reaction, A_{geo} is the geometric surface area, h_g is the mass-transfer coefficient for the prevailing conditions (Ghiaasiaan, 2014), and $p_{i\,0}$ and $p_{i\,ash}$ are the reactant partial pressures at the bulk gas phase/fluid boundary layer and fluid boundary layer/ash layer, respectively. Proceeding to the ash layer the overall reaction rate is given similarly by applying Fick's law

$$\dot{m}_C = \nu_i \cdot A_{geo} \cdot D_{i\,ash} \cdot \left(\frac{dp_i}{dx}\right), \tag{7.99}$$

which gives after integration

$$\dot{m}_C = \nu_i \cdot A_{geo} \cdot \left(\frac{D_{i\,ash}}{\delta_{ash}}\right) \cdot (p_{i\,ash} - p_{i\,surface}). \tag{7.100}$$

Here $D_{i\,\text{ash}}$ is the effective diffusion coefficient of the reactant in the ash layer, δ_{ash} is the thickness of the ash layer, and $p_{i\,\text{surface}}$ is the partial pressure of the reactant at the surface of the solid porous char phase. Finally, for the diffusion into the porous structure

$$\dot{m}_{\text{C}} = \nu_i \cdot A_{\text{pore}} \cdot h_{\text{pore}} \cdot (p_{i\,\text{surface}} - p_{i\,\infty}) \tag{7.101}$$

can be written, where A_{pore} are the cross-sectional areas of all pores, h_{pore} is the mass-transfer coefficient for the diffusional mass transport into the pores, and $p_{i\,\infty}$ is the reactant partial pressure at the pore end. It should be noted that for A_{pore} a correlation with the geometric area or volume of the char must be provided and that the mass-transfer coefficient is a complicated function of the diffusion mechanism within the pores, the structure of the pores (tortuosity), pore size (Knudsen number), and the type of surface reaction. Assuming for simplicity cylindrical pores and molecular diffusion and a reaction of first order with respect to the reactant, which may be suitable for a wide range of reaction conditions (see reaction rate expressions discussed in Sections 7.2.3.1–7.2.3.5) and $p_{i\,\infty} = 0$

$$h_{\text{pore}} = \frac{D_{i\,\text{pore}}}{L_{\text{pore}}} \cdot \Phi \quad \text{with} \quad \Phi = L_{\text{pore}} \cdot \sqrt{\frac{2 \cdot k_{\text{chem}}}{D_{i\,\text{pore}} \cdot R_{\text{pore}}}}. \tag{7.102}$$

Φ is the Thiele modulus for the specified assumptions. For other conditions as specified by the earlier assumptions the Thiele modulus attains different forms and, hence, the mass-transfer coefficient for the diffusion into the pores (Crank, 1964). Combining Eqs. (7.98), (7.100), (7.101) to eliminate the unknown partial pressures at the internal boundary surfaces, we obtain

$$\dot{m}_{\text{C}} = \nu_i \cdot h_{\text{total}} \cdot p_{i\,0}, \tag{7.103}$$

where

$$\frac{1}{h_{\text{total}}} = \left[\left(\frac{1}{A_{\text{geo}} \cdot h_{\text{g}}} \right) + \left(\frac{1}{A_{\text{geo}} \cdot \dfrac{D_{i\,\text{ash}}}{\delta_{\text{ash}}}} \right) + \left(\frac{1}{A_{\text{pore}} \cdot h_{\text{pore}}} \right) \right]. \tag{7.104}$$

With this simplified approach we treat the overall molar flux, which is equivalent to a reaction rate given by the time change of the molar amounts of carbon, in terms of a series of mass-transfer resistances which add to a total resistance. Eq. (7.104) clearly reveals that the process with the highest resistance dominates the overall reaction rate. It should be noted that this approach may be extended referring to the statistical structure of the porous char and the appropriate mechanisms of surface reactions and pore diffusion. However, the principle characteristic of the overall reaction rate with the superposition of the different transport processes, affecting the surface reaction, is reflected by Eqs. (7.103), (7.104). Further discussion is presented in Laurendeau (1978) and Bell et al. (2011).

The combustion of char via reaction (7.84) provides to the largest part the energy necessary for the other endothermic gasification reactions (7.57), (7.68) as well as for devolatilization and drying. Combustion and gasification reactions consume the solid phase so that the char gasification zone migrates through the coal seem. The migration rate may be estimated with the help of energy balances as sketched in Section 7.2.2.5 introducing the appropriate reaction rates and temperatures. The heat fluxes from the gasification zone into the pyrolysis zone and further into the drying zone, extension and location of the different zones, evolution rate of gasification products and volatiles as well as migration rates of the zones adjust interdependently to variations of the local state and conditions as discussed in Sections 7.2.1 and 7.2.2.5.

7.2.4 Homogeneous secondary reactions of gasification and pyrolysis products

The intended product of underground gasification is a mixture of CO and H_2. According to the composition of coal, the content of volatiles, and the amount of water the required energy for drying, devolatilization and gasification necessitates the combustion of varying amounts of coal so that the product gas contains a certain level of CO_2. Products from devolatilization and pyrolysis can also survive the gasification zone, because air/oxygen is not applied in excess. Typical gas composition from underground gasification is given in Table 7.7 (Bell et al., 2011, see also Perkins and Sahajwalla, 2008).

The product gas components constitute a highly combustible mixture which reacts with oxygen via homogeneous reactions, for example

$$CO + O_2 \quad \rightarrow CO_2 \tag{7.105}$$

$$H_2 + O_2 \quad \rightarrow H_2O \tag{7.106}$$

$$CH_4 + 2O_2 \quad \rightarrow CO_2 + 2H_2O \tag{7.107}$$

and also among each other via, for example

$$H_2 + CO_2 \rightarrow H_2O + CO \tag{7.108}$$

$$CH_4 + CO_2 \rightarrow 2CO + 2H_2. \tag{7.109}$$

The earlier-listed homogeneous combustion and gasification reactions occur via complex mechanism of parallel and consecutive reactions including radical chain initiation, chain propagation, and chain branching reactions. An example for this kind of mechanism for the combustion of H_2 according to reaction (7.106) is given in Table 7.8 (Maas and Warnatz, 1988). The reactions listed in Table 7.8 take place in forward and reverse directions. The rate coefficients for the reverse reactions can be calculated from thermodynamic data. Reaction mechanisms for the combustion and gasification of CO and hydrocarbons, comprising several hundreds of elementary

Table 7.7 Typical product gas composition on a dry basis in % by volume from underground coal gasification (Powder River Basin, Wyoming)

Component	Air-blown	O_2-blown
CH_4	5.4	10.6
$C_2H_6 + C_2H_4$	0.4	0.8
$C_4H_8 + C_3H_6$	0.2	0.4
CO	16.1	31.5
CO_2	11.8	23.1
H_2	16.7	32.7
N_2	48.8	–

Table 7.8 Reaction mechanism and reaction rate coefficients for the combustion of H_2 (Maas and Warnatz, 1988)

Reaction	$k_{0\text{ for }i}$	$b_{\text{for }i}$	$E_{A\text{ for }i}$
Chain branching reactions			
$O_2 + H = OH + O$	2.20E+14	0	70.30
$H_2 + O = OH + H$	1.50E+07	2	31.60
$H_2 + OH = H_2O + H$	1.00E+08	1.6	13.80
$OH + OH = H_2O + O$	1.48E+09	1.14	0
Three-body recombination/dissociation reactions			
$H + H + M = H_2 + M$	1.80E+18	−1	0
$H + OH + M = H_2O + M$	2.20E+22	−2	0
$O + O + M = O_2 + M$	2.90E+17	−1	0
$H + O_2 + M = HO_2 + M$	2.00E+18	−0.8	0
HO_2 reactions			
$HO_2 + H = OH + OH$	1.50E+14	0	4.20
$HO_2 + H = H_2 + O_2$	2.50E+13	0	2.90
$HO_2 + O = OH + O_2$	2.00E+13	0	0
$HO_2 + OH = H_2O + O_2$	2.00E+13	0	0
H_2O_2 reactions			
$HO_2 + HO_2 = H_2O_2 + O_2$	2.00E+12	0	0
$OH + OH + M = H_2O_2 + M$	3.25E+22	−2	0
$H_2O_2 + H = H_2 + HO_2$	1.70E+12	0	15.70
$H_2O_2 + H = H_2O + OH$	1.00E+13	0	15.00
$H_2O_2 + O = OH + HO_2$	2.80E+13	0	26.80
$H_2O_2 + OH = H_2O + HO_2$	7.00E+12	0	6.00

Notes: The rate coefficients are given as $k_i = k_{0\ i} \cdot T_i^b \cdot \exp(-E_{A\ i}/R \cdot T)$ for forward reactions only. The rate coefficients for the reverse reactions can be calculated from thermodynamic data. Units are mole, s, and kJ/mol.

reactions between large numbers of species, can be found in the literature, see for example, Gardiner (2000), Battin-Leclerc et al. (2013), and Smith et al. (2017).

Reaction rates for this part of the underground gasification process consisting of homogeneous reactions can be expressed as outlined briefly in Section 7.1.1. Referring to Eq. (7.5) the forward reaction rate for a single reaction j of species i can be written as

$$r_{ij} = k_{\text{for } j}(T,p) \cdot \prod_1 c_1^{\nu_{\text{for } l}}. \tag{7.110}$$

As the reactions listed in the mechanism given in Table 7.8 are elementary reactions, the reaction order with respect to the single reactants is the respective stoichiometric coefficient. An analogous expression holds for the backward reaction and the net reaction rate of species i in reaction j then is given by

$$r_{ij} = k_{\text{for } j}(T,p) \cdot \prod_1 c_1^{\nu_{\text{for } l}} - k_{\text{back } j}(T,p) \cdot \prod_k c_k^{\nu_{\text{back } k}}. \tag{7.111}$$

The conversion of the single components i in this kind of multireaction system is given by the sum of the reaction rates of all the single reactions where the specific component is involved in

$$r_{i \text{ total}} = \sum_{j=1}^{R} k_{\text{for } j}(T,p) \cdot \prod_1 c_1^{\nu_{\text{for } l}} - k_{\text{back } j}(T,p) \cdot \prod_k c_k^{\nu_{\text{back } k}}. \tag{7.112}$$

The progress of the earlier reactions is strongly determined by temperature, pressure, and the oxygen partial pressure in the gas mixture and compared with the different processes in underground coal gasification occurs on a different time scale. While the formation of H_2O during combustion according to the reaction mechanism listed in Table 7.8 occurs on a time scale of the order of magnitude of 0.1 ms, the time scale for the formation of H_2O during devolatilization at 773 K is about 3.5 s (see Section 7.2.2 and Table 7.2). The time scale for gasification of char by oxygen at 1000°C is of the order of magnitude of 30 s (Laurendeau, 1978), the one of gasification by CO_2 is of the order of magnitude of 4000 s (per g/m^2 of internal-specific surface area), compare Section 7.2.3. Due to the wide variation of time scales for the different processes, temperature gradients in the diverse zones in underground coal gasification, their extension and the migration rate of the entire production zone and the product composition thereof adjust interdependently depending on the operating conditions of the process.

7.3   Summary

The kinetics of underground coal gasification have been analyzed and discussed in this chapter. Underground coal gasification is characterized as a zonal process with time- and space-dependent state variables. This creates boundary conditions for the

different gasification processes, which cause changes in the reaction mechanisms and, hence, the kinetic rate laws. In addition due to the heterogeneity of the processes mass transport and energy transport limitations can occur.

For the drying process heat flux, extension, and location of the drying zone as well as migration rate of the drying zone adjust interdependently to variations of the influx and content of water. The flux of steam from the drying zone and the temperature gradient at the surface of vaporization in the drying zone are linearly related. Therefore, the time change of the molar amount of water in the drying zone volume, which represents a reaction rate for the "drying reaction" can be interpreted as being of first order in temperature.

Reaction rates for the formation of volatiles in the pyrolysis zone mostly are formulated with simple rate expressions, which lump all the different formation reactions in an overall reaction. The formation rates are coupled with the temperature gradient at the surface of reaction in the pyrolysis zone.

Due to the temperature gradient in the pyrolysis zone the pyrolysis reactions occur at higher temperatures at the hot end of the pyrolysis zone and at lower temperatures at the cold end of the pyrolysis zone. The different temperature dependency of the formation reactions of the single gaseous and liquid pyrolysis products and the different ultimate amounts of the single components cause a varying product distribution in the pyrolysis zone with time and from the hot side to the cold side.

Different molecular mechanisms of the heterogeneous reactions occurring in the gasification zone—chemisorption, surface migration, and surface reaction—lead to similar rate expressions. However, they all are characterized by a change in reaction order with increasing reactant partial pressure and inhibition by inert components, reactants, and even products.

Reactions in the gasification zone of the porous char structure are superposed by transport processes. Reaction rates can be treated in terms of a series of mass-transfer resistances, which add to a total resistance. Then the process with the highest resistance dominates the overall reaction rate.

The combustion of char provides to the largest part the energy necessary for the endothermic gasification reactions as well as for devolatilization and drying. Combustion and gasification reactions consume the solid phase so that the char gasification zone migrates through the coal seem. The heat fluxes from the gasification zone into the pyrolysis zone and further into the drying zone, extension and location of the different zones, evolution rate of gasification products and volatiles as well as migration rates of the zones adjust interdependently to variations of the local state and conditions.

References

Battin-Leclerc, F., Simmie, J.M., Blurock, E., 2013. Cleaner Combustion. Springer Verlag, London.

Bell, D.A., Towler, B.F., Fan, M., 2011. Coal Gasification and Its Applications. Elsevier Inc., Oxford.

Blackwood, J.D., 1962. The kinetics of the system carbon-hydrogen-methane. Aust. J. Chem. 15, 397–408.

Bockhorn, H., Hornung, A., Hornung, U., 1999. Mechanisms and kinetics of thermal decomposition of plastics from isothermal and dynamic measurements. J. Anal. Appl. Pyrolysis 50, 77–101.

Bockhorn, H., Hornung, A., Hornung, U., Löchner, S., 2000. Pyrolysis of polystyrene as the initial step in incineration, fires, or smoldering of plastics: investigations of the liquid phase. Proc. Combust. Inst., vol. 28, pp. 2667–2673.

Crank, J., 1964. The Mathematics of Diffusion. Oxford University Press, London.

Emig, G., Dittmeyer, R., 1997. Simultaneous heat and mass transfer and chemical reaction. In: Ertl, G., Knözinger, H., Weitkamp, J. (Eds.), In: Handbook of Catalysis, vol. 3. VCI Verlagsgesellschaft, Weinheim, pp. 1209–1252.

Ergun, S., 1961. Kinetics of the reactions of carbon dioxide and steam with coke. US Bureau of Mines Bulletin 598.

Frank-Kamenetzkii, D.A., 1969. Diffusion and Heat Transfer in Chemical Kinetics. Plenum Press, New York.

Gardiner, W.C., 2000. Gas-Phase Combustion Chemistry. Springer-Verlag, New York.

Ghiaasiaan, S.M., 2014. Connective Heat and Mass Transfer. Cambridge University Press, New York.

Grant, D.N., Pugmire, R.J., Fletcher, T.H., Kerstein, A.R., 1989. Chemical model of coal devolatilization using percolation lattice statistics. Energy Fuel 3, 175–186.

Hayward, D.O., Trapnell, B.M.W., 1964. Chemisorption. Butterworths, London.

Jupudi, R.S., Zamansky, V., Fletcher, T.H., 2009. Prediction of light gas composition in coal devolatilization. Energy Fuel 23, 3063–3067.

Kajitani, S., Suzuki, N., Ashizawa, M., Hara, S., 2006. CO_2 gasification rate analysis of coal char in entrained flow coal gasifier. Fuel 85, 163–169.

Kobayashi, H., Howard, J.B., Sarofim, A.F., 1977. Coal devolatilization at high temperatures. Proc. Combust. Inst. 16, 411–425.

Laurendeau, N.M., 1978. Heterogeneous kinetics of coal char gasification and combustion. Prog. Energy Combust. Sci. 4, 221–270.

Maas, U., Warnatz, J., 1988. Ignition processes in hydrogen-oxygen mixtures. Combust. Flame 74, 53.

Mathews, J.P., Chaffee, A.K., 2012. The molecular representations of coal—a review. Fuel 98, 1–14.

Mentser, M., Ergun, S., 1973. A study of the carbon dioxide-carbon reaction by oxygen exchange. US Bureau of Mines Bulletin 664.

Merrick, D., 1987. The thermal decomposition of coal: mathematical models of the chemical and physical changes. In: Volborth, A. (Ed.), Coal Science and Chemistry. Elsevier, Amsterdam, pp. 307–342.

Müllen, H.J., van Heek, K.H., Jüntgen, H., 1985. Kinetic studies of steam gasification of char in the presence of H_2, CO_2 and CO. Fuel 64, 944–949.

Nagle, J., Strickland-Constable, R.F., 1962. Oxidation of Carbon between 1000–2000°C. Proc. Fifth Carbon Conference, Pergamon Press, New York, p. 154.

Olzmann, M., 2013. Statistical rate theory in combustion: an operational approach. Cleaner Combustion, Springer Verlag, London. Chapter 21.

Perkins, G., Sahajwalla, V., 2008. Steady-state model for estimating gas production from underground coal gasification. Energy Fuel 22, 3902–3914.

Roberts, D.G., Harris, D.J., 2000. Char gasification with O_2, CO_2, and H_2O: effects of pressure on intrinsic reaction kinetics. Energy Fuel 14, 483–489.

Roberts, D.G., Harris, D.J., 2006. A kinetic analysis of coal char gasification reactions at high pressures. Energy Fuel 20, 2314–2320.

Roberts, D.G., Harris, D.J., 2007. Char gasification in mixtures of CO_2 and H_2O: competition and inhibition. Fuel 86, 2672–2678.

Serio, M.A., Peters, W.A., Sawada, K., Howard, J.B., 1984. Global kinetics of primary and secondary reactions in hydrocarbon gas evolution from coal pyrolysis. ACS Div. Fuel Chem. 29 (2), 65.

Serio, M.A., Hamblen, D.G., Markham, J.R., Solomon, P.R., 1987. Kinetics of volatile product evolution in coal pyrolysis: experiment and theory. Energy Fuel 1, 138–152.

Smith, G.P., Golden, D.M., Frenklach, M., Moriarty, N.W., Eiteneer, B., Goldenberg, M., Bowman, C.T., Hanson, R.K., Song, S., Gardiner, W.C.J., Lissianski, V.V., Qin, Z., 2017. GRI-Mech[TM]. http:/www.me.berkeley.edu/gri_mech/.

Solomon, P.R., Hamblen, D.G., Carangelo, R.M., Serio, M.A., Deshpande, G.V., 1988. General model of coal devolatilization. Energy Fuel 2, 405–422.

Solomon, P.R., Serio, M.R., Suuberg, E.M., 1992. Coal pyrolysis: experiments, kinetic rates and mechanisms. Prog. Energy Combust. Sci. 18, 113–220.

Spokes, G.N., Benson, S.W., 1967. Oxidation of a Thin Film of a Carbonaceous Solid at Pressures Below 10-4 Torr, Fundamentals of Gas-Surface Reactions. Academic Press, New York, p. 318.

Steinfeld, J.L., Francisco, J.S., Hase, W.L., 1989. Chemical Kinetics and Dynamics. Prentice Hall, Englewood Cliffs, NJ.

Strange, J.F., Walker, P.L., 1976. Carbon-carbon dioxide reactions: Langmuir-Hinshelwood kinetics at intermediate pressures. Carbon 14, 345.

van Krevelen, D.W., 1961. Coal. Elsevier, New York.

Veras, C.A.G., Carvalho, J.A., Ferreira, M.A., 2002. The chemical percolation devolatilization model applied to the devolatilization of coal in high intensity acoustic fields. J. Braz. Chem. Soc. 13, 358–367.

von Fredersdorf, C.G., Elliott, M.A., 1963. Coal Gasification. Wiley, New York, p. 892.

Wright, M.R., 2005. Introduction to Chemical Kinetics. John Wiley & Sons, Hoboken.

Zogala, A., 2014. Critical analysis of underground coal gasification models, part II: kinetic and computational fluid dynamic models. J. Sustain. Min. 13, 29–37.

Zsakó, J., 1976. The kinetic compensation effect. J. Therm. Anal. 9, 101–108.

The role of groundwater as an important component in underground coal gasification

8

E.V. Dvornikova
Ergo Exergy Technology Inc., Montreal, QC, Canada

8.1 Introduction

Groundwater plays a very important role in mining mineral deposits. Development of coal deposits is accompanied by groundwater influx into mine workings, which can significantly complicate the development of mine workings and coal mining, even with conventional mining methods. In underground coal gasification, excess groundwater influx into the gasifier can completely disrupt the gasification process or result in low process yields (the calorific value of UCG gas and the efficiency of the gasification process). Influx of gravitational groundwater may occur both in the coal seam itself and the aquifers overlying and underlying the coal seam.

The amount of groundwater ingressing into gasifiers is determined not only by the natural conditions of the coal deposit but also by those specific (man-made) factors that arise during coal gasification: high temperatures in the gasifier, excess pressures of injected air and gas, and deformation of the roof rock above the gasification cavity.

Given a high-temperature environment, in addition to the gravitational groundwater (free water), the gasification process incorporates bound water. These are molecules of water bound by electromolecular forces with the surfaces of particles in the coal seam floor and roof and directly with the coal seam (Tsitovich, 1983). Detailed consideration of the types of bound water and its participation in underground coal gasification is presented below.

In addition, high temperature alters the physical and mechanical properties of rock in the coal seam floor, and roof rocks of the coal seam change. Clays, which in a natural undisturbed setting function as aquitards, dry and crack during gasification, even becoming permeable to water with fracturing at some depth intervals and no longer preventing water influx into the gasifier. Conversely, excess injected air and gas pressure acts to prevent groundwater influx into the gasifier.

The influx of gravitational groundwater into the gasification cavity is possible if:

- The overlying aquifers are hydraulically interconnected with the coal seam, provided the coal seam roof is composed of rock sufficiently permeable to conduct groundwater. The influx is a function of groundwater residing in the coal seam and groundwater contained in the overlying aquifers.

- After the aquitard layers in the overburden collapse, the zone of groundwater-transmitting fractures extends to the overlying aquifers. The influx is a function of groundwater residing in the coal seam and groundwater contained in the undermined overlying aquifers.
- Because of the confined nature of the aquifer underlying the coal seam and its water levels (head) stabilize above the coal seam floor elevation and as a result of heat penetration into floor rock that causes fracturing, the underlying aquifer becomes hydraulically connected with the underground gasifier. The influx is a function of groundwater residing in the coal seam and groundwater contained in the underlying aquifer.
- The overlying and underlying aquifers are hydraulically connected with the coal seam. The influx is a function of groundwater residing in the coal seam and simultaneously groundwater contained in the overlying and underlying aquifers.

For a successful implementation of UCG, the preferred natural hydrogeologic conditions are those in which:

A. The coal seam is adequately isolated from the overlying aquifers that are located a considerable distance from the coal seam; this distance should be greater than the extent of the zone of groundwater-transmitting fractures that form as a result of deformation of the overlying rock.
B. The underlying aquifer is sufficiently separated from the coal seam by aquicludes, with groundwater levels stabilized below the coal seam floor, with coal not under water.

Hydrogeologic conditions pose a greater challenge when the coal seam is not adequately isolated from the overlying and underlying aquifers at the sites of active gasification operations. The underlying formation contains a confined aquifer or if aquifers in the overburden are located inside the zone of rock deformation-induced discontinuities, that is, inside the zone of groundwater-transmitting fractures.

Of important note is that the lithology of the surrounding strata also has a significant effect on UCG. Varying lithologic composition of the surrounding rock will vary how groundwater inflows into the gasification channel. For instance, groundwater inflowing from sandy rocks will have in a dispersed flow pattern (seepage from overlying strata), while groundwater flow pattern from fractured limestones, sandstones, shales, etc. will be in the form of concentrated flows. The dispersed groundwater inflows provide uniform cooling of the rock surrounding the coal seams, entering the gasification cavity largely as steam. Concentrated flows result in nonuniform cooling of the surrounding rock and may even influx into zones of gasification as liquid water (Klimentov, 1963).

The mechanism of groundwater influx impacting underground coal gasification is well understood; with excess groundwater influx into the gasification zone, heat losses sharply increase due to the heating of water and its evaporation, bringing down the temperature inside the in-seam gasification channel.

Creating the most favorable hydrogeologic conditions and managing excess groundwater influx into the gasifier entail either preliminary or concurrent dewatering of the gasification site including water extraction. Water extraction implies using dewatering wells to pump out groundwater that influxes by gravity into the gasifiers, both into the initial gasification channel and into the gasification cavity. Dewatering essentially involves drainage of the aquifers by intercepting groundwater headed toward the gasification (gasifier) and toward the fire face by pumping water up to the surface through dewatering wells.

One of the major challenges often encountered during groundwater extraction from the underground gasifier's gasification cavity is the high temperature of the water and contamination with products of thermal decomposition of coal, mainly phenols, benzene, ammonia, and hydrogen sulfide (Skafa, 1960).

A large body of literature exists on dealing with the issues of dewatering in various mining, geologic, and hydrogeologic settings of UCG sites in the former USSR (the Moscow, Kuznetsk, Donetsk, Dnepr, and Angren coal basins) (Troyansky et al., 1961; Antonova et al., 1967, 1990a,b, 1992; Shilov, 1960; Bogoroditsky, 1961) and is not considered further in this chapter. However, it bears noting that various kinds of drainage mining excavations were used in dewatering underground gasifiers as follows: vertical dewatering wells, initial horizontal gasification channels connected to the dewatering wells, horizontal directional wells, directional production wells linked to dewatering wells, gasification cavities of spent, and operating gasifiers.

Dewatering activities were generally a two-stage process: prior to ignition of the coal seam and as part of UCG operations. The best outcomes in dewatering were achieved in depths down to 200 m. Dewatering of deeper intervals is rather complicated. This is due to the fact that as depth increases, so do groundwater heads, while transmissivity and groundwater yield, which determine the efficiency of groundwater abstraction, decrease.

In addition to drainage operations that permit the reduction in excess groundwater influx into underground gasifiers, the following activities can have a positive effect on process-related outcomes:

(1) Increase the flow rate of the injected air, thereby increasing the rate of dissociation of water vapor.
(2) Increase the oxygen content of the injected air, thereby increasing the rate of decomposition of water vapor.
(3) Increase the air injection pressure, thus displacing groundwater from the gasifier.

As borne out by many years of successful UCG experience in the USSR, with low rates of groundwater inflow (up to about 1 m^3/h) into gasifiers located both on plateau and geosynclinal areas of coal deposition, water extraction measures should suffice. In certain conditions, water extraction is needed not so much to preclude the possibility of flooding the fire face, but rather to mitigate and minimize adverse impacts to the gasification processes and to preempt any possibility of flooding the bottom of the injection wells. Otherwise, if dewatering is not conducted, the air injected into the injection wells absorbs great quantities of moisture, resulting in disruptions to the normal operation of the gasification process.

With low rates of groundwater influx into the gasifier (below 0.5 m^3/h), groundwater may experience complete evaporation and is produced along with the gas, without impacting the gasifier operation.

However, even in coalfields with low rates of groundwater influx (the Donetsk and Moscow coal basins), groundwater had a negative impact on the UCG process. For example, groundwater influx into the underground gasifiers at the Lisichanskaya UCG plant (the Donetsk coal basin) in excess of 10–15 m^3/h had an extremely adverse

effect on the gasification processes, often leading to a complete stoppage of the UCG process (gasifier nos. 10, 14, and 15 and pilot gasifier no. 3).

Impacts of groundwater on UCG can be differentiated into groundwater that has a continuous impact and intermittent impact (gravitational water).

The constant effect of the first type of groundwater is a function of its physical and chemical bonding with the coal and rock, as a result of which groundwater continuously and in specific quantities participates in the processes of underground coal gasification.

Bound water is continuously participating, as it closely interacts with rock and is retained in it by a force greater than the force of gravity. One distinguishes chemically bound water (inherent water and crystallization water) and physically bound water (hygroscopic, film, and capillary water).

Groundwater participation—continuous or otherwise—in UCG is treated in detail in general hydrogeology. It should be noted that during UCG virtually all bound water is changed into vapor, participates in forming gas/vapor mixtures, and is characterized by a specific chemical composition. The amount of bound water is usually determined from the maximum molecular storativity of rock. In addition to bound water, UCG also involves pyrogenic water that forms during the combustion of hydrogen. The pyrogenic and bound water content constitutes 10%–20% of the total amount of water entering the underground gasifier (Bogoroditsky, 1961). The amount of continuously acting water is determined by the size of the zone of heat penetration of rock and the lithology of the coal seam floor and the roof, which in turn depends on the specific mining and geologic conditions of the coal deposit. Based on the results of post-gasification opencasting of underground gasifiers, the maximum depth of heat penetration into rock of up to 100°C was recorded at a distance of 4 m in the coal seam floor and 7–8 m in its roof (Dvornikova, 2011).

The main source of groundwater influx into underground gasifiers is intermittently active (free) gravitational water, which does not have any appreciable bonding with rocks and moves through rock under gravity. The inflow of gravitational water is a function of permeability of both the coal seam and the lithologies in contact with coal, their thickness, groundwater head, and the degree of hydraulic interconnection of the aquifers with the coal seam and with surface streams.

If the amount of gravitational water together with continuously active groundwater does not exceed the optimal water content for coal combustion, the gasification process operates within normal tolerances. Alternatively, the operation of the gasifier is disrupted, the high-temperature environment and gas quality deteriorate, which slows down the rate of gasification until its complete cessation.

In the event of an insufficient moisture content of coal in the gasifier, the decrease in calorific value of gas can occur due to the reduction of the primary combustible component, that is, hydrogen.

Using the common hydrodynamic methods to calculate the optimal amount of groundwater for UCG is not possible, since during UCG parameters of the gasification cavity continually change, with hydraulic conductivity values changing sharply; however, in existing calculation formulas, hydraulic conductivity is a constant value. In addition, calculating intermittent inflows from the coal seam roof is challenging,

given rock deformation above the gasification cavity. In view of the above, calculations of the amount of water taking part in the gasification process, which is required for the process, were carried out using gas chemistry calculations and methods developed at the Laboratory of Hydrogeological Problems of the Academy of Sciences of the USSR (K. F. Bogoroditsky, A. I. Silin-Bekchurin, and V. I. Kononov) and at the VNII Podzemgaz (A. A. Agroskin, N. A. Fedorov, T. M. Sukhotinskaya, P. I. Kalashnikov, N. Z. Brushtein, V. S. Zagrebelnaya, and G. O. Nusinov). Gasifier moisture balances were developed and computed. The optimum amount of water for the gasification process depends on specific natural conditions and changes in them. For the Podmoskovnaya UCG plant, the amount of groundwater influx into the gasifiers was 62 kg/100 kg of coal and for the Lisichanskaya UCG plant at the Donetsk coal basin 139 kg/100 kg of coal (Bogoroditsky, 1957).

Water participates in UCG by entering the gasification zone and reacting chemically with the hot coal, releasing the hydrogen of decomposition into the gas phase, while part of water evaporating without reacting with carbon. With excess groundwater influx into the gas generation zone, the heat produced by the combustion of carbon is expended on the evaporation of moisture, thereby bringing down the temperature in the gasification channel, while it has an adverse effect overall on the heat balance of UCG.

During combustion of coal, the potential heat (Q_c) is distributed between the latent (Q_{la}) and sensible heat (Q_s) of products of combustion of coal as follows (Antonova and Kreinin, 1975):

$$1 = \frac{Q_x}{Q_y} + \frac{Q_\phi}{Q_y} = \eta + \varphi \qquad (8.1)$$

where η is the gasification efficiency and φ is the degree of heat release.

Given the high heat losses in the underground gasifier, including for the evaporation of groundwater, $Q_x \to 0$ and $\eta \to 0$ and $Q_\phi \to Q_y$ and $\varphi \to 1$. Thus, as heat losses in the underground gasifier increase, gasification of the coal seam shifts predominantly to combustion and semicombustion processes.

Despite a multitude of possible hydrogeologic conditions characterizing the depositional setting of the coal seam being gasified, evaporation of both bound and gravitational water takes place in all zones inside the gasification channel walls during UCG. Evaporation of water ultimately causes a decrease in temperature of the coal surface and gas.

During UCG in the gasification channel, three zones of the gas phase are differentiated: the zones of the injected air, the zone of gas generation (heterogeneous gasification reactions), and the zone of gas transport (homogeneous gasification reactions) (Fig. 8.1).

Inside the injected air zone, the temperature of the injected air and the coal surface generally rises and reaches the point of spontaneous combustion of coal. The injected air is often heated by the heat that was retained inside the gasification cavity. As the injected air is heated, it is humidified by water vapor. Considering that the critical temperature of spontaneous combustion of coal exceeds 300°C in most cases, the
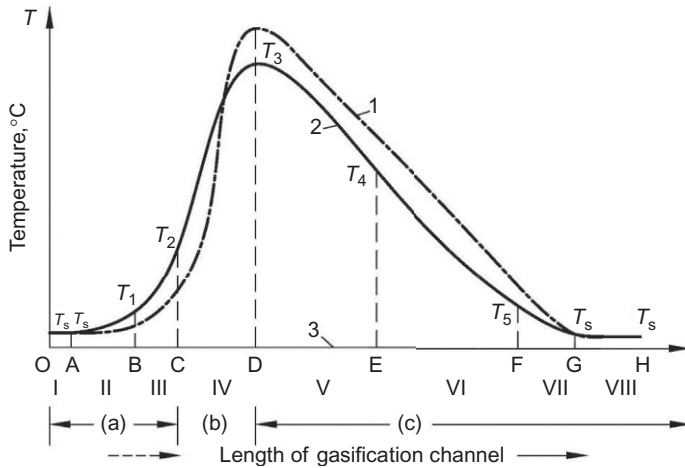
Fig. 8.1 Temperatures in gasification channel: I—injection zone, II—injection flow drying zone, III—ignition preparation zone, IV—exothermic reaction zone, V—endothermic reaction zone, VI—pyrolysis zone, VII—gas flow drying zone, VIII—gas zone, 1—gas-phase temperature variations, 2—coal surface temperature variations, and 3—coal surface, moisture entering gas phase.

water vapor content at the end of this zone can be measured in kilograms per 1 m^3 of the injected air. In some cases, the injected airstreams may entrain the airborne water droplets and carry water along the airflow path.

The water vapor entering the oxygen zone from the channel walls brings down the temperature of the gas and the coal surface. The airborne water droplets that are carried out of the injected air zone exert a similar effect.

An increase in the water vapor content in the gas also leads to a slowing down of the combustion rate. This leads to the oxygen zone becoming extended, increased heat losses into surrounding strata and, eventually, a drop in the gas temperature.

The following water balance accounting procedures have been developed for analysis of the groundwater parameters:

- Moisture balance of water used in the formation of gas.
- Moisture balance of water evaporated by gas (water balance of the gasifier).
- Moisture balance of the underground gasifier.
- Balance of gravitational water of the section being gasified.

The moisture balance of water participating in the formation of gas is used to determine the amount of moisture entering the zone of heterogeneous gasification reactions. This balance is extremely important, since studies established that the greatest adverse effect on the calorific value of gas is associated with water entering the zone of heterogeneous reactions where the formation of combustible components CO and H_2 takes place (Zibalova, 1956). Experiments demonstrated that heterogeneous reactions that produce CO proceed readily at a temperature of $\geq 800°C$. The concentration of CO and H_2 in the gas when leaving the zone of reduction reactions is determined by the heat content of the

channel at 800°C or above, that is, by the maximum temperature in the channel at the end of the oxidation zone and at the beginning of the reduction zone (Shishakov, 1948). However, excess water vapor in the gas stream at a temperature of more than 800°C inhibits the rate of heterogeneous reactions and promotes the conversion of carbon monoxide. The formation of the main combustible components inside the zone of heterogeneous reactions is a function of heat losses due to the inflow of water vapor into the gasification channel within the boundaries of this zone. The moisture saturating the gas in different zones of the gasification channel does not have the same effect on the calorific value of gas. The drop in the calorific value of gas due to moisture entering the zone of heterogeneous reactions is 3–20 times greater than the decrease in the calorific value of gas due to the same amount of moisture entering the zone of homogeneous reactions. Therefore, calculation of the balance of moisture participating in gas formation is performed to establish the correlation between the calorific value of gas and moisture entering the zone of heterogeneous reactions.

The balance of moisture evaporated by gas is used to determine the amount of water participating in the formation of gas in all the zones as it leaves the zone of homogeneous reactions. The latter moisture balance differs from the former only in that the calculation of disassociated moisture is performed only for the zone of heterogeneous reactions, assuming that the water-gas shift reaction occurs only in this zone. The latter balance includes the entire amount of disassociated moisture (entering all the zones), while the former only part of it.

The moisture balance of the underground gasifier is computed to assess the groundwater parameters for the entire underground gasifier. Not all moisture entering the gasifier evaporates or carried out in the gas flow. Part of it, in the liquid phase, especially during underground coal gasification in geosynclinal deposits, collects in the lower part of the gasification cavity and is removed from the gasifier by water extraction. The moisture balance of the underground gasifier takes into account all the water that enters the gasifier, regardless of whether it is carried out in the gas flow or pumped out through drainage dewatering well or dewatering well. This balance takes into account process water, condensed moisture, water that is pumped out or collects in the gasification cavity. This moisture balance is needed for proper selection of dewatering equipment and conducting dewatering activities.

At sufficiently dewatered gasification sites, the preponderance of the balance consists of bound water of the coal seam and the heated floor and roof rocks, while in areas with insufficient dewatering, gravitational water forms the bulk of the moisture balance.

Balance of gravitational water of the area gasified is calculated to assess the efficiency of dewatering activities. This balance also accounts for dynamic and static groundwater resources. The assessment is completed based on the efficiency factor of the dewatering equipment. A gasification site is defined as a ground surface area under which one or more gasifiers, and a dewatering system are located.

The first two types of balances are incorporated in subsequent balances. The objective determines the choice of the balance calculated. Below is the methodology for calculating the second type of balance.

8.1.1 Balance of moisture evaporated by gas

Moisture balance of the gasifier consists of two columns, one for input and another for output.

The moisture balance input data contains ingressing groundwater (gravitational water) that participates in the gasification process, bound water of the coal seam and the floor and roof rock, as well as the moisture of the injected air.

Despite the fact that the volume of water in the vapor phase contained in the atmospheric air and entering the underground part of the gasifier with it is relatively small (compared with the amount of ingressing groundwater), but given the significant amounts of injected air required for the UCG processes, the moisture of the injected air (moisture fraction of air) has a certain effect on the calorific value of gas and is factored into the calculations of the moisture balance of the underground gasifier. The moisture content of the injected air is a function of the humidity of the air, while with steam/oxygen/air injection, it is determined by the amount of water vapor injected. At UCG plants, the moisture content of the injected air fluctuated across the months of the year from 18–20 to 70 g/m^3. The moisture content of the injected air enriched with oxygen was 250–300 g/m^3 at the Lisichanskaya UCG Plant.

In a high-temperature environment, pyrogenic water may also form during combustion of hydrogen as the UCG processes are ongoing. Sixty percent of oxygen in coal is generally assumed to bind with hydrogen to form pyrogenic moisture (Silin-Bekchurin et al., 1960). However, Kalashnikov (1966) proved that factoring pyrogenic moisture into the calculations is unnecessary, as the intermediate reactions of the gas generation, during which pyrogenic moisture is formed, do not determine the final outcome, to wit, the final gas composition. In performing calculations of the values of disassociated moisture, all the combustible constituents in the coal are assumed to convert to gas.

Thus, whether or not pyrogenic moisture ought to be factored into the calculations is disputed. Some researchers deem it advisable to account for it, others do not.

As syngas is produced through production wells and cooled, process water used for cooling should also be included in the water balance calculations. Water injected for cooling purposes is measured by direct measurements.

The abovementioned types of water—inflowing (gravitational) water, bound water of the coal seam and floor and roof rocks, moisture content of the injected air, pyrogenic and process water—constitute the gasifier water balance input.

The *moisture balance output data* contains the following:

- Moisture content of gas.
- Dissociated moisture content, which dissociates chemically and is converted to gas.

Water carried out by the gas stream (moisture content of gas). Water of this type does not dissociate during UCG, but is produced in the vapor phase along with gas. The amount of this type of water is determined by the nature of inflow of water into the fire source and by the overall groundwater influx into the gasification area. A particularly high content of water in the vapor phase in the gas is observed with groundwater bursting into the gasifier, such as when roof rocks collapse. During such

events, the moisture content of gas can sometimes exceed 3000–4000 g/m^3. Any sharp variations in the moisture content of gas points to poor stability of the coal gasification process and must be eliminated by adjusting the operating mode of the gasifiers.

The disassociated moisture content is formed by the interaction of hot carbon with water vapor, forming an intermediate complex, which then disassociates to form CO, CO_2, and H_2.

The amount of hydrogen formed during this process is a useful indicator of the absolute amount of disassociated water.

A relative characteristic of this type of water can be obtained by dividing the amount of disassociated water by the amount of water entering the fire source. This ratio is known as the steam disassociation coefficient.

The latter is not a constant value, but rather it is determined by extent of groundwater influx into the fire source and the gasifier mode of operation and undergoes significant changes over time. At the Podmoskovnaya UCG plant, the steam dissociation coefficient varied between 0.1 and 0.4, while at the Lisichanskaya UCG plant, it fluctuated within a greater range.

8.1.2 Calculation methodology for the evaporated moisture balance

These calculations of moisture balance are in grams divided by 1 m^3 of the gas produced or 1 kg of coal gasified. The following designations are used:

W_c—moisture content of coal
W_f—moisture content of floor rock
W_r—moisture content of the roof rock
W_i—moisture content of the injected air
W_{gwi}—groundwater influx (gravitational water from aquifers)
W_{dis}—disassociated moisture (reacted in the gasification channel)
W_g—moisture carried away by the gas stream as undissociated water vapor

The moisture balance equation can be written as follows:

$$W_c + W_f + W_r + W_i + W_{gwi} = W_{dis} + W_g \tag{8.2}$$

If gas is cooled as it is produced through the production well, then process water used for cooling should be included in the water balance input data (W_{cool}). Then, the above Eq. (8.2) is rewritten as follows:

$$W_c + W_f + W_r + W_i + W_{gwi} + W_{cool} = W_{dis} + W_g \tag{8.3}$$

This equation permits the calculation of the amount of gravitational water (W_{gwi}) influxing into the gasifier that is difficult to determine using hydrodynamic methods owing to the variability of the water permeability of undermined rock strata, the effect of high temperature, and the changes in the parameters of the gasification cavity.

This equation does not take into account the ingressing groundwater that, bypassing the fire face, collects in the gasification cavity and is pumped out through the drainage wells and the water that is pumped out by the dewatering wells located outside of the gasifier boundaries. The amount of water pumped out is included both into the input data and the output column of the water balance and does not affect the results of the calculation of other line items of the water balance.

Calculations of specific line items of the water balance, which are needed to solve the equation in g/m^3 of gas, are provided below.

I. LINE ITEMS OF WATER INFLUX

1. To determine each line item of the water balance, an initial calculation is performed of the sum of combustible constituents of gas in volume percent:

$$\sum C^g = CO_2 + CO + CH_4 + 2C_mH_n \tag{8.4}$$

$$\sum H_2^g = H_2 + H_2S + 2CH_4 + 2C_mH_n \tag{8.5}$$

$$\sum O_2^g = CO_2 + 0.5CO + O_2 \tag{8.6}$$

The coal composition is in weight percent.

2. The moisture content of coal (W_c) is determined by the amount of moisture of coal on an air-dried basis (W^{ad}) divided by the amount of gas (V^g) produced from 1 kg of coal gasified:

$$W_c = A \frac{W^{ad} \sum C^g}{C^{ad}} \tag{8.7}$$

where

W^{ad}—moisture content of coal on AD basis, wt%
C^{ad}—carbon content in coal, wt%
$\sum C^g$—carbon content in gas, wt%
A—coefficient calculated from gas chemistry formulas

3. The moisture content of floor and roof rock is calculated from the amount of bound moisture contained in the zone of heat penetration up to a temperature of 100°C divided by gas output:

$$W_{rfr} = B \frac{\omega_f l_f \sum C^g}{m \gamma_c C^{ad}} \tag{8.8}$$

where

ω_f—volumetric groundwater storativity of floor rock, kg/m^3
l_f—thickness of the zone of heat penetration into floor rock, m
m—thickness of the coal seam gasified, m
γ_c—specific weight of coal, g/cm^3
B—coefficient calculated from gas chemistry formulas

4. Moisture content of roof rock

$$W_r = B\frac{\omega_r l_r \sum C^g}{m\gamma_c C^{ad}}$$

(8.9)

  where
  ω_r—specific groundwater storativity of roof rock, kg/m^3
  l_r—thickness of the zone of heat penetration into roof rock, m
  m—thickness of the coal seam gasified, m
  γ_c—specific weight of coal, g/cm^3
  B—coefficient calculated from gas chemistry formulas

5. The moisture content of the injected air is calculated from the average monthly absolute humidity of the injected air:

$$W_i = \frac{w_a^o N_2^g}{N_2^i}$$

(8.10)

  where
  w_a^o—absolute humidity of air, kg/m^3
  N_2^g—nitrogen content of gas, vol%
  N_2^i—nitrogen content in the injected air (in the air $N_2^i = 79\%$)

6. Water used to cool the gas (W_{cool}) is measured by the water level meter.

II. LINE ITEMS OF OUTPUT

1. The moisture content of gas (W_g) is measured with a moisture meter in g/m^3.

2. Dissociated moisture is calculated based on the coal composition on an air-dried basis, injected air and the gas produced from the oxygen balance equations and hydrogen balance equations that participate in the coal gasification processes.

  Dissociated moisture per unit of hydrogen

$$W_{H_2}^{dis} = 8.03 \sum H_2^g - 48\frac{H_2^{ad} \sum C^g}{C^{ad}}$$

(8.11)

  Dissociated moisture per unit of oxygen

$$W_{O_2}^{dis} = 16.1 \sum O_2^g - 4.27 N_2^g - 6.02\frac{\sum C^g O_2^{ad}}{C^{ad}}$$

(8.12)

  where
  $\sum H_2^g$, $\sum O_2^g$, and N_2^g—the content, respectively, of hydrogen, oxygen-containing constituents, and nitrogen in gas in vol%
  O_2^{ad}, and H_2^g, content of, respectively, oxygen and hydrogen, in coal on an air-dried basis, wt%

3. The amount of dissociated water vapor is calculated as an average value:

$$W_{dis} = \frac{W_{O_2}^{dis} + W_{H_2}^{dis}}{2}$$

(8.13)

III. The amount of groundwater influxing into the gasification zone is calculated from the difference between the output and the sum of all other line items of the input data of the water balance:

$$W_{\text{gwi}} = W_{\text{dis}} + W_{\text{g}} - W_{\text{c}} - W_{\text{f}} - W_{\text{r}} - W_{\text{i}} \qquad (8.14)$$

The results of the calculations are presented in a table.

To convert the moisture content from g/m^3 to m^3/t of coal gasified:

(A) Calculate the gas yield from 1 kg of coal (V^c) from the formula

$$V^{\text{g}} = 1.87 \frac{C^{\text{ad}}}{\sum C^{\text{g}}} \, (\text{m}^3/\text{kg}) \qquad (8.15)$$

where

C^{ad}—carbon of coal on AD basis, wt%

$\sum C^{\text{g}}$—carbon content in gas, wt%

(B) During gasification of 1 kg of coal, the influx of free gravitational water is:

$$W_{\text{gwi total}} = W_{\text{gwi}} \times V^{\text{g}} = \text{kg/kg} = \text{m}^3/\text{ton} \qquad (8.16)$$

IV. To determine the specific groundwater influx, which is the general criterion for groundwater influx into the gasifier, the following is calculated:

(A) The amount of coal gasified (V^{I}) over a certain period, kg or ton

$$V^{\text{I}} = \frac{V}{V^{\text{g}}} \qquad (8.17)$$

where

V, volume of gas produced per month, m^3

V^{g}, gas output from 1 kg of coal, m^3/kg or m^3/ton

(B) Gasification rate (J)

$$J = \frac{V^{\text{I}}}{T} \, (\text{tons/h}), \quad \text{where } T - \text{time in hours} \qquad (8.18)$$

(C) Calculate the total influx of free gravitational water per month from the formula

$$w_{\text{gwi}} = V \times W_{\text{gwi}} = \left(\text{m}^3/\text{h}\right) \qquad (8.19)$$

where V, volume of dry gas for a certain period

(D) Specific groundwater influx is calculated from the formula

$$q = \frac{w_{\text{gwi}}}{J} \left(\text{m}^3/\text{ton}\right) \qquad (8.20)$$

Thus, the degree of groundwater influx into the gasifier is calculated from the specific groundwater influx to the gasification site.

Given that the process of underground gasification takes place in conditions of natural occurrence of the coal seam, the nature and course of the UCG process, in addition to technological factors, are influenced by a large number of different natural factors:

- Degree of groundwater saturation of rock.
- Lithologic makeup of rock in the coal seam roof and floor.

- Coal seam thickness.
- Coal quality (ash content, porosity, moisture content, and results of ultimate analysis of coal), etc.

To determine the effect of these factors on UCG parameters (mainly on the calorific value of gas and its chemical composition), and to select the optimal gasification mode of operation, extensive examination of long-term production data was conducted focusing on operation of underground gasifiers at the Yuzhno-Abinskaya UCG plant and Lisichanskaya UCG plant, conducting UCG operations in steeply dipping coal seams of the Kuznetsk and Donetsk coal basins, were systematized and processed. The analysis also included the production data from the Angren UCG plant and Podmoskovnaya UCG plant operating in subhorizontal lignite coal seams.

There is a great deal of literature concerned with investigating the issues of the effect of various natural factors. In some cases, the effect of moisture content of coal on the chemical composition and calorific value of gas was studied in laboratory conditions (Farberov and Yuryevskaya, 1959; Nusinov et al., 1960; Zvyagintsev, 1962). Other researchers studied the effect of groundwater influx in natural in situ conditions (Antonova et al., 1967; Silin-Bekchurin et al., 1960; Kalashnikov, 1966; Brushteyn and Zagrebelnaya, 1957; Efremochkin, 1964; Antonova and Kreinin, 1975).

An example of the effect of high moisture content of coal on the temperature profile are laboratory experiments using samples of brown coals from the Dneprovsky basin (Zvyagintsev, 1962). During these experiments, the moisture content of coal varied from 5% to 58% (Figs. 8.2 and 8.3).
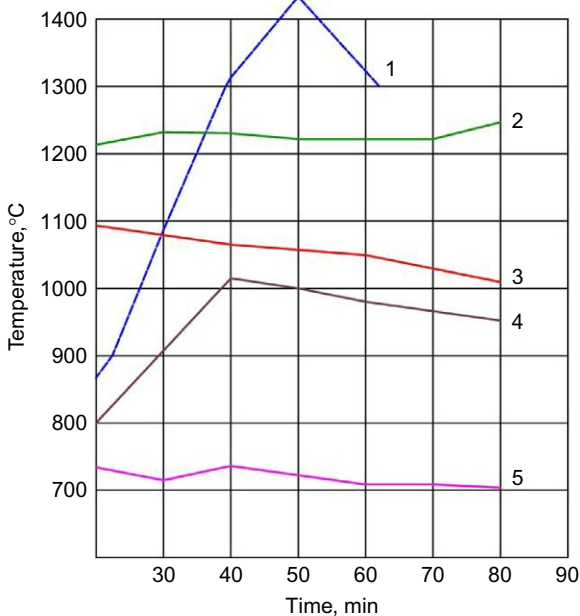
Fig. 8.2 Effect of the moisture content of coal on temperature within the gasification channel: 1—moisture content of coal 5%; 2—moisture content of coal 15%; 3—moisture content of coal 46%; 4—moisture content of coal 52%; 5—moisture content of coal 58%.

Fig. 8.3 Variations in the calorific value of gas relative to the moisture content of coal.
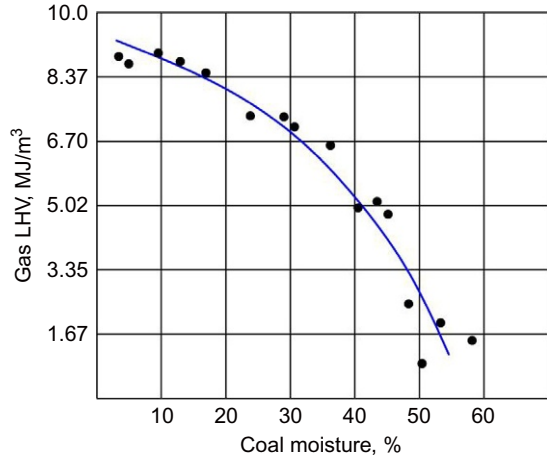
As the figure shows, as the moisture content of coal increases, the temperature decreases from 1350 to 700°C (Fig. 8.2), while the calorific value of gas decreased from 9.66 MJ/m³ (2300 kcal/m³) to 1.68 MJ/m³ (400 kcal/m³) (Fig. 8.3). The experiments were carried out with the use of a gaseous oxygen feed.

Direct measurements of temperature profiles during changes in groundwater influx in natural in situ conditions were not performed. However, a large set of data were aggregated over an extended period of on-site UCG operations on variations in the calorific value of gas relative to the moisture content of gas and groundwater influx into the gasification zone.

In analyzing and interpreting the data on UCG trials, it was important not only to establish the nature of variability of the major process parameters relative to changes in groundwater influx and thickness of the coal seam but also to establish correlation patterns between these quantitative variables.

By grouping the corresponding parameters of UCG and hydrogeologic factors, the causes and repeating patterns of the coal gasification process were revealed relative to variations in natural in situ conditions for different types of coals: lignite and bituminous coal. Data from over 200 different modes of plant operation in bituminous coals of Yuzhno-Abinskaya UCG plant and Lisichanskaya UCG plant were processed and analyzed, approximately 100 modes of plant operation in brown coal at the Angren UCG plant, as well as 50 modes of plant operation at the Podmoskovnaya UCG plant. The most in-depth, comprehensive analysis was conducted of the data sets from UCG operations in two coal seams at the Kuznetsk coal basin (Seam VIII Inner 2 m in thickness and Seam IV Inner with a thickness of 8.5 m). Empirical correlations for operational data were identified between the following:

- Calorific value and moisture content of gas and specific groundwater influx.
- Calorific value of gas, gasification rate, and groundwater influx.
- Calorific value of gas and thickness of the coal seam.
- Chemical composition of gas and specific groundwater influx.
- Dissociated moisture content and specific groundwater influx.

8.1.3 Effects of groundwater influx and the rate of UCG processes on the moisture content of gas

The moisture content of gas (W_g) is one of the initial parameters of groundwater influx into the coal seams gasified and must be established for effective management and control of the UCG processes. To that end, the correlation between the calorific value of gas and its moisture content needed to be identified first. However, comparison of the rates of groundwater influx into the gasification sites solely on the basis of the moisture content of product gas can be conducted only for gasification modes characterized by the same rate of UCG processes. Given a consistent gasification rate, the higher moisture content of gas will be in zones with a greater absolute groundwater influx.

As can be seen from formula (8.20), the value of the specific groundwater influx is significantly affected by the rate of gasification (gasification "intensity"). As the rate of UCG processes increases, the specific groundwater influx into the site decreases.

Operational data from different modes of plant operation at the Yuzhno-Abinskaya UCG plant were analyzed in order to identify the correlation between the moisture content of gas and the rate of gasification; the data set was split into two subsets characterized by the consistency of absolute groundwater influx: 0.5, 2.5, 3.5, 6–7, and 8 m³/h (Antonova et al., 1967). The results of data processing are presented in Fig. 8.4. As the figure shows, a power-law correlation between the moisture content
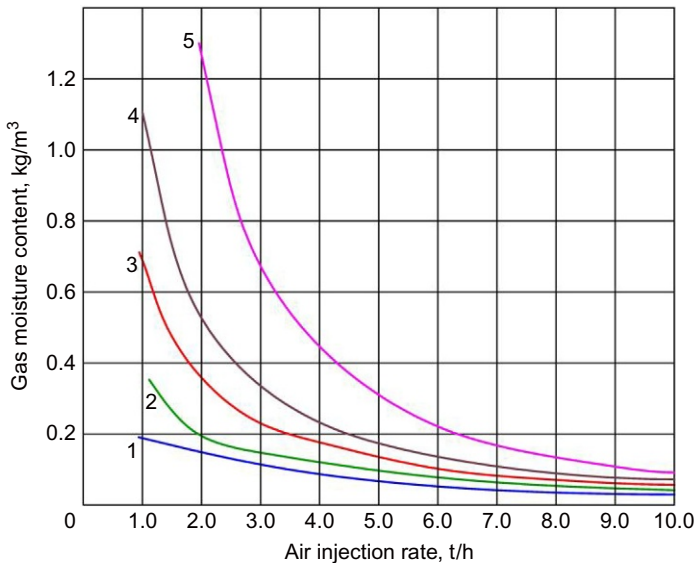
Fig. 8.4 Correlation between the moisture content of gas and the gasification rate and groundwater influx into gasification zones: 1—0.5 m³/h; 2—2 m³/h; 3—4 m³/h; 4—6 m³/h; 5—up to 8 m³/h.

of gas and the rate of gasification was found to exist that, depending on the increase of groundwater influx, is expressed as the following approximated empirical equations:

$$W_g = 186J^{-0.55} \tag{8.21}$$

$$W_g = 336J^{-0.81} \tag{8.22}$$

$$W_g = 705J^{-1.02} \tag{8.23}$$

$$W_g = 1120J^{-1.11} \tag{8.24}$$

$$W_g = 3929J^{-1.61} \tag{8.25}$$

The moisture content of gas decreases most sharply with changes in the gasification rate from 1 to 5 t/h, and further, as the rate of the process increases, the curves in question get closer together (Fig. 8.4). The lowest moisture content of gas was recorded with the lowest rate of groundwater influx into the gasification site. The maximum efficiency of intensifying the rates of gasification is noted with high absolute groundwater influx values.

Identifying causes and repeating patterns permits the selection of modes of UCG operation and predicting the anticipated moisture content of gas when determining the groundwater influx into the gasification site. In addition, it becomes clear that one of the ways to reduce the specific contribution of groundwater to the process of underground coal gasification may be through intensification of the rate of gasification.

8.1.4 Correlation between the calorific value and moisture content of gas

The nature of the correlation between the calorific value of gas Q_g and its moisture content W_g, irrespective of the type of coal being gasified, has a logarithmic correlation and is expressed as the following general form equation:

$$Q_g = A - B \lg W_g \tag{8.26}$$

where A and B are constant coefficients, which are determined by the thickness of the coal seam being gasified and the coal quality.

Fig. 8.5 shows this correlation for lignites at the Podmoskovnaya UCG plant that were 3–4 m in thickness. As can be observed in the figure, as the moisture content of gas increases, the calorific value decreases. The maximum gas calorific value of 3.77 MJ/m^3 (900 kcal/m^3) correlates with the gas moisture content of 150 g/m^3, with a further reduction of the calorific value by 0.54 MJ (130 kcal) that is observed with an increase in the moisture content of 100 g/m^3.

A similar correlation was noted for a 10 m-thick coal seam at the Angren UCG plant (Fig. 8.6) and is calculated with the empirical expression (Lavrov et al., 1967).
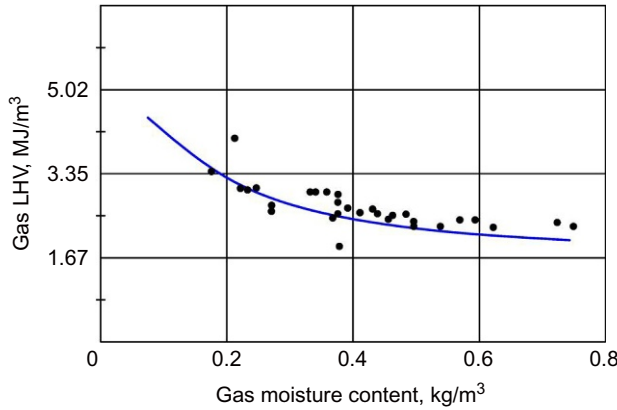
Fig. 8.5 Correlation between the calorific value of gas and its moisture content (Podmoskovny coal deposit).
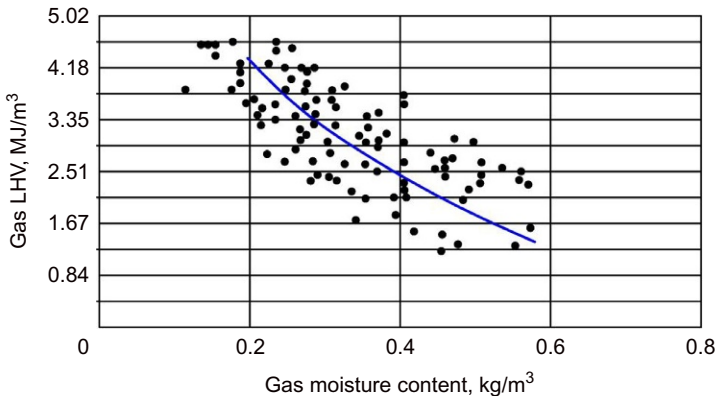
Fig. 8.6 Correlation between the calorific value of gas and its moisture content (Angren coal deposit).

$$Q = 4202 - 1389 \lg W_g \tag{8.27}$$

The correlation between the CV and moisture content of gas is logarithmic within the range of variation of moisture content of gas from 150 to 600 g/m³. The correlation shows that the maximum gas calorific value of 4.19 MJ (1000 kcal/m³) can be obtained with a gas moisture content of 200 g/m³ and a CV of 3.77 MJ/m³ (900 kcal/m³) with a gas moisture content of 250 g/m³.

A similar trend of correlation was found in analyzing UCG modes of operation in the bituminous Kuzbass coal seams with thicknesses of 2 and 8.5 m (Antonova et al., 1967). For a 2-m-thick coal seam, the CV to moisture content correlation (Fig. 8.7) is expressed by the equation

Fig. 8.7 Correlation between
the calorific value of gas and its
moisture content (Yuzhno-
Abinsk coal deposit).
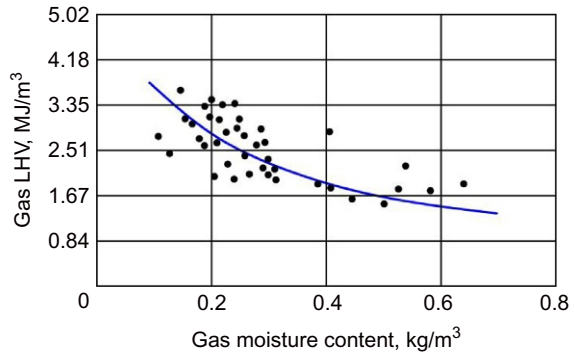
$$Q = 2650 - 720 \lg W_g \tag{8.28}$$

while for a coal seam 8.5 m in thickness by the equation

$$Q = 2650 - 695 \lg W_g \tag{8.29}$$

As can be seen from Fig. 8.7, on-specification gas with a calorific value of
3.77 MJ/m^3 (900 kcal/m^3) in coal seams with a thickness of 2 m is achieved with
a moisture content of gas being no more than 200 g/m^3, while in a coal seam
with a thickness of 8.5 m, given the same moisture content, the calorific value
is 4.4 MJ/m^3 (1050 kcal/m^3). This can be attributed to the thickness of the coal
seam; the greater the thickness of the coal seam, the less the amount of heat loss
into surrounding rock.

8.1.5 Correlation of the calorific value of gas with the specific groundwater influx

The physical moisture content of gas, which is one of the more easily measured param-
eters of UCG, indicates only the amount of evaporated moisture, while the total amount
of water participating in the process is composed of evaporated moisture and dissociated
moisture minus bound water. The total moisture content, expressed in m^3/ton of coal
gasified is a specific value, which is generally referred to as the specific groundwater
influx. The specific groundwater influx into the gasification zone, calculated from the
water and gas balance, indicates the total amount of water participating in the UCG pro-
cesses, which also takes into account the gasification rate (Formula 8.20).

The correlation of the changes in the calorific value with the specific groundwater
influx for the Kuzbass coal seam with a thickness of 2 m over the entire period of oper-
ation of the gasifiers is shown in Fig. 8.8. As can be seen in the diagram, the relation-
ship is correlative and within the range of variability of the calorific value from 4.19
(1000 kcal/m^3) to 1.88 MJ/m^3 (450 kcal/m^3) is expressed by a power-law empirical
equation

$$Q = 893 q^{-0.5} \tag{8.30}$$
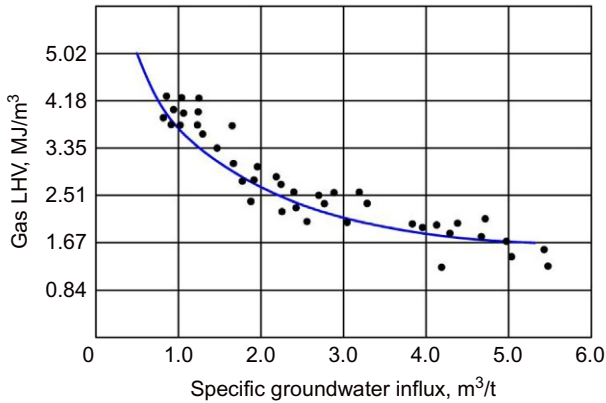
Fig. 8.8 Correlation between the calorific value of gas and specific groundwater influx (Yuzhno-Abinsk coal deposit).

From the expression found, the maximum calorific value of gas is 4.19 MJ/m^3 (1000 kcal/m^3) was achieved with a specific groundwater influx of about 0.8 m^3/t. With increasing specific groundwater influx up to 2.5 m^3/t, the calorific value of gas is reduced to 2.09 MJ/m^3 (500 kcal/m^3).

For the initial period of gasifier operation in a 2-m-thick coal seam, this correlation is expressed as follows:

$$Q = 1107q^{-0.465} \tag{8.31}$$

A similar correlation was found for the Lisichansk bituminous coal seam that is 1 m in thickness:

$$Q = 816q^{-0.395} \tag{8.32}$$

The correlations clearly show that increasing specific groundwater influx results in sharply decreasing calorific value of gas.

For beds of bituminous coal, the correlation between the calorific value of gas Q and the specific groundwater influx q within the range of the variability of the calorific value of gas of 4.06–1.88 MJ/m^3 (1100–450 kcal/m^3) is expressed by an empirical correlation of the power-law form:

$$Q = Kq^{-a} \tag{8.33}$$

where K and a are constant coefficients that are determined by the thickness of the coal seam gasified.

According to the correlations revealed, producing an on-specification gas with a calorific value of 4.19 MJ/m^3 (1000 kcal/m^3) during UCG in coal seams with a thickness of 1.0, 2.0, and 8.5 m, the specific groundwater influx should not exceed 0.6, 1.0, and 1.6 m^3/t, respectively.

The causes and repeating patterns revealed permit the determination of the allow-able groundwater influx into the coal seam. Thus, it is possible to predict the calorific value of gas and to implement all the necessary dewatering activities and to select the gasification mode of operation.

8.1.6 Correlation between the calorific value of gas, thickness of the coal seam, moisture content of gas and groundwater influx

As was shown above, the effect of groundwater influx on the calorific value of gas with different thicknesses of the coal seam manifests itself in different ways, despite equivalent specific groundwater influx. Commensurate with decreasing thickness of the coal seam, the calorific value of gas likewise decreases. Correlations between the effect of the coal seam thickness (m) on the calorific value of gas (Q) during UCG in bituminous coals given different moisture content of gas (W_g) and different values of specific groundwater influx (q) are presented in Fig. 8.9. Correlation $Q = f(W_g)$ is expressed by an empirical equation within the range of the variability of the coal seam thickness from 1.0 to 8.5 m and moisture content of gas from 100 to 600 g/m^3:

$$Q = \left(1e^{1.54\,m}\right)\left(1510 - 2.29W_g 0.001485W_g^2\right) \tag{8.34}$$

The diagram shows that the most significant impact of the coal seam thickness on the calorific value of gas is observed in the range of 1.0–4.0 m. In this range, the calorific value of gas increases by approximately 1.0–1.5 MJ/m^3 (238–357 kcal/m^3). Further increases in the thickness of the coal seam have a lesser impact.

As can be seen in Fig. 8.9, during gasification of bituminous coal using air as the injected oxidant, an on-specification gas with a calorific value of 3.36 MJ/m^3 (800 kcal/m^3) can be produced in coal seams with a thickness of less than 1.0–1.5 m with a minimum specific groundwater influx (1 m^3/t). The actual thickness of the coal seams gasified at the Lisichanskaya UCG plant was 0.85 and 1.2 m. The calorific value varied within 2.93–3.36 MJ/m^3 (700–800 kcal/m^3) with groundwater influx ranging 1–1.5 m^3/t.

In an effort to produce on-specification syngas, the UCG process at the Lisichanskaya UCG plant was mainly conducted using oxygen-enriched injection agent (air).

At the Yuzhno-Abinskaya UCG plant in Kuzbass, UCG was conducted in coal seams with a thickness of 2.0, 3.5, and 8.5 m with rates of groundwater influx into the gasification zone of 2–3 m^3/t, exceeding the maximum allowable (Fig. 8.8). The calorific value of gas was 600–700 kcal/m^3.

Therefore, the calorific value during gasification of the above layers was frequently below 4.2 MJ/m^3 (1000 kcal/m^3). The cold gas efficiency of the UCG process in coal seams with a thickness of 1 and 10 m was 45%–50% and 65%–68%, respectively.
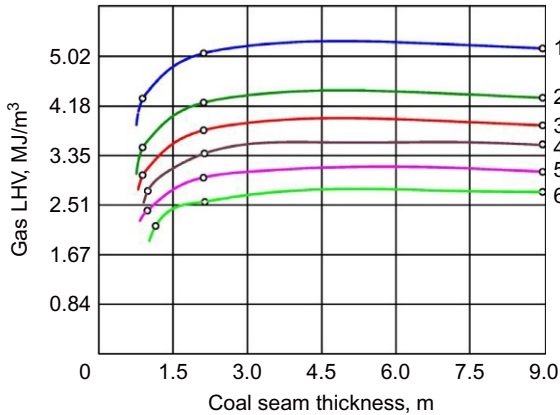
Fig. 8.9 Effect of the coal seam thickness, moisture content of gas and specific groundwater influx on the calorific value of gas. (A) $1 = 100$ g/m^3; $2 = 200$ g/m^3; $3 = 300$ g/m^3; $4 = 400$ g/m^3; $5 = 500$ g/m^3; $6 = 600$ g/m^3. (B) $1 = 1$ m^3/ton; $2 = 2$ m^3/ton; $3 = 3$ m^3/ton; $4 = 4$ m^3/ton.
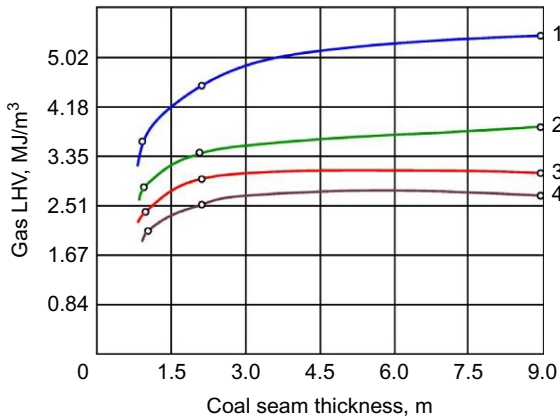
For seams of lignite coal, the effect of the seam thickness on the calorific value of gas was established for the period when the moisture entering the fire face was only from bound water in the coal seam and the heated floor and roof rock. In the absence of an influx of gravitational groundwater, the calorific value of gas during UCG in Angren coals ranging in thickness from 2 to 10 m may increase, respectively, from 3.36 (800 kcal/m^3) to 4.6 MJ/m^3 (1000 kcal/m^3). The actual specific groundwater influx at the Angren UCG plant often exceeded 1.5–2.0 m^3/t, while the calorific value of the coal seam 4–10 m in thickness was decreased, averaging about 3.14–3.56 MJ/m^3 (750–800 kcal/m^3). It should be noted that the air injection and gas production systems had a significant impact on the UCG processes. In view of this, the correlations in question could only be identified with all other parameters being constant.

Thus, the relationship between groundwater influx and the thick of the coal seam being gasified has a significant effect on UCG outcomes. Consequently, with decreasing thickness of the coal seam, the efficiency of dewatering should be increased, while the UCG process should be conducted with a rate that reduces the specific groundwater influx into the gasification zone to 0.5–1.0 m^3/t.

8.1.7 Effects of gasification rate on the calorific value of gas

Based on the correlations between the calorific value of gas, moisture content and the specific groundwater influx (Formulas 8.26, 8.33), the effect of the gasification rate on the calorific value of UCG gas was established. The general the correlation between the calorific value (Q) and the gasification rate (J) or gasification "intensity" (tons/h) is expressed by the equation:

$$Q = a + b\lg J \tag{8.35}$$

where the ratio a decreases as the rates of absolute groundwater influx into the gasification zone increase while the coefficient b increases.

As an example, a particular solution of this equation is considered for coal seams with a thickness of 2 m (Fig. 8.10). In the investigated range of variability of the gasification intensity of a coal seam from 1 to 9 t/h with a groundwater influx into the gasification zones from 1 to 8 m³/h, the calorific value of gas increases, while the sharpest increase in the calorific value of gas in the area of increasing gasification intensity is up to 5 t/h. With a gasification intensity of 9 t/h, the calorific value of gas tends toward its maximum value.
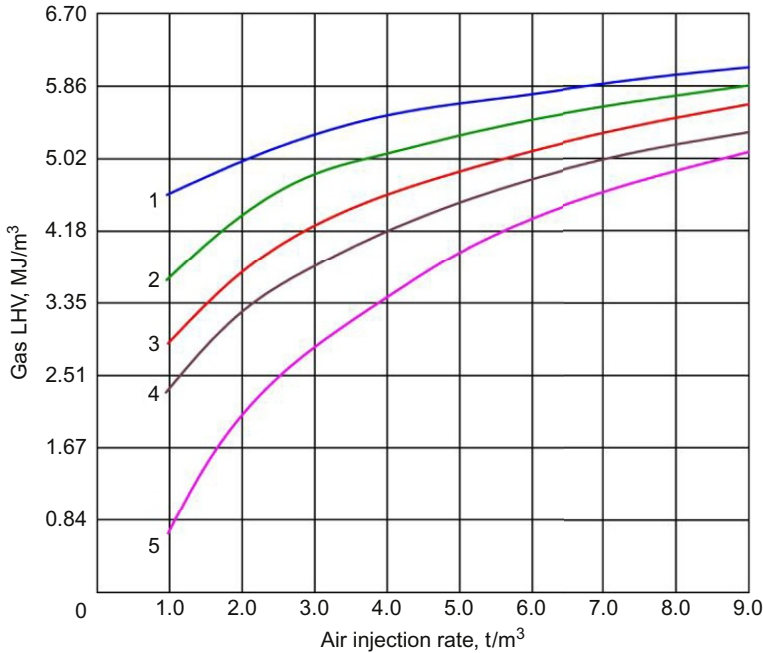
Fig. 8.10 Effect of the gasification rate on the calorific value of gas at different values of groundwater influx into gasification zones: 1—groundwater influx into the gasification zone 0.5 m³/h, $Q = 1080 + 332 \lg J$; 2—2 m³/h, $Q = 395 + 594 \lg J$; 3—4 m³/h, $Q = 670 + 710 \lg J$; 4—530 m³/h, $Q = 530 + 765 \lg J$; 5—8 m³/h, $Q = 160 + 1200 \lg J$.

The causes and repeating patterns revealed are valid for conditions of a properly organized mode of gasification without any gas combustion occurring directly after gas formation at the fire face.

For lignites of the Angren UCG plant, the correlation between the calorific value of gas and gasification intensity is of a different type. What sets it apart is a certain limit of gasification intensity, whereby after a general increase in the calorific value of gas, a decrease is observed. According to this correlation, a certain optimum range of gasification intensity inside the channel varies from 6000 to 10,000 m^3/h (per unit of injected air) (Lavrov et al., 1967).

8.1.8 Effect of specific groundwater influx to gasification zones on the chemical composition of gas

In order to understand the mechanism of moisture having an effect on the UCG process and, in particular, on the chemical composition of the product gas, it should be noted that the main reaction during the gasification of coal is the reaction of reduction of carbon dioxide that is formed in significant amounts in the oxygen zone to carbon monoxide:

$$CO_2 + C = 2CO \tag{8.36}$$

This reaction is reversible and is determined by the energy level of the system. An increase in temperature in the reduction zone contributes to an increase in the CO yield, while a decrease in temperature results in its decrease (Chukhanov, 1957; Lavrov et al., 1966). Simultaneously with the reduction reaction, a second reaction of water vapor with carbon occurs:

$$H_2O + C = CO + H_2 \tag{8.37}$$

Per Chukhanov (1957), the overall rates of these reactions are largely determined by the initial concentrations of CO_2 and H_2O.

Based on actual data on the average composition of gas during UCG in seams VIII and IV in Kuzbass and specific groundwater influx, an assessment was conducted of changes in the principal constituents of gas CO, H_2, CO_2, and CH_4 depending on the increase in groundwater influx into the gasifier. As can be seen in Fig. 8.11, decreasing concentrations of CO and H_2 occur in a different manner and are expressed by the following empirical equations.

The decrease in the concentration of CO in the syngas is expressed by an equation of the type:

$$C_{co} = a - b \lg q \tag{8.38}$$

while the concentration of H_2 is expressed by the equation

$$CH_2 = dq^{-n} \tag{8.39}$$

where a, b, d, and n are constant coefficients.
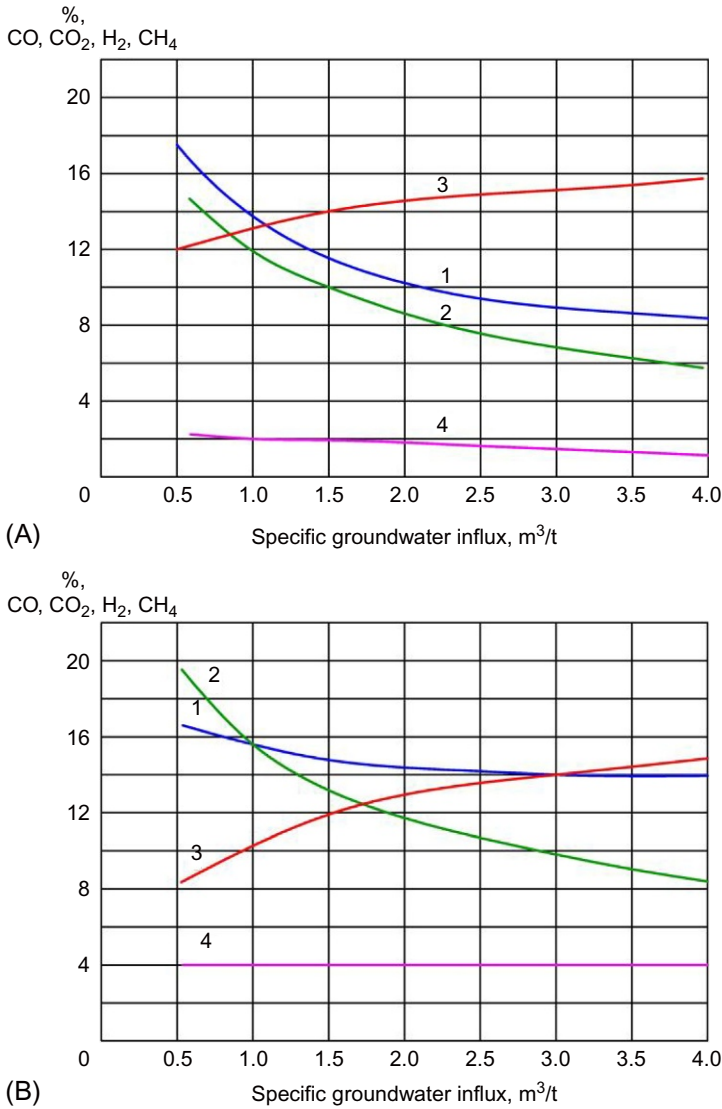
Fig. 8.11 Correlation between the chemical composition of gas and groundwater influx: (A) Coal seam VIII—Vnutrenny, 1—$C_{H_2} = 13.8\,q^{-0.365}$; 2—$C_{CO} = 12.1$–$10.57\lg q$; 3—$C_{CO_2} = 13.6 + 3.65\lg q$; 4—$C_{CH_4} = 2.74$–$0.43\lg q$. (B) Coal seam VIII—Vnutrenny, 1—$C_{H_2} = 15\,q^{-0.103}$; 2—$C_{CO} = 15.6$–$12.4\lg q$; 3—$C_{CO_2} = 10.82 + 6.97\lg q$; 4—$C_{CH_4} = 4$.

Different expressions of Eqs. (8.38), (8.39) indicate that in the zone of relatively low rates of specific groundwater influx (0.5–2.0 m³/t), the reaction rate $H_2O + C$ is much higher than that of $CO_2 + C$. As groundwater influx increases and with it the concentration of H_2O in the gas stream, the reaction rates of both become comparable.

When comparing the correlations characterizing the rate of decrease in the concentration of CO and H_2 in thick Seam IV Inner (8 m) and thin Seam VIII Inner (2 m), it is evident that in the thin coal seam, the concentration of CO and H_2 is slightly lower, while the rate of decrease of H_2 with increasing groundwater influx is much greater. The latter is due to the fact that in the thin seam the energy level of the process is lower owing to the relatively higher heat losses. Increasing concentration of CO_2 with increasing groundwater influx is easily accounted for and is attributable to the reaction of conversion of carbon monoxide.

According to the results of processing a large amount of data on UCG in bituminous and lignite coals in various hydrogeologic conditions, the main causes and repeating patterns were identified in the variability of the following process parameters of UCG: calorific value of gas and its moisture content, chemical composition of gas, cold gas efficiency of the UCG process, rate of gasification given variability groundwater influx into gasification zone, thickness of the coal seam, and coal quality.

Additional data processing and joint solution of the empirical equations (8.26), (8.33)–(8.35) allowed a generalized equation to be derived for bituminous coal that relates the rate of gasification and calorific value of gas with groundwater influx into the gasification zone and the thickness of the coal seam:

$$J = \frac{W_{\text{abs gwi}}}{0.506 \left(\dfrac{Q_H^g V_g}{Q_H^c} \right) - 1.9 \times m^{\left(0.702 - 0.659 \frac{Q_H^g V_g}{Q_H^c} \right)}} \tag{8.40}$$

where

  J—gasification rate (gasification "intensity"), tons/h
  $W_{\text{abs gwi}}$—absolute groundwater influx to the gasification zone, m^3/h
  Q_H^g—calorific value of gas, $kcal/m^3$
  Q_H^c—calorific value of coal gasified, kcal/kg
  V^g—gas yield from 1 kg of coal, m^3
  m—thickness of the coal seam, m

From this equation, the rate of the UCG process (gasification "intensity"), which is required to produce syngas of a certain calorific value, depends on the absolute groundwater influx into the gasification zone, the coal quality, and thickness of the coal seam (Antonova et al., 1990a,b).

In Fig. 8.12, this dependence is represented as a nomogram. Specific groundwater influx is plotted on the vertical axis, and the thickness of the coal seam is given on the horizontal axis, with each of the curves represents a certain value of the cold gas efficiency of the UCG process:

$$\eta = \frac{Q_H^g V_g}{Q_H^c} \tag{8.41}$$

Provided the predicted groundwater influx and coal quality are known, and given the cold gas efficiency of the UCG process, the generalized correlation permits the
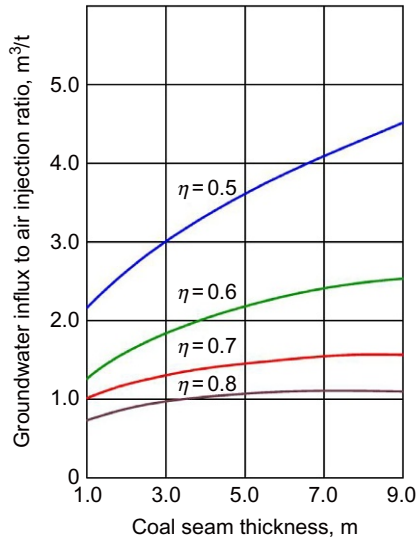
Fig. 8.12 Summary correlation diagram.

determination the optimal UCG modes of operation, thus ensuring management and control over the complex process of underground coal gasification.

8.1.9 Permeability of coal, surrounding rock and groundwater pressure head

Natural gas permeability of coal has a significant impact on the UCG process. It has a significant effect on the gasification process due to the fact that the faster the coal gives up its moisture and dries, the greater the reactivity of coal, the faster the reaction rate of the oxidation and reduction reactions (Zibalova, 1958).

Coal seams with a wide range of gas permeability values from 0.001 to 1–2 darcy were gasified at the UCG plants. Among the brown coals, the least permeable were the Angren coals, whose permeability did not exceed 0.001 darcy, while the Podmoskovnaya coals were characterized by permeability 2–3 orders of magnitude higher, about 1 darcy. The Lisichansk coals had the highest permeability values, up to 0.3–0.5 darcy (Kreinin et al., 1982).

The variations in coal permeability values had a significant impact on the methodology of creating the initial gasification channels. At coal deposits with a natural fracture system, the creation of reactive coal channels was mainly carried out using a combination method with the use of Aquasplitt™ and combustion linking, as well as in-seam drilling of coal channels. The process of opening up reactive coal channels is impacted by the permeability of the surrounding rock; with higher permeability values of rock, the parameters of linking deteriorate due to dispersal of injection air resulting in injected air losses. The permeability

values of the coal seam and surrounding rock rocks also affect groundwater influx into the gasification site and the effectiveness of dewatering activities. However, groundwater influx is also determined by the amount of head, the thickness of groundwater saturated rock, and the thickness of aquicludes separating the aquifers; for this reason, their impact should be examined in toto, taking into account the overall hydrogeologic conditions of the coalfield.

The amount of the groundwater head in the coal seam generally determines the pressure setting and the mode of operation during combustion linking of the wells and the selection of the equipment. Permeability properties and groundwater saturation of the surrounding rock determine the extent of gas leakage. The main reason for extensive gas leakage at the Podmoskovnaya UCG plant was the presence of dewatered, highly permeable rock in the coal seam floor. Gas leakage into karsted limestones in select gasification zones occurred over a wide area and spread within a radius of up to 3 km. For this reason, UCG operations on such sites were ended and transferred to those sections of the coalfield where the coal seam was underwater. The latter approach indicates that the integrity of gasifier systems is determined not only by lithology and permeability of rock but also by the degree of groundwater saturation; in other words, by the general hydrogeologic setting of the coal deposit. Hydrogeologic investigations conducted in the course of ongoing underground coal gasification operations present unique challenges due to possible gas saturation of aquifers, high temperatures and pressures in the gasification cavity, and migration of heated waters.

References

Antonova, R.I., Bezhanishvili, A.E., Blinderman, M.S., Grabskaya, E.P., Gusev, A.F., Kazak, V.N., et al., 1990a. Underground Coal Gasification in the USSR. Central Research Institute of Economics and Scientific Information of Coal Industry, Moscow.

Antonova, R.I., Garkusha, I.S., Gershevich, E.G., et al., 1967. Investigation of causes and repeating patterns in underground coal gasification. Solid Fuel Chem. USSR Acad. Sci. 01, 86–96.

Antonova, R.I., Kreinin, E.V., 1975. Author's Certificate No. 710245 (USSR). The Underground Coal Gasification Methodology. Promgaz Research Institute (Inventor's Certificate). Filed: 02.04.1975, No. 2115205/03.

Antonova, R.I., Shvetsova, N.I., Dvornikova, E.V., 1990b. Experience with dewatering of underground gasifiers at the Yuzhno-Abinskaya UCG Plant. Nonconventional coal mining and coal utilization methods. Scientific Bulletin. Skochinsky Institute of Mining, Moscow, pp. 23–33.

Antonova, R.I., Shvetsova, N.I., Dvornikova, E.V., 1992. Dewatering methods in commercial underground gasifiers at the Yuzhno-Abinskaya UCG Plant. In: Collection of Reports: Seminar on Underground Coal Gasification, Kemerovo, pp. 89–96.

Bogoroditsky, K.F., 1957. The extent and nature of hydrogeological investigations in coal deposits under development as a UCG mining operation. Underground Coal Gasificat. 01 Promgaz Research Institute, Moscow, pp. 65–67.

Bogoroditsky, K.F., 1961. The role of groundwater in chemical component transport at underground coal gasification sites. Geochemistry USSR Acad. Sci. 01, 75–83.

Brushteyn, N.Z., Zagrebelnaya, V.S., 1957. The effect of moisture on UCG. Underground Coal Gasification. 03 Promgaz Research Institute, Moscow, pp. 33–38.

Chukhanov, Z.F., 1957. Gasificaton of Coke and Challenges of Coal Gasification. USSR Academy of Sciences, Moscow.

Dvornikova, E.V., 2011. Important features of chemical contaminant migration from the underground gasifier: mitigation of environmental impacts. Coal 11, 63–68.

Efremochkin, N.V., 1964. Investigation of Groundwater Influx and Dewatering of Coal Seams During UCG Mining Operations (Extended Abstract of Dissertation for the Degree of Cand Tech Sci). Promgaz Research Institute, Moscow, p. 19.

Farberov, I.L., Yuryevskaya, I.P., 1959. An investigation of the impact of the moisture content of the Podmoskovny Basin coal on the composition of gas produced inside a gasification channel. Underground Coal Gasification. 01 Promgaz Research Institute, Moscow, pp. 39–42.

Kalashnikov, P.I., 1966. The Study of the Groundwater Setting in the Underground Part of the Gasifier and the Effect of the Hydrogeological Setting on the Process of Underground Coal Gasification in Lignite Deposits (Extended Abstract of Dissertation for the Degree of Cand Tech Sci). Promgaz Research Institute, Moscow, p. 21.

Klimentov, P.P., 1963. Hydrogeological investigations in underground coal gasification. izvestia news publication for higher educational institutions. Geol. Explor. 09, 104–119.

Kreinin, E.V., et al., 1982. Underground Coal Gasification of Coal Seams. Nedra Publishers, Moscow.

Lavrov, N.V., Kreinin, E.V., Revva, M.K., et al., 1966. The effect of the coal seam thickness on the calorific value of gas in underground coal gasification (UCG). Proc. Acad. Sci. USSR 171, 656–658.

Lavrov, N.V., Kulakova, M.A., Kazachkova, C.I., et al., 1967. Underground coal gasification at the Angren lignite deposit. Solid Fuel Chem. USSR Acad. Sci. 01, 86–96.

Nusinov, G.O., Brushteyn, N.Z., Miringof, H.C., 1960. A study of the interrelationship between gas quality and moisture content of the coal undergoing gasification. Nauchnye Trudy [Scientific Works], vol. 3. Promgaz Research Institute, Moscow, pp. 13–18.

Shilov, Y.S., 1960. Gasifier dewatering diagram for the Yuzhno-Abinskaya Podzemgaz UCG Plant. Nauchnye Trudy [Scientific Works], vol. 3. Promgaz Research Institute, Moscow, pp. 91–96.

Shishakov, N.V., 1948. Basics of Fuel Gas Production. Gosenergoizdat, Moscow.

Silin-Bekchurin, A.I., Bogoroditsky, K.F., Kononov, V.I., 1960. The Role of Groundwater and Other Natural Factors in Underground Coal Gasification. USSR Academy of Sciences, Moscow, p. 125.

Skafa, P.V., 1960. Underground Coal Gasification. State Publishing House of Technical Literature on Mining, Moscow, p. 322.

Troyansky, S.V., Fisenko, N.E., Efremochkin, N.V., 1961. Evaluation of the applicability of various dewatering systems in underground gasifiers. Nauchnye Trudy [Scientific Works], vol. 04. 04 Podzemgaz UCG Research Institute, Gosgortekhizdat, pp. 79–83.

Tsitovich, N.A., 1983. Soil Mechanics. Survey Course. Course Manual, fourth ed. Visshaya Shkola Publishing House, Moscow, p. 288.

Zibalova, G.P., 1956. Further to the issue of gas formation over time in underground coal gasification at the Podmoskovnaya UCG plant. Underground Coal Gasificat. 08 Promgaz Research Institute, Moscow, pp. 65–67.

Zibalova, G.P., 1958. Changes in permeability characteristics of the Angren coal during drying and preheating. Underground Coal Gasification. 01 Promgaz Research Institute, Moscow, pp. 28–31.

Zvyagintsev, K.N., 1962. An investigation of the impact of the moisture content of Dnepropetrovsk coal on oxygen-blown UCG of the same. Nauchnye Trudy [Scientific Works], vol. 07. Promgaz Research Institute, Moscow, pp. 41–46.

This page intentionally left blank

The effects of rock deformation in underground coal gasification

9

G.V. Orlov
Ergo Exergy Technologies Inc., Montreal, QC, Canada

9.1 Rock deformation and subsidence in conventional shaft coal mining

9.1.1 General considerations of the effects of underground mining on subsurface rock deformation and subsidence

Rock overlying a mineral deposit is in a state of natural equilibrium. Unsupported mine voids created during underground mining cause a disequilibrium in rocks, leading to their displacement and deformation. Rock displacement that occurs in the vicinity of an underground mine working extends upward to the upper layers of the overburden. Once the underground working reaches a sufficiently large size, the displacement of rock strata will extend to the ground surface, which will in turn undergo deformation. As early as the mid-19th century, subsidence began to cause severe damage to buildings, facilities, transportation links, and agricultural land in a number of European coalfields. This led coal mine surveyors to install monitoring stations and conduct systematic monitoring of subsurface rock deformation and subsidence. Based on the summary of the results of this monitoring and theoretical understanding, a new subfield was formed within mining science—rock deformation.

Rock deformation and subsidence during underground mining developments of coalfields are among the most extensively investigated processes. Therefore, the presentation of material will be based primarily on the results of studies conducted in the coal-mining regions of the Commonwealth of Independent States (CIS).

In underground coal gasification, the immediate roof strata not only undergo displacement and deformation involving a loss of continuity but also change their mechanical properties, chemical, and mineralogical composition and its aggregate state. This results in a loss of integrity of the underground UCG gasifier cavity, increased losses of oxygen supply (injected air) and gasifier gas losses, and a heat loss to the surrounding strata, with some peripheral process air leakage occurring that can disrupt the entire UCG plant process.

Technological process parameters and the specifics of a coal-mining operation determine the shape of the depleted UCG cavity and the nature of overburden deformation, which in turn have a direct impact on process consistency and stability and on process performance and economic sustainability. It is for this reason that monitoring and research into rock deformation and subsidence during underground coal

gasification and conventional underground coal mining is of great importance not only for prediction of the undermining of surface structures and their protection but also for the continued improvement of these methodologies.

As research results showed, the principal processes of rock deformation during UCG or conventional shaft mining of coal are driven by a common set of mechanisms. It is therefore useful to begin by considering the general principles that were identified in relation to conventional coal-mining settings.

9.1.2 Types and modes of rock deformation

The selection of precautionary measures to mitigate the adverse effects of rock deformation on surface structures is determined by the nature of deformation, which is defined as displacement of rock and changes in the stress-strain state of rock strata following undermining and overmining.

According to data on mining developments and a review of monitoring data on rock deformation in numerous coalfields, it was determined that the principal forms of rock deformation during underground extraction of coal seams are as follows: bending of rock strata, caving, displacement along the bedding plane, coal sloughage, coal creep (or plastic flow), and sliding along the bedding plane.

Of the above, bending, sloughage, and creep or plastic flow of rock mass manifest themselves in varying degrees virtually at all times. Displacement of rock along the bedding plane occurs during mining in inclined and steeply dipping coal seams. Caving and sliding of rock have to do with roof control methods and may be prevented by backfilling mined-out workings.

Below is a brief description of the principal types of rock deformation.

Bending of rock is the sequential separation of rock layers from the formation and their displacement toward the gasification cavity without causing discontinuities in the rock stratification. Rock deformation above underground mine workings invariably begins in the form of bending of some rock layers directed along the normal to the bedding plane.

Caving of rock takes place in the immediate roof rock layers above the mined-out area. Caving is characterized by rock becoming detached from the overlying strata and randomly collapsing in the form of discrete rock blocks and fragments. Caving is necessarily preceded by the maximum critical bending of rock layers. As rock caves in, volumetric bulking of rock material diminishes the magnitude of overlying strata deformation.

Rock displacement along the bedding occurs simultaneously with the bending of layers in inclined and steeply dipping coal seams. Rock displacement is caused by the deformation of layers along the bedding plane being acted upon by the weight of the rock mass as the formation segregates into layers and by shear stresses acting as layers bend.

Sloughage is a type of deformation that occurs in the coal seam whereby the lithostatic pressure crushes a part of the coal seam causing it to slough off into the mined-out cavity. Sloughage of the coal seam is accompanied by rock deformation processes that

begin to occur within the rock formation and on the ground surface outside the boundaries of the mined-out cavity.

Creep deformation or plastic flow of rock from the formation in the direction of the mined-out cavity manifests itself as swelling of floor rock in a mine working. During plastic flow, a decrease is noted in the thickness of the rock layers within the formation outside the cavity boundaries, while it increases above and below the cavity. An increase in rock layer thickness inside the zone of relaxation will also occur owing to elastic recovery of rock. Plastic flow occurs principally in clays, argillaceous (carbonaceous) shales, and coal. Plastic flow is one of the major causes of deformation of the overburden and the ground surface above the barrier pillar of unmined coal outside the solid-coal boundaries of the mined-out cavity.

Rock sliding occurs in the mined-out cavity during coal extraction in inclined and steeply inclined coal seams with mine roof collapse. As rock slides, displacement takes place of the collapsing hanging-wall rock and the footwall rock that is being rendered discontinuous.

Mining operations create several zones in the rock mass that differ in nature and the degree of rock deformation. The number of these zones is determined by the geologic and mining setting of the coal resource being developed. Our current state of knowledge of this issue allows us to differentiate three regions and 16 zones (17 zones in steeply dipping seams) each bearing different characteristics specific only to that zone (Fig. 9.1).
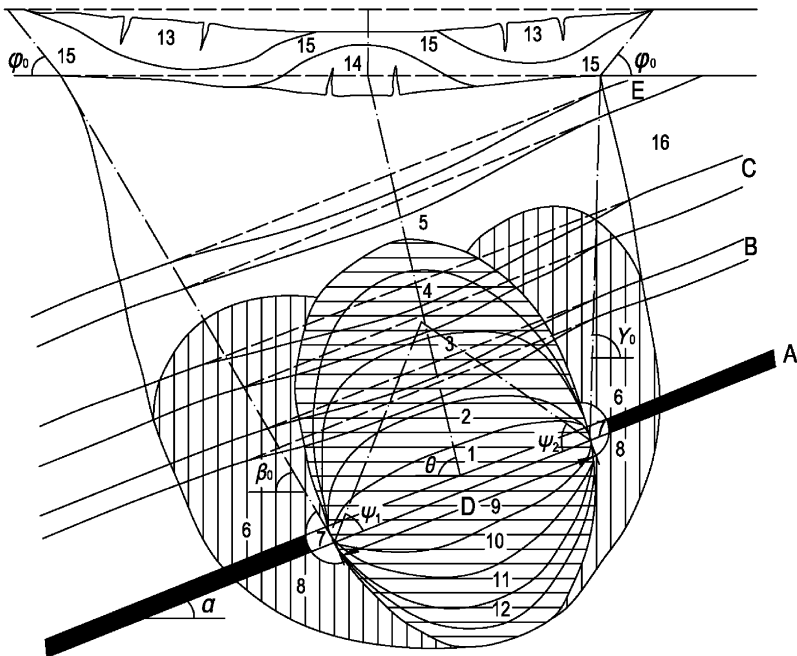
Fig. 9.1 Schematic diagram of rock deformation during mining of coal seams.

The zone of rock stress relaxation is characterized by decreased normal stresses (compared with intact rock) that act perpendicular to bedding. It is located above and below the mined-out cavity (shown crosshatched in Fig. 9.1) and resembles two semiellipses in cross section, whose shared axis is equal to the width of extraction cavity D. The values of semiaxes that characterize the semiellipses in both undermined and overmined portions of the formation are determined by the dimensions of the underground working, dip, thickness and depth of extraction, and measures to control the effects of the lithostatic pressure, lithologic structure, and mechanical properties of rocks. Rock masses inside the zone of relaxation expand and are displaced toward the mined-out cavity. Rock bulking occurs thanks to elastic recovery and stratification of rock, with voids forming under the hanging layers. In undermining overlying rock, stratification and hanging of rock play an important role in the overall loosening of the rock mass; hence, the entire process has a distinctly discrete character.

Most nonuniform deformation occurs at contacts of rock layers of varying strength, especially if the more rigid layer overlies an easily bending or collapsing layer. During overmining, stratification voids will relatively seldom form, predominately in cases of steeply dipping coal seams.

The zone of elevated lithostatic pressure (ELP), also referred to as the zone of rock-bearing pressure, is bordered by the zone of relaxation and is located above and below the undisturbed mineral deposit or above and below the coal pillar left for support. Fig. 9.1 shows the ELP zone hatched by vertical lines. In this zone, stresses normal to the bedding plane are higher than in undisturbed rock. Rock-bearing pressure parameters are determined by the depth of mining operations, physical and mechanical properties of rock, thickness and dip of the coal seam, and dimensions and spatial configuration of the mined-out cavity, among other factors. Based on monitoring data, the width of the rock-bearing pressure in the plane of the coal seam varies between 0.1 and 0.3 H (where H is the depth of mining operations).

The zone of complete deformation is characterized by displacement of the layers parallel to the original bedding. Displacement vectors inside this zone are normal to the bedding plane and have maximum values for these conditions (thickness and dip of the coal seam, measures to control the effects of the lithostatic pressure, etc.). Once deformation stops, rock layers come to rest on the floor of the coal seam being mined. The zone of complete deformation is located above the mined-out cavity and is delineated on the strike-perpendicular vertical section (Fig. 9.1) by lines drawn from the boundaries of the mined-out cavity at angles of complete deformation ψ_1 and ψ_2 while on the strike-parallel cross section, at angle ψ_3.

The greatest amount of rock deformation occurs *inside zone 1*, which is located directly above the working, resulting in fragmented pieces and smaller blocks of rock. It is generally referred to as the *caving zone*.

In shaft mining of coal deposits, the height of the caving zone is usually taken to be 3–6 m.

Zone 2, which adjoins the caving zone, is characterized by the development of fractures normal to the bedding plane and stratification fractures in bending layers that break up the formation into large blocks forming a system of water- and

gas-transmitting channels with low gas flow resistance, which has virtually no impact on the fluid and gas flow through the channels. This zone is generally referred to as the *zone of contiguous fractures*.

Inside zone 3, subvertical fractures, which transect the bending layer from the upper and bottom portions, reach the stratification fracture, thereby forming a system of water- and gas-transmitting fractures with a considerable gas flow resistance that increases in proportion to the distance away from the coal seam. *Zone 3* may be termed *the zone of active fractures*.

Inside zone 4, tensile deformation induced by the bending layer reaches a critical value in the microlayers bordering the top and bottom surfaces of the layer. Concurrently, shear stresses induced by the bending layer bring about shear deformation that gives rise to stratification fractures. However, since the extent and depth of the subvertical fractures inside zone 4 is insignificant, no system of water- and gas-transmitting fractures is formed. *Zone 4* may suitably be termed *the zone of discontiguous fractures*.

Zone 5 is characterized by a bending of rock with virtually no loss of continuity. The zone is appropriately referred to as the *zone of plastic bending*.

Zones 6 and 7 are located inside the zone of elevated lithostatic pressure. Zones 6 exhibits predominantly elastic deformation, while zone 7 exhibits inelastic deformation (irreversible). *Zone 6* is generally referred to as the zone of rock-bearing pressure, as the same characteristics are used to describe it as the zone of rock-bearing pressure. *Zone 7* is conventionally known as the *maximum stress zone*, although deformation at outcrop is generally above the elastic limit. Inside this zone, rock material undergoes all the stages of deformation from considerable uniform compression on the boundary of the elastic deformation zone to significant decompaction in the vicinity of the outcrop. Permanent deformation occurs along systems of natural fractures accompanied by displacement along the surfaces of structural elements. The above zones (with the exception of zone 7) are located in the undermined rock strata. Zone 7 extends both to the undermined and the overmined strata, but it manifests itself most strongly in the coal seam being mined. Five zones are distinguished within the overmined strata (no caving zone is present), while zones 9, 10, 11, 12, and 8 correspond qualitatively to zones 2, 3, 4, 5, and 6 in the undermined strata, but all the zones that are created in the overmined strata are located in closer proximity to the coal seam than those in the undermined strata.

Owing to bending stresses, tensile stress zones and compressive stress zones form within the rock layer closest to the ground surface (or within a multilayer rock unit that undergoes deformation as a single unit), with tensile stress zones being isolated from one another and compressive stress zones virtually merging.

Zone 13 is characterized by maximum tensile stresses of the upper microlayers of the bending layer (multilayer rock unit) and a gradual attenuation of tensile stresses from the upper microlayers toward the lower, with zone 14, conversely, with maximum tensile stresses in lower microlayers of this layer (multilayer rock unit) and a gradual attenuation of tensile stresses starting from lower microlayers toward the upper. Zone 15 is noted for compression of the layer (multilayer rock unit). This zone incorporates virtually merging zones in which bending-induced strike-parallel compression of the layer (rock unit) occurs.

At a certain dip, rock layer sliding occurs (predominately along the bedding plane), with zone 16 manifesting itself within the formation, which is located mainly in the hanging wall of the mined seam. In steeply dipping (less frequently, inclined) layers, this zone also extends toward the footwall of the seam in question.

Depending on mining conditions, roof control methods and other factors, the number and location of zones may vary from the zoning differentiation described above. Thus, during backfilling of the mined-out cavity and when employing roof control measures such as gradual roof support removal, the caving zone is generally absent.

The condition of surface infrastructure and natural features is determined by which deformation zone they fall into. These considerations are of particular importance when undermining surface water bodies and underground aquifers. If a water body is located within zones 1 and 2, a catastrophic ingress of water will occur, resulting in underground workings becoming completely flooded. If a water body is located within zone 3, an intensive water influx into mine workings will occur, with the water influx rate being inversely proportional to the M/m ratio, where M is the distance from the working roof to the floor of the water body.

9.1.3   Displacement and deformation proper in the principal sections of the subsidence trough

Monitoring data showed that the subsidence follows complex, nonlinear patterns. Displacement vectors, their horizontal and vertical components for different points on the ground surface vary in their magnitude and, not infrequently, in direction. The displacement vector of the subsidence trough can be decomposed into its three components: vertical (subsidence) η, horizontal (horizontal displacement) ξ, and perpendicular to the sectional plane ς. Due to its negligible magnitude in the principal cross sections of the subsidence trough, the latter component is rarely, if ever, used in practice.

Therefore, the main indicators characterizing subsidence in the subsidence trough are *settlement and horizontal displacement*.

Nonuniform displacement of adjacent points leads to vertical (inclines and curvature) and horizontal (compression and tensile stresses) deformation of areas of the ground surface within the subsidence trough.

Fig. 9.2 shows points 1, 2, and 3 representing the locations of the markers on the ground surface prior to undermining; $1', 2', 3'$—position of the same markers after undermining has taken place; η_1, η_2, η_3—downward displacement of the corresponding markers; ℓ_{1-2}, ℓ_{2-3}—horizontal distance between markers prior to undermining; and ξ_1, ξ_2, ξ_3—horizontal displacement of the corresponding markers.

Slope of the interval along the surface is calculated as the ratio of the difference in subsidence between two adjacent points within the subsidence trough to the original distance between them (nondimensional, 10^{-3})

$$i_{1-2} = \frac{\eta_2 - \eta_1}{\ell_{1-2}} \tag{9.1}$$
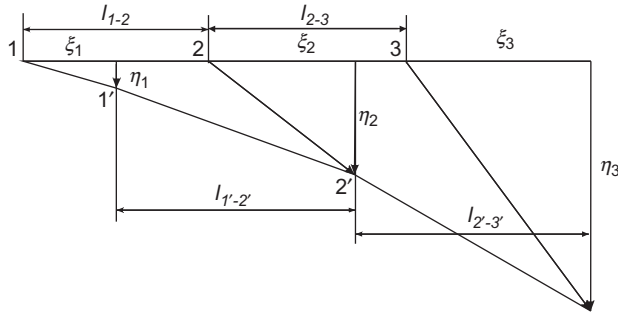
Fig. 9.2 Schematic diagram of deformation calculation.

The resulting slope value i_{1-2} is an average value for the interval and is assigned to/plotted on the interpoint center. The slope is also noted for being the first derivative of the subsidence function $\eta = f(x)$. The slope values in both the updip and along-strike directions are considered to be positive, while in the opposite direction, the values are assumed to be negative.

Curvature is caused by the nonuniformity of slopes of adjacent areas within the subsidence trough. Curvature is estimated as the ratio of the difference between the slopes of two adjacent subsidence trough intervals to the semi-totals of the original lengths of these intervals (10^{-3} 1/m).

The mean curvature at the boundary of intervals 1–2 and 2–3 is calculated from expression (9.2)

$$K_{1-2-3} = \frac{i_{2-3} - i_{1-2}}{\frac{1}{2}(\ell_{1-2} + \ell_{2-3})}, \quad \frac{1}{M} \times 10^{-3} \tag{9.2}$$

and is assigned to/plotted on point 2. Curvature is the first derivative of the slope function di/dx or the second derivative of the subsidence function $d^2\eta/dx^2$.

The radius of curvature R is the reciprocal of curvature: $R = 1/K$ (m or km). In areas of the subsidence trough with an up-facing convex, the curvature and the radius of curvature are taken to be positive, while in areas with a down-facing convex, they are assumed to be negative.

Nonuniform horizontal displacement of points within the subsidence trough gives rise to horizontal compressive and tensile deformation (see Fig. 9.2). The magnitude of horizontal deformation ε over an area of the subsidence trough ℓ_{1-2} is calculated as the ratio of shortening or lengthening of the interval to its original length:

$$\varepsilon_{1-2} = \frac{\ell_{1'-2'} - \ell_{1-2}}{\ell_{1-2}}, \tag{9.3}$$

where ℓ_{1-2} is the original length of the interval and $\ell_{1'-2'}$ is the length of the interval after deformation.
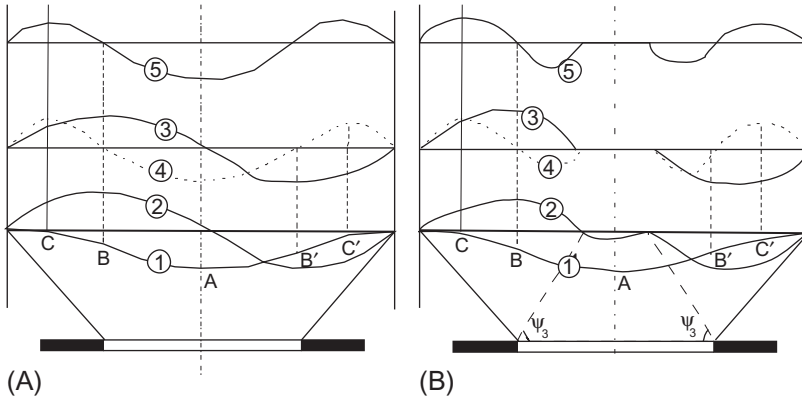
Fig. 9.3 Schematic diagram of patterns of distribution of deformation above a mine working with partial (A) and full (B) undermining: (1) subsidence and (2) horizontal displacement, (3) slopes, (4) curvature, and (5) compression and tensile extension.

Sign convention of the stresses is as follows: tensile stress as positive and compressive stress as negative. They are plotted in the center of the intervals.

Horizontal and vertical displacement that occur within the subsidence trough affect surface structures and natural features; hence, establishing deformation values is imperative.

In order to address issues related to the choice of measures to mitigate the detrimental impact of deformation on structures located inside the zone of influence of undermining operations, the pattern of distribution of deformation in the principal cross sections of the subsidence trough must be known after all extraction is completed as well as postdeformation (Fig. 9.3).

The predominant mode of rock deformation above mine workings in mining subhorizontal coal seams is sequential bending of overburden strata. This is the expected mode of deformation of the ground surface. In steeply dipping coal seams, shear deformation occurs perpendicular to the strike direction. Sinkholes and terraced subsidence may result from working steeply dipping seams that show $\alpha < 45$ degrees dipping at relatively shallow depths using mining methods with mine roof collapse.

9.1.4 Main parameters of rock deformation and their practical application (based on the results of research conducted in the CIS countries)

The part of the formation that is subjected to deformation resulting from underground mining is generally termed the rock deformation zone, while the area of the ground surface located inside this zone is referred to as the *subsidence trough*.

Maximum values of displacement and deformation proper are reached in *the principal sections of the subsidence trough*: vertical cross sections of the subsidence trough along the strike and across the strike of the coal seam passing through the points
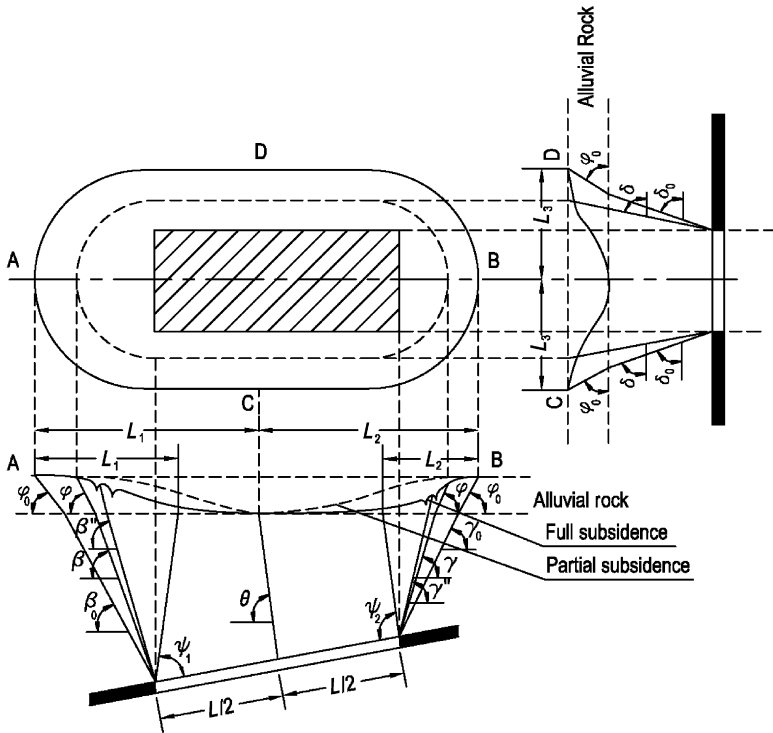
Fig. 9.4 The subsidence trough and deformation angles are as follows: $\beta_0, \gamma_0, \delta_0, \varphi_0$, boundary angles; $\beta, \gamma, \delta, \varphi$, deformation angles; ψ_1, ψ_2, ψ_3, angles of full deformation; θ, angle of maximum subsidence; β'', γ'', angles of break (or angles of subsidence).

of maximum subsidence. All deformation angles are calculated in the vertical sections of the principal cross sections of the subsidence trough.

The boundaries of the zone of influence of underground mining on the ground surface are determined by boundary angles (β_0, γ_0, and δ_0; Fig. 9.4), which are external angles relative to the mined-out area formed by horizontal lines and lines (sequentially drawn in bedrock, Mesozoic rock, and alluvial deposits) connecting the solid-coal boundaries of the mined-out working with points on the ground surface where slopes and bending do not exceed 0.5×10^{-3}. Boundary angles are also used in coal pillar design for deep vertical shafts.

Deformation angles (β, γ, δ) are one of the major parameters of deformation. The value of the deformation angles is used in delineating the zone of damaging subsidence effects inside the subsidence trough and solid-coal pillar boundaries left to protect surface structures.

Boundaries of the zone of damaging subsidence effects are defined as areas where the slope $i = 4 \times 10^{-3}$, curvature $K = 0.2 \times 10^{-3}$ 1/m, and tensile stress $\varepsilon = 2 \times 10^{-3}$ (with an average interval between adjacent markers being 15–20 m).

To find the measure of deformation angles, boundaries of the mined-out workings are connected to points on the ground surface that satisfy all the above conditions. As with boundary angles, deformation angles that delineate the zone of damaging effects inside the subsidence trough from the downdip direction β, γ—from the updip direction, δ—along the strike of the coal seam, and deformation angles in alluvial deposits—φ. It should be noted that the deformation angles and boundary angles are intended for informational use only and should not be considered as the actual incline of surfaces along which rock deformation activity occurs.

Deformation angles are calculated after the ground surface is fully undermined, where the constant maximum subsidence value characterizes the undermining process as the dimensions of the mined-out area increase. In subhorizontal coal seams, the subsidence trough has a flat bottom, with the trough resembling a saucer in cross section (Fig. 9.3). *Partially undermined* ground surface is manifested in the form of a trough that has a cup-shaped bottom, with changing maximum subsidence values as the mined-out area increases.

The shape of the subsidence trough determines the patterns of distribution of deformation values in its principal cross sections. The degree of undermining of the ground surface is expressed as the *subsidence coefficient n*, which is the ratio of the actual size of the mined-out area D to the minimum dimensions D_o for complete undermining of the ground surface to occur. Two subsidence coefficients are differentiated: downdip (updip)—n_1 and along the strike of the coal seam—n_2: $n_1 = D_1/D_{01}$ and $n_1 = D_2/D_{02}$. With the ground surface fully undermined, the values of the subsidence coefficients n_1 and n_2 are equal to or greater than 1. In the latter case, in performing all calculations, the value of these coefficients is taken to be equal to 1.

Angles of full deformation (ψ_1, downdip; ψ_2, updip; and ψ_3, along the strike of the coal seam)—angles that are internal relative to the mined-out cavity and formed by the plane of the coal seam and the line connecting the boundaries of the cavity with the boundaries of the flat bottom of the subsidence trough. In practice, angles of full displacement are used to delineate the zone of full undermining within the rock formation and on the ground surface.

In the absence of a flat bottom of the subsidence trough (partial undermining), the location of the point of maximum subsidence is defined by the *angle of maximum subsidence θ*, which is formed from the downdip direction by the horizontal line and the line connecting the center of the mine working with the point of maximum subsidence (see Fig. 9.4).

In calculating the subsidence values, the length of semitrough is taken into account, that is, the distance on the principal cross section across the strike (L_1, L_2) or along the strike (L_3) between the boundary of the subsidence trough and the point of intersection with the ground surface by the line drawn at the angle of maximum subsidence (in partial undermining) or at the angle of full deformation (in full undermining). The length of the flat bottom is not included in the calculations of the semitrough value.

Coal mining under surface water bodies (rivers, canals, water reservoirs, aquifers, etc.) and protection of the water bodies from damaging effects of undermining are conducted with adequate measures for allowable water ingress into the mine workings. Inside the zone of damaging effects of underground mining fissures can form

in the ground surface, which should be considered when delineating the zone of groundwater transmitting fractures underneath the water body being undermined or in the case a coal pillar being left underneath. The outer boundaries of the fracture zone inside the subsidence trough are delimited by *angles of break*, which are external angles relative to the mined-out cavity formed by horizontal lines and lines connecting the boundary of the mined-out area with the fractures nearest the boundary of the subsidence trough (β'' and γ'' across the strike on the cross section and δ'' along the strike on the cross section).

Timely implementation of measures designed to protect surface structures and ensuring continued ability to build facilities above the undermined area involves having a thorough understanding of the specifics of deformation over time. Rock deformation and subsidence inside the zone of influence of underground mining occur nonuniformly over time and are characterized by the overall extended duration of the process of deformation and a period of deformation causing adverse effects.

The overall extended duration of deformation refers the period of time during which the ground surface undergoes deformation.

The period of deformation causing adverse effects refers to the period of the active stage of deformation during which the subsidence rate exceeds 30 mm/month for inclined and steeply dipping coal seams and 50 mm/month for subhorizontal coal seams. Surface structures undergo the most significant deformation specifically during this period.

The period of harmful effects (t) is determined when mining operations are conducted above the safe depth of mining:

$t = 0.65T$, with H down to 300 m, and $t = 0.55T$, with $H = 500$ m.

The starting point of subsidence is set on the date when the ground surface settlement reaches 15 mm, while the end point is set on the date 6 months after which the total subsidence does not exceed 10% of the maximum, but not more than 30 mm.

The starting point of subsidence preceding the advancing coal face is set on the date when the distance in plan view from the coal face to this point is $\ell_1 = H_{cp}.ctg\delta_0$, with the start point of the period of harmful deformation is set on the date by which the distance in plan view from the coal face to the point reaches $\ell_2 = H_{cp}.ctg\delta$.

9.1.5 Factors influencing the nature and parameters of rock deformation and subsidence

Both natural and technological factors have an impact on deformation and determine deformation parameters, on the dimensions and location of deformation zones in the undermined formation and on the ground surface. Among the *natural factors* are the geologic structure of the formation; the physical and mechanical properties of rocks; the dip, thickness, and depth of the coal seam; the tectonic features of the coal deposit; the hydrogeologic setting; and the topographical features.

The impact of the major factors is as follows:

The *total thickness extracted* is one of the main factors determining the magnitude of rock deformation and subsidence. With increasing extracted thickness, the caving

zone within the undermined overburden also increases. The greater the thickness extracted at a time, the more intense the deformation creating adverse conditions for surface structures.

The depth of mining is one of the main natural factors determining the size of the subsidence trough, the nature and extent of ground surface deformation. As the depth of mining increases, subsidence decreases, with deformation occurring more gradually and over a more extended period of time. Thus, with the depth of mining changing from 100 to 1000 m, the duration of deformation increases from 5 to 44 months.

Physical and mechanical properties, thickness, and interbedding of different rock layers have a considerable impact on all the parameters and the nature of deformation. Based on the physical and mechanical properties, Prof. S. G. Avershin divides all rock types into four groups: (1) hard and dense, (2) plastic, (3) loose, and (4) groundwater-saturated sand.

Rocks of the first group are typical of coal deposits (sandstones) and usually collapse in sizable rock mass in a short period of time after having been undermined over a large area. Rocks belonging to the second group (e.g., clays and mudstones) are conducive to smooth bending of undermined layers, with the area of the subsidence trough increasing. Deformation of rocks belonging groups 3 and 4 occurs by plastic-like flow.

Interbedding and thickness of rock layers within the formation have an impact on the manifestation of deformation on the ground surface. Layers of hard rock can hang, in which case deformation does not reach the ground surface. Deformation of loose rock on the ground surface will generally produce sinkholes, with rocks belonging to group 4 serving to shallow out boundary angles and deformation angles.

The dip of the coal seam and the overburden is one of the major factors determining the parameters and nature of subsurface rock deformation and subsidence. The role of the dip of the mined coal seam is by far not limited to its effect on deformation angles. The nature of subsurface rock deformation and subsidence varies depending on the dip of the strata. In steeply dipping coal seams, horizontal displacement will occur exceeding the vertical displacement, while the ground surface undergoes deformation with resultant discontinuities (surface depressions or sinkholes, benches, and cracks in the ground surface); in inclined and steeply dipping coal seams, deformation curves are asymmetrical relative to the boundaries and the center of the mined cavity and skewed toward the downdip direction. In mining subhorizontal coal seams, the subsidence trough is symmetrical relative to the boundaries of the mined cavity, with its center located above the center of the cavity.

Tectonic faults are surfaces of weakening along which displacement of some rock layers occurs causing changes in the values of deformation angles and boundary angles. Cracks and benches may form on the ground surface in the vicinity of disjunctive dislocations.

The presence and thickness of alluvial deposits—A considerable (over 5 m) thickness of alluvium has a favorable effect on deformation, smoothing out nonuniform displacements and minimizing the likelihood of fractures initiating. In the alluvial deposits, boundary angles and deformation angles are smoothed out.

Process-induced (technogenic) factors impacting the nature of deformation are produced in the course of mining operations and may vary. The type of mining method employed plays a particularly significant role. In some cases, the mining method used

ensures a gradual rate of subsurface rock deformation and subsidence, yet in other cases, subsidence will result in discontinuities in the ground surface (surface depressions, benches, etc.). Lastly, there are cases where deformation does not reach the ground surface.

The measures to control the effects of lithostatic pressure are a major technogenic factor determining the magnitude and nature of deformation. When applying measures to control the effects of lithostatic pressure by means of mine roof collapse, deformation reaches its maximum with respect to all linear and angular parameters. *The dimensions of the mined cavity and the presence of coal pillars inside* have a major effect on the nature of deformation (shape and size of the subsidence trough, magnitude of deformation, and other parameters) in the setting of partial undermining. In conditions of full undermining, changing dimensions of the mined cavity have virtually no impact on the nature and parameters of deformation. *However, in conditions when coal pillars are left in the mined-out area*, the patterns of distribution of deformation within the undermined overburden are altered. At a certain ratio of the coal pillar size to mined-out cavity dimensions, deformation may not reach the ground surface. Leaving smaller-size coal pillars complicates considerably the nature of deformation of immediate overburden and results in the concentration of stresses above coal pillars and the presence of zones of localized deformations.

9.1.6   Methods of studying rock deformation

Investigating rock deformation and subsidence generally involves the use of methods that are subdivided into three categories: *field monitoring and measurements, physical and mathematical modeling*, and *analytic studies*.

In situ field monitoring is key, as it is otherwise impossible to identify major factors of deformation and properly define the criteria for analytic studies and modeling. In situ field monitoring entails visual observation and instrumented monitoring.

Visual observation permits one to identify, over a relatively short period of time and overextensive areas, the scope of manifestations of rock deformation within mined cavities and on the ground surface, gaining a preliminary understanding necessary to select an appropriate methodology for deformation monitoring and modeling. Combining visual observation with instrumental measurements assists in selecting the sites for measurements and define areas of application of the results. In situ (field) observations and measurements define the parameters of deformation and are used to solve specific problems.

Physical and mathematical modeling is widely used in conducting investigations of rock deformation.

For physical modeling of deformation of rock strata composed of elastic, plastic, and unconsolidated rocks, the method of *nominally equivalent materials* proposed by Prof. G. N. Kuznetsov is generally applied in the CIS countries. Deformation experiments are conducted using 2-D and 3-D deformation apparatus and nominally equivalent materials, that is, artificial materials whose mechanical characteristics in the geometric scale used for the model satisfy the requirements for rock types modeled: $m_\ell = \ell_M / \ell_N$

$$\sigma_M = \frac{\ell_M}{\ell_H} \cdot \frac{\gamma_M}{\gamma_H} \cdot \sigma_H, \tag{9.4}$$

where σ_M and σ_H, ℓ_M and ℓ_H, γ_M and γ_H are stresses, dimensions of the cavity, and specific weight of the material, respectively, both the model and in situ.

The method of nominally equivalent materials with great precision permits an understanding of the mechanism of deformation within the rock formation and to determine characteristics of deformation that is unobtainable through either in situ or analytic methods.

However, modeling cannot reproduce all the parameters of the formation, such as microfracturing and small-block fracturing; rather, deformation modeling allows only a certain degree of schematic representation of in situ conditions and extending (considering the scale of the model) the quantitative model results to actual in situ conditions is not always warranted.

Mathematical modeling is used to predict the stress-strain state of the undermined strata and mined cavities located inside the zone of influence of underground mining operations, process wells, and other wells. The problem is solved by using numerical methods as follows: mechanical and mathematical models, algebraization (discretization) of the problem, algorithm development, and programming- and computer-based implementation.

For mechanical and mathematical models, the physical and mechanical properties of rocks are tested in the study area. Based on the results of these tests, the type and parameters of the equation of the condition of rocks is fitted to specific conditions.

Investigating the issues of rock deformation and subsidence using the analytic method requires a very substantial mathematical treatment and schematic representation of deformation. The impact of fracturing, stratification, nonuniform mechanical properties of rocks in different directions is not factored in, which greatly complicates the development of engineering calculation methods and their application in specific mining and geologic conditions. The use of the analytic method studies with generalization of data on specific features of structure and strength properties of the material under study makes it possible to predict the general nature and preliminary parameters of deformation and subsidence, while contributing to the introduction of new theoretical notions.

It should be noted that none of these research methods is universal to the study of rock deformation and subsidence issues. Only through comprehensive studies (in situ, laboratory, and analytic) can these problems successfully be solved.

9.2   Rock deformation and subsidence in conventional underground coal mining

9.2.1   Effects of rock deformation on the production process during underground coal gasification operations

Underground coal gasification is a complex physicochemical process involving in situ conversion of coal into combustible gas with the help of free or bound oxygen. The principal stages of the UCG process are as follows:

- Drill vertical or directional wells to the coal seam to supply injection agent (process air) and produce syngas.
- Run casing and create an in-seam link between the wells.

- Ignite coal and operate the coal gasification process by injecting process air into some wells and produce syngas from other wells.

The underground gasifier is the main onsite system at the UCG plant comprising a host of process equipment and monitoring tools that make it possible to gasify a certain working section of the coal seam. The gasifier consists of a surface plant and an underground gasification cavity. The aboveground plant includes pipework installations to supply injection agent (process air, water vapor/oxygen mixture, etc.) and to produce syngas. The wellhead assembly is fitted with monitoring tools for operation, supervision, and control of the UCG production process. The underground part of the gasifier is made up of drilled wells with an in-seam connection via channels among themselves and with the fire source. A schematic diagram of the UCG operation in a subhorizontal coal seam using vertical wells is shown in Fig. 9.5. In order to develop the initial gasification channels and link the wells to them, AquaSplitt of the coal seam is most frequently used, as well as combustion linking and horizontal drilling of the channels in the coal seam.

The effects of rock deformation during the specific stages of UCG include the following: as wells are drilled into the coal seam and the initial gasification channels are created, drilling is conducted in an intact formation. With the enlargement of gasification channels, the immediate roof rocks cave in, resulting in deformation of the overburden rocks. Subsequently, as part of ongoing UCG operations, drilling of vertical wells preceding the advancing fire face (rows II and III) is performed in undermined rock.

Research in the patterns of gas production over time, the location of combustion zones, recovery, and convection during UCG showed that, as a rule, narrow gasification channels appear in the vicinity of the coal seam floor extending into the zone immediately in front of the advancing fire face over a distance not exceeding one-third of the coal seam thickness. Most of the coal reserves are located above the gasification channel. As it is undermined, the first signs of deformation begin to appear in the form of bending of rock layers. Upon reaching the maximum stable dimensions of the
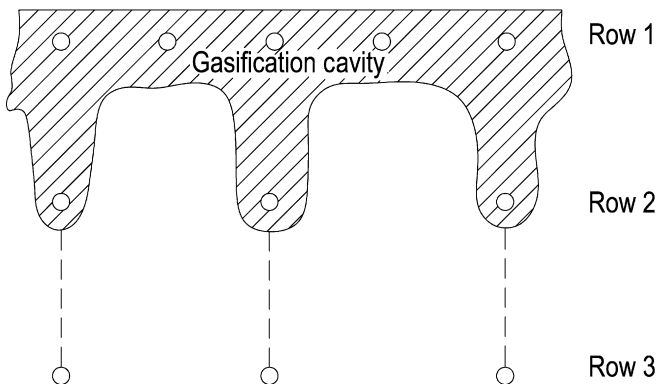
Fig. 9.5 Schematic diagram of UCG operations being carried out in a subhorizontal coal seam with the use of vertical wells.
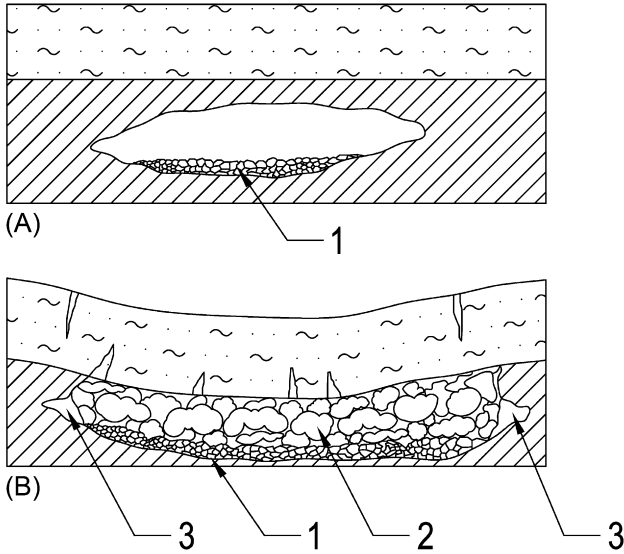
Fig. 9.6 The gasification channel depicted in cross section: (A) Prior to coal caving in and (B) after the coal and rock collapse: (1) ash and slag, (2) collapsed coal, and (3) voids.

exposed face of coal, coal and rock within the immediate roof begin to cave into the cavity (Fig. 9.6). Coal and rock collapsing results in reduction of space in the channel and changes in the gas flow resistance. Subsequent open casting of spent gasifiers revealed that the cavity boundary contours move toward the coal seam roof and extend areally. The thickness of the coal seam that has actually been gasified has a maximum value at the center decreasing toward the boundary edge.

Random caving of the immediate roof rock leads to a reduction of the reactive surface area of coal, losses of the injection agent (process air) and gas, heat loss within the rock rubble, giving rise to peripheral process air and gas flowstreams inside the underground gasifier, adversely affecting process efficiency. Groundwater transmitting fractures can cause a rapid influx of water from the overlying aquifers into the gasification channel and disrupt the process of gasification.

Gradual gasification of a working section of the coal seam and gradual settlement of the coal seam roof without collapse allows for a uniform filling of the gasification cavity by the rock layers undergoing deformation. This contributes to the compaction of loose ash residue inside the gasifier and the movement of flow streams of the injection agent (air) and gas along the reactive surfaces and to the consistency of gas composition and facilitates a more complete gasification of the remaining coal reserves. Thus, the mode of deformation of undermined immediate roof rock has a significant impact on the gas production as early as the earliest stages of gasification.

When the gasification cavity reaches a certain size, following the immediate roof rock collapse, deformation begins to affect the overlying rock layers that are subjected to bending. This results in bedding-perpendicular rock displacement that may or may

not cause discontinuities. The bending of the rock strata causes tensile (compressive) strains that are a function of both bending curvature radius and thickness of each discrete rock layer. When strata with distinctly different strength characteristics undergo bending, stratification voids may develop within the formation that may allow accumulation of groundwater or gas. The latter phenomenon may have a negative impact on the gasification processes and the environment.

Rock deformation during gasification of a 2–4 m thick coal seam at a depth of 40–50 m had, in rare cases, caused well casing breaches. The greater the coal seam depth and thickness, the shorter the service life of the vertical process wells, with the stability of the gasification processes, gas composition, and completeness of extraction of the coal reserves being determined by the specific features of deformation of undermined rock layers. Studies carried out at the Angren UCG plant on a thick coal seam at a depth of 100–200 m revealed that a *significant* number of vertical wells experienced premature rock deformation related failure.

Prediction of possible rock-deformation-related casing failure not only is part and parcel of the successful operation of a UCG processes producing consistently on-spec gas but also is crucial in preventing possible contamination caused by gasification by-products of the overlying aquifers through possible casing breaches of production wells.

During UCG activities conducted in thick, steeply dipping seams (Yuzhno-Abinskaya UCG Plant), one important characteristic of rock deformation was that it produced ground surface depressions as the seam was gasified in the updip direction and the fire face neared the ground surface. Surface depressions will generally disrupt the UCG process due to increasing injection agent (air) and gas leakage blowing agent and gas, partial loss of the underground gasifier integrity. Rock deformation encountered during UCG activities in a coal sequence determines the order in which the seams will be mined.

Thus, process parameters and specifics of the UCG process determine the shape of the gasification cavity and the nature of deformation of the overlying rocks, which, in turn, has a direct impact on the stability of the gasification process and its technoeconomics.

9.2.2 Goals, objectives and methods of studying rock deformation and subsidence

Trends and parameters of rock deformation and subsidence during UCG should be established in order to determine the extent of the impact on the mining technology and to improve its efficiency, as well as to protect surface structures, the ground surface and to minimize adverse environmental impacts.

During UCG activities in subhorizontal and steeply dipping coal seams, the following major objectives were recognized and accomplished:

- Establish basic parameters and repeating patterns of rock deformation and subsidence and compare the results with available shaft mining data.

- Identify the mechanism of subsidence of rock mass during different stages of a UCG mining operation.
- Develop methods to control the mode and extent of coal seam gasification.
- Establish the level of impact of subsurface rock deformation and subsidence on process well casing integrity and surface structures.
- Identify the mechanism of surface depression formation and determine the requisite size of coal pillars to protect from surface depressions (during UCG in steeply dipping coal seams).

Objectives were accomplished using a comprehensive method that included in situ observations of subsurface rock deformation and subsidence, laboratory-based simulation of deformation in an undermined rock mass, and analytic studies.

In situ investigations included systematic monitoring of the displacement of surface markers and borehole extensometers deep frames, visual inspections of failed well casings, open casting of and drilling into spent underground gasifiers, monitoring for ground surface depressions above active UCG mines, and data collection on sinkhole-type subsidence above shaft mines.

In contrast to the monitoring stations above coal mine workings, which are generally installed on the ground surface as multiple monument profiles, surface makers above active UCG zones were installed at the vertices of a square (rectangular) grid over the entire area of the anticipated subsidence. The areally extensive coverage of a monitoring station was shaped by the need to control the coal seam gasification in area and thickness, since during UCG the gasification cavity boundary contours are irregular in shape both in plan view and in side view.

Based on the data collected during systematic monitoring of the displacement of surface markers, subsidence diagrams, horizontal displacement diagrams, and deformation diagrams were plotted, and plan view outlines of subsidence, subsidence rates, and the curvature of the subsidence trough were produced. The diagrams were used to generate gasification boundary contour lines and to determine the percentage extraction of the coal seam by UCG in area and thickness.

Monitoring of the rock deformation depth profile was conducted with the aid of extensometers, while bulking factors were calculated for the undermined rock mass.

Diagnostics of failed well casings were performed by running in a lead impression stamp. Borehole inspections were performed determine the depth of the casing failure point, type of casing deformation, and magnitude and direction of the casing displacement.

Abandoned gasification cavities (gasification sites) were accessed and surveyed by core drilling. Any changes in the rate or total loss of drilling fluid circulation indicated the presence of voids (drill string dropping abruptly) and discontinuities in the formation made it possible to determine the extent and nature of deformation within the rock mass and to delineate zones with distinctive features.

Subsequent open casting of cooled underground gasifiers is an extremely labor-intensive and costly but the most reliable method to determine the nature and extent of gasification of the coal seam in area and thickness, as well as the shape of the gasification cavity, zones of heated rock and coal, the degree of deformation of the undermined rock mass delineating zones with distinctive features, shape and area of the cross sections of the gasification channels, and distribution patterns of the residual

ash and slag inside the underground gasifier, along with other parameters. This method permits the direct comparison of the mutually interdependent relationship of operational process modes of gasification and geomechanical processes occurring within the rock mass. Open casting of the spent gasifiers was carried out during UCG of steeply dipping coal seams in the Donetsk and Kuznetsk coal basins.

A laboratory simulation of UCG-induced rock deformation was conducted using the equivalent materials method using 2-D and 3-D deformation apparatus. The 2-D deformation apparatus was employed to investigate the influence of the coal pillars left in the underground gasifier on the nature of subsurface rock deformation and subsidence and the role of the coal seam dip on the initial collapse of the unsupported roof span. The 3-D deformation apparatus was used to study the impact the coal seam thickness, the dimensions of the gasification cavity, the lithology of the formation, and the nature of rock deformation during mining of steeply dipping seams have on the size of coal pillars at which ground surface depressions will occur.

The following principal factors determining the geomechanical processes taking place in the undermined formation were used in the models: stratified rock layers of the formation, size of the gasification cavity, the direction of mining, and other parameters. The selection of equivalent materials was effected based on strength characteristics. Modeling using equivalent materials makes it possible to determine the impact of specific geologic and mining factors on the deformation of the stratified formation.

Analytic methods were used in assessing the strength and resilience of process well casings.

9.2.3 Specific features of subsurface rock deformation and subsidence during underground coal gasification of a subhorizontal coal seam and their practical applications

9.2.3.1 General causes and repeating patterns of subsidence during shaft mining and underground coal gasification of coal seams defining the solid-coal boundary contours of the gasification cavity and the amount of coal gasified

We start this section by considering general causes and repeating patterns of subsidence above mine workings and underground gasifiers. Detailed data on the percentage of coal gasified from a coal seam in area and thickness, on the location of gasification channels, coal pillars and the solid-coal boundaries of the gasification cavity are an important prerequisite for effective UCG process control. The data are also indispensable during the final stage of UCG to estimate coal loss and resource recovery percentage.

The method of delineating the boundary contours of the depleted gasification cavity and gasification rate was put forward by Prof. S. G. Avershin and later refined by Prof. I. A. Turchaninov for underground coal gasification in coal seams 2.5–3.5 m in thickness at depths up to 60 m in the Podmoskovnaya lignite basin. This method is based on the general causes and repeating patterns of subsidence above mine

workings. Additional investigations of subsurface rock deformation and subsidence were needed to determine whether this method can be applied at the Angren commercial UCG plant where underground coal gasification operations were underway in a thick (20 m) lignite coal seam. Research and development (R&D) efforts were continuing to explore new methodologies that would permit control of the gasification rate in a more complex setting.

Investigations of rock deformation in the Angren lignite coal deposit focused on revealing causes and repeating patterns as well as any differences in deformation behavior of the ground surface above conventional mine workings versus UCG sites (underground gasifiers), which were located in the vicinity of the coal mine (Prof. G.V. Orlov). The research objectives included defining the main parameters of deformation (angles of draw, maximum subsidence and horizontal displacement, deformation, etc.), identifying the location of peak points of the subsidence curve relative to the cavity boundaries, and examining the possibility of using the causes and repeating patterns identified for subsidence by UCG mine surveyors to provide surveying control by calculating production from the UCG operation in a thick subhorizontal coal seam.

Each monitoring site had to meet several requirements: First, longwall workings and underground gasifiers must be located in similar geologic conditions and adjoin the coal pillar rather than a mined-out cavity, and second, mining of the first and second layer should be ongoing in the longwall working. Based on the above requirements, monitoring was started above two longwall working of Mine 9 of Sredazugol Industrial Group and five underground gasifiers of the Angren UCG plant.

The Jurassic deposits were composed of a coal-bearing and a kaolin sequence (Fig. 9.7). The average thickness of the coal-bearing sequence, which was made up of alternating layers of clay and sandstones, was 10 m inside the boundaries of UCG sites and 27 m in the vicinity of the mine workings. The kaolin sequence had the same thickness almost uniformly (35–37 m) and was composed of kaolin clay, clay with high sand content and sandstone. Overlying the kaolin sequence inside the boundaries of UCG sites were Cretaceous and Suzak deposits consisting of sands, sandstones, and siltstones, with a total aggregate thickness of 38 m. No such overburden existed above the longwall workings. The Alai deposits consisted of limestones of uniform thickness (about 18 m). The marls of the Turkestan units are absent in the geologic cross sections above the longwall workings; marl layers overlying UCG sites were 15 m in thickness. Quaternary deposits in the research sites consist of 10 and 23 m thick loams.

Laboratory tests showed that the majority of clay and sand samples making up the coal seam had a uniaxial compressive strength of 1.12–1.32 MPa or less. The strong rock types (sandstone and limestone) also had relatively low UCS values of 7.4–14.9 MPa. Limestone is highly fractured, which greatly reduces its strength in the formation. The depth to the coal seam roof in UCG sites was 120–140 m, while it was 105–110 m at the mine. Therefore, despite some differences in the thickness of the overburdens, monitoring sites shared largely comparable geologic and mining conditions.

The thickness of the coal seam at the mine was 18 m, with a dip of 8 degrees. During the monitoring period, the coal seam was worked in two 2.6–3.0 m thick layers.
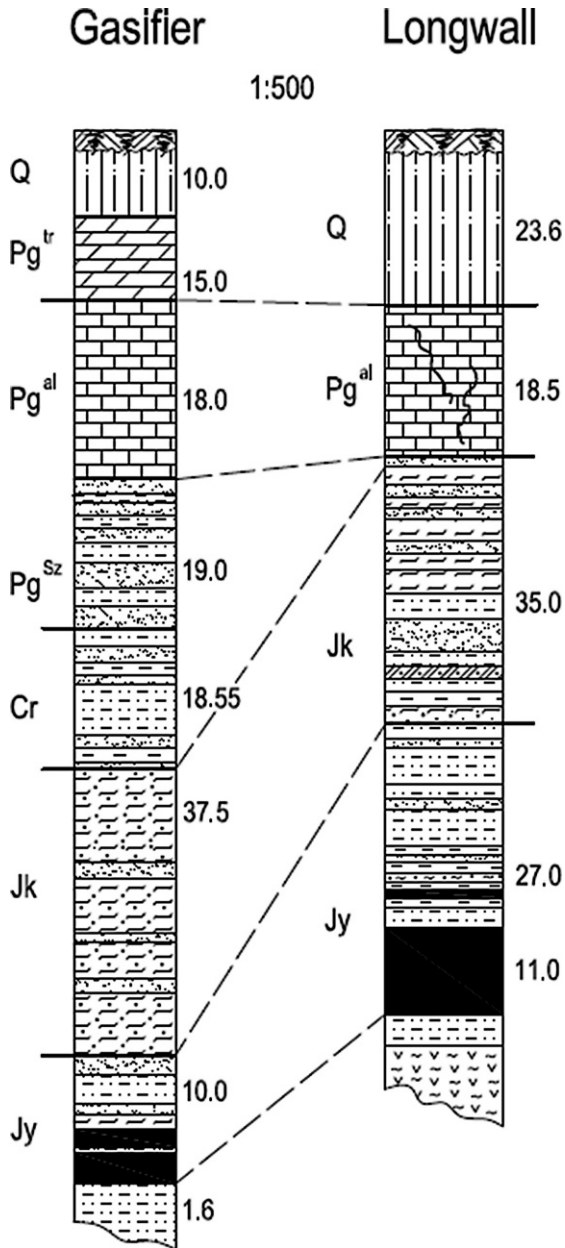
Fig. 9.7 The geologic structure of the formation at the monitoring sites.

The mining method used long pillars along the strike in descending order. The length of the longwall working was 110 m. The coal face advance rate per cycle was 2.4 m. The roof control method was complete roof collapse. The thickness of coal seam in UCG sites was 3–6 m, with a dip of 5 degrees. The coal seam was mined using the UCG method with panels (gasifiers) 100–200 m in width. Wells of the ignition row were drilled first, with a fire face initiated between them. Next, the fire face was advanced on one or both sides of the ignition row. Gasification of the coal seam occurred gradually in area and thickness.

Active surface markers were installed along the profiles with an interval of 10 m along the horizontal distances. For high-frequency monitoring of every 1–3 h and temporal correlation with the roof settlement, a specialized monitoring station was installed consisting of two monument profiles with a monument interval of 4–5 m. The surface markers above UCG gasifiers were installed on a rectangular 10×20 m $\times 15 \times 15$ m grid.

The determination of gasification cavity boundaries and gasification rate was based on the rock deformation values recorded at the coal mine. In this regard, the physical, geologic, or mining-related differences should be considered in comparing the conventional coal-mining method with UCG and the extent to which these differences can affect the recorded values of subsidence.

In the case of longwall mining, the width of the longwall face is in the range of 100 m, with a straight and steplike long mining face that advances parallel to itself. During UCG, the width of the gasification front (fire face) is generally no less than that of the gasification cavity. The fire face may not advance uniformly across the entire gasification front inside the gasifier forming a nonlinear face. However, the irregularly shaped fire face should be relatively smooth, as lithostatic stress concentration on any sharp protrusions from the coal pillars will result in their destruction and gasification.

Uneven coal seam gasification in the vertical z-direction. As the coal seam is mined in successive layers, the thickness removed varies within a relatively small range. These variations in thickness gasified may be significant during UCG and are a function of changes in the thickness of the coal seam, its ash content, the presence of any rock partings, and nonuniform distribution of the gasification zones.

The structure of the gasification cavity. In a coal-mining excavation, the part of the working adjacent to the coal face remains supported at all times with pitprops. Mining relies on controlled collapse of the seam roof outside the timber-supported zone. The timber props that were not retrieved during the roof collapse remain in the cave-in zone (around 10% of the mined seam thickness).

During underground coal gasification, ash and slag remain in the cavity, as well as ungasified units of coal. Research showed that the volume of slag is below 10%–20% (13% on average), while the amount of unconsolidated ash varies from 2% to 12% (5% on average) of the total volume of coal gasified.

The physical state of the coal seam in conventional shaft mining of coal, the near-face part of the coal seam becomes fractured and, under lithostatic pressure, partially squeezed into the working. Inspection of the condition of mine props in the initial workings driven into the longwall working revealed that the lithostatic pressure exerts the greatest force on the coal seam some 10 m preceding the advancing longwall face.

During underground coal gasification, in addition to lithostatic pressure, the shallow preheating devolatilization (drying and pyrolysis) zone further promotes fracture development inside the near-face zone.

Physical and mechanical properties of the immediate roof rock. During underground coal gasification, the rocks of the immediate roof are subjected to drying and pyrolysis that alters their structure and chemical composition. Investigations showed that the depth of heat penetration of rocks due to thermal conductivity does not exceed 1–2 m.

In considering the impact of these factors on subsurface rock deformation, it should be noted that both in underground mining and during underground coal gasification, the major factor in rock deformation is lithostatic pressure. Consequently, the causes and repeating patterns of rock deformation as a physical process involved in underground coal gasification cannot differ significantly. As verified by monitoring, the location of the vertical and horizontal displacements, deformation, inflection points on the subsidence curves above underground gasifiers, and mine workings bear the same characteristics.

When the mine-working width reached about 10 m, evidence of subsidence became observable on the ground surface. Monitoring series above longwall workings confirmed that the upward deformation propagation from the underground longwall workings to the ground surface occurred in as few as 4–5 h after the initial undermining and less than 1 h after the secondary undermining of the overburden. Therefore, deformation propagation velocity within the formation makes it possible for subsidence values to be used for real-time operational control of coal seam gasification.

During underground coal gasification in a thick coal seam, gasification is vertically nonuniform inside the gasifier. Depending on the mode of UCG operation, there are times when zones of intense gasification through the thickness of the coal seam propagate across the entire gasifier area, so the ground surface undergoes repeated subsidence. This explains the need to define parameters and reveal repeating patterns of subsurface rock deformation and subsidence during the initial and subsequent undermining (mining of the second layer of the coal seam) in a conventional underground mining operation.

Monitoring above longwall workings indicated that the most stable position relative to the contours of the gasification cavity is located in the points of inflection on the subsidence curves, which at the Angren lignite deposit were located virtually over the border between the gasification cavity (± 5 m) and the solid-coal block yet to be gasified. The location of the inflection point of the subsidence curve should be consistent (as confirmed by monitoring), since the subsidence curves proved to be smoother than those in longwall mining.

Of note, the fire face is not a clearly delineated border between the gasification cavity and solid coal ahead of the face. It has to do with a certain thickness of the thermally preconditioned coal seam where the reactions of gas production occur. The location of the point of inflection is determined relative to a certain boundary from which the bending of the immediate roof strata occurs.

In underground mining, a timbered working space is maintained between the coal face and goaf. The immediate roof over the mine working bends downward, with the

magnitude of bending depending on a number of factors. In this case, as with underground coal gasification, deformation propagates from the bend line of the immediate roof rock. The distance from the boundary to the solid block of coal yet to be gasified in longwall mining and UCG varies over a small range. This is confirmed by the good convergence of the values of the displacement parameters (angles of draw, boundary angles, etc.) established for both mining methods (Table 9.1)

9.2.3.2 Delineating the boundary contours of the gasification cavity and the extent of gasification of the coal seam

Considerable changes occur in the physical and mechanical properties of the roof rock in the underground gasifier under high temperature stress but only inside the caving zone; hence, the causes and repeating patterns of the undermined rock strata and ground surface are the same in longwall mining and UCG. Thus, as suggested by investigations conducted at the Podmoskovnaya lignite basin showed (I. A. Turchaninov) and the Angren lignite deposit in Central Asia (G. V. Orlov), the distinctive points of the subsidence curves, points of inflection maintain a stable position relative to the boundaries of the gasification cavity given the cavity dimensions of $D \geq 0.7D_o$ (D, *actual size of the gasification cavity, and* D_o, *minimum size of working that causes full undermining of the ground surface*). As the boundaries of the gasification cavity move, so do the points of inflection. Based on monitoring data collected above mine workings at the Angren coal deposit, it was determined that the point of inflection is located above the border between the boundary of the longwall mine and the coal pillar; while preceding the advancing coal face, it is displaced from the boundary by 2–4 m toward the mined-out cavity.

Similar results were obtained during verification core drilling into underground gasifiers post shutdown. The error in determining the location of the point of inflection relative to the cavity boundaries was below ± 5 m.

The slope of the subsidence curves is the steepest at points of inflection where the change of curvature from convex to concave takes place. The slope of the subsidence curve is expressed by the first derivative of the deformation function $i = \partial\eta/\partial x = \max$.

The curvature of the subsidence curve is calculated from the formula

$$K = \frac{\partial^2\eta/\partial x^2}{\left[1 + (\partial\eta/\partial x)^2\right]^{2|3}}. \tag{9.5}$$

For subsidence trough curves, when the value of $\partial\eta/\partial x$ is low, $(\partial\eta/\partial x)^2$ can be omitted from the calculation; to calculate the curvature, the second derivative of the subsidence function may be used. At points of inflection, the curvature equals zero: $K = \partial^2\eta/\partial x^2 = 0$.

The points of inflection are located not only at the edges of the subsidence trough but also in the central part, which indicates nonuniform gasification of the coal seam along the vertical thickness. Connecting the inflection points in the center of the

Table 9.1 Rock deformation parameters, Mine No. 9, and the Angren UCG plant

Subsidence trends and parameters	In shaft mining		During underground gasification coal of the coal seam $m = 3.0–6.0$
	Initial undermining (mining of the first layer) $m = 2.6$	Repeat undermining (gasification of two layers) $m = 2.9–3.0$	
Boundary angles, degrees			
Along the strike of the coal seam δ_0	57	57	57–58
From the downdip direction β_0	57	57	57–58
From the updip direction γ_0	–	–	62–64
Deformation angles, degrees			
Along the strike of the coal seam δ	63	59	59–65
From the downdip direction β	66	61	64–72
From the updip direction γ	–	–	65–74
Angles of break, degrees			
At the boundary of the cavity	75	–	78
Along the strike δ''	–	–	78
At the bottom boundary of the cavity β''	26	67	6–31
Maximum subsidence rate, mm/day			
The maximum subsidence value η_M, mm	1800	2950–3000	1700
Maximum value of horizontal deformation ξ_M, mm	485	1450	400
Ratio $\alpha = \xi_0/\eta_0$	0.27	0.48	0.24
Ratio $q_0 = \eta_0/m$	0.68	1.0	0.3–0.85
Time rock deformation propagates from the working to the ground surface, hours	4	1	–

subsidence trough and at the edge of the subsidence trough indicates the location of zones with varying degrees of gasification of the coal seam.

Apart from delineating boundary contours of the gasification cavity during UCG, the extent and characteristics of coal extraction by UCG method should be established, as well as the direction of gasification channels. Meeting these challenges allows operational management and control measures to be put in place to ensure maximum coal recovery and to implement process control in the gasifier. The results from the combined analysis of data obtained through monitoring of subsidence above underground gasifiers and process data and the amount of coal gasified suggest that ground surface settlement is determined by the extent and nature of coal seam gasification in area and thickness. Different rates and duration of gasification operations lead to different numerical rates of subsidence and deformation values.

A qualitative visualization of the coal seam thickness gasified in different parts of the gasifier can be obtained by producing contour plans of the subsidence rate. Centers of maximum rates of subsidence for each monitoring period permit an understanding of the locations of intense gasification of the coal seam, while the direction along which the contour lines are elongated and the contour line interval indicate the location of the gasification channels and the extent of the coal seam gasification in area and thickness over the period between monitoring events. Using superimposed contour maps that show the rates of subsidence throughout the entire monitoring period and having delineated the areas with constant intense ground surface settlement, the tentative contours of the boundaries of the gasification cavity are obtained where gasification along the vertical height of the seam has the highest value.

To delineate the boundary contours and extent of gasification of the coal seam, contour plans are produced showing the curvature of the ground surface as of each date of monitoring. The outer boundary contours of the gasification cavity are delineated using the tendency of the inflection points to occupy a permanent position relative to the boundaries of gasification cavity. When delineating the coal pillars inside the gasification cavity, only the qualitative picture of coal gasification is obtained, since positive curvature of the subsidence trough will be present both with coal pillars and with partial gasification along the vertical height of the seam. The distribution, interval, and configuration of the contour lines permit judgment to be made as to the extent and nature of the coal gasification over the vertical thickness of the seam and the direction of the gasification channels.

Fig. 9.8 shows an example of delineating the boundary contours of the gasification cavity and the degree of gasification of the coal seam along the isolines of the subsidence trough curvature as recorded at one of the gasifiers of the Angren UCG plant. The distribution of contour lines indicates a nonuniform gasification of the coal seam along the vertical thickness. In the central part of the gasifier (borehole 39 - gas/cav 6), the most complete gasification was observed along the vertical height of the coal seam through a comparatively narrow gasification channel. Areas of the ground surface with a positive curvature of the trough located above the gasification cavity indicate the presence of coal pillars underneath, which was confirmed by verification drilling.

Determining the extent of coal seam gasification based on contour lines of the subsidence curvature permits control of UCG mining of the coal seam in area and
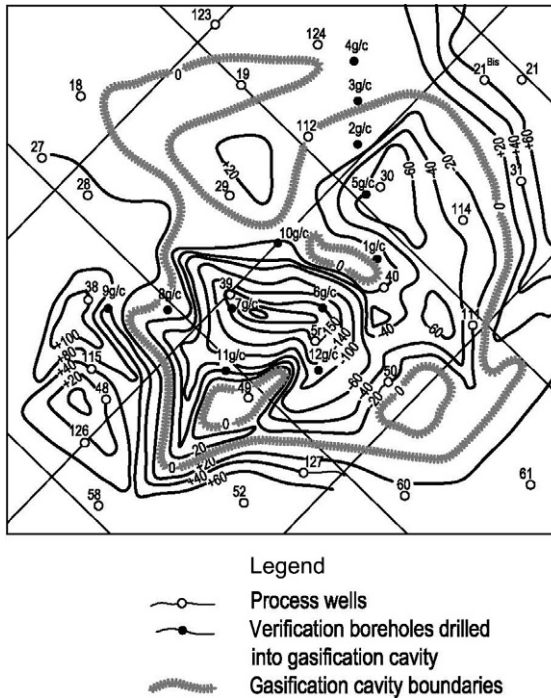
Fig. 9.8 Delineating the boundary contours of the gasification cavity using the isoline contours of the subsidence trough: o ⌐, 61—process wells; ● ⌐, 11 gas/cav—background wells completed into gasification cavity; ⌐, the boundaries of the gasification cavity.

thickness, of the location of coal pillars inside the gasification cavity, and direction of the gasification channels during UCG activities. This information is needed to identify reasonable modes of operation, to ensure maximal coal gasification, and to improve underground gasifier design.

Analysis of subsidence monitoring above longwall workings indicated that the magnitude of the subsidence trough is directly proportional to the amount of coal extracted. The coefficient k_v describing the ratio has different values for the active part of the deformation processes versus the attenuation stage during initial and secondary undermining of rock formation. In a conventional underground mining operation, the initial undermining value was 0.65. This value describes the ratio of the volume of the subsidence trough to the volume of the mined-out cavity during advancement of the longwall coal face at a rate of 1.5–1.8 m/day. Once deformation attenuated, the average value of the factor was 0.73. During secondary undermining and the same rate of fire face advancement, the average value of coefficient $k_v = 0.83$. Variations in the value of the coefficient k_v during deformation and after attenuation of deformation during secondary undermining, are negligible (0.01–0.02). Coefficient values k_v stabilized once the mined-out cavity reached the width of

$D \geq (0.7 - 0.8)D_0$ (D_0—span of complete undermining of the ground surface/critical unsupported span).

In underground coal gasification, the amount of the subsidence trough was determined from mine surveying data, while the amount of coal gasified was estimated based on the volume and carbon content of syngas. Based on core-drill data, the average volume of ash residue is 13% of the coal gasified. V_3 Ash residue left during UCG and remnants of the mine props inside the longwall working were taken into account when computing the volume of the gasification cavity.

It should be noted that the average value for areas of gasification where coal gasification was conducted with a broad gasification front was close to that of a longwall working during initial undermining of the ground surface $k_v^2 = 0.64$. At UCG panels with a few select dominant gasification channels, the value did not exceed 0.45. Discrepancies in the coefficient values k_v^2 are due to variations in the configuration of the gasification cavity. The stability of the coal seam roof depends on the shape and the extent of the exposed face. After the maximum critical size of the void is reached, the immediate roof rock caves in, and deformation propagates up through the overburden.

In shaft mining of coal, a contiguous mined-out void is formed, which is filled with caved-in rock, causing a subsidence trough or a change in the subsidence trough. In underground coal gasification, apart from the main area of complete gasification, narrow channels form inside which one of the dimensions is less than the maximum stable unsupported span. Coal gasification in such zones is not manifested on the ground surface or shows only a marginal manifestation. The amount of coal gasified inside narrow gasification channels can be computed solely by using a process-based analytic method, that is, by performing gas chemistry and chemical reaction calculations; surveying method in this case yields an erroneously low result (i.e., negatively biased).

Thus, from the volume of the subsidence trough V_M, the volume of coal gasified V_y (computed from process data), the volume of ash residue and slag V_3 (for Angren coal and computed from the coal gasified for some coal deposits of the Moscow basin $V_3 = 13\%$) and from the parameter range for longwall mining k_v, the coal gasification rate in underground gasifiers can be calculated for various UCG methods.

The mine surveyor calculates coal losses within the entire underground gasifier post gasification and after rock deformation stops. To calculate the amount of coal gasified, the ratio of the volume of the subsidence trough V_M to the amount of coal extracted V_y, which is estimated both for above the mine workings and the pilot UCG plant.

$$K_v = \frac{V_M}{V_y}, \quad \text{for the longwall working;}$$
$$K_v = \frac{V_M}{V_y - V_3}, \quad \text{for the underground gasifier,}$$

(9.6)

where K_v is the rock volume expansion during undermining and V_3 is the volume of compacted ash residue.

The volume of compacted ash residue is calculated from the expression

$$V_3 = K_3 \cdot A_6^c \cdot V_y, \tag{9.7}$$

where K_3- is a coefficient reflecting the increase of relative volume of the ash residue compared with the weight content of ash in coal (for the Podmoskovnaya coal basin); $K_3 = 1.4$; A_6^c is the average ash content, wt% (dry basis)

Considering Eqs. (9.6) and (9.7), the formula used to calculate the volume of coal gasified takes the form

$$V_y = \frac{V_M}{K_v \left(1 - K_3 \cdot A_6^c / 100\right)}. \tag{9.8}$$

The relative error in determining the volume of coal gasified in lignite deposits was 10%–15%.

The possible application of the methodology used in delineation of the gasification cavity boundaries and the nature and extent of coal seam mining is generally confined to subhorizontal coal seams with overburden strata that ensure the deformation is propagated to the ground surface without significant hanging of undermined rock strata.

To determine the value of displacement of points on the ground surface above the underground gasifier, a specialized areal monitoring network is installed. The error in determining the solid-coal boundaries of the gasification cavity is +2–8 m, with the overburden depth being 30–200 m and the distance between the monitoring station markers 5–15 m.

For operational monitoring and control of the location of gasification channels, when the channel dimensions are too small to cause subsidence or if there is significant hanging of the undermined strata, it is recommended that the method developed at the Moscow State Mining University (MSMU) be applied, which uses high-precision gravimetric survey data (with a mean quadratic deviation of 0.03 mGal) of a subhorizontal coal seam in area and thickness. *The gravimetric method* is based on the effect of decompaction of the formation resulting from coal gasification on the gravitational field of the Earth. When a coal seam is mined using the UCG method, a redistribution of the gravity field occurs with a gravity high (positive anomaly) showing above the zone of rock-bearing pressure and gravity lows (negative anomalies) occurring above the gasification cavity. This leads to an increase in the gravity anomaly range above the boundary contours of the gasification cavity whose position is determined by the inflection point of the gravity change curve along the monitoring profile. The error in determining the gasification cavity boundaries at the depth to the coal seam of up to 200 m is below ±5 m. Other techniques of operational management and control of fire face advancement and the gasification cavity boundaries, such as geophysical, geochemical, and thermometry methods, did not become practical applications due to the need to drill special purpose wells for probe, receiver, and transmitter placement, as well as due to the difficulty of installing equipment above an active gasifier where it is difficult to eliminate noise contamination.

9.2.3.3   The mechanism of rock deformation above the gasification cavity

In this section we investigate the factors that influence the integrity of casing in vertical wells.

Let's focus on the mechanism of rock deformation above the gasification cavity. An investigation of the geomechanical response of overburden during underground coal gasification and shaft mining was carried out to address the following key issues: identifying the type of rock deformation above the gasification cavity and distribution of the displacement vector components relative to the gasifier boundaries in plan view and along the vertical projections and defining the mechanism of rock deformation ahead of the advancing fire face. These issues are raised because of the need to ensure a stable, efficient UCG process in the underground gasifier and extend the service life of process wells that are located inside the zone of rock deformation.

Monitoring rock deformation along the vertical axis was conducted using extensometers installed in special boreholes. The wells were drilled with a 150–180 mm bit, and surface casing was installed. Next, wells were drilled uncased, with coring of selected intervals of anticipated installation of markers. Surface markers were installed as soon as drilling and geophysical logging were completed before the walls of the uncased portion of the hole cave in.

In situ investigation of the type of rock deformation taking place in the formation was conducted based on the inspection of the casings from failed wells. The investigation methodology is as follows. The failed well is isolated from the system. The depth to the obstruction with rock fragments is measured. The well is cleaned and flushed as needed. After that, the lead impression stamp is run in. The drilling rig is set up over the well. A wooden cylinder block 0.3–0.5 m long with a lead plate at the bottom is attached to the bottom of the drill string (2–3 cm smaller diameter than the casing). The alignment accuracy of the lead impression block in the horizontal plane was achieved with the help of a theodolite. The impression taken enables a judgment to be made as to the extent, nature, and magnitude of deformation and direction of displacement of specific casing pipe joints.

The investigation methodologies described above led to a greater understanding of change in deformation patterns over time in the formation as well as discrete parts of the rock mass during undermining. The data obtained can be correlated with the parameters of longwall mining: location of the fire face, boundaries of the gasification cavity, percent of the seam thickness extracted, etc.

This cannot be achieved in UCG without using specialized methodologies that would make it possible to investigate the structure of the gasification cavity and define its shape and dimensions. To conduct these activities and to delineate zones of deformation, control wells were drilled and cored at spent gasifier sites. Rock deformation zones with varying degrees of discontinuity of rock layers were delineated based on the rate of drilling fluid circulation during drilling and by the presence of voids (recorded when the drill string drops abruptly) and discontinuities in the core recovered. The extent and nature of coal seam gasification in area and thickness, the degree of the cavity volume being filled with rubble, and the cavity structure were determined

by performing core analysis studies on samples recovered from the spent parts of the underground gasifier.

One of the simplest and most effective methods for laboratory-based investigations of the extent and type of rock deformation during underground mining is modeling using equivalent materials. Modeling was performed on a flat, 4.5×20 cm deformation apparatus. The purpose of the investigations was to determine the type of rock deformation during longwall mining versus at the nearby UCG plant. Longwall mining and UCG using gasification channels separated by coal pillars were modeled. As the coal seam was gasified, monitoring rock deformation was conducted using time-lapse photography.

The modeling experiments showed that in longwall mining (initial undermining), the distribution of the displacement vector components follows the expected distribution: maximum vertical displacement occurs above the mined-out area and decreases closer to the coal yet to be gasified; the horizontal displacement values are at their lowest above the center of the mined-out area, while the maximum values are in the upper part of the formation, above the boundary between the mined-out area and the coal to be gasified.

From analysis of the modeling data, it can be concluded that the first rocks to start moving are the rocks above the center of mined-out cavity. Then, rock located above the peripheral areas is displaced in the direction of the rock layers that had undergone deformation. The upper layers of the formation follow the most complex deformation path where the maximum horizontal displacements are concentrated.

Rock deformation of the immediate roof during mining of the coal seam has the following distinctive features: in the initial moment of departure from the cutting face of the furnace on the elaboration of a zone of a disorderly collapse of the rocks. The height of the caving zone varies depending on the seam thickness mined. In a coal seam 2 m in thickness, it is below 1–1.5 times the thickness of the seam. Further advancement of the face does not cause an increase in the height of the caving zone, with the roof undergoing bending deformation that may or may not give rise to discontinuities.

Horizontal displacement causes fractures in the formation and on the ground both at the fixed boundary and preceding the advancing face. Stabilization of the zone of horizontal displacement occurs from the stationary border. Ahead of the advancing coal face, the location of the zone of maximum horizontal displacement shifts, resulting in new fractures. The magnitude of the horizontal component of the displacement vector in the vicinity of a stationary boundary is greater than that of an advancing mining face.

Imitation coal seam gasification in individual channels on the models was carried out with working layer leaving pillars between them. Rock deformation above smaller-scale underground workings is characterized by the same repeating patterns that are observed in longwall "total extraction" mining. Above the center of the mined-out area, displacement of rock layers occurs along the normal. Horizontal displacement leads to displacement from direction of the coal pillars that are located in between the extraction workings. No horizontal displacement occurs directly above the central part of the coal pillars. The type of overburden deformation during mining

in strips and longwall mining are the identical only in the upper layers; deformation of the lower part of the formation during longwall mining of the coal seam in slices (or webs) are more complex owing to the formation and reciprocal influence of discontiguous zones of deformation above the mining zones (Fig. 9.9).

Special features of the horizontal displacements of select rock layers and subsidence as the longwall coal face advances are as follows. Initially, at a distance of 10–5 m preceding the advancing fire face, the rocks move toward the face, and then, after the fire
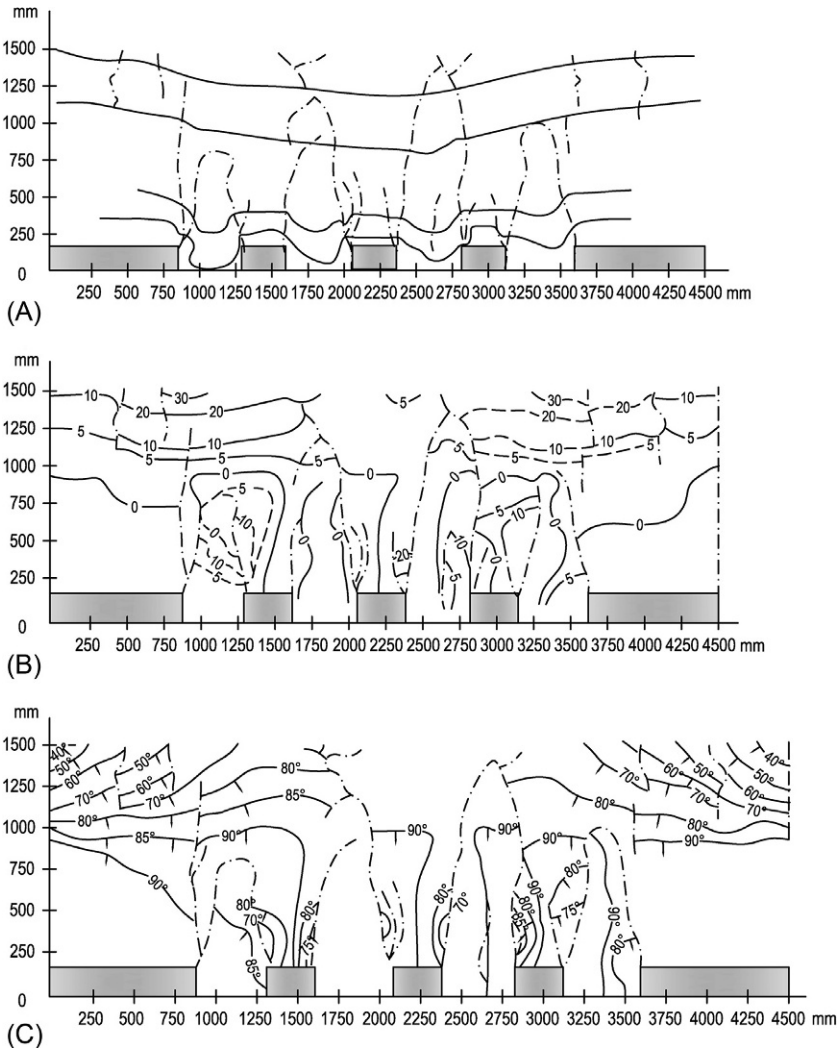
Fig. 9.9 The nature of subsurface rock deformation in mining the coal seam in strips: (A) subsidence profiles, (B) contour lines of horizontal displacement, and (C) contour lines of displacement vectors.

face passes below the rocks, the direction of the horizontal displacement is reversed. Above the mined-out area, a secondary reversal of direction takes places, with rocks eventually returning to their original position. The greatest horizontal displacement takes place in the ground surface and the limestone layer immediately below.

Of the remaining rock occurring in the upper part of the formation, the strongest rock types such as siltstones experience the most significant displacement. The horizontal displacement values of siltstones are 2–2.5 times greater than those of the overlying loose sand layers. Modeling data on the maximum horizontal displacement preceding the advancing fire face were confirmed by the results of results of downhole surveys of failed process well casings.

Core barrel drilling was used to drill background wells into the gasification cavity, which made it possible to delineate zones with varying degrees of rock deformation. Thus, the zone of random caving extended vertically as much as 1.5–1.6 m (m—thickness of the seam gasified factoring in the values of ash residue), while the zone of rock deformation, in which a total loss of drilling fluid circulation occurs, was 5.5–6.6 m. Rock deformation with discontinuities, when a temporary total loss of drilling fluid circulation (*fracture zone characterized by fluid flow resistance*) were observed above the gasification cavity at a distance of 14.4–15.0 m. Investigation of the gasification cavity structure indicated that rock from the immediate roof of the coal seam fills a large part of the cavity along its height. The thickness of the residual ash and slag generally ranges 10%–16% of the coal seam thickness gasified.

The results of laboratory and in situ investigations permitted elucidation of the rock deformation mechanism above mine workings during mining of a subhorizontal coal seam as follows. As the fire face moves further away from the ignition row and after the gasification cavity reaches the maximum unsupported span length, the immediate roof rock will cave in. The characteristic feature of this stage is the collapse of rock strata resulting finally in a stable arch configuration. Following the rock collapse, the overlying rock layers are subjected to displacement by bending resulting in subsidence. The initial stage of rock caving is common to both in longwall mining and UCG. Further displacement of the roof rock in the mining methods being considered, has some distinctive features.

Another type of rock deformation takes place above the underground gasifier. When only vertical wells are used in UCG, after the gasification channel has been created between the wells in the ignition row, linking channels are created in a plane perpendicular to the ignition row (Figs. 9.5 and 9.6). As coal is gasified and the gasification channels become enlarged, the immediate roof rock caves in. During UCG, preceding the contiguous gasification front, which is created as the ignition row channel is enlarged, discontiguous zones of collapsing immediate roof rock are formed within narrow channels ahead of the fire face. The main overburden response to longwall undermining is rock layers bending. Bending of rock layers occurs without hanging of layers and leads to significant horizontal displacement above the coal pillar in the upper part of the rock formation. Maximum horizontal displacement affects stronger rocks: limestones and siltstones.

It is critically important to investigate the factors that influence the integrity of casing in vertical wells.

Specific well design requirements exist for UCG process wells in view of severe service conditions. First, the integrity and good seal of a process well must be ensured including under high pressure. These conditions are necessary to create linking gasification channels that are accomplished by injecting water or air at high pressure. Loss of cement seal integrity of the casing may lead to gas and injected air leakage, groundwater transmission from the aquifer into the gasifier, and a disruption of desired the moisture balance. A process well is designed and constructed to ensure the coal seam, fractured rock layers, and groundwater aquifers are isolated. This serves to prevent gas and air leakage from the gasifier and groundwater influx through the annular space. The process well should remain operational throughout the period of gasification of the coal resource it exposes and prepares for gasification.

The results of the above investigation have been applied in designing process wells used in underground gasifiers. Operational lessons learned from past UCG mining experience in the thick (up to 20 m) coal seam at the Angren coal deposit at depths of 110–220 m, highlighted serious complications stemming from premature well failure. Depending on the thickness, dip, depth of the coal seam, among other factors, relating to the underground gasifier design, either vertical or horizontal directional process wells are installed. At the pilot/commercial Angren UCG plant, vertical wells (at 12 gasifiers) accounted for 92% of the total wells used, horizontal directional wells 5%, and directional wells less than 3%.

Vertical wells are used during all stages of UCG: intersect and provide initial access to the coal seam, create borehole-to-borehole link (linkage channels), supply injection agent (air), and produce gas from the underground gasifier. Vertical wells are generally drilled using 349, 298, and 244 mm drill bits and cased with 273, 219, and 168 mm steel pipes that are no less than 7–8 mm thick. The annular space is filled with the cement slurry.

The main advantages of vertical wells are simplicity of design and being economical; the main drawback is premature failure due to rock deformation. The required service life of process wells is determined by the amount of coal reserves accessed by them and the gasification rate. For example, given the mining conditions at the Angren UCG plant and the average thickness of the coal seam being 6 m, with process wells drilled 15–20 m apart, the coal reserves accessed by one well are 2200 t. At the injection flow rate of about 3000 m^3/h (gasification rate of about 25 t of coal per day), gasification of this quantity of coal requires 90 days. The total service life of the well should be no less than 300–360 days, including time in service as a gas production well.

HDD wells are used on a limited basis because of the complexity of construction and high cost. Wells must be drilled outside the deformation zone to ensure integrity of casing. The disadvantages of directionally drilled wells are uneven thickness of the cement seal, the high cost and technological complexity of directional drilling and casing. Table 9.2 shows key operating and performance parameters of drilling and completing various types of wells and the average performance parameters relative to their operation at the four commercial Angren UCG plants.

Directional drilling rates are only half those typically seen in vertical drilling, while costs are higher. The operational lifetime and the amount of coal gasified using directionally drilled wells is 1.5 times greater than with vertical wells.

Table 9.2 Key operating and performance parameters of drilling and completion of wells at the Angren UCG plants

Parameter name	Vertical	Horizontal directional	Directional
Rig total operating speed, m/month	379	211	102
Duration of operation, days, including the	187	311	386
following: used as an injection well used as a	69	74	352
production well	118	237	28
Amount of coal gasified well, ton	1690	2440	9220
Cost per running meter, rubles (up until 1990)	17.9	33.7	52.6

Directional wells are designed mainly to create linkage channels and supply injection agent (air) and are cased with a cement seal down to the coal seam. The advantages of this well type are increased speed of linking and structural stability given that the directional part of the wellbore is located outside of the undermined rock zone. The disadvantages include difficulties drilling of nonvertical and horizontal sections of the borehole and a nearly fourfold increase over vertical well construction costs.

The average service life of underground gasifiers is 5–7 years. The actual service life of production wells is measured, on average, in months (4–6 months) and in some cases in weeks and even days. Causes of reduced service life of well casings include well construction quality, the effects of high temperature and chemical potential of UCG gas, and the impact of deformation of undermined strata. Summarized below is an analysis of the degree of influence of these factors on the integrity of well casings during their operation.

An important factor in the service life of the well is the quality of casing and cementing installation: connection makeup of casing joints and installation of the annular cement seal. Downhole surveys conducted at the Podmoskovnaya UCG plant revealed cases of improper casing connection makeups. Of the 39 casing joints surveyed, 16 joints had proper connection makeup (7 + turns from stab in to full makeup), 13 had satisfactory connection makeup (7–5 turns), while in 10 acceptable connection makeup was not achieved (2–5 turns). Such couplings cannot maintain their integrity under the smallest load applied. At the Angren UCG plant, where the number of joints in the drill string was several times greater than at the Podmoskovnaya UCG plant, this factor takes on an even greater importance.

An assessment of the quality of the casing cement job revealed that cementing was performed to accepted industry standards. The techniques used including vibrating the cement during cementing operations ensured good returns of cement slurry from the coal seam to the surface and uniform distribution of cement slurry along the length of the casing, that is, a well-executed cement seal.

Thus, provided proper casing tubing connection makeup and cement seal protocols are adhered to, a UCG process well constructed to engineering specifications will perform as expected during linking, injection of process air to the fire face (injection wells), or gas production over the entire service life of the well.

Effects of high temperature on casing integrity have been a subject of multiple studies. Underground coal gasification involves using temperatures of up to 1100–1300°C. Production well casings remain exposed to long-term high temperature stress, especially when the UCG processes are at work in the vicinity of the bottom of the wells. Inspection of wells during direct access into the gasifier cavity post gasification revealed a number of cases where the bottom part of the casing pipes were burned. In the vast majority of cases, the bottom part of the casing pipe will have burned areas but without any physical damage. Therefore, the possibility of burning the bottom of the casing exists, albeit unlikely.

Prof. V. I. Sheinin established a correlation between the wellhead gas temperature and the temperature at the bottom of the well:

$$T_{(H)} = T_{(o)} \cdot e^{-KH}, \tag{9.9}$$

where $T_{(H)}$—temperature at the wellhead; $T_{(o)}$—temperature at the bottom of the well; e—base of the natural logarithm; H—distance from the top to bottom point of measurement; K—coefficient calculated from the expression.

$$K = \frac{\lambda}{r} \cdot 0.5 F_0^{-0.5} \cdot B_i^{0.5} \cdot \frac{2\pi r}{G \cdot C_p},$$

where $F_0 = \dfrac{a\tau}{r^2}$ —Fourier's criterion, which is calculated from the duration of well operation under normal conditions; $B_i = \dfrac{\propto \cdot r}{\lambda}$ —boundary conditions criterion; a—temperature conductivity coefficient of rock surrounding the well (for lignite deposits $a = 25 \times 10^{-4}\,\text{m}^2/\text{h}$; r—radius of the well; λ—thermal conductivity coefficient (for lignite deposits); $\propto$—heat output coefficient from gas to the borehole wall, kcal/m²/h °C; G—amount of gas passing through the borehole per unit time, м³/h; C_p—gas heat capacity at constant pressure $\left(C_p = 0.27 - 0.32\,\dfrac{\text{kcal}}{\text{kg}}\,°C\right)$.

In the vicinity of the fire face, the bottom portion of the casing may reach 800–900°C.

Estimated data versus actual measurement data indicate that at the Angren UCG plant the gas temperature range at the wellhead was 100–400°C.

The production well casings are subjected to high temperature stresses. The effect of high gas temperature may manifest as follows: decrease of strength of the steel casing pipe, disintegration of the cement seal, and vertical elongation of casing pipes.

The strength properties of casing pipe steel are adversely affected by exposure to high temperature. The yield strength of steel is known to be greatly reduced as the temperature rises to 350°C; at temperatures above 350°C, the yield strength decreases at a slower rate than the tensile strength. Stress on metal at high temperatures over extended periods leads to its gradual plastic deformation, while resistance of steel to brittle fracture is significantly reduced.

Steel casing pipes expand and lengthen on heating.

$$\Delta l = \alpha \cdot t \cdot l, \tag{9.10}$$

where Δl—pipe extension, mm; α—linear expansion coefficient; t—average heating temperature, °C; and l—casing length, m.

At the Angren UCG plant, the vertical elongation of the casing reached as much as 1.0 m at a depth of 200 m.

The cement seal and the compressive pressure from surrounding rock preclude the casing string from elongating freely, which causes stresses exceeding the yield strength of the casing steel. Studies have shown that the stress values occurring in casing pipes due the temperatures ranging 800–1000°C may under certain conditions exceed the maximum allowable ranges by three times. These conclusions are based on the assumption that very good bonding exists of the cement seal to casing and formation. However, the results of a verification shaft being completed to the spent gasifier cavity (post shutdown) revealed that the cement seals around the production well casings were highly fractured with fractures up to 3 mm wide and virtually no contact with them. Experimental investigations conducted during oil production operations also indicated that bonding of cement to casing and rock is poor (weak).

Depending on the nature of compression on casing in the wellbore, manifestations of thermal expansion of the casing can be quite varied. In the event of compression on casing at the wellhead through the weak rock intervals, some sections of casing may become distorted, while most casing joints under lengthening in the direction of the bottom of the well. If the adhesive bond between annular cement and casing is lost, the entire casing string will lengthen and jut out at the surface.

Along with the effects of high temperature on the casing of a production well, the possibility of chemical erosion of casing pipes and solid particles suspended in the gas stream should also be taken into account. The rate of oxidation reactions increases with increasing temperature.

The impact of this factor at the Angren UCG plant. Syngas from Angren coal using injected air has the following average composition: H_2S, 0.4; CO_2, 19.5; C_mH_n, 0.3; O_2, 0.6; CO, 5.4; H_2, 17.0; CH_4, 2.0; and N_2, 54.8. The presence of water vapor and carbon dioxide in gas exacerbates the corrosion of carbon steel, while increased content of carbon monoxide reduces it.

The solid particles suspended in the gas stream have an abrasive effect on the casing. The casings at the Podmoskovnaya UCG Plant were noticeably affected by sand carried out in the gas stream. Analysis of data on the tar content and solid particulates in the product gas (data obtained from measurements taken at a pilot gasifier of the Angren UCG plant) revealed a lack of correlation between the duration of borehole operation and tar levels and other contaminants in the product gas. Although the chemical potential of UCG gas and solid particles are recognized as causes of internal casing wear, they are not among the factors likely to significantly shorten the service life of the well.

Possibly the most important factor affecting the integrity of the process well casing is deformation of the rock mass in which the casing is placed. As coal is gasified over a

more a less extensive area, the equilibrium of geologic materials is disturbed; rock strata are displaced into the depleted gasification cavity, which subjects the casing to nonlinear stresses along the length of the well. Types and magnitudes of these loads depend on the extracted seam thickness, strength characteristics of roof rock, and location of the process wells relative to the gasification cavity.

Depending on the type of impact on process wells, three zones within the rock mass are differentiated, which are the following:

- Above the central part of the gasification area: the zone where the process well is mainly subjected to stresses due to vertical displacement (zone 1).
- Above the section of coal seam to be gasified, ahead of the fire face where the casing is subjected mainly to horizontal displacement and negligible vertical displacement (zone 2).
- Intermediate zone where horizontal and vertical displacement reach considerable values (zone 3).

During underground coal gasification of a coal seam, the location of process wells relative to the fire face can vary considerably. Therefore, when it comes to the well service life, it is important to provide for the possibility of casings sustaining damage in all three zones of undermined rock strata.

Two major types of rock deformation of undermined beds of stratified rock are differentiated based on generalized findings of monitoring in in-situ conditions: rock caving, which manifests itself as discrete blocks separating from the formation and becoming displaced into the gasification cavity, and bending of rock strata, which occurs as displacement of rock layers along the direction normal to the bedding plane that may or may not give rise to discontinuities. The bending of the rock strata causes tensile (compressive) strains that are a function of both the bending curvature radius and thickness of each discrete rock layer. The rock collapse occurs over the central area of the gasification cavity and over narrow gasification channels that precede zones of contiguous gasification. In addition to the two types of deformation that takes place during mining in subhorizontal and inclined coal seams, other types of possible deformation include compression of rock and coal seam associated with changes in volume and displacement deformation.

Based on subsidence monitoring data, delineation of the solid-coal boundaries of the gasification cavity in plan view permitted a more in-depth analysis of reasons for premature well failure. The borehole survey results in damaged wells along with mine surveying data at gasification sites were used to conduct the analysis (Table 9.3).

For purposes of revealing the causes and repeating patterns in well failure, data were collected and consolidated into sets characterizing the casing failure points relative to the boundaries of the gasification cavity in plan view d and relative to the coal seam roof along the vertical height of the coal seam H. It was determined that most frequently (75%) wells experienced failure at a depth of 50–90 m from the coal seam roof and 20–35 m ahead of the advancing fire face (zone 2). The second group of wells (25%) underwent deformation in the depth interval of 10–47 m from the coal seam roof and 8–20 m from the gasification area solid-coal boundaries (zone 3).

Table 9.3 **Locations of well casing failure on commercial Gasifiers 1, 1-bis, III (Angren UCG plant)**

Borehole name	Horizontal distance from the point of failure to bottom of the well, dm	Vertical distance from the point of failure to coal seam roof coal seam, H, m	Borehole name	Horizontal distance from the point of failure to bottom of the well, dm	Vertical distance from the point of failure to coal seam roof coal seam, H, m
a	Group 1		78-III	22	78
109-I			118-Ib	20	79
95-Ib	25	52	16-III	33	80
82-Ib	20	54	77-III	32	81
21-III	25	59	86-Ib	32	81
101-III	28	63	6-Ib	25	84
38-III	30	64	159-Ib	30	84
123-III	28	65	72_2-Ib	35	84
23-III	25	67	7-Ib	35	84
48-III	20	70	158-Ib	35	86
126-III	30	71	71-1b	35	89
62-I	30	71			
17-III	35	73	Group 2		
58-III	20	74			
98-Ib	30	74	117_1-III	10	8
59-III	27	75	134-III	15	19
211-III	32	75	72_1-1b	8	22
61-III	29	76	141-III	20	29
137-I	25	76	44-III	10	21
109-Ib	32	76	56-III	8	32
121 Ib-	28	76	115-III	20	39
88-I	35	76	119-Ib	15	40
	33	77	147-III	30	40
			103-I	30	47

A run was made with a lead impression block, which revealed that the displacement of the upper part of the casing of the group 1 wells occurred in the direction of the advancing fire face. All wells in this group failed on the interface of relatively strong and weak rocks. Most casing strings failed in weak sandstones below a thick layer of limestone, while some wells failed on the siltstone-sandstone interface. In the first instance, the thickness of sandstone below the limestone was over 5 m and, in the latter case, less than 3 m. The limestone layer, separated from siltstone by a relatively thick sandstone layer, is displaced independently from siltstone; deformation of well casings occurs at the limestone/sandstone interface. If the thickness of sandstone does not exceed 3 m, the limestone and siltstone are displaced as a

rock unit, with maximum casing deformation occurring at the siltstone/underlying sandstone contact.

Casing breaches in wells 20–35 m ahead of the advancing fire face is explained by the following. As revealed by field monitoring and modeling, the zone of maximum horizontal displacement of the ground surface is formed in this interval. With a certain degree of approximation, these data can be applied to a limestone layer that occurs near the ground surface. The mechanism of geomechanical response of rock is such that the formation is subjected to maximum vertical displacement above the center of the gasification cavity; horizontal displacement is concentrated in the upper portion of the formation adjoining, in plan view, the mined-out cavity. The deeper into the rock mass the more attenuated the horizontal displacements. In view of the above conclusions, it is evident that the group of wells in question failed as a result of horizontal displacement of rock.

Using mathematical statistics, an equation was developed to describe the relationship between d and H, which makes it possible to delineate the zone of the most damaging effects of rock deformation preceding the advancing fire face:

$$d = 0.25\,H\,10\,m. \tag{9.11}$$

Practical application of the formula is as follows: knowing the location of the specific layers of hard rock relative to the coal seam roof, that is, the value of the H parameter, the horizontal distance preceding the advancing contiguous fire face d, where deformation of the well casings is anticipated.

Having sustained deformation damage to casings some 8–20 m from the boundary of contiguous gasification front, wells of group 2, unlike wells of group 1, were located on gasification sites as discontiguous narrow channels. The zone of random caving forms above each gasification channel, with overlying rock being displaced along the normal, pulling the casing string along with it. If a well casing is rigidly grouted into rock casing, failure will occur. Judging by the distance from the contiguous fire face, horizontal displacement of rock during gasification in the adjoining narrow gasification channels also had an impact on the deformation-induced damage to the wells.

Casing with partial cementing are recommended to extend the service life of wells including expansion joints for steel casing pipes capable of absorbing vertical displacements. The location of uncemented lengths of casing and sections for expansion joint installation is determined based on the coalfield-specific geologic structure and anticipated features of rock deformation.

9.2.4   Specific features of rock deformation during underground gasification of steeply-dipping coal seams

During underground coal gasification of subhorizontal coal seams, no ground surface depressions were recorded. In a shallow (30–40 m) coal seam in the Podmoskovnaya coal basin, the zone of collapse above some gasifiers reached the ground surface as sinkholes (surface depressions). With the increasing depth to the 5–10 m thick

coal seam (Angren coal deposit) to 100–160 m, earth fissures formed at the edges of the subsidence trough leaving small 10–20 cm benches. Ground surface depressions were most frequently recorded during UCG in bituminous Kuzbass coal seams.

Ground surface depressions lead to significant injection agent (air) and gas leakage and disrupt the technological process. Identifying and defining the conditions of their formation is an important task whose solution is a prerequisite for the efficient operation of a UCG plant. Comprehensive studies (V. N. Kazak and V. N. Kapralov) of conditions of the formation of ground surface depressions during underground coal gasification were conducted in the Prokopyevsko-Kiselevsky district of Kuzbass, including an analysis of the results of investigations of the conditions of formation of depressions in shaft mining, simulations using equivalent materials, and field studies at the Yuzhno-Abinskaya UCG plant (Kiselevsk, Kemerovo Region).

Data obtained through monitoring ground surface depressions at the UCG site (using instrument-based observations and extensometers and postgasification verification open casting of spent gasifiers) were used to establish a correlative link between rock deformation above the gasification cavity and subsidence. Control wells were drilled into the gasification cavity of spent gasifiers to determine the type and extent of rock deformation with different thicknesses of the coal seam as well as varying sizes of coal pillars, in the vicinity of which surface depressions appeared.

Studies conducted on 3-D and 2-D models using equivalent materials focused on investigating the effect of specific factors in generating ground surface depressions that are difficult to account for in in situ conditions.

9.2.4.1 The effect of mining and geological factors in generating ground surface depressions

Based on analysis of data on the magnitude, location and time surface depressions occurred during mining of coal deposits using various mining methods, several critical geologic, mining and technological factors were defined.

The shape, size, location, and time of formation of the surface depressions are determined by coal seam thickness and depth of mining, dip, physical and mechanical properties of rock, composition of rock, mining method employed, distance between the coal seams, and size of coal pillars.

The dip of the coal seams has a significant impact on the location of the zone of ground surface depressions. When the upper seams are mined, the zone of ground surface depressions is delimited from the direction of the footwall by a line drawn from the point where the coal seam floor intersects the alluvium at an angle of 75 degrees and from the direction of the hanging wall by a line running through the bottom boundary of the longwall working. The width of the zone of ground surface depressions across the strike of the coal seam dipping more than 75 degrees is equal approximately to five times its thickness. The surface depression boundary along the strike is not determined by the dip of the coal seam, but rather by a vertical line drawn from the boundary of the longwall working to the alluvial deposits and within the alluvial deposits by a line at an angle of 45 degrees to the horizontal.

Depressions forming on the ground surface may be attributable to the possibility of rock rolling downdip leaving the upper part of the cavity empty. Rolling of collapsed rock downdip occurs if the following condition is satisfied ($T_g\alpha \geq f'$ (α, dip, and f', friction coefficient during the movement of collapsed rock along the coal seam floor). In the Kuzbass coalfield, rolling of caved-in rock was observed at $\alpha = 31$–35 degrees, if $f = 0.7$–0.8.

Sedimentary rocks that make up the coal-bearing strata consist of alternating layers of sandstone, siltstone, and mudstone, which have a distinct stratified texture. The thickness of the layers, which the formation splits into, largely determine the stability of exposed areas, the nature and extent of deformation and the size of the rock caving zone. If there are weak rocks in the coal seam roof that are located inside the caving zone, the contours of the ground surface depression coincide with the outcrop of the weak rock below the alluvium. If the coal seam roof is composed of strong rock, then the depression will reach the ground surface either along the coal seam as a weaker layer or along the coal seam floor in cases of weaker rock and dip in excess of 83 degrees.

If the roof rock is composed of medium strength to weak rock and is less than 1 am in thickness, no depression-related displacement was observed toward the hanging wall of the coal seam. With unstable roof rock or weak rock partings 1 m in thickness or more, surface depressions are significantly shifted. It was established that the determining conditions for the formation of depressions during mining in steeply dipping coal seams are the height of the rock caving zone and the size of the coal block yet to be gasified and rock that are inside the caving zone.

9.2.4.2 Mechanism of formation of surface depressions and calculation methodology of coal pillars

Specific features of rock deformation in mining thin (0.5–1.3 m) and medium (1.3–3.5 m) steeply dipping seams are displacement of the roof layers along the normal to the bedding plane, smooth transition of the caving zone to the zone of orderly rock deformation, and sliding of the rock layers as the mined-out void nears the ground surface.

Based on drill data from background wells drilled in the gasification site with a 2.2 m thick coal seam dipping 64 degrees, it was determined that the height of the caving zone along the normal to the bedding plane is 4–5 times the coal thickness gasified. In the lower part of the zone that is 1–2 times the thickness of the gasified coal seam, there are voids and rock mixed in with coal and slag. This indicates a nonuniform nature of the gasification cavity being filled, with partially collapsed rock into the bottom of the cavity.

When mining thick (over 3.5 m) steeply dipping coal seams, the caving zone consists entirely of randomly collapsed rock. Caving stops when the amount of empty space between the collapsed rock and the exposed roof downdip is less than the span of roof collapse, that is, the largest amount of empty space is in the upper part of the working.

The condition whereby the caving zone ceases to expand along the direction normal to the coal seam may be calculated from the expression

$$\frac{mH - H(k_p - 1)\sum_{1}^{i} h_i}{m + \sum_{1}^{i} h_i} \leq l_{o\delta p.(i+1)}, \tag{9.12}$$

where m is the seam thickness extracted, m; H is the size of the working up dip, m; k_p is the bulking factor of the collapsed roof rock; $\sum_{1}^{i} h_i$ is the sum of collapsed rock layer thicknesses, m; $l_{o\delta p.(i+1)}$ is the caving span of the $(i+1)$th layer.

The expression (9.12) can be used for approximate calculation of the value of the rock collapse zone $\sum_{1}^{i} h_i$ in mining thick, steeply dipping seams.

Analysis of the conditions preceding the development of surface depressions, which was based on the modeling data and in situ studies, provided important insights into the mechanisms responsible for ground surface depressions during UCG in steeply dipping coal seams as follows.

During stage 1 of UCG, bending of the immediate roof strata occurs, followed by rock collapse into the bottom part of the gasification cavity. During this period, rock collapse spreads ahead of the fire face along the weak rock layer that is located inside the caving zone. This is attributable to the rock-bearing pressure crushing the edges of the layers of weak rock.

After the mined-out cavity dimensions increase in the updip direction to such a degree that condition (9.12) is met, caving of rock layers will occur in the form of breaking of a cantilever beam as the fire face advances.

As coal is gasified, the solid block of coal yet to be gasified and surrounding rock affected by the caving zone reach their maximum critical values resulting in their breakdown and ground surface depression.

The surface depression forming is preceded by the solid block of coal breaking off the formation. After the coal pillar breaks off, it is displaced downdip, with rock strata splitting up into discrete blocks, which cave into the gasification cavity.

The task of calculating the size of coal pillars to protect from ground surface depressions during mining of steeply dipping coal seams entails the estimation of the height of the rock collapse zone. At the Kuzbass coalfield, the ratio of the coal pillar size h' to the height of the rock collapse zone $\sum h$ and the seam thickness extracted m is as follows:

$$h' = 1.72\left(\sum h + m\right). \tag{9.13}$$

Factoring in C the maximum value of the caving zone $\sum h = 5\,m$, the size of the coal pillar for the conditions will be $h' = 10\,m$.

During underground coal gasification of coal seams, the coal pillar size that will ensure that the leak integrity of the underground gasifier is maintained is determined not only by the lithostatic pressure but also by the degree of fracturing of coal and rock inside the weathered zone. When calculating the dimensions of coal pillars that protect from gas or injection agent (air) outbursts or leakage from the underground gasifier, the depth and degree of weathering of rock and coal should be factored in such calculations.

The greatest extent of coal gasification in thick, steeply dipping coal seams takes place in the vicinity of the coal seam roof, depending on the degree of weathering of coal, rock-bearing pressure, and process modes of operation. Based on the results of a postgasification verification survey conducted through a shaft driven into the spent gasifier, the fire face is preceded by 12–28 m inside the zone of weathered rock in the roof rock of a coal seam 9–10 m in thickness.

The reactive surface of the coal seam, along which coal is gasified, is sloped toward the roof. The angle made with the horizontal δ_u changes in the range 65–85 degrees. Based on these data, the correction to the size of coal pillars left as the fire face approaches the zone of weathered rocks is calculated from the formula

$$\Delta h' = mtg(\delta_u - 90° + \alpha), \tag{9.14}$$

where δ_u—slope of the reactive surface of the coal seam, degrees, $\delta_u = 85°$; α—dip of coal seam, degree.

In UCG, the size of the coal pillar is calculated from the expression

$$h' = 10\,m + \Delta h' \tag{9.15}$$

The steps of calculation methodology for the size of coal pillars during UCG in a sequence of steeply dipping seams (regardless of the order gasification) are as follows:

1. The interburden thickness is determined between the coal seams in the sequence $M_1, M_2, ..., M_n$.
2. The ratio of interburden thickness to the maximum possible height of the zone of collapsed rock is computed:

$$\frac{M_1}{5m_1}, \frac{M_2}{5m_2}, ..., \frac{M_n}{5m_n}.$$

3. If $M/(5m) > 1$, calculations of coal pillar values are performed as for a single seam $h' = 10m$.
4. If $M_1/(5m_1) \leq 1$, a $M_2/(5m_2) > 1$, then the value of the coal pillar for both seams m_1 and m_2 is calculated: $h' = 1.72(M_1 + m_1 + 5m_2 + m_2)$, that is, taking into account the formation of a common caving zone during the mining of seams m_1 and m_2.

Similar calculations of coal pillar values are performed if a common caving zone forms encompassing several coal seams.

Further reading

Avershin, S.G., 1947. Rock Deformation During Mining Operations. Ugletkhizdat, Moscow, p. 245.

Bukrinsky, V.A., Orlov, G.V. (Eds.), 1984. Rock Deformation and Subsidence in Conventional Underground Coal Mining. Nedra, Moscow, p. 247.

Kazak, V.N., Kapralov, V.K., 1986. Deformation of the Roof Rock During UCG Activities in Thick, Steeply-Dipping Coal Seams, vol. 244 Academic Association. The Skochinsky Institute of Mining, A.A. Skochinsky, pp. 55–60.

Kazak, V.N., Orlov, G.V., Popov, V.I., 1969. Rock deformation above the gasification cavity (based on data collected during post-gasification open-casting of Gasifier 3 at the Angren UCG plant). Use of Gas, Underground Storage of Liquid Gases, Oil Products, Thermal Mining of Minerals, vol. 4 Nedra, Moscow, pp. 162–165.

Orlov, G.V., 1969. The effect of rock deformation on well casing failure at the Angren coal field. Use of Gas, Underground Storage of Liquid Gases, Oil Products, Thermal Mining of Minerals, vol. 3 Nedra, Moscow, pp. 171–177.

Orlov, G.V., 1986. Mine surveying control of the extent and nature of coal seam gasification based on subsidence monitoring data. Rocks Deformation and Protection of Surface Structures During Mining. KarPTI, Karaganda, pp. 72–78.

Orlov, G.V., 2010. General Considerations of the Effects of Underground Mining on Subsurface Rock Deformation and Subsidence: Educational Manual for University Students. Gornaya Kniga Publishing House, Publishing House of Moscow State Mining University, Moscow, p. 198.

Orlov, G.V., Kisurkin, A.F., 1987. Use of gravimetric survey in mine surveying during mining mineral ore deposits using borehole-based mining techniques. Mine Design and Exploitation of Mineral Resources in Complex Mining and Geological Conditions. Moscow State Mining University, Moscow, pp. 89–92. Collection of Scientific Papers.

Orlov, G.V., Trost, V.M., 1988. Development drilling methods under the supervision of a mine surveyor compilation of reports. In: VII International Surveyor Conference (Leningrad, 28.06–27.07.88), Collection XIII, pp. 119–124.

Orlow, G.W., Szewczyk, J., 1989. Geodezyjne metody kontroli resultato'w otworowej eksploatacyi surowco'w stalych. Prz. Go'r. T.45 nr 10 S.16-22.

Scheinin, V.I., 1963. Temperature distribution along the length of a production well casing. In: Proceedings of the Podzemgaz Institute, вып. 10, pp. 32–38.

Semenenko, D.K., Turchaninov, I.A., 1956. Mine surveying method for determining the location of the fire face in underground coal gasification at the Podmoskovny Coal Basin. Undergr. Gasific. Coals 7, 18–22. Ugletkhizdat.

Skafa, P.V., 1960. Underground Coal Gasification. Gosgortekhizdat, Moscow, p. 322.

Smirnov, V.G., 1959. Calculation of thermal stresses in casing pipes of production wells. Undergr. Gasific. Coals 4, 46–49. Ugletkhizdat.

Turchaninov, I.A., 1957. The nature and extent of coal seam gasification and overburden deformation during UCG operations in the Podmoskovny Coal Basin. Undergr. Gasific. Coals 2, 74–78. Ugletkhizdat.

This page intentionally left blank

Underground coal gasification (UCG) modeling and analysis

10

M.A. Rosen, B.V. Reddy, S.J. Self
University of Ontario Institute of Technology, Oshawa, ON, Canada

10.1 Introduction

The global supply of energy is composed of many sources, including fossil fuels, nuclear fuels, and various alternative and renewable sources. As of 2012, approximately 82% of the global energy supply was derived from fossil fuels, and a continued high fossil-fuel dependency appears likely in the immediate future (García-Olivares and Ballabrera-Poy, 2015; International Energy Agency, 2014; World Energy Council, 2013). The amount of energy required globally is projected to increase due to growing population and industrialization (Birol, 2014; Energy Information Administration, 2014). Birol (2014) estimates that the total global energy use will grow by 40%, relative to levels today, by the year 2040. Given the increases in global energy demand, the current dependence on fossil-fuel technologies, and the finite amount of fossil fuels available, it has been predicted that fossil-fuel shortages will occur in the future (García-Olivares and Ballabrera-Poy, 2015).

Hammond (2000) argues that fossil-fuel depletion is a significant factor for the future when considering sustainable energy systems. Fossil-fuel resources are finite and being consumed rapidly, especially the most economically attractive ones (oil and gas) (Aleklett et al., 2010). Fossil-fuel resource extraction and production rates are expected to peak and begin to decline in the foreseeable future (Chapman, 2014; World Energy Council, 2013; Aleklett et al., 2010). When fossil-fuel demand approaches supply levels, the cost of energy is anticipated to increase drastically, prompting research and technological developments for improved ways to convert more fossil-fuel resources into useable reserves (Ghose and Paul, 2007).

In 2012, coal was the largest source used for electricity generation, accounting for approximately 40% of the world's electricity production (World Energy Council, 2013). Coal exhibits the largest global reserves of any fossil fuels and is abundant in many countries. The world's recoverable coal reserve is estimated at close to 150 years at current production rates, but this only represents only 20%–25% of the entire resource (International Energy Agency, 2014; Birol, 2014; World Energy Council, 2013). Global coal resources have recently been estimated to be 18 trillion tonnes (Couch, 2009), which contrasts significantly with the typical figure of tens of billions of tonnes for recoverable reserves (Birol, 2014). If unrecoverable coal can be shifted to recoverable reserves, the lifetime of the resource could be extended by a couple hundred years. For this to be realized, new economic extraction techniques need to be implemented. Much research related to coal processes and use has been

reported (Rosen et al., 2015; Mehmood et al., 2015; Mehmood et al., 2014; Gnanapragasam et al., 2010; Gnanapragasam et al., 2009).

Coal is conventionally extracted by mining, both underground and open pit. Mining operations require much time, personnel, and natural resources. Coal reserves usually lie too deep underground or are too costly to exploit using conventional mining methods. Conventional mining also has other challenges including land subsidence, high machinery costs, hazardous work environments, coal transport requirements, localized flooding, and methane buildup in cellars of nearby homes (Blinderman, 2015; Bhutto et al., 2013).

Underground coal gasification (UCG) is a newer type of coal extraction that is being investigated and implemented around the world. Underground coal gasification is a combination of mining, exploitation, and gasification that eliminates the need for mining; UCG involves the conversion in situ coal into synthetic gas (syngas) for use in power generation or as chemical feedstock (Brown, 2012). Underground coal gasification can avoid most of the problems of mining coal while expanding recoverable coal reserves (Nakaten et al., 2014). Underground coal gasification limits the amount of underground work required by personnel, lowering risks of harm relative to conventional mining. Power generation and chemical processing plants can be built directly above a coal resource and use the syngas produced through UCG, avoiding coal transport. Underground coal gasification has the ability to significantly widen the resource base, since it permits the energy contained within previously inaccessible coal reserves to be recovered economically (Blinderman, 2015). It has been estimated by the underground coal gasification partnership that around 4 trillion tonnes of otherwise unusable coal could be suitable for UCG (Ghose and Paul, 2007).

UCG is appealing for expanding recoverable coal reserves, but as with the combustion of all fossil fuels, there are associated greenhouse gas emissions. Coal is the most carbon-intensive of all fossil fuels and has high associated CO_2 emissions per unit of thermal energy produced (Roddy and Younger, 2010). If coal is to continue to be a major contributor in the future global energy supply, CO_2 capture and storage techniques almost certainly need to be incorporated. Underground coal gasification has good potential for CO_2 emissions reduction. During gasification, CO_2 is produced, which can be captured from the syngas and stored for long terms (Schiffrin, 2015). If UCG is successfully linked to such carbon capture and storage (CCS), a method will be available for exploiting the energy in previously unrecoverable coal reserves while satisfying standards for reducing CO_2 emissions.

The aim of this chapter is to review concepts, technologies, and models related to underground coal gasification and carbon capture in UCG systems. This chapter also presents a case study that illustrates the modeling and analysis of UCG and investigates the feasibility of using an auxiliary power plant, utilizing the thermal energy removed during the cooling gasification products, to provide the energy required for CCS, through amine-based chemical absorption and compression within a UCG system. The overall objective of the chapter, which draws heavily from prior work by the authors (Self et al., 2013; Self et al., 2012), is to improve the general understanding of UCG technology and modeling while presenting a method for analyzing UCG systems with CCS.

10.2   UCG processes

UCG is similar to surface gasification with syngas produced through the same chemical reactions (Pana, 2009; Burton et al., 2006). The main difference is that surface gasification occurs in a manufactured reactor, whereas the reactor for a UCG system is a natural geologic formation containing unmined coal (Pana, 2009). Underground coal gasification also has similarities to in situ combustion processes applied in heavy-oil recovery and oil shale retorting, with such common operational parameters as roof/floor stability, seam continuity and permeability, and groundwater influx (Lee et al., 2014; Pana, 2009).

10.2.1   UCG process overview

UCG has been approached in numerous ways. The oldest and most basic UCG approach utilizes two drilled wells that act as injection and production wells as illustrated in Fig. 10.1. The basic method involves three main steps. Initially, the injection and production wells are drilled to the coal seam, and a permeable flow path is established between the wells. In situations where the natural permeability of a coal seam is low, it can be increased using techniques including forward combustion linking (FCL), reverse combustion linking (RCL), electrolinking, hydrofracturing, and directional drilling (Blinderman et al., 2008).
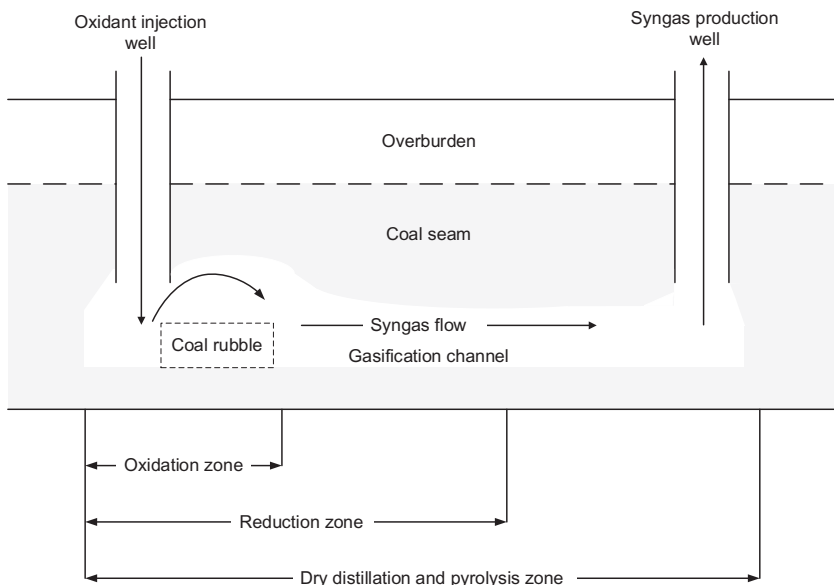
Fig. 10.1 Underground coal gasification approach.

Once a flow path between the wells has been created, the second step is ignition. Gasification begins with ignition of the coal and introduction of gasifying agents into the coal seam through the injection well. This triggers an in situ substoichiometric combustion process, producing syngas (Kempka et al., 2011). Coal ignition is initiated through the use of an electric coil or gas firing near the face of the coal seam (Daggupati et al., 2011a). Gasifying agents can be in the form of air, oxygen, steam/air, and steam/oxygen (Perkins and Sahajwalla, 2007). Continuous oxidant flow through the injection well allows for gasification to be sustained (Daggupati et al., 2011a).

Syngas is extracted through the production well and is cleaned prior to use (Van der Riet, 2008). The quality of the product gas is influenced by several parameters—such as the pressure inside the coal seam, coal properties, feed conditions, kinetics, and heat and mass transport within the coal seam—and the product of the UCG process is a multicompound, high-temperature, and high-pressure syngas (Daggupati et al., 2011a). When the syngas reaches the surface, it is cleaned, and undesired by-products are removed from the product stream (Perkins and Sahajwalla, 2008). Removal techniques are similar to those used with surface gasifiers. Once the by-products are removed, they can be disposed of safely or used for other chemical processes (Shafirovich and Varma, 2009). The degree of cleaning required is dependent on the use of the syngas; syngas is cleaned either to meet the specification for input into a gas turbine (for electricity generation) or to be of sufficient purity for use as a chemical feedstock for conversion to synthetic fuels (Walker, 1999).

Over time, the gasification process creates a cavity. Eventually, the coal near to the injection well will be completely converted to syngas, and steps one and two are repeated in order to access new coal and maintain syngas production. Once a coal seam has been exhausted, the last step is to clean and cool the cavity in an attempt to return the environment back to its original state (Imran et al., 2014). The cavity is flushed using steam and water to remove pollutants, preventing them from entering into the local environment.

10.2.2   UCG techniques

Two standard techniques of preparing a coal seam for gasification have been utilized successfully, shaft and shaftless. The method implemented is dependent on parameters such as the natural permeability of the coal seam, geochemistry of the coal, seam thickness, depth, width and inclination, proximity of urban developments, and amount of mining desired (Wiatowski et al., 2012).

10.2.2.1   Shaft UCG methods

Shaft methods use coal mine galleries and shafts to transport gasification reagents and products, which sometimes entail the creation of shafts and the drilling of large-diameter openings through underground labor (Wiatowski et al., 2012). The shaft method was the first technique utilized within UCG systems. Currently, the shaft

method is only employed in closed coal mines for reasons of economics and safety (Wiatowski et al., 2012). Examples of common UCG shaft methods include chamber or warehouse method, borehole producer method, stream method, and long and large tunnel gasification method.

Chamber or warehouse method

This method utilizes constructed underground galleries with brick walls separating coal panels. Gasification agents are supplied to a previously ignited coal face on one side of the wall, and the syngas is removed from a gallery on the other side. The chamber method strongly relies on the natural permeability of the coal seam to allow for sufficient oxidant flow through the system. The syngas composition may vary during operation, and the gas production rates are often low. To improve system output, coal seams are often outfitted with explosives for rubblization prior to the reaction zone (Lee et al., 2014).

Borehole producer method

For this method, parallel underground galleries are created within a coal seam with sufficient distance between them. The galleries are connected by drilling boreholes from one gallery to the other (Wiatowski et al., 2012). Remote electric ignition of the coal in each borehole is used to initiate the gasification process. This method is designed to gasify considerably flat-lying seams. Some variations exist where linking of the galleries is accomplished through hydraulic and electric linking (Lee et al., 2014; Wiatowski et al., 2012).

Stream method

This method is designed for sharply inclined coal beds. Parallel pitched galleries following the contour of the coal seam are constructed and are connected at the bottom of the seam by a horizontal gallery also known as a fire drift. To initiate gasification, fire is introduced within the horizontal gallery. The hot coal face moves up the seam slope with oxidant fed through one inclined gallery and syngas leaving through the other. The main advantage of this method is that the ash and roof material drop down fill the void space created during the process, which prevents suffocating the gasification process at the coal front (Lee et al., 2014).

Long and large tunnel gasification method

This method utilizes mined tunnels or constructed roadways to connect the injection well to the production well (Roddy and Younger, 2010). Typical long and large tunnel (LLT) systems consist of a gasification channel, injection and production wells, two auxiliary wells, and tunnels connecting the wells to the gasification channel (Fig. 10.2). The auxiliary wells are arranged between the injection and production wells and are used as malfunction wells for the injection of air and water vapor or to discharge gas that increases gasifier control. LLT also includes an auxiliary tunnel constructed of bricks, which is a supplementary installation for air injection that
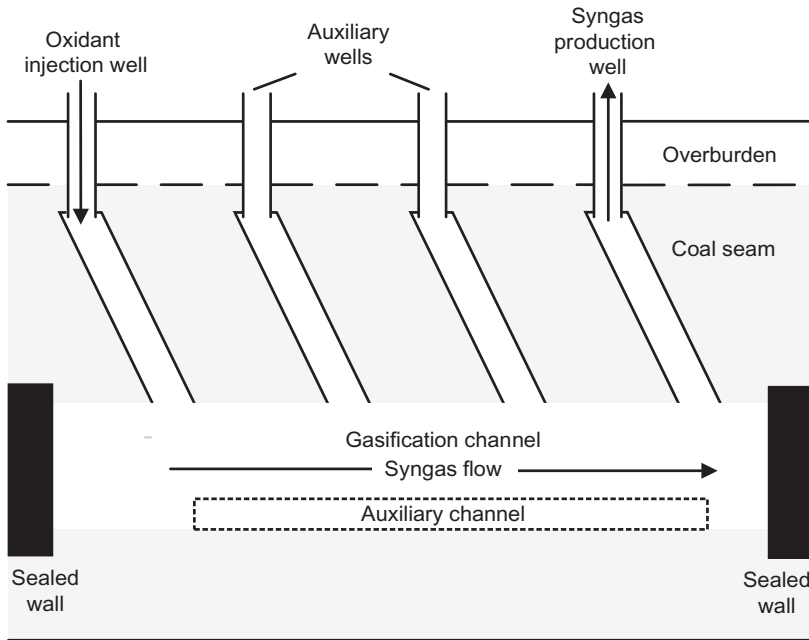
Fig. 10.2 Structure of a long and large tunnel underground gasifier.

prevents blockage in the gasification channel. The mined tunnels are isolated by sealing walls to prevent leakage of combustible gases from the gasifier (Liang et al., 1999). The location and height of the oxidant injection points and gas outlet points can be adjusted, allowing for two-dimensional control of oxidant injection and gas production (Yang et al., 2003).

10.2.2.2 Shaftless UCG methods

Recently, most of the focus of UCG research has been on shaftless methods, which employ directional drilling techniques (Hammond, 2000). With shaftless methods, all preparation and operational processes are carried out through a series of boreholes drilled from the surface into a coal seam and do not require underground labor. Preparation of a shaftless reactor consists of the creation of dedicated in-seam boreholes for oxidant injection and product collection using drilling and completion technology that has been adapted from oil and gas production (Wiatowski et al., 2012); the approach generally includes drilling inlet and outlet boreholes into a coal seam, increasing the coal permeability between the inlet and outlet boreholes, igniting the coal seam, introducing an oxidant for gasification, and extracting the product gas from the outlet well (Lee et al., 2014).

Currently, there are two main classifications of shaftless UCG methods, linked vertical well (LVW) and controlled retractable injection point (CRIP).

Linked vertical well method

The LVW method is one of the oldest methods for UCG and is derived from technology developed in the former Soviet Union (Shafirovich and Varma, 2009). Vertical wells are drilled into a coal seam, and internal pathways in the coal are utilized to direct the oxidant and product gas flow from the inlet to the outlet borehole. Internal pathways can be naturally occurring or constructed (Liang et al., 1999). In its simplest form, the LVW method has inlet and outlet borehole locations that are static for the life of the system. During operation, the coal face migrates, and it is found that system control, performance, and syngas quality are affected negatively as the distance from the coal face to the oxidant injection point increases (Roddy and Younger, 2010); this factor greatly reduces the feasibility of simple LVW systems.

A more advanced LVW approach involves a series of dedicated injection boreholes located along the length of a coal seam (Lee et al., 2014). Over the life of a UCG reactor, the coal face, being gasified, travels as localized coal is exhausted (Roddy and Younger, 2010). Having multiple boreholes for injection allows for improved static operating conditions. A more complex variation of the LVW method also exists where multiple inlet and outlet boreholes are drilled into a coal seam, forming inlet and outlet borehole pairs. Parallel inlet and outlet manifolds are connected to the boreholes to provide a path for oxidant and syngas flows, respectively. Coal between each pair of inlet and outlet boreholes forms a zone. When the coal in a zone has been exhausted, new boreholes are drilled in a location of fresh coal, forming new zones (Lee et al., 2014).

Low-rank coals, such as lignites, have considerable natural permeability and can be exploited for UCG without the need for linking technologies. However, high-rank coals, such as anthracites, are far less permeable, making the gas production rate more limited if UCG is employed (Liang et al., 1999). For the use of high-rank coals in UCG, a method of linking must be employed to increase the permeability and fracture the coal seam (Blinderman and Klimenko, 2007). The boreholes in traditional LVW gasifiers are linked by through forward combustion, reverse combustion, fire linkage, electric linkage, hydrofracturing, and directional drilling to create sizable gasification channels (Blinderman et al., 2008; Liang et al., 1999).

Controlled retractable injection point method

Over the span of a coal seam, the geometry may change, resulting in variable UCG operation and system performance (Nourozieh et al., 2010). In the past, this problem was solved by having multiple injection and/or production wells so that static operating conditions could be accomplished through moving the gasifier zones to fresh coal (Shafirovich and Varma, 2009). CRIP offers an alternative approach where the vertical injection well is not moved, but the injection point is moved within the coal seam to fresh coal when necessary (Klimenko, 2009).

The CRIP method relies on a combination of conventional drilling and directional drilling to access the coal seam and physically form a link between the injection and production wells, without the use of linking technologies utilized in LVW methods (Nourozieh et al., 2010). A vertical section of injection well is drilled to a predetermined depth, after which directional drilling is used to expand the hole and drill along the bottom of the coal seam creating a horizontal injection well (Wang et al., 2009). At the end of the injection well, a gasification cavity is initiated in a horizontal section of the coal seam, creating a localized reactor. The CRIP system utilizes a burner attached to retractable coiled tubing that is used to ignite the coal (Klimenko, 2009). The burner burns through the borehole casing to ignite the coal. The ignition point can be moved to any desired location along the horizontal injection well for the creation of a new gasification cavity after a deteriorating reactor has been deserted (Nourozieh et al., 2010). Typically, the injection point is retracted using a gas burner, which burns a section of the liner at a desired location (Klimenko, 2009). In this manner, accurate control of the gasification process can be obtained. This UCG method has gained popularity in Europe and the United States, but the use of the CRIP method for UCG is fairly new and currently has not become commonly employed (Roddy and Younger, 2010).

10.2.3   Chemical processes

UCG is similar to surface gasification where syngas is produced through the same chemical reactions (Ludwik-Pardała and Stańczyk, 2015; Pana, 2009). The main chemical processes occurring during coal gasification are drying, pyrolysis, combustion, and gasification of the solid hydrocarbon (Stańczyk et al., 2012).

Temperature, pressure, and gas composition vary along the gasification channel. As a result, the chemical reactions that occur in the channel vary with location. Based on the chemical reactions occurring, the gasification channel can be divided into three zones: oxidization, reduction, and dry distillation and pyrolysis (Ludwik-Pardała and Stańczyk, 2015; Yang et al., 2010) as seen in Fig. 10.1. The oxidation zone is located where the gasification agents are introduced to the ignited coal face. In the oxidization zone, multiphase chemical reactions occur between the oxygen in the gasification agents and the carbon in the coal. The highest temperatures in the gasification channel occur in the oxidation zone, due to the degree of exothermic reactions occurring (Lee et al., 2014). The temperature of the coal face in this zone typically ranges from 900 to 1500°C (Bhutto et al., 2013; Perkins and Sahajwalla, 2008). The main chemical reactions, specific to the oxidation zone, include

$$C + O_2 \rightarrow CO_2 + 393.8\,kJ \tag{10.1}$$

$$2C + O_2 \rightarrow 2CO + 231.4\,kJ \tag{10.2}$$

$$2CO + O_2 \rightarrow 2CO_2 + 571.2\,kJ \tag{10.3}$$
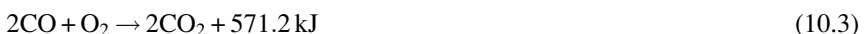
As the oxygen is consumed, the gas stream enters the reduction zone. The reduction zone begins at the same location of the oxidation zone and is typically 1.5–2 times the length. Temperatures typically range from 600°C to 1000°C. In this zone, water vapor and carbon dioxide are reduced to hydrogen gas and carbon monoxide due to high temperatures (Bhutto et al., 2013; Perkins and Sahajwalla, 2005).

The following endothermic reactions occur in the reduction zone (Lee et al., 2014; Yang et al., 2003):

$$C + CO_2 \rightarrow 2CO - 162.4 \, kJ \tag{10.4}$$

$$C + H_2O(g) \rightarrow CO + H_2 - 131.5 \, kJ \tag{10.5}$$

Coal ash and metallic oxides are formed in the gasifier, which act as catalysts, allowing for methanation to occur in the reduction zone:

$$C + 2H_2 \rightarrow CH_4 + 74.9 \, kJ \tag{10.6}$$

Due to the endothermic reactions that occur in the reduction zone, the temperature in the reduction zone decreases until the reduction reactions cannot be sustained.

Once the temperature is reduced, the gas then enters the dry distillation and pyrolysis zone. This zone can extend the entire length of gasification channel, and the temperature in this zone typically ranges from 200°C to 600°C. The main process that occurs in this zone is dewatering of the coal, where water is vaporized, causing the coal to dry and crack. At the beginning of the dry distillation and pyrolysis zone, when temperatures are over 550°C, H_2, CO_2, and CH_4 are still produced. As the flow progresses through the gasification channel, the temperature drops due to heat transfer with the surrounding coal (Yang, 2008). When the temperature is between 350°C and 550°C, high degree of tar and a limited amount of combustible gases are created. Chemical reactions and light polymerization and depolymerization continue to occur as temperatures decrease to approximately 300°C (Bhutto et al., 2013). Within the dry distillation and pyrolysis zone, the coal seam is decomposed into multiple possible volatiles including H_2O, CO_2, CO, C_2H_6, CH_4, H_2, tar, and char (Lee et al., 2014; Yang et al., 2003). As the temperature decreases, some of these volatiles are separated out and become viscous. The UCG process can also have other by-products, including H_2S, As, Hg, Pb, and ash depending on the coal quality, oxidant, and operating conditions (Yang et al., 2010; Shu-qin et al., 2007; Liu et al., 2006a). At the exit of the gasification channel, syngas is typically extracted from the production well between 200°C and 400°C with the volatile composition consisting mostly of CO, CO_2, H_2, and CH_4 (Liu et al., 2006b). The composition of syngas at the end of the gasification channel is highly dependent on the gasification agent, air injection method, and coal composition (Prabu and Jayanti, 2012; Stańczyk et al., 2011).

During operation, the three gasification zones move along the coal seam, ensuring continuous reactions throughout the channel (Lee et al., 2014). A distinguishing feature of UCG, compared with surface gasification, is that drying, reduction, pyrolysis, and oxidation can occur simultaneously within the coal seam (Perkins and Sahajwalla, 2005), and the areas where these reactions occur in the gasification channel overlap.

10.2.4   Physical processes

The high temperatures associated with UCG cause the formation of temperature fields in the coal, localized rock mass, and strata. This leads to changes in the physical and mechanical properties of the coal and rock mass. Differences in thermal expansion between coal grains cause the formation of cracks, which can contribute to the overall gasification cavity and increase gas permeability (Yang, 2003).

Yang and Song (2001) found that the coal and rock densities are greatly affected by temperature and pressure and do not remain constant during operation. Small changes in the physical properties of the coal and rock affect the temperature field and the seepage of underground water. Coal and rock are deformed by fluid pressure in pores and cracks. The fluid content in cracks and pores changes the stress and strain forces within the coal, which changes the elastic modulus and compressive strength of the coal and rock (Bhutto et al., 2013).

The entire process is confined to the space of the coal seam and is sealed from the surface by natural geologic formations or man-made barriers; the coal seam and strata serve, to some extent, as a natural groundwater cleaning system. In general, systems have active pressure control, in which the cavity pressure is held in equilibrium or below that of the surrounding strata (Van der Riet, 2008; Shu-qin et al., 2007). The pressure difference induces flow into the reactor space, which inhibits gasification products from leaking away from the cavity (Wiatowski et al., 2012; Yang, 2008).

10.3   UCG modeling

Though UCG is similar to surface gasification, there are many chemical and physical phenomena that occur during UCG including combustion, gasification, fluid flow, and rock mechanics, and these cannot be controlled or easily monitored (Khan et al., 2015; Seifi, 2014). With UCG, the quantifiable parameters are typically limited to coal and seam properties, gas production rate, gas composition, localized temperature, and operating conditions, which vary between sites and systems (Elahi, 2016; Golec and Ilmurzyńska, 2008). The combination of complex phenomenon, limited measurable parameters, and site specificity makes operation and control of UCG systems difficult compared with surface gasifiers. These difficulties motivated the creation of quantitative models to predict the effects of various physical and operating parameters on system operation and performance.

Numerous laboratory coal block experiments have been conducted including those by Hamanaka et al. (2017), Bhaskaran et al. (2015), Stańczyk et al. (2011), Prabu and Jayanti (2011), Daggupati et al. (2010), Yang (2003), Yeary and Riggs (1987), and Poon (1985). Experiments investigated the effect's oxidant type, injection rate, temperature and pressure, steam-to-oxygen ratio, combustion time and distance between wells on the product gas composition, extraction rate, and temperature. Temperature distribution throughout the coal and cavity formation have also been investigated. Although laboratory-scale experiments can provide insight into the processes involved with UCG, applying the data and creating accurate UCG models have limited

scope since all phenomenon associated with UCG and the interactions between them may not be accurately represented (Upadhye et al., 2006). There are two main types of UCG models, process and global. Process models involve studying specific UCG processes or phenomena, and global models consider the entire UCG process. Early UCG development was limited, and research involved isolated processes including heat transfer, mass transfer and combustion rate, and development of process models (Gunn and Krantz, 1987). As UCG research developed, there has been increased interest in the creation of a global model to simulate UCG.

A global model that encompasses all the processes and phenomena associated with UCG would be composed of submodels that represent injection/production linkage, UCG reactor, groundwater hydrology, ground subsidence and surface facilities, and gas processing. Using these submodels simultaneously would hypothetically provide a complete description of the UCG process but would require significant effort. As such, the submodels have focused on analysis of the characteristics individually using several simplifying assumptions (Khan et al., 2015). Overall, an effective global model would

1. analyze transient temperature profiles within the coal seam;
2. calculate the rate of gas and coal consumption;
3. analyze the influence of coal shrinkage or swelling on UCG operation;
4. determine the pressure and velocity of the gases produced in a coal seam of known porosity and permeability;
5. predict the advancing shape of the combustion front;
6. simulate the cavity growth with time;
7. analyze the effect of reactor pressure, oxidant temperature, injection rate, feed mixture ratio and well spacing on production rate, gas composition, heating value, and cavity dimensions;
8. predict the influence of coal seam dimensions and ash and moisture content on production rate, gas composition, heating value, and cavity dimensions.

There are various approaches to modeling UCG including packed-bed models, coal block models, and channel models (Khan et al., 2015; Seifi, 2014), and numerous quantitative models have been created utilizing these methods. Early models were one-dimensional, but with the improvement of computer hardware and software, two dimension and three dimension have also been created. The following sections describe the various modeling methods and approaches.

10.3.1 Packed bed models

Packed-bed models are the earliest UCG models created. Packed-bed models define the UCG reactor as packed-bed reactor and are primarily applicable to laboratory-scale projects. Packed-bed models simulate gasification in a highly permeable porous medium with a stationary coal bed that is consumed over time (Seifi, 2014). Early models considered the creation of a permeable region between two boreholes through such processes as reverse combustion and hydrofracturing (Uppal et al., 2014).

One-dimensional models were first developed by Winslow (1977) and Thorsness et al. (1978) through the use of a finite difference approach. They achieved good

predictions of gas production, gas composition, and coal consumption from laboratory experiments on crushed coal (Seifi, 2014). Later, Abdel-Hadi and Hsu (1987) and Thorsness and Kang (1986) developed packed-bed models in two-dimensional and compared their results with Thorsness et al. (1978). Recent one-dimensional packed-bed models have been developed by Uppal et al. (2014) and Khadse et al. (2006).

Packed-bed models can accurately represent coal gasification at the laboratory scale; however, they are not appropriate for field-scale UCG processes. The majority of pack-bed models are one-dimensional. Modeling field-scale gasifiers would require three-dimensional analysis, and due to increased reactor size, the computation time would grow significantly (Khan et al., 2015). In addition, packed-bed models do not incorporate geomechanical considerations, including thermomechanical failure, which may have significant effect on UCG operation and cavity growth. Thorsness et al. (1978) made some predictions for field-scale UCG, but a comparison between their results and field-scale data was not performed.

10.3.2   Coal block models

Some models attempt to describe a UCG coal seam as a coal block. In coal block models, it is assumed that gasification begins from one end of a semi-infinite block of coal with lower permeability than in the packed-bed model. Unlike other models, coal block models consider different layers, and for each layer, separate mass and energy balances are typically analyzed resulting in governing equations for mass and energy balances of split boundary types. These models describe the process by movement of defined regions in a coal slab perpendicular to the flow of the injected oxidant gas. These regions usually include the gas film, ash layer, char region, dried coal, and virgin coal. The presence of various regions is due to a low heating rate of the UCG. At a very high heating rate, there is a possibility of drying and combustion fronts existing simultaneously (Tsang, 1980). Mass flux is considered to be diffusion dominant.

Tsang (1980) was the first to use this approached considering the observation of the development of drying, pyrolysis, and gas-char reactions zones around the most permeable path in the coal seam. Tsang (1980) based the approach on the profiles of temperature and saturation and the direction of heat and mass transfer exhibited from the pyrolysis experiments performed by Westmoreland and Forrester (1977). Coal block models that have been created recently include Elahi (2016); Khan et al. (2015); Seifi (2014); Perkins et al. (2003); Perkins and Sahajwalla (2005, 2006); Beath et al. (2000); Van Batenburg et al. (1994).

The main feature of the coal block model is the ability to track the drying and combustion front movement. This model can effectively determine the drying and devolatilization behavior of large coal particles; however, this model approach has not been validated using UCG field trial data (Khan et al., 2015). Numerous coal block models have been created under atmospheric conditions. However, the pressure is significantly higher than atmospheric in UCG field trials (Seifi, 2014). Also, by assuming a semi-infinite coal block, models are typically limited to use with thick coal seams. The majority of the coal block models only include one-dimensional analysis, so information on cavity shape cannot be accurately determined using them (Seifi, 2014; Khan et al., 2015).

10.3.3 Channel models

Channel models overcome the limitation associated with determining UCG cavity shape and size. In channel models, a coal seam is assumed to have a cylindrical geometry with a cylindrical or rectangular channel in the middle of the seam. The channel model assumes that coal is gasified at the perimeter of an expanding permeable channel, and all heterogeneous reactions take place on the channel wall (Seifi, 2014). When determining cavity shape and size, the channel model is preferred (Khan et al., 2015). The channel model is found to better calculate sweep efficiency (Seifi, 2014).

With channel models, the UCG process is characterized by an expanding channel where two separate zones of rubble/char and open channel exist. The approach was developed through the observation that an open-channel structures have developed in different UCG field tests (Van Batenburg et al., 1994; Kuyper and Bruining, 1996). Recent channel models include those developed by Plumb and Klimenko (2010), Luo et al. (2009), Perkins and Sahajwalla (2007), Pirlot et al. (1998), and Kuyper et al. (1994).

For the majority of channel models, there is a high degree of concentration on heat transfer related to UCG. The consideration of natural convection is found to be one of the main phenomena in channel model development. Some models successfully incorporate water influx (Elahi, 2016). Most channel models neglect drying and pyrolysis, which are considered significant in other UCG model approaches. Few channel models include thermomechanical failure. Even without these considerations, many of the channel models have been validated with data from field trials. Most existing channel models are in two dimensions; however, a few three-dimensional models exist that allow cavity shape and size to be visibly obtained (Seifi, 2014).

10.4 UCG with CO_2 capture and storage

Mitigating global climate change is a substantial problem currently. Carbon dioxide (CO_2) emissions associated with fossil-fuel combustion are a significant contributor to global warming. The energy sector is one of the main sources of CO_2 emissions due the predominant use of fossil fuels (International Energy Agency, 2014). A technology that can help decrease emissions is carbon capture and storage. CO_2 is captured, transported to suitable storage location, and typically injected into underground geologic formations (Schiffrin, 2015; Selma et al., 2014). Coal is commonly used throughout the world for energy production; however, coal has the highest CO_2 emissions, per unit energy produced, of the fossil fuels when combusted (Khadse et al., 2007; Nag and Parikh, 2000). To maintain and expand the use of coal, implementation of CCS technologies is becoming vital (Selosse and Ricci, 2017). According to the International Energy Agency, CCS could account for up to 19% of the global emission reductions by 2050 (International Energy Agency, 2010).

CO_2 capture can be performed in three main fashions: precombustion, post combustion, and oxy-firing (Göttlicher and Pruschek, 1997). A broad range of technology options are available for capturing CO_2 including physical absorption, chemical absorption, membrane separation, and cryogenic separation (Ho et al., 2006;

Göttlicher and Pruschek, 1997). In UCG, the syngas compositions, temperatures, and pressures of production streams at the exit of a production well are comparable with those of surface gasifiers, which allow similar methods of CO_2 capture. Due to the similarities to surface gasifiers, it is believed that the CO_2 contained in the UCG syngas could be processed and separated using physical sorbents, within a precombustion arrangement, which has costs comparable with capture technologies commonly utilized in integrated gasification combined cycles (Selosse and Ricci, 2017; Roddy and Younger, 2010; Burton et al., 2006). Postcombustion methods are also applicable and would be directly comparable in terms of cost and performance with typical postcombustion systems utilized in power plants. Oxy-firing options are possible for UCG as well, and within a power-generating scenario, an air separation unit can generate O_2 streams for injection into the UCG and for use in an oxy-fired plant utilizing the syngas (Burton et al., 2006).

The spatial coincidence of geologic carbon storage (GCS) options with UCG opportunities suggests that designers could collocate and combine UCG and GCS systems with high potential for effective CO_2 storage (Roddy and Gonzalez, 2010). In general, these storage options would be the same for conventional carbon sequestration operations, including saline formations and mature oil and gas fields (Friedmann et al., 2009). For UCG systems with CCS, there could exists commonality in site characterization and monitoring for both UCG and CCS projects, where work performed during the design and implementation of one project could be used within the other. Coordinating UCG and CCS designs would improve economics for both projects.

If UCG and CCS are coupled, there is an attractive carbon management scheme that could be implemented, where the produced CO_2 emissions are sequestered back into a coal seam void that has been recently created through UCG activities using existing injection and production wells (Lee et al., 2014; Khadse et al., 2007). When voids are created, they typically collapse, similar to voids produced during longwall coal mining, leaving zones of artificial breccias with high permeability. Suitable containment zones prevent vertical flow of CO_2 to the surface, where storage locations are isolated from the surface by low-permeability strata (known as seals or caprocks, often shales or evaporites) (Roddy and Younger, 2010; Orr, 2009). For a spent UCG system to accommodate CO_2 storage, the void must be at depths below approximately 800–1000 m (Budzianowski, 2012; Friedmann et al., 2009; Orr, 2009). These depths are required so that supercritical pressures and temperatures exist allowing the CO_2 density to be high enough (approximately 500–700 kg/m^3) to limit the storage volume required (Orr, 2009).

The UCG-CCS approach, if successfully implemented, could offer an integrated energy recovery and CO_2 storage system, which exploits a new sequestration resource created during UCG operation. A significant challenge with CCS is the large energy requirement associated with CO_2 capture and compression (Gibbins and Chalmers, 2008; Steinberg, 1999). The pressure after compression is generally high enough to allow for a reduction in pressure during transport while allowing the fluid to be in a liquid state (Ghose and Paul, 2007). If CO_2 storage is accommodated in spent UCG reactors, CO_2 transport and compression requirements decline. CO_2 transport typically accounts for 5%–15% of conventional CCS costs for systems with long

transport distances. Costs could be significantly lowered through the reduced piping and shipping requirements associated with a self-contained UCG-CCS project (Roddy and Gonzalez, 2010). A large portion of the cost for a CCS project is allotted for CO_2 storage, typically 10%–30%, which is mostly used for geologic and geophysical studies and drilling injection wells (Roddy and Gonzalez, 2010; Gibbins and Chalmers, 2008). These tasks are commonly completed during UCG construction and would not necessarily need to be repeated for the implementation of CCS, thus reducing system cost relative to conventional storage methods (Roddy and Gonzalez, 2010).

An important CCS challenge relates to the significant energy requirements associated with removing CO_2 from a gas stream and compressing it to a state suitable for transport and storage. Similar to surface gasifier units, the implementation of precombustion CO_2 removal can be adopted, using current technology. For conventional fossil-fuel power-generating plants, the energy requirements are typically in the range of 10%–40% of the total net plant output, which results in a reduction in plant efficiency (Romano et al., 2010; Thambimuthu et al., 2005; Herzog and Drake, 1998).

As of 2009, it remains unclear if CCS using UCG-produced voids is viable (Friedmann et al., 2009). Until recently, this alternative has received little attention, and there remains substantial scientific uncertainty associated with the technological challenges and environmental risks of storing CO_2 in this manner (Friedmann et al., 2009; Khadse et al., 2007). For full-scale commercialization, extensive research and development is needed to alleviate the uncertainties. Currently, CO_2 sequestration is under development internationally by such organizations as the Intergovernmental Panel on Climate Change and Carbon Sequestration Leadership Forum (Khadse et al., 2007). Recent research studies into CCS and UCG include those by Yang et al. (2016), Kasani and Chalaturnyk (2017), McInnis et al. (2016), Sheng et al. (2016), Prabu and Geeta (2015), Schiffrin (2015), and Verma and Kumar (2015).

10.5   UCG with CCS and auxiliary power plant: case study

One advantage of UCG is the potential for CO_2 emission reductions through the use of CCS technologies. Precombustion CO_2 processing systems used in industry commonly utilize physical absorption-based plants to capture CO_2 from the syngas stream; though less common, chemical absorption, with amine-based solvents, is also used for precombustion carbon capture (Padurean et al., 2012). Amine-based systems are the oldest and most well-understood CO_2 capture technology on the market but are mostly used in postcombustion applications, due to their high efficiency under low-pressure conditions (Letcher, 2008). Even though the efficiency is reduced when amine systems are used in high-pressure applications, Padurean et al. (2012) found that these systems have higher carbon capture rates than physical absorption methods, which would be beneficial within UCG systems due to their large scale and potential for high syngas production rates. The benefit of using amine chemical absorption within UCG systems is increased when the coal, in underground gasifier, is at shallow depths allowing for lowered operating pressures.

Amine systems require a significant amount of thermal energy to separate CO_2 from the amine fluid, in a splitter reboiler, prior to compression (Harkin et al., 2010). The thermal requirements for current and developing amine-based technology range from 1.2 to 4.8 GJ/t CO_2 (1.20–4.80 MJ/kg CO_2), which is supplied by saturated steam at pressures of 310 kPa or higher (Harkin et al., 2010; Romeo et al., 2008; Kvamsdal et al., 2007). In general precombustion systems currently employed in industrial plants can capture 85%–95% of the total CO_2 in a flow (Romano et al., 2010; IPCC, 2005; Thambimuthu et al., 2005). CO_2 compression requires mechanical work to increase its pressure to levels suitable for transport, which typically range from 324 to 432 kJ/kg CO_2 (Aspelund and Jordal, 2007).

The UCG process produces a high-temperature, high-pressure syngas, which can contain many chemical components depending on the coal quality and operating conditions (Liu et al., 2006b). Before the syngas can be used in power generation, it requires processing to remove unwanted gasification products, which requires the syngas to be cooled to a suitable temperature, coinciding with the processing technology utilized. Conventional gas processing temperatures range from 150°C to 600°C (Hamelinck and Faaij, 2002; McMullan et al., 1997).

This case study examines the feasibility of implementing an auxiliary power plant, utilizing the thermal energy removed during the cooling of the syngas, to provide the energy required for CO_2 capture, through amine-based chemical absorption and compression within a UCG system. The amount of power produced by the auxiliary plant is compared with the energy requirements of a UCG system with CO_2 processing, including air injection, CO_2 capture and compression, and pump work within the auxiliary plant. Parametric studies are performed to investigate the effects on system performance of air injection flow rate, power requirements for CO_2 capture and compression, and syngas cooling.

10.5.1 System description

The system considered here for UCG system with CO_2 capture and compression is based on the Newman Spinney P5 field test and illustrated in Fig. 10.3. The Newman Spinney P5 field test is theoretically combined with precombustion CO_2 capture and compression and auxiliary Rankine cycle, as seen in Fig. 10.3. Air is compressed and fed to an underground reactor, where syngas is produced through gasification and conveyed to the surface via a production well. The syngas is cooled in a single-pressure heat recovery steam generator (HRSG). Cooled syngas flows from the HRSG to the gas processing, including water-gas shift and CO_2 capture sections. The cleaned syngas enters a plant to be combusted and used in electricity production. CO created within the underground gasifier is converted to CO_2 within a water-gas shift reactor. The CO_2 from the gasifier and water-gas shift reactor is captured using an amine solvent-based capture process, which requires thermal energy for separating the CO_2 from the working fluid in a splitter reboiler. CO_2 enters a compression process to prepare the CO_2 stream for pipeline transport.

Steam produced in the HRSG is utilized within a Rankine cycle to drive a turbine arrangement producing work. A portion of the steam is extracted from the turbine, as
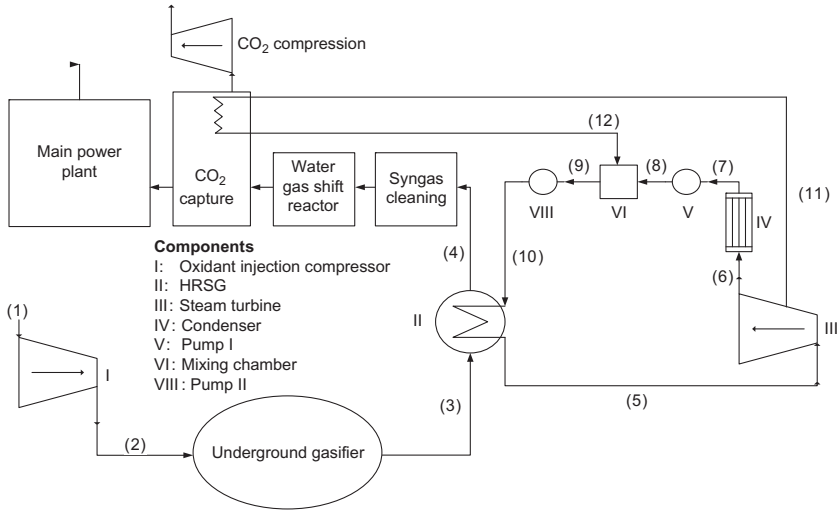
Fig. 10.3 Schematic of UCG system with CO_2 capture and compression and auxiliary plant. Numerical values represent state points in the system.
From Self, S.J., Rosen, M.A., Reddy, B.V., 2013. Energy analysis of underground coal gasification with CO2 capture and auxiliary power production. Proc. Inst. Mech. Eng. A: J. Power Energy 227 (3), 328–337. Used with permission.

saturated steam at an intermediate pressure, to supply thermal energy to the splitter reboiler. The remaining steam exits the turbine and is condensed. The pressure of the condensed steam is raised to the extracted steam pressure. The condensed steam and extracted steam streams are mixed in a mixing chamber, and the fluid pressure is raised to the HRSG pressure by a second pump prior to entering the HRSG.

The Newman Spinney P5 field test is a shallow depth UCG trial that was conducted at Newman Spinney, Derbyshire, during 1958 and 1959. The Newman Spinney P5 field test utilized an open-channel gasifier setup that consisted of four injection bore-holes feeding air at a rate of 1.0–3.0 kg/s per borehole and at injection pressures of 120–190 kPa (Perkins et al., 2003). Typical injection conditions include a flow rate of 2.5 kg/s per borehole at 150 kPa, which are utilized within the study. The generating plant originally connected to the Newman Spinney P5 field test had an output of 1–2 MW and a steady-state value of 1.75 MW (Gibb, 1964).

The syngas composition leaving the gasifier is illustrated in Table 10.1.

10.5.2 Data and assumptions

For the base system, a temperature of 400°C is assumed for the syngas after cooling, which is approaching the upper temperature limit that is appropriate for syngas cleaning technologies (Hamelinck and Faaij, 2002; McMullan et al., 1997). Limited thermal energy is available for transfer across the HRSG under this condition, which helps to demonstrate the practicality of the illustrated system. Selected system parameters used in the case study are shown in Table 10.2.

Table 10.1 Composition of syngas based on dry-gas quantities, at Newman Spinney UCG test plant

Species	Fraction	
	Mass	**Molar**
O_2	0.003	0.001
CO	0.080	0.037
CO_2	0.150	0.044
H_2	0.094	0.606
CH_4	0.008	0.006
N_2	0.665	0.306

Perkins, G., Saghafi, A., Sahajwalla, V., 2003. Numerical Modeling of Underground Coal Gasification and Its Application to Australian Coal Seam Conditions. Australia: University of New South Wales; Gibb, A., 1964. Underground Gasification of Coal. London: Sir Isaac Pitman and Sons.

Table 10.2 System parameters utilized in analysis

Parameter	Value	State point(s)[a]
Isentropic efficiency (%)		
Air compressor	80	n/a
Turbine isentropic	85	n/a
Pump isentropic	90	n/a
Temperature (°C)		
Hot syngas	727	3
Cooled syngas	400	4
HRSG exit steam	500	5
Pressure (kPa)		
HRSG steam	10,000	5, 10
Turbine intermediate exhaust	330	11
Condenser	10	6, 7
Others		
CO_2 removed from syngas stream (% of total)	90	n/a
Splitter reboiler-specific thermal requirement (MJ/kg CO_2)	1.60	n/a
Compression-specific work requirement (kJ/kg CO_2)	378	n/a

[a]State points refer to Fig. 10.3.

The following general assumptions are made in the analysis:

- The system is at steady state.
- Heat transfer from process components to the surroundings is negligible.
- Pressure drops are negligible within the gasifier, HRSG, condenser, and pipe sections.

- All carbon monoxide contained within the syngas stream is converted to carbon dioxide in the water-gas shift reactor.
- The steam/oxidant ratio within the gasifier remains constant.
- The gasifier product gas composition remains constant (Daggupati et al., 2011b).

10.5.3 Analysis

In this and following sections, the state points coincide with states shown in Fig. 10.3.

The air compressor work rate $\dot{W}_{air,comp}$ is determined as follows:

$$\dot{W}_{air,comp} = \dot{m}_{air}(h_2 - h_1) \tag{10.7}$$

where $\dot{m}_{air}$ is the mass flow rate of air entering the compressor and h_1 and h_2 are the specific enthalpies at the inlet and exit of the compressor, respectively.

The syngas composition of a known UCG system is utilized, which allows the mass flow rate of the syngas to be found using the air injection rate, under the assumption that nitrogen within the product gas is introduced entirely through air injection. Using the composition of atmospheric air, the air and nitrogen molar injection rates to the reactor are calculated as follows:

$$\dot{N}_{air} = \frac{\dot{m}_{air}}{M_{air}} \tag{10.8}$$

$$\dot{N}_{N_2} = 0.79\,\dot{N}_{air} \tag{10.9}$$

where $\dot{N}_{air}$ is the molar flow rate of air injected, $\dot{m}_{air}$ is the mass flow rate of air injected, M_{air} is the molar mass of air, and $\dot{N}_{N_2}$ is the molar flow rate of nitrogen gas injected.

Assuming the nitrogen does not react within the gasifier, the flow rate of nitrogen at the inlet of the reactor is the same as at the exit. The mass flow rate of nitrogen $\dot{m}_{N_2}$ is

$$\dot{m}_{N_2} = \dot{N}_{N_2} \cdot M_{N_2} \tag{10.10}$$

where M_{N_2} is the molar mass of nitrogen.

The syngas mass flow rate $\dot{m}_{syngas}$ is estimated using the mass fraction and flow rate of nitrogen in the syngas:

$$\dot{m}_{syngas} = \dot{m}_3 = \frac{\dot{m}_{N_2}}{x_{N_2}} \tag{10.11}$$

where x_{N_2} is the mass fraction of nitrogen.

The specific enthalpy of a mixture of gases is expressed as the sum of the specific enthalpies of each component and their mass fractions. The specific enthalpy at the gasifier exit is evaluated as

$$h_3 = \sum_{i=1}^{n} x_i h_{i,3} \tag{10.12}$$

where h_3 is the total specific enthalpy at state 3, x_i is the mass fraction of species i, and $h_{i,3}$ is the specific enthalpy of species i at state 3. The specific enthalpy at state 4 is found similarly.

The temperature of the water entering the HRSG is set high enough to prevent low-temperature acid formation on the gas side of the HRSG. Steam temperature and pressure at the exit of the HRSG are set to allow for steam formation rates that facilitate power production from the steam turbine while allowing the flow rate and temperature of the steam leaving the turbine, at the intermediate pressure, to be suitable for use in the splitter reboiler. The steam generation rate is calculated using an energy balance:

$$\dot{m}_3(h_3 - h_4) = \dot{m}_5(h_5 - h_{10}) \tag{10.13}$$

where $\dot{m}_3$ and $\dot{m}_5$ are the syngas and steam mass flow rates, respectively. Also, h_3 and h_4 are the specific enthalpies of the syngas across the HRSG, while h_{10} and h_5 are the specific enthalpies of steam at the inlet and exit of the HRSG, respectively.

The work rate produced by the turbine $\dot{W}_{turb}$ is calculated via an energy balance:

$$\dot{W}_{turb} = \dot{m}_5 h_5 - (\dot{m}_{11} h_{11} + \dot{m}_6 h_6) \tag{10.14}$$

The system has two pumps. Pump work rate is calculated for the pressure difference across the pump and specific volume of the fluid at the pump inlet. Specific enthalpy values at the pump outlets are estimated using specific pump work.

The enthalpy at state 9 is found with an energy balance for the mixing chamber:

$$\dot{m}_9 h_9 = \dot{m}_8 h_8 + \dot{m}_{11} h_{12} \tag{10.15}$$

where $\dot{m}_9$ is the mass flow rate of water leaving the mixing chamber, h_9 is the specific enthalpy at the mixing chamber outlet, and h_{12} is the specific enthalpy of condensed steam leaving the splitter reboiler.

The thermal energy rate required for capturing the CO_2 from the syngas stream is estimated using typical thermal requirements for amine absorption:

$$\dot{Q}_{cap} = q_{cap} \cdot \dot{m}_{CO_2,cap} \tag{10.16}$$

where $\dot{Q}_{cap}$ is the thermal energy consumption rate, q_{cap} is the specific thermal energy consumed, and $\dot{m}_{CO_2,cap}$ is the mass flow rate of CO_2 removed from the syngas stream.

The water-gas shift reactor converts CO within the syngas stream into CO_2 prior to the carbon capture process. The chemical reaction for the water-gas shift reaction is

$$CO_{(g)} + H_2O_{(v)} \rightarrow CO_{2(g)} + H_{2(g)} \tag{10.17}$$

It is assumed that 100% of the CO in the syngas stream is converted to CO_2.

The mass flow rate of CO_2 captured is a percentage of the total CO_2 in the syngas stream:

$$\dot{m}_{CO_2,cap} = y_{CO_2} \dot{m}_{CO_2} \tag{10.18}$$

where y_{CO_2} is the percentage of CO_2 extracted from the syngas steam and $\dot{m}_{CO_2}$ is the mass flow rate of CO_2 in the syngas stream after the water-gas shift reactor.

The compression work input rate $\dot{W}_{CO_2,comp}$ is determined using

$$\dot{W}_{CO_2,comp} = w_{CO_2,comp} \cdot \dot{m}_{CO_2,cap} \tag{10.19}$$

where $w_{CO_2,comp}$ is the specific work per kg CO_2 compressed.

The total work input rate is the sum of work rate inputs for the system. That is,

$$\dot{W}_{Required} = \dot{W}_{pump1} + \dot{W}_{pump2} + \dot{W}_{CO_2,comp} + \dot{W}_{air,comp} \tag{10.20}$$

where $\dot{W}_{pump1}$ and $\dot{W}_{pump2}$ are the rate of power consumption of pumps one and two, respectively.

The net work output of the entire UCG system is determined as

$$\dot{W}_{UCG,net} = \dot{W}_{turb} - \dot{W}_{Required} \tag{10.21}$$

To quantify the degree to which the auxiliary plant can supply the work consumed within the system, a parameter called coverage ratio (CR) is introduced. Coverage ratio compares the turbine work output rate to the work consumption rate of the system:

$$CR = \frac{\dot{W}_{turb}}{\dot{W}_{Required}} \tag{10.22}$$

$CR < 1$ implies the output of the auxiliary plant does not meet the requirements, $CR = 1$ implies the auxiliary plant meets the requirements exactly, and $CR > 1$ implies the auxiliary plant output exceeds the requirements.

The energy efficiency of the auxiliary plant, including the reboiler thermal requirements, is defined as

$$\eta_{aux} = \frac{\left(\dot{W}_{turb} + \dot{Q}_{cap}\right) - \left(\dot{W}_{pump1} + \dot{W}_{pump2}\right)}{\dot{m}_5(h_5 - h_{10})} \tag{10.23}$$

10.5.4 Results and discussion

Using the original assumptions and operating conditions, it was found that the mass flow rate of carbon dioxide captured after the water-gas shift reaction is 13.6 kg/s. The work rate requirements for air compression, feedwater pumping, and CO_2 compression are 454 kW, 176 kW, and 5.13 MW, respectively, with a total work requirement of 5.76 MW. The thermal energy rate requirement of the CO_2 capture process is 21.7 kW. The work output rate of the auxiliary plant is 12.1 MW, and the net power output of the system is 6.38 MW, which renders a coverage ratio of 2.11. The thermal

load of the stripper reboiler in the CO_2 capture process is also fulfilled through the extraction of steam at an intermediate pressure within the steam turbine. The auxiliary plant efficiency is 77%.

Overall, the implementation of a Rankine cycle with steam extraction, which provides syngas cooling, within a UCG system appears to be feasible and provides a reasonable net power output. The introduction of this system arrangement could possibly allow for elimination of energy penalties associated with CO_2 capture and compression that would otherwise be incurred by the original power production plant. Inclusion of an auxiliary Rankine cycle also allows an increase in the net output of UCG systems; this would be especially beneficial if the syngas produced by the UCG system has a low heating value, resulting in low power plant outputs. The combination of a Rankine cycle and UCG could improve the economic feasibility of UCG use and environmental impacts, while increasing recoverable coal reserves.

10.5.4.1 Effect of air injection flow rate on system performance

The effect of changing the air injection flow rate on system performance is investigated for air flow rates of 1–3 kg/s per borehole (4–12 kg/s total). It is assumed that the steam/oxidant ratio within the gasifier and all other operating conditions remain constant, allowing for constant syngas composition. The effect of varying air injection flow rate is presented in Table 10.3.

As the injection rate increases, the total energy requirements of air compression, CO_2 capture, CO_2 compression, and feedwater pumping increase linearly, which allows for a constant coverage ratio. This indicates that the air injection rate has a direct relationship with the plant power production and the work rate required by the consuming processes. The change in auxiliary plant output is attributed to the varying amount of energy available for transfer across the HRSG. The increase in work and

Table 10.3 **Effect of air injection rate on selected plant parameters**[a]

$\dot{m}_{air}$ (kg/s)	Work rate (MW)			$\dot{Q}_{cap}$
	$\dot{W}_{Required}$	$\dot{W}_{turb}$	$\dot{W}_{UCG,net}$	
4.00	2.30	4.86	2.55	8.68
4.89	2.82	5.94	3.12	10.6
5.78	3.33	7.01	3.69	12.5
6.67	3.84	8.09	4.25	14.5
7.56	4.35	9.17	4.82	16.4
8.44	4.86	10.3	5.39	18.3
9.33	5.38	11.3	5.96	20.3
10.2	5.89	12.4	6.52	22.2
11.1	6.4	13.5	7.09	24.1
12.0	6.91	14.6	7.66	26.1

[a]Coverage ratio is 2.11 for all air flow rates.

thermal requirements are caused mostly by increased CO_2 flow rates. Although larger injection flow rates do not affect the work coverage ratio, the net work output of the system is found to increase, which implies that for elevated power outputs, increased injection rates are favorable. In contrast, higher injection rates imply that system components have to be larger to accommodate the various loads, which affects the economic feasibility.

10.5.4.2 Effect of varying power requirement for CO_2 capture and compression on system performance

The effect of CO_2 capture and compression energy requirements on the coverage ratio are illustrated in Fig. 10.4. The thermal requirements of the splitter boiler are much higher than the work requirements of the CO_2 compression process; therefore, the variation in the coverage ratio is more significant over the range of applicable CO_2 capture requirements. As thermal requirements of the amine solvent capture process increase, the amount of steam available for use in the turbine beyond the extraction point decreases. This results in a reduced turbine output and associated CR. It is found that the Rankine cycle arrangement, with the given operating conditions, cannot support the entire thermal load of the capture process when the thermal requirement
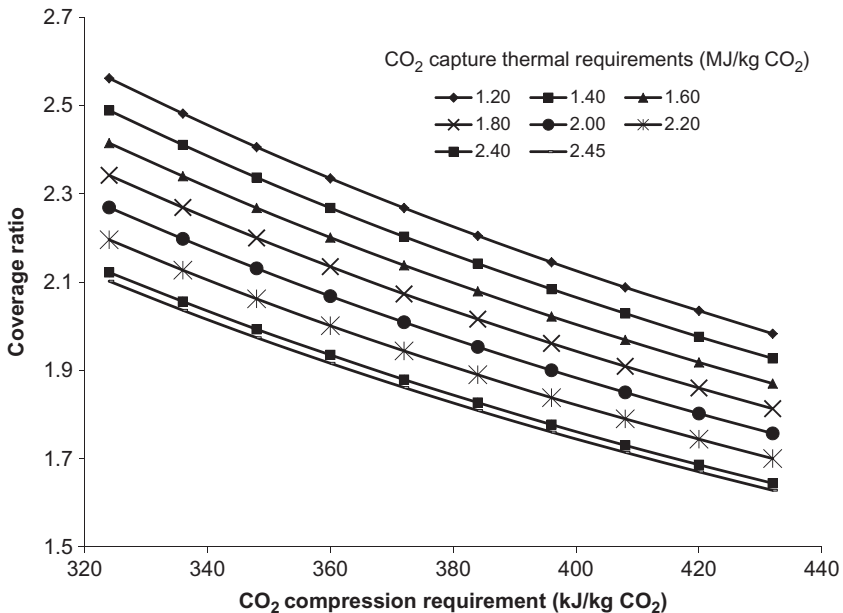
Fig. 10.4 Effect of CO_2 capture and compression requirements on coverage ratio. From Self, S.J., Rosen, M.A., Reddy, B.V., 2013. Energy analysis of underground coal gasification with CO2 capture and auxiliary power production. Proc. Inst. Mech. Eng. A: J. Power Energy 227 (3), 328–337. Used with permission.

approaches 2.46 MJ/kg CO_2. The conditions set for the extracted steam require the flow rate to be higher than that produced by the HRSG. Possible methods of increasing the maximum thermal load the auxiliary system can encounter include increasing the intermediate pressure at which steam is extracted from the turbine and reducing the steam pressure within the HRSG. The effect of using the above options is a reduction in turbine output and CR. As an alternative to reducing turbine output, extracted steam from the Rankine cycle could be used to supply only a portion of the thermal requirements through reducing the flow rate of the extracted steam.

The effect of compression requirements on system performance is not as significant as the thermal requirements of CO_2 capture, because the range of typical compression requirements is considerably less than that of CO_2 capture. The trends resulting from varying the compressor requirements are identical, which suggests that the compression process has an effect on the coverage ratio independent of the thermal requirements within the capturing process. Compared with the base system, the arrangement with the greatest energy requirements reduces the CR and net work output by 26% and 44%, respectively. Utilizing the lowest power requirements can increase CR and net work output by 19% and 20%, respectively. Reducing the energy requirements for the capture and compression processes is preferred in order to maximize the turbine output of the auxiliary plant and the net work output of the system. Exploiting reduced energy requirements is technologically possible but could require increased process complexity and cost.

10.5.4.3   Effect of syngas temperature at the HRSG exhaust on system performance

The effect of varying syngas temperature at the exit of the HRSG on coverage ratio and net work rate is shown in Fig. 10.5. It is found that decreasing the syngas temperature at the HRSG outlet causes CR and net work output rate of the UCG system to increase. Marrero et al. (2002) attained comparable results in a study investigating optimal operating conditions of a triple power cycle that incorporated an HRSG, connected to a Rankine cycle similar to the one in the present study. Similar to the work by Marrero et al. (2002), it is found that reducing the syngas temperature at the HRSG outlet allows for increased thermal energy utilization within the HRSG, resulting in increased steam production and steam turbine output.

Higher HRSG exhaust temperatures reduce the amount of energy available for steam production, resulting in lowered steam flow rates at the turbine inlet. The thermal requirement of the CO_2 capture process remains static, and the energy transferred to the auxiliary plant is decreased, with increasing temperature, which increases the portion of steam used for CO_2 processing compared with the steam produced in the HRSG. As the portion of steam extracted from the turbine at an intermediate pressure increases, the flow rate through the turbine from the inlet to the low-pressure outlet is reduced, which contributes to the reduction in turbine output. In terms of power production, employment of low-temperature gas processing systems would be preferred, to allow power production to be optimized.
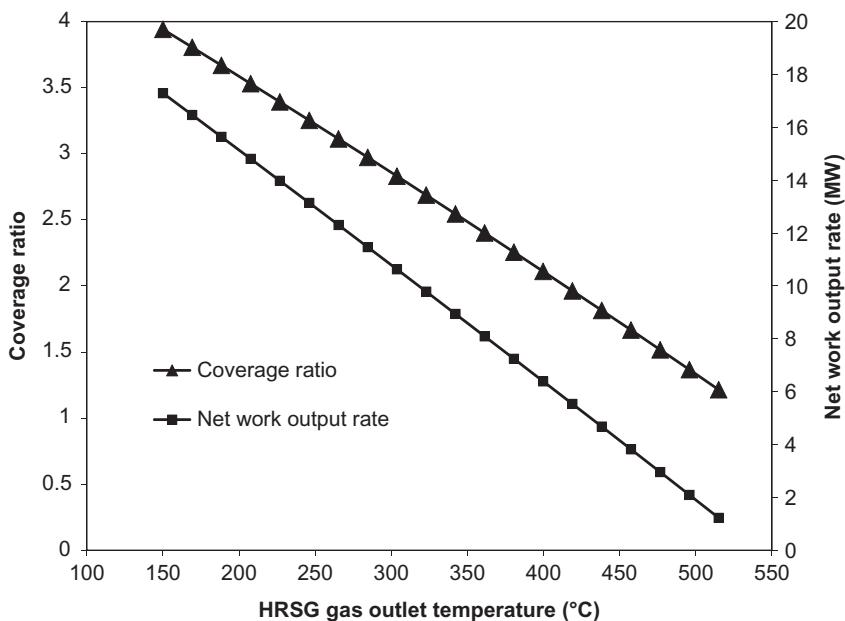
Fig. 10.5 Effect of HRSG outlet syngas temperature on coverage ratio and UCG system net work output.
From Self, S.J., Rosen, M.A., Reddy, B.V., 2013. Energy analysis of underground coal gasification with CO_2 capture and auxiliary power production. Proc. Inst. Mech. Eng. A: J. Power Energy 227 (3), 328–337. Used with permission.

The system arrangement and operating conditions impose restrictions on the upper HRSG exhaust temperature. The temperature must remain below 515°C to provide the steam required by the splitter reboiler with the current model. This is a result of inadequate steam production rates within the HRSG in comparison with the requirements of the splitter reboiler. The restriction could be varied through the use of different turbine extraction conditions and reducing the process requirements. Extracting steam from the turbine at higher pressures would allow for the flow rate to the splitter reboiler to be reduced and the HRSG exhaust temperature restriction to be increased. Increasing the extraction pressure would reduce the turbine work output.

The effect of HRSG exhaust gas temperature on the auxiliary plant efficiency is illustrated in Fig. 10.6. Higher HRSG syngas outlet temperatures result in increased auxiliary plant efficiency (Eq. 10.18). Over the range temperatures considered, the efficiency varies from 59% to 99%. The efficiency increases with syngas temperature because of a reduction in the condenser losses that is a result of reduced flow rates within the condenser. The flow rate through the condenser associated with the highest exhaust gas temperature is zero, and all of the steam produced in the HRSG is used by the splitter reboiler. This suggests that the auxiliary plant could exclude the typical condenser unit and use the splitter reboiler for condensing the steam exiting the
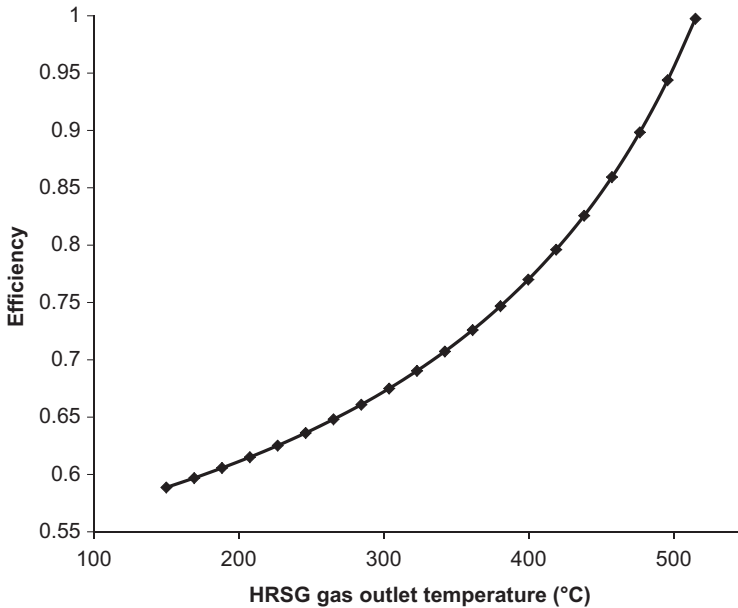
Fig. 10.6 Effect of HRSG outlet syngas temperature on overall plant efficiency. From Self, S.J., Rosen, M.A., Reddy, B.V., 2013. Energy analysis of underground coal gasification with CO_2 capture and auxiliary power production. Proc. Inst. Mech. Eng. A: J. Power Energy 227 (3), 328–337. Used with permission.

turbine. The efficiency approaches 100% due to the model utilized within this study; the assumptions made allow for all of the thermal energy transferred to the steam to be utilized in the associated processes.

10.5.4.4 Concluding comments for case study

When heat is recovered from hot syngas to supply an auxiliary Rankine cycle, sufficient thermal and electric energy are made available for use by processes associated with UCG with CCS. The combination of UCG with CCS and an auxiliary power plant demonstrates benefits in terms of reduced CO_2 emissions and associated energy requirements. The combination of a Rankine cycle and UCG can mitigate CO_2 emissions while improving UCG economic feasibility and increasing recoverable coal reserves.

The turbine output of the auxiliary plant, for the circumstances investigated, is greater than that required by the power-consuming processes, allowing a greater net power delivery from the UCG system considered compared with UCG systems not utilizing this arrangement.

The air injection rate affects the syngas production rate and, therefore, the energy flow rate through the HRSG. The air injection rate also affects the CO_2 production rate and the associated capture and compression energy use rates. Varying the air injection

rate does not affect the coverage ratio of the auxiliary plant, suggesting a linear relationship between air injection rate and the operating conditions for the plant processes. Increasing the air injection rate raises the net work output of the auxiliary system. It appears advantageous to operate this system arrangement with high air injection rates to increase the produced power, although caution is required since high air injection rates require elevated process capacities and component sizes, resulting in increased costs (even though there may be some advantages associated with economy-of-scale effects for larger systems). Air injection rates can be adjusted to optimize the system economic feasibility.

Utilization of CO_2 capture and compression processes with high energy requirements has a negative effect on the coverage ratio of the auxiliary plant, which reduces the system net work output. Under certain operating conditions, an upper limit exists for the thermal requirements of the CO_2 capture process; if exceeded, the system cannot supply all the required thermal energy. When CO_2 capture requirements are below this limit, the auxiliary plant operates correctly and has a positive net work output over the entire range of CO_2 compression energy requirements.

The temperature to which the syngas is cooled, prior to cleaning, has a significant effect on system performance. The temperature of the cooled syngas is a major factor in determining the amount of thermal energy available for steam production. When the syngas is cooled to the lowest temperature typically used in industry, the coverage ratio and the net power output of the UCG system are significantly increased relative to the base system. An upper temperature limit exists, above which the rate of steam production is too low to support the CO_2 capture requirements. When the syngas temperature is set to the upper limit, the overall auxiliary plant efficiency, which includes the CO_2 capture requirement, is increased due to reduced thermal losses in the condenser.

10.6   Closing remarks

Although the earth is an abundant source of coal, a significant amount is currently unrecoverable using conventional mining techniques. Coal is likely to remain used in many countries, increasing the needs for new technologies that permit more environmentally benign extraction and utilization. The use of UCG can help expand recoverable coal reserves, and the syngas it produces can be used as a fuel or chemical feedstock. Fossil fuels typically utilized in power production can then be used for other purposes, or their consumption rates can be reduced.

Numerous models have been created to simulate UCG and the various processes and phenomenon involved. Packed-bed models are applicable for highly permeable porous media. Most of the packed-bed models consider detailed physical and chemical factors, based on experimental and theoretical comparisons. The packed-bed models exhibit good agreement for gas compositions measured from laboratory experiments, but the overall relating of these models to field trials is difficult. The packed-bed and coal block approaches are mostly developed by considering one-dimensional behavior. As a result, information on cavity shape cannot be obtained from these

models. The channel models have the ability to determine cavity shape and size using two- or three-dimensional analysis.

The production of excess power through implementing an auxiliary power plant, utilizing rejected heat from syngas cooling, can help provide the necessary energy requirements for CO_2 capture and compression and other auxiliary processes. The combination of UCG with CCS and auxiliary power plant appears beneficial in terms of reducing CO_2 and providing the associated energy requirements while potentially improving the economic feasibility of UCG and carbon capture.

UCG has the potential to store CO_2 within voids created during its operation, which reduces the need for transport and storage site identification. In essence, UCG could provide a cost-effective, near-zero-carbon energy source through the use of a self-contained system with a closed carbon loop.

UCG offers a coal extraction and conversion method in a single process that avoids many of the challenges associated with conventional mining practices. Underground coal gasification has a high potential for integration with CCS using conventional methods utilized in power production due to similarities with surface gasifier units. Although the technology is not widely employed currently, additional research and testing of UCG systems will likely improve modeling and analysis methods and expand the use of UCG systems globally.

Acknowledgments

References

Abdel-Hadi, E.A.A., Hsu, T.R., 1987. Computer modeling of fixed bed underground coal gasification using the permeation method. J. Energy Resour. Technol. 109 (1), 11–20.

Aleklett, K., Hook, M., Jakobsson, K., Lardelli, M., Snowden, S., Soderbergh, B., 2010. The peak of the oil age: analyzing the world oil production reference scenario in World Energy Outlook 2008. Energy Policy 38, 1398–1414.

Aspelund, A., Jordal, K., 2007. Gas conditioning: the interface between CO_2 capture and transport. Int. J. Greenhouse Gas Control 1 (3), 343–354.

Beath, A., Wendt, M., Mallet, C., 2000. Underground coal gasification method for reducing the greenhouse impact of coal utilization. In: Proceedings of Fifth International Conference on Greenhouse Gas Control Technologies, Cairns, QLD, Australia, 13 August 2000, pp. 1307–1312.

Bhaskaran, S., Samdani, G., Aghalayam, P., Ganesh, A., Singh, R.P., Sapru, R.K., Jain, P.K., Mahajani, S., 2015. Experimental studies on spalling characteristics of Indian lignite coal in context of underground coal gasification. Fuel 154, 326–337.

Bhutto, A.W., Bazmi, A.A., Zahedi, G., 2013. Underground coal gasification: from fundamentals to applications. Prog. Energy Combust. Sci. 39, 189–214.

Birol, F. (Ed.), 2014. World Energy Outlook 2014. International Energy Agency, Paris.

Blinderman, M.S., 2015. Underground coal gasification: commodity: coal. Inside Mining 8 (2), 10–11.

Blinderman, M.S., Klimenko, A.Y., 2007. Theory of reverse combustion linking. Combust. Flame 150, 232–245.

Blinderman, M.S., Saulov, D.N., Klimenko, A.Y., 2008. Forward and reverse combustion linking in underground coal gasification. Energy 33, 446–454.

Brown, K.M., 2012. In situ coal gasification: an emerging technology. J. Am. Soc. Min. Reclam. 1 (1), 103–122.

Budzianowski, W.M., 2012. Value-added carbon management technologies for low CO_2 intensive carbon-based energy vectors. Energy 41, 280–297.

Burton, E., Friedmann, J., Upadhye, R., 2006. Best Practices in Underground Coal Gasification. Lawrence Livermore National Laboratory, Livermore, CA.

Chapman, I., 2014. The end of peak oil? Why the topic is still relevant despite recent denials. Energy Policy 64, 93–101.

Couch, G., 2009. Underground Coal Gasification. IEA Clean Coal Centre, London.

Daggupati, S., Mandapati, R.N., Mahajani, S.M., Ganesh, A., Mathur, D.K., Sharma, R.K., Aghalayam, P., 2010. Laboratory studies on combustion cavity growth in lignite coal blocks in the context of underground coal gasification. Energy 35 (6), 2374–2386.

Daggupati, S., Mandapati, R.N., Mahajani, S.M., Ganesh, A., Pal, A.K., Sharma, R.K., Aghalayam, P., 2011a. Compartment modeling for flow characterization of underground coal gasification cavity. Ind. Eng. Chem. Res. 50 (1), 277–290.

Daggupati, S., Mandapati, R.N., Mahajani, S.M., Ganesh, A., Sapru, R.K., Sharma, R.K., Aghalayam, P., 2011b. Laboratory studies on cavity growth and product gas composition in the context of underground coal gasification. Energy 36 (3), 1776–1784.

Elahi, S.M., 2016. Geomechanical Modeling of Underground Coal Gasification. Doctoral DissertationUniversity of Calgary.

Energy Information Administration, 2014. International Energy Outlook 2014. U.S. Department of Energy, Washington, DC.

Friedmann, S.J., Upadhye, R., Kong, F.M., 2009. Prospects for underground coal gasification in carbon-constrained world. Energy Procedia 1 (1), 4551–4557.

García-Olivares, A., Ballabrera-Poy, J., 2015. Energy and mineral peaks, and a future steady state economy. Technol. Forecast. Soc. Chang. 90, 587–598.

Ghose, M.K., Paul, B., 2007. Underground coal gasification: a neglected option. Int. J. Environ. Stud. 64 (6), 777–783.

Gibb, A., 1964. Underground Gasification of Coal. Sir Isaac Pitman and Sons, London.

Gibbins, J., Chalmers, H., 2008. Carbon capture and storage. Energy Policy 36, 4317–4322.

Gnanapragasam, N.V., Reddy, B.V., Rosen, M.A., 2009. Hydrogen production from coal using coal direct chemical looping and syngas chemical looping combustion systems: assessment of system operation and resource requirements. Int. J. Hydrog. Energy 34 (6), 2606–2615.

Gnanapragasam, N.V., Reddy, B.V., Rosen, M.A., 2010. Hydrogen production from coal gasification for effective downstream CO_2 capture. Int. J. Hydrog. Energy 35 (10), 4933–4943.

Golec, T., Ilmurzyńska, J., 2008. Modeling of gasification process. In: Borowiecki, T., Kijeński, J., Machnikowski, J., Ściążko, M. (Eds.), Clean Energy, Chemical Products and Fuels from Coal: Evaluation of the Development Potential Clean Energy, Chemical Products and Fuels from Coal: Evaluation of the Development Potential. Institute for Chemical Processing of Coal, Zabrze, Poland, pp. 170–187.

Göttlicher, G., Pruschek, R., 1997. Comparison of CO_2 removal systems for fossil-fuelled power plant processes. Energy Convers. Manag. 38, 173–178.

Gunn, R.D., Krantz, W.B., 1987. Underground coal gasification: development of theory, laboratory experimentation, interpretation, & correlation with the Hanna field tests. Final Report No. DOE/LC/10442–2545. U.S. Department of Energy, Morgantown, WV.

Hamanaka, A., Su, F.Q., Itakura, K.I., Takahashi, K., Kodama, J.I., Deguchi, G., 2017. Effect of injection flow rate on product gas quality in underground coal gasification (UCG) based on laboratory scale experiment: development of co-axial UCG system. Energies 10 (2), 238–259.

Hamelinck, C.N., Faaij, A.P.C., 2002. Future prospects for production of methanol and hydrogen from biomass. J. Power Sources 111 (1), 1–22.

Hammond, G.P., 2000. Energy, environment and sustainable development: a UK perspective. Trans. Inst. Chem. Eng. B 78, 304–323.

Harkin, T., Hoadley, A., Hooper, B., 2010. Reducing the energy penalty of CO_2 capture and compression using pinch analysis. J. Clean. Prod. 18 (9), 857–866.

Herzog, H.J., Drake, E.M., 1998. CO_2 capture, reuse and sequestration technologies for mitigating global climate changeCO2 capture, reuse and sequestration technologies for mitigating global climate change. In: Proc. 23rd International Technical Conference on Coal Utilization and Fuel Systems, Clearwater, FL, March 9–13, 1998, pp. 615–626.

Ho, M.T., Allinson, G., Wiley, D.E., 2006. Comparison of CO_2 separation options for geo-sequestration: are membranes competitive? Desalination 192, 288–295.

Imran, M., Kumar, D., Kumar, N., Qayyum, A., Saeed, A., Bhatti, M.S., 2014. Environmental concerns of underground coal gasification. Renew. Sust. Energ. Rev. 31, 600–610.

International Energy Agency, 2010. Energy Technology Perspectives, 2010: Scenarios and Strategies to 2050. International Energy Agency, Paris.

International Energy Agency, 2014. Key World Energy Statistics. International Energy Agency, Paris.

IPCC, 2005. IPCC Special Report on Carbon Dioxide Capture and Storage. Cambridge University Press, Cambridge.

Kasani, H.R., Chalaturnyk, R.J., 2017. Coupled reservoir and geomechanical simulation for a deep underground coal gasification project. J. Nat. Gas Sci. Eng. 37, 487–501.

Kempka, T., Plötz, M.L., Schlüter, R., Hamann, J., Deowan, S.A., Azzam, R., 2011. Carbon dioxide utilisation for carbamide production by application of the coupled UCG-urea process. Energy Procedia 4, 2200–2205.

Khadse, A.N., Qayyumi, M., Mahajani, S.M., Aghalayam, P., 2006. Reactor model for the underground coal gasification (UCG) channel. Int. J. Chem. React. Eng. 4 (1), A37.

Khadse, A., Qayyumi, M., Mahajani, S.M., Aghalayam, P., 2007. Underground coal gasification: a new clean coal utilization technique for India. Energy 32, 2061–2071.

Khan, M.M., Mmbaga, J.P., Shirazi, A.S., Liu, Q., Gupta, R., 2015. Modelling underground coal gasification: a review. Energies 8 (11), 12603–12668.

Klimenko, A.Y., 2009. Early ideas in underground coal gasification and their evolution. Energies 2, 456–476.

Kuyper, R.A., Bruining, J., 1996. Simulation of underground gasification of thin coal seams. In Situ 20, 311–346.

Kuyper, R.A., Van Der Meer, T.H., Hoogendoorn, C.J., 1994. Turbulent natural convection flow due to combined buoyancy forces during underground gasification of thin coal layers. Chem. Eng. Sci. 49 (6), 851–861.

Kvamsdal, H.M., Jordal, K., Bolland, O.A., 2007. Quantitative comparison of gas turbine cycles with CO_2 capture. Energy 32 (1), 10–24.

Lee, S., Speight, J.G., Loyalka, S.K., 2014. Handbook of Alternative Fuel Technologies, second ed. CRC, Boca Raton, FL.

Letcher, T.M., 2008. Future Energy: Improved, Sustainable and Clean Options for our Planet. Elsevier, Oxford.

Liang, J., Liu, S., Yu, L., 1999. Trial study on underground coal gasification of abandoned coal resourcerial study on underground coal gasification of abandoned coal resource. In: Xie, H., Golosinki, T.S. (Eds.), Proceedings of the '99 International Symposium on Mining Science and Technology. Beijing, August 1999. A.A. Balkema, Rotterdam, pp. 271–275.

Liu, S., Wang, Y., Yu, L., Oakey, J., 2006a. Thermodynamic equilibrium study of trace element transformation during underground coal gasification. Fuel Process. Technol. 87, 209–215.

Liu, S., Wang, Y., Yu, L., Oakey, J., 2006b. Volatilization of mercury, arsenic and selenium during underground coal gasification. Fuel 85 (10–11), 1550–1558.

Ludwik-Pardała, M., Stańczyk, K., 2015. Underground coal gasification (UCG): an analysis of gas diffusion and sorption phenomena. Fuel 150, 48–54.

Luo, Y., Coertzen, M., Dumble, S., 2009. Comparison of UCG cavity growth with CFD model predictions. In: Proceedings of the 7th International Conference on CFD in the Minerals and Process Industries, CSIRO, Melbourne, Australia, 9–11 December 2009.

Marrero, I.O., Lefsaker, A.M., Razani, A., Kim, K.J., 2002. Second law analysis and optimization of a combined triple power cycle. Energy Convers. Manag. 43 (4), 557–573.

McInnis, J., Singh, S., Huq, I., 2016. Mitigation and adaptation strategies for global change via the implementation of underground coal gasification. Mitig. Adapt. Strateg. Glob. Chang. 21 (4), 479–486.

McMullan, J.T., Williams, B.C., Sloan, E.P., 1997. Clean coal technologies. Proc. Inst. Mech. Eng. A: J. Power Energy 211 (1), 95–107.

Mehmood, S., Reddy, B.V., Rosen, M.A., 2014. Analysis of emissions and furnace exit gas temperature for a biomass co-firing coal power generation system. Res. J. Environ. Sci. 8 (5), 274–286.

Mehmood, S., Reddy, B.V., Rosen, M.A., 2015. Exergy analysis of a biomass co-firing based pulverized coal power generation system. Int. J. Green Energy 12 (5), 461–478.

Nag, B., Parikh, J., 2000. Indicators of carbon emission intensity from commercial energy use in India. Energy Econ. 22, 441–461.

Nakaten, N., Islam, R., Kempka, T., 2014. Underground coal gasification with extended CO_2 utilization: an economic and carbon neutral approach to tackle energy and fertilizer supply shortages in Bangladesh. Energy Procedia 63, 8036–8043.

Nourozieh, H., Kariznovi, M., Chen, Z., Abedi, J., 2010. Simulation study of underground coal gasification in Alberta reservoirs: geological structure and process modeling. Energy Fuel 24, 3540–3550.

Orr, F.M., 2009. Onshore geologic storage of CO_2. Science 325 (5948), 1656–1658.

Padurean, A., Cormos, C.C., Agachi, P.S., 2012. Pre-combustion carbon dioxide capture by gas–liquid absorption for Integrated Gasification Combined Cycle power plants. Int. J. Greenhouse Gas Control 7, 1–11.

Pana, C., 2009. Review of Underground Coal Gasification With Reference to Alberta's Potential. Energy Resources Conservation Board, Edmonton, AB, Canada.

Perkins, G., Sahajwalla, V., 2005. A mathematical model for the chemical reaction of a semi-infinite block of coal in underground coal gasification. Energy Fuel 19, 1679–1692.

Perkins, G., Sahajwalla, V., 2006. Numerical study of the effects of operating conditions and coal properties on cavity growth in underground coal gasification. Energy Fuel 20 (2), 596–608.

Perkins, G., Sahajwalla, V., 2007. Modelling of heat and mass transport phenomena and chemical reaction in underground coal gasification. Chem. Eng. Res. Des. 85 (3), 329–343.

Perkins, G., Sahajwalla, V., 2008. Steady-state model for estimating gas production from underground coal gasification. Energy Fuel 22, 3902–3914.

Perkins, G., Saghafi, A., Sahajwalla, V., 2003. Numerical modeling of underground coal gasification and its application to Australian coal seam conditions. University of New South Wales, Australia.

Pirlot, P., Pirard, J.P., Coeme, A., Mostade, M., 1998. A coupling of chemical processes and flow in view of the cavity growth simulation of an underground coal gasifier at great depth. In Situ 22 (2), 141–156.

Plumb, O.A., Klimenko, A., 2010. The stability of evaporating fronts in porous media. J. Porous Media 13 (2), 145–155.

Poon, S.S.K., 1985. The Combustion Rates of Texas Lignite Cores. Masters Thesis, The University of Texas at Austin, Austin, TX.

Prabu, V., Geeta, K., 2015. CO_2 enhanced in-situ oxy-coal gasification based carbon-neutral conventional power generating systems. Energy 84, 672–683.

Prabu, V., Jayanti, S., 2011. Simulation of cavity formation in underground coal gasification using bore hole combustion experiments. Energy 36 (10), 5854–5864.

Prabu, V., Jayanti, S., 2012. Integration of underground coal gasification with a solid oxide fuel cell system for clean coal utilization. Int. J. Hydrog. Energy 37, 1677–1688.

Roddy, D., Gonzalez, G., 2010. Underground coal gasification (UCG) with carbon capture and storage (CCS). In: Hester, R.E., Harrison, R.M. (Eds.), Issues in Environmental Science and Technology. vol. 29. Royal Society of Chemistry, Cambridge, pp. 102–125.

Roddy, D.J., Younger, P.L., 2010. Underground coal gasification with CCS: a pathway to decarbonising industry. Energy Environ. Sci. 3, 400–407.

Romano, M.C., Chiesa, P., Lozza, G., 2010. Pre-combustion CO_2 capture from natural gas power plants, with ATR and MDEA processes. Int. J. Greenhouse Gas Control 4 (5), 785–797.

Romeo, L.M., Espatolero, S., Bolea, I., 2008. Designing a supercritical steam cycle to integrate the energy requirements of CO_2 amine scrubbing. Int. J. Greenhouse Gas Control 2 (4), 563–570.

Rosen, M.A., Bulucea, C.A., Mastorakis, N.E., Bulucea, C.A., Jeles, A.C., Brindusa, C.C., 2015. Evaluating the thermal pollution caused by wastewaters discharged from a chain of coal-fired power plants along a river. Sustainability 7 (5), 5920–5943.

Schiffrin, D.J., 2015. The feasibility of in situ geological sequestration of supercritical carbon dioxide coupled to underground coal gasification. Energy Environ. Sci. 8 (8), 2330–2340.

Seifi, M., 2014. Simulation and Modeling of Underground Coal Gasification Using Porous Medium Approach. Doctoral Dissertation, University of Calgary.

Self, S.J., Reddy, B.V., Rosen, M.A., 2012. Review of underground coal gasification technologies and carbon capture. Int. J. Energy Environ. Eng. 3 (16), 1–8.

Self, S.J., Rosen, M.A., Reddy, B.V., 2013. Energy analysis of underground coal gasification with CO_2 capture and auxiliary power production. Proc. Inst. Mech. Eng. A: J. Power Energy 227 (3), 328–337.

Selma, L., Seigo, O., Dohle, S., Siegrist, M., 2014. Public perception of carbon capture and storage (CCS): a review. Renew. Sust. Energ. Rev. 38, 848–863.

Selosse, S., Ricci, O., 2017. Carbon capture and storage: Lessons from a storage potential and localization analysis. Appl. Energy 188, 32–44.

Shafirovich, E., Varma, A., 2009. Underground coal gasification: a brief review of current status. Ind. Eng. Chem. Res. 48, 7865–7875.

Sheng, Y., Benderev, A., Bukolska, D., Eshiet, K.I.I., Gama, C.D., Gorka, T., Green, M., Hristov, N., Katsimpardi, I., Kempka, T., Kortenski, J., 2016. Interdisciplinary studies on the technical and economic feasibility of deep underground coal gasification with CO_2. Mitig. Adapt. Strateg. Glob. Chang. 21 (4), 595–627.

Shu-qin, L., Jing-gang, L., Mei, M., Dong-lin, D., 2007. Groundwater pollution from underground coal gasification. J. China Univ. Min. Technol. 17 (4), 467–472.

Stańczyk, K., Howaniec, N., Smoliński, A., Świadrowski, J., Kapusta, K., Wiatowski, M., Grabowski, J., Rogut, J., 2011. Gasification of lignite and hard coal with air and oxygen enriched air in a pilot scale ex situ reactor for underground gasification. Fuel 90, 1953–1962.

Stańczyk, K., Kapusta, K., Wiatowski, M., Swiadrowski, J., Smolinski, A., Rogut, J., Kotyrba, A., 2012. Experimental simulation of hard coal underground gasification for hydrogen production. Fuel 91 (1), 40–50.

Steinberg, M., 1999. Fossil fuel decarbonization technology for mitigating global warming. Int. J. Hydrog. Energy 24, 771–777.

Thambimuthu, K., Soltanieh, M., Abanades, J.C., 2005. Capture of CO_2. In: Metz, B., Davidson, O., De Coninck, H., Loos, M., Meyer, L. (Eds.), Carbon Dioxide Capture and Storage. Cambridge University Press, New York.

Thorsness, C.B., Kang, S.W., 1986. General-Purpose, Packed-Bed Model for Analysis. Lawrence Livermore Laboratory, Livermore, CA. UCID-20731.

Thorsness, C.B., Grens, E.A., Sherwood, A., 1978. One-Dimensional Model for In Situ Coal Gasification. Lawrence Livermore Laboratory, Livermore, CA. UCRL-52523.

Tsang, T.H.T., 1980. Modeling of Heat and Mass Transfer During Coal Block Gasification. Ph. D. ThesisUniversity of Texas at Austin, Austin, TX.

Upadhye, R., Burton, E., Friedmann, J., 2006. Science and Technology Gaps in Underground Coal Gasification. Lawrence Livermore Laboratory, Livermore, CA. 222523.

Uppal, A.A., Bhatti, A.I., Aamir, E., Samar, R., Khan, S.A., 2014. Control oriented modeling and optimization of one dimensional packed bed model of underground coal gasification. J. Process Control 24 (1), 269–277.

Van Batenburg, D.W., Biezen, N., Bruining, J., 1994. New channel model for underground gasification of thin, deep coal seams. In Situ 18 (4), 419–451.

Van der Riet, M., 2008. Underground coal gasificationUnderground coal gasification. In: Proceedings of the SAIEE Generation Conference, 19 February 2008, Eskom College, Midrand, South Africa.

Verma, A., Kumar, A., 2015. Life cycle assessment of hydrogen production from underground coal gasification. Appl. Energy 147, 556–568.

Walker, L., 1999. Underground coal gasification: a clean coal technology ready for development. The Australian Coal Review 8, 19–21.

Wang, G.X., Wang, Z.T., Feng, B., Rudolph, V., Jiao, J.L., 2009. Semi-industrial tests on enhanced underground coal gasification at Zhong-Liang-Shan coal mine. Asia-Pac. J. Chem. Eng. 4, 771–779.

Westmoreland, P.R., Forrester, R.C., 1977. Pyrolysis of large coal blocks: implications of heat and mass transport effects for in-situ gasification. ACS Div. Fuel Chem. 22 (1), 93–101.

Wiatowski, M., Stańczyk, K., Świądrowski, J., Kapusta, K., Cybulski, K., Krause, E., Grabowski, J., Rogut, J., Howaniec, N., Smoliński, A., 2012. Semi-technical underground coal gasification (UCG) using the shaft method in Experimental Mine "Barbara." Fuel 99, 170–179.

Winslow, A.M., 1977. Numerical model of coal gasification in a packed bed. International Symposium on Combustion 16 (1), 503–513.

World Energy Council, 2013. Survey of Energy Resources 2013. World Energy Council, London.

Yang, L.H., 2003. Model and calculation of dry distillation gas movement in the process of underground coal gasification. Numer. Heat Transf. B: Fundamentals 43 (6), 587–604.

Yang, L.H., 2008. A review of the factors influencing the physicochemical characteristics of underground coal gasification. Energy Sources, Part A 30 (11), 1038–1049.

Yang, L.H., Song, D.Y., 2001. Study on the Method of Seepage Combustion in Underground Coal Gasification. China University of Mining and Technology Press, China.

Yang, L.H., Liang, J., Yu, L., 2003. Clean coal technology: study on the pilot project experiment of underground coal gasification. Energy 28, 1445–1460.

Yang, L.H., Pang, X.L., Liu, S.Q., Chen, F., 2010. Temperature and gas pressure features in the temperature-control blasting underground coal gasification. Energy Sources, Part A 32, 1737–1746.

Yang, D., Koukouzas, N., Green, M., Sheng, Y., 2016. Recent development on underground coal gasification and subsequent CO_2 storage. J. Energy Inst. 89 (4), 469–484.

Yeary, D.L., Riggs, J.B., 1987. Study of small-scale cavity growth mechanisms for UCG. In Situ 11 (4), 305–327.

Further reading

Breault, R.W., 2010. Gasification processes old and new: a basic review of the major technologies. Energies 3, 216–240.

Mohr, S.H., Evans, G.M., 2009. Forecasting coal production until 2100. Fuel 88, 2059–2067.

Peng, F.F., Lee, I.C., Yang, R.Y.K., 1995. Reactivities of in situ and ex situ coal chars during gasification in steam at 1000-1400°C. Fuel Process. Technol. 41, 233–251.

Shackley, S., Mander, S., Reiche, A., 2006. Public perceptions of underground coal gasification in the United Kingdom. Energy Policy 34, 3423–3433.

Environmental performance of underground coal gasification

<div style="text-align:right">**11**</div>

E.V. Dvornikova
Ergo Exergy Technology Inc., Montreal, QC, Canada

11.1 Introduction

In modern-day industrial applications, with sustained growth of production and energy consumption, the issues related to the impact on the environment gain prominence in analyzing the fuel and energy complex, including the effects on the hydrosphere, whose protection has over the last several decades been one of the pressing tasks confronting contemporary society.

Today's technological level of mining and use of solid fuels often results in a gradual transformation of some coal mining areas into ecological disaster zones.

It is well known that during blasting operations in open-pit mines, for each ton of explosives, depending on its type and specific consumption rate, 0.090–0.282 t of dust is thrown up into the air and 0.001–0.104 t of carbon oxides (A collection of methods for calculating air emissions in various industries, 1986).

When operating heavy mining machinery, such as excavators, bulldozers, conveyors, belt elevators, and dumpers, dust emissions range from 200 to 3000 kg/t of coal (accounting for dust suppression).

Burning waste rock spoils emits a significant amount of noxious gases: CO, from 0.8 to 1.0 t per day; CO_2, from 2.0 to 7.5 t per day; O_2, from 0.03 to 0.1 t per day; H_2, 0.02 t per day; and O_X, from 0.03 to 0.13 t per day. The total aggregate concentration of these gases in the air can reach 12–76 mg/m^3 (Chekina, 1994).

Effluent with acidic pH and containing high concentration of TDS, often resulting from metamorphosed groundwater during coal mining, is one of the major contributors to environmental degradation. The amount of waste water with a concentration of TDS above 1000 mg/L is 44%, while groundwater with TDS values over 3000 mg/L constitutes as high as 34% of the total volume of water pumped from the mine drainage sumps. Mine drainage related to coal mining in Russia accounts for more than half of all industrial waste water discharge. US data show that acid mine drainage carries out more than 4 million tons of acid per year from operating and abandoned coal mines, with nearly 10,000 km of rivers and streams, and about 12,000 ha of water surface contaminated with acidic or alkaline water from coal mines.

The main groundwater contaminants in mine and quarry operations are the concentration of TDS and total suspended solids (TSS) (Parakhonsky, 1992). According to the VNIIOS Ugol Research Institute, only 5% of underground and open-pit coal mines have groundwater with a concentration of TDS up to 1 g/L (Technological schemes of

cleaning from suspended solids and disinfection of mine waters, 1985). For the Kuzbass mines, the concentration of TSS in mine water can be as high as 1500 mg/L, with TDS values ranging from 0.5 to 1.5 g/L.

The most common organic contaminants found in mine and quarry water are phenols and petroleum compounds. The concentration of phenols can be as high as 0.01 mg/L and petroleum compounds as high as 13 mg/L. In some cases, exceedances of the concentration of concern were recorded for the following trace elements: cadmium 3–11 times, nickel 2–18 times, copper 10–20 times, zinc and manganese 2–200 times, chromium 5–123 times, and cobalt 2–27 times (Technological schemes of cleaning from suspended solids and disinfection of mine waters, 1985).

Both surface water and groundwater may be susceptible to contamination. Groundwater resource depletion may extend over enormous areas. For example, after the design depth of the open-pit mine was reached (500 m) in the Gubkinsko-Stoylensky oblast of the Kursk Magnetic Anomaly, the cone of regional groundwater depression had a radius of over 50 km.

One of the directions in improving the environmental performance of coal mining is the development of alternative, nonconventional techniques of in situ processing of coal into more ecologically friendly fuels (liquid and gaseous hydrocarbon products). One promising avenue is development and implementation of coal mining involving well drilling, of which underground coal gasification (UCG) is a prominent mining method.

In addition, the obvious and prodigious advantage of UCG is the feasibility of mining uneconomic coal resources that are not suitable for conventional mining and coal that occurs as local lenses.

11.2   UCG and environment

The suitability of employing the UCG method in a specific mining and geologic setting is largely a function of the effects that the UCG activities might have on the environment during all of the process stages.

Protection of the environment during UCG operations entails protection of the air, land, surface water, and groundwater.

Beyond doubt, the UCG technology offers advantages such as preserving the earth's surface and fertile topsoil; no additional stockpile areas are required for waste rock spoils or for coal storage. Using conventional mining techniques, the latter two represent one of the principal sources of environmental contamination.

The UCG method is also intrinsically socially beneficial compared with conventional coal mining techniques, as it eliminates the need for miners to be exposed to the extreme dangers and risks of underground coal mining.

UCG product gas is scrubbed and cooled and gas condensate treated and utilized in a closed-loop process without discharging gas directly to the atmosphere. A biological dephenolization unit was operated at the Yuzhno-Abinskaya UCG plant at the Kuznetsk coal basin since 1976 scrubbing 99.5% of phenols from the condensate,

reducing the concentration of phenols from 2000 to 5 mg/L. Diluted treated water was discharged into the main city sewer interceptor line.

To prevent the ground surface depressions from forming, a special methodology was developed for calculating the safe dimensions of the coal pillars, which must be left in place. The optimal correlation between the depth of coal mining and coal seam thickness was determined, whereby no groundwater and gas-transmitting fractures developed within the overburden all the way up to the ground surface, which prevents significant gas leakage and gas bursts into the atmosphere. The spent wells are plugged and abandoned properly.

In addition, at the energy consumption stage, most of the environmental impact factors are deemed as less detrimental than solid fuels.

As a fuel, UCG product gas contributes to atmospheric contamination considerably less than coal. Table 11.1 displays the comparative values of the concentrations of air pollutants during combustion of various types of fuels. As can be seen from the table, no solid particles are present in the combustion products of syngas, while the nitrogen and carbon oxide content is lower than when burning solid and liquid fuels. The concentration of nitrogen oxides does not exceed 0.2 g/m^3, with carbon oxides at 0.15–1.1 g/m^3 (Antonova and Dvornikova, 1992).

During gasification of high-sulfur coal, sulfur is converted to gas as hydrogen sulfide, which can relatively easily be isolated and used to recover chemically pure sulfur and sodium thiosulfate. Throughout the operation of the Podmoskovnaya UCG plant where lignite containing up to 3% sulfur was mined by UCG process, about 22,000 t of sulfur and 44,700 t of sodium thiosulfate were recovered (Antonova and Dvornikova, 1992). The gas was purified by the arsenic-soda method (Antonova et al., 1991).

In Russia, the sulfur oxide emissions of coal-fired boiler plants were as high as 7420 mg/mJ, with nitrogen oxide emissions of 4930 mg/mJ (Chekina, 1994). Data presented in (Corazon, 1991) showed that at coal-fired power plants, specific sulfur emissions were in the range of 720–2200 mg/mJ and nitrogen oxide emissions at 245 mg/mJ.

In addition, burning coal at coal-fired thermal power plants (TPPs) leads to a serious ecological problem, as significant amounts of ash and slag waste (ASW) are generated. According to the Russian Ministry of Energy, 30.4 million tons of ASW are generated annually by coal-fired TPPs. Coal ash disposal and storage sites containing 1.7 billion tons of ash and slag occupy a storage area of 28,500 ha (Kalachev, 2016). Ash storage facilities generally contain coal combustion residuals (unburned carbon), with ongoing chemical oxidation processes that often lead to fires in the coal ash impoundments. Oxidation and the interaction of ash impoundments with atmospheric precipitation lead to leaching of the mineral mass and active migration of many components, which leads to contamination of the hydrosphere.

UCG does not require waste rock stockpiling, thus providing a distinct advantage over conventional coal mining methods.

While protection of the ground surface from ground surface depressions and the air from contamination due to loss of gasifier seal integrity and water treatment of the surface plant are all part and parcel of the UCG technology, protection of groundwater

Table 11.1 **Hazardous components in combustion products of UCG gas, solid, and liquid fuels**

| | Concentration of hazardous components | | | | | |
| | Coal | | Liquid fuel | | UCG gas | |
Fuel type	vol%	g/m^3	vol%	g/m^3	vol%	g/m^3
Particulate matter, ash, soot	–	1.45–4.5	–	0.2–0.3	–	–
Sulfur oxides	0.05–0.34	1.6–11	0.031–0.2	1.0–7.0	–	–
Nitrogen oxides	0.02–0.07	0.6–2.0	0.007–0.04	0.2–1.0	0.007	0.2
Carbon monoxide	0.035–0.35	0.44–4.4	0.035–0.35	0.44–4.4	0.01–0.09	0.15–1.10

resources presents the greatest challenge. Given the dynamic nature of groundwater, contaminants can be transported over great distances and enter aquifers located far away from the gasification sites.

Is it possible to minimize or prevent contamination of the hydrosphere? After all, groundwater present in the coal seam is brought into direct contact with the fire source during UCG.

The impact of the UCG processes on groundwater varies and is determined primarily by the specific geologic and hydrogeologic conditions of the coal deposit. The specific process conditions during UCG may also have a significant impact.

In the former Soviet Union, more than half a century of experience had been accumulated in scientific development and practical implementation of the UCG technology and environmental assessment of UCG plant operations. The experience acquired is unique and unsurpassed anywhere in the world. In situ coal gasification projects were operated in coal fields characterized by varying degrees of complexity of geologic and hydrogeologic conditions. These were flat-lying to subhorizontal deposits such as Basovskoe, Gostevskoe, and Shatskoye coal deposits in the Moscow coal basin and the Yuzhno-Sinelnikovskoye coal deposit in the Dneprovskoe coal basin and geosynclinal-type coal deposits: Lisichanskoye coal deposit in the Donetsk coal basin and Kiselevskoye (the Yuzhno-Abinsk site) in the Kuznetsk coal basin. The Angren lignite deposit in Central Asia (Uzbekistan) belongs in an intermediate position in the classification.

Two short-term UCG trials were conducted on bituminous coal with a low volatile matter content: anthracite (A) in Shakhty City and semianthracite (SA) in Kamensk. As a result of these trials, such coals (anthracite and semianthracite) proved nonsuitable for UCG due to mechanical instability of the heated reactive surface of the gasification channel underground.

Research programs in UCG were initiated and conducted in the United States (Hoe Creek, Hanna, Carbon County, Centralia, and Rawlins) and in Western Europe.

During the period between 1999 and 2003, a commercial UCG project was operated at the Chinchilla coal field in Australia (Walker et al., 2001).

A pilot scale UCG project at the Majuba coal field, South Africa, to supply a combined steam-gas cycle power plant continues to operate in a subhorizontal bituminous coal seam. The new UCG site with a capacity of about 3 PJ per year was completed and ready for commissioning; planned shutdown is still ongoing at the old site where UCG activities were concluded.

Based on years of experience in operating UCG projects, the principal process parameters were defined, and patterns of man-made hydrolithosphere change were identified during UCG operations (Table 11.2) (Dvornikova, 1996a,b,c).

Three major types of human impact on the hydrolithosphere are differentiated:

1. In situ conversion of coal to a gaseous fuel consisting of multiple physical and chemical reactions under conditions of high temperature and pressure leading to contamination of groundwater, which reduces the total amount of coal resources, with formation of gasification cavities;
2. Abstraction of groundwater that may lead to an overall drawdown in freshwater reserves and changes in hydrostatic pressure of aquifers;
3. Operation of aboveground condensate storage facilities, which may create conditions for the formation of man-made aquifers and sediment.

Table 11.2 **The main indicators of human impacts on the hydrolithosphere during UCG operations**

Type of human impact	Nature of impact	Type of man-made change	Nature of man-made change	Nature of physical and chemical processes
1	2	3	4	5
Conversion of solid coal using the UCG method	Thermal (thermobaric/ PT)	Extraction of solid fossil fuel deposits	Changes in geodynamic conditions	Increase in transmissivity of overburden (hydraulic conductivity, porosity)
			Changes in thermobaric conditions (temperature and pressure)	UCG product gases dissolving in groundwater (saturation)
				Heat penetration of rock and groundwater, decreased density and viscosity of water Emergence of thermal springs Increase in groundwater storativity (sorptive capacity) of rock, the formation of ash, slag, calcined, or sintered rock
	Chemical	Increased rates of geochemical processes	Changes in geochemical conditions	Increase in the chemical potential (dissolving ability) of groundwater
				Transition of chemically and physically bound groundwater and fracture groundwater, as well as gravitational groundwater, to a vapor state, transformation of water to superheated steam Formation of pyrogenic water
		Contamination of groundwater in aquifers by gasification products	Changes in groundwater chemistry, influx of contaminants	Solid rock, gases, organic components dissolving in groundwater
				Increase in the concentration of TDS, macro- and microcontaminants in groundwater

				Suspended and emulsified materials trapped by rocks
			Increase rates of physical, chemical and biochemical processes of interaction between contaminated groundwater and naturally occurring groundwater	
				Dilution of contaminated groundwater by clean naturally occurring water
				Molecular diffusion, dispersion, absorption of specific components (physical and chemical sorption), gas production, heat transfer
		Contamination of rock material	Changes in physical and chemical properties of soil and rock	Elevated tar and silt content of soil and rock
				Ash and slag waste, calcined rock, tars, oils accumulate in the depleted gasification cavity
	Geodynamic	Deformation of the overburden	Rock deformation	Subsidence
			Rock deformation zone propagates up to the ground surface with resultant discontinuities	Increased fracture density of rock
			Changes in transmissivity of the overburden	Increase in the zone of gas leakage, increased aquifer recharge from infiltration

Continued

Table 11.2 **Continued**

Type of human impact	Nature of impact	Type of man-made change	Nature of man-made change	Nature of physical and chemical processes
1	2	3	4	5
Abstraction of groundwater	Hydrodynamic	Increased rates of man-made geodynamic processes	Increased rates of suffusion/suffosion and karsting	Connectivity of the gasification cavity with gas-permeable rock layers and aquifers Increased transmissivity, storativity, and sorption properties of rock Rock dissolving or subjected to leaching
		Decreased operational freshwater resources	Changes in hydrostatic pressure	Changes in hydraulic connectivity between aquifers Changes in groundwater flow direction Increased piezometric gradient (hydraulic gradient) and flow velocity of groundwater Lower boundary of oxidation-reduction potential A deep groundwater depression Area of dewatered rock
Operation of aboveground liquid waste storage facilities	Chemical	Contamination of rock in the vadose zone (aeration zone)	Changes in the chemical composition and transmissivity of the overburden strata	Increased silt and tar content of rock Precipitation of contaminants at the bottom of the settling pond Changes in permeability and transmissivity values of the overburden strata

		Man-made aquifers forming	Changes in the chemical composition of alluvial groundwater due to contaminant infiltration	Increased hydrostatic pressure
				Increased rates of rock dissolution
				Increased concentration of TDS, groundwater contaminants
			Increased rates of physical, chemical, and biochemical processes	Molecular diffusion, dispersion, absorption (sorption) of select components

The types and nature of man-made changes to the hydrolithosphere were identified, as well as the nature of the physiomechanical and physiochemical processes inherent in the UCG technology, which largely determine the degree of groundwater contamination. The latter include changes in geodynamic, hydrodynamic, thermobaric, and geochemical conditions in gasification areas, accompanied by various physical and chemical processes occurring in the rock formation.

UCG activities generate contaminants as unwanted by-products that can adversely affect the environment at the UCG plant location. Significant aspects of impact of the UCG process on the environment are presented in Fig. 11.1.

Potential sources of contamination of the geologic setting and groundwater in particular are

−the fire source of the operating gasifier and gas leakage,
−gasification cavities of spent gasifiers,
−aboveground condensate discharge and storage dams and discharge of condensate along gas pipelines.

The principal sources of contamination are the fire source proper within the coal seam and gasification products (CO_2, CO, H_2, CH_4, C_mH_n, and H_2S) and gasification by-products (phenols, tars, ammonia, cyanides, benzenes, pyridine compounds, etc.) as well as the residual products of gasification in spent gasifiers (ash, slag, and tar) that can enter groundwater and migrate over considerable distances.

Untreated hot UCG product gas as it is collected at the surface from the production well is a mixture of steam/water vapor products of both complete and incomplete carbon combustion, dioxide and water vapor reduction reactions, reactions of coal pyrolysis, and conversion reactions of water vapor and combustion reactions of gaseous products.

The above reactions involve not only the injection agents fed into the coal seam from the surface but also groundwater, moisture, and carbon-containing components of rock surrounding the coal seam.

Sulfur compounds contained in the coal and rocks undergo conversion to gaseous state as they come into contact with oxygen, hydrogen, and water vapor.

As the vapor/gas mixture cools, it separates into a liquid (condensate) and gaseous phase. When left standing, the condensate settles out into an above-the-tar water solution layer containing multiple chemical compounds and tar. The highest concentrations of noxious components are found in the gas condensate: approximately 1–2 g/L of phenols, 4–25 mg/L of cyanides, 2–5 g/L of dissolved ammonia, tars, and pyridine compounds.

Gas condensate enters the surface storage, which can also be a source of contamination of both the atmosphere and the hydrosphere. However, when the condensate storage dam is installed properly and condensate is treated and utilized, which can be achieved through relatively simple means, contamination from the surface-based contamination source can be reduced to zero.

An important characteristic of UCG is the production of most contaminants along with hot gas to the ground surface as condensate. As can be seen from Table 11.3, samples collected simultaneously had a concentration of phenols, rhodanides, and
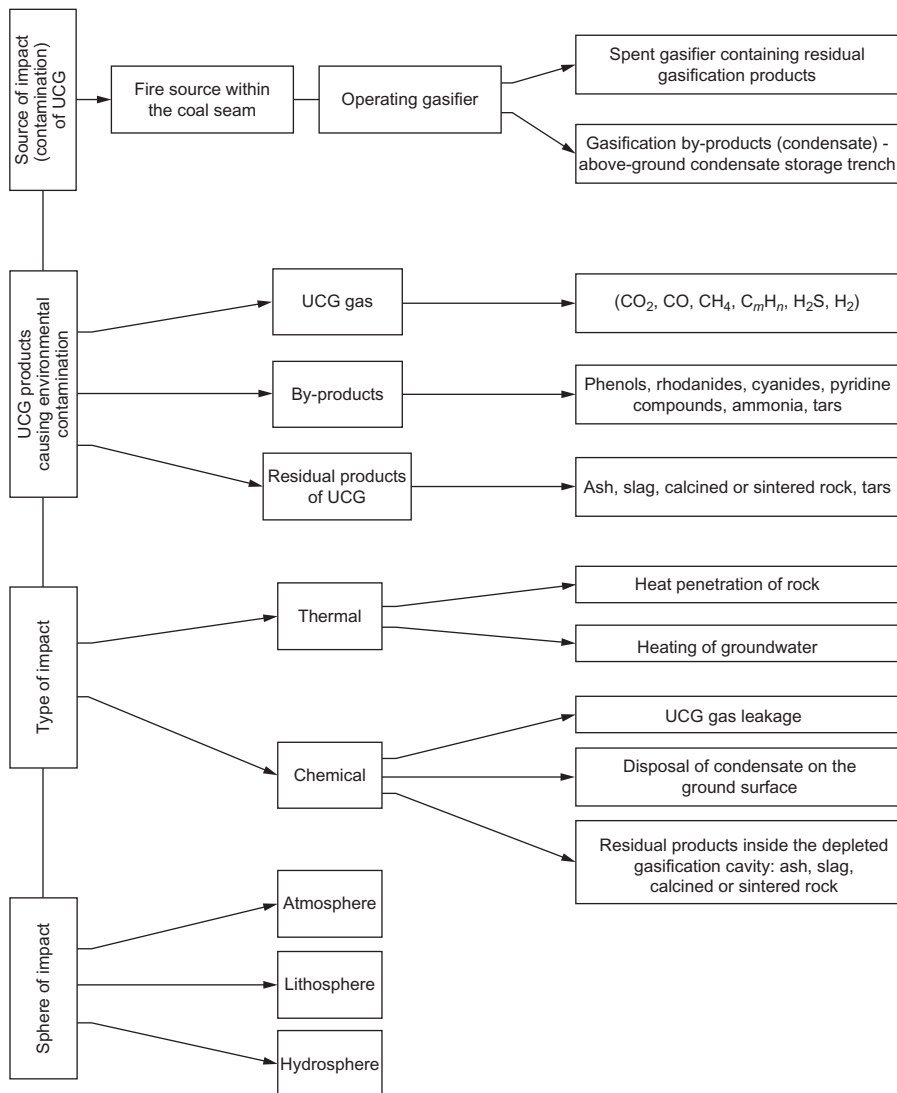
Fig. 11.1 Impact of UCG on the environment.

cyanides thousands of times higher in the condensate than in water pumped out from the underground gasifier (Table 11.3).

However, the really important question is what percentage of contaminants remains in the underground gasifier. Assessing the degree of contamination of ground-water and determining the extent of the plume and the rate of its migration require that both the naturally occurring and man-made factors (mining, geologic, and hydrogeologic conditions of the coal field) be evaluated in each specific case, as they determine the degree of contamination.

Table 11.3 Contaminants in gas condensate and water samples collected from Gasifier 17 of the Yuzhno-Abinskaya UCG plant (Kuznetsk coal basin)

No	Sampling point, Date	Phenols (mg/L)		Cyanides (mg/L)	Rhodanides (mg/L)	Ammonia (mg/L)
		Volatile matter	Nonvolatile matter			
1	Gas condensate produced from Well 7G, May 1991	1366.4	32.9	75.8	530.7	2602
2	Groundwater From Well 39, which had connectivity with production Well 7 May 1991	0.09	Not detected	0.18	Not detected	8.2

11.3 Major factors affecting the groundwater chemistry and contamination of groundwater during UCG

Generalizing from many years of experience in in situ coal gasification at UCG stations located in various coal basins, it can be stated that the degree of impact of UCG on aquifers varies and is determined not only by the specifics of the UCG process itself but also by natural factors characterizing the deposit.

The classification of the factors contributing to groundwater contamination is presented in Fig. 11.2 (Dvornikova, 1996a,b,c; Dvornikova and Kreinin, 1993).
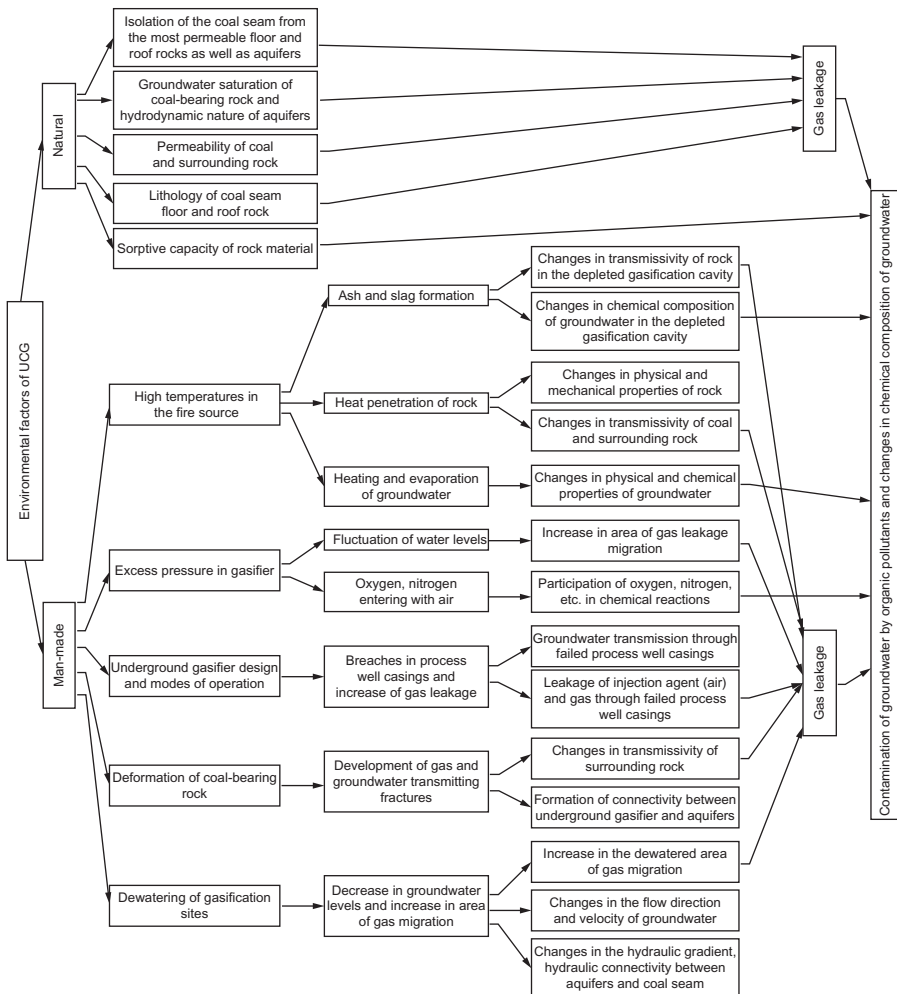
Fig. 11.2 Classification of environmental impacts of UCG on groundwater.

During UCG, the possibility of environmental contamination including groundwater is mainly related to gas losses from underground gasifiers. Gas leakage at the operating UCG plants was generally between 7% and 30%.

Important man-made factors that have a significant impact on groundwater include the following:

I High temperatures at the fire face (up to 1200–1300°C) and inside the gasification cavity
II Overpressure in the underground gasifier
III Gasifier design and gasification mode of operation
IV Deformation of coal-bearing rocks of the roof and floor due to the processes of rock deformation and impact of high temperature
V Gasification site dewatering and water extraction from gasification cavities (Dvornikova and Kreinin, 1993)

A high-temperature profile at the fire source and long-term temperature anomalies have a significant impact on the hydrogeochemical groundwater conditions and their variations over time.

High temperatures cause changes that affect physical and chemical properties of rock and groundwater. A gas/vapor mixture zone forms in the immediate proximity to the fire source of combustion. Pyrogenic waters are formed, which are characterized by a different chemical composition. Part of the water transitions from the droplet liquid phase to steam, which comes into contact with the gasifier gases, becomes saturated with organic components, migrates through the rock strata and, after condensing once again, enters the aquifers.

As the groundwater temperature rises, its physical and chemical properties change:

−Dissolving ability (chemical activity) of water increases.
−Water density decreases (the volume of the liquid increases).
−Water viscosity decreases.

Various chemical components are carried out with vapor-phase water as it migrates through heated rock.

High temperatures cause changes that affect physical and chemical properties of overburden and underburden strata. Rock generally fractures and loses its aquitard properties. Hydraulic conductivity values increase and so do permeability and reservoir properties of heated rock strata, which can result in increasing gas leakage and its migration over considerable distances, thus potentially increasing the possibility of aquifer contamination. Therefore, the presence of aquitards of certain thicknesses and weakly permeable strata in the coal seam floor and roof, which is an integral part of operating the UCG process, is conducive to minimizing the environmental impacts on the hydrosphere.

Due to rock deformation in overburden strata and the impact of high temperature, zones of higher permeability and open groundwater-transmitting fractures form, which can lead to larger plume dispersions of migrating gas. The presence of poorly permeable, groundwater-saturated rock in the overburden generally prevents the spread of gas leaks.

Variations in the degree of environmental contamination may be attributed to overpressure in the underground gasifier, which determines the amount of gas leakage.

Increasing pressure in the gasifier may result in increased gas losses. The greater the additional flow resistance created by weakly permeable groundwater-saturated rock, the lower the gas loss increase rate. As the pressure in the gasifier increases and as the conductivity properties of heated rock mass increase, as concurrent dewatering activities in the gasification site result in increasing area of dewatered rock, gas leakage can increase dramatically. However, as a result of drainage activities and water extraction in the vicinity of the UCG site, a cone of groundwater depression will develop, which precludes migration of contaminants beyond its boundaries. Contaminated groundwater is pumped via water extraction wells to the surface, where it is treated with all known available and reasonable technology. Contamination of groundwater is contained within the vicinity of water extraction wells.

UCG modes of operation and the gasifier design of the gasifier may have a significant effect on groundwater contamination. As can be seen from Table 11.4, the chemistry of the gas condensate collected at the same gasification site but during different gasification modes of operation is different (samples 1–3). The gasifier design also has a significant effect on possible contamination of the hydrosphere. As vertical wells are drilled in the gasifier, aquifer contamination may occur through breaches in process well casings due to rock deformation of overlying strata. New designs of underground panels and vertical production wells have successfully resolved this problem and ensure excellent environmental performance of UCG systems built using vertical process wells.

Leaks from an underground gasifier are detected not only using process-related parameters, pressure, viscosity of the gas losses, dimensions of the gasification cavity, temperature, etc., but also primarily by the distance from the gasification cavity to the plume boundaries, the thickness and permeability of the surrounding layers, the degree of isolation of the coal seam, the amount of groundwater saturation of the rock strata, that is, by the naturally occurring conditions, or, alternatively, the geologic and hydrogeologic conditions of the coal deposit.

There is a varying degree of impact of UCG on groundwater conditions and its contamination in different mining and geologic settings. Important natural factors that determine the degree of groundwater contamination include the following:

  I. Isolation of the coal seam from the most permeable floor and roof rocks and aquifers
 II. Permeability of the surrounding rock and coal seam
III. Groundwater saturation of coal-bearing rock and hydrodynamic nature of aquifers
IV. Lithology of the floor and roof rock of the coal seam
 V. Sorption properties of coal and surrounding rock

One of the most important natural factors is the isolation of the coal seam. When a thick layer of dense, virtually aquiclude rocks (clays) occurs in the floor and roof of the coal seams, which are persistent along the strike and thickness, which serve to isolate the coal seam, the possibility of contamination is effectively excluded (Antonova and Dvornikova, 1992).

The permeability of the surrounding rock and coal seam has a significant impact on the contamination of groundwater. Rocks with high gas permeability (karsted fractured limestone and sandstone) occurring in the roof and floor of the coal seam

Table 11.4 **The chemistry and gas composition of the condensates**

UCG site	Sample no.	Date sampled	pH	Dry solid residue (mg/L) Total	After calcination	Sulfur content (mg/L)	Oxidation resistance in O_2 (mg/L)	NH_4	Na^+	K^+	Ca^{2+}	Mg^{2+}	Al^{3+}	$Fe^{2+}+Fe^{3+}$	Cl^-	F^-	SO_4^{2-}	HCO_3^-
Podmoskovny (sandy clay rocks)	1	3 Sep 1958	6.6	2272	643.5	1056	1692.0	715.0	2.21	Not measured	25.8	2.41	15.0	240.0	2.0	2.0	1.0	738.0
	2	22 Jun 1959	5.2	27,810	2415.0	6325	5724.0	4112	11.0	25.0	55.0	21.0	120	681.0	248.0	18.0	4.0	-
Lisichansky (sandy shale rocks)	3		6.4	14,705	1388.0	3976	5317.0	4333	8.0	24.0	19.0	19.0	100	997.0	255.0	Not measured	4.0	227.0
	4		8.2	2342	2204	2480	1480	1258	14.0	Not measured	59.0	58.0	4.5	15.0	152.0	–	289.0	212.0

UCG site	$S^{2-}+HS^-$	SO_4^-	$S_2O_4^{2-}$	Si	Ti	Mn	Cu	Zn	Sr	Ba	Ag	Be	V	Sn	Cr	Pb	Ge
Podmoskovny (sandy clay rocks)		488.0		11.0	0.02	12.0	0.1	1.0	0.5	15	0.03	None	None	0.005	0.001	Not detected	
	858.0	780.0	4598	Not measured												Not detected	
Lisichansky (sandy shale rocks)	775.0	10.0	5604	28.0	0.3	1.1	0.03	Not detected					0.006	0.006	0.001	0.11	–
	Trace	732	2461	13.0	0.05	0.11	0.05	0.45	Not detected			–	Not detected			1.1	–

may lead to significant gas leakage from gasifiers, leading to contamination of groundwater over a wide area.

If rocks with low permeability (siltstone, mudstone, and clays) occur in the roof and floor of the coal seam, the possible resulting contamination of groundwater is insignificant. The coal seam and surrounding rock with low permeability ensure the underground system integrity of the gasification panels and reduce gas leaks, which reduces the degree of negative impact of UCG on the environment including groundwater and also minimal rates of migration of the contaminated flow over considerable distances.

Essential for mitigating the negative impact of UCG is groundwater saturation, the pressurization of the system encompassing the entire coal-bearing rock unit with very low hydraulic conductivity values (hydraulic conductivity of 0.0001–0.01 m/day), which serve as hydrolock of sorts preventing gas leakage.

Such factors as the hydrodynamic nature of aquifers, the zone of groundwater recharge, groundwater flow, and discharge that affect the variations of possible contamination over time and determine the rate and direction of groundwater flow play a significant and deciding role in contaminant migration.

The lithology of the floor and roof rock of the coal seam determines the groundwater chemistry. As mentioned above, when considering man-made factors, high temperatures cause vapor-phase water to leach chemical elements from the surrounding rock, which affects the chemistry of the condensate and the chemical composition of the groundwater.

In addition, the main lithologies of floor and roof rock influence the formation of gas-transmitting fractures in the overlying and underlying rock strata. When dense and plastic rocks (clays) occur in the roof of the coal seam, smooth subsidence of the overlying rock and filling of fractures were noted, which reduces gas leakage from the underground gasifier and mitigates the risk of groundwater contamination.

The natural sorption properties of coal and surrounding rock have a significant influence on the degree of aquifer contamination and affect the processes of self-purification of groundwater. In addition, high temperatures generated from combustion of plant remains and decompaction occurring in the coal-bearing formation causes an increase in rock porosity, storativity, and sorption properties. Increasing permeability and porosity of rocks results in a large reactive surface area, which in turn leads to an increase in the sorptive capacity of rock.

11.4 Environmental performance of UCG in the former USSR

Comparative analysis of the results of hydrogeochemical studies in various geologic and hydrogeologic settings and environmental impact analysis of UCG plants suggest that in areas where there are no aquitards of persistent thickness occurring in the floor and roof of the coal seam, and with presence of an unconfined aquifer in the floor of the coal seam, situated in fractured, karsted rocks, the upper 10 m of which was not under water, it was not possible to prevent contamination of groundwater. In such gasification sites, migration of gas leaks through aerated rock was recorded over a wide
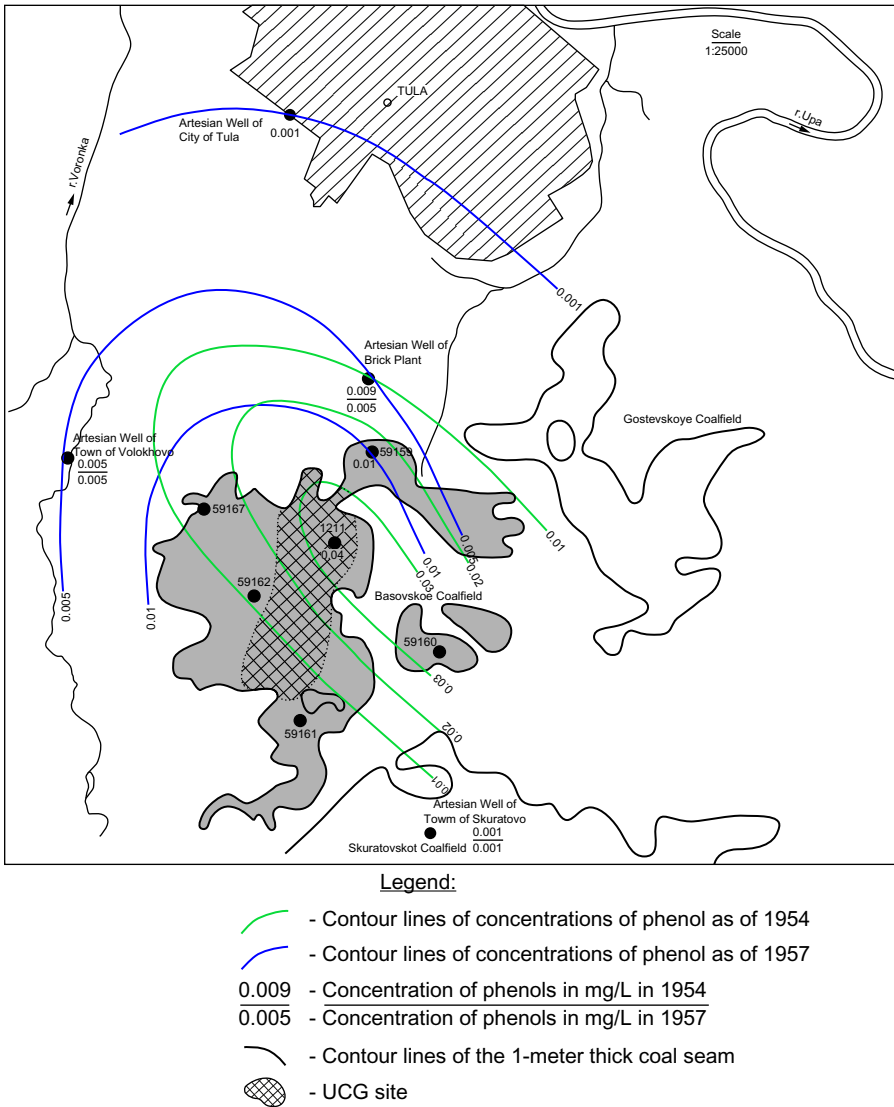
Fig. 11.3 Schematic map of the concentration of phenols in groundwater of the Upinsky aquifer at the Basovskoe coal deposit of the Podmoskovny Coal Basin.

area, which led to contamination of the aquifer. Gas leakage was as high as an average of 30% and less frequently, 40%. As can be seen from Fig. 11.3 (Kononov, 1965), the concentration of phenol in the immediate vicinity of the gasification site in the under-lying Upinsky aquifer was as high as 0.04 mg/L. The farther away the location of monitoring wells from the gasification site, the lower the concentration of phenol in the samples all the way to values below the maximum allowable concentration

levels. So, the concentration of phenols did not exceed 0.009 mg/L within a radius of 1.5 km, while at a distance of 3 km, the concentration of phenols did not exceed the maximum allowable concentration for drinking water (MAC = 0.001 mg/L). These UCG panels at the Podmoskovnaya UCG plant were not deemed suitable for mining using the UCG method.

Comparative analysis of the results of geochemical studies in the adjacent panels at the Podmoskovnaya UCG plant showed that in select zones where the coal seam was flooded under confined groundwater conditions by groundwater of the underlying aquifer, with clay layers of sufficient thickness occurring in the floor and roof of the coal seam, contamination was minimal. Confined groundwater of the underlying Upinsky aquifer served as a natural hydrolock precluding contaminant migration. Water extraction from the underlying aquifer ensured the containment of contaminated water within the vicinity of water extraction wells. Subsequent to the completion of gasification and water extraction operations, the concentration of phenols decreases to values below the MAC. This finding proved that contamination may remain localized.

It is important to underscore that as compared with conventional mining methods, the UCG technology as applied in the Podmoskovny Coal Basin (open-pit development) is the safest and most environmentally friendly. In the Podmoskovny Coal Basin, the UCG sites and open-pit mines share the same mining and geologic conditions. As can be seen from Table 11.5, compared with open-pit development, change in the groundwater chemistry was less significant during UCG within the deep coal seam aquifer in depleted gasification panels. The pH of groundwater is neutral (pH 7.0–7.5) both in the zone of circulating gas/vapor mixture and at a distance of 30–40 m from the gasifier, which is consistent with the baseline values for the deposit. However, the condensate sample collected from the production well is characterized by extremely high concentration of TDS (12,473 mg/L), slightly acidic pH (pH 6.4), and high iron content (997 mg/L), which indicates that during UCG, the preponderance of contaminants is brought up to the surface where it is collected in the condensate storage dam. During UCG activities in the deep coal seam aquifer, inside the zone of influence of UCG, a certain amount of increase in the concentration of TDS is recorded, from 253 mg/L (baseline value) up to 1243–1373 mg/L (Kononov, 1965). In comparison, at the Ushakovsky and Kimovsky open-pit coal mines located in the Moscow region, where the same lignites were mined in similar geologic and hydrogeologic conditions, there exist to the present day dozens of man-made "dead" water reservoirs that had formed in depleted areas, that is, in the cutting trenches. The pH of water in such reservoirs is highly acidic environment, with a pH of 2.7–5.0, concentration of TDS from 1500 to 4460 mg/L, and extremely high iron content (25–531 mg/L) and SO_4 ions (1000–3100 g/L) (Dvornikova et al., 2001). The trace element composition shows high concentrations of highly hazardous lithium, extremely harmful beryllium, dangerous manganese, iron, aluminum, nickel, and cobalt. The sulfur content is as high as 725 mg/L. Figs. 11.4 and 11.5 show the presence of ferruginous sediments and sulfur deposits, which in arid years crystallized during evaporation in the riparian zones of the "dead" water reservoirs, and an absolutely lifeless, lunar-like landscape at the abandoned sites (Fig. 11.6).

Table 11.5 **The chemical composition of groundwater in open coal mining sites and in areas of underground coal gasification in the suburban coal basin**

Aquifer	Coal mining method	Variations in groundwater conditions	Prevailing temperature (°C)	pH	TDS (mg/L)	HCO$_3$ (mg/L)	SO$_4$ (mg/L)	Fe (mg/L)
Coal seam	Underground coal gasification	Naturally occurring	6–8	7.0	252.2	147.0	–	6.8
		Inside the zone of influence of UCG—at a distance of 30–40 m from the gasifier	20	7.5	1373.0	703.0	346.0	–
		Inside the zone of influence of UCG—inside the gasifier, inside the zone of the circulating gas/water vapor mixture	Up to 114	7.0	1243.0	738.0	–	52
		Condensate from the production wellhead	400–600	6.4	12,473.1	–	4.0	997.0
	Open-pit coal mining (opencast coal mining sites)	Man-made "dead" pond with an acidic and very acidic environment	20	2.7–5.0	1500–4460	–	1000–3100	25–531
		Man-made water reservoir with a neutral and alkaline environment	20	7.22–7.94	1480–1740	–	810–1010	0.05–3.2

Fig. 11.4 Benthic ferrous sediments of the "dead" man-made water reservoir at the Ushakovsky open-pit mine in the Podmoskovny Coal Basin.

Fig. 11.5 Sulfur crystals along the banks of the "dead" man-made water reservoir at the Ushakovsky open-pit mine in the Podmoskovny Coal Basin.

As the table shows, in open-pit coal mining, even in man-made reservoirs with a neutral and alkaline pH, the presence of high concentrations of sulfates, iron, and TDS is recorded, which is significantly higher in comparison with during UCG operations.

The localized nature of the UCG-induced contamination was confirmed in studies conducted at the Yuzhno-Abinskaya UCG plant (Kuznetsk coal basin) and the Lisichanskaya UCG plant (Donetsk coal basin). As can be seen in Fig. 11.7, during water extraction, the concentration of phenol decreases, dropping below the MAC

Fig. 11.6 "Moonlike" landscape at the Ushakovskoe coalfield of the Podmoskovny Coal Basin.
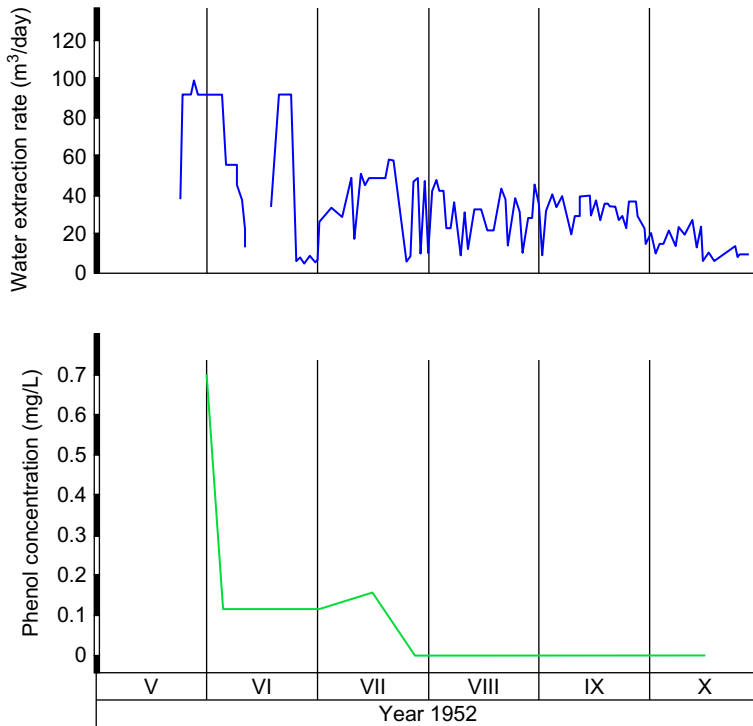
Fig. 11.7 Decreasing trend of phenol concentration in groundwater extracted during dewatering of Gasifier 29 at the Lisichanskaya UCG plant.

values post gasification and with continuing water extraction activities. Thus, it was proved that UCG-induced groundwater contamination was negligible and can be reduced to a minimum by means of adequate engineering and process measures.

The Angren UCG site at the Angren lignite deposit (Uzbekistan) is another example with relatively suitable conditions. The lignite deposit is noted for its low coal seam permeability and surrounding rock and a confined groundwater system within the coal-bearing strata. The main Cretaceous-Paleogene aquifer system occurs at a considerable distance above the coal seam and is securely isolated from it by a thick layer of kaolin clays impermeable to groundwater and gas. However, during certain stages of the Angren UCG plant operation when gas was produced through vertical production wells, gas leakage occurred through breaches in process well casings. During certain periods of plant operation, gas leakage was as high as 24%. Gas migrated through the Cretaceous-Paleogene aquifer overlying the coal seam at a distance of 100 m. Phenols were occasionally detected in groundwater at the gasification panel at a concentration below 0.01–0.02 mg/L (Dvornikova, 2005). The gasifier design was subsequently modified at the Angren UCG plant. The updated design led to a reduction of the number of vertical wells with failed casings with gas leakage and virtually eliminated this as the source of contamination.

The above examples illustrate that the degree of aquifer contamination is a function not only of natural factors but also of the gasifier design, the condition of process wells, and UCG modes of operation.

Since 1990, large-scale environmental studies were conducted over 6 years at the UCG sites at the Yuzhno-Abinskaya UCG plant in the Kuznetsk coal basin, which have relatively favorable geologic and hydrogeologic conditions. A total of 2906 m of a network of groundwater monitoring wells was drilled as part of the studies. A systematized monitoring process was put in place to record changes in groundwater temperature, level, chemistry, and concentration of dissolved gas. The purpose of these studies was to determine the extent and variations over time of the contaminant migration beyond the boundaries of gasification sites. Also of considerable interest were the questions what percentage of contaminants remained in the underground gasifier and what amount flew out with groundwater flow post gasification. In addition to the results of studies obtained as part of this groundwater monitoring program, the monitoring results of previous years were used in the assessment and analysis of groundwater contamination.

Of important note is that the mining lease area of the Yuzhno-Abinsk UCG plant as a study area is quite complex due to the fact that as of the launch of the research study, the in situ gasification of coal seams of varying thickness and depth had been in operation for over 37 years in 21 gasifiers. The coal-bearing unit that is composed of steeply dipping coal seams and interbedded mudstones, siltstones, and sandstones has very low permeability and groundwater saturation. It is classified as intermediate between aquitards and aquifers. A gas condensate storage trench was installed in loam soil without a plastic liner and operated over a long period. There were some periods when the condensate was collected in spent gasifiers.

Studies were carried out in operating and spent gasifiers, in the vicinity of surface gas condensate storage, and outside of the mining lease boundaries. The monitoring period was 9 years for an operating gasifier and 4.5 years for depleted panels.

The following results were obtained:

1. The main source of the hydrosphere contamination was the condensate storage trench. At a distance of 12 m from the storage site, the concentration of phenols and ammonium ion was 15 and 225 mg/L, respectively, while 60 m away, their values were as low as 0.9 and 21 mg/L (Figs. 11.8 and 11.10B). The study showed that loam soil neither serves as a screen nor prevents contaminant migration (Dvornikova, 1996a,b,c, 2011). Condensate must be disposed into specially designed storage dams or properly lined condensate ponds.

2. During UCG, groundwater undergoes significant changes throughout the gasifier panel. The concentration of carbon dioxide is as high as 90–150 mg/L; the concentration of TDS in groundwater pumped from the gasifier increases (from 400–600 to 1700–2000 mg/L); there is an increase in the concentration of iron ions (up to 2.0 mg/L) and sulfates (from 20 to 800 mg/L); the pH shift is down. The concentration of phenols does not exceed 0.02 mg/L (MAC = 0.001 mg/L), with ammonium ion at 40–60 mg/L (Fig. 11.9). The maximum contamination was recorded during the period of the most intensive stage of the UCG process and maximum gas leakage into the surrounding rock strata, while a deep groundwater depression cone persisted in the operating gasifier due to evaporation of groundwater and water extraction activities. The contaminated groundwater flow direction was toward the water extraction wells, toward the zone of decreased pressure.
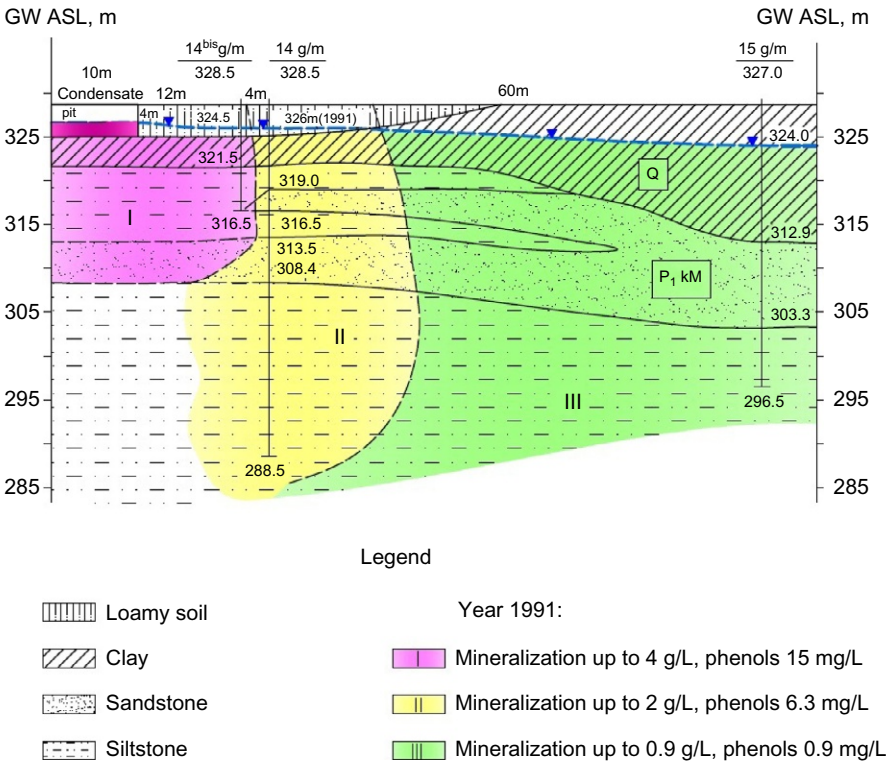
Fig. 11.8 Dynamics of technogenic metamorphization of groundwater as a result of the ingredient inflow from the condensate pit.
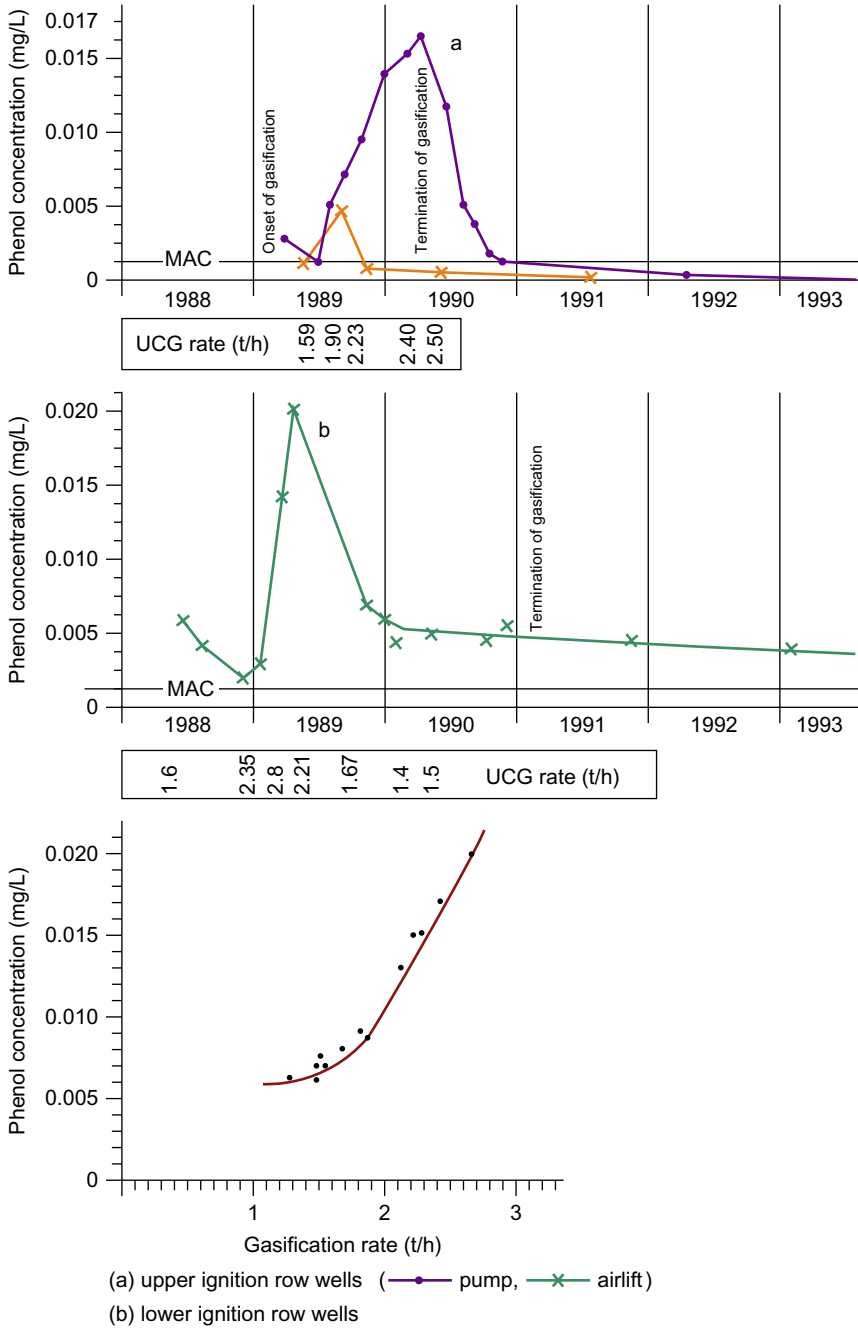
Fig. 11.9 Phenol concentration changes in ground water during dewatering and correlation between phenol concentration and gasification rate.

By the use of a specially devised tower experiment during the gasification process, phenols were shown to be subject to rapid oxidation. Water extraction was performed from the depleted cavity through two wells drilled only 10 m apart, using a pump in one and airlift in the other. During groundwater airlift, the concentration of phenols decreased sharply (Fig. 11.9A), which indicated active oxidation of phenols. In the water extraction well where a pump was used, the concentration of phenol was as high as 0.017 mg/L, while at a distance of 10 m from the well, in the airlift well, the phenol concentration did not exceed 0.0045 mg/L (Dvornikova, 1996a,b,c, 2011). Subsequently, the results of the experiment were used to develop a method for clean UCG.

Some 90 m from the operating gasifier, inside the zone of condensation of vapor-phase water, the concentration of phenols and ammonium did not exceed 0.006 and 4.5 mg/L, respectively (Fig. 11.10A), while at a distance of 350–500 m from the operating gasifier, there were no exceedances of MAC values. This suggested that moisture was condensed to water near the fire source within a radius of no more than 250 m, where migration of gas leakage was at its most intense and a cone of groundwater depression formed. It was thus proved that thanks to the cone of groundwater depression, groundwater contamination was restricted to a localized area at an operating gasifier under conditions of the Yuzhno-Abinsk UCG plant.

As is known, UCG-induced contamination is directly related to gas leakage. Analysis of gas leakage showed that during UCG, gas leakage values averaged 7%–10% but at certain periods was as high as 15%. Maximum leakage values were recorded during periods when the ratio between the pressure in the underground gasifier (P) and the hydrostatic pressure in this section (H) exceeded 1.1. A series of experiments were conducted at an operating gasifier using a range of ratios between pressure P within the underground gasifier and hydrostatic pressure H of 0.5–1.1. Optimal (from the point of view of minimal impact on the ecosystem) modes of operation of the gasifier were devised, which generated gas with a calorific value of about 1000 kcal/m^3 (Dvornikova, 1996a,b,c). The invention was then patented (Patent No. 2090750 "Method of underground coal gasification") (Kreinin and Dvornikova, 1997). In order to reduce gas leakage (Kreinin and Dvornikova, 1997), the LPUCG method was also recommended (Blinderman, 1995), which ensures minimum pressure in the underground gasifier system and, consequently, minimal contamination of the hydrosphere. A comprehensive process solution was developed to minimize groundwater contamination and subsequently patented (Karasevich et al., 2009a,b). As a result of large-scale, multiobjective environmental studies, it was proved that improving the environmental impact during UCG is possible through achieving optimal operating conditions and the gasifier design.

3. After the completion of UCG operations while water extraction was still ongoing, the concentrations of the contaminants were reduced to values below the MAC (Fig. 11.9A).

4. Immediately after the cessation of UCG and water extraction activities from the depleted gasification cavity, groundwater levels recover naturally over time. A gradual decrease in the concentration of TDS was recorded: 3 years post gasification, from 2000 to 1100 mg/L, and at a 5-year mark, down to 800 mg/L (baseline value 400–600 mg/L). Without forced inflow of groundwater (no ongoing water extraction), the concentration of phenol in the depleted gasification cavity does not exceed four times the MAC (0.0037 mg/L), while the concentration of ammonium ion is 7.3 mg/L.

5. Groundwater in the depleted cavities of abandoned gasifiers is metamorphosed. A common finding among them is an increased content of carbon dioxide at a concentration of an average of 70 mg/L, ammonium ion 4–8 mg/L, and phenols 0.002–0.005 mg/L. The maximum degree of contamination was recorded in UCG panels with thick coal seams (4 and 8 m). Beyond the boundaries of depleted UCG panels, concentrations of contaminating components do not exceed the MAC, which suggests self-purification of groundwater due to sorption processes occurring in the rock formation (Fig. 11.10B).
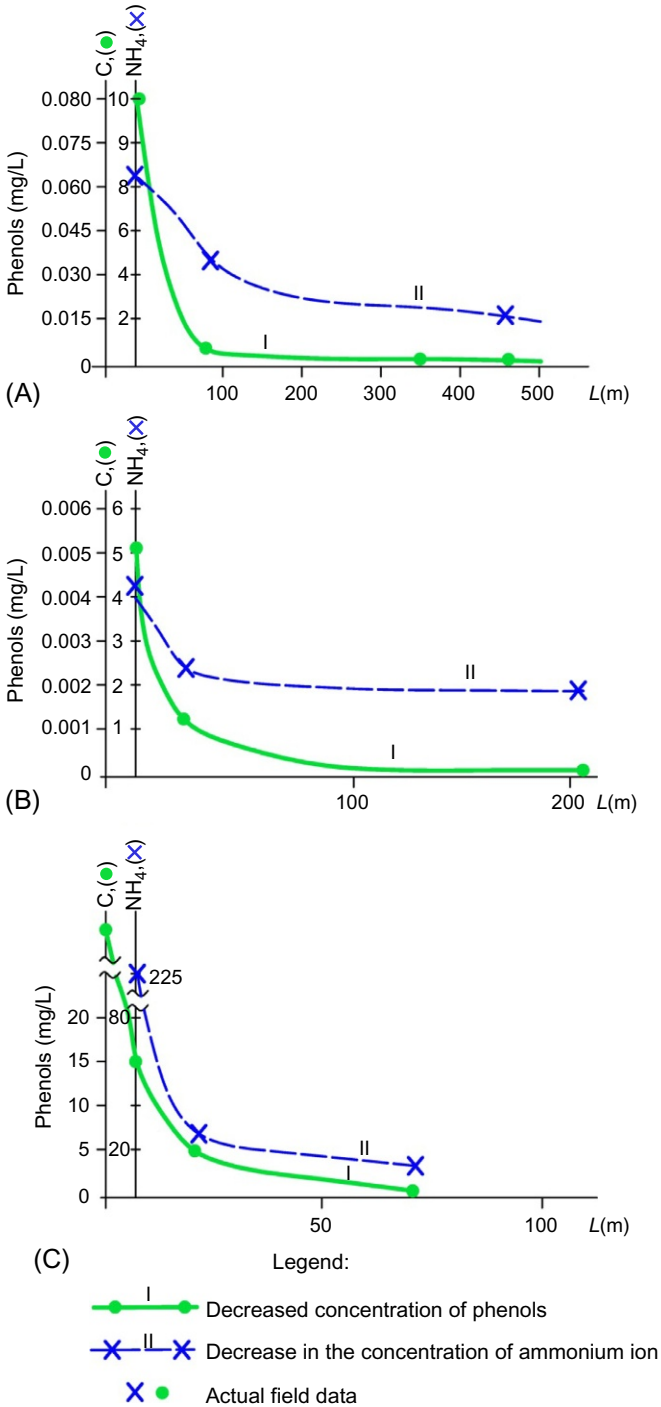
Fig. 11.10 Migration of chemical contamination: (A) during gasification, (B) from the spent gasifier, and (C) from the aboveground condensate storage trench.

To evaluate and validate the theory of self-purification of groundwater, special laboratory studies of the sorption properties of coal sampled from a depth of 300 m were conducted. The assumption as to high sorption capacity of Yuzhno-Abinsky coal was confirmed. The adsorption capacity of raw and heated coal with the initial concentration of the solution of 0.04 mg/L was 2.5 and 9.0 µg/g, respectively. By way of comparison, the adsorption capacity of activated carbon is 13 µg/g. With equilibrium concentrations of phenol being 0.7–0.8 mg/L, the adsorption capacity of raw and heated coal was 0.13 and 0.22 mg/g, respectively (Dvornikova, 1996a,b,c).

The contaminated groundwater flow in the coal seam from the direction of depleted UCG panels moves primarily through heated coal that is subject to water vapor exposure, through the zone where processes of the sorption of contaminated components are actively going on, resulting in self-purification of groundwater. The results of long-term and large-scale field studies proved that at the Yuzhno-Abinskaya UCG plant, groundwater contamination in the depleted gasification panels was confined to a localized area, with contaminants being adsorbed by the heated rock whose sorptive capacity properties increase sharply as the heat penetrates through coal and the surrounding rock material.

The Henry's isotherm constant and distribution coefficient β, which were obtained as a result of laboratory studies of high volatile bituminous grade coal, were used in calculations and predictions of the migration of contamination plumes. Calculations were performed using the conductivity profile model "ρo" from the spent gasifier and condensate discharge site. The calculations took into account the hydrodynamic and conductivity properties of the rock strata, as well as the spent gasifier sites characterized by increased sorption capacity values (Dvornikova, 1994).

Presented in Fig. 11.11A are the calculation curves of phenol concentrations in groundwater for different periods of time and patterns of their decrease in the center of the contamination plume during migration from the spent gasifier. Analysis of the data confirmed a decrease in the concentration of phenols along the migration path of the plume and over time (Kreinin and Dvornikova, 1999). The results of calculations based on the conductivity profile model "ρo" are reasonably consistent with the actual data recorded during the long-term groundwater monitoring period. Fig. 11.11B shows data on the calculated concentrations of phenols in different sections located 30, 90, and 210 m away from the spent gasifier, respectively. The variation curves of the phenol concentration over time show extreme amplitudes. A slight increase in the concentration of phenols (0.0017 mg/L) was recorded at a distance of 90 m from the abandoned gasifier 8 years post gasification.

To minimize residual contamination (phenols) in the depleted cavity, a groundwater treatment method was developed using biochemical oxidation of organic compounds in alkaline conditions, whereby special bacteria and oxygen of air were injected through process wells (Karasevich et al., 2009a,b).

The studies conducted at the Yuzhno-Abinskaya UCG plant located in the Kiselevsk coal deposit showed the following:

1. Groundwater contamination during the operation of the UCG gasifier is localized to the gasification site.
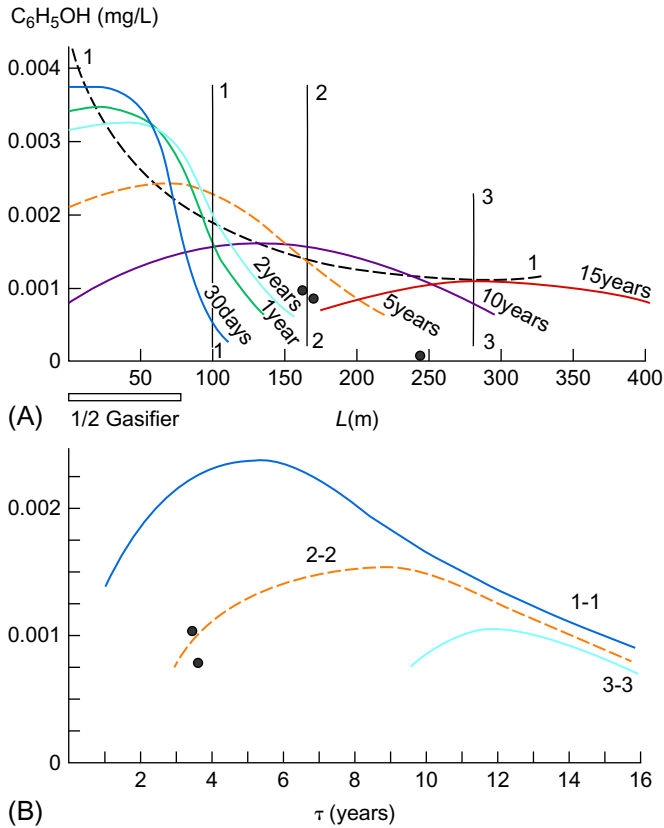
Fig. 11.11 Calculation curves for changes in phenol concentration in ground water: (A) during migration in time, (B) in different cross-sections (at 30 m, 1–1; 90 m, 2–2; and 210 m, 3–3). ● Actual well data at 90 m over 3.5 years.

2. The principal contaminants of concern (phenols, tars, rhodanides, cyanides, and ammonium) are volatile, become entrained gas mixture, and are to the surface as condensate.
3. The maximum contaminant concentration is noted during the gasification period, with a cone of groundwater depression surrounding the gasifier, which prevents the spread of contamination. It was experimentally proved that three months after the cessation of gasification, with continuous water extraction, the concentrations of phenols do not exceed the maximum allowable concentration.
4. UCG should be applied using optimal (in terms of minimum damage to the ecosystem) modes of operation of the gasifier with a certain ratio between the pressure in the underground gasifier (P) and the hydrostatic pressure (H).
5. After the UCG processes have run their course, it is necessary to pump the groundwater out of the gasification cavity to ensure a thorough removal of contaminants to the ground surface followed by their treatment.
6. Once water extraction activities are completed, localized sources of contamination should be eliminated by flooding, with processes of oxidation and decomposition of phenols activated.

7. Post gasification, the degree of groundwater contamination in abandoned sites is negligible (2–5 MAC).
8. As contaminants migrate beyond the boundaries of depleted UCG panels, their concentration levels decrease to values close to the MAC due to sorption by coal and rock. Natural self-purification of groundwater ensues. Outside the mining lease area, groundwater contamination was not recorded.
9. UCG site is selected first and foremost from the standpoint of possible environmental impacts, assessing primarily the mining, geologic, and hydrogeologic conditions of the coal field.

Analysis of long-term ecological studies conducted at the Yuzhno-Abinskaya UCG plant and at certain periods at the Lisichanskaya, Podmoskovnaya, and Angren UCG plants showed that the UCG-induced environmental impacts are predictable and can be controlled and mitigated using relatively simple engineering measures. A set of measures was developed to protect groundwater from contamination, which makes it possible to reduce the UCG impacts to a minimum.

11.5   Environmental performance in recent UCG projects

In the United States, first UCG trials were conducted at the Gorgas, Alabama site. In 1975, Texas Utilities obtained a UCG technology license in the former USSR, and its subsidiary Basic Resources, Inc. conducted the first UCG trial in Texas assisted by Soviet experts. The results of the first experiments became the basis and comparative criteria for subsequent theoretical and laboratory studies and field tests conducted during the ensuing years. Prior to 1992, around 30 experiments were conducted in natural conditions in coal deposits in five states (Wyoming, West Virginia, Illinois, New Mexico, and Texas).

The largest research project was implemented at the Rocky Mountain 1 site in the Hanna coal deposit. The coal seam had a thickness 10 m occurring at the depth of 130 m. The seam was subhorizontal. The test project duration was 100 days. A special program was designed to assess the environmental impacts, which included the following:

−Development of requirements for environmental protection
−In-depth studies of the hydrogeologic conditions at the UCG site prior to the start-up of operations
−Monitoring of the experiment
−Water extraction from depleted gasification cavities
−Geochemical studies of groundwater and condensate

The experiment was successfully completed in 1988.

The results of these studies confirmed some conclusions reported previously in the USSR:

−UCG-induced groundwater contamination is localized to depleted gasification cavities.
−The cone of groundwater depressions is still present in the vicinity of the cavity, with groundwater flow direction toward the cavity.

- After the depleted cavity was allowed to flood, water extraction was conducted from two cavities with the help of submersible pumps, followed by water treatment in an aboveground three-stage water treatment system and subsequent discharge to the ground surface.
- During water extraction activities, a decrease in the concentration of phenol was recorded (Fig. 11.12), as well as boron and ammonia to below detection limit, 0.02 mg/L.
- The bulk of groundwater that was subjected to the impacts of UCG is pumped out from the cavity, thereby reducing or eliminating the possibility of aquifer contamination (Speight and Covell, 1989).
- The water treatment system selected for removing ammonia and phenols was successful, but for the removal of other contaminants, the water treatment system should be improved.
- During site selection, attention should be given to the mining, geologic, and hydrogeologic conditions of the site.

Therefore, favorable environmental impacts of the UCG technology were confirmed.

A study of the possible UCG-induced groundwater contamination was carried out in the Surat coal basin in Australia. The pilot UCG project was launched in 1999 by Linc Energy and Ergo Exergy near Chinchilla, some 350 km from Brisbane. The pilot UCG plant was operational for more than 30 months. The controlled shutdown of the gasifier was commenced in January 2002. The UCG project in Chinchilla was the largest in scale and longest-operating in the West. It should be noted that since the UCG project at Chinchilla was the first of its kind outside the former Soviet Union and was developed on a commercial basis, strict confidentiality standards were maintained, with only limited disclosure of findings (Blinderman and Fidler, 2003).

The coal deposit is characterized by quite favorable conditions for UCG. The coal seam is 10 m thick at a depth of 140 m surrounded by low-permeability rock strata composed of clays, clay sandstone, mudstone, and siltstone. The dimensions of the gasifier were 200 by 150 m.
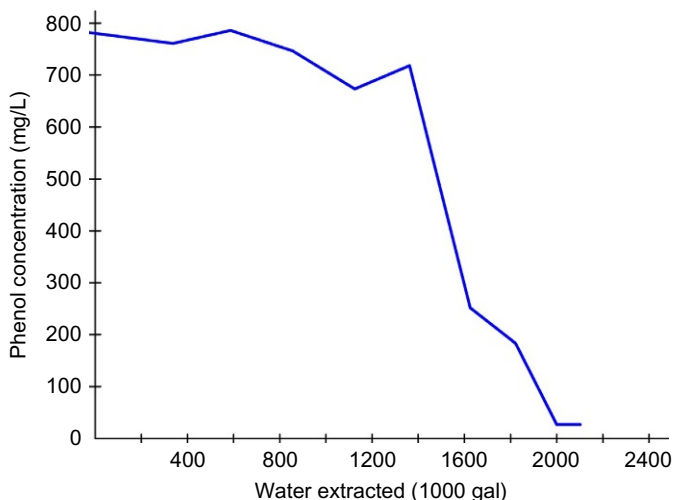
Fig. 11.12 Variations over time of the concentration of phenol in groundwater in depleted gasification cavities during water extraction activities.

Environmental monitoring studies of groundwater systems were conducted at the coal deposit. Prior to initiation of UCG operations at the pilot gasifier, 13 groundwater monitoring wells were drilled. Monitoring occurred in two zones:

−Inner zone with a radius of 300 m from the center of the gasifier containing six groundwater monitoring wells, two of which within 50 m and the rest at a distance of 130–180 m
−Outer zone at a distance of 350–1750 m from the gasifier containing seven groundwater monitoring wells

Inside the inner zone, five wells were drilled and instrumented with piezometers (Fig. 11.13).

Gasification was carried out at pressures below the hydrostatic pressure throughout the service life of the gasifier.

To stop gasifier operation, a special program of controlled shutdown was developed. The shutdown program entailed a continued gasification phase under reduced pressure. Eventually, air injection into the underground gasifier was cut in mid-April 2002, with UCG operations completion in April 2003.

Monitoring of hydrodynamic and geochemical groundwater conditions supported the findings obtained previously in the USSR and the United States as follows:

1. During UCG, the groundwater flow direction is toward the underground gasifier area. Contamination is localized.
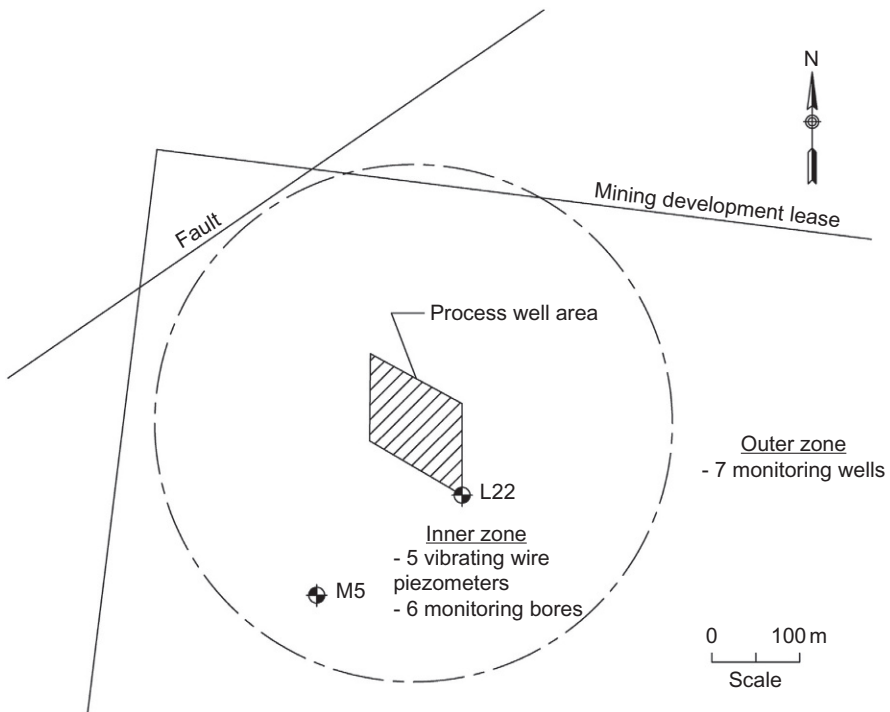
Fig. 11.13 Groundwater at the underground coal gasification site at Chinchilla, Australia.
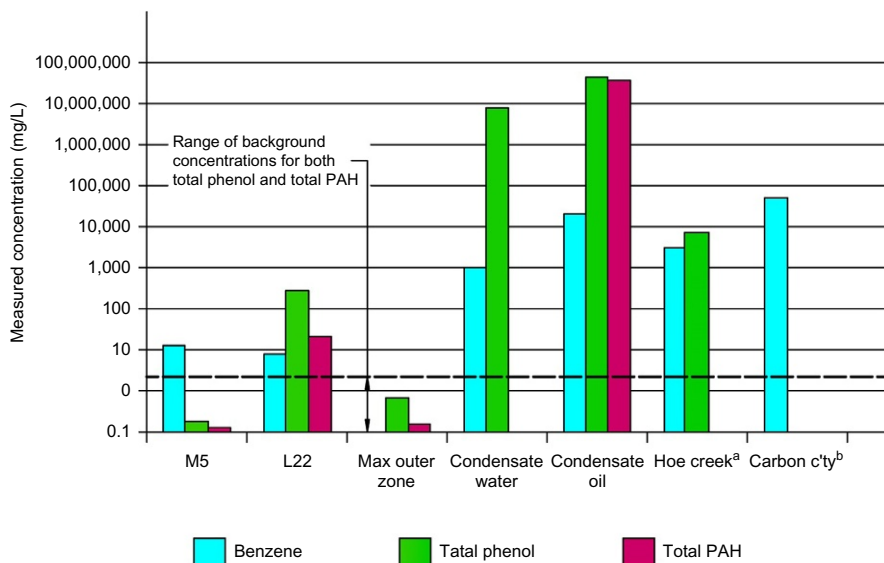
Fig. 11.14 Results of groundwater quality monitoring. [a]Phenol concentration measured adjacent to gasifier at 6 months after gasification. Benzene concentration for unknown location and time. [b]Maximum measured concentration 3 years post-gasification

2. The maximum contaminant concentration levels are found in the condensate (Fig. 11.14), which confirms the conclusion that during UCG operations, most contaminants are entrained with the gas mixture and brought up to the surface where it can be treated.
3. The increased concentration of contaminants was noted only in wells connected into gasification cavity. No contamination was detected in the groundwater monitoring wells. After termination of UCG operations, the concentration of contaminants inside the gasification cavity was consistently decreasing.

One of the important aspects of the project was the proprietary system of groundwater protection using hydraulic circulation system developed by Ergo Exergy. This system consisted of several wells with an in-seam interconnectivity. This technique permitted cleaning the spent gasifier from contaminants using water injection or by injection of biological agents into one of the wells.

In 2002, Eskom Holding (South Africa) entered into an agreement with the Canadian-based technology provider Ergo Exergy to develop the Majuba coal field in the province of Mpumalanga. Hydrogeologic and environmental investigations in the mining lease were initiated in 2005 and continue to the present.

At the pilot UCG site, the subhorizontal coal seam with a thickness of 4.2–5.35 m was intersected at a depth of 266–300 m (coal seam floor). Four aquifers are identified at the study site. Groundwater monitoring wells were installed in the shallow aquifer that is nearest to the ground surface, the intermediate upper and intermediate lower aquifers, and the deep coal seam aquifer.

The investigations bore out the results of previous studies conducted in the former USSR, the United States, and Australia:

1. During UCG, the cone of groundwater depression was continuously present localizing the contamination.
2. After termination of UCG operations, the groundwater level gradually recovered. Thanks to the water level recovery, a zone of decreased groundwater heads persists in the vicinity of the gasifier for a long time. The groundwater flow direction is toward the spent gasifier cavity. Decreased contaminant concentration is noted.
3. Environmental protection measures, including hydrodynamic impacts on the aquifer, were instituted making it possible to control the groundwater contamination.

Thus, large-scale studies conducted in various mining, geologic, and hydrogeologic conditions, at commercial UCG plants in the former USSR, and during experimental and research programs in the United States, Australia, and South Africa showed that with an adequate mode of operation of a UCG gasifier, gasifier design, gasification, and dewatering regimes and complying with environmental protection measures, it is possible to conduct coal mining operations using the UCG method without detriment to the environment.

11.6 Conclusions

Presently, the world's coal consumption in electricity generation is significant: 70% in China, 56% in the United States, and 40%–60% in Western Europe. Coal resource tonnage significantly exceeds the total oil and natural gas resources. Considering the growing shortage of natural gas, the use of coal for energy production can be expected to increase in the near-term future. However, as was discussed above, the use of conventional coal mining methods has considerable environmental disadvantages. Modern environmentally friendly coal technologies, notably including UCG, will permit a reduction in stress to the environment in coal mining regions.

This chapter discusses the formation of the zone of man-made impacts on the hydrolithosphere and defining principal parameters. The types and nature of man-made changes in the hydrolithosphere are identified, as well as the nature of the physiomechanical and physiochemical processes inherent in the UCG, which largely determine the degree of groundwater contamination. The chapter also incorporates a classification of the major factors that determine the chemical composition of groundwater and the contamination plume, which together constitute the main environmental impact factors of UCG. For convenience, all factors are subdivided into two main groups: man-made and naturally occurring factors. Each factor and its effects on the hydrosphere are described individually, although during the actual operation of the UCG gasifier, the factors are not isolated from one another but rather interrelated. It should be emphasized that depending on the natural setting, some factors may play a pivotal or secondary role, while others may not play any distinctive role in groundwater chemistry. Not infrequently, major impacts of some factors may give

way to the influence of other, more dominant factors under different conditions, which is a common occurrence in UCG, with continual changes in temperature, pressure, hydrodynamic, and geomechanical conditions.

Analysis of large-scale environmental studies conducted in the USSR, where a number of commercial and pilot UCG plants were in operation, and select pilot studies in the United States, Australia, and South Africa showed that potential groundwater contamination by the products of in situ coal gasification products is restricted to a localized area and can be completely removed or reduced to a minimum.

The model prediction contamination plume spread using the conductivity profile model that takes into account the anisotropy and conductivity nonuniformity of rock, gravitational differentiation, and physiochemical interaction of the contaminated stream with rock (sorption) is solidly backed up by the results of long-term studies.

Most contaminants are carried along with the gas flow to the surface in the form of condensate. The maximum contaminant concentration is recorded during the in situ coal gasification period, with a cone of groundwater depression surrounding the gasifier, which prevents the spread of contamination. Once the UCG operations have been completed, continued water extraction brings the concentration of contaminants down to levels below the maximum allowable concentration for drinking water. After groundwater levels recover, migration of contaminants from the depleted gasifier occurs primarily through heated coal, which is noted for high sorption capacity, contributing to the self-purification of groundwater. Specialized studies of the adsorption properties of raw and heated coal showed high phenol adsorption values.

UCG site selection should first and foremost consider possible environmental impacts. The classification of environmental impact factors should serve as a basis for the choice of an appropriate UCG mining method, gasifier design, mode of dewatering and gasification operation, and the need to develop environmental programs.

The investigation results presented highlight the multifaceted nature of protecting groundwater from contamination during UCG operations. Future efforts would do well to pursue development in the following areas:

−Investigate transport of solutions through heated and burned rock and coal in laboratory conditions and determine their sorption properties.
−Conduct field studies of groundwater flow and transport in specific geomechanical aquifer settings, specialized tracer testing.
−Study physical and chemical parameters of the coal seam, which are necessary to predict contaminant dispersal velocity and for the development of environmental protective procedures.

To provide effective solutions to eliminate possible adverse effects of UCG technology, close attention is required to the scientific and methodological aspects as early as the site evaluation and exploration stage, as well as gasifier design and operation.

The geologic and hydrogeologic conditions of each coal deposit mined using the UCG method offer a unique set of challenges both in determining the extent and scale of potential adverse effects on the hydrosphere and developing methods of prediction to develop cost-effective, environmentally protective solutions.

References

A collection of methods for calculating air emissions in various industries, 1986. Leningrad: Gidrometeoizdat.

Antonova, R.I., Dvornikova, E.V., 1992. Effects of underground coal gasification on the environment. Seminar reports. In: Seminar on Underground Coal Gasification, Kemerovo, pp. 52–59.

Antonova, R.I., Dvornikova, E.V., Kreinin, E.V., Guryanova, E.V., 1991. Underground Coal Gasification and Environmental Protection. Izvestia. vol. 1. Skochinsky Institute of Mining, Moscow, pp. 199–201.

Blinderman, M.S., 1995. Underground coal gasification in abandoned mines. Coal Sci. 1, 739–743.

Blinderman, M.S., Fidler, S., 2003. Groundwater at the underground coal gasification site at Chinchilla, Australia. In: Proceedings of the Water in Mining Conference, Brisbane, Australia.

Chekina, V.B., 1994. Environmental assessment of underground coal gasification in comparison with conventional coal mining methods. Scientific Bulletin, 295, Skochinsky Institute of Mining, pp. 112–123.

Corazon, M., 1991. Energy Policy and Planning Seminars. Training Material. Economic Development Institute, The World Bank.

Dvornikova, E.V., 1994. Investigations of specifics of interaction of products of underground coal gasification and groundwater. Science Bulletin, vol. 295. Skochinsky Institute of Mining, Moscow, pp. 48–56.

Dvornikova, E.V., 1996a. Analysis of the formation and prediction of the distribution of groundwater contamination zones during underground coal gasification (Ph.D. thesis). Moscow, p. 251.

Dvornikova, E.V., 1996b. Major factors impacting the groundwater conditions and contamination of groundwater during underground coal gasification. Scientific Bulletin, vol. 304. Skochinsky Institute of Mining, Moscow.

Dvornikova, E.V., 1996c. Role of sorption capacity of high volatile bituminous coals in self-purification of groundwater. Ugol 5, 45–47.

Dvornikova, E.V., 2005. Ecological aspects of underground coal gasification. Scientific Bulletin, vol. 330. Skochinsky Institute of Mining, Moscow, p. 330.

Dvornikova, E.V., 2011. Specifics of contaminant migration from the underground gasifier: mitigation of environmental impact. Ugol 11, 63–69.

Dvornikova, E.V., Kreinin, E.V., 1993. On the interaction of groundwater with the fire source during underground coal gasification. Physical and Process-Related Challenges in Researching Fossil Fuels, 5, Academy of Sciences of the Russian Federation, Novosibirsk, pp. 73–78.

Dvornikova, E.V., Strock, N.I., Bankovskaya, V.M., 2001. Specifics of man-made metamorphosing of surface water in open-pit coal mining in the Moscow coal basin. Mining Bulletin, vol. 2.

Kalachev, A.I., 2016. Problems and solutions for the conversion of coal-fired power plants to SSZHShU-100 (system of dry ash and slag waste removal) designed for optimal utilization of ash and slag waste. In: UgolEco Conference, Moscow, September 27–28.

Karasevich, A.M., Kreinin, E.V., Dvornikova, E.V., Streltsov, S.G., Sushentsova, B.Y., Zorya, A.Y., 2009a. Method of environmentally friendly underground coal gasification. Patent (Russian Federation) No. 2360106.

Karasevich, A.M., Kreinin, E.V., Dvornikova, E.V., Streltsov, S.G., Sushentsova, B.Y., Zorya, A.Y., 2009b. Method of cleaning groundwater in the depleted cavity of an underground gasifier. Patent (Russian Federation) No. 2358915.

Kononov, V.I., 1965. Effects of Natural and Man-Made Heat Sources on Groundwater Chemistry. Nauka, Moscow, p. 146.

Kreinin, E.V., Dvornikova, E.V., 1997. Method of underground coal gasification. Patent No. 2090750.

Kreinin, E.V., Dvornikova, E.V., 1999. Distribution prediction of zones of interaction of the contamination source with groundwater. In: Proceedings of the Academy of Sciences, Part 365. vol. 3. pp. 371–373.

Parakhonsky, E.V., 1992. Protection of Water Resources in Underground and Open-Pit Mines. Nedra Publishers, Moscow, p. 191.

Speight, J.G., Covell, J.R., 1989. Rocky Mountain 1 groundwater restoration: first treatment. In: International Underground Coal Gasification, Delft University of Technology, October 9–11. pp. 515–533.

Technological schemes of cleaning from suspended solids and disinfection of mine waters, 1985. Catalog. Central Research Institute of Economics and Scientific Information of Coal Industry, Moscow, p. 120.

Walker, L.K., Blinderman, M.S., Brun, K., 2001. An IGCC Project at Chinchilla, Australia based on Underground Coal Gasification (UCG). In: Paper to 2001 Gasification Technologies Conference, San Francisco, October 8–10.

This page intentionally left blank

Part Three

Modern underground coal gasification (UCG) projects, scaling up and commercialization

This page intentionally left blank

What makes a UCG technology ready for commercial application?

12

M.S. Blinderman, A. Blinderman, A. Taskaev
Ergo Exergy Technology Inc., Montreal, QC, Canada

12.1 Introduction

Underground coal gasification (UCG), proposed by Wilhelm Siemens as early as in 1868 as a large-scale industrial process for extracting coal energy that can replace conventional coal mining, has not achieved wide commercial deployment to date, following almost 150 years of its worldwide development. This may be countered by pointing out several commercial-scale UCG plants that have operated in Soviet Union for many years, one of which, the Angren UCG plant commissioned in 1960, is still operational (Saptikov, 2017). While acknowledging the value of Soviet experience of designing, building, and operating large UCG plants for decades, we should emphasize that investment decisions for those plants were made in Soviet central planning system, which is hard to correlate with modern, economically driven investment decisions. A good indicator of commercial readiness of UCG technologies is the fact that no commercial plant was commissioned anywhere in the world in the last 50 years. We will discuss here the technical, environmental, and regulatory reasons for this lack of commercialization progress and the ways to change the trend and make the technology more prepared for commercial application.

Let's briefly consider current condition of the nascent UCG industry. A long period of global UCG development spawned by the energy crisis that started in 1973 was completed by the Rocky Mountain 1 trial in the United States in 1988 and the European UCG trial in Spain in 1992. Following several years of lull and uncertainty, the Chinchilla UCG project in Australia marked the beginning of new era of UCG development in Australia, New Zealand, South Africa, Europe, Canada, and the United States. Spanning almost 20 years, this latest stage of UCG development was distinguished by a preponderance of privately funded projects with a significant share of the capital raised from stock markets.

It appears that this latest stage of UCG development has suffered considerably from the drop in fossil-fuel prices in the world markets and from the general global commodity market slowdown. Whereas the reduced oil and natural gas prices seem to have affected new and existing UCG projects by decreasing projected sale prices of UCG products, the corresponding precipitous drop in coal price robbed many UCG proponents of the revenue that was intended for investment into new UCG projects.

An example of the latter was the shutdown of the Huntly West UCG plant in New Zealand.

The commodity market slowdown led to the slower development of the Majuba UCG project in South Africa. Reduced economic performance and suppressed energy prices in, for instance, North American markets seem to have led to closure of the Swan Hills ISCG project and deterred the start-up of the Parkland County UCG project in Canada.

The other factor in limiting UCG activity in the world is the lack of preparedness of environmental regulations and a gross misunderstanding and misinformation on UCG within environmentally concerned communities, caused no doubt by scarcity of factual information on UCG. This regrettable state of public awareness has led to reluctance by local authorities to approve new UCG projects in several jurisdictions, in particular, in Queensland, Australia, and Scotland, the United Kingdom.

Along with these objective reasons for a slowdown in the global UCG development, there also have been other possibly more subjective technical grounds for a slowdown or demise of several widely anticipated UCG commercialization projects.

12.2 Requirements to commercial UCG technology

Commercialization of UCG must deal with the issues similar to any other new large-scale fossil-fuel-based energy technology, namely,

- capital intensity;
- carbon footprint;
- scarcity of long, large-scale demonstration runs;
- availability of competent technology providers;
- availability of skilled workforce;
- awareness and maturity of expert community;
- the lack of industry standards;
- the absence or insufficiency of regulatory framework;
- perceptions of technical, environmental, and financial risk;
- the lack of political support.

These similarities, however, don't mask the differences inherent in UCG process: a UCG reactor is built and operated hundreds of meters below the surface by remote control, and the operator has no efficient means to monitor its shape or the processes within the reactor. The difference in scale and ability of the operator to control and intervene into the process is illustrated by Fig. 12.1.

Despite the differences, to be applied in commercial projects, UCG must meet common criteria of a commercial technology. These are to include at least the following criteria, *all* of which must be met *all the time*:

1. Consistent quality of the product (syngas). For instance, for a CCGT application the variation of the syngas quality parameter, Wobbe index should not exceed 5%. Obviously, for any application the consistent gas quality must be within inlet specifications of the customer plant.
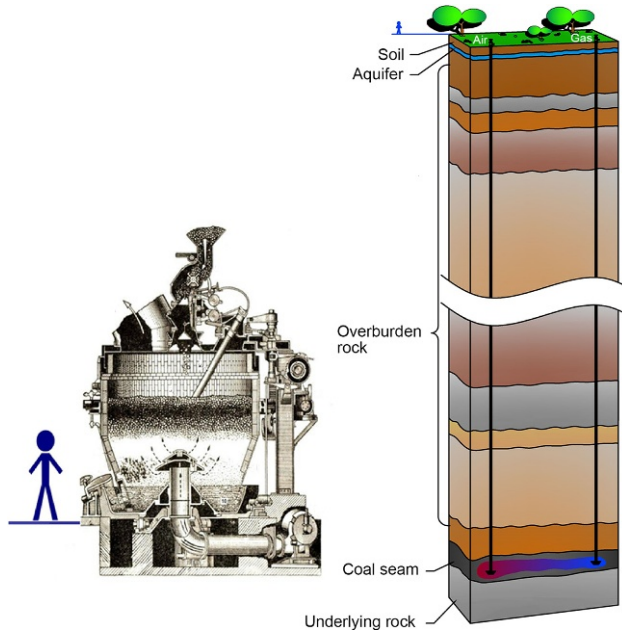
Fig. 12.1 The difference between UCG and conventional gasification reactor in scale and access.

2. Requirement of consistent quantity of the product may be formalized by limiting variations of the energy output of UCG plant by say 1%, if the plant consuming the syngas can operate with this inlet capacity tolerance.
3. The size of UCG operation must be sufficiently large and scalable to meet the input requirements of a world-scale consuming plant, for example, at least 1 million metric tonne per annum. It is required to maintain this capacity consistently for 25–30 years to allow time for repaying capital and receiving return on investment.
4. Environmentally clean, carbon-efficient operation that protects groundwater, air, and other potential environmental receptors.

12.3 Syngas quality

The main question to a UCG technology provider is always that—can UCG deliver reliability of supply to a modern power or chemical plant, in other words, is the quality of the gas consistent and stable? Apart from obvious concerns with access and control of UCG reactor, there is a simple technical reason why UCG should demonstrate the ability to produce consistent quality gas. It is illustrated in Fig. 12.2.

The mechanism of inherent inconsistency of gas quality in linear (1-D) UCG reactors is easy to understand. Unlike conventional gasification reactors, UCG reactor has no steel vessel walls to contain the reagents and products. It is built within coal seam, which serves as walls of the reactor. Coal, the main raw material for the reactions, is consumed
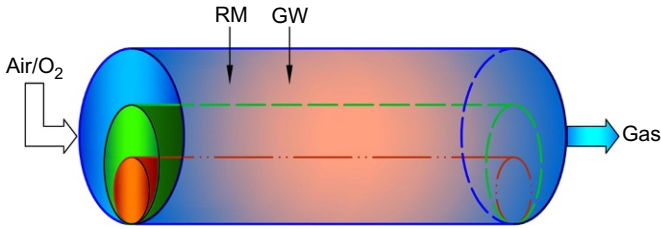
Fig. 12.2 Inherent variation of reaction conditions in a UCG reactor; RM, rock mechanics inputs; GW, groundwater inputs.

off the walls of the reactor; water is supplied by groundwater influx sipping through the reactor walls. As the process proceeds, coal walls of the reactor are consumed, and the cross section of the reactor keeps growing. Since the flow rate of injection agent is constant, the increase in reactor diameter leads to a lower gas velocity in the reactor. This corresponds to dropping Reynolds number, a criterion of flow turbulence. As turbulence subsides, the mass and heat exchange in the reactor weakens, which means that the oxygen of the injection agent is less effectively delivered to reactor coal walls where it should be consumed in heterogenic reactions. This in situ process results in visible deterioration of syngas quality produced at the ground surface. In field operations, this process takes only 10–15 days for the gas to start losing quality and to show unreacted oxygen. Before the concentration of unreacted oxygen in the produced syngas starts approaching a dangerous level, the gasification must be stopped.

In order to alleviate the effects of described process, a technique of controlled retracting injection point (CRIP) was proposed by researchers of Lawrence Livermore National Laboratory (LLNL) in the United States (Hill and Shannon, 1981). It is illustrated in Fig. 12.3. The horizontal channel between injection and production wells is
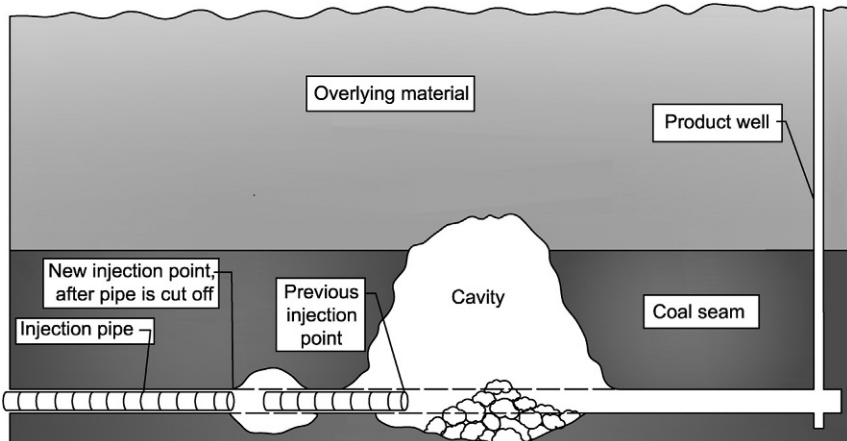
Fig. 12.3 CRIP technique.

lined with a perforated steel pipe and fitted with a burner inserted on a flexible tube from injection well, that may be moved back toward injection well by pulling out the flexible tube. The injection well is normally a directional well with horizontal in-seam portion, connected to a vertical production well (this version of CRIP technique is also referred to as linear CRIP). Initial reactor is started by using the burner to ignite coal seam. As the reactor growth reaches the point when the gas quality shows first signs of deterioration, the burner is pulled back, and a new reactor is created by second ignition, upstream from the first one (this operation is called a CRIP maneuver). Multiple CRIP maneuvers should be used for a prolonged gas production. This way, the size of the currently active reactor is limited, which should be evidenced by a stable quality of produced gas.

The best demonstration of CRIP technique to date is the Rocky Mountain 1 trial conducted in 1986–88 in Wyoming (RM1, 1989). Two UCG modules—one with CRIP and the other (ELW) without it—were run in parallel to highlight the benefits of CRIP operation. The time variation of product gas heating value for CRIP and ELW modules is shown in Fig. 12.4.

In this graph, red lines correspond to CRIP module and blue ones to ELW module, with solid lines for actual variation of gas heating value and dashed lines for the average heating value trends. Roman numerals I, II, and III show times of consecutive CRIP maneuvers. It is clear that although gas quality achieved in CRIP module is almost always better than ELW, it also deteriorates significantly with time despite three performed CRIP maneuvers. Explanation is obvious: the gas, produced in active CRIP reactor with optimal gasification conditions, must pass through all the old, depleted CRIP reactors on its way to the production well. These reactors are cold
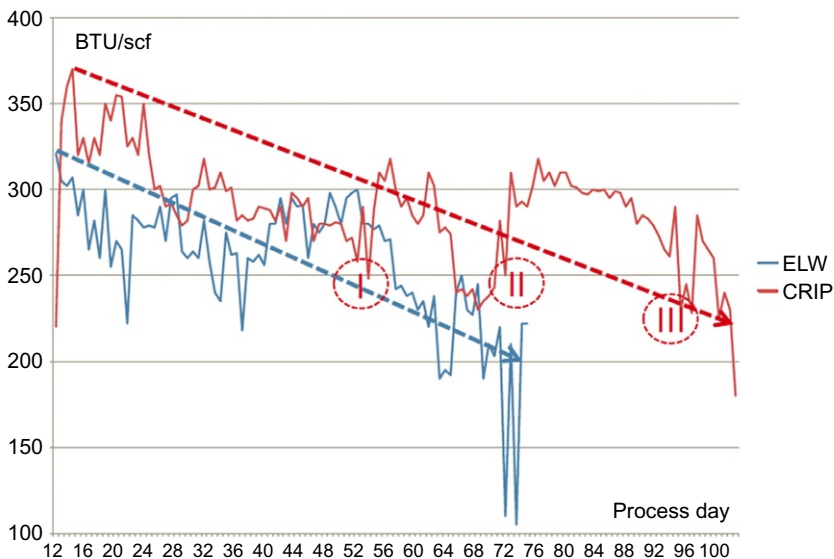
Fig. 12.4 Time variation of gas heating value, ELW and CRIP modules, RM 1 UCG trial.
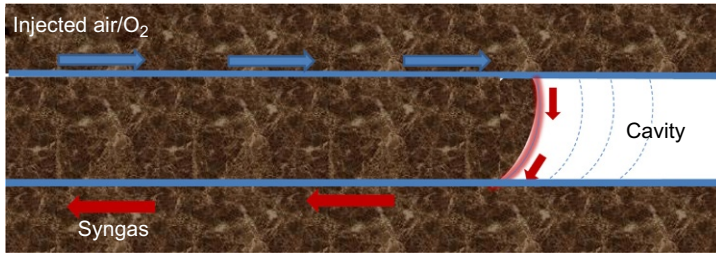
Fig. 12.5 A plan view of a parallel CRIP reactor.

and filled with ash, slag, and condensate liquids or vapors, so the gas continues to dete-
riorate there as it passes through. The longer is the chain of old reactors that gas must
flow through before it can be produced, the deeper is the negative effect on its quality.
It is this prominent feature that seems to have prevented commercialization of the
CRIP-based UCG plant following the success of Rocky Mountain 1 trial.

An attempt to correct CRIP deficiencies was made in proposals of "parallel CRIP."
In this technique, production well is not vertical but rather directional, with a long
in-seam portion drilled parallel to injection well (Davis, 2012). A plan view of the
parallel CRIP reactor can be seen in Fig. 12.5.

The idea behind the parallel CRIP was to eliminate the long gas passage through
multiple depleted CRIP reactors and instead give it a chance to be produced through a
horizontal production well. It was thought that the injected oxygen would flow along
the coal wall between injection and production points and participate in heterogenic
reactions with coal, thereby forming high-quality syngas. Retraction of injection point
may be performed by pulling ignition burner along the injection well or by installing
the injection well liner made of disposable sections that are supposed to achieve a
similar effect.

Parallel CRIP has been trialed by Carbon Energy and Linc Energy in Queensland,
Australia (Davis, 2012). Numerical modeling of this process was conducted by
researchers of University of Queensland and Ergo Exergy (Blinderman et al., 2016).
Selected results of simulations are presented in Figs. 12.6 and 12.7.

The modeling was conducted for a wide range of parameters such as pressure, flow
rates, and temperature and for reactor geometries reported by developers. The results
are clear. In case of the 3 m wide reactor, injected oxygen is in vigorous contact with
coal surface, and heterogenic reaction there dominates the process. However, when
reactor grows to a 25 m width, injected oxygen flows into the volume of the reactor
and does not have a chance to reach coal face until after it has reacted with product gas
that fills up the reactor. In fact, this type of oxidant flow is typical for reactors wider
than 10 m. For reactors wider than 10 m, simulation has found no practically signifi-
cant conditions when oxidant flow is held against the coal and does not pass through
the cavity, except for the oxidant flows with $Re < 50$, which corresponds to flow
rates measured in units of cubic meters per hour. These flow rates, of course, have
no relevance to a practical UCG process.
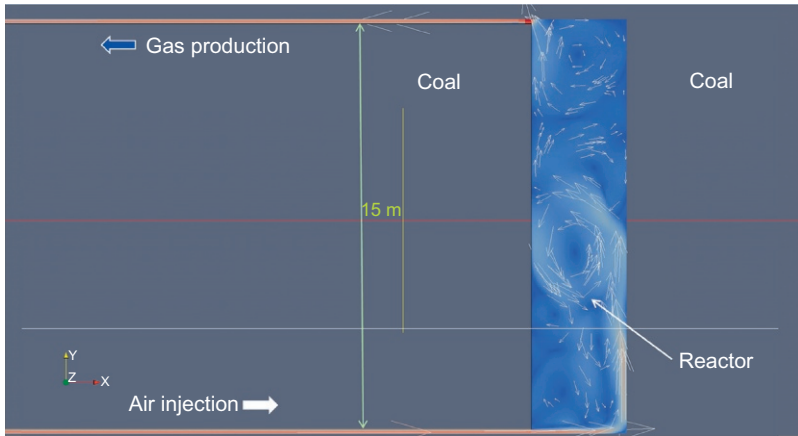
Fig. 12.6 Mass and energy exchange in the parallel CRIP 3 m-wide reactor (plan view).
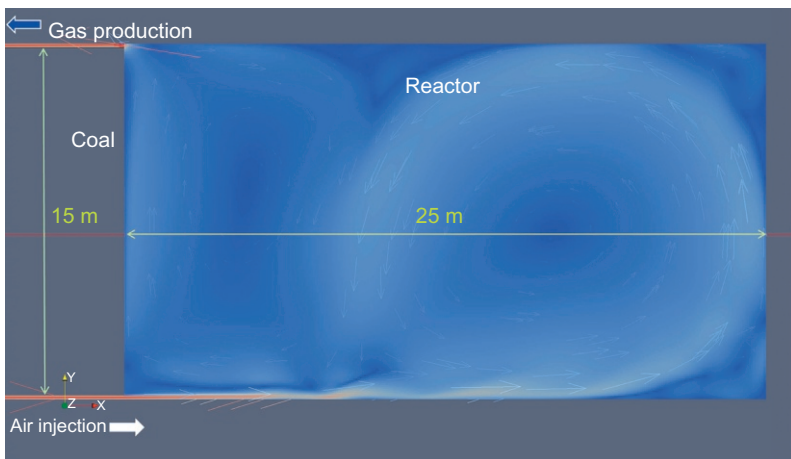
Fig. 12.7 Mass and energy exchange in the parallel CRIP 25 m-wide reactor (plan view).

Another way of assessing the effectiveness of heterogenic reactions of oxidant on the coal face versus its homogenic reactions with the preformed gas in the reactor volume, for various widths of reactor, is to calculate the yield of CO in these reactions. The more oxidant is consumed in reactions with coal, the higher yield of CO in the production well. The more oxidant is consumed in homogenic reactions with CO in the volume of reactor, the less CO will be found in the product gas. In Fig. 12.8, the ratio of CO/CO_2 in production well is plotted as a function of reactor width for three values of preexponential factor in the Arrhenius equation of the reaction ($A = 1$, 5, and 10 $mol^{-1}\,s^{-1}$). For slower reaction rate, the drop of concentration of CO in the product gas with increasing width of the reactor is quite prominent: at
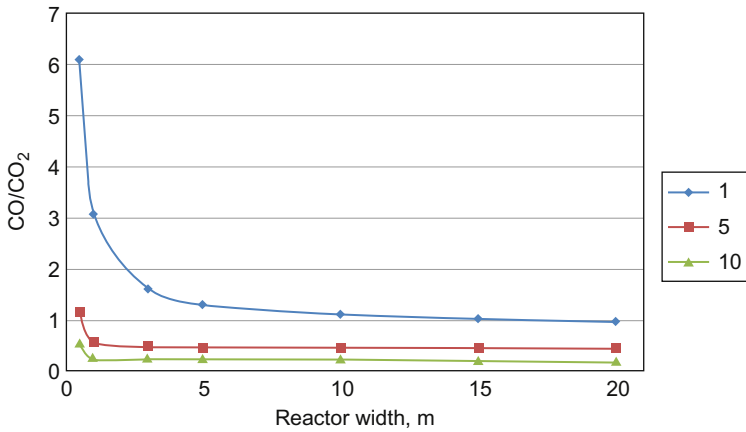
Fig. 12.8 CO/CO_2 in product gas versus reactor width for three reaction rates.

$A = 1$ mol^{-1} s^{-1}, as reactor expands from 0.5 m up to 20.0 m, the ratio of CO/CO_2 in the gas is reduced dramatically from 6.07 to 0.97. This effect is less prominent but still clearly pronounced for higher reaction rates ($A = 5$ and 10 mol^{-1} s^{-1}): In these conditions, the process is dominated by reaction kinetics rather than diffusion, so effects of mass exchange are suppressed. This outcome confirms an intuitively obvious conclusion: the growth of gasification cavity caused by continuous coal consumption in gasification process inevitably results in substantial decline in product gas quality.

In terms of syngas quality being suitable for modern industrial plants, extensive work including testing and field demonstrations has confirmed that efficient power generation is feasible using syngas from either air-blown or O_2-blown UCG processes (Blinderman, 2006; Blinderman and Anderson, 2004). Both air and oxygen syngas are suitable for a wide range of power generation plants, including gas engines, conventional boilers with steam turbines, and CCGT—gas turbines combined with heat recovery steam generators and steam turbines. These plants can be supplied by a variety of reputable international vendors. Syngas quality demonstrated in recent UCG operations has been shown to be suitable as a feedstock for various chemical syntheses (Blinderman et al., 2011).

12.4 Syngas quantity

What are the typical flow rates of syngas to be produced by a UCG to meet standard commercial plants demand? Table 12.1 may offer an idea of the UCG production scales that may be considered suitable.

The hourly flow rates in Table 12.1 are quite substantial and significantly higher than flows of natural gas the same plants would require, because of different composition and much lower heating value of syngas.

Table 12.1 Syngas quantity requirements for world-scale plants

Product	Capacity	Syngas demand, $10^3 \times N$ m^3/h
Synthetic gasoline	10,000 bblpd	380
IGCC power plant	300 MW$_e$	456
Urea	3500 tpd	390
Synthetic methane	25 BCF per annum	380
Synthetic diesel	10,000 bblpd	490

These quantities of syngas set specifications for the size of UCG production, number of injection and production wells, size of ASU or total compressor capacity, requirements for cleanup plant, etc. For example, the amount of syngas that can be produced through one production well is limited by the diameter of its casing, syngas production pressure, metallurgy of casing material, design of the cooling system, and the distance from underground reactor to the bottom of production well. Capacity of typical production well, be it vertical or directional, built to API standards and without forced gas cooling, would be limited to 2000–5000 N m^3/h (Blinderman et al., 1995). Comparing this flow rate with the ones indicated in Table 12.1 might be of concern for developers considering a UCG system with limited number of production wells, which is characteristic of CRIP-based designs.

Table 12.2 lists the key factors that, most frequently, tend to limit production capacity of UCG plant. They include gasification efficiency, availability of coal for gasification process, reliability of oxidant supply, and availability of production

Table 12.2 Key factors affecting production capacity of UCG plant

Target	Controlling factors
Gasification efficiency	Syngas yield per unit of oxidant
	Process intensity
	Control of injection point
	Syngas transport path
Coal availability	Timely commissioning of new reactors
	Availability of injection wells
	Control of injection point
Oxidant supply reliability	Compressor and ASU redundancy
	Availability of injection wells
	Timely well linking
Production availability	Production well integrity
	Condensate management
	Timely well linking
	Temperature control
	Workover capabilities

capacity. Next to these parameters, one can find the factors that help controlling them, thereby ensuring steady production rates of the plant.

Roles of most factors grouped in Table 12.2 are self-explanatory. They have to be taken into account in designing and operating the plant in a way that would provide necessary redundancy and maximize system flexibility in meeting syngas demand. The most important of them, in our estimate, are the ones related to process well integrity. Redundancy and flexibility in process well availability are the most critical for operational stability of UCG plant. It is fair to say that most operational failures in recent UCG projects, such as El Tremedal, Kingaroy, first panel of Bloodwood Creek, Swan Hills and some panels of Linc Energy's trial in Chinchilla (post 2006) that eventually led to a shutdown and abandonment of the trial, were related to failure of injection or production wells that left the operator unable to access the reactor and inject oxidant or produce gas from underground reactor.

It is important to remember that the factors listed in Table 12.2 play out on the background of ever-varying conditions: coal and surrounding rock geology, groundwater influx, and overburden cave-in accompanied by the deformation of surrounding rock. A meaningful and effective control of the process, necessary for ensuring stability and consistency of gas production, would be therefore only possible with using adequate geologic, hydrogeologic, and rock mechanics models of the formation and applying a comprehensive, practically validated model of gasification process itself. Even with these tools at hand, an effective UCG process control remains an art; experiences of process designer and operator are of utter value in ensuring reliability of syngas supply.

12.5   Extraction efficiency and coal resource

Criterion of scale and extraction efficiency is also vitally important for deciding on commercial application of UCG technology. Table 12.3 shows an example of coal consumption requirements of world-scale plants consuming UCG syngas, calculated for Texas lignites (Blinderman et al., 2011). Given contingences allowing for uncertainties of geologic structure, this information suggests that it would seem necessary to consider for a world-scale UCG plant a coal resource exceeding 50 million tonne. This

Table 12.3 **Coal requirements for UCG-supplied world-scale plants**

World-scale plant capacity	UCG coal consumption, million tonne per annum
10,000 bblpd of synthetic gasoline	3.0
300 MW$_e$ IGCC power plant	1.7
3500 tpd of urea	2.0
25 bcf of SNG	3.0
10,000 bblpd of diesel	4.0

assumes a very high extraction efficiency of UCG technology. For a 300 MW$_e$ IGCC plant, the extraction efficiency assumed in Table 12.3 was 95%. Should the efficiency drop to the level typical for underground mining (<50%), the plant's annual coal resource requirement would grow from 1.7 to 3.5 million tonne.

Considering extraction efficiency and resource requirements for CRIP-based systems, let's once again turn to experiences of Rocky Mountain 1 trial (RM1, 1989). A plan view of CRIP and ELW modules is presented in Fig. 12.9. The largely parallel modules spaced by about 100 m of virgin coal were run concurrently, with CRIP module running for 100 days and EVW module completing gasification 24 days earlier.

Material and heat balance of Rocky Mountain 1 trial were considered in detail in Gas Research Institute Report (Boysen et al. 1990). ELW module consumed 3,961 tonne and CRIP module—10,155 tonne of coal. Despite a roughly 100 m wide coal barrier between the modules, material balance shows significant cross flow of oxidant and syngas between the modules, which in this case could reach 2%–3%. Similar effects were reportedly observed in Bloodwood Creek trial between panels 1 and 2 and in a series of Linc Energy trials in Chinchilla (post 2006). Interaction and cross flow of oxidant and syngas between adjacent gasification cavities is well-known from operations of commercial-scale plants in the Soviet Union.

Let's assess a plant-average extraction efficiency of a CRIP-based UCG plant. The plant would include multiple CRIP modules running in parallel with nonrecoverable barrier pillars left between them to prevent cross flow of oxidant and syngas.
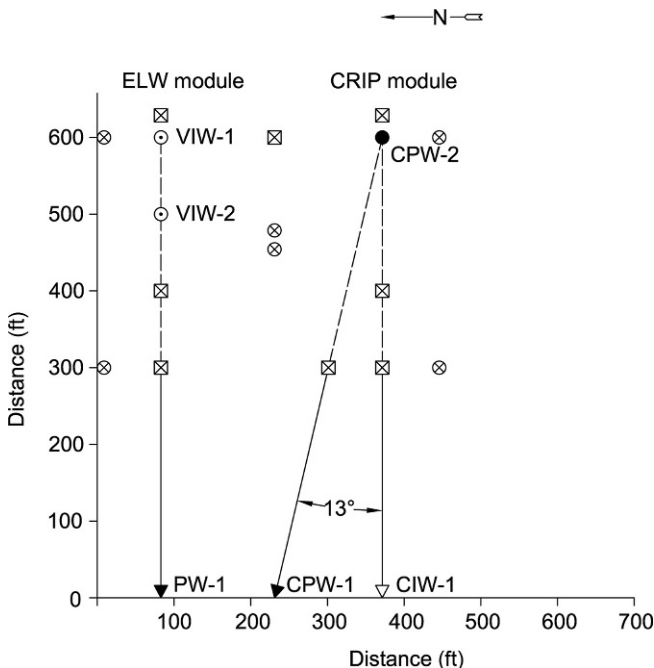
Fig. 12.9 Plan view of ELW and CRIP modules of Rocky Mountain 1 UCG trial.
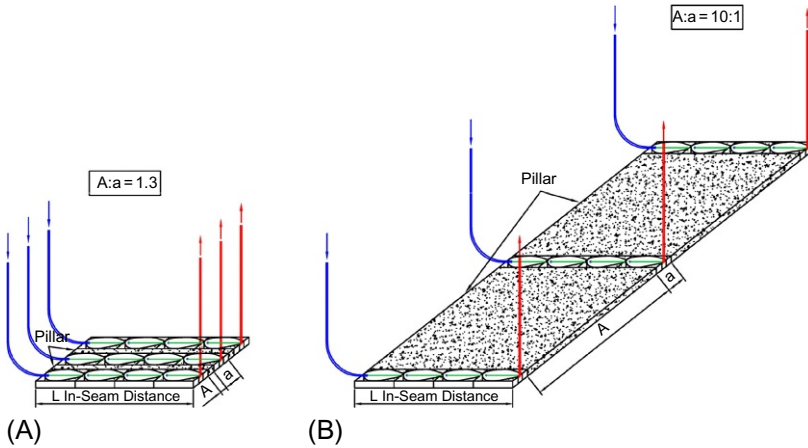
Fig. 12.10 CRIP mine plan: (A) as proposed by proponents and (B) preventing cross flow.

Extraction efficiency within one linear CRIP module has been recently estimated at approximately 28% (McVey, 2011). The width of the module is 30 m; this coincidentally corresponds to the width of a parallel CRIP panel as well (Mallett and Hains, 2015). Let's assume that the width of protective barrier pillar between CRIP modules is a conservative 100 m (according to the Soviet UCG experience, the width of the pillar must be at least 10 times as wide as the cavity). In these conditions the mine-average extraction efficiency could be calculated at 9.2%. This is illustrated in Fig. 12.10, depicting two versions of CRIP mine plan—one proffered by its proponents and another, more realistic one as described here.

Returning to coal requirements for commercial plants in Table 12.3, it is clear that with the extraction efficiency achievable for CRIP mine plans (less than 10%), a CRIP-based UCG operation supplying a 300 MWe IGCC power plant would require an annual coal resource allocation in excess of 16 million tonne. For 25 years of mine life, this amounts to more than 400 million tonne, which for obvious reasons may not be feasible. Note that this is valid for both linear and parallel CRIP designs. This seems to suggest that CRIP-based systems would require further work on mine planning and, most particularly, on incorporating this technique for controlling injection point into a broader context of UCG technology implementation.

To be attractive for commercial applications, a UCG technology should demonstrate extraction efficiencies close or exceeding those of conventional coal-mining industry, for which a 50% would be a good benchmark.

There is another very important reason why the mine plans like the ones shown in Fig. 12.10 cannot and should not be used in UCG. Since it is related equally to both coal resource requirement and environmental performance of UCG plant, we discuss it in the next section.

12.6   Environmental performance

No technology may be applied commercially unless its environmental performance is well understood and proven, and for simple reason, since no environmental clearances for such plant would be forthcoming. Besides, the plant would be met with a formidable opposition of local community and environmental groups, which would make its development impossible.

So UCG technology must demonstrate good environmental performance and provide convincing proof that its performance at a commercial scale would be as benign as demonstrated.

Along with routine environmental issues of any other industrial plant such as prevention of air and soil pollution, noise, management of hazardous materials, and handling of effluent water, which are dealt with in UCG by means similar to any other industry, UCG has two specific environmental aspects as its key concerns, namely, subsidence and protection of groundwater.

Subsidence in UCG is somewhat analogous, in principle, to subsidence in conventional underground mining, although there are important differences as discussed in Chapter 9 of this book. There are two general approaches to subsidence management in conventional mining:

- Partial extraction of coal seam, which leaves behind coal pillars, supporting overburden and thereby preventing roof collapse over extracted areas and limiting propagation of overburden deformation to the surface, that is, preventing subsidence; a typical example of this approach is a "bord-and-pillar" mining method, illustrated in Fig. 12.11.
- Continuous extraction, which requires complete and continuous removal of coal seam and avoids leaving pillars, thereby causing managed collapse and cave-in of overburden and eventual, full in its extent, subsidence of the surface. This approach is implemented by a long-wall mining method, widely employed in high-productivity underground coal mines.
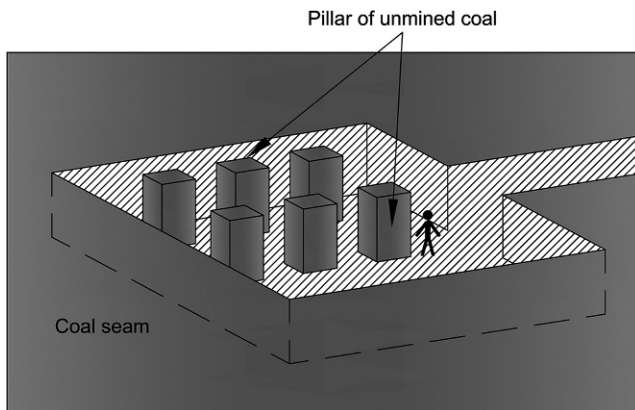
Fig. 12.11 "Bord-and-pillar" coal-mining method.

The CRIP-based mine plans reviewed in previous section seem to be an incarnation of the "bord-and-pillar" method. These mine plans are intended to prevent subsidence at the ground surface by leaving sufficiently large coal pillars between adjacent CRIP modules. We believe that this approach to subsidence management is flawed, not reliable, and is likely to lead to serious environmental problems.

It is well documented that, in many current and abandoned coal-mining areas around the world, for example, Witbank in South Africa; Ipswich in Queensland, Australia; Jharia in Jharkhand, India, supporting pillars in old coal mines are a source of major environmental concerns:

–   The pillars fail mechanically that results in random and unpredictable collapse of overburden and sudden subsidence that endangers lives and property.
–   Collapsed pillars are prone to spontaneous combustion that has caused sustained underground fires that turned out to be impossible to extinguish for a very long time.

These areas are examples of a failed subsidence management method. Whether the size and condition of protective pillars left by old mining was not adequate to begin with or time effects on the pillars had not been properly allowed for in the design, the result is obvious—the pillars lost their ability to support the roof, which caused major environmental events. In most cases, the owners of old mines are long gone and responsibility of dealing with environmental consequences is left to local communities and governments. Note that these pillars were left by underground mining, where their size and condition were easily monitored and controlled by miners underground.

UCG's ability to control the size and condition of protective pillars is limited—only so much can be done by remote control. Besides, depleted UCG cavities are abandoned at a still-elevated temperature and usually filled with groundwater and ash, which also may affect conditions of the pillars. UCG technology even with CRIP's advantages would have only limited control over shape, size, and mechanical strength of the pillars. In a long term, it is reasonable to expect gradual deterioration of pillar strength, while no direct inspection is possible, and only limited opportunities for monitoring of the pillar strength may be available. All this justifies a negative prognosis for long-term stability of the pillars, resulting in almost certain overburden deformation and unpredictable timing, specific location, and severity of subsidence. What confidence in the long-term environmental performance of a postgasification site may a regulator have? What in this case should be operator's pathway to complete rehabilitation and abandonment of the site?

With this in mind, it should be clear that since the pillars left by UCG mining would be even less reliable than those left in conventional underground mining, they should not be relied upon in managing subsidence at a commercial UCG plant. The UCG pillars are formed by combustion and gasification process without the presence of an operator, so their exact shape, condition, and location are hard to ascertain.

This seems to leave UCG operator with only one realistic option for responsible environmental management of subsidence—the continuous extraction method. In this case, the underground depleted cavity that contains ash, slag, groundwater, and small amount of residual coal char is filled with collapsed overburden rock, and deformation propagates toward the surface to its full extent. If this causes subsidence, full

subsidence is completed within the time frame of cavity rehabilitation, while the UCG plant still continues to operate. Any viable approach to subsidence management in a commercial-scale UCG plant should be based on the following:

– Continuous total coal seam extraction with no barrier pillars left behind;
– Controllable, predictable, and complete overburden deformation above depleted cavities, to be concluded within operational life of the plant.

It is obvious that mine plans of CRIP-based technologies (Fig. 12.10) are not suitable for this kind of subsidence management.

In terms of protecting groundwater, a UCG plant can be treated as a complex combination of coal mine and chemical plant placed into geotechnical environment underground. As such, it has no clear boundaries, thus entailing possibility of direct exposure of its surroundings to syngas and by-products of gasification process. No UCG process can operate in dry environment, the geological formation within which UCG is performed must be water-saturated. Since no direct access to underground environment by a human operator is feasible, the interaction of UCG process with groundwater is hard to monitor. In case groundwater contamination does happen, the nature of the plant makes it difficult to mitigate or eliminate consequences of such an event. Another important aspect of the interaction of UCG plant and groundwater is the following: UCG plant consumes sizable amounts of groundwater in the gasification process; this water should be accounted for and, in some jurisdictions, expressly licensed to UCG plant by the regulators.

The key mechanism of groundwater protection in a UCG operation is illustrated in Fig. 12.12.

Gasification pressure in the active cavity must be maintained lower than hydrostatic pressure in the surrounding aquifers, so that groundwater pressure gradient is always directed toward the cavity. This causes groundwater to flow into the cavity, where it reacts with coal and gas to form hydrogen and its compounds in the product syngas. The same gradient prevents the escape of syngas and by-products from the cavity into surrounding aquifers. Specific magnitude of the hydraulic gradient is a
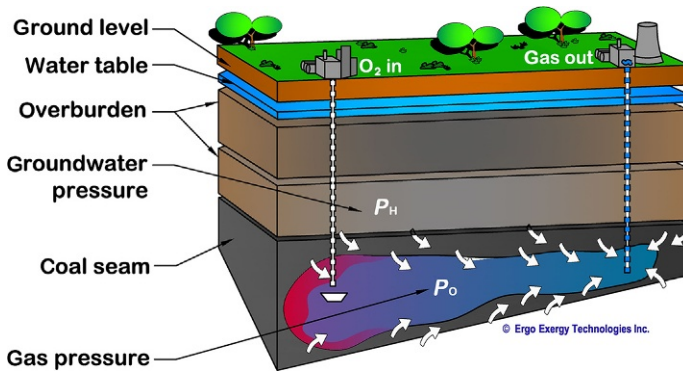
Fig. 12.12 Mechanism of groundwater protection in UCG operations.

Table 12.4 **Groundwater protection factors**

Potential impact	Control and mitigation factors
Local GW consumption	Planning and licensing of GW resources
	Reuse of cleaned condensate (UCG is net producer of water)
GW contamination by gas and condensate	Site selection and characterization—protect aquifers
	GW gradient toward cavity, extraction, and treatment of condensate
	Reliable underground circulation system
	Cavity steaming, flushing; forced and natural bioremediation
	Natural attenuation
Ash leaching in post gasification	Containment—slagging, gelling, and GW flow restraints
	Forced and natural dilution
	Sorption on residual coal char and injected sorbents

function of coal and rock permeability and depth, process water requirements, and many other factors.

Table 12.4 lists potential groundwater impacts and corresponding control and mitigation factors (Blinderman and Fidler, 2003). The first potential impact is groundwater abstraction. For example, to supply a 300 MW_e IGCC power plant, UCG operation would need to consume annually about 500,000 tonne of groundwater.

A large part of this would come from inherent moisture content of coal in situ, whereas the balance would have to be the groundwater influx into the UCG reactor from surrounding rock. Although in many cases this groundwater is saline or otherwise unsuitable for beneficial use, it must be accounted for and, in some cases, licensed. Fortunately, the water phase of the condensate delivered to surface with hot syngas flow can be separated from gas flow, cleaned up, and reused in the process, thereby significantly reducing overall groundwater consumption.

By far the most significant concern with groundwater in UCG is its potential contamination by syngas and condensate. There have been two well-known cases when UCG operations caused groundwater contamination with by-products of gasification (Carbon County UCG Inc., 1996; FETC, 1997). Although both sites have been fully rehabilitated and are now clean, there were important lessons learned as a result of those tests. As shown in Fig. 12.12, the most important controlling factor preventing groundwater contamination is maintaining positive groundwater gradient toward the cavity at all times of operation. This must be accompanied by thorough continuous extraction of condensate with hot syngas flow via production wells to the surface plant where it should be separated and processed. Neither positive gradient toward the cavity nor uninterrupted removal of condensate from the cavity is possible if there is no underground circulation system that is composed of a set of injection wells, underground reactor of low hydraulic resistance, and a set of production wells,

interconnected so that the flow of large quantities of gas through the system is possible to maintain with only limited pressure drop across underground gasification plant. As the reactor reaches the end of its life after all the available coal is consumed, a controlled shutdown and rehabilitation must be conducted to ensure that there are no residual sources of organic contaminants related to UCG process. The methods of steaming the cavity, flushing it of liquids and gases, pumping out of liquids for treatment at the surface cleanup plant, and bioremediation of depleted cavity have been demonstrated to be quite effective at this stage. It has been also noticed that there is a degree of natural decay of contaminants in depleted postgasification cavities, explicable by their sorption and by dilution of cavity water by regional flows. Ash leaching in postgasification cavity filled with groundwater may be of concern if physical and chemical properties of ash make it a potential source of inorganic contaminants. This process may be controlled or attenuated by conducting UCG in a slagging-favored mode, by adding into the cavity the agents that may limit mobility of leachate, and by using natural, and creating artificial, constrains for groundwater flow through the depleted reactor. Besides, leaching effects may be diminished by dilution of groundwater in the cavity and by sorption of leachate on coal char or on a purposefully injected sorbent.

As any other fossil-fuel-based technology, UCG must be concerned with its carbon footprint. An LCA assessment of GHG emissions of an UCG-IGCC power plant, for specific geologic conditions, and the eUCG™ technology, has shown the emissions to be significantly less than those of other coal-based power plants (BHP Billiton, 2002; Blinderman and Anderson, 2004). Further analysis of this issue is presented in Chapter 13 of this book.

A commercially applicable UCG technology must demonstrate reliable control of environmental performance during gasification and after it has been completed. It is therefore clear that a commercially applicable UCG technology must meet at least the same criteria that apply to coal-mining technologies: large scale and scalability, environmental acceptability, reliability of supply, and consistency of product quality. In this regard, UCG should be considered a coal-mining technology producing gaseous and liquid hydrocarbons, which is equally justified for other, more process-related reasons.

12.7   Feasibility and pilot plant

As for any other commercial project, a bankable feasibility study of some description is necessary to obtain an investment decision to build a commercial UCG plant. Given that a UCG plant may be considered as a "hybrid" of coal mine, chemical plant, and often power plant (at least to meet UCG's own needs) and that UCG is not a commonly well-understood technology, proving feasibility of such plant may become a daunting task.

The UCG feasibility study should accomplish the following:

– Define coal resources and technical reserves.
– Specify geologic and hydrogeologic settings.

–   Determine design base parameters for commercial plant.
–   Prove environmental performance.
–   Provide data for environmental impact assessment (EIA) of commercial plant.
–   Suggest design parameters and protocols for environmental monitoring of commercial plant.
–   Assess and prove economic viability of commercial plant.

In summary, feasibility study must sufficiently prove commercial plant's performance in terms of product quality and consistency, process efficiency, CO_2 footprint, and environment protection. All this is impossible without running a demonstration or pilot plant.

In order to commercialize a UCG technology, its performance must usually be proved and demonstrated at a pilot scale. The pilot plants are supposed to demonstrate technical parameters of the technology, such as syngas yield per a unit of coal mass, syngas yield per a unit of injection agent flow rate, cold gas efficiency, carbon conversion efficiency, and the overall thermal efficiency of the process. Besides, pilot plant should prove environmental performance of the technology by demonstrating controlled and limited environmental impacts and the operator's ability to control and mitigate environmental risks. Pilot plant is also relied upon to show competitiveness of capital and operational costs and to provide cost data for financial modeling of a full-scale, commercial plant. This presumes that the pilot plant in its design, scale, and duration is representative of the process to be used at a commercial scale and is capable to demonstrate the key salient features of the full-scale process in terms of its technical, environmental, and financial parameters.

In previous sections, we argued that only a large-scale, continuous extraction UCG plant with consistent quality and quantity of syngas may be suitable for commercial application. For pilot plant operation, this means that the scale of pilot plant, its design, and duration of testing should allow achieving conditions dominant at a commercial scale; most significantly, the effects of rock deformation and accompanying changes in groundwater flow patterns and influx into operating reactors. For example, if commercial plant design calls for a long-wall UCG panel that would inevitably lead to overburden deformation, then pilot plant's scale should be sufficient to see and manage the same rock mechanics effects, a resulting change in groundwater flow, and the specific way in which these processes affect gasification process proper and environmental performance of the panel. In other words, pilot plant performance and results should be scalable to commercial size in a clear and meaningful way.

This requirement is in a sharp contrast with an absolute majority of UCG trials conducted outside of the former Soviet Union. Most of them were designed to demonstrate gas production as such and possibly study some elements of the technology, for example, CRIP or reverse combustion linking, and had not operated for a duration or at a scale that could lead to a convincing demonstration of rock deformation effects on gasification process or groundwater flow. The size of the pilot plants was as a rule limited to 2–3 process wells; the surface area of operation would not exceed a couple of hectares, with total coal extraction almost never above 10,000 tonne and with total cumulative coal conversion, achieved in all UCG trials outside the former Soviet Union by 1997, less than 70,000 tonne (Walker, 2007). This explains why

most of these trials not only didn't find answers to questions of commercial-scale UCG operation but also never had a chance to realize what exactly those questions were.

The Soviet UCG program, with all its limitations related to distorted economics of central planning system and sometimes the lack of focus on environmental performance, at least could not be blamed for the small scale: approximately 24 million tonne of coal have been extracted by UCG there with plants varying in installed capacity between 0.1 and 0.75 million tonne of coal per annum. We believe that it was this large size that decided success of Soviet program in bringing about commercial-scale UCG operations: several UCG plants there operated commercially for decades, and one of the Soviet plants, commissioned in 1960, is still operating commercially today.

Apart from this general requirement of scalability of pilot plant, there are many technical tasks to be fulfilled in tests during its operations. Some of them are listed in Table 12.5. It is imperative to design the pilot testing program in such a way that the outcomes can be applied to a commercial UCG operation. What this really means is that all salient features of commercial plant must be well understood in advance, before designing and planning pilot tests. In practice, the flow of work in the project development should include the following in the displayed order:

- Screening of coal resource
- Scoping of commercial project
- Site selection for commercial and pilot plant
- Prefeasibility study
- Site characterization
- Pilot plant design, construction, testing, decommissioning, site, and cavity rehabilitation
- Bankable feasibility study
- Construction of commercial plant

Missing in this sequence is the work on obtaining regulatory and environmental approvals and fundraising.

Selection of the pilot plant scale is a very important decision. From our discussion above, it should be clear that a larger pilot plant has a better chance to reproduce the features and effects to be expected at a commercial scale. However, the larger the pilot operations, the higher are environmental risks associated with it. Small pilot plant with short duration of operations has the lowest potential environmental impact. Besides, capital and operational costs of the pilot plant are directly proportional to its size and life time. The necessary conclusion from this is that the selection of pilot plant scale is a crucial decision that should be made based on expert advice and careful analysis of technical, environmental, and financial aspects of the project.

12.8 Recent CRIP-based pilot plants

The Swan Hills UCG trial has been conducted in Alberta, Canada, in 2009–11. It targeted a 7 m thick seam of subbituminous coal at the depth of 1450 m. The UCG technology employed was described as linear CRIP. The underground system has

Table 12.5 **Some of technical objectives of pilot tests**

Optimization target	Variables
Syngas composition and its consistency (noncondensable, liquids, hydrocarbons, trace elements, etc.)	Oxidant composition, flow, pressure, and injection point
	Coal-seam thickness, coal quality, faults, and intrusions
	Groundwater influx
	Production temperature, flow, and pressure; production point
	Inert rock cave-in or heave-in
Drilling, process well design, construction, and operation	Drilling techniques, diameter versus operational pressure
	Type and number of casings
	Cement recipe and cementing procedure
	Cooling and condensate handling
	Integrity breach detection
	Workover convenience
	In-well instrumentation
	Wellhead design
Ignition methods	GW at ignition point
	High-pressure versus low-pressure ignition
	External versus incorporated oxidant
	Exhaust and product gas removal
Linking methods	Speed versus cost
	Oxidant composition, flow, pressure, and injection point
	Coal-seam thickness, coal quality, faults, and intrusions
	Groundwater influx
	Start/end pressure drop
Injection point control	Trigger selection
	Displacement distance
	Continuous versus discrete step

been constructed by drilling directional hole with a 1400 m long in-seam section and a vertical production well (Swan Hills Synfuels, 2012).

The information reported by the project operators was scarce. There were no data on the quantity, quality, temperature, pressure, flow rate, liquid components, and mechanical impurities of the syngas produced. Equally, no data are provided for the duration of gas production or parameters of injected agent such as oxygen-water ratio, flow rate, and pressure. No mention has been made of the process efficiency, extraction rates, and total amount of consumed coal. Environmental performance

has not been considered in the report, and no mention of environmental monitoring system has been made except for a microseismic monitoring well that seems to have been used for process monitoring.

It appears that no detailed site characterization had been undertaken prior to the commencement of gasification and no obligation of monitoring the potential underground impacts had been required by the plant permit conditions. As we understand from the report, the gasification process lasted not more than several days in the row, and it is unclear how many gasification attempts had been made. Some operational information can be drawn from a government regulator's incident investigation report (AER, 2014). On the sixth day of an apparent resumption of the process, there was a blowout, explosion, and fire in the directional injection well resulting in the loss of wellhead, release of gas and liquids into atmosphere, and fires in the nearby woods. The plant has been shut down and eventually abandoned.

Linear CRIP system attempted in this trial, as discussed above, has the following inherent limitations:

1. Despite CRIP maneuvers, efficiency of gasification and quality of the syngas inevitably deteriorate with each subsequent maneuver, primarily due to the detrimental influence of multiple previously depleted CRIP reactors, downstream from the active reactor, through which the syngas must flow to reach production well.
2. One linear CRIP module trialed in Swan Hills is too small to support a commercial use of the syngas. Multiple modules would be required to feed a standard size power or chemical plant. These modules must be separated by barrier pillars to ensure independent operation of the modules and prevent cross flow of injection agent and produced syngas. Extraction efficiency within one linear CRIP module has been recently estimated at approximately 28% (McVey, 2011). Taking into account the necessary width of the barrier pillars, the overall extraction efficiency of a mine plan comprising multiple CRIP modules with barrier pillars would be less than 10%—far below the coal-mining industry average.
3. Combined effect of syngas quality deterioration and very low extraction efficiency results in low reliability and poor use of natural resource, which, in our view, renders the method of linear CRIP unacceptable as a commercial coal extraction and conversion technology.

Although the project proponents seemed to claim that the results of Swan Hills pilot operation might be useful in commercializing UCG at a great depth, given what is known about operational results and in the absence of any news on the project for the last 3 years, we believe that commercialization of the process trialed at Swan Hills is unlikely.

The Chinchilla II project was operated from 2007 to 2013. Unlike the Chinchilla I UCG project that was developed and operated using the εUCG™ technology, between 1997 and 2006 within the same coal lease (Walker et al., 2001; Blinderman and Jones, 2002), the Chinchilla II was designed, constructed, operated, and managed with no involvement or knowledge of Ergo Exergy Technologies Inc.

The Chinchilla II pilot plant is located near the town of Chinchilla in southeastern Queensland, Australia. It targeted a 135 m deep, 10 m thick seam of subbituminous coal. Although technical information about the operations is very limited, it seems that the project attempted the application of both linear and parallel

CRIP methods (Davis, 2012). There were four consecutive attempts at UCG at four different locations within the same property. Details of the process at any of these trials have not been made public, so there is no information on the composition of injection agent (air/oxygen flow rates and pressure), nor there is any clear information on flow rates, pressures, temperatures, composition, impurities, or stability of syngas production, which would not give one a chance to appraise the process efficiency. Total coal resource converted by four trials combined apparently had not exceeded 8000 tonne. Starting from 2013, Queensland government announced a major investigation into environmental performance of the Chinchilla II plant. Department of Environmental and Heritage protection (DEHP) reported that in the course of this investigation,

– over 230 boreholes were drilled, and water and soil samples were collected from 13 surrounding farms;
– laboratory tests confirmed the presence of carbon monoxide, hydrogen, hydrogen sulfide, BTEX, and other chemicals in the collected samples;
– there was "scientific evidence of operation above hydrostatic pressure, fracturing the landform, and excursion of contaminants."

Queensland DEHP also alleged that plant owner failed to report numerous plant incidents, including several listed below:

– Fire that caused site evacuation in 2007
– Persistent leaks of toxic gas into air and groundwater from 2007 to 2011
– Worker's claims about their ill-health as result of "uncontrolled releases" of gas at site in 2007–13

As a result of this investigation, QEHP charged the company with irreversible damage "to more than one environmental receptor (the atmosphere, vegetation, water, and soil)" and laid five criminal charges against the plant owner. A 320 km^2 exclusion zone around 1 km^2 plant was established restricting farming activities there (the surface area of this zone reportedly to be extended further). According to recent reports, five officers of the company are also on trial for similar charges (Queensland DEHP, 2017). In the meantime, the company that owns and operates the plant has declared bankruptcy and is in the process of liquidation.

In light of all the above, one would tend to believe that commercialization of the UCG process trialed in the Chinchilla II project is unlikely.

Bloodwood Creek is the name of another UCG pilot project conducted in Queensland, Australia, in 2008 through 2012 (Mallett and Hains, 2015). It targeted a 200 m deep, 8–9 m thick subbituminous coal seam. The method of parallel CRIP has been employed with a 500 m long in-seam directional drilling. Two trials of gasification have been run with the first panel abandoned early in operations, apparently due to irreversible problems with injection well, caused by explosion and blockage. Second trial reportedly produced gas of stable quality for an extended period of time. There has been one reported instance of GW contamination during operations. Following the panel shutdown, residual contaminants were reported to remain in the cavity water.

Serious concerns with material balance in the demonstration of parallel CRIP technology have been expressed based on CFD modeling of the gas flow within a parallel CRIP panel (Blinderman et al., 2016). The modeling based on reported operational parameters shows that in the conditions described above, the oxygen of injected air could not effectively react with the coal seam close to injection point. The oxygen would rather proceed into the volume of created cavity to be consumed in parasitic homogenic reactions with syngas created in the cavity previously, thereby causing deterioration of produced gas quality (a process colloquially known as *cannibalizing syngas*). This means that the raison d'être of CRIP method—to improve stability of the process while increasing size of underground cavity—does seem unattainable in either linear or parallel CRIP configurations. Besides, all the issues with extraction efficiency discussed above for linear CRIP are equally valid for its parallel incarnation. Uncontrollable variability of gas quality and quantity together with low extraction efficiency appear to be the technical barriers that the proponents are still to overcome on the path to commercializing the CRIP-based UCG methods.

12.9 The εUCG™ based pilot plants

Several UCG plants, operated in the past 20 years, have been based on the **ε**UCG™ technology. The Exergy UCG™ (**ε**UCG™) technology is a specific set of approaches, means, tools, techniques, methods, devices, apparatus, models, algorithms, procedures, standards, recipes, formulations, specifications, and norms for extracting the energy and hydrocarbons from underground unminable fossil-fuel deposits, such as coal, lignite, peat, oil, tar, or shale, by converting them into gaseous and liquid hydrocarbons in a gasification process performed in situ, whereby drilled wells are used for delivering oxidant for gasification process and transporting products to the surface for processing and beneficial use. The **ε**UCG™ technology was developed by Ergo Exergy Technologies Inc. (Ergo Exergy) and has been applied in several international UCG projects.

The **ε**UCG™ technology is a large-scale, scalable, and modular mining technology with a typical panel capacity of about 0.3 million metric tonne per annum and combined hydrocarbon output of 2.0–5.5 PJ/a (in certain conditions, a smaller capacity panel may be feasible). Each panel would normally have a life span of 3–5 years, although there are geologic conditions where a single panel can last a life of the typical consumer plant (20–30 years). Unlike UCG techniques described in the previous sections, the **ε**UCG™ process is not designed to avoid roof collapse. Instead, it is designed to purposefully incorporate controlled rock deformation and groundwater influx. Depending on the quality of coal and specifications for required products, the process may include injection of compressed air, oxygen, steam and water, carbon dioxide, and other oxidants. Injection of oxidants and production of syngas are effected via drilled boreholes, design of which is suited to geologic condition and

includes vertical, inclined, and directional wells. Several techniques of controlling and changing injection point form an integral part of εUCG™.

The versatility of the $\boldsymbol{\varepsilon}$UCG™ technology may be illustrated by Table 12.6 that shows coal quality and geology at the plants, where various elements of the $\boldsymbol{\varepsilon}$UCG™ technology have been applied.

Of projects listed in Table 12.6, we here briefly consider two, the largest and the second largest UCG plants outside of the former Soviet Union. More detailed discussion of the $\boldsymbol{\varepsilon}$UCG™-based projects can be found in other chapters of this book.

12.9.1   Chinchilla I (Australia)

The Chinchilla I UCG project was commenced in 1997 when Ergo Exergy experts selected the Chinchilla site, some 300 km west of Brisbane, for the first UCG pilot plant in Australia (Walker et al., 2001, Blinderman and Jones, 2002).

The project intended to demonstrate technical and environmental performance of $\boldsymbol{\varepsilon}$UCG™ in the geologic conditions of Chinchilla site: a 10–11 m thick subbituminous coal seam at the depth of 135–250 m, with an average LHV of 21.7 MJ/kg. The pilot ran in close proximity to a significant fault with a 40 m throw. Ergo Exergy supervised design, construction, commissioning, operation, and shutdown of the pilot plant.

The plant was built as a single panel with nine vertical process wells linked by reverse combustion linking (RCL). Its design capacity reached 80,000 Nm^3/h. The plant was operated with continuous uninterrupted gas production for 30 months straight. As a result, approximately 35,000 Mt of coal has been converted to approximately 80,000,000 Nm^3 of raw syngas of consistent quality: the average LHV of 5.0 MJ/N m^3 with maximum variation of 4.7%, the average wellhead gas temperature of 120°C, and stable gas pressure of 1100 kPa. The plant demonstrated 95% of extraction efficiency within the targeted resource and the cold gas efficiency of 75%. Throughout all 30 months of operation, gasification pressure in the cavity had been maintained at the level consistently lower than hydrostatic pressure of the aquifer, so that groundwater pressure gradient had been always toward the gasification reactor, which is always critical to ensure for protection of groundwater from potential contamination.

In the late 2001, due to shortage of funds, construction of power plant to monetize syngas production was canceled, and the Chinchilla UCG panel was required to shut down. Ergo Exergy designed and supervised the implementation of a three-phase gradual shutdown procedure that ended in 2003. By the end of controlled shutdown, the cavity was cooled to 47°C by groundwater influx; no forced cooling was required. No gasification or pyrolysis occurred in the cavity post shutdown.

Environmental monitoring during operation, shutdown, and post shutdown complied with rigorous requirements of Queensland EPA; quarterly environmental performance reports prepared by Golder Associates have been submitted to Queensland government. Annual environmental audits had been conducted by the independent auditor Sinclair Knight Merz—during all seven audits, no environmental issues had been reported, for example, Ref. Sinclair Knight Merz (2004).

Table 12.6 Conditions in which the *ε*UCG™ technology has been applied

UCG plant	Coal rank	Thickness, m	Depth, m	Dip°	LHV, MJ/kg
Lisichansk	Bituminous	0.4–2.0	60–250	38–60	20.1–23.0
Yuzhno-Abinsk	Bituminous	2.2–9.0	130–380	35–58	28.9–30.7
Podmoskovnaya	Lignite	2.5	30–80	<1	11.8
Angren	Lignite	3.0–24.0	110–250	7	15.3
Shatskaya	Lignite	2.6	30–60	<1	11.0
Sinelnikovo	Lignite	3.5–6.0	80	<1	8.0
Chinchilla	Subbituminous	10.0–11.0	135	<1	21.7
Majuba	Bituminous	3.5–4.5	285	3	20.3
Kingaroy	Subbituminous	17.0	200	5	23.5
Huntly West	Bituminous	4.0–22.0	220–540	0–75	24.5
CC Alberta	Subbituminous	7.0	150–260	6	20.5–23.0
Alaska SHR	Subbituminous/lignite	1.0–12.0	50–1650	0–75	11.0–16.5

In November 2006, Ergo Exergy ceased provision of the εUCG™ technology to Chinchilla I project owner and permanently left the Chinchilla UCG site. At that time, no environmental issues have been detected on or around Chinchilla I UCG site, the cavity was fully quenched, and the plant was shut down completely.

As discussed elsewhere, following Ergo Exergy's departure Linc Energy made several attempts at UCG within the same site, which allegedly led to a significant contamination of several environmental receptors in a large area surrounding Linc Energy site (Queensland DEHP, 2017). These operations have been conducted without any knowledge or participation of Ergo Exergy.

12.9.2   Majuba (South Africa)

The Majuba UCG project (Van der Riet et al., 2006) has been developed by Eskom Holdings Limited, using the εUCG™ technology, with continuous and comprehensive support of Ergo Exergy. It is situated in the province of Mpumalanga, next to the Majuba power plant. It targets 3.0–4.5 m thick coal seam at the depth of 280–300 m, which was proved impossible to mine by conventional underground mining. The plant has been in continuous operation since January 2007. At the moment, it comprises two εUCG™ panels with 1.0–3.7 PJ/a capacity. The panels were built by drilling one directional in-seam well and a number of vertical process wells, linked by Aquasplitt™ and RCL methods. At the moment, the first panel is undergoing controlled shutdown. The other, fully built, piped, instrumented, and connected to the boilers of the Majuba power station by a 7 km dedicated syngas pipeline, has passed cold commissioning and, pending a grant of water use license, is prepared for starting syngas production.

The first panel was operated at capacity from January 2007 to September 2011 after which controlled shutdown operations started. It demonstrated εUCG™ performance in the coal seam of very complex geology with multiple unresolved faults and volcanic intrusions. The first panel of the Majuba UCG plant was the longest running UCG plant outside the former Soviet Union; during its operation, it consumed over 50,000 tonne of coal. The plant confirmed suitability of the produced gas for power generation in a boiler of coal-fired power plant. Tests conducted in operations of the first panel produced valuable information necessary for the design of commercial-scale plant, which enables preparing design specifications for the commercial plant.

Extensive groundwater monitoring program confirmed that groundwater in the monitoring wells drilled and completed in representative aquifers surrounding UCG cavity is clean.

Both Chinchilla I and Majuba UCG projects have demonstrated key elements of the εUCG™ performance—optimal process well design, gas composition, process efficiency, extraction efficiency, linking techniques, etc. Together with the core content of the εUCG™ technology—design of the underground gasification panel and geometry of gasification reactors—the outcomes of each of these trials are necessary and sufficient for confident design of commercial plant in the respective geologic

conditions, characterized by parameters specified in the beginning of this section—a panel capacity of 3–5 pJ/a and an extraction efficiency of 95%.

12.10 Regulating UCG

Regulatory framework for the development of commercial UCG plant is supposed to codify the vital issues of the plant's creation and existence, related to

– licensing the mineral and petroleum resource;
– minimal exploration requirements for a UCG operation;
– technical and safety rules, specifications, norms and procedures for design, construction, commissioning, and operation of the plant;
– royalty regime;
– environmental monitoring and permitting.

12.10.1 Petroleum or mining rights

In terms of licensing of rights for UCG exploration and operation, there is a critical question: should UCG be regulated as coal mining, based on the extractable resource, or as petroleum and gas production activity, based on the products? Also note that in many jurisdictions there are two kinds of rights that can be granted over the same coal deposit—mining rights to extract coal and petroleum rights to extract coal-bed methane (CBM). Which of these does a UCG developer require? There have been many occasions when respective rights were given to different developers, causing conflicts and an impasse for both projects and eventually forcing governments to interfere. Some regulators attempted to resolve the controversy by granting coal and petroleum prospecting rights over the same lease area to two respective developers and declaring that commercial license would be available on a "first-come, first-served" basis, that is, to whoever is ready first to apply for it. To avoid these existential complications, it seems the safest to secure both mining and petroleum rights over the project area, although this decision must be made individually for each project.

12.10.2 Exploration requirements

Exploration for UCG is different from that for underground coal mining since UCG requires much better understanding of coal geology and hydrogeology. As in exploration for coal mining, the rules and specifications are dependent on local geologic conditions. The main difference lies in defining requirements for hydrogeologic testing. UCG needs a comprehensive hydrogeologic model that would allow calculating groundwater influx into reactor for a commercial-scale operation. This level of detail is rarely required for mining. In anticipation of specific UCG regulations, the needs for adequate exploration within the project area must be decided in negotiations with the regulator. Inadequate exploration has proved in the past to be one of the first reasons for technical or environmental failure of UCG projects.

12.10.3   Regulating UCG operations

For regulatory purposes, a UCG operation may be considered as consisting of under-ground plant (everything under the ground surface) and surface plant (Fig. 12.13).

Several overlapping regulations may apply for various parts of UCG plant. For example, the underground plant includes coal extraction, which in our view is most convenient to regulate as a coal mine. Injection, production, and monitoring wells of this plant may require the application of petroleum and gas regulations, dealing with hot, high pressure, and sometimes toxic fluids. Groundwater monitoring and consumption may need regulation for environment protection and water licensing. Surface plant upstream of injection wellhead may consist of air compressors, steam generators, ASU, and panel- and well piping and instrumentation. These would be regulated as an industrial plant and gas plant. Downstream of production well, the plant includes gas gathering pipelines, cleanup plant, and end-user plant, where a chemical plant regulation seems most suited. Protection of air, soil, and surface water streams would be subject to environmental regulation. If there are pipelines to carry oxidant, syngas, and by-products, pipeline regulation would apply. All this seems quite obvious and intuitive, but experience shows that there are many persisting uncertainties, for example,

- the means to accurately measure coal extraction rates of the plant when plant produces only syngas;
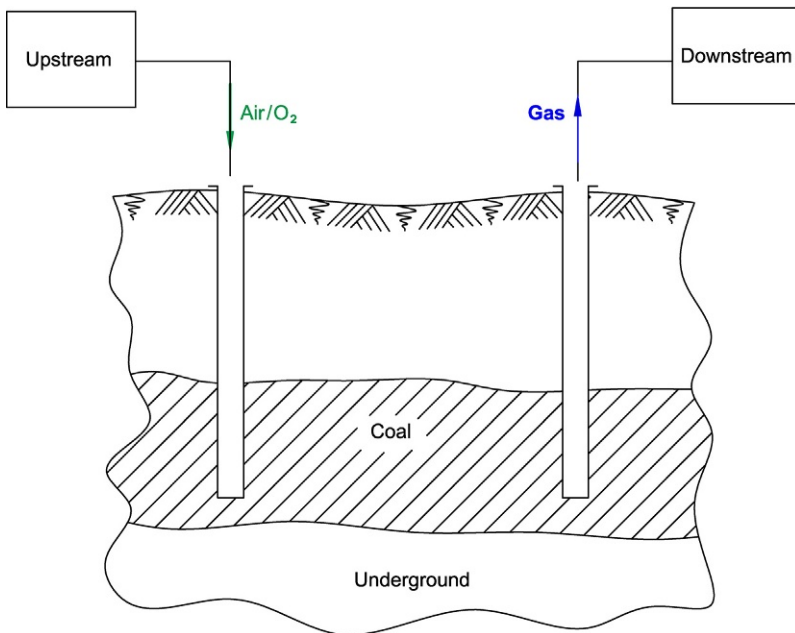
Fig. 12.13 UCG plant from regulatory standpoint.

– oil and gas well regulations are difficult to apply: UCG process wells have distinct design and operational needs;
– in licensing water—UCG consumes groundwater from mostly unaccountable sources, which normally would not be counted as aquifers.

All this leads to a conclusion that in every jurisdiction a new integral UCG regulation would be necessary to support operations of the UCG industry that otherwise may not be possible to develop.

12.10.4 Royalty regime

For obvious reasons, the royalty regime can make or break a new developing industry. The issues to consider here are as follows:

– What should be the base for royalty calculation, resource (coal) or product (syngas)?
– Since UCG is the extraction of coal, it is reasonable to use coal royalty regime, but how to measure the amount of coal extracted when you are producing hydrocarbons (syngas)?
– Natural gas royalty rules are hardly applicable since syngas is of much lower energy content and value;
– By-products contain hydrocarbon liquids that are very similar to petroleum—how to charge royalty on those?
– By-products contained in water phase of the condensate include phenols, ammonia, naphthalenes, and other products that may be marketed, possibly after significant workup and processing—what should be royalty on these?
– Since syngas by itself is usually a nonmarketable product, should royalty be based on the value of marketable end product, such as electricity and chemicals?
– Actual royalty rates are obviously crucial for a nascent industry and may perchance reflect the great difference in the value of the UCG resource—unmineable coal—compared with the market value of oil and gas.

12.10.5 Environmental permitting

Environmental permitting is necessary to ensure the protection of groundwater, managing subsidence (prediction, monitoring, and mitigation) and more conventional aspect of air emissions (including GHG), noise, surface streams, flora, and fauna. Experience of regulating coal mining, oil and gas operations, and chemical and manufacturing plants would certainly help; however, given the poor understanding of UCG by regulators and complex nature of the technology itself, the following is essential:

– An extensive body of data on the project conditions and plant operations should be made available.
– Special training and education of regulators, possibly in consultation with jurisdictions where UCG has been permitted before, is very advantageous.
– A collaborative approach should be favored when regulator is given early and open access to environmental and operation data so that regulatory approvals for the next step of the project may be based on the findings of the preceding stage.

12.11   Investing in UCG

In order to develop a commercial UCG project, apart from operators' competence and availability of an expert technology provider with a workable technology, many other factors have to come together. Nothing would happen without government and community support, without goodwill and understanding on the part of local and international environmental groups, without the interest of syngas-consuming industries, and without a degree of competence and insight within expert communities. Besides, building a commercial UCG plant is impossible without growing robust base of skillful UCG technologists: experts combining working knowledge of chemical engineering, coal mining, drilling, drilling, and hydrogeology and other skills necessary to design, build, and run commercial UCG plants.

And yet, all this may be in vain, if investors are reluctant to invest into the new technology. Investment decision will depend on the quality of feasibility study, whether it answers clearly and verifiably the questions on technical, environmental, and financial performance of the plant. Even if all this is in place, there still is the question of investing substantial capital into something for a first, second, or third time; and the perceived risk of doing that is quite real. These questions face every innovative and disruptive technology (Moore, 1991) and are eventually answered by any or a combination of the following:

– Participating in government-sponsored programs—UCG is of strategic interest to many nations.
– Serving a burning need:
   · Stranded end-user plants (e.g., methanol plant that lost dedicated natural gas supply)
   · Countries with great shortage of energy (e.g., South Africa in 1948 and Germany during the Second World War)
– Spread the risk:
   · International development institutions (IMF, World Bank, etc.)
   · Stock exchange participation
   · Public-private partnerships
– Power of greed—UCG project must offer a formidable return on investment.
– Finally, every new disruptive technology succeeded, first of all, by attracting obsessive enthusiasts. Fortunately, there certainly seems to be no shortage of dedicated believers of UCG.

12.12   Conclusion

Completing the discussion of the attributes necessary to achieve acceptance of UCG technology as a modern commercial-scale supplier of hydrocarbons for power generation and chemical feedstock, we would like to point out that the efforts to commercialize UCG at current stage of its development benefit greatly from referring to experiences of commercial-scale UCG operations in the former Soviet Union, where a number of such plants operated for decades. However, current requirements to technical, environmental, and financial performance of commercial UCG plants have

of course changed significantly, and more work is necessary to improve acceptance of UCG for commercial projects. This work should focus on increasing the scale of UCG demonstrations with a view of achieving cost neutrality or even producing commercial returns while working on testing and demonstrating the technology. Recent work completed by Ergo Exergy with Laurus Energy Inc. in the United States has confirmed that a very small UCG panel feeding a small 10 MW_e power plant may be commercially viable in certain markets. This size of a UCG operation is much more conducive to providing confidence in a larger, scaled-up plant performance, which would serve to convince investors, regulators, and the public in benign nature and economic credentials of UCG technology.

It is impossible to overestimate the value of adequate UCG regulation for successful commercializing of UCG. The work on new regulations as a rule takes a long time. It is therefore imperative that the countries that plan to use UCG as one of new indigenous sources of energy establish working groups within regulating agencies that may start early preparation of regulatory documents in consultation with public, industry, and international experts.

There are many parts of the world where there seem to be no alternatives to a large-scale commercial deployment of UCG. A diligent development of UCG regulations should make it possible to move more decisively on commercializing UCG there.

References

AER, 2014. AER Investigation Report. Swan Hills Synfuels Ltd., Well Blowout, 10 October 2011 (Calgary: Alberta Energy Regulator).

BHP, 2002. Case study B20: Electricity Production Using Underground Coal Gasification (UCG). BHP Billiton, Newcastle, Australia.

Blinderman, M.S., 2006. The Exergy underground coal gasification technology as a source of superior fuel for power generation. In: Proc. ASME 2006 Power Conference, Atlanta, Georgia, USA, 2–4 May, pp. 437–444.

Blinderman, M.S., Anderson, B., 2004. Underground coal gasification for power generation: high efficiency, and CO_2-emissions. In: Proc. ASME 2004 Power Conference, Baltimore, Maryland, USA, 30 March–1 April, pp. 473–479.

Blinderman, M.S., Fidler, S., 2003. Groundwater at the underground coal gasification site at Chinchilla, Australia. In: Proc. Water in Mining Conference, 13–15 October 2003, Brisbane, Australia. Australasian Institute of Mining and Metallurgy, Carlton.

Blinderman, M.S., Jones, R.M., 2002. The Chinchilla IGCC project to date: underground coal gasification and environment. In: Paper to Gasification Technologies Conference, San Francisco, USA, 27–30 October.

Blinderman, M.S., Shifrin, E.N., Taskaev, A.V., 1995. Gas flow and pressure loss in a UCG reactor. Izv VUZov-Gorniy Zhournal (Min. J.) 1, 1–5.

Blinderman, M.S., Gruber, G.P., Maev, S.I., 2011. Commercial underground coal gasification: performance and economics. In: Proc. 2011 Gasification Technologies Conference. Gasification Technology Council, San Francisco.

Blinderman, M.S., Dvornikova, E.V., Orlov, G.V., Sundaram, B., Klimenko, A.Y., 2016. Overburden collapse as defining factor in performance of large underground coal gasification reactors. In: Proc. 8th Int. Freiberg Conference on IGCC & XtL Technologies. Bergakademie Freiberg, Cologne, p. 64.

Boysen, J.E., Covell, J.R., Sullivan, S., 1990. Rocky Mountain 1: Underground Coal Gasification Test, Hanna, Wyoming. Results From Venting, Flushing, and Cooling of the Rocky Mountain 1 UCG Cavities. Gas Research Institute Report GRI-90/0156. 87 pp.

Carbon County UCG, Inc., 1996. Carbon County UCG Site Reclamation Interim Report. Received by the WY Department of Environmental Quality, Land Quality Division on 13 February 1996.

Davis, B., 2012. UCG technology developments. In: Proc. 2012 Gasification Technologies Conference. Gasification Technology Council, San Francisco.

FETC, 1997. Environmental Assessment, Hoe Creek UCG Test Site Remediation, Campbell County, WY. Report DOE/EA-1219, October 1997.

Hill, R.W., Shannon, M.J., 1981. Controlled retracting injection point (CRIP) system: a modified stream method for in situ coal gasification. In: 7th Underground Coal Conversion Symposium, Fallen Leaf Lake, CA, USA, 8 September.

Mallett, C., Hains, J., 2015. Carbon Energy's underground coal gasification pilot in Queensland, Australia. In: Proc. the Seventh Int. Conference on Clean Coal Technologies. IEA, Krakow.

McVey, T., 2011. Final Report: Technoeconomic Evaluation of Underground Coal Gasification (UCG) for Power Generation and Synthetic Natural Gas. Lawrence Livermore National Laboratory, Livermore.

Moore, G.A., 1991. Crossing the Chasm: Marketing and Selling Technology Products to Mainstream Customers. Harper Business, New York, NY.

Queensland DEHP, 2017. http://www.ehp.qld.gov.au/management/linc-energy/ (accessed 20.04.17).

RM1, 1989. Rocky Mountain 1: Underground Coal Gasification Test, Hanna, Wyoming. Volume 1. Operations. Summary report, United Engineers and Constructors, Inc., Denver, CO Stearns-Roger Div.

Saptikov, I.M.L., 2017. History of UCG development in the USSR. In: Blinderman, M.S., Klimenko, A.Y. (Eds.), Underground Coal Gasification and Combustion. 1st ed. Elsevier, London.

Sinclair Knight Merz, 2004. Chinchilla Underground Coal Gasification EMP Audit—December 2003. Environmental Performance Report, 04 January 2004.

Swan Hills Synfuels LP, 2012. Swan Hills In-Situ Coal Gasification Technology Development—Final Outcomes Report. Swan Hills Synfuels LP, Alberta, Canada.

Van der Riet, M., Gross, C., Fong, D., Blinderman, M., 2006. Underground coal gasification at Majuba. In: Proc. Workshop on Potential for Underground Coal Gasification, Houston, June.

Walker, L.K., 2007. Commercial development of underground coal gasification. Proc. Inst. Civ. Eng. Energy 160 (EN4), 175–180.

Walker, L.K., Blinderman, M.S., Brun, K., 2001. An IGCC project at Chinchilla, Australia, based on underground coal gasification. In: Proc. 2001 Gasification Technologies Conference. Gasification Technology Council, San Francisco.

Further reading

Blinderman, M.S., Shifrin, E.I., 1993. Flow of fluids through a UCG reactor. Gorniy Vestnik (Min. Herald) 1993 (3), 33–45.

Skafa, P.V., 1960. Underground Coal Gasification. Gosgortechizdat, Moscow.

Underground coal gasification (UCG) to products: Designs, efficiencies, and economics

13

S. Maev*, M.S. Blinderman†, G.P. Gruber‡
*Laurus Energy Inc., Edmonton, AB, Canada, †Ergo Exergy Technology Inc., Montreal, QC, Canada, ‡Black & Veatch Corp., Kansas City, KS, United States

13.1 The need for reference costs

It has been discussed at length that syngas manufactured with underground coal gasification (UCG) can be used as a feedstock for manufacture of great many products and used as boiler fuel and gas turbine fuel or converted into methanol, gasoline, diesel, etc.

There are certain criteria regarding the technical aspects of a UCG project that should be satisfied—coal seam depth, thickness, quality, structure of overburden, hydrogeologic conditions, and many others.

The economic parameters of a UCG-based project that includes the user's plant are not readily available in the literature. All commercial-scale UCG plants that operated to this day had been developed in the former USSR, and their economics is hard to understand in modern accounting terms or applied to modern projects: Soviet plants were developed in a completely different economic system. Nevertheless, it is clear that every potential UCG development in the modern world would have to justify investment into the project by creating a marketable product at a competitive cost. Otherwise, there is no basis for such a development.

Most parameters of the end-user plants, be it a power generation or a chemical synthesis facility, are well-known. With multiple reference plants in operation today, their designs, performance, and economics are well understood and offered for replication by technology vendors and engineering companies.

However, when it comes to a UCG plant, its design, performance, and economics have no reference analogues in the Western world. As a result, only few UCG practitioners such as Ergo Exergy Technologies Inc. (Ergo Exergy) have practical understanding of what it costs to develop a UCG project and produce UCG syngas. The fact is that every UCG development is unique because of variance in geologic conditions, essentially or at least partially different for every particular project location.

As to the syngas treatment plant that forms a part of any UCG-based project, a somewhat greater understanding of technologies, efficiencies, and costs may be available. The raw syngas produced at the wellhead of a UCG plant should be treated in such a way that the processes syngas is acceptable by the end-use plant. Even though

all requisite technologies, such as gas-liquid separation, hydrogen sulfide removal, and particulate filtration, have multiple reference installations and are in general well understood, specific composition and parameters of syngas that determine type, size, and combination of the treatment equipment would be different from location to location. Consequently, the gas treatment plant must be custom fitted to specific syngas composition, project location, and requirements of the end-use plant.

Few available estimates of the UCG syngas cost have been generated without relevant experience of commercial UCG project development and operation and should therefore be approached with caution.

Still and despite all the difficulties, an answer to the question of cost—capital, operational, cost of an end product—remains critical in deciding the project fate before any significant funds can be invested.

In 2011, amid all described confusion about UCG costing and after lengthy preparations, three companies with an interest in UCG projects decided to conduct a study to produce reliable reference costs of several marketable end products to be manufactured from UCG syngas as a feedstock. These were Ergo Exergy Technologies Inc. (Ergo Exergy), a UCG technology provider; Laurus Energy Inc. (Laurus), a UCG project developer; and Black & Veatch Corporation (Black & Veatch), a renowned US engineering company with rich experience in coal gasification and petrochemical projects.

13.2   The εUCG technology

UCG is a gasification process carried on in unminable coal seams using injection and production wells drilled from the surface, enabling the coal to be converted in situ into a product gas. The process has produced commercial quantities of gas for chemical processes and power generation.

A simplified illustration of the UCG process is given in Fig. 13.1.

As in CG methods, in UCG[1], process coal in the ground reacts with an oxidant, and a part of released sensible heat is used in coal drying, pyrolysis, and endothermic reactions with coal that reduce the products of combustion. The resulting mixture is called UCG gas or UCG synthesis gas (syngas). The obvious differences with a conventional gasifier include the following:

– Coal is not mined, and chemical processes are arranged to occur in the virgin coal seam in situ.
– Contact between coal and oxidant is maintained through boreholes drilled from the surface into the coal seam, while other boreholes are used to conduct the product gas to the surface. These boreholes are called injection and production wells, respectively, and collectively— process wells.
– Process wells must be connected within the coal seam by the links of low hydraulic resistance to allow the production of commercial quantities of gas.

---

[1]From this point on, unless indicated otherwise, any mention of "UCG" refers to the εUCG technology.
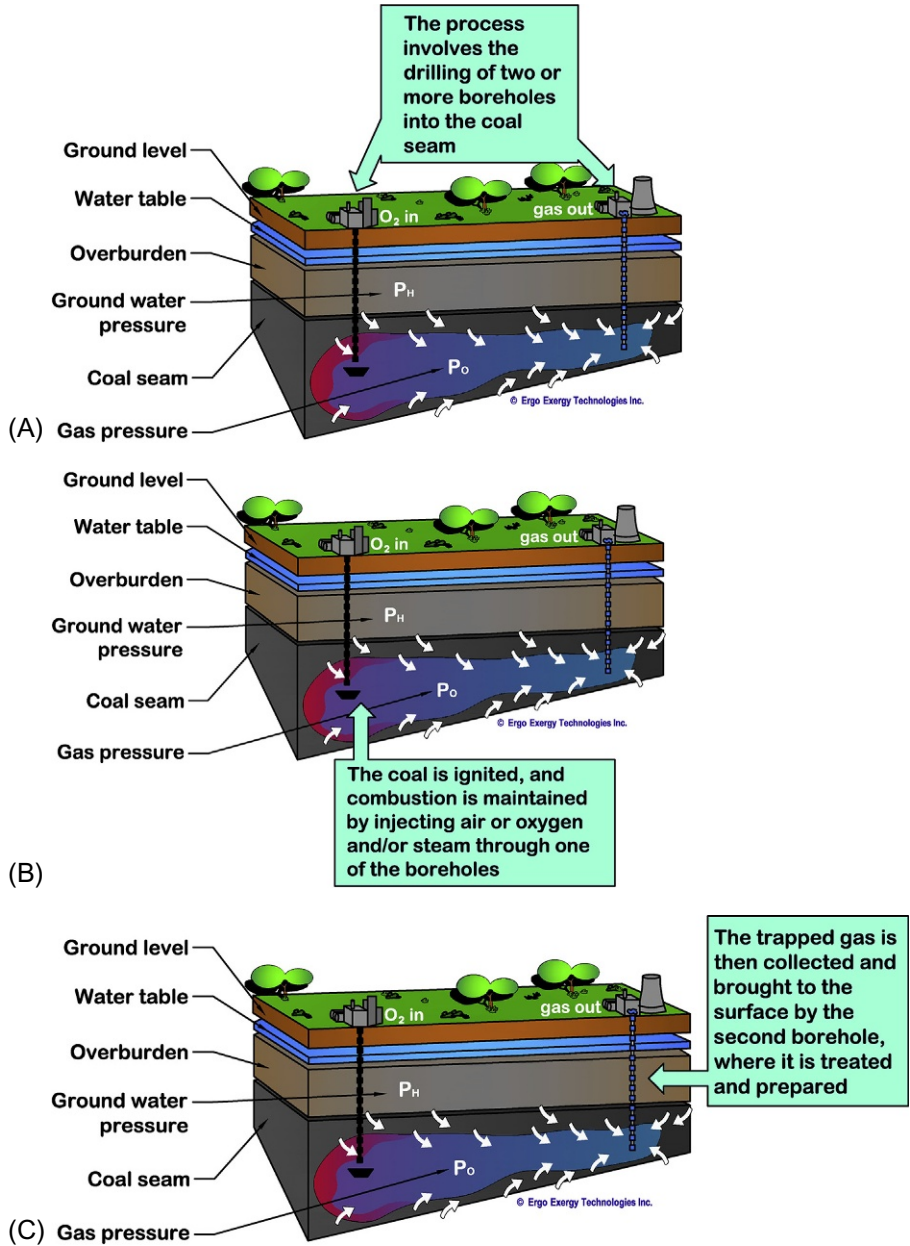
Fig. 13.1 Schematics of the εUCG process.

– Process water for gasification usually comes from the coal itself and surrounding rocks, and its influx must be carefully controlled.
– The process must be confined within a reactor system created in the coal seam so that no leakage of the product is possible and no contamination of the underground environment can occur. Such a reactor system is called an underground gasifier, and its design is the most crucial part of a UCG operation.

Process parameters, such as operating pressure, outlet temperature, and flow, are governed by the coal and rock properties that vary with time and location. Information on the process conditions must be constantly monitored and updated as the gasifier develops. Process parameters should be adjusted accordingly to accommodate ever-variable conditions of gasification.

Unlike CG methods, not only UCG is a method of coal conversion, but also it is first of all a method of extracting coal from underground beds, that is, a mining technique. There are various similarities between UCG and underground mining techniques; for example, UCG is concerned with typical mining issues such as sweep efficiency, roof stability, and groundwater influx. As a coal recovery method, UCG supplements conventional mining by utilizing coal seams impossible or uneconomical to mine.

The UCG process developed, refined, and practiced by Ergo Exergy is called the Exergy UCG technology or εUCG technology. It differs from generic UCG by virtue of its higher exergy efficiency and lower exergy dissipation into the environment. Selected distinctive features of εUCG technology are shown in Table 13.1.

Table 13.1 **Some distinctive features of Exergy UCG technology**

The Exergy UCG technology
Coal mining technology with a syngas product
Large scale (coal conversion of at least 300,000 t/a)
Adaptable to widely varying geology and hydrogeology
High sweeping efficiency (ca. 95%)
Directional, inclined, and vertical drilling
Well linking: RCL, Aquasplitt, directional drilling, electrolinking
Controlled multiple injection points
Ignition of coal in high-groundwater-pressure conditions
High-capacity production well designs
Comprehensive environmental management
Groundwater protection and cavity influx control
Subsidence and rock deformation management
Air/O_2/CO_2 injection flexibility
Tailored syngas composition for end-use requirements
Stability and consistency of syngas quantity and quality
Spontaneous combustion management
Comprehensive models of εUCG process
CO_2 management autonomy
Applicable to coal seams to the depth of 2000 m

The εUCG technology has a proved record of successful and efficient energy production. It is the only UCG process outside of the former Soviet Union (FSU) that has demonstrated continuous, consistent production of consistent quantities of quality fuel gas.

The Chinchilla I UCG project (1997–2006) was the first to demonstrate εUCG as the technology for gas production (Blinderman and Jones, 2002). The project was located at Chinchilla, Australia (350 km west of Brisbane, Queensland). Ergo Exergy provided εUCG technology for the project and designed and operated the εUCG plant.

Altogether, the εUCG technology has been used in four syngas production projects in the last 16 years:

– Chinchilla (Australia), 1999–2006.
– Eskom (South Africa), 2007–present.
– Kingaroy (Australia), 2010.
– Huntly West (New Zealand), 2012.

Exergy UCG technology is practical and based on hands-on experience of running commercial UCG plants. It uses all drilling methods available today, including high-precision directional wells and conventional, vertical, and inclined (angled) wells. Its arsenal includes multiple methods of well linking, various oxidant injection (air, O_2/H_2O, etc.), and various designs of underground gasifiers. It can be applied to coal in a wide range of geologic and hydrogeologic conditions. In every geologic setting, specific εUCG design is tailor-made to fit the unique conditions of a target coal seam.

13.3   Experience with different types of coal and geological conditions

Every coal deposit in the world is unique in its geologic setting and coal quality. Even within the same coalfield, there may be very significant differences in coal quality and geologic parameters between sites located a few hundred meters apart.

The εUCG technology can be adopted and applied to a large variety of coal qualities and geologic settings due to its flexibility in design and multiple methods and techniques utilized by Ergo Exergy.

Ergo Exergy experts have hands-on experience with application of UCG technology to various coals in various geographic locations including design and operation of multiple projects listed in the Table 13.2.

The εUCG can be applied to practically all coal ranks—from lignite to bituminous coal.

Its elements have been successfully applied for gasification of coal seams with the following:

– Thickness from 0.44 m (Lisichansk) to 25 m (Angren).
– Depth from 30 m (Podmoskovnaya and Shatskaya) to 370 m (Huntly West).
– Dip from horizontal to steeply dipping (e.g., Huntly West 0°–75°).
– LHV of 8.0 MJ/kg (Sinelnikovo) to 30.5 MJ/kg (Yuzhno-Abinsk).

Table 13.2 ε**UCG application in a variety of coal conditions**

UCG plant	Rank	Thickness, m	Depth, m	Dip°	LHV, MJ/kg
Lisichansk	Bituminous	0.44–2.0	60–250	38–60	20.1–23.0
Yuzhno-Abinsk	Bituminous	2.2–9.0	130–380	35–58	28.9–30.7
Podmoskovnaya	Lignite	2.5	30–80	< 1	11.8
Angren	Lignite	3.0–24.0	110–250	7	15.3
Shatskaya	Lignite	2.6	30–60	< 1	11.0
Sinelnikovo	Lignite	3.5–6.0	80	< 1	8.0
Chinchilla	Subbituminous	10	135	< 1	21.7
Majuba	Bituminous	3.5–4.5	285	3	20.3
Kingaroy	Subbituminous	17	200	5	23.5
Huntly West	Bituminous	4.0–22.0	220–540	0–75	24.5
CC Alberta	Subbituminous	7	150–260	6	20.5–23.0
Alaska SHR	Lignite/subbituminous	1.0–12.0	50–650	0–75	11.0–16.5

The coalfields in Table 13.2 are located all around the world:

- Ukraine (Lisichansk and Sinelnikovo).
- Moscow region (Podmoskovnaya and Shatskaya).
- Siberia (Yuzhno-Abinsk).
- Uzbekistan (Angren).
- Australia (Chinchilla and Kingaroy).
- South Africa (Majuba).
- New Zealand (Huntly West).
- Canada (CC Alberta).
- The United States (Alaska SHR).

Ergo Exergy experts participated in operation of UCG plants in the FSU under the Soviet UCG program and since 1994 have worked from the Company's headquarters in Montreal, Canada, on commercialization of εUCG technology in international projects.

13.4   Conceptual life cycle of the εUCG production unit—A panel

Similar to one of the conventional methods of coal mining, namely, longwall mining, εUCG technology is performed within modular individual panels, the εUCG panels. A εUCG panel is an independent production unit capable of converting about 300,000 tonnes of coal into syngas per year.

Longwall mining is a form of underground coal mining where a long wall of coal is mined in a single slice. The longwall panel (the block of coal that is being mined) is typically 3–4 km long and 250–400 m wide (Fig. 13.2).

Longwall mining machines consist of multiple coal shearers mounted on a series of self-advancing hydraulic ceiling supports. The entire process is mechanized. Massive shearers cut coal from a wall face, which falls onto a conveyor belt for removal. As a longwall miner advances along a panel, the roof behind the miner's path is allowed to collapse.

εUCG process works in a similar fashion, but instead of mechanical miners and shearers, it uses high-temperature heat to consume the coal of the wall face, layer by layer, along the whole width of the panel and convert it into a mix of gases comprising syngas.

A εUCG panel undergoes the following phases during its life:

1. Exploration drilling
2. Modeling and design

    Using models of the target coal seam geology, hydrogeology, and rock mechanics, the developer establishes design parameters to achieve intended panel outputs so it can fulfill its role in the system. According to these parameters, the number, location, and design of the production and monitoring wells are determined. The response of the environment to the UCG operation is also predicted at this stage. All the outcomes of the previous panel construction and operation are taken into account in designing each new panel.
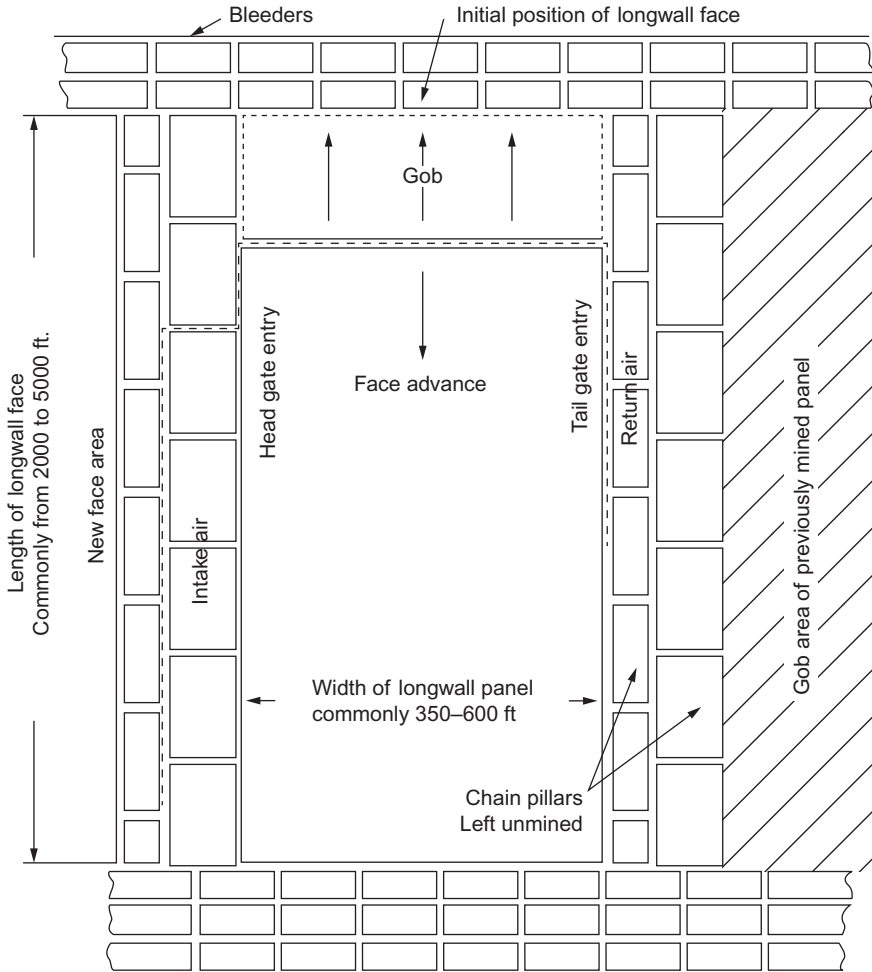
Fig. 13.2 Example of a longwall coal mine in plan view (Meyers, 1981).

3. Development

Production and monitoring wells are drilled and completed. Surface pipelines are assembled; control systems are established. In-seam linking of production wells and channel conditioning are completed. Some syngas generation will occur at this phase.

4. Commissioning

The panel is commissioned and starts independent production of syngas with design quality and volumes required by the schedule of introduction phase. Production is ramped up to compensate for the loss of production of the other panel that is at the end of its life and is being phased out. When the outgoing panel stops syngas generation, the newly introduced panel reaches its full design capacity and transitions into the next phase.

5. Introduction

Production is ramped up to compensate for the loss of production of the other panel in the system that is at the end of its life and is being phased out. The panel is being introduced into

the overall syngas production process, and its output is integrated (both quality and volume) with other panels' outputs.

By the time the "outgoing" panel stops syngas production, the newly introduced panel reaches its full design capacity and transitions into the next phase.

6. Full capacity mining

Panel generates syngas at full design capacity.

7. Phasing out

Panel phaseout usually coincides with a new panel introduction in such a way that the combined output of the two panels is kept at the level of full capacity of a single panel and the overall syngas output is stable.

8. Panel shutdown

During the process of panel shutdown, the panel is cooled down, syngas production is completely stopped, and all remaining products of gasification are removed from the underground cavity. The operator ensures that there is no contamination at source in the postgasification cavity.

Wells not required for further use are plugged and abandoned; surface pipework is taken apart and reused or scrapped. After a while, when the process of subsidence (if ever present) is complete and surface stability is established, the land above the panel can be returned to its previous use.

9. Rock mechanics and groundwater (RM and GW) monitoring

Monitoring is maintained throughout the life of the panel and a few years after shutdown (depending on the local environmental regulations).

13.5   Choosing coal resource

Interest in UCG technology and its potential is expressed by many parties around the globe. To satisfy that interest, one needs to create an internationally accepted benchmark easily adaptable to various locations, countries, and states. A commonly accepted location for such a benchmark in relation to construction and operation of various sorts of energy and chemical plants is the US Gulf Coast (USGC). The reason for this location being accepted as a benchmark is the fact that on and in proximity to the Texas and Louisiana Gulf of Mexico shorelines, numerous gas processing, chemical, energy, and other industrial plants were built in the last 100 years. This history of construction and operation provides a variety of industries with sufficient data related to costs of materials, equipment, labor, and productivity for the area. It allows generation of economic estimates based on average values collected from hundreds of executed projects. Accepted standards among industry publications, for example, Compass International (Global Construction Costs Yearbook, Richardson Location Factors, etc.), continuously track and update their database of projects around the world and publish location factors. Using these factors, an estimator is able to assess the costs associated with a specific location (e.g., another country) using the base costs computed for USGC.

Consequently, for the purpose of this evaluation, the authors decided to locate a hypothetical reference project in Texas and utilize local coal resources for the production of syngas and end-use products.
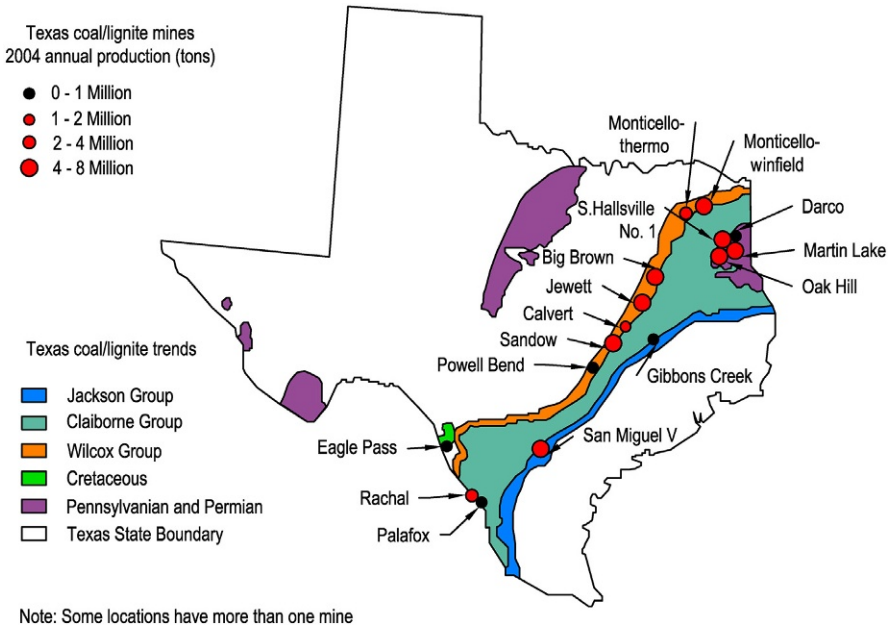
Fig. 13.3 Texas lignite map.

In Ergo Exergy and Laurus estimates, Texas contains about 35 billion tonnes of deep coal resources suitable for UCG application. Those resources are located within the depths of 60–600 m and in coal seams over 1.5 m in thickness. The coal is classified as lignite.

Major lignite resources are represented by the Wilcox and Jackson groups and deposited in a wide swath extending from Texas northeast to southwest.

The Wilcox group contains about 70%, while the Jackson group represents about 30% of Texas deep-sitting lignite resources (Fig. 13.3).

13.6 Adopted approach

13.6.1 Method, technologies, products

The evaluation of the costs was done by comparing UCG- and CG-based end-product plants, situated in the same geographic location and operating in identical conditions, such as production capacity, product mix, and lignite quality.

The location is the state of Texas. There are a number of reasons for this choice:

– Texas has large resources of lignite.
– Texas is a state with well-developed infrastructure, power, and petrochemical industries.
– Due to the vast number of various industrial plants built in the state over the last 100 years, most of them in proximity to the Gulf of Mexico, there is a very large amount of data related to capital costs, labor productivity, O&M costs related to the construction, and operation of those plants.

– USGC is universally accepted as a reference point for the cost of construction and operation of all sorts of industrial plants, cost of materials, cost of equipment delivery, and cost of labor as well as labor productivity.
– There are a number of publications, for example, Compass International Index, tracking and updating costs and other relevant data, and calculating location factors. Those factors are published annually and serve as a guide for estimators preparing various project assessments. Using those factors, one can easily adjust the cost of construction or product from USGC to any other location in the United States or in any part of the world.

UCG technology in this evaluation is represented by the Exergy UCG technology (εUCG). For conventional coal gasification (CG) technology, the data from generic dry feed technologies, for example, Shell, Siemens, or Uhde, were used.

The following products, among others, were included into the study scope:

– electricity
– synthetic natural gas (SNG)
– methanol
– synthetic gasoline
– synthetic diesel
– synthetic naphtha
– urea
– ammonia
– synthetic liquefied petroleum gas (LPG)

13.6.2   Lignite and lignite seam parameters

The fuel (feedstock) for all the products in the study was Texas lignite with the following characteristics:

Geology:
– Coal seam thickness: 21 ft (7 m).
– Depth to coal seam floor: 600 ft (200 m).
Quality:
– 6500 BTU/lb wet HHV (15,119 kJ/kg).
– 10,000 BTU/lb dry HHV (23,260 kJ/kg).
– 56.2 wt % dry carbon.
– 21.7 wt % dry ash.
– 2.9 wt % dry sulfur.

13.6.3   Financial parameters

Financial conditions were assumed as those for an independent power producer building the second or third project using a relatively new technology.

Capital cost parameters are as follows:

– Debt/equity ratio: 60%–40%.
– Interest on debt: 10%.
– Capital cost: overnight construction cost.

13.6.4   Cost of electricity for synfuel and chemical production

Cost of power for any chemical plant's operation is one of the critical parameters, as it may represent a significant portion of the ultimate product cost.

For this study, the cost of electricity for εUCG-based products was assumed at the cost of electricity produced by an adjacent εUCG-IGCC generation unit. The study started from evaluating the cost of such electricity supply, produced at a stand-alone εUCG-IGCC power plant built at the study location.

The cost of electricity supply for CG production was assumed as the cost of electricity produced by an adjacent CG-IGCC generation unit. This cost was estimated among the first in the study.

The cost of electricity produced by a CG-IGCC generation unit is relatively high. This electricity turned out to be more expensive than electricity purchased in the power market in Texas. For fairness of comparison, both costs—of own electricity and market sourced electricity—have been used for CG-based product plants, the latter case scenarios denoted "CG M."

13.6.5   Size of plant

In determining the production unit size, the following were considered:

– In order to use the benefits of economy of scale for all the major plant components, the plant should employ a standard single-train process.
– For the same reason, the size of the largest vessel in the train should not exceed the limits imposed by existing fabricators' abilities and transportation requirements. In other words, it should not be uniquely large and should not require equipment that does not routinely exist.

The size of the power plant for electricity generation was determined by the largest existing turbine for the syngas application. For Texas market, it is the General Electric Frame 7FB turbine coupled with an appropriate steam turbine (ST) in a 1×1 configuration—nominal size of 300 MW net.

For all chemical products, the chosen size was the plant capacity equivalent of 10,000 bar/day of synthetic gasoline. The corresponding syngas production would be 30 PJ p/a on the LHV basis.

13.6.6   CO$_2$ emissions

The approach to CO_2 emission management for power generation case scenarios was to satisfy the California standard of 1080 lb/MWh sent-out. The requisite amount of CO_2 is removed from the syngas stream, compressed to 2000 psig (138 barg), and made ready to be shipped for enhanced oil recovery (EOR) to a nearby location.

13.6.7   Other study parameters and assumptions

CO_2 sales to EOR and sales of other marketable by-products, for example, naphtha and LPG, were considered as offset to the annual cost of production, thereby impacting ultimate product costs. The selling prices for respective by-products were assumed as the local market prices.

In this study, the value of some condensate-derived by-products, for example, sulfur, ammonia, and phenols, was not credited to production costs. These products were assumed to be released; free of charge and at no cost, to third parties "over the fence" for processing; and therefore cost neutral.

13.7   Raw syngas production

Fig. 13.4 illustrates simplified schematics of raw syngas production.

The production process begins with the oxidant, for example, air, oxygen, or oxygen-enriched air, being continuously injected into underground εUCG modules at an appropriate pressure. Each UCG module is an independent unit of syngas production referred to as a panel. A εUCG plant utilizes simultaneously as many panels as required in order to achieve its design capacity. Each panel operates its own gasification process with independent input and output parameters. Each panel may produce syngas of different volume and quality as compared with the other panels in operation. Typical raw syngas at the production wellhead contains water-phase and oil-phase vapors in addition to gaseous components. The main components of raw syngas are hydrogen, carbon monoxide, and carbon dioxide. In addition to the main components, raw syngas contains certain minor components: nitrogen, methane and some higher hydrocarbons, water, hydrogen sulfide, carbonyl sulfide, hydrogen cyanide, hydrogen chloride, mercury, ash, pyrolysis products, etc. The operator has the ability to influence and control the production of each panel in order to achieve
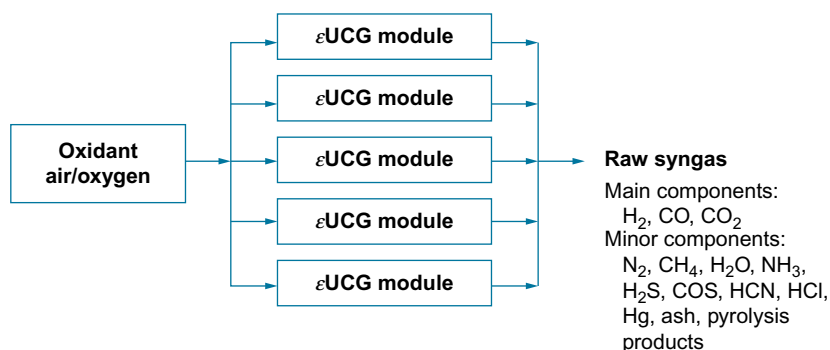
Fig. 13.4 Raw εUCG syngas production (Blinderman et al., 2011).

specific output parameters, for example, syngas volume and quality. The outputs of the multiple individual panels can be blended together in order to achieve stable production volumes and consistent quality of syngas.

13.8   Syngas treatment (cleanup and conditioning)

In order to produce optimal syngas feed for various products and ensure low environmental impact of the production, raw syngas coming from underground gasifier should undergo certain treatment—cleanup and conditioning before it can be delivered to the end-use production unit.

The block flow diagram of syngas treatment process is shown in Fig. 13.5.

The following stages of syngas treatment were considered and modeled in this study:

1. Syngas scrubbing entails liquids and particulate matter removed from the stream. Liquids are then separated into a water-phase stream and an oil-phase stream. The water-phase stream will be directed to the wastewater treatment plant where it will pass through ammonia stripper and phenol removal equipment. Sufficiently, clean water can be reused in the production process. As mentioned above, utilization of oil-phase liquids, ammonia, and crude phenol is not reviewed here. In CG case scenarios, ash is disposed of in ash dams.

2. During syngas compression, raw syngas coming to the surface at the pressure of 11 bar should be recompressed to 33 bar in order to optimize processing equipment size for syngas treatment.
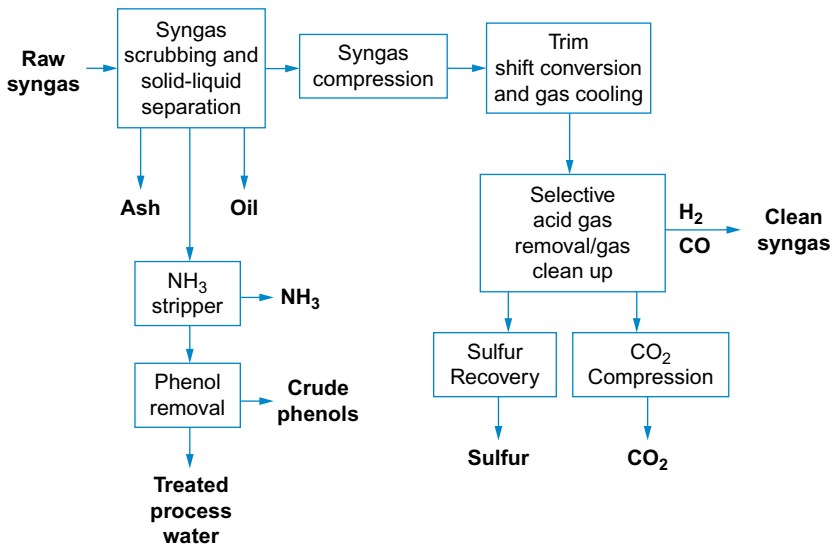
Fig. 13.5 Syngas treatment plant (Blinderman et al., 2011).

3. Trim water-gas shift conversion and gas cooling.

   Depending on the application, syngas may need to be conditioned to adjust the hydrogen-to-carbon monoxide (H_2-to-CO) ratio to meet downstream process requirements. A slipstream of syngas will undergo the shift reaction, and this will bring H_2-to-CO ratio of the entire gas stream to the required level. After this, syngas is cooled.

4. Dried and cooled syngas will pass through the selective acid gas removal (AGR) equipment where sulfur compounds and CO_2 will be removed from the gas stream. H_2S is to be converted to pure sulfur, and CO_2 is to be compressed to the level of 2000 psig (138 barg) to ready it for geologic sequestration or EOR operations. The option of CO_2 self-sequestration in depleted εUCG panels has not been considered in this study due to shallow depth of lignite occurrence.

5. Treated syngas consisting of H_2 and CO in requisite ratio and some other constituents will be delivered to the downstream plant for conversion to the end-use product.

13.9   Synthesis products

Among the multitude of products that can be manufactured from εUCG syngas, electricity stands out as the only product that can be produced using air as an oxidation agent. Other products included in the study are the result of chemical synthesis and cannot be economically produced with an air-blown syngas. For this reason, the feedstock for these products should be an oxygen-blown syngas. Instead of air compressors, in the εUCG upstream plant for syngas production, an air separation unit (ASU) is installed. The ASU will supply the operation with oxygen at the required pressure; air compressors for injection are not utilized in these cases.

Even though in this study we assumed single composition of syngas for all synthesis products, it should be noted that each product reviewed would benefit from optimization of syngas composition to suit each specific process needs. The syngas optimization can be done in part during the production of the raw syngas in the underground gasifier and in the process of syngas treatment above ground. This optimization would result in a greater efficiency of the synthesis process and should offer an additional cost reduction.

The following block flow diagram in Fig. 13.6 illustrates a variety of syngas compositions to match the requirements of different products.

The main components of syngas participating in chemical synthesis are H_2 and CO. Production of ammonia and urea utilizes only H_2 from the syngas stream. Therefore, the CO should be converted to CO_2 via the water-gas shift reaction and removed from the gas stream.

Production of diesel, naphtha, and LPG via F-T synthesis is optimal when the ratio of H_2 content to CO is from 1:1 to 2:1.

Production of DME, gasoline, and all products of alcohol synthesis, for example, methanol and ethanol, is efficient when H_2/CO equals 2:1.

The production of SNG is optimal when H_2/CO equals 3:1.
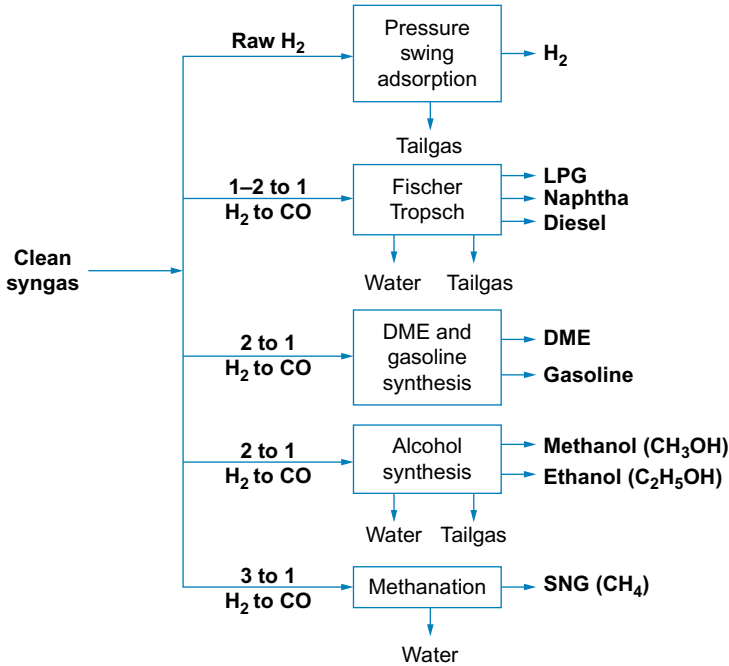
Fig. 13.6 Syngas products (Blinderman et al., 2011).

13.10 Electricity

The most common use of coal is electricity generation. In this study, we investigated various options of using coal for the purpose of producing power:

1. UCG-IGCC with air-blown syngas and partial CO_2 removal.
2. UCG-IGCC with air-blown syngas and maximum CO_2 removal.
3. UCG-IGCC with O_2-blown syngas and maximum CO_2 removal.
4. CG-IGCC with O_2-blown syngas and maximum CO_2 removal.

13.10.1 Case 1

Case 1 represents the cheapest way to build a UCG-based IGCC with respect to capital expenses.

The process starts with the air compressors pumping air into underground gasifier at 11 barg, thus supplying gasification process with the oxidant. Syngas generated underground comes to the surface where it is cooled down and delivered to the gas scrubbing and oil/water separation unit. Both oil-phase and water-phase liquids are separated from the gas stream. Gas is then scrubbed, and particulate matter, condensed tars, etc. are removed. The water-phase liquids are sent down to the wastewater treatment plant.

Syngas is then recompressed to the pressure required by the AGR unit—the MDEA solvent in this case—where sulfur compounds and a part of the CO_2 content will be removed from the gas stream.

The MDEA solvent is chosen for this case because the main purpose of AGR is to remove sulfur and very little of CO_2—just so that syngas would be of an acceptable quality to be used in a gas turbine. Only 11.6% of total CO_2 equivalent contained in coal will be removed in this case, resulting in 88.4% of CO_2 equivalent in coal being emitted in the process of power generation. H_2S removed in AGR will be processed further in sulfur recovery unit (KLAUS plant in this and all other considered cases). Captured CO_2 is recompressed to 2000 psig and made ready for EOR.

Clean syngas is delivered to the GE Frame 7FB combustion turbine (CT) with installed capacity of 232 MW (on syngas fuel). Hot turbine exhaust gas from CT is directed to the heat recovery steam generation unit (HRSG) that is supplied with boiler feedwater and produces superheated steam. Steam from HRSG feeds a 100 MW generic ST.

There is a special feature in this setup that makes it a true integrated gasification combined cycle (IGCC) that is different from the conventional combustion turbine combined cycle (CTCC). Air extracted from the compressor of the CT is looped back to the air injection supply line. It may partially or entirely perform the duty of air supply to the underground process. This will reduce or, in the best case, eliminate the air compressors, leading to a significant reduction in CAPEX.

The total CAPEX for this case is the lowest of four cases, and the resulting cost of electricity is $33.3/MWh sent-out.

13.10.2   Case 2

This case is identical to case 1 in most aspects. The same BFD as in case 1—Fig. 13.7—can be used to illustrate the setup. The difference is in the amount CO_2 removed from syngas in the AGR unit. The purpose of this setup is to produce electricity with associated CO_2 emissions complying with the California standard of 500 kg/MWh (1100 lb CO_2/MWh).

In order to achieve this goal, a different type of solvent was used in the AGR unit: Selexol replaced MDEA. The Selexol process is more effective in CO_2 capture than MDEA and costs about three times more. With this change, the CO_2 captured in the AGR unit represents 57.4% of the CO_2 equivalent in coal, and the resulting CO_2 emissions are 443 kg/MWh sent-out (974 lb CO_2/MWh). Also, due to the different process, it is possible to produce more steam energy in HRSG and therefore use a larger CT of 112 MW, bringing the total gross generation capacity to 344 MW.

CAPEX in this case is 10% higher than in case 1, due to an increase in the CO_2 processing equipment capacity and higher capital and operating costs. However, the resulting cost of electricity is lower than in case 1, that is, $29.9/MWh sent-out. This can be explained in part by a larger volume of electricity produced and mainly by a larger amount of CO_2 sold to EOR and therefore more significant cost of power offset.
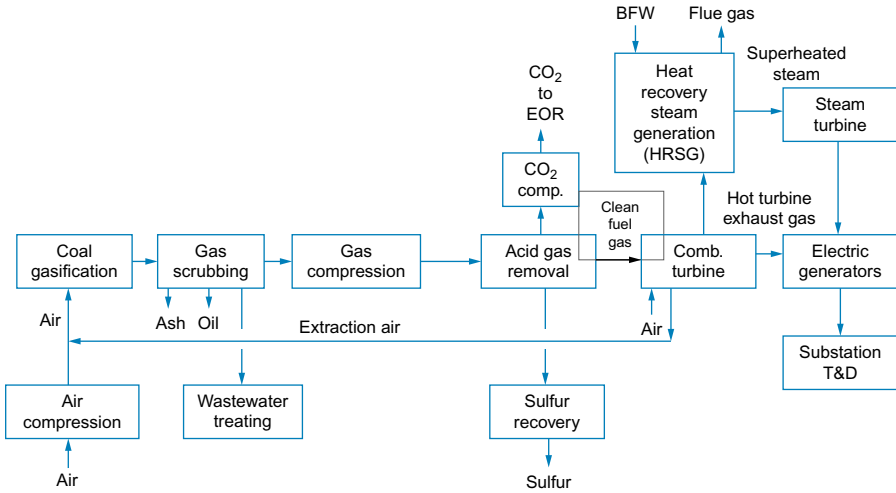
Fig. 13.7 Air-blown εUCG-IGCC power generation BFD (Blinderman et al., 2011).

13.10.3   Case 3

In this case, we investigated the option to produce electricity using oxygen instead of air in the process of underground gasification. The changes in setup are more significant if compared with cases 1 and 2 (Fig. 13.8).

Supplying oxygen requires replacement of air compressors with an ASU that produces oxygen for injection underground. The ASU also supplies nitrogen as an additive to syngas prior to combustion in CT in order to control combustion temperature and NOx emissions.

The environmental footprint of the plant is much smaller than in case 1 but only marginally better than in case 2. The captured CO_2 is as high as 63.1% of the CO_2 equivalent in coal vs 57.4% in case 2.

The changes in the syngas production and treatment processes also result in a gross power generation increase and simultaneous internal load increase, so as a result, the net power production in case 3 is less than that in cases 1 and 2. The change of equipment brings a substantial increase in CAPEX and OPEX of syngas production and treatment (67% and 43% over case 1, respectively), resulting in different costs of the end product—power (Fig. 13.9).

Comparing the outcomes of all three cases of power generation with the UCG syngas feedstock, it is quite clear that case 2 presents the best results in both cost and environmental footprint and will be compared with CG as representative of the UCG-IGCC technology.

13.10.4   Case 4

In this case, we investigated performance and economics of conventional above-ground gasification coupled with a CTCC power island (Fig. 13.10).
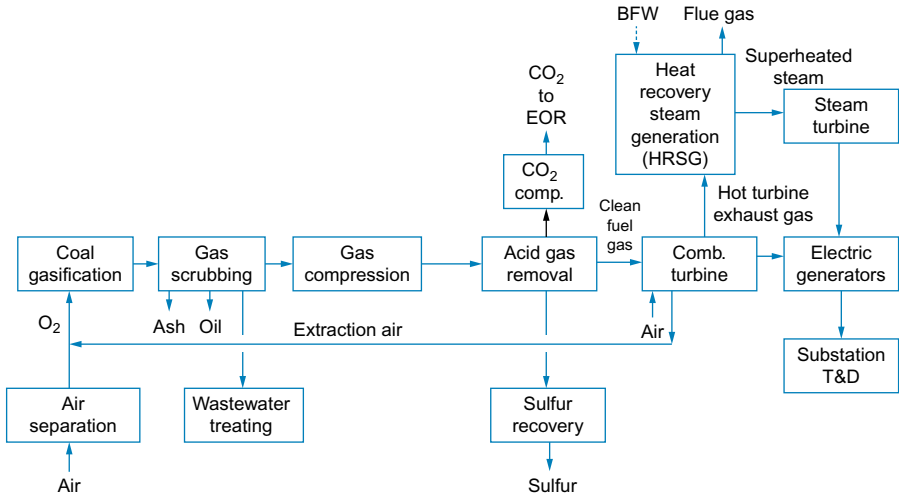
Fig. 13.8 O_2-blown εUCG-IGCC power generation BFD (Blinderman et al., 2011).
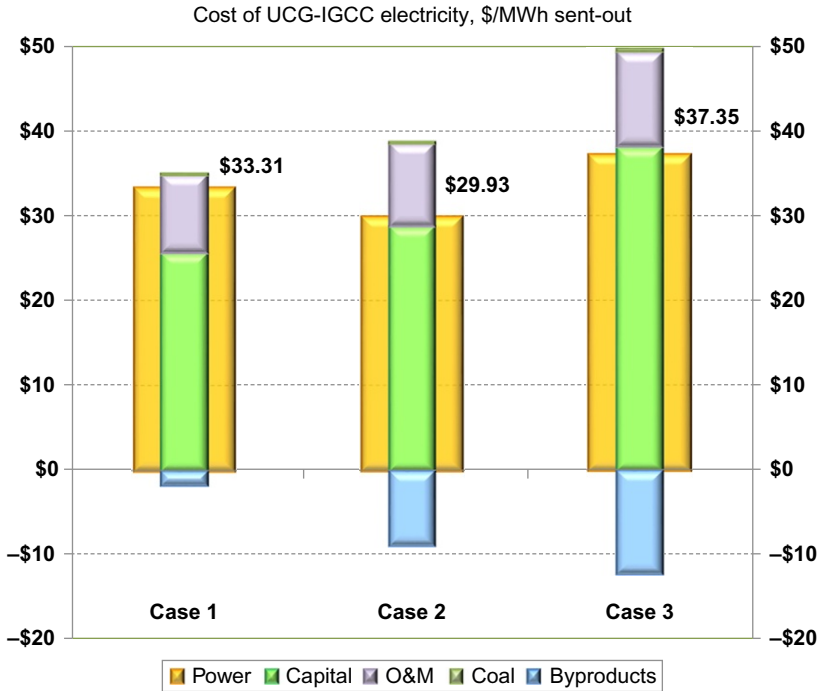
Fig. 13.9 Cost of electricity comparison for UCG-based cases (Blinderman et al., 2011).
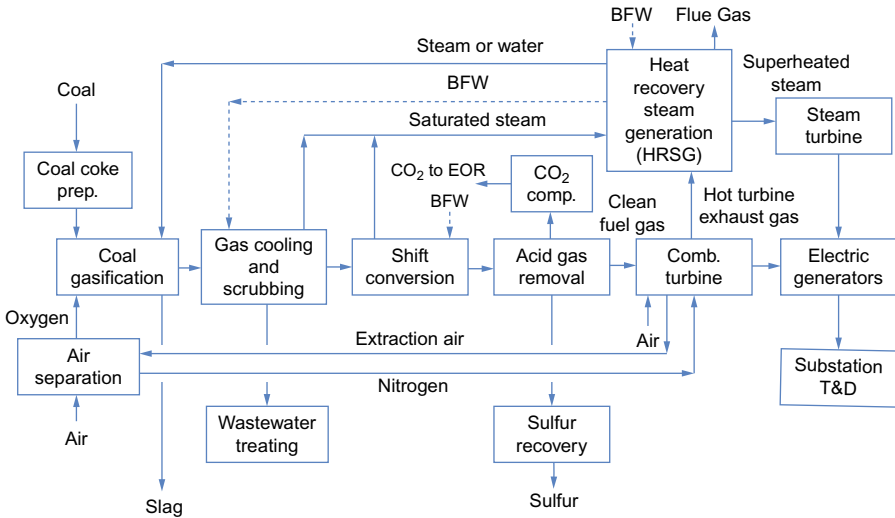
Fig. 13.10 CG-IGCC power generation BFD (Blinderman et al., 2011).

The process flow is similar to case 3 in some aspects, but the changes are significant. All the process units are above the ground and that is the most significant change. While the UCG process is using coal and water in situ, this process starts with storage and preparation of the coal delivered from the coal mine. The coal, oxygen, and water are then fed into the gasifier. After the gas cooling and scrubbing unit, syngas goes through the water-gas shift conversion in order to adjust the H_2-to-CO ratio. Recompression of syngas as in cases 1–3 is not required because syngas comes out of the gasifier at high pressure.

The rest of the units are the same as in case 3.

The environmental performance is not as good as in case 3. Only 43.2% of the CO_2 equivalent in coal is captured. Net power generation is 20% higher than in case 3, but the massive increase in CAPEX (35% higher than in case 3) results in a cost of syngas (Fig. 13.11) increased over 6 times and cost of electricity 2.3 times higher (Fig. 13.12) than in case 3.

As can be seen in the graph, the largest driver of the electricity cost is the cost of capital, followed by the cost of coal in the case of CG-IGCC.

13.11 Synthetic natural gas

One product that consistently interests various entities is SNG. The ability to manufacture this staple feedstock from coal in places where there is no other hydrocarbon sources is important in many parts of the world.

In this study, we model a SNG production plant with capacity of 26 bcf of SNG per annum (Fig. 13.13).
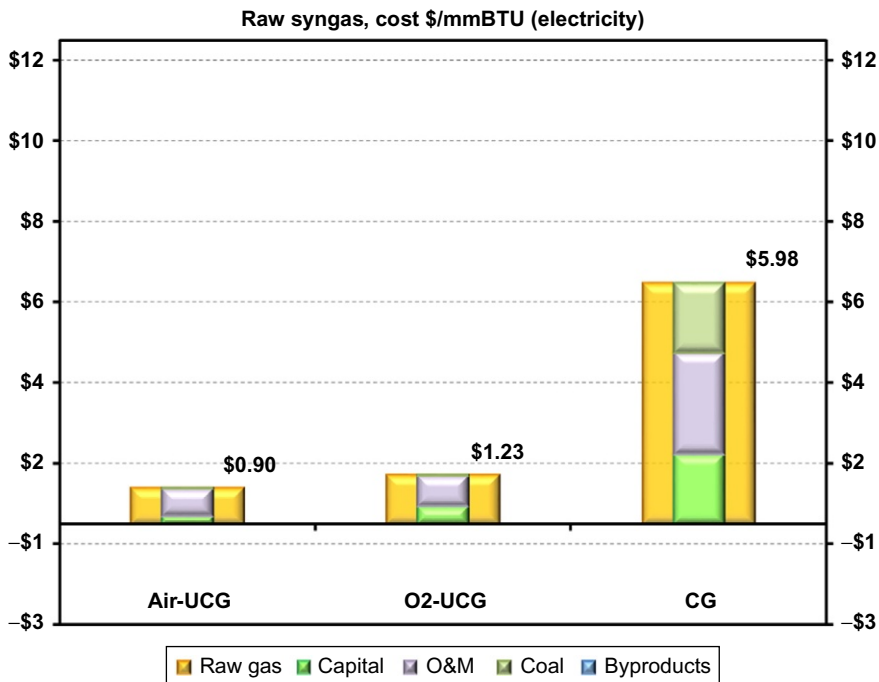
Fig. 13.11 Cost of syngas comparison (Blinderman et al., 2011).
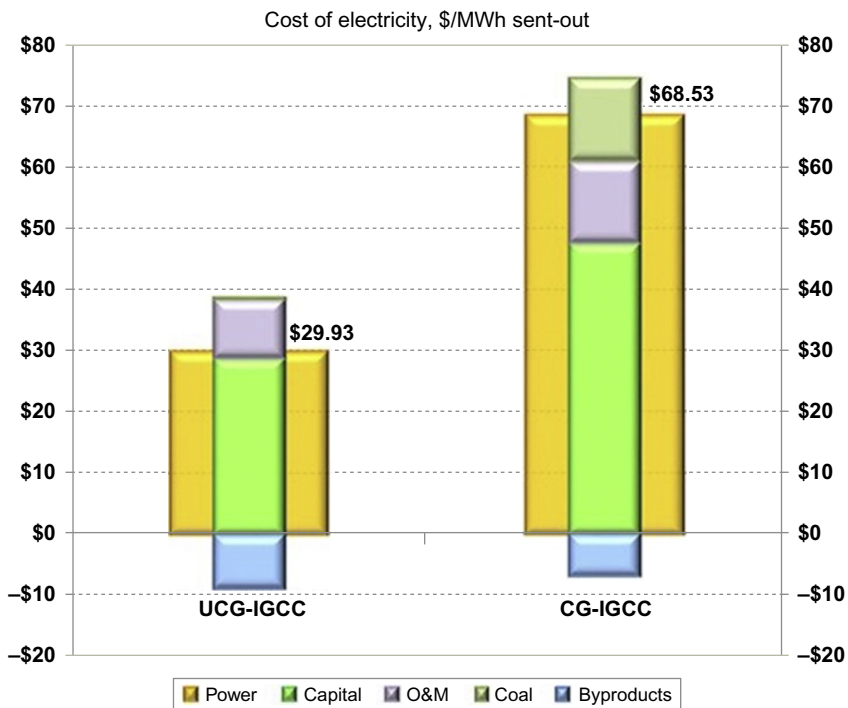
Fig. 13.12 Cost of electricity comparison (Blinderman et al., 2011).
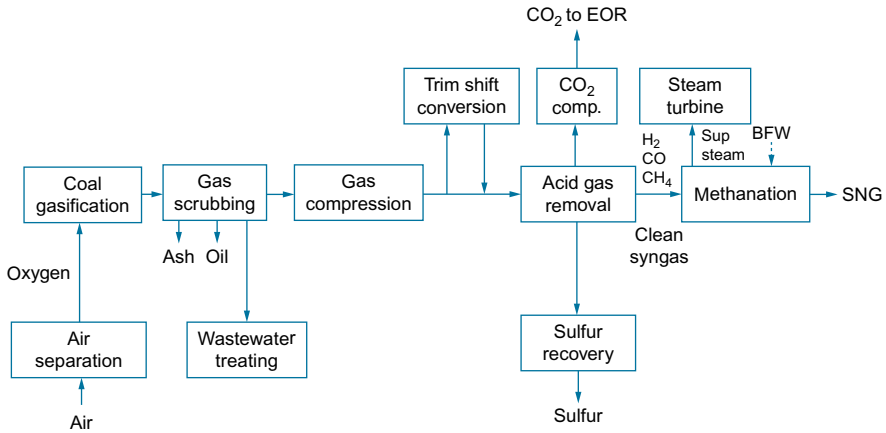
Fig. 13.13 εUCG-SNG production BFD (Blinderman et al., 2011).

First, it should be noted that the size of the plant is nearly double that designed for electricity generation. The requirement to produce more energy (30 vs 16 PJ p/a) leads to a similar increase in coal use and increases in capital costs across the board.

In other respects, the process flow is very similar to electricity production with oxygen injection (case 3) reviewed earlier.

The differences in the process are as follows:

a. Trim shift conversion unit to adjust the H_2-to-CO ratio. This trim shift was not required in power generation but is necessary in the chemical synthesis process.
b. A Rectisol unit replaces the Selexol unit in AGR.
c. Double the amounts of effluents like H_2S and CO_2 will be processed, produced, and used or released.
d. Clean syngas after AGR is delivered to the methanation unit instead of CT.
e. Methanation is an exothermic process, and the released heat will create a significant amount of steam. As a result, a ST using this steam can produce about 60% of overall power required for the plant.
f. The balance of power is purchased from the adjacent UCG-IGCC unit (case 2) at cost.

The capital cost of SNG production is relatively low. It is essentially the same as in electricity production case 2, despite SNG operation being about twice the size.

The outcome is a low-cost SNG that can be produced at $3.06/MMBtu.

Let's review of a similar process using CG for syngas production. The process flow is again very much the same as in power generation case 4. Clean syngas from the AGR unit is delivered to the methanation unit, and the resulting SNG cost is $9.10 (Fig. 13.14).

In this and in all the following cases, we considered that the actual market price of electricity in Texas at the time was about $50.00/MWh, which is quite lower than $68.50/MWh projected for CG electricity, and therefore, comparing the UCG-based process with two options for CG cases, the balance of required power either is procured from adjacent CG-IGCC at cost ($68.5/MWh) (CG) or purchased in the market at $50.0/MWh (CG(M)). The market priced electricity improves outcomes but only marginally—by less than 3% (Fig. 13.15).
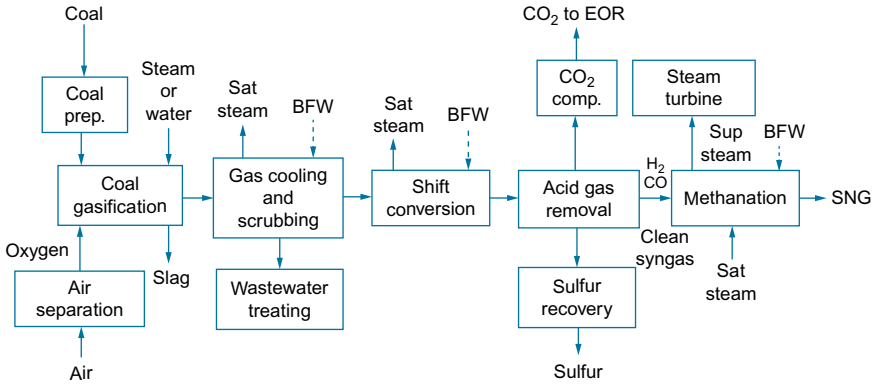
Fig. 13.14 CG-SNG production BFD (Blinderman et al., 2011).
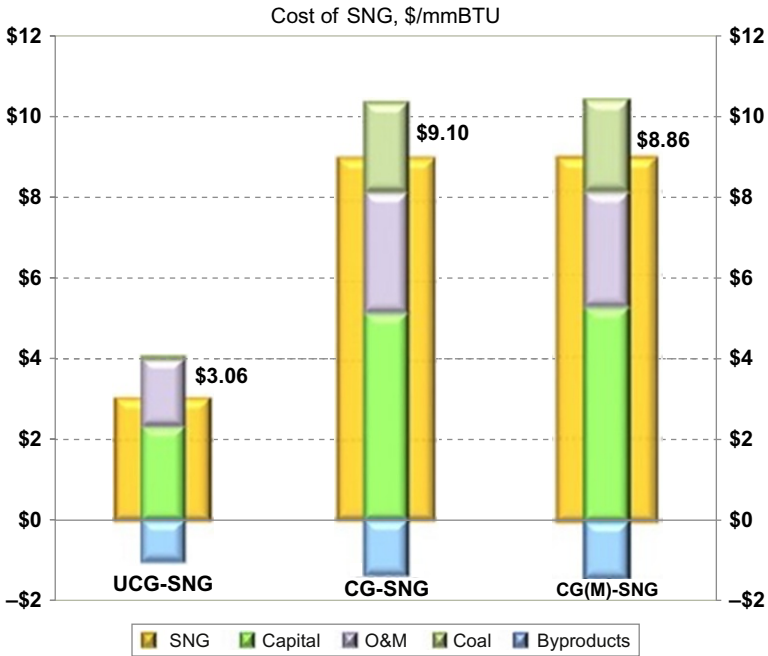
Fig. 13.15 Cost of SNG comparison (Blinderman et al., 2011).

13.12   Methanol

Methanol is one of the most common industrial hydrocarbon commodities in the world. It can be used as is or as a precursor to the production of other valuable products.
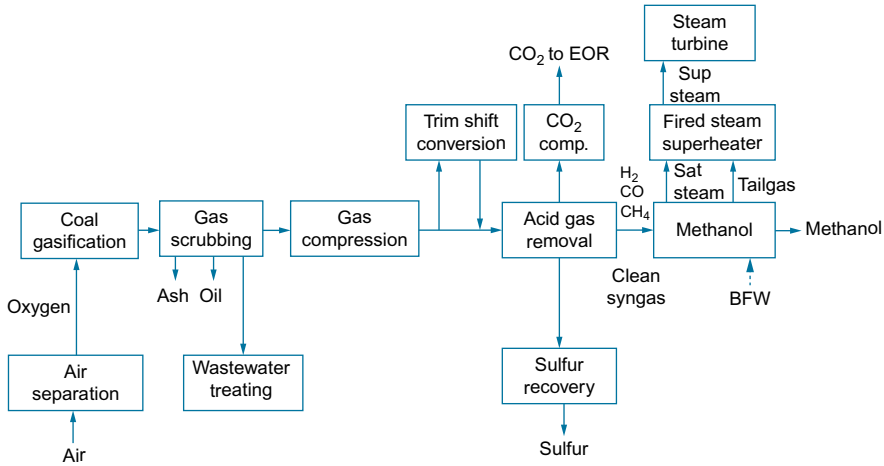
Fig. 13.16 εUCG-methanol production BFD (Blinderman et al., 2011).

The preparation of clean syngas for methanol synthesis is no different from an analogous preparation for SNG synthesis. A methanol unit replaces an SNG unit, and a fired steam superheater unit is put in place prior to the ST to improve output of the ST. The feedstock for the fired steam superheater unit is saturated steam and tail gas from the methanol unit (Fig. 13.16).

However, the energy balance and costs are quite different here. Despite a similar size, methanol production requires 12% more electricity for process needs, but internal generation is only 57% of that in the SNG case. The resulting balance of power demand will increase electricity purchase requirements and bring up the cost of production. This increase is less noticeable in UCG scenarios and quite significant in GC scenarios given the cost of power difference reviewed in electricity cases.

Changes in the CG process are exactly the same as in the UCG case. The internal power load though is 17% higher than in UCG (Fig. 13.17).

The resulting cost of methanol reflects these differences in process parameters and costs.

The cost of methanol in CG is over 2.5 times higher than in UCG, and switching to market power shows a small gain of 7% (Fig. 13.18).

13.13 Gasoline

Production of gasoline utilizes the ExxonMobil methanol-to-gasoline (MTG) process, so in terms of the process flow, it is a methanol synthesis process that we reviewed in the previous section with addition of an MTG unit. This addition results in a CAPEX increase of about 30% as compared with methanol production in the UCG case and 17% in the CG case (Figs. 13.19–13.21).
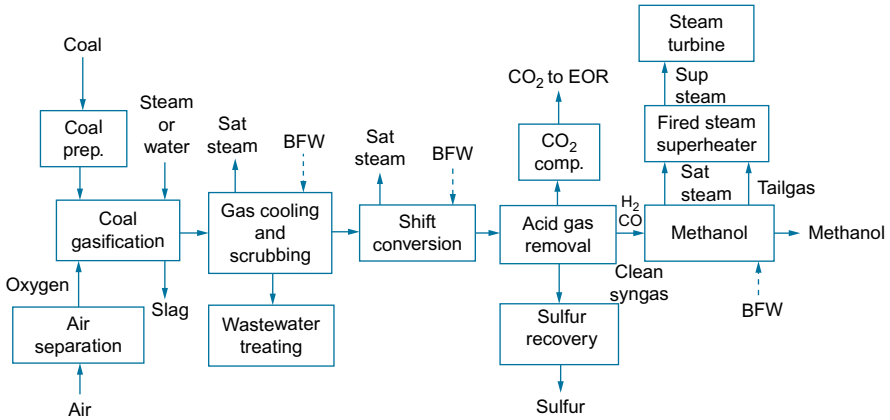
Fig. 13.17 CG-methanol production BFD (Blinderman et al., 2011).
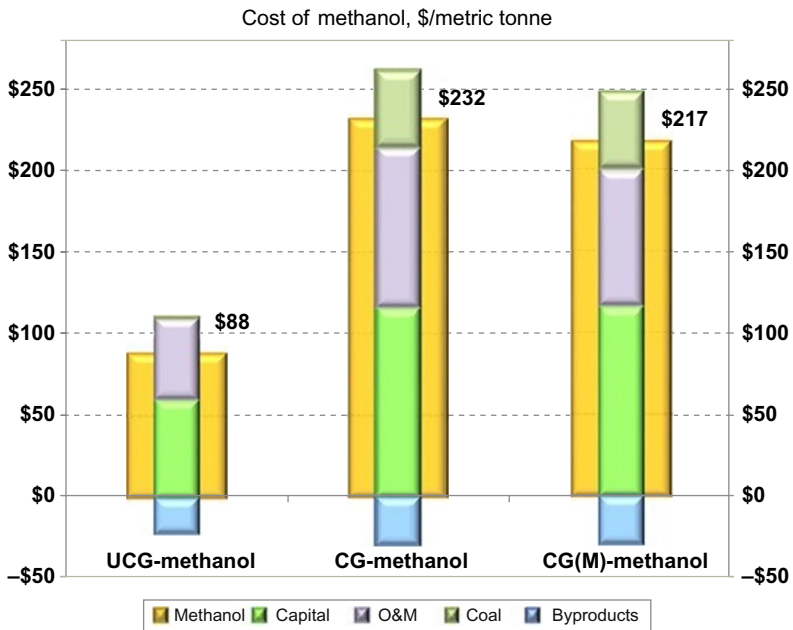
Fig. 13.18 Cost of methanol comparison (Blinderman et al., 2011).

The gasoline cost in all cases was quite lower than the market price at the time. The UCG-based gasoline is more than two times cheaper than gasoline manufactured using CG. The difference between CG and CG(M) is quite small—about 5%.
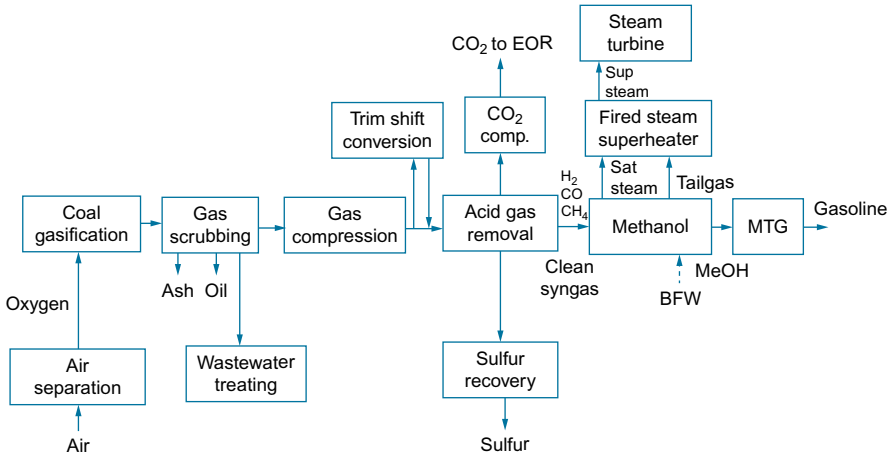
Fig. 13.19 εUCG-gasoline production BFD (Blinderman et al., 2011).
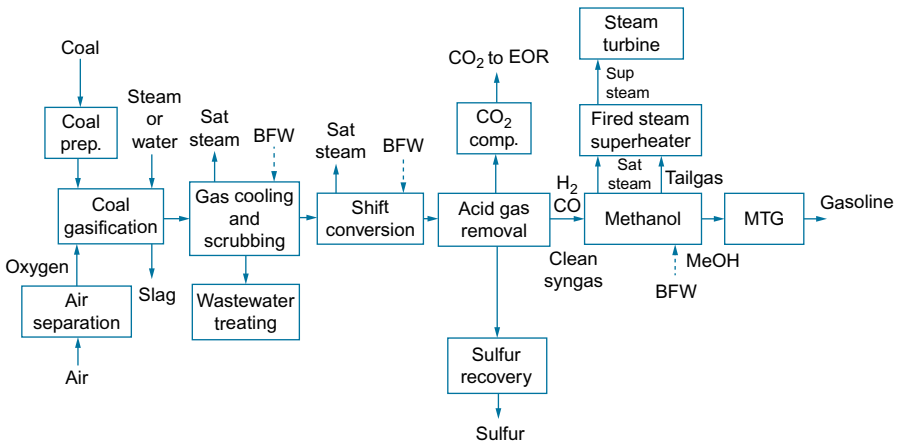
Fig. 13.20 CG-gasoline production BFD (Blinderman et al., 2011).

13.14 Ultra-low-sulfur diesel

Production of ultra-low-sulfur diesel (ULSD) is based on the Fischer-Tropsch (F-T) reaction. Syngas is converted into two products: ULSD and LPG.

The block flow diagram depicting the process is essentially the same as in all synthesis cases. The end-use block is an F-T unit.

An additional processing step unique to this process is tail gas recycling in the partial oxidation (POx) unit via the POx process. Installation of this unit requires an additional feed of oxygen and the tail gas for unit operation. Oxygen comes from
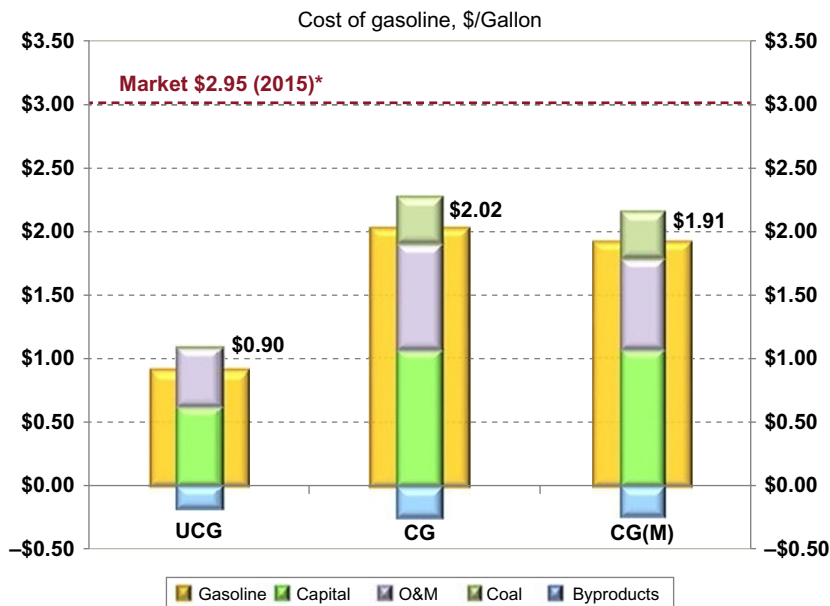
Fig. 13.21 Cost of gasoline comparison (Blinderman et al., 2011).

the ASU and tail gas—from the back end of the F-T reactor. The syngas produced is added to the primary syngas stream prior to the syngas compression unit.

Installation of a POx unit is required for both UCG and CG plants (Figs. 13.22–13.24).

The ULSD plant is the most expensive plant in this review, with CAPEX close to $2 billion or about twice the SNG CAPEX in the UCG case and 150% in the CG case. The resulting cost of diesel is $1.24/gal in the UCG case and $2.70/gal in the CG case (220% more expensive) or $2.56/gal (210%) in CG(M) case scenario.

There is a technological option to reduce both CAPEX and product costs if the plant is designed to produce three products such as ULSD, naphtha, and LPG, but this is achieved by reducing volume of diesel and a respective increase in naphtha production.

13.15   Ammonia/urea

The production of urea and its precursor ammonia is based on the production of SNG. For UCG base plant, the process flow is the same as for SNG except for the following significant changes:

1. Oxidizing agent

Instead of pure oxygen injection as in all previously reviewed synthesis products, this plant uses oxygen-enriched air. This change is required because for the synthesis of ammonia; a
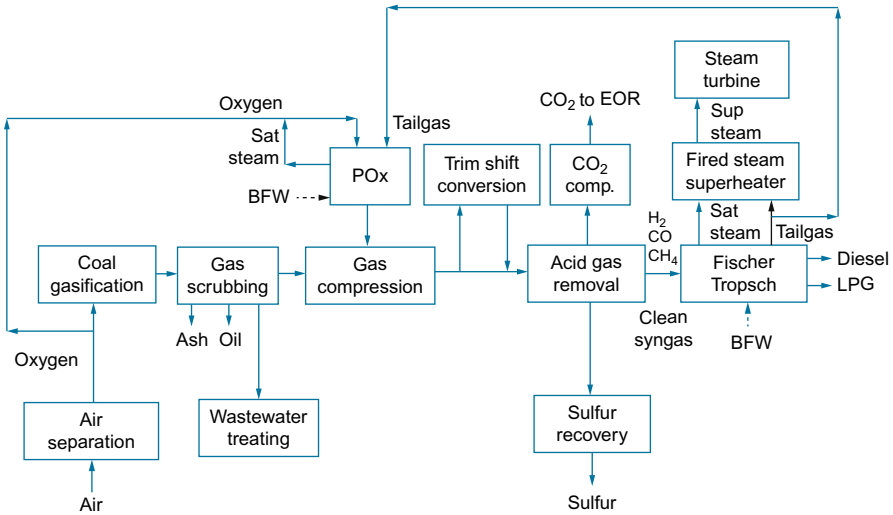
Fig. 13.22 εUCG-ULSD production BFD (Blinderman et al., 2011).
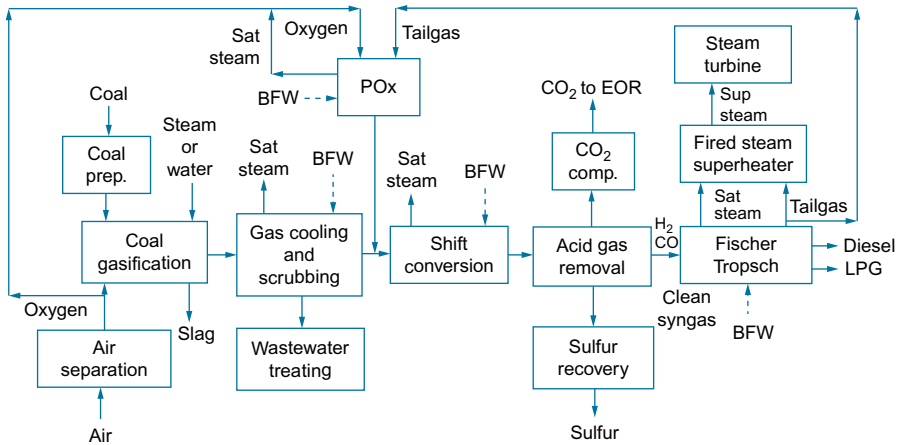
Fig. 13.23 CG-ULSD production BFD (Blinderman et al., 2011).

certain amount of nitrogen must participate in the synthesis reaction and therefore should be delivered to the reactor together with H_2. N_2 as a constituent part of air in the oxidizing agent will enter the process, eventually separate from oxygen, and then flow unreacted until it reaches the ammonia synthesis unit where it will enter catalytic reaction with H_2 to form anhydrous liquid ammonia. This step is known as the ammonia synthesis loop (also referred to as the Haber-Bosch process):

$$3H_2 + N_2 \rightarrow 2NH_3$$
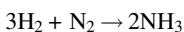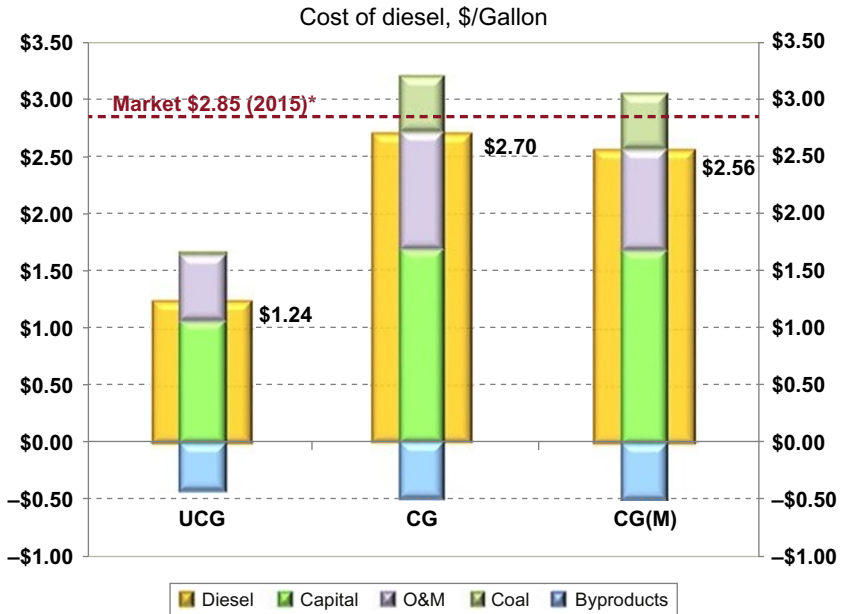
Fig. 13.24 Cost of ULSD comparison (Blinderman et al., 2011).

2. Shift conversion

In all previously reviewed cases of UCG-based synthesis products, the plants were employing a trim shift conversion unit in order to adjust the H_2-to-CO ratio. Ammonia synthesis does not need CO for the process, and therefore, all CO has to be converted to CO_2 and H_2 prior to CO_2 extraction in AGR.

3. CO_2 captured in AGR

Components of urea synthesis are NH_3 and CO_2. NH_3 is delivered to the urea synthesis unit from the ammonia unit and CO_2 from the volume of CO2 captured in AGR.

4. The methanation unit in the SNG production process was a large unit capable of converting all the syngas feed to SNG. The purpose of the methanation unit in the ammonia plant is the final removal of carbon oxides from the stream of H_2, as they are considered to be a poison to ammonia catalysts. Therefore, the methanation unit is much smaller in size and has a different purpose (Fig. 13.25).

The process of ammonia synthesis based on CG is organized differently:

1. A conventional gasifier is not designed to work with oxygen-enriched air, and the oxidizing agent used in the UCG-based case cannot be applied here. As in all previously reviewed synthesis cases, pure oxygen should be supplied in coal gasification.

2. Shift conversion, as in the case of the UCG-based process, must shift all available CO, rather than adjust the H_2-to-CO ratio.

3. For the final H_2 purification, it was decided that the pressure swing adsorption (PSA) unit will suit the CG-based ammonia production process better than the methanation unit, so after AGR, syngas is delivered to the PSA unit.

4. Pure H_2 extracted from PSA is then blended with pure N_2 delivered from ASU, and the mix enters the ammonia synthesis unit.
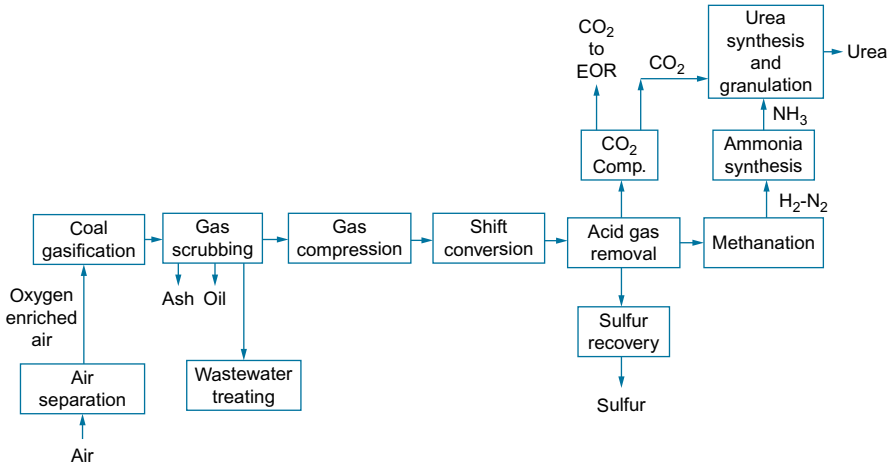
Fig. 13.25 εUCG-urea production BFD (Blinderman et al., 2011).

5. Part of the tail gas is delivered to the fired steam superheater as fuel gas. Superheater supplies the superheated steam to the ST that produces about 12% of the internal load requirement. The rest of the tail gas from the PSA unit is looped back, recompressed, admixed with the stream of the primary syngas, and delivered to the shift conversion unit (Fig. 13.26).

Resulting CAPEX of GC-based urea plant is close to $2 billion, about 27% higher than CAPEX for a UCG-based urea plant. O&M in the same comparison is 73% higher. The cost of produced urea reflects the differences in complexity and costs of installation and operations between UCG-based and CG-based plants as well. CG-urea costs are 80 and 67% higher than the cost of UCG product in respective CG and CG(M) cases (Fig. 13.27).

13.16 εUCG vs CG cost reduction

Direct comparison of major economic and environmental parameters of UCG and CG production reveals a significant benefit of employing UCG-based plants.

Capital requirements for UCG-based production are between 29% and 55% less than that of CG across the whole range of reviewed products, with the largest reduction for SNG and the smallest reduction for urea.

It can be explained by the fact that the capital cost of processing and end-use equipment above ground in relation to the syngas production is the largest in case of urea and smallest in case of SNG.

O&M reduction is between 28% and 49%, with the smallest for electricity and the largest for methanol.

The cost of feedstock reduction is invariable at 98% for all cases reviewed.

Lastly, the reduction in the product cost is between 44% for urea and 66% for SNG.
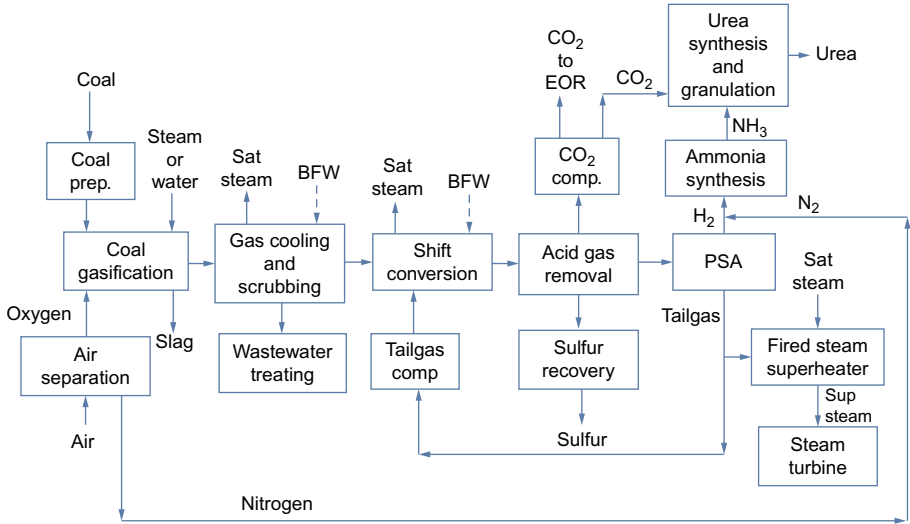
Fig. 13.26 CG-urea production BFD (Blinderman et al., 2011).
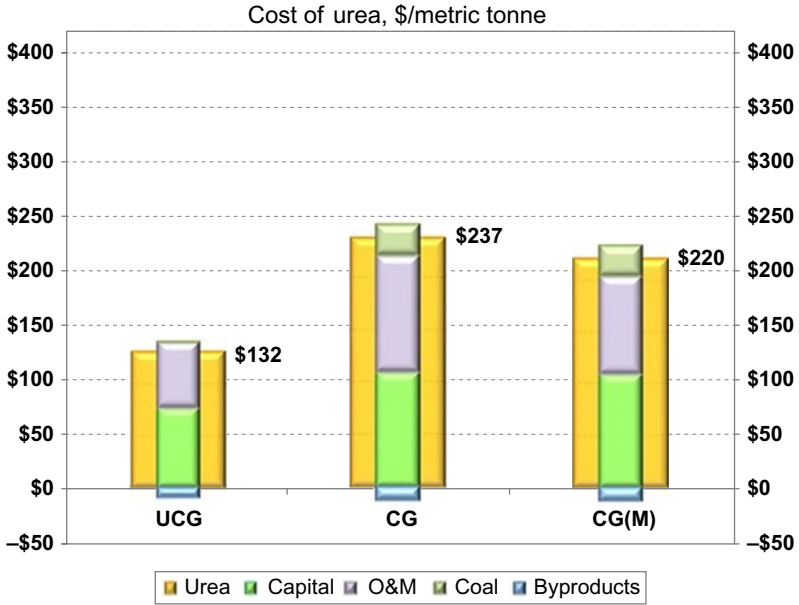
Fig. 13.27 Cost of urea comparison (Blinderman et al., 2011).

Table 13.3 εUCG vs CG cost reduction (Blinderman et al., 2011)

	Capital (%)	O&M (%)	Coal (%)	Product (%)
Electricity	39	28	98	56
SNG/CH$_4$	55	43	98	66
Methanol	52	49	98	62
Gasoline	42	44	98	55
Diesel	36	44	98	54
Urea	29	42	98	44

In terms of CO_2 emissions, CG-based plants capture more CO_2 in all cases except for electricity (Table 13.3).

13.17 Further work

Every production unit reviewed in this work comprises three major components:

1. Syngas production.
2. Syngas treatment.
3. End-product manufacturing.

All the modeling cases with respect to syngas treatment and end-use products were based on standard engineering equipment designed over the years for the multitude of projects and installed in many locations all over the world. This equipment represents tried and true engineering solution proved many times over. However, it does not mean that it is most economic or optimal solution for UCG syngas. The design of this equipment does not reflect specific parameters of UCG syngas, is not optimized, and can be improved leading, for example, to a significant reduction of syngas treatment costs.

In order to determine the most beneficial area of improvement and focus on it in the future work, we review the relative share of cost components in overall capital cost for each UCG-based case. The average CAPEX distribution for tree production components across all the cases is as follows:

1. UCG syngas production—12%.
2. Syngas treatment—33%.
3. End-product manufacturing—56%.

It is clear that while the UCG plant can be improved and cost of it reduced, it would result in only marginal reduction in overall project cost. The end-product plants use mature designs, and cost improvement there may be slow and incremental at best. However, the syngas treatment part that represents one-third of total capital cost is similar in all reviewed case scenarios and should be a primary target for major improvement in design and cost. In this study, it invariably includes the same technological blocks, namely, AGR, SRU, and sour gas stripping. This appears to be the most

promising field for technological improvements resulting in ultimate cost reductions. For example, recently, we studied a new solution for acid gas treatment and sulfur recovery that can reduce the cleanup cost compared with conventional Rectisol and Klaus units modeled in this study by up to 50%. This technology is offered by a large international technology provider and represents excellent opportunity for capital cost reduction across all UCG-based end-product plants.

The other area of potential improvements is the end-use product equipment. In this study, we modeled the world-class plant sizes, the largest available equipment in a single production train configuration, with the goal to maximize effect of the economy of scale. At the same time, there are a number of new manufacturers offering smaller, modular skid-mounted equipment. The unit of end product may be more expensive compared with world-scale plant output but still below the market prices, given the use of inexpensive UCG syngas as a feedstock. And the overall cost of the plant that is 10–15 times smaller than world-class installations becomes manageable, especially for an entry stage project.

The third area of the future work is the development of new products based on UCG syngas. There are a number of high-value products unrelated to energy applications that may become primary movers for UCG-based projects in modern market.

13.18   Conclusions

Electricity and most of hydrocarbon-based commodities, such as SNG, methanol, and gasoline, can be produced from coal as a feedstock.

With the exception of electricity generated at conventional coal-fired boiler plants, all uses of coal for energy or chemical synthesis require coal to be converted to syngas via coal gasification process. Syngas is then cleaned up and converted to its intended product using an appropriate technology.

The familiar method of producing syngas from coal is conventional coal gasification in a purpose-built aboveground gasifier. The conventional method requires coal to be mined, delivered to the gasifier site, stored, and prepared (conditioned) before being fed into the gasifier. It also requires a significant amount of water to be supplied for gasification. All effluents of coal gasification such as ash, slag, and water streams should be collected, treated, and disposed of.

UCG utilizes coal and water in situ and does not require collection, treatment, and disposal of all the effluents mentioned above, because ash and slag are left underground and not produced at the surface.

In this study, we reviewed the economic outcomes of replacing CG with UCG for syngas production. This change stipulates certain changes in syngas cleanup and downstream processes and equipment. The resulting economic impacts and outcomes change as well.

Six major products have been reviewed in the study:

- Electricity
- Fuels and chemicals

- – SNG
- – Methanol
- – Gasoline
- – Diesel
- • Fertilizers
  - – Urea

The technological processes, equipment, and operational parameters were modeled, evaluated, and costed for each product with the use of CG and UCG.

Apart from gasification method, most other conditions were the same for each compared case, specifically plant location, production capacity, lignite quality, financing parameters, etc.

In each case scenario, end-product plant using UCG was found to have significantly better efficiencies, less capital requirement, lower operational and maintenance expenses, and lower resulting costs of the product as compared with CG.

The findings suggest that products based on UCG syngas are 44%–66% less expensive than the same products manufactured with CG-based syngas. More importantly, the cost of UCG-derived products is much lower than market prices—for all end products included in the study.

The study clearly demonstrates superior economic performance of UCG-based energy and chemical synthesis plants in comparison with CG-based technologies. All considered UCG-based products are inexpensive enough to successfully compete at the current market prices.

References

Blinderman, M.S., Jones, R.M., 2002. The Chinchilla IGCC project to date: underground coal gasification and environment. In: Proceedings of 2002 Gasification Technologies Conference, San Francisco, USA.

Blinderman, M.S., Gruber, G.P., Maev, S., 2011. Commercial underground coal gasification performance and economics. In: Proceedings of 2011 Gasification Technologies Conference, San Francisco, USA.

Meyers, R.A., 1981. Coal Handbook. Marcel Dekker, New York, NY.

Majuba underground coal gasification project

14

S. Pershad, J. Pistorius, M. van der Riet
Eskom Research, Testing & Development, Johannesburg, South Africa

14.1 Introduction

South Africa is well endowed with coal, solar, wind, and nuclear energy resources but less so with hydro, gas, and oil. This is changing as new discoveries are confirmed, such as the potential of shale gas in the Karoo region of South Africa. In the regional context, South Africa has a broader diversity of energy resources, with a far greater proportion of gas and hydro (including the enormous potential of the Inga river in the Democratic Republic of Congo). All these indigenous energy resources compete, and their competitiveness is judged by factors such as their accessibility, cost, environmental footprint, and proximity to market. Furthermore, imported energy resources (such as LPG, LNG, and nuclear fuel) could be competitive.

Underground coal gasification (UCG) presents a significant future energy source opportunity for South Africa. Within the South African context, this is recognized in two key energy documents, namely, the National Development Plan (NDP) 2030 (2012) and the recently released draft Integrated Resource Plan (IRP) 2016.

With specific reference to coal, UCG and electricity, the NDP states the following:

> *Cleaner coal technologies will be supported through* research and development *and technology transfer agreements in ultra-supercritical coal power plants, fluidized-bed combustion,* underground coal gasification*, integrated gasification combined cycle plants, and carbon capture and storage, among others.*

The draft RSA IRP (November 25, 2016) states the following:

> *UCG technology therefore allows countries that are endowed with coal to continue to utilize this resource in an economically viable and environmentally safer way by converting coal into high value products such as electricity, liquid fuels, syngas, fertilizers and chemical feedstock. While the process has previously been criticized for generating large quantities of hydrogen as a useless by-product, hydrogen is now in demand as a feedstock for the chemical industry and shows potential as an alternative fuel for vehicles. The development of this technology and the viability of its implementation are still at a nascent stage and ongoing research needs to be undertaken.*

Research and development:

> *Research and development should focus on innovative solutions and in particular on solar energy, as this has the greatest potential to address electricity challenges for small-scale energy consumers in a fairly short timeframe. Solar energy also has the potential to address the need for energy access in remote areas; create semi-skilled jobs; and increase localization. More funding should be targeted at long-term research focus areas in clean coal technologies such as CCS and UCG as these will be essential in ensuring that South Africa continues to exploit its indigenous minerals responsibly and sustainably. Exploration to determine the extent of recoverable shale gas should be pursued and this needs to be supported by an enabling legal and regulatory framework.*

The Department of Energy is accountable for the compilation of a draft South African Integrated Energy Plan (IEP). A draft (IEP) (DOE, 2016), was released in 2016 for public comment with a view to replace the previous IEP 2010, which comprises many elements as indicated in Fig. 14.1. These elements govern the need for, and timing of, all energy technologies. The primary factors considered when proposing any energy technology would be its commercial maturity, cost, and emissions. Secondary factors such as water consumption, localization, job creation, and technology transfer also determine technology suitability.

The South African IEP (and specifically the IRP component for electricity) sets the entrance criteria for all energy technologies, including UCG.
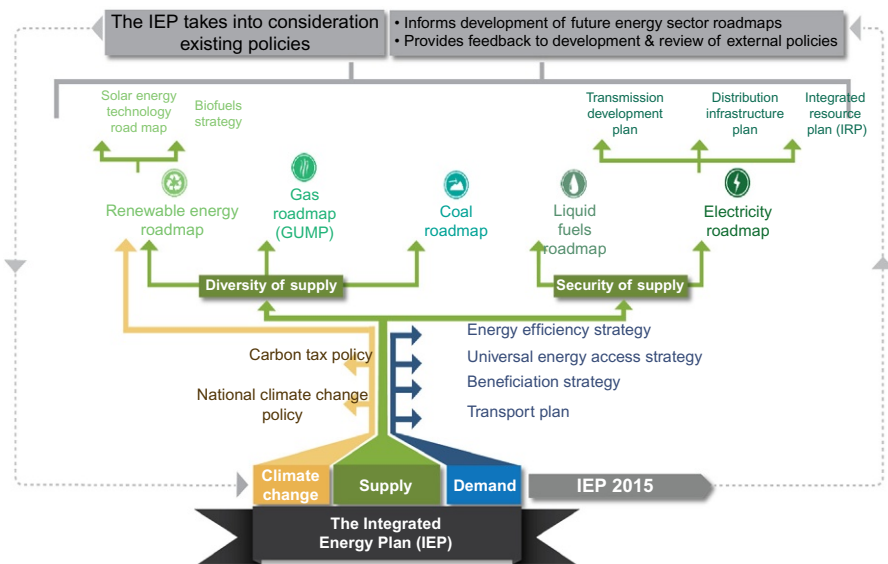
Fig. 14.1 Integrated Energy Plan (IEP) (DOE, 2016).

Eskom Holdings SOC Ltd (Eskom) is a vertically integrated public electricity utility in South Africa, with primary energy provided by coal, nuclear, hydro, wind, photovoltaic, and biomass. Eskom Holdings SOC Ltd is South Africa's primary electricity supplier and is a state-owned company (SOC) as defined in the Companies Act, 2008. The company is wholly owned by the South African government, through the Department of Public Enterprises (DPE). Eskom generates ∼90% of the electricity used in South Africa and ∼40% of the electricity used on the African continent.

The electricity supply industry in South Africa consists of the generation, transmission, distribution and sale of electricity, and importation and exportation thereof. Eskom is a key player in the industry, as it operates most of the baseload and peaking capacity, although the role played by independent power producers (IPPs) is expanding. Eskom operates 28 power stations, with a total nominal capacity of 42,810 MW, composed of 36,441 MW coal-fired stations, 1860 MW of nuclear power, 2409 MW of gas-fired, 600 MW hydro and 1400 MW pumped storage stations, and 100 MW Sere Wind Farm.

It includes four small hydroelectric stations, which are installed and operational, but not considered for capacity management purposes (Eskom Holdings SOC Ltd, 2016).

UCG is one of several potential clean coal technologies being researched and developed by Eskom, to align with the South African IRP for electricity generation.

14.2 Overview of Eskom's Majuba UCG project

Eskom's UCG research project was initiated by the South African UCG pioneer Dr. Mark van der Riet in 2002 to develop the science of UCG technology against modern standards and regulations. Eskom highlighted UCG's potential in an internal Coal Technology Conceptual Study in 2002, and this led to a site selection and Prefeasibility Study in 2003, a Site Characterisation Study in 2005, the successful commissioning of a pilot plant in the Majuba coalfield in January 2007, and the successful testing of the equipment for cofiring of UCG gas in one of the Majuba Power Station boilers in October 2010. Eskom's Pilot Plant ran successfully through to September 2011, after which decommissioning commenced as the pilot had successfully qualified the technology performance, and the following step was to quantify performance with a demonstration plant (Table 14.1).

Eskom licensed the εUCG technology from Ergo Exergy Technologies Inc. (Canada). Ergo Exergy's UCG experts have been closely involved in all technical aspects of Majuba UCG project since its inception; successful gradual transfer of εUCG technology expertise and know-how helped to build up the skill set of Eskom UCG team.

The lengthy technology gestation period unfortunately occurred during a time in South Africa when the country evolved from having surplus generating capacity to where there were critical shortages. Likewise, within the same time frame, the international community evolved from having scant regard for carbon emissions to the current imperative of decarbonizing. These evolving circumstances affected

Table 14.1 **Eskom Majuba UCG project phases**

Activities	Period	Milestones/KPI's/results
Technology scans	2001	To identify UCG potential
Conceptual study	2002	Highlight the potential of UCG technology
Site selection and prefeasibility study	2003	Majuba coalfield identified
Site characterization study	2005	To quantify UCG potential
Commissioning and operating of an initial 5000 Nm^3/h pilot plant in the Majuba coalfield	2007–10	Successful—first UCG gas production providing qualitative results
Preliminary engineering (40 MW)	2009–10	Concluded that it was necessary to increase the demonstration plant scale to between 100 and 140 MW (with the mine operating at 250,000 Nm^3/h) due to the unavailability of a suitable 40 MW turbine size
Increase pilot plant capacity to 15,000 Nm^3/h	2010–11	Prove the concept of cofiring gas in the Majuba boilers and demonstrate power generation, that is, prove UCG as a baseload power option
Demonstration phase studies, basic engineering studies of the 100–140 MW demonstration plant	2010–13	Concluded that while the conceptual gas specification is technically viable, it has limitations with specifically carbon footprint due to the Majuba site geologic setting (relatively shallow coal depth). The carbon footprint was not initially an objective at research inception in 2002, but evolving national priorities and legislation necessitated its inclusion in 2010. This was due to South Africa's commitment to a low-carbon trajectory at the COP15 in Copenhagen in December 2009, subsequent inclusion in IRP2010 and IRP2016, and carbon taxes proposed by Treasury for 2018 The gas specification therefore requires improvement and needs to be proved on a larger pilot plant scale more representative of commercial-scale application

Table 14.1 Continued

Activities	Period	Milestones/KPI's/results
Due diligence, by external independent third party, of cofiring safety	2011	Complete—an expert review, by VGB PowerTech (Germany), concluded the competence of the pilot plant installation and readiness for cofiring
Commencing shutdown of gasifier G1	September 2011	This was a necessary regulatory and research motivation prior to any further expenditure
• Continued shutdown of G1 • Planning key research questions and activities • Costing and scheduling • Site legal compliance • Postgasification drilling	May 2013 onward	These activities are continued at a different level of complexity, on a continuum of the Eskom pilot's and demonstration project life-cycle model (PLCM), such as concept, basic design, and detail designs

Eskom's UCG project significantly, and the project therefore needed to also change its strategic drivers.

The strategic drivers applicable in the period 2007–12 are illustrated in Fig. 14.2.

In 2012, the project strategic objectives again changed to be in step with local factors and South Africa's international commitment to decarbonize electricity production. The new strategic drivers and progress therein are reflected in Fig. 14.3.
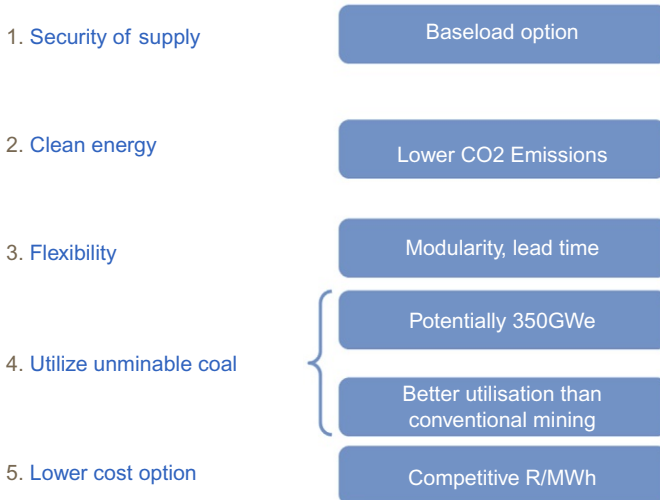
Fig. 14.2 UCG strategic drivers for Eskom (approved for period 2007–12).

UCG strategic drivers	Progress
• Independent, long-term fuel source	Proven at concept level
• Total environmental footprint (including Carbon)	In progress
• Low cost energy source	In progress
• Mining efficiency	Proven at pilot level
• Security of supply—baseload or mid-merit option	In progress
• Technology transfer	In progress
• Mining safety	Proven at pilot level
• Broader geographic distribution for new generating capacity	Proven at concept level
• Job creation in rural locations	Proven at pilot level
• Valuable by-products	Proven at pilot level
• Ash left underground	Proven at pilot level

Fig. 14.3 UCG strategic drivers for Eskom (approved for period 2012 onward).

Table 14.1 illustrates the various phases of Eskom's Majuba UCG project.

Eskom's initial intent and the objective of the pilot plant was to firstly produce and secondly cofire the UCG gas, at the Majuba UCG site, into the adjacent Majuba Power Station boilers. This would naturally not have added new generating capacity to the grid, but merely swopped fuel source from coal to coal-derived syngas. However, due to the shortage of generating capacity in South Africa that became apparent in the early 2000s, Eskom's UCG commercial objective evolved to adding new generating capacity by firing the gas produced at the Majuba UCG site in an open-cycle gas turbine (OCGT) or a combined-cycle gas turbine (CCGT), depending on the load required.

In 2015, the project encountered circumstances within the country and company that led to company-wide budget restrictions, affecting all noncore operations. Owing to the success of the UCG project and its continued strategic importance, Eskom board granted a revised mandate to seek partnership and to convert the existing UCG infrastructure into a commercially viable power-generating plant. This phase intent is still currently in the internal commercial and regulatory process, with the end objectives and scale to be defined with the new partner(s).

14.3   Site selection & prefeasibility phase, 2002–03

In 2002, Eskom completed a scoping study report, which described the technology review, communications with UCG technology suppliers, and potential sites considered (Van Eeden et al., 2002). The study identified and recommended Ergo Exergy Technologies Inc. of Canada (*Ergo Exergy*) as the technology supplier. Ergo Exergy's variation of UCG technology is based on lessons learnt in the extensive UCG research

and operations in the former-Soviet Union and successfully trialed in the Chinchilla **I** UCG project, Australia (1997–2006) and several others international projects. The Ergo Exergy variation of UCG technology is termed the Exergy UCG or εUCG. With Ergo Exergy's assistance, six potential sites were short-listed as suitable for UCG.[1] The Majuba site located on farm Roodekopjes 67HS, in the Amersfoort district of Mpumalanga, South Africa, was the site eventually chosen from the selection process, for reasons given below:

1. Eskom owned the mineral rights and substantial surface rights.
2. The proximity of Majuba Power Station enabled consideration of cofiring the gas in to the boilers, to offset coal imports.
3. The Majuba coal seam met the UCG conceptual technology requirements, as the coal seam had an ~250 m average depth and 3 m average thickness. The coal seam was also known to have low permeability, which was also seen as an advantage for containing the UCG process.
4. Dolerite intrusions were acknowledged to have broken the coal reserves into smaller blocks, which were anticipated to be a benefit (from the point of view of containing the process) or possibly a problem (from the point of view of disrupting UCG mining).
5. The Majuba coal deposits were extensive, with many adjacent blocks, capable to support a large UCG-based power generation development.

The very difficult geologic conditions in the coalfield were a concern to Ergo Exergy. Eskom noted this but concluded that from a research perspective, this was a suitable challenge for UCG, implying that if it worked successfully in this coalfield, then it could conceivably work in any other more favorable coalfield.

Many other favorable features became apparent after the studies with the Majuba site began, such as given below:

– Eskom had access to an extensive geologic database of more than 400 exploration boreholes drilled in the coalfield, for the defunct Majuba colliery.
– Eskom also had access to extensive hydrogeologic study data, and geophysics conducted on the site.
– There was existing Majuba colliery infrastructure, comprising extensive and unused buildings, workshops, living quarters, etc.
– The proximity of Majuba Power Station proved invaluable, due to their frequent assistance and support, from the use of their medical and emergency services, through to the loan of heavy equipment such as mobile crane.
– Majuba Power Station also had an extensive hydrocensus of surrounding water bodies, compiled over many decades and updated regularly. There were also two ambient air monitoring sites in proximity, with several decades of data. In addition, there was also an existing meteorologic database over several decades.
– During the construction of Majuba Power Station, a detailed flora and fauna study had identified endangered red book species living in the area, the sungazer lizard (*Cordylus giganteus*). A special sanctuary had been successfully established adjacent to Majuba Power Station for the relocation of this and other animal species.
– No cultural heritage places or archeological finds were identified.

---

[1] From this point on in this chapter, unless specifically indicated, abbreviation "UCG" in relation to Majuba project refers to εUCG™.

Fig. 14.4 Sun gazer lizard (*Cordylus giganteus*), Red Data Book species.

The Majuba site was subsequently approved for development of the project into the next phase, site selection and prefeasibility (Blinderman and Van der Riet, 2003) (Fig. 14.4).

14.4   UCG site description

The Karoo Supergroup hosts all South African coal deposits and ranges from the Late Carboniferous to Middle Jurassic age (320–180 Ma). It was formed in the great Gondwana basin that is composed of parts of South Africa, Antarctic, Australia, India, and South America. Coal deposits in South Africa are restricted to the area east of 26°E and in relation to the Majuba area, falls within the Vryheid Formation of the lower Ecca Group (Snyman, 1998).

The Majuba coalfield is situated in Amersfoort district of the Mpumalanga province in South Africa and comes into the immediate vicinity of Eskom's 4100 MW Majuba Power Station in the south. The surface of the area consists of rolling hills, with drainage courses forming occasional cliff features. Elevation varies between 1593 and 1775 AMSL. The relief in the northern area is greater with deeper incision of water courses, resulting in occasional large cliff features and rocky terrain. Drainage is generally good via numerous intermittent streams. Average annual rainfall is ~490 mm. The rainy season is generally from October to March with peak season falling in January. There may be 125–150 mm rainfalls in one single day.

Most of the area is pastoral land, providing grazing for sheep and to some extent cattle. Small areas are under cultivation, generally for maize.

The Majuba coal deposit forms a part of the Ermelo coalfield, which covers an area of 115,000 km^2. The coal resources for conventional mining in the coalfield have been estimated in the range of 8 billion t, with most resources being undeveloped.

The coal measures consist of three sequences: (a) the underlying Dwyka Formation, a tillite, which lies unconformably on the basement rocks and varies in thickness from 1 to 25 m; (b) the Pietermaritzburg Formation, a massive dark shaley siltstone about 20 m thick; and the Vryheid Formation, which is the thickest unit that consists of predominately upward coarsening cycles that are capped by coal seam formation. The only seam of economic importance is named the Gus seam, which is a subbituminous seam attaining a maximum thickness of nearly 5.0 m.

The floor of the Gus seam is a laminated carbonaceous siltstone and the roof a coarse grained interpreted as an erosive fluvial channel but changes laterally to a laminated siltstone and finer grained sandstone, which represents the interchannel zones.

Above the Gus seam the Alfred seam, if present, can develop up to 1.5 m in thickness. The parting between the Gus and the Alfred seams varies from 0 to more than 10 m.

The coal resources are severely intruded by Jurassic and early Cretaceous dolerite units. These intrusive events are divided into three categories:

- Near-horizontal sheets
- Transgressive sills
- Near-vertical dikes

Fig. 14.5 illustrates a simplified stratigraphic column for the Majuba coalfield.

The intrusion of dikes and sills was governed mainly by lithostatic pressure, and intrusions occurred along cracks and fissures caused by tension. These dolerite intrusions form a complex network within the coal bearing Vryheid Formation of the Ecca Group, leaving these sedimentary rocks of sequences of succession structurally and metamorphically disturbed. The structural disruptions of the coal seams are mainly due to the intrusion of dolerite dikes and sills. However, small-scale graben-type faulting and fracturing within the coal seams also occur (Du Plessis, 2008).

The Majuba coal deposit, and specifically the selected site, was found to be technically suitable for applying UCG technology. Calculated primary reserves for UCG operations within the farm Roodekopjes 67HS amounted to ~106 million t, enough to supply UCG gas for 400 MWe of power generation in Majuba Power Station for ~43 years (or 28 years for 600 MWe; 28 years being similar to the remaining life of Majuba Power Station).

The application of UCG technology to the Alfred/Gus coal seam of this deposit was deemed technically justified and feasible. Specific conditions of the Majuba coal deposit, such as multiple dolerite intrusions, were considered not to create insurmountable problems for UCG operations. A multitude of technical issues concerning the UCG application and adaptation were intended to be resolved during the next research phase, that is, site characterization and pilot plant operations on the selected site.

Detailed process modeling of UCG proper, gas cleanup, transportation, and boiler performance showed that cofiring UCG gas with coal in the boilers of Majuba Power Station was technically feasible and likely to lead to confirmation of an alternative and abundant local fuel supply. It was concluded to be technically feasible to reticulate and integrate UCG.
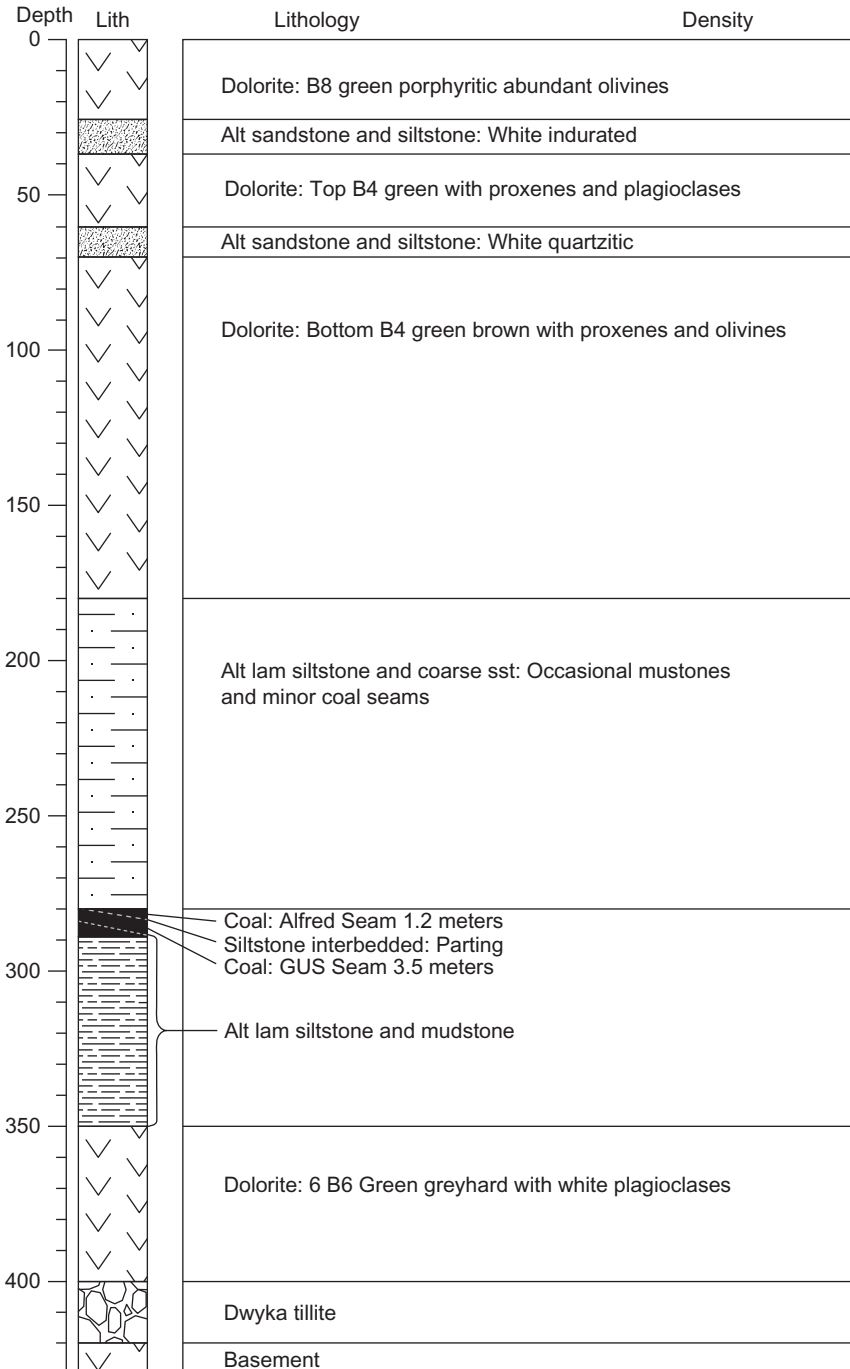
Fig. 14.5 Simplified stratigraphic column in the Majuba area.

It was found that at the selected site, the conditions of coal occurrence would be conducive to conducting UCG operations in the Alfred/Gus seam at the depth below 250 m, without causing an impact on valuable groundwater resources. The subsidence would be managed in order to minimize the surface disturbance and avoid undermining surface-water sources and alluvial aquifers.

14.5   Site characterization phase, 2005

In 2005, a detailed characterization of the site was conducted (Blinderman et al., 2005).

The site characterization phase covered prospecting, geologic and hydrogeologic investigations, and rock mechanics modeling of the overburden behavior at the target UCG site. The coal seam in the process area was also tested under "cold" conditions with controlled air and water injection to evaluate UCG potential, and extensive UCG-specific program of laboratory gasification testing of coal core samples were completed (Figs. 14.6 and 14.7).

The results of site characterization indicated that the site was favorable for applying εUCG technology at Majuba, and they create a solid foundation for design and construction of a UCG pilot plant. They also confirmed the findings and recommendations of the site selection and prefeasibility report produced in 2003 as follows:

– The Majuba coal deposit, and specifically the selected site, was found to be technically suitable for applying εUCG technology for gas production.
– The application of εUCG technology to the Alfred/Gus coal seam of this deposit was deemed technically justified and feasible. Specific conditions of the Majuba coal deposit such as multiple dolerite intrusions were not anticipated to create insurmountable problems for UCG operations.

Fig. 14.6 "Cold air" tests at Majuba UCG site.

Fig. 14.7 First Majuba "cold air testing" UCG well.

– It was found that at the selected site, the conditions of coal occurrence would be favorable for conducting UCG operations in the Alfred/Gus seam at the depth below 250 m without causing an impact on valuable groundwater resources. The subsidence would be managed to minimize the surface disturbance and rule out a possibility of undermining surface-water sources and alluvial aquifers.

In conclusion, from a technical perspective Ergo Exergy recommended proceeding to construction and commissioning of the pilot plant using the newly created test wells in the target area for process and monitoring wells.

The commercial in-house review concluded that the energy cost compared very favorably with the Eskom baseline power-generating technology of pulverized fuel combustion. The spacing of εUCG wells and electricity draw were identified as major technical risks influencing the energy cost, and the subsequent phases focused on optimizing these factors.

The site characterization phase recommended the following specific actions:

1. Further work should be done to evaluate water quality in the actual coal seam and in any aquifers that may be identified in the overlying or underlying rock.
2. Future packer tests should be conducted at higher water injection pressures to produce more extensive data on coal seam permeability.
3. Supervision of the drilling and logging and reporting of any significant events are critical.
4. Water and rock mechanics monitoring systems will be essential.
5. The high yield of polyaromatic hydrocarbon (PAH) compounds arising from the laboratory coal pyrolysis tests indicated caution in handling UCG tars and condensate as such compounds could be toxic.
6. Further research into the pyrolysis behavior of the coal was required using larger sample masses.
7. The overall conclusion was that the project is viable from technical and environmental viewpoints. It was recommended to proceed with the project to pilot plant operation.

The following findings motivated the request for approval of the pilot phase of the Majuba *ε*UCG project:

1. The geologic interpretation of the UCG site area remained unchanged, after the drilling of eight additional boreholes. Drilling difficulties included deteriorating dolerite and fissures in the overburden, which dictated the requirement for the drilling, reaming, and casing to take place within 10 days to avoid borehole deterioration and collapse. Vertical drilling and coring produced samples of rock and coal that enabled evaluation of seam and overburden properties with detailed analyses and testing.

   One nearly vertical dolerite dike had been intercepted by directional drilling, and from general understanding of the microgeology, it was perceived beneficial for UCG operations. The directional hole was still advancing at the time of the report. It was anticipated to form a backbone of the future pilot plant design and assist larger UCG operations in the future.

2. The old hydrogeologic study had very scarce information on the aquifers existing in the area, with exception of the alluvial upper aquifer that is well-known and easily accessible. There were insufficient data at that time on occurrences of groundwater in the coal seam and the deep aquifers in the overburden and underburden. The groundwater monitoring system was finished prior to construction of the Pilot plant in the next phase. The main findings at that stage were the following:
   – Water levels in the upper alluvial aquifer did not differ from those anticipated in the site selection and prefeasibility report
   – Holes into the coal seam filled with water within several days and water levels reached ∼50 m from the surface. This evidence indicated the presence of a confined aquifer associated with the coal seam.
   – Packer tests using the standard methodology for conventional mining exploration are not relevant to UCG. Tests need to be conducted at injection pressures that allow an extended water flow to render the results more representative.
   – There were not enough data to suggest any trends in regional groundwater flow, anisotropy of the permeability in the coal and the upper aquifer.
   – There were multiple occasions when drilling water circulation had been lost in the overburden rock, specifically within the overlying dolerites. It was deemed important to understand the structure and extent of the fractured zones that served as the water sinks.

3. Based on the rock mechanics modeling, both analytic and numerical, the following conclusions were drawn:
   – Immediate roof collapse could be expected to initiate from (at most) a 20 m UCG cavern span. Indications were, however, that caving would initiate from (at most) an 8 m cavern span.
   – The worst-case scenario indicated that the thick intact layers of overlying dolerite would fail beyond a 100 m cavern span.
   – The maximum height of collapse was not reasonably expected to exceed 110 m (for a 250 m cavern span).
   – No caving through to surface was expected if the "intact" dolerite layers did not contain major jointing or geologic structural weaknesses.
   – As the UCG cavern span reaches 10–15 m, the *first* immediate roof layers will collapse. As the span increases, the extent of the goaf will reach a height of 15–40 m. The overlying rock layers will then tend to become dislodged along preexisting joints and settle on the goaf, recompressing it, when the span is ∼80–100 m. Due to the presence of thick and strong sandstone layers and the thick dolerite sills, no meaningful surface subsidence is expected. The cavity below the base of the sill will gradually fill up by progressive failure of the overlying sill over a long period of time, continuing for several months or years.

4. εUCG air and water pressure cold tests were conducted using three process wells and surrounding exploration and monitoring holes. The primary purpose of the testing was to obtain data on gas and water permeability of the coal seam and surrounding strata. Results of air testing showed considerable gas permeability of the coal seam in the areas between process wells. This indicates that reverse combustion linking (RCL) can be used for linking the process wells during the pilot plant stage. The water test results confirmed the very high permeability of the coal seam between the process wells. Due to limitations of water pumping equipment and unexpectedly high-water permeability of the coal seam in the process area, it was impossible to reach high pressures required to achieve Aquasplitt linking conditions.

5. Bench-scale testing compared the gasification of Majuba coals with Chinchilla coal from the then Ergo Exergy εUCG site in Queensland, Australia. The CO_2 gasification reactivity of the Chinchilla coal as measured by a thermogravimetric analyses (TGA) was four times higher than Majuba coal. However, in the Ergo Exergy fixed-bed reactor, the Chinchilla coal took more than twice as long to burn through the same distance along the reactor length. The Australian coal peak combustion temperature was also lower by some 160°C than the Majuba coal, and rate of combustion was 2.6 times slower. The Majuba coal had higher levels of CO and H_2 but lower levels of CH_4 compared with the Australian coal. The Australian coal produced more aliphatic volatile organic compounds (VOCs), whereas Majuba coal produced more PAH compounds and light gases (H_2 and CH_4).

6. In summary, from a technical perspective the results confirmed suitability of the Majuba test site for UCG operation, in accordance with εUCG technology.

14.6 Pilot phase (2007—present)

14.6.1 Introduction

The findings and recommendations from the preliminary investigations and site characterization studies were considered when developing the strategic objective of the pilot plant. Fig. 14.8 illustrates the intent of the pilot plant and the out-of-scope items that were not intended to be researched. It is important to understand the out-of-scope items as these often lead to an overexpectation of technology development outcomes.

The objective of the pilot phase was to qualitatively determine the feasibility of the application of εUCG technology at the Majuba field and within the South African economic and legislative environment. This was done by the construction, commissioning, operation, and controlled shutdown of a pilot εUCG plant at the Majuba site.

In order to prove the εUCG technology via performance qualification, the pilot plant objectives were as follows:

1. Production of a synthesis gas via the means of UCG. The key sub activities were the following:
   - Drill, case, and complete injection and production wells.
   - Link injection and production wells.
   - Ignite the coal seam.
   - Develop and sustain the gasification reaction.
   - Collect and further analyze the UCG gas.
2. Determine gasifier operational responses and parameters.
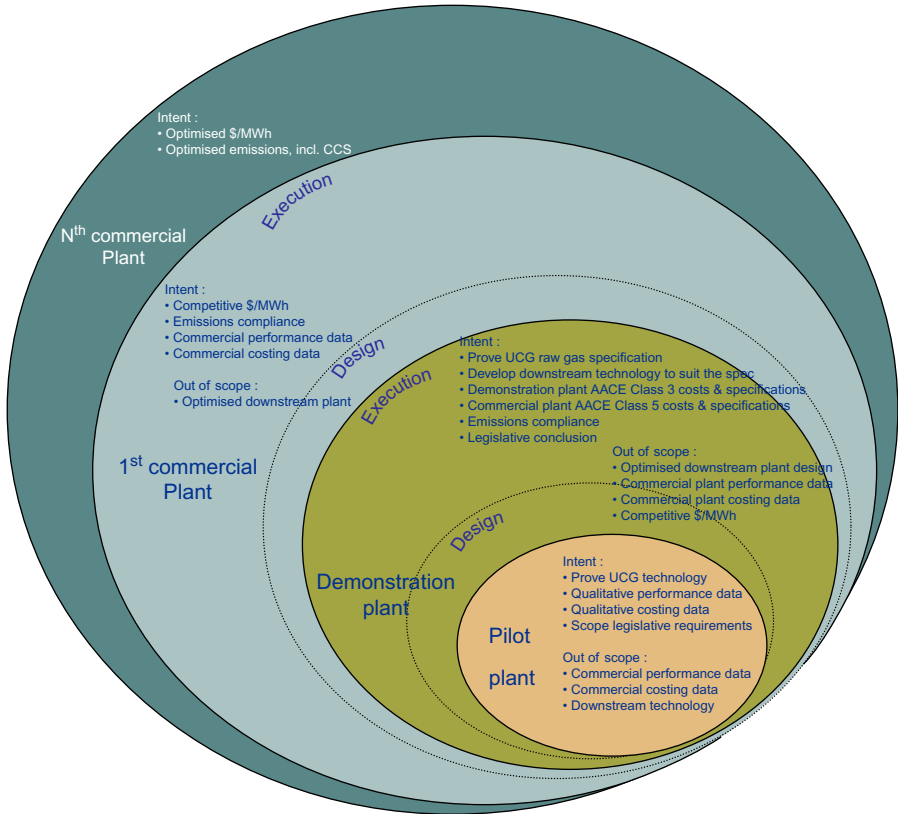
Fig. 14.8 Onion-skin diagram showing pilot plant intent during development.

3. Determine the properties of gaseous and liquid products.
4. Controlled shutdown, with postgasification drilling and monitoring of impacts.
5. Prove environmental and safety performance of the technology.
6. Develop and maintain the pilot facility for training, experimentation, and data generation.
7. Controlled shutdown, with postgasification drilling and monitoring of impacts.

14.6.2 Methodology

The pilot plant was broken into three phases in order to meet the objectives at various stages and scale through the life of the project, as described in Table 14.1. The scope of work of the pilot phase 1a and pilot phase 1b was the construction, commissioning and operation of a 5000 and 15,000 Nm^3/h εUCG pilot plant, respectively (Fig. 14.9). The UCG pilot plant can be generically broken down into two areas of operation:

1. UCG mine
2. UCG surface plant

Fig. 14.9 Aerial view of Eskom Majuba εUCG pilot site, October 2006.

The mining operation consisted of various wells that were drilled and cased to ensure that the gasification chamber was sealed off from the surrounding environment. The wells either were fed with air (as an oxidant for the gasification process) or were gas producers (Figs. 14.10–14.12).

Surface plant infrastructure included the air compressor plant, gas and air piping network, gas-liquid separation plant, condensate treatment plant, raw water dam, and condensate evaporation pond.

Fig. 14.10 Vertical drilling rig.

Fig. 14.11 Directional drilling rig with Majuba Power Station in the background.

Fig. 14.12 Well casing cementation unit.

For the design and construction of surface plant equipment, a model gas specification was developed by Ergo Exergy using proprietary εUCG model based on the unique characteristics of the Majuba UCG site, such as coal quality, geology, hydrogeology, and rock mechanics. The specification for the 5–15,000 Nm^3/h pilot plant included noncondensable gases (C_nH_m, CO_2, CO, H_2, H_2S, Ar, and N_2), condensable vapors (H_2O, NH_3, C_6H_6O, C_7H_8O, $C_{10}H_8$, and C_7H_8), and particulates (coal fines, ash, and solidified tar). Process modeling produced gas composition at well head and at the gas treatment plant (GTP) outlet. The modeling showed notably low particulate content of the gas (1.5 mg/Nm^3) that in practice turned out to be much lower.

14.6.3   Findings

In January 2007, following extensive preparation fieldwork, the coal was successfully ignited. Hours after ignition, the first εUCG syngas was produced from the Majuba coalfield.

During the first year of operation, gas production was stable, proving the feasibility of producing εUCG syngas from the Majuba coalfield.

Operational parameters were altered within the limits of the available plant and equipment to determine the gas properties at various operating conditions and thereby optimize the syngas quality and production. In June 2007, a 100 kW power generator was modified to run on 80% UCG gas and 20% diesel. The diesel was predominantly required for lubrication; however, the generator ran on 100% syngas for a period of 2 weeks. This is remarkable as an example of using syngas for power generation in technically simple and very cost-effective manner (Figs. 14.13 and 14.14).

By 2008, the UCG operations needed to expand to a larger scale. This was done without interrupting the gas production, by drilling additional production wells in the G1 panel and systematically linking them to the existing underground reactor.

Gas field operational parameters were again tested at a larger scale with multiple injection and production points. UCG gas production was sustained at a consistent production rate and stable gas quality for an extended period of time. An initial strategic objective of the Majuba UCG project was to cofire syngas into a 710 MW pulverized coal boiler at Majuba Power Station. In October 2010, the first syngas was successfully cofired for a period of time. During that period, the infrastructure and controls of cofiring syngas and coal had been tested (Fig. 14.15).

During the pilot plant operation from 2007 until shutdown initiated in 2011, key research questions were answered, within the capability and scale of the pilot plant (Table 14.2).

Fig. 14.13 January 20, 2007 first ignition of εUCG gas in Africa.

Fig. 14.14 Modified diesel generator operating on εUCG gas.

Fig. 14.15 UCG gas pipeline to Majuba Power Station.

There were also a number of operational problems encountered and successfully resolved:

1. Drilling through the horizontally layered sugary dolerites, penetrating the vertical dolerite intrusions intercepting the coal seam, gasifier entering combustion state, and autoignition of the coal seam.
2. The cofiring trial successfully proved the capability of the installed equipment. Subsequent expert review by the VGB (Germany) concluded the competence of the installation and readiness for cofiring.
3. No UCG-related safety and health accidents have been recorded during pilot plant operations. The pilot plant proved to be a steep learning curve in terms of safety. UCG essentially

Table 14.2 **Key research questions and answers**

Key questions	Answers
Suitability of Majuba coalfield for UCG	– Total coal consumption of $\sim$50,000 t
Quality and consistency of UCG gas	– Average gas production per kg coal $\sim$4.2 Nm^3/kg – The maximum flow rate achieved and sustained $\sim$11,000 Nm^3/h – Calorific value proved to be sustainable at $\sim$4.2 MJ/Nm^3
By-products from UCG production	– Production rate varied significantly during start-up, normal operation, and shutdown of the gasifier – Analysis method development was required due to the complexity in analyzing the products – Variability in production rate and composition led to complications with the gas treatment plant
Ignition	– Ignition conducted at two separate points of underground panel
Linking	– Successfully linked 10 production wells – Reverse combustion linking (RCL) was proved. The combination of Aquasplitt linking and RCL appears more appropriate for the low coal seam permeability – The 400 m in-seam hole was drilled, utility of which for linking is problematic due to microfaulting and frequent displacement of the coal seam
Combustion of UCG gas	– In diesel generator and in cofiring with pulverized coal, but more testing required with cofiring in a pulverized coal boiler
Environmental performance	– The pilot plant reported several soil contamination events, due to accidental diesel and oil surface spillages – One soil contamination event was due to a production casing failure, and seepage of gas into the surrounding soil in immediate vicinity. This was proved to be contained within the surrounding soil, and the casing failure was diagnosed as being due to inadequate casing pipe. This has been fully rehabilitated

combines three industries (mining, petrochemical, and power), with their attendant standards and applicable legislation. The Eskom UCG pilot plant was the first in South Africa and the longest running in the Western World. UCG does not easily fit within existing mining regulations and acts and has required negotiation, leniency, and concessions from regulators. The overall response and support for the technology has been very positive, and there has been a willingness to allow it to proceed as a research endeavor due to the tremendous potential it offers while learning regulatory requirements. This is necessary for any first-of-a-kind (FOAK) plant (Figs. 14.16–14.18).

Fig. 14.16 Surface piping scaling—
solidified organic condensate
deposits.

Fig. 14.17 Heat-exchanger
corrosion.

Fig. 14.18 Flare stack replaced due to corrosion.

4. The specific technical lessons learnt from the UCG pilot research plant include the following:
   – Thorough site characterization is essential for assessing UCG viability at a conceptual level (comprising geologic, hydrogeologic, rock mechanic, and geotechnical).
   – Baseline environmental tests are essential prior to commencing any UCG activities on a site. These comprise testing of soil, water (surface and subsurface), air, flora and fauna, and noise.
   – Site characterization and pilot plant are absolutely necessary to determine the potential of a coalfield for UCG technology.
   – A water monitoring system is essential prior to any UCG activity, so as to establish baseline and production data. The Majuba UCG water monitoring strategy is described in more detail in the following subsection.
   – UCG generally offers an inventory of methodologies for each activity, not all of which will work on a specific field or at a specific location. Their selection is based on skill, and furthermore, they must be trialed during the pilot phase to select the appropriate approach for each site.
5. The generic lessons learnt from the Majuba UCG pilot plant have been extensive:
   – A core team of competent and multitasking professionals and support staff is essential for a UCG pilot plant, as the technology crosses many different disciplines and traditionally separate industries.
   – There is serious concern with regard to mineral rights, due to overlapping property licenses (such as coal-bed methane) for a given single coal resource.
   – The rapid evolution of legislation (particularly in the South African context) requires the attention and dedication of a senior professional, to continuously monitor compliance. This is essential even for a UCG pilot plant.
   – Evolving legislation during the UCG piloting period proved significant enough to change the research scope and strategic drivers with corresponding budget and schedule impacts.
   – Stakeholder engagement is critical to inform and consult. Stakeholders include staff, management, the community, NGOs, academics, regulators, legislators, and even other UCG developers nationally and worldwide.
   – The Eskom UCG project set out to prove several strategic drivers, and the project findings confirmed that the technology works and is operationally and strategically relevant for Eskom and South Africa.
   – Any UCG developer needs to accept the inherent challenges with commercializing technology in their own, unique coal geology. While proved on many sites internationally, technology should not be transferred to other sites without substantial studies, testing, and piloting.
   – The potential value of the technology far outweighs its uncertainties.
   – Based on the performance of εUCG technology during feasibility and pilot studies that were conducted under a special Ergo Exergy *MFS License*, Eskom acquired from Ergo Exergy a *General εUCG License* for development of commercial εUCG-based power projects in South Africa (Fig. 14.19).

14.6.4   Recommendations

1. A revised 70,000 Nm^3/h pilot plant was motivated and approved by the Eskom board in December 2012 (and ratified in January 2013), to continue the research and quantify UCG performance at adequate scale for commercial uptake.

Fig. 14.19 15,000 Nm^3/h gas treatment plant.

2. The intent of this size panel was to prove the technology performance for subsequent commercial plant development. The specific reasons for this size are outlined below:

   – The 5000–15,000 Nm^3/h pilot plant is operated as a linear (one-dimensional) gasifier. As the coal is consumed, the cavity grows and the quality of the gas decreases. The reason for the decrease in quality is the large cavity reduces the velocity of air and the airflow pattern is not turbulent; thus, the air does not contact fresh coal surface, and all the air is therefore not consumed in the process. Essentially, a three-dimensional reactor is required that makes use of multiple injection and production points. This ensures that new sources of oxidant and gas offtake points are available as needed and that sufficient gas velocity is maintained to ensure turbulence across a face of fresh coal. Once the coal has been consumed, roof cave-in must be facilitated, essentially keeping the cavity at an optimal size for intense air/coal contact. Without cave-in, over time, the gasification reaction will deteriorate as the reaction consumes its own products, due to the constantly expanding "dead space" in a larger cavity and abundance of unused free oxidant and syngas at high temperatures.

   – The concept engineering design was completed to provide an indication of what has been done and what still needs to be done in terms of the operation of a nominal 70,000 Nm^3/h UCG power plant. The plant design consisted of UCG mining, gas and condensate treatment and power generation. The plant intended to generate 28 MW (gross) electricity, making use of reciprocating engines (Fig. 14.20).

14.6.5 Water monitoring strategy

The establishment of a water monitoring system is essential prior to any UCG activity, to establish baseline data and to plan production. The Majuba UCG water monitoring and protection strategy was designed by the εUCG technology provider Ergo Exergy during early stages of prefeasibility and site characterization based on the then available hydrogeologic information. It was further adjusted to site conditions taking into account new hydrogeologic information gathered during pilot plant operation in collaboration of hydrogeology advisor Golder Associates, Ergo Exergy, and Eskom (Love et al., 2015).

Fig. 14.20 15,000 Nm^3/h gas flare stack with Majuba Power Station in background.
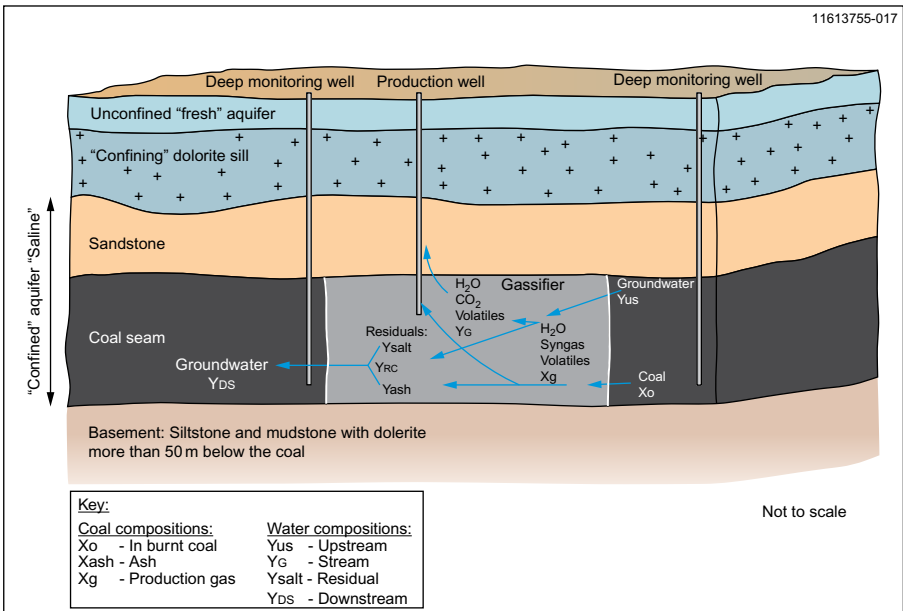
Fig. 14.21 Majuba UCG conceptual hydrogeology model (Love et al., 2015).

The groundwater system at the Majuba UCG site comprises a deep coal seam aquifer, a lower intermediate aquifer, an upper intermediate aquifer and a shallow aquifer (see Fig. 14.21). The preUCG baseline water quality studies proved the coal seam aquifer is unsuitable for domestic or agricultural use. The potential source sits within the coal seam aquifer, and the principal receptor is the shallow aquifer, which is used for agricultural purposes—although not at the Majuba UCG site. The overlaying

dolerite sill is seen as a natural confining layer between the source—the coal seam aquifer where gasification is taking place—and the receptor, the shallow aquifer. Pathways from the source to the receptor could, in principle, be developed in preparation to, or during gasification, allowing interconnectivity between the coal seam aquifer and the shallow aquifer.

Different hydrogeology monitoring zones are identified, as indicated in Table 14.3.

The layout of these monitoring zones will obviously need to be expanded as UCG production develops. Within the process control zone, the approach is to detect signs of possible contamination and to investigate and mitigate such contamination immediately. The compliance zone contains groundwater that should be minimally affected by the UCG operation and to which compliance standards apply. Once UCG has ceased, monitoring will continue to be required during the post-operation recovery phase. During this phase, the water table will be recovering (rebounding), and it is expected that water quality in the production zone will be recovering due to dilution. It is proposed that during this phase, the production zone becomes part of process control zone and the compliance zone is retained without alteration. Once the site enters the closure and long-term monitoring phases, the monitoring zonation and approach depends on the closure plan approved by the legal regulator.

14.7 Demonstration phase studies

14.7.1 Introduction

The Eskom UCG pilot plant ran successfully for 4½ years, purposefully sited on one of the most geologically complex coalfields in the country so as to test the technology suitability. The positive findings of the pilot plant led to the subsequent approval of the feasibility study into a demonstration plant. A basic front-end engineering design (FEED) of a 100–140 MW demonstration plant (250,000 Nm^3/h) was undertaken in the period 2010–12 with Black & Veatch (the United States).

Eskom's demonstration plant intent was to prove the potential of using the Majuba coalfield to sustainably produce sufficient UCG gas to fuel a 2100 MW (gross) integrated gasification combined cycle (IGCC) plant. The risks associated with such a large FOAK technology investment would be mitigated by designing, building and operating a demonstration plant of sufficient scale to form a module of the commercial plant, and proving operations of the high-risk units such as the gas turbine (in open-cycle mode only) and GTP.

14.7.2 Methodology

A power plant basic engineering design and GTP FEED was performed with the following scope. The GTP would treat 250,000 Nm^3/h of UCG syngas for use as fuel in a 100–140 MW OCGT demonstration scale plant.

Table 14.3 Majuba UCG hydrogeology monitoring zones

UCG zone during operations	Conventional mine equivalent	Conceptual basis	Monitoring purpose	Zone in shallow and intermediate aquifers	Zone in coal seam aquifer
Production	Underground mine workings or open pit—"process water"	Operational area	Observe levels "process water" against operations summary	150 m zone around production well collars	500 m zone around production well bottoms
Process control	Safety zone around mine workings or open pit	Buffer zone for early warning of any problems	Monitor for significant changes in early warning indicators	150 m zone outside the production zone—300 m from production well collars	500 m zone outside the production zone—1000 m from production well collars
Compliance	External environment	Area expected to be unaffected by UCG operations	Compliance required against agreed WUL quality standards	150 m zone outside the Process Control zone—450 m from production well collars	500 m zone outside the Process Control zone—1500 m from production well collars

The tasks performed during the power plant basic engineering design were as follows:

– A site arrangement drawing for the demonstration plant, which included the power plant, GTP, common area, and evaporation ponds.
– Heat balance calculations for several load conditions and lower syngas heating values.
– A water mass balance diagram that depicted the water usage and flow rates of the various water and wastewater streams in the facility.
– Preliminary process flow diagrams for the major plant systems that depict typical system configuration, equipment redundancy, major flow paths and valves, etc.
– Overall demonstration plant electric one-line diagrams showing the generator, transformers, and auxiliary electric system down to the 400 V level.
– A major equipment list to show the required pieces of equipment for the open-cycle power plant.
– An AACE Level 3 cost estimate and schedule.
– It is critically important to conduct the engineering design study at the appropriate level, with the above details to fully appreciate the overall project complexity, risk mitigation, and total project costs.

14.7.3   UCG gas specification

The gas specification for the demonstration pilot plant was modeled by Ergo Exergy based on previous results and the outcomes of pilot plant operation and adjusted to operational conditions of a large-scale demonstration plant. The optimal gas composition produced by modeling was within limits given in Table 14.4.

14.7.4   Findings

The function of the GTP in Fig. 14.22 was to treat the raw UCG syngas and its associated condensate to meet the OCGT feed requirements while adhering to environmental and safety requirements.

A Level 1 milestone schedule was developed based on an engineer, procure, and construct (EPC) execution methodology. An overall project schedule duration of 44 months was calculated, starting with preliminary engineering activities and ending with final acceptance of the plant in month 44. An approximate ±25% accuracy capital cost estimate was developed for the OCGT, GTP, and common facilities, based on the level of accuracy of information available. Costs for equipment, systems, materials, etc. that are shared between the OCGT and GTP were placed in the common category.

The following major risks were identified during the design process:

– UCG syngas and condensate specification and consistency: The demonstration plant design was completed based on a model gas specification, the sustainability of which had not been adequately tested during the pilot plant operations. The initial pilot plant was operated as a one-dimensional reactor; however, during commercial operations, the UCG would be operated as a three-dimensional reactor. This will have a major effect on the gas and condensate specification and consistency. Deviations from the model gas specification will therefore have a direct influence on the process efficiency of the demonstration plant. As a consequence of this uncertainty, the demonstration plant design had to cater for a worst-case scenario and was consequently overdesigned.

Table 14.4 ε**UCG demonstration plant syngas specification**

	Min ($\%_{v/v}$)	Max ($\%_{v/v}$)
Gas components		
C_nH_m	3.10	4.89
CO	7.36	11.57
H_2	14.72	18.93
H_2S	0.21	0.21
O_2	0.10	0.10
H_2O	0.10	0.10
NH_3^{gas}	0.11	0.11
N_2	54.63	46.52
Ar	0.11	0.11
CO_2	19.45	17.35
	Min (mg/Nm^3)	**Max (mg/Nm^3)**
Dry condensate components		
NH_3^{liq}	300.00	1000.00
C_6H_6	10.00	22.50
C_7H_8	1.00	4.25
C_8H_{10}	0.50	1.25
$C_{10}H_8$	10.00	36.25
C_6H_6O	2000.00	4000.00
C_7H_8O	300.00	1050.00
Other organics	0.10	50.00
Anions and cations	0.10	151.57

– Technology selection: None of the technologies specified in the secondary treatment plant had been specifically tested on the UCG condensate before. Of specific concern was the sequencing batch reactor that caters for biological treatment of hydrocarbons, due to the selection of the microorganisms to be used. This selection is dependent on the quantity and quality of ammonia, sulfur, chloride, and phenol in the condensate and the aeration requirements.
– Auxiliary power consumption: The auxiliary requirements of the GTP and OCGT are relatively high and should be optimized in future plant design.

A power plant basic engineering design was produced for the 100–140 MW UCG OCGT demonstration project. The following risks were identified for the power plant basic engineering design:

– UCG syngas and condensate specification and consistency: The water and salt balances are based on a model specification and have not been adequately tested. Thus, if there is a significant change in the condensate composition during operation, the demonstration plant would not be able to effectively process the condensate produced.
– Auxiliary power requirements were high, and optimization led to a higher-quality gas specification.
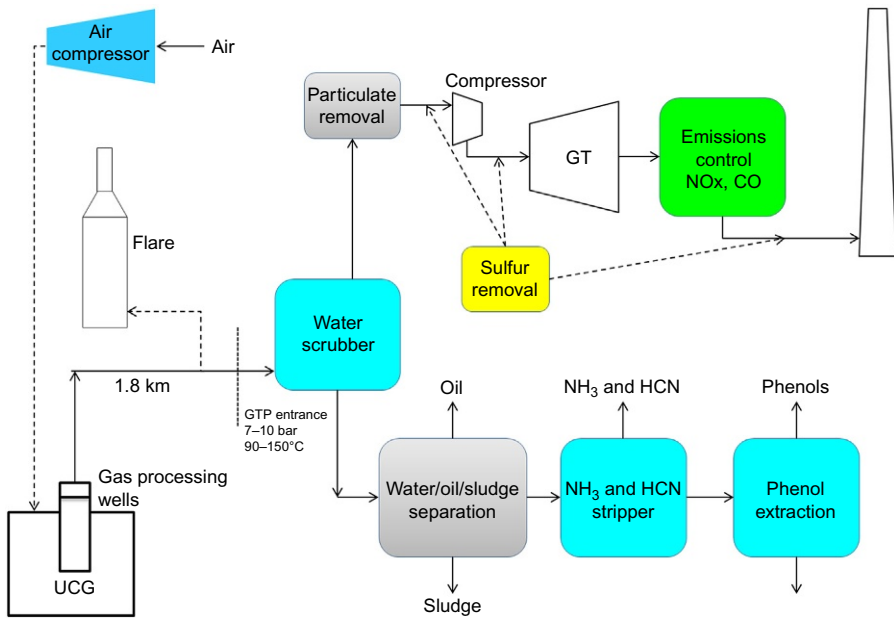
Fig. 14.22 Schematic representation of the proposed OCGT Power Plant.

The above findings are to be expected with the evolutionary development for FOAK technology.

14.8 Majuba gasifier 1: Shutdown & verification drilling

14.8.1 Introduction

The verification drilling together with environmental monitoring of the UCG post-gasification system forms a final, critical part in proving the hydrogeologic integrity of the spent gasifier in a mining technology "cradle to grave" approach. In order to apply UCG on a commercial basis, it needs to be proved that the used UCG cavities are hydrogeologically stable and that no contamination plume spread can occur from the cavity to surrounding groundwater sources over substantial periods of time (as determined by the South African water and mining regulators). Part of the controlled shutdown process forming a part of εUCG technology and long-term rehabilitation and monitoring strategy is to prove that the coal side walls, char, and ash residue in the cavity is capable of absorbing any remaining contaminants (if any) and that the level of contaminants decrease over time.

Even with existing experience of what actually remains in the UCG cavity and what the long-term effects and impacts of this could be on the surrounding environment, projections for any specific geology and hydrogeology settings must be tested at the specific site.

Eskom's UCG project successfully completed the operation of a pilot facility near Majuba Power Station. Further research activities together with environmental monitoring are being carried out to gain a full understanding of the requirements for safe shutdown and assist in finalizing of future UCG plant shutdown procedures. The initial approach was to allow the cavity to be cooled down by natural influx of the surrounding groundwater into the cavity. This shutdown process took longer than originally anticipated and eventually had to be assisted with supplementary water injection. Water injection required a lengthy process with fully detailed mitigation strategies to obtain the necessary approval from the South African water regulator. The UCG cavity was officially declared shutdown in June 2015.

14.8.2   Verification drilling objectives

Verification drilling was subsequently initiated (and is still ongoing) as part of the postgasification research program, in order to investigate the gasification area and to establish the following:

– The extent of the gasification cavity by confirming the boundaries of the cavity. This would indicate control over the growth, direction, and size of the cavity and that mining was not "blind." The information is also required to provide regulatory feedback for prospecting and mining rights to confirm the extent of the reserves utilized and payment of royalties.
– The physical and chemical properties of the postgasification cavity in various positions. This information will be used to verify the understanding of the main mechanisms driving the UCG process, its extraction efficiency, and overall performance.
– The upper lithology's changes in physical and chemical properties. This information will be used to verify the initial geologic, hydrogeologic, and rock strength models that are required for safe and successful long-term mine planning of commercial operations.

The verification wells that are being drilled will also subsequently serve as environmental monitoring wells to fully understand the long-term impacts of a depleted UCG cavity.

14.8.3   Verification drilling interim conclusions

This section presents interim conclusions from the verification drilling program as it is still ongoing as this text is being prepared. Key conclusions to date are as follows:

– The verification drilling program has been successfully initiated to address key UCG technology "cradle to grave" operational an environmental issues.
– The first three wells have been successful in verifying the gasification cavity boundaries and showing control over the process reliably limited location of fire within the coal seam. This information will be used in discussions with the South African regulators for Minerals, Environment and Water in order to clarify new legislation that will be required to govern UCG processes in the future.
– The deformation and softening of the upper lithologies in the test core samples indicate that sufficient information from the following three wells will be obtained to verify

characterization phase rock strength models. These models are greatly important during the mine planning stages and operation of the UCG process. Hence, validation of them at the end of gasification is critical for future use.

– The packer testing to establish changes in the porosity and permeability of the different lithologies was unsuccessful to date. The methodology has been revised going ahead to incorporate the use of the drill rig to perform the tests on the remaining wells. This information is critical in validating and finalizing the project hydrogeologic models.

– The chemical results of the liquid samples provide confidence of UCG technology viability going forward, since there is no plume migration out of the cavity. This means that both the gasification process and the subsequently accumulated water body have been safely contained within the spent UCG cavity.

– The liquid samples from the verification wells analysis are relatively clean when compared with typical gasification reaction related chemicals and contaminants. It has always been assumed that some contaminants would be trapped in the spent cavity, post gasification; however, an estimation of these levels was very difficult. The results are providing the first quantifiable insights into what really remains within an old UCG cavity. The extended shutdown period promotes the breakdown, dilution, and absorption of some of the chemicals leading to very low observed levels. This is extremely significant for continual development of the UCG technology. Monitoring of these wells will be continued for any changes in composition over time as part of the long-term water use license requirements.

– In summary, the postgasification conditions of the UCG cavity are stable, with no signs of plume spread. The overall composition of the liquids remaining in the cavity is in line with typical coal seam aquifers, and the baseline analyses performed on the site prior to any UCG activity. Water quality monitoring will be continued over time to refine and assure the water quality models used to predict long-term impacts.

– To date, no postgasification UCG technology contamination risks have been identified. The results indicate that the controlled shutdown and rehabilitation operational design is adequate and functional.

The verification drilling program should be completed in order to fully address the outstanding key post gasification UCG technology conclusions (Fig. 14.23).

14.9 Commercialization phase

14.9.1 Introduction

Due to current capital constraints within Eskom, a mandate was granted for the UCG project to secure a partnership to the following:

– Leverage the substantial Majuba UCG pilot plant asset and intellectual property and commercial module design completed.
– Secure funding to complete the current project.
– Assist with commercializing the technology.

The guiding principle assumed is that the partnership intends to be profitable, and the first phase of development will deliver an acceptable return on equity in order to attract a suitable partner.

Fig. 14.23 Verification drilling and sampling.

14.9.2 Methodology

In preparation for executing the partnership mandate, it was necessary to constitute a team that would analyze and evaluate the business proposition ahead of seeking a partner via Eskom's commercial process. This team also included external business analysis experts to critically assess the project status. The analysis considered the following aspects:

1. Market situational analysis describing the UCG value chain, regulatory requirements, competitor technologies, and UCG development competitors in SA.
2. Strategic alignment outlining the changes in the environment that has had an impact on the strategic drivers, the project life-cycle model, the strategic drivers, and the alignment of these with Eskom's strategy.
3. Market context and opportunities analysis highlights the benefits and opportunities that development of the UCG project would have.
4. UCG competitive positioning aims to demonstrate that UCG has the potential to be competitive in terms of gas supply and UCG to power at a generating cost comparable with other technologies.
5. UCG development status and research intent providing background to the development from inception to date and the research approach and potential development options.
6. Majuba UCG development asset valuation providing information on the cost to date and the potential value that could be extracted.
7. Business model options that describe the high-level options to extract maximum value from the development.

8. Majuba UCG partnership plant estimated cost that provided the high-level capital and operating cost to develop the UCG partnership plant based on a set of assumptions forming the base case.
9. Commercial considerations highlighting some of the key factors that would need to be elaborated in continuing the development path or road map.
10. Advocacy strategy providing high-level guidance on the partnership options that will be explored further in the partnership and procurement strategy.
11. Risks and timescales

14.9.3   Key finding

The key finding of the partnership assessment is that there is sufficient information derived from the Majuba UCG project to demonstrate that the project and technology are attractive and should be commercially developed.

With the above finding in mind, Eskom will pursue the development of UCG technology with a partner.

14.10   Conclusions

The following conclusions can be drawn from Eskom's 14 years investment in UCG research and development:

1. The 2007–10 pilot plant operation has successfully proved the application of UCG technology on the Majuba coalfield at the maximum scale of 15,000 Nm^3/h.
2. The demonstration feasibility study proved that UCG gas is technically feasible for power generation. However, the design of the demonstration plant could not be optimized without a further, adequate scale demonstration of UCG technology.
3. A larger (nominal 70,000 Nm^3/h) gas production was proposed and built to complete the quantification of the technology performance and prepare the technology for a large-scale commercialization.
4. The initial economics and financial computations completed in-house demonstrate that the technology is commercially viable in comparison with competing technologies, from a gas production and electricity generation perspective.
5. UCG can have a synergistic relationship with conventional coal mines, as the technology requires coal resources that conventional miners would not consider economically viable. Conventional miners target coal seams at less than 300 m depth for economic reasons, whereas UCG is the converse as it can work at deeper levels and in fact requires depth for higher process efficiency.
6. Eskom has acquired a εUCG technology license from Ergo Exergy Technologies Inc. of Canada for South Africa, which enables it to develop as many UCG plants as required. Given Eskom's accumulated experience at the Majuba pilot site and advancement down the learning curve, subsequent sites can be developed more rapidly and in partnership with Eskom.
7. UCG brings opportunity for using the εUCG gas for several different industries (i.e., polygeneration), with significant capability of capitalizing on synergies between them.

References

Blinderman, M., Van der Riet, M., 2003. Majuba UCG Site Selection and Prefeasibility Study. Eskom Holdings SOC Ltd., Johannesburg.

Blinderman, M., Van der Riet, M., Fong, D., Beeslaar, M., 2005. Site Characterisation Report. Eskom Holdings SOC Ltd., Johannesburg.

DOE, 2016. www.energy.gov.za. Retrieved from Department of Energy—South Africa.

Du Plessis, G., 2008. The Relationship Between Geological Structures and Dolorite Intrusions in the Witbank Coalfield, South Africa (M.Sc. Thesis). University of Bloemfontein, Bloemfontein.

Eskom Holdings SOC Ltd, 2016. Integrated report. 31 March 2016. http://www.eskom.co.za/IR2016/Documents/Eskom_integrated_report_2016.pdf.

Love, D., Beeslaar, M., Blinderman, M., Pershad, S., Van der Linde, G., Van der Riet, M., 2015. Ground Water Monitoring and Management in UCG. South African Underground Coal Gasification Association. SAUCGA, Secunda.

Snyman, C.E., 1998. The Mineral Resources of South Africa. In: Handbook, sixth ed. vol. 16. Council for Geoscience, Cape Town.

Van Eeden, F., Keir, J., Van der Riet, M., 2002. Scoping Report: Underground Coal Gasification. Eskom Holdings SOC Ltd., Johannesburg.

UCG commercialization and the Cougar Energy project at Kingaroy, Queensland, Australia

<div style="float:right; font-weight:bold; font-size:2em;">15</div>

L. Walker
Phoenix Energy Ltd., Melbourne, VIC, Australia

15.1 Introduction

The Kingaroy project was developed by Cougar Energy Ltd., a company founded in 2006 with the sole purpose of commercializing the UCG process in Australia, with an initial focus on power generation in Queensland. The company's activity formed part of the resurgence of interest in UCG technology, which occurred in Australia between 1999 and 2013 and had flow-on effects internationally.

While the Kingaroy project was short-lived, as described later in this chapter, it served the purpose of concentrating attention on the range of factors involved in advancing an initial "pilot burn" into a commercially viable project, of which none has yet been established outside the historical work undertaken in the former Soviet Union (FSU), which reached its peak some 50 years previously. Factors such as government regulation and project finance are only fully addressed when a commercial project is planned, as are technical requirements such as the design of a commercial UCG facility and the matching of gas composition to end use.

To understand the genesis of the Kingaroy project and its impact on the commercialization of UCG technology in a wider context, it is necessary to review the prior history of UCG activity in Australia and its impact on planning for the project. An appreciation of this history is likely to be significant for successful project developments in the future.

15.2 Historical background in Australia

Although a number of studies of the UCG process and its potential in Australia were undertaken in the 1980s (Walker, 1999), the first active trial was undertaken by Linc Energy Ltd., which was founded by the writer in 1996. The approach to applying the technology in Australia rested on the conclusion that the only commercial sized UCG operation ever developed was that undertaken as part of the long-term UCG program in the FSU, which reached its peak in the 1960s. At the Angren UCG facility (now in Uzbekistan), syngas was produced (in 1965) at a rate of approximately 1200 billion kcal/a (Gregg et al., 1976) that, in a modern combined cycle

power plant, would generate approximately 60 MW of power, and overall, more than 10 million tonnes of coal were gasified at that location (Burton et al., 2006). This compared with less than 100,000 tonnes of coal gasified in all UCG trials undertaken outside the FSU up to the late 1990s (Burton et al., 2006).

As a result of this assessment and after a number of visits to the Angren site, Linc Energy negotiated a technology agreement with Ergo Exergy Technologies Inc. of Canada to apply their expertise gained in the FSU to Linc's projects. This culminated in the planning for the first UCG field trial in Australia at a site near Chinchilla, Queensland.

After grant of a coal exploration license, then a mineral development license (MDL) as required under the then current mining law, Linc Energy entered into an agreement in June 1999 with CS Energy Ltd., a Queensland Government-owned power generator, to cofund (with the assistance of an Australian Government research grant) the development of a pilot UCG demonstration plant at Chinchilla, which, if successful, was to be expanded to produce gas for use in a gas turbine with an output of approximately 40 MW (Walker et al., 2001).

At that time, the initial focus was almost exclusively on ensuring that quality syngas production was achieved. Given the gap of some 10 years since the end of the major US research program on UCG and cessation of the European effort some 3 years earlier, it was clear that failure to produce syngas on a consistent basis would most likely result in a rapid termination of UCG interest in Australia. Following signing of the agreement with CS Energy and preliminary site characterization and site investigation work, air injection, and subsequent ignition, the first gas production was achieved in December 1999 (Walker et al., 2001). The continuous nature of gas production at the Chinchilla site is illustrated in Fig. 15.1, with the gas calorific value averaging about 5 MJ/m^3 over this period. Approximately 35,000 tonnes of coal were gasified, making it by far the largest UCG demonstration undertaken outside the FSU at that time.

Perhaps more importantly, it was undertaken with no evidence of any environmental impact, particularly in relation to potential contamination of groundwater aquifer systems from the products of gasification. Blinderman and Fidler (2003) reported
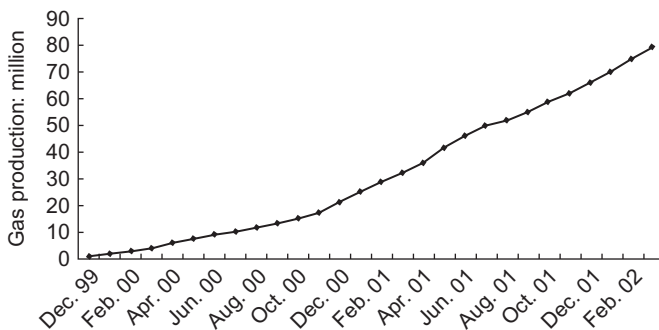
Fig. 15.1 Gas production at Chinchilla UCG site (Blinderman and Jones, 2002).

benzene levels in the coal seam within 50 m of the UCG gasifier area of approximately 10 ppb, and a similar reading was obtained approximately 200 m away as a result of the high directional permeability resulting from cleat structures in the coal seam. These data were obtained after completion of the controlled shutdown process in 2002. While no subsequent data have been published to indicate potential longer-term decay of this benzene level, there have been no reports of residual benzene in the coal resulting from the demonstration. The authors at the time quoted experience in the FSU showing that chemical concentrations in the coal seam "tend to return to the baseline levels over 3–5 years after the end of gasification," which supports the concept of rehabilitation of the coal seam over a period of time.

By mid-2000, when the initial goal of successful gas production had been achieved, Linc Energy and CS Energy commenced discussions about advancing the demonstration plant into the power generation phase. Additional process wells were added to maintain the operation at minimal cost, while CS Energy undertook an in-house review of the technical and economic issues involved in advancing the project. These discussions culminated in the preparation of a joint review report early in 2002 confirming the viability of the technology; however, CS Energy required Linc Energy to seek third-party funding for the agreement to be maintained. Such funding was unable to be provided in the time required by CS Energy, who subsequently took effective control of Linc Energy in mid-2002, ordered a controlled shutdown of the operation, and subsequently sold out from the project to new investors. Ergo Exergy terminated its agreement with Linc Energy for the project at Chinchilla in November 2006.

The inability to raise project funding at the time could be attributed to a number of factors:

- An unfavorable investment climate, post the events of 9/11 in 2001 in the United States.
- Low energy prices (oil price at US $20–30 per barrel).
- Perceived investment risk, with Linc Energy being the first mover with a commercial UCG project development proposal.
- Lack of the demonstration of syngas cleanup to confirm its suitability for gas engines or gas turbines.
- Low rate of return for a first phase 40 MW power plant due to low energy prices in Queensland, with competition from much larger coal-fired power stations.
- Growing competition from coal seam gas (CSG) explorers for use of local coal deposits.
- Lack of clear regulation for UCG project development.

These factors combined to effectively delay the international development of UCG technology for several years, although publication of the results of the demonstration (Walker et al., 2001; Blinderman and Jones, 2002) generated growing interest in the prospects of a revival of the technology in the Western world. This resulted from the size and longevity of the demonstration, its successful environmental outcomes, and the attractive cost estimates for producing power using combined cycle gas turbine systems (Walker et al., 2001). The Chinchilla experience also confirmed that commercial factors such as government regulation and project finance were likely to play a significant part in the rate of UCG development in Australia.

As a result of the experience at Chinchilla, the writer formed Cougar Energy early in 2006 and continued his association with Ergo Exergy to develop a new commercial

power project using gas from a UCG facility as the fuel. The new company acquired rights to a coal lease near Kingaroy, also in Queensland, but modified its approach to commercial development by the following:

- Arranging for the company to be listed on the Australian stock exchange (ASX) in order to provide better access to capital.
- Developing longer-term plans for a phased 400 MW power project to achieve economies of scale to improve investment attractiveness.
- Designing a small gas treatment plant to demonstrate that the process would produce clean gas suitable for combustion in a gas turbine.
- Confirming that coal at Kingaroy could not be used for competing CSG production.

Following resource definition and site characterization work, development of the Kingaroy project was planned in the following stages:

- Ignition and syngas production, gas cleaning, and flaring for a period of 6–12 months.
- Power generation by gas engines or gas turbine up to 30 MW.
- Expansion of power generation to 200 MW, then 400 MW.

This phased program was not greatly different from that contemplated for the Chinchilla site; however, it was more clearly defined at an early stage in Cougar Energy's life, and with the technical experience gained from the past demonstration and the availability of progressive funding from the ASX listing, it was considered to be realistic.

15.3   Site characterisation

15.3.1   Resource definition and site selection

The location of the Kingaroy project (shown as MDL 385 on Figs. 15.2 and 15.3) was some 10 km south of the town of Kingaroy in Queensland, being part of a larger coal exploration permit (EPC882). The area was selected on the basis of a number of historical drill holes showing good coal intersections at depth.

A new exploration drilling program at Kingaroy was undertaken by Cougar Energy over the period late 2007/early 2008. Twenty-three holes were drilled with a total length of 4933 m, with 336 m of coring being undertaken, predominantly in the coal seams. Two main seams were identified, being the Kunioon and Goodger seams, separated by an interburden generally in the range 30–100 m. The Kunioon seam ranged in thickness from 7 to 17 m, at depths from 60 to 206 m, while the Goodger seam thickness ranged from 3 to 13 m at depths from 160 to 270 m.

A typical geologic profile is presented in Fig. 15.4, which shows the Tarong coal beds lying beneath Tertiary basalt flows and the two main seams (Kunioon and Goodger) interbedded within sedimentary rock layers.

In July 2008, the company completed a JORC resource statement, resulting in indicated and inferred coal resources of 45 and 28 million metric tonnes, respectively, with approximately 70% of the resource being in the Kunioon seam. This resource size was considered to be sufficient to provide syngas to fuel the proposed
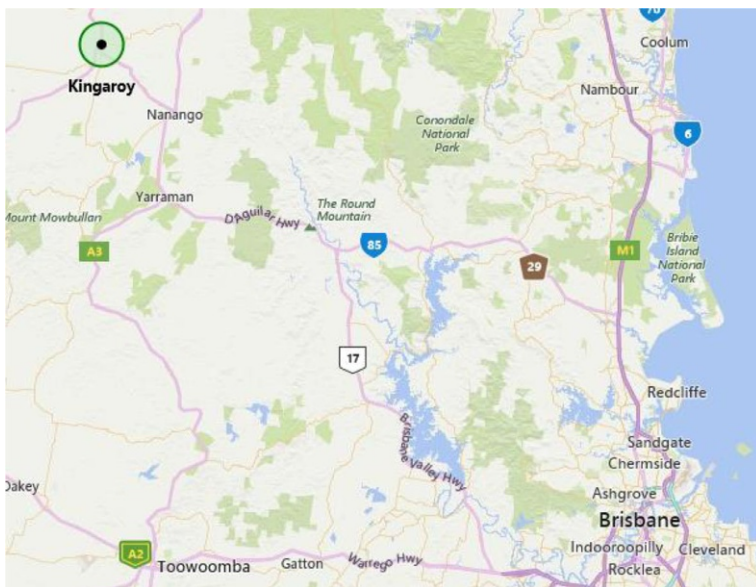
Fig. 15.2 Kingaroy project location.

400 MW power station for 30 years. The average properties of the Kunioon coal seam are summarized below.

Kunioon coal seam properties (as received—% by weight)	
Relative density	1.59
Inherent moisture	4.85%
Ash	35.1%
Volatile matter	25.2%
Fixed carbon	32.6%
Total sulfur	0.25%
Specific energy	19.1 MJ/kg

Following a detailed evaluation of the drilling data, Cougar Energy selected the initial location for UCG development in the southeast corner of the exploration permit, largely because of its greater distance from local residents and a greater depth to the coal seam resulting from increased elevation in the area.

Fig. 15.5 shows the location of holes drilled in the ignition site area, together with water sampling and early warning bores. The locations of the first three injection/production wells (numbered 1, 2, and 3) are also shown in the figure.

Across the ignition area, the top of the Kunioon coal seam varies from 185 to 200 m below ground level. While the seam thickness over the area is generally around 15 m, there are a number of consistent partings within the seam that could potentially enable a thinner coal section to be utilized, to protect against potential overburden cracking allowing transmission of gas to the surface during larger-scale operations.

Fig. 15.3 Kingaroy tenement location.

15.3.2 Hydrogeology studies

As part of the early evaluation of the Kingaroy UCG site, Cougar Energy undertook a desktop study of regional hydrogeology in April 2007. The study provided a broad appreciation of the geologic profile, regional groundwater conditions, like groundwater chemistry and potential direction of regional groundwater flow.
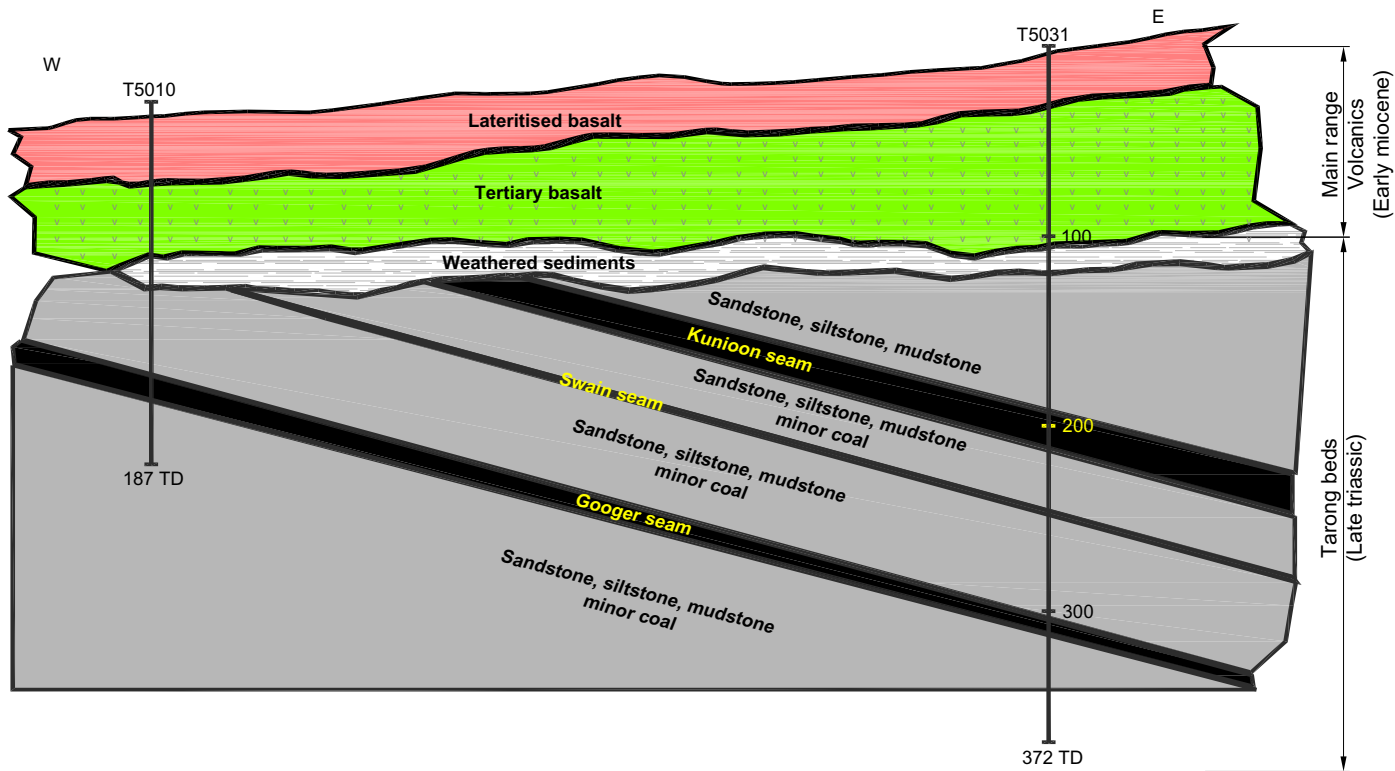
Fig. 15.4 Typical Kingaroy geologic profile.
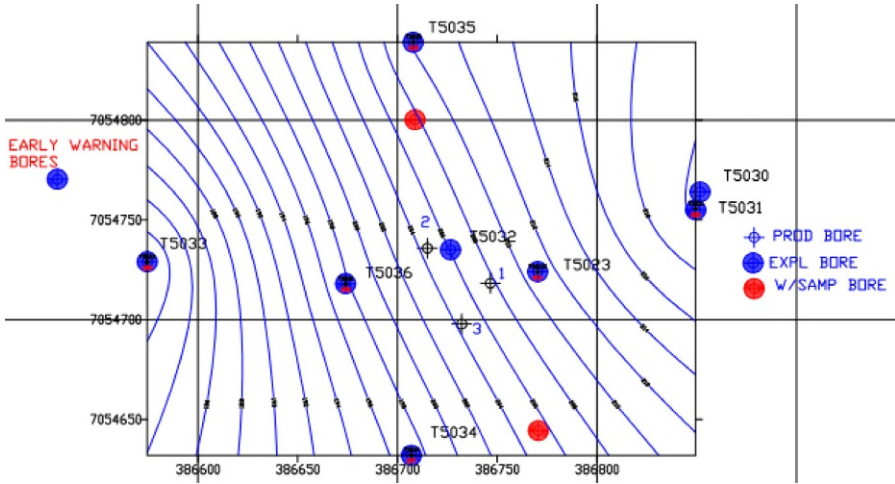
Fig. 15.5 Location of drill holes and production wells.

Following confirmation from resource drilling completed in early 2008 that

- A significant coal resource existed suitable for application of the UCG process.
- No major aquifer systems were evident in the geologic profile.
- A preferred site for initiation of the first phase of the project could be identified.

A detailed hydrogeological investigation program was initiated late in 2008 in accordance with the consent conditions for the project agreed with the Queensland Department of Environment and Resource Management (DERM) and contained in an environmental authority (EA) issued by DERM in April 2008. The conditions included the requirement for an independent hydrogeological report, which was subsequently undertaken and completed in March 2010 after a program of field and office work.

The program of hydrogeological work undertaken for the area in the vicinity of the proposed pilot burn site included

- Collation and review of all existing drilling and groundwater data.
- Preparation of geologic cross sections and a 3D geologic model.
- Packer testing of selected test sections within exploration boreholes to derive hydraulic parameters for specific rock/coal layers within the profile.
- Installation of six water quality monitoring bores around the proposed ignition area.
- A network of 23 vibrating wire piezometers (VWPs) installed as part of the test pumping of the Kunioon coal seam and also subsequently used during the air acceptance testing program. These were contained in five boreholes located around the pump test well.
- Test pumping from a purpose constructed well to capture the hydraulic response of a large area of the local groundwater system under groundwater extraction conditions.
- Air acceptance testing to test the response of the Kunioon coal seam to air injection.

- A groundwater model constructed to allow evaluation of response to conditions imposed during the UCG process, for example, groundwater consumption in the underground cavity.
- A baseline program for water quality monitoring, initiated in December 2009.

15.3.3   Hydrogeological profile

The hydrogeology of the Kingaroy test site is defined by the main geologic layers in the profile shown in Fig. 15.4:

- The Tertiary volcanic layer of low groundwater yield, consisting of multiple lava flows with interbedded sediment layers, and a basal contact layer with the Tarong beds consisting of montmorillonitic clay of low permeability. This basal clay layer was described as having a prime characteristic of "tight, squeezing clay behavior and an expansive nature," which caused significant drilling problems and made it difficult to penetrate using typical drilling techniques.
- The Triassic Tarong beds, consisting of sandstone and conglomerate layers with very low groundwater yield and containing the coal seams of higher yield. Within the Tarong beds, detailed analysis of data from the pump testing indicated permeabilities ranging between 5 and 10×10^{-6} m/s for the Kunioon coal seam and 3×10^{-6} m/s for the overburden to the coal seam.

With respect to hydrogeology, the volcanic layer was determined to be spatially discontinuous as evidenced by dry conditions observed in several monitoring wells and the highly variable recovery rates observed during well installation and development. This was assessed as being a result of the size, persistence, infilling, and orientation of the relatively isolated pockets of water-bearing fractures in the rock structure.

The suite of groundwater measurements indicated a significant downward gradient from the volcanic layers to the Tarong beds, maintained by the relatively impermeable intermediate clay layer below the basalt. With respect to horizontal groundwater flow, the Kunioon coal seam dipped to the south, and this was interpreted as the groundwater flow direction in the seam, whereas groundwater measurements in the volcanic layers indicated a flow direction to the west.

The following relative hydrochemical features of the three hydrogeological units beneath the UCG pilot site were determined:

- Lateritic clay—High in Cu and Ni, low in bicarbonate (generally < 50 mg/L), slightly acidic (pH generally 5.5–6.5), brackish (TDS generally 1500–2500 mg/L).
- Basalt—Low in Cu and Ni, high in bicarbonate (generally 700–750 mg/L), slightly to highly alkaline (pH generally 7.3–11), brackish (TDS 1500–2000 mg/L).
- Kunioon coal—Low in Cu and Ni, moderate bicarbonate (generally 150–300 mg/L), slightly alkaline (pH generally 7–8.5), fresh (TDS generally 500–1000 mg/L).

Thus, the lateritic clay is distinguished from the other units by relatively elevated Cu and Ni concentrations, lower pH, and low bicarbonate. The basalt aquifer is characterized by relatively high bicarbonate and higher pH. The Kunioon coal aquifer is characterized by lower salinity (TDS and EC). The observed differences in the geochemistry suggest a reasonable degree of hydraulic separation of the hydrogeological units.

15.3.4   Hydrogeological impacts on Kingaroy pilot burn

The hydrogeological study provided evidence that the pilot burn could be undertaken with no significant impact on the groundwater system likely to occur. Factors supporting this conclusion can be summarized as follows:

- The Kunioon coal seam exhibits a permeability 2–3 times higher than its overburden.
- A relatively impermeable clay layer beneath the basalt provides a good aquitard to groundwater flow.
- There are no significant permeable aquifers above the coal seam in the geologic profile.
- Water quality in overburden layers is brackish and unsuitable as drinking water.

The pilot burn itself was limited in size to the gasification of a maximum of 20,000 tonnes of coal under the EA issued by the Queensland Government. With this limit, there was no concern about the possibility of subsidence occurring in a manner that might induce overburden cracking to reach the ground surface and potentially release chemical by-products into near-surface groundwater layers.

However, the thickness of the Kunioon coal seam (up to 17 m) was such that a detailed future evaluation would be necessary in relation to the interaction between cavity size and the depth and thickness of coal to ensure that this concern was fully addressed for the proposed commercial scale plant.

15.4   Government and community interaction

15.4.1   Government permits and approvals

In order to commence preparations for initiation of the first phase of its UCG project, Cougar Energy required approvals to advance the regulatory status of the relevant part of its exploration permit. The procedure applicable at the time in Queensland involved the following steps:

- Application for a MDL to permit small-scale noncommercial gas production to commence. Application for the MDL was made in December 2007, and it was eventually granted on 22 February 2009.
- During this period, Cougar Energy negotiated an EA that was issued by DERM in April 2008.
- Once the MDL was granted, a further application was required to enable the MDL to be utilized for UCG operations, the so-called "mineral (f)" classification under a clause (section 6 (2) (f)) in the Mineral Resources Act of 1989. The mineral (f) application was made in March 2009 and was granted in August 2009.
- Further expansion of gas production would require a mining license to be applied for and granted, with additional approvals required to allow power generation.

With a suitable coal resource being defined at Kingaroy late in 2007 and the MDL application being made in December 2007, it thus took a further 20 months for approval of the first stage of gas production to be achieved.

15.4.2   Government policy

A matter of considerable significance occurred on 18 February 2009 (4 days before the grant of Cougar Energy's MDL after a 14-month wait from the date of application). On that day, the Queensland Government released an Underground Coal Gasification Policy Paper (Queensland Government, 2009), which stated that "the Minister for Natural Resources, Mines and Energy, if asked to determine a coordination or preference decision between the developer of a CSG resource and the developer of a UCG resource, the decision will be made in favour of the CSG tenure holder under the P&G Act, so as to allow the CSG tenure to progress to production stage." The impact of this policy was amplified by the fact that, at that time, virtually all coal basins in Queensland were covered by CSG (coal seam gas) tenure.

This Policy Paper also confirmed that the government would review the progress of UCG projects, with a decision on the future of UCG in Queensland to be determined in 2011–12. Earlier, in August 2008, press reports had circulated claiming that the "government had no intention of granting production tenures for UCG for at least 3 years." While there was some question of the accuracy of these reports at the time, the Policy Paper effectively achieved the same outcome.

The Policy Paper also provided for the establishment of a "scientific expert panel" to assist the government in preparing a report on UCG technology for consideration by Cabinet. The Policy Paper concluded that "…should the government report produce adverse findings on the UCG technology, on-going constraint, or even prohibition of UCG activities may be recommended." Regrettably, when the panel was formed, its members had no previous experience in UCG technology and no international representation and gave little regard to the success of numerous demonstrations overseas and, more specifically, the success of the Chinchilla test 10 years earlier.

It is noted that the Policy Paper was issued at a time when Cougar Energy had completed its resource evaluation process, had negotiated an EA, and had made significant progress on its hydrogeological testing program and pilot plant design. It was only after some internal consideration that the company elected to continue with its proposed project despite the newly created regulatory uncertainty.

15.4.3   Community relations

The Chinchilla test burn initiated in late 1999 was undertaken with the support of the Queensland Government at its operating level in the relevant departments and the support of the landowner on whose property the test was undertaken—less than 500 m from his house.

During preparations for initiation of the Kingaroy project, Cougar Energy undertook a program of community relations, involving meetings with those landholders within the proposed area of development, and a project presentation evening for local residents. In October 2009, after the commencement of site preparation for construction of the pilot burn, an open day was held for all residents to explain the proposed development sequence.

However, it became progressively evident that the level of support at Chinchilla could not be reproduced at the Kingaroy site because of the following:

- The increasing political influence on the government of the CSG industry, which was in its infancy in 1999.
- The resultant change instance of the state government to the UCG industry, as expressed in its 2009 UCG policy, by raising issues as to whether the technology would be "acceptable" in Queensland.
- The development of a local group protesting against the technology and its impact on the local state political representative.

While each item appeared to the company to be manageable at that time, circumstances following ignition conspired to bring them together in a manner that ultimately led to the termination of the project, as described in later sections.

15.5   Preparations for ignition

Following completion of the resource evaluation, the site selection, and the receipt of the EA in April 2008, Cougar Energy commenced detailed design of the UCG pilot plant facility. This was undertaken to meet objectives required to support later expansion to the commercial facility, which included

- Sufficient syngas production and processing capacity to produce a power output of up to 30 MW.
- Gas processing plant capable of producing a cleaned syngas suitable for meeting gas turbine specifications.
- Site layout (both gas production and gas processing plants) capable of being expanded in modular form to increase output.
- Preliminary feasibility study for the medium-term design case of a nominal 200 MW syngas/power generation project.

The company had undertaken some preliminary treatment plant design work early in 2008 and in May 2008 appointed consulting engineers to undertake detailed design for the pilot plant project as a whole. This work was completed late that year, by which time construction of long lead-time items of plant had commenced, with contract packages for all other work being assembled in January 2009.

All of this work was undertaken in expectation of an imminent grant of the MDL (applied for in December 2007), which was ultimately granted in February 2009, but only after release of the Queensland Government's UCG policy with its associated uncertainties. After the company made a considered decision to proceed with the project, the contract packages were put out to tender, with the company now awaiting grant of the "mineral (f)" attachment to the existing MDL. This was received late in August 2009, and the successful contractor was appointed a few days later. By this time, the first three UCG production wells had been installed and tested, with commissioning of the plant being scheduled for February 2010.

During the latter half of 2009, design staff were appointed in the company's Brisbane office to undertake the preliminary feasibility study for a nominal 200 MW

UCG/power plant, with the majority of this work being completed by mid-2010 with favorable economic results. Thus, by early 2010, Cougar Energy had largely completed its objectives for pilot plant design and construction and for the large-scale project feasibility analysis.

15.6   Syngas production, cessation and the events leading to project shutdown

15.6.1   Gas production operations

The first three production wells (P1–P3) at the Kingaroy site were installed in April/May 2009 at locations shown in Fig. 15.5. A fourth well (P4) was installed in October 2009 placed to give a minimal connection distance to P1 for starting the UCG process.

Ignition was achieved in the afternoon of 15 March 2010, and gas production developed using the reverse combustion linking process, which was completed by the evening of 17 March. At that time, compressed air was being injected into well P1, with syngas produced from well P4.

The underground gasifier operating conditions were monitored indirectly and continuously. All wells were equipped with flow, temperature, and pressure measurement instruments on the pipe leading into the ground. The dry gas composition was measured using a gas chromatograph, with water and heavy hydrocarbons removed from the gas prior to measurement.

The groundwater pressure at a number of locations and in a number of geologic layers was measured using the 23 installed VWPs. During forward gasification and reverse combustion linking, these data were required to ensure that the pressure in the cavity was kept lower than the local groundwater pressure to ensure flow of water was maintained toward the cavity.

Gas production from P4 continued until the morning of 20 March (113 h in Fig. 15.6), when it ceased, indicating blockages in both P1 and P4, at which time air injection was stopped, and the surface pipework at P4 was dismantled and blockages removed. Air injection into P4 was then continued for some 3 weeks, until 9 April, when a groundwater sampling well (T5037) located some 250 m from P4 was observed to be bubbling air and water to surface. Air injection into P4 was immediately ceased and a review of all information made.

A detailed investigation of well P4 followed, including the use of a downhole camera, which established that at 62.5 m depth in the well, the coupling between casing strings had separated and the casing below this level had been deformed.

15.6.2   The casing string design

In the installation of P4, three strings of casing were utilized as outlined in Table 15.1. Each of the three casing strings was cemented into place. The 14 and 10 in strings were cemented in using a standard Portland cement mix with specific gravity 1.72, while the 7 in casing was cemented using a cement containing silica flour.
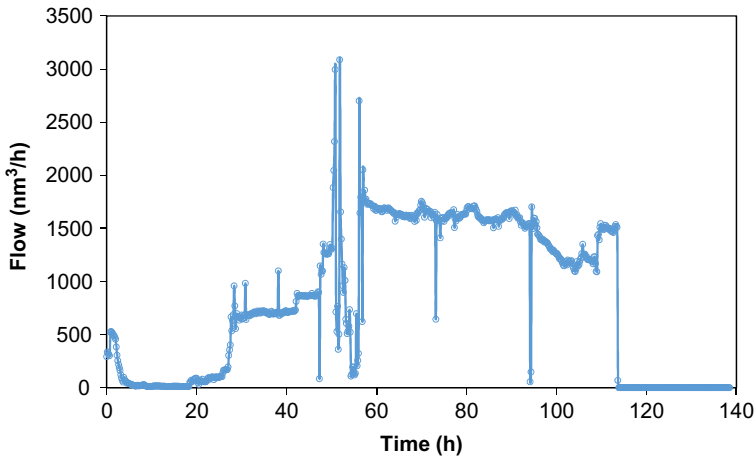
Fig. 15.6 Gas production flow rate.

Table 15.1 **Casing string design**

Casing diameter (in)	Hole diameter (mm)	Casing thickness	Material	Connections	Depth to (m)
14	404	9.53 mm	A53B CS	Welded	5
10	333	9.27 mm	A53B CS	Sharpe flush joint	13
7	254	API 5CT 26 ppf seamless	API 5CT K55	Buttress thread	205.8

The reason for using a multiple casing string design is related to the geologic conditions. Cougar Energy's geologists, in conjunction with various drillers that were engaged in the exploration drilling programs over the previous 2 years, had evaluated the best techniques for drilling holes down to the coal seams of interest. The main problems they encountered related to the expansive clay formations above and below the basalt. Experience showed that if these formations were not cased off (by using the first and second casing strings shown in Table 15.1), then the clays would expand and block the hole while drilling through them. The technique used for drilling these exploration holes was then translated across to installation of the production holes.

As it transpired, the use of multiple casings created complexities in cementing the casings into place. A detailed assessment of all possible failure mechanisms for well P4 concluded that residual water was left behind between the 7 and 10 in casings at a depth of about 63 m, which expanded on heating, causing the inner casing to collapse.

As a result of this experience, two new wells were planned for installation (P5 and P6) using a larger rig and a single continuous casing. These wells were successfully installed, and operations were scheduled to recommence in late July 2010.

15.6.3   Events leading to shut-down notice

With evidence of the well casing failure in P4 and some groundwater response (bubbling of air) in monitoring bore T5037, Cougar Energy increased the frequency of monitoring bore water sampling and testing, specifically for the chemicals benzene and toluene. The monitoring focused on T5037, screened over the interval 35–47 m, and a nearby bore (T5038) 10 m away, screened over the interval 64–76 m, each about 250 m from the gasification zone.

Groundwater samples from T5037 exhibited benzene levels of 2 ppb (parts per billion) from samples taken on 11 and 27 May 2010 and 1 ppb (the laboratory limit of detection) from samples taken on 6 June and 16, with subsequent readings being below the level of detection. No toluene was measured in this bore. No benzene was measured in T5038, although toluene was measured at levels well below trigger levels. The difference in observations between these two sets of results led to some uncertainty in interpretation of the data.

In relation to trigger levels, the EA applicable to the Kingaroy pilot burn stated that

> In the event that contaminant trigger levels (as identified in the groundwater moni-
> toring program) are exceeded, or the groundwater monitoring program detects a
> likely material failure of the production water containment system, or migration of
> contaminants from the coal seam that is being or has been gasified, the authority
> holder shall promptly assess and report to the administering authority on potential
> environmental impacts investigation of the causes and remedial measures to be
> implemented.

Groundwater trigger levels for shallow monitoring bores had been recommended by Cougar Energy's groundwater consultants as being those applicable in the Australian water drinking limits, namely, 1 ppb (parts per billion) for benzene, and for deep monitoring bores those covered by the Australian and New Zealand guidelines for fresh and marine water quality (2000)—950 ppb for benzene. The World Health Organization recommendation for benzene in drinking water is 10 ppb.

After receipt of the initial data (some 10 days after sampling) and a subsequent review, the company prepared a report to DERM that was submitted on 10 June. The data were discussed with DERM officials at a meeting in late June, and it was concluded that no environmental threat was present, especially given that baseline quality of groundwater at the monitoring bores was not suitable for drinking. As a result, the company was allowed to continue with its earlier planned reignition of the coal seam scheduled for late July 2010. However, the company was requested to table any trigger level exceedances more rapidly than had been done on this occasion.

On 13 July 2010, Cougar Energy received from the testing laboratory a reading of 84 ppb purported to come from T5038, in which no previous measurement of benzene had been recorded. In providing these data rapidly to the government authorities, the company advised of the likelihood that it was an erroneous reading and supported this on 14 July 2010 with a further check test result from the same bore that showed no benzene at the level of detection (Cougar Energy, 2011a).

On 16 July, Cougar Energy forwarded to DERM a letter from the independent testing laboratory confirming that the reading was the result of a mix-up of samples and that the correct sample recorded no detectable benzene. This result was confirmed by DERM's own sample test results; however, on 17 July 2010, DERM issued a shutdown notice on the site. Evidence (Cougar Energy, 2011b) suggests that this was a result of pressure from a number of local residents expressed through their local member of parliament. No subsequent readings of benzene above the detection limit were recorded at the site despite widespread monitoring over the following years; however, the shutdown order was confirmed and enforced.

15.7   Environmental issues

15.7.1   The environmental evaluation process

The shutdown notice triggered off a lengthy process involving the preparation by Cougar Energy of reports requested by DERM using its powers under the Environment Act. These reports were prepared in response to a series of questions raised by DERM following the service of the shutdown notice. The reports covered topics such as operations prior to the well blockage, analysis of the casing failure, and interpretation of the groundwater mechanisms involved in the transport of chemicals. In the period August to December 2010, 16 separate environmental evaluation reports were submitted to the government, containing more than 650 pages of detailed data and analysis.

During this period, DERM had also requested the independent select panel (ISP) to review the performance of Cougar Energy on the Kingaroy project. This panel had been set up by the government in October 2009 and was given the task of reviewing all current UCG projects in Queensland and making recommendations on the future of the technology in that state. In January 2011, the ISP produced a public report with criticisms of much of Cougar Energy's work.

The company responded in February with a public critique of this report (Cougar Energy, 2011b), recording errors of fact, disputing many of its findings, and providing evidence that it may have been prepared without reference to the voluminous reports submitted by the company in the previous year. As an example, the ISP report stated that "It is unclear why the trial was not located in a more simple hydrogeological setting, which was available not too distant from the existing site." No evidence or technical discussion was given to support this conclusion.

Ultimately, in early July 2011, DERM notified the company of its decision to amend the company's existing EA to prevent it from restarting UCG gas production on the site and restricting activity to rehabilitation and monitoring.

Despite the acceptance by all parties that the limited and localized (in time and space) benzene levels reported in no way caused any environmental harm, the government in July 2011 issued charges under the Environment Act relating to failure of the production well, the evidence of benzene and toluene in monitoring wells, and a claimed delay in reporting these readings. The company responded in October 2011 by issuing proceedings against the government and its officials in the Supreme Court of Queensland claiming A\$34 million in damages. As events transpired, the Supreme Court proceedings were eventually discontinued by agreement between the parties in July 2013.

At that time, it was clear that the future development of UCG in Queensland, and certainly Cougar Energy's potential role in such development, had little chance of advancing for the foreseeable future. As it transpired, the government in April 2016 announced a permanent ban on UCG technology in the state.

15.7.2 The environmental authority

At the time of preparation of the EA by the Queensland Government, the task was undertaken by the relevant regional office in Maryborough, 250 km north of Brisbane, the state capital. Cougar Energy management met with environmental staff in their office to discuss UCG technology and the proposed project development schedule, commencing with the pilot burn phase. The resulting EA was tabled in April 2008 and restricted the test to the gasification of no more than 20,000 tonne of coal. Subsequent events underscored significant deficiencies in the EA and its wording that played a part in the eventual termination of the Kingaroy project.

The introductory clauses in the EA carry the following wording:

> In carrying out the activities to which this approval relates, you must take all reasonable and practicable measures to prevent and/or minimise the likelihood of environmental harm being caused.

This clause and its use of the term "likelihood of environmental harm" provided the opportunity for a range of possible interpretations as to its meaning. The general nature of the term was exacerbated by the reference to the term "trigger levels" in the EA as described in Section 15.6.2 and the actions required if they were exceeded. No trigger levels were defined in the EA, and both the company and MEMR relied on the general recommendations contained in the company's hydrogeological report, viz.

> *For* "shallow on-site monitoring bores: Drinking Water Criteria (ANZECC 2000)" *and*
> *For* "Deep on- and off-site monitoring bores: Protection of Aquatic Ecosystems at 95% level of protection"

These general recommendations were not translated into trigger levels for specific chemicals nor related to the location and depth of specific monitoring bores and the possible use of water in any monitored aquifer systems. It is evident from the events that occurred in the Kingaroy project with respect to the benzene level readings that the company and DERM had quite different interpretations of the actions necessary with respect to using the trigger levels to meet the requirements of the EA, with significant technical and financial consequences.

15.8   Rehabilitation and monitoring

Under the revised EA, Cougar Energy was required to rehabilitate the UCG site, involving both surface plant and groundwater conditions. This work involved conventional activities such as plugging of production wells, removal of pipework, decommissioning and removal of the gas treatment plant, and cleaning and backfilling of the water storage dams. It was completed by mid-2015.

Rehabilitation of the groundwater in the vicinity of the gasification area proved rather more complex, largely because no clearly defined requirement for residual chemical compositions for benzene and toluene was defined in the EA. The company had always argued that, as none of the layers in the geologic profile could be considered as an existing or potential aquifer for potable water, the Australian drinking water standards (1 ppb for benzene) should not apply as a residual level, but rather the guidelines for fresh and marine water quality (950 ppb for benzene). It is understood that this issue is yet to be resolved.

Cougar Energy had previously installed three groundwater monitoring bores in the coal seam relatively close (4–10 m) to the gasification zone. It was in one of these bores that the reading of 84 ppb was obtained, which was erroneously attributed by the testing laboratory to T5038 some 250 m away and which led to DERM's actions in issuing the shutdown notice. Monitoring of benzene levels in these bores continued from shutdown in July 2010 to the present (December 2015), when the highest level was 2 ppb.

In relation to potential decay of benzene levels in coal, Cougar Energy had undertaken a study to establish the principles of monitored natural attenuation whereby benzene levels attenuate over time naturally as they are degraded by microbial activity. The success of this procedure at Kingaroy is illustrated in Fig. 15.7, which shows the benzene decay curves over time for the three wells closest to the gasification zone. Each of these curves is realistically represented by a logarithmic decay curve, as might be expected from theoretical considerations. As is evident from the curves, once the benzene level is below 10 ppb, further reductions are extended in time. However, given that the World Health Organization's drinking water limit is set at 10 ppb and it is unlikely that any coal seams would double as potable aquifers, reductions in benzene concentration below this level would have no practical environmental significance.
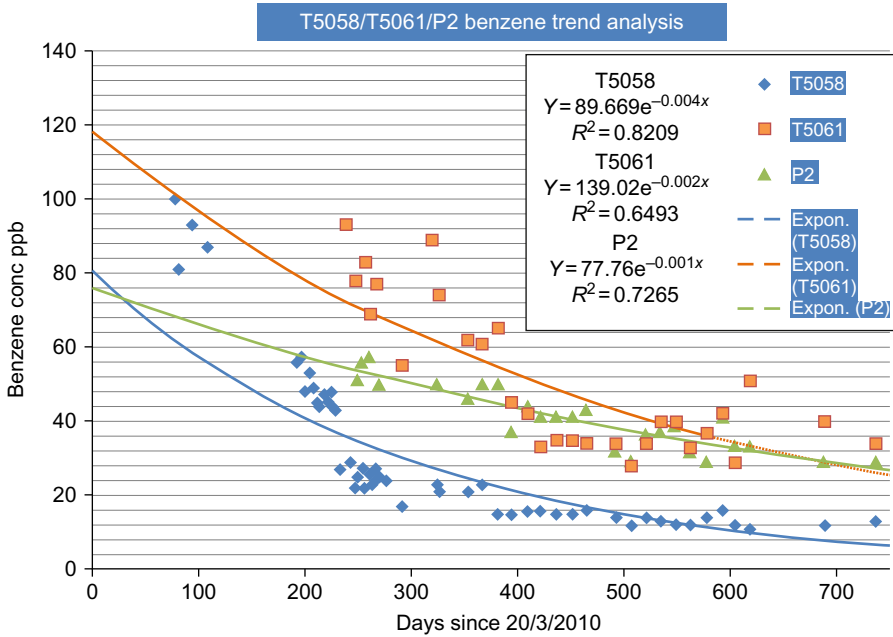
Fig. 15.7 Benzene level decay curves.

15.9 Conclusions from the Kingaroy UCG project

15.9.1 General

The initial concept for the Kingaroy project involved the phased construction of a 400 MW power project, starting with an initial phase of about 2–5 MW equivalent of gas production prior to installation of the power plant. The concept, initiated in late 2006, was supported technically by the long gas production experience of Cougar Energy management on the Chinchilla project and financially by the economic analysis contained in the Cougar Energy preliminary feasibility study. Subsequent analyses have confirmed this view (Walker, 2014). In the early stages of the Kingaroy project development, there appeared to be strong support from the Queensland Government to see the project develop.

The outcome was gas production lasting only 5 days, gasifying an estimated 20 tonne of coal, before the production well blockage and failure on 20 March 2010, and the subsequent events involving two measurements of benzene in one monitoring well at a level of 2 ppb, barely above the level of detection of 1 ppb. While these readings were considered by the government at the time to be of no concern, a subsequent erroneous reading 1 month later (due to a laboratory sampling mix-up) was used by the government as a justification for shutting down the site, despite a lengthy

period of report preparation by the company assessing the well failure and describing measures taken to prevent a recurrence.

As a result, Cougar Energy wrote off some A$20 million of direct expenditure on the project, apart from associated additional head office expenditure. Commercial development of the technology in Queensland at that time was thus no further advanced than it was at the time of the first test at Chinchilla 15 years earlier, despite the expenditure of substantial funds by Cougar Energy and the two other UCG companies active in the state, together investing a total estimated at more than A$300 million. Conclusions to be drawn from the Kingaroy project can best be considered under the separate headings of technical and regulatory issues.

15.9.2   Technical issues

There are two technical issues flowing from the Kingaroy project that can be identified as impacting on the successful achievement of its original goals—the failure of the casing in production well P4 and the lack of preparation and acceptance by government of a detailed plan covering monitoring, reporting, and remedial actions associated with potential groundwater contamination.

While the "triple casing" design was justified by the experience from previous drilling campaigns, its use for the production wells introduced greater complexity in the installation and cementing procedures. While these issues could have been eventually overcome, they resulted in high water pressure developing behind the casing in well P4 that contributed to its collapse. The system used for wells P5 and P6, installed but not utilized, confirmed the advantages of a simpler design. The experience reinforces the care required in selecting a casing system that is best adapted to both the geologic conditions encountered and the requirements of achieving successful in-place grouting.

Of greater significance to the project, however, were the implications associated with groundwater monitoring and the interpretation of the data obtained. The lack of clearly defined and agreed groundwater guidelines between the company and the regulatory agency allowed widely different interpretations of the recovered data to be made, despite the fact that all parties agreed that no threat of environmental harm existed at the site.

A practical groundwater protocol that should have avoided the complications resulting from the use of the Kingaroy groundwater data could have consisted of

- The definition of an operating gasification zone around the immediate cavity, within which high concentrations in groundwater would result from the chemical processes occurring during operations.
- Around this gasification zone, definition of an inner (monitoring) and outer (compliance) ring of groundwater monitoring bores each with their own trigger levels for water quality.
- Definition of responses required in each case of trigger level being exceeded, including alternatives involving repeat measurements to establish trends, remedial actions, or ultimately operational shutdown.
- Acceptance of groundwater standards for acceptable long-term levels of relevant chemical compounds (e.g., WHO, ANZ guidelines for fresh and marine water quality).

A schematic interpretation of the above requirements is shown in Fig. 15.8, with the specifics dependent on local site conditions.
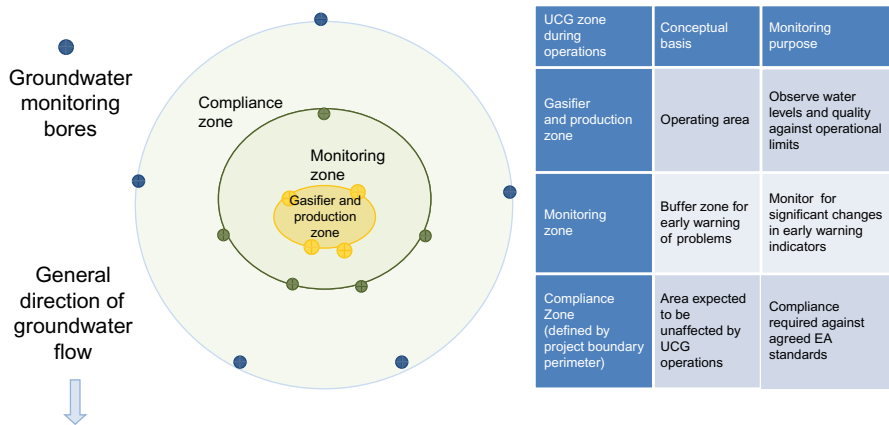
Fig. 15.8 Schematic of groundwater monitoring regime.

For the specific case of benzene, the starting point for assessing the significance of acceptable permanent levels is the classification/zoning of any overlying water resource or aquifer. Where the water resource is used for human consumption, reference should be made to the level acceptable for drinking water. This level is measured in micrograms/liter or parts per billion (ppb). Different countries have different standards required for drinking water with the WHO adopting a figure of 10 ppb. This standard is based on an assessment that a human, drinking 2 L of water a day for 70 years, will have a 1 in 100,000 extra chance of developing cancer (World Health Organisation, 2011).

Assessing an acceptable permanent level for benzene in a coal seam that is impacted by the UCG process, but is not classified as a water abstraction aquifer, is a more difficult exercise. The reference commonly used is the "Guidelines for Fresh and Marine Water Quality" (Australian Government, 2000). Under these guidelines, recommended trigger levels for benzene at the 95% level of species protection are 950 ppb (freshwater) and 700 ppb (marine water).

With the acceptable levels of benzene in groundwater potentially varying from 10 to 950 ppb, it is evident that each specific UCG location requires individual consideration in the selection of a relevant benzene trigger level. Factors of relevance include the following:

- Whether the water is in the coal seam or overburden. If in the coal seam, natural decay of levels of benzene with time after completion of operations is likely.
- Whether the water is being used for drinking or is likely to be used for drinking, in the period of process operations or in the longer term.
- The regional groundwater hydrological system. If contaminants do escape, data are required to show where they will be carried and how rapidly and whether dilution will occur.
- What is the level of any observed contaminant in relation to the approved trigger level?
- If contaminants are observed, how will they be treated and over what time period?

An installed monitoring system such as illustrated in Fig. 15.8, combined with a reporting and action response plan, will give the regulatory authorities the mechanism to enforce the agreed environmental management plan and should form the basis for an open and transparent integration of all stakeholders in the compliance reporting process.

15.9.3   Issues of regulatory control

A major issue in the acceptance of the UCG technology by the regulators in any country is the extent to which they are prepared to accept the experience gained elsewhere in developing the technology. Although this past experience is largely at a demonstration level, the range of data available from tests in a number of countries can be utilized to allow acceptance of the value of the technology and enable the development of a regulatory regime for a commercial project. This would avoid the necessity for the regulatory approach of "reinventing the wheel" by demanding a further demonstration project prior to acceptance of potential commercial development, with the financial risks that this entails for the developer, as was well illustrated by the Queensland experience.

The Chinchilla demonstration of 1999–2004 was undertaken in a cooperative spirit between government and developing company, with regular environmental reporting being utilized to ensure that no environmental threat existed. For the Kingaroy project, a change in government attitude to the technology occurred late in 2008 after various financial commitments by a number of UCG companies had been made, presumably as a result of political factors that can only be inferred from evidence available, including

- The declared preference for CSG technology wherever conflicts with UCG occur (February 2009).
- The predominance at the time of CSG tenement applications over all coal basins in Queensland.
- The delay in granting approval of the MDL required for the first Kingaroy phase (22 months).
- The establishment of a scientific panel to review all aspects of UCG technology to assess whether it should be permitted in Queensland (October 2009), despite its proved success in development internationally.
- The lack of consistency between the technical arm of the Queensland Government that accepted the negligible and short-lived benzene readings and the political arm, which initiated the shutdown on an erroneous report of one high benzene reading.

Regrettably for each of the UCG project developers in Queensland, who (from 1999 onward) had commenced developing their projects in good faith and with the support of officers in the relevant Queensland government departments, the political arm of government chose (early in 2009) to introduce a major uncertainty as to the future of the UCG industry in the state. The technical and financial impacts on each of the developers have been significant, more especially because of the government's decision in April 2016 to ban the technology in the state.

15.9.4   Summary of conclusions

The lessons that arise from the Kingaroy project relate more to the establishment of practical government regulations rather than specific technical issues about the UCG process itself. These might be summarized as follows:

- Some well failures might be expected as for any other drilling-related activity. Provided adequate site, health, safety, and environmental controls are in place, these should be accepted by the regulator as in other industries.
- In relation to groundwater issues, environmental regulations require definition of operating project areas within which temporarily acceptable contaminant levels are defined, as exists for conventional mining/chemical projects.
- Regulations should also provide a precise definition of site-specific trigger and rehabilitation levels for potential contaminants in groundwater, which take into account the relevant chemical and its measurement location, the groundwater end use, and the period of time by which rehabilitation will be required.
- Development of coal using the UCG process should be clearly defined in relevant legislation in a way that permits development as for other mining-related projects, with appropriate support from government for UCG companies working with local communities.

In addition to the above factors, education of government regulatory staff in the UCG process, using the vast amount of data available in the public domain, is an integral part of ensuring a minimum of difficulty in resolving the many operating issues likely to arise from commercial development of UCG technology in the future.

References

Australian Government, 2000. Australian and New Zealand Guidelines for Fresh and Marine Water Quality, The Guidelines, Australian and New Zealand Environment and Conservation Council, Agriculture and Resource Management Council of Australia and New Zealand, vol. 1, pp. 3.4–6, October.

Blinderman, M.S., Fidler, S., 2003. Groundwater at the underground coal gasification site at Chinchilla, Australia. In: Proceedings of the Water in Mining Conference, Brisbane, October.

Blinderman, M.S., Jones, R.M., 2002. The Chinchilla IGCC project to date: UCG and environment. In: Gasification Technologies Conference, San Francisco, October.

Burton, E., Friedmann, J., Upadhye, R., 2006. Best practices in underground coal gasification. Contract No. W-7405-Eng-48, Lawrence Livermore National Laboratory, University of California.

Cougar Energy Ltd (renamed Moreton Resources Ltd), 2011a. AGM address and slide presentation, released to Australian Securities Exchange 28 October, p. 5.

Cougar Energy Ltd (renamed Moreton Resources Ltd), 2011b. Cougar Energy challenges Queensland Government shutdown—independent scientific panel report disputed. Presentation released to Australian Securities Exchange, 1 March 2011 (accessed 11/1/2016).

Gregg, D.W., Hill, R.W., Olness, D.U., 1976. An overview of the Soviet effort in underground gasification of coal. USERDA Contract No. W-7405-Eng-48, Lawrence Livermore Laboratory, University of California.

Queensland Government, 2009. See http://www.services.dip.qld.gov.au (accessed 11/1/2016).

Walker, L.K., 1999. Underground coal gasification: a clean coal technology ready for development. Aust. Coal Rev. (October), 19–21.

Walker, L.K., 2014. Underground coal gasification—issues in commercialisation. Proc. Inst. Civ. Eng. Energy (November), 188–195.

Walker, L.K., Blinderman, M.S., Brun, K., 2001. An IGCC project at Chinchilla, Australia, based on underground coal gasification (UCG). In: Gasification Technologies Conference, San Francisco, October.

World Health Organisation, 2011. Guidelines for Drinking-Water Quality, fourth ed., WHO Geneva Switzerland, p. 38.

Underground gasification of oil shale

16

A. Reva, A. Blinderman
Ergo Exergy Technology Inc., Montreal, QC, Canada

16.1 Underground gasification of oil shale

Oil shale is a sedimentary rock of organic origin containing predominantly inorganic components and organic matter called kerogen. Not to be confused with tight oil and gas, they may occur in oil shale and can be produced by fracturing and drilling the shale, whereas kerogen may be produced only by the process of oil shale pyrolysis.

Kerogen is a product of the conversion under natural conditions of various materials of plant and animal origin that formed the sapropel and humus deposits.

In considering oil shales as one of the types of fossil fuels, the properties of peat, shale, and lignite should be examined (Table 16.1).

Oil shales are laminated, rarely hard, oversized sedimentary rock deposits, which may split into thin plates, dark gray in color or various hues of brown; if ignited, they burn with a sooty, smoky flame (Rudina and Serebryakov, 1988).

Oil shales are noted for varying degrees of hardness, but do not exceed 3 on Mohs' scale. Sometimes very loose structures are encountered. Saturated with water oil shale does not swell, but water acts to loosen the rock.

Oil shales containing inherent moisture are darker in color, and when exposed to air, they exhibit fissility, splitting into thin sheets.

For the most part, oil shales are uniform but may have relatively large inclusions of nonorganic rock or rock containing very small amounts of organic material. Due to the presence of sulfur compounds and a highly reducing environment in shales, various copper, zinc, and other metal (sulfide) ores can occasionally be found.

The density of shales is determined by the kerogen content, mineral composition of shale, porosity, and moisture content. The density of pure kerogen is 1200 kg/m^3.

All fossil fuels (encountered in solid, liquid, and gas phase) originate from plant or animal remains and are collectively referred to as caustobioliths (from the Greek "kaustus" combustible, "bios" life, "lithos" stone).

Mineral constituents (acaustobioliths) combine with organic sediment (caustobioliths) to form oil shales. The acaustobiolith components are frequently mixed in with mineral compounds. Acaustobioliths (the mineral phases present in the oil shale) are mainly composed of limestones, dolomites, some sandstones, and often clays containing a substantial proportion of silicic acid. The inclusions are generally represented by gypsum, phosphorites, marcasite, iron oxides, and pyrite.

The organic components of shale are subdivided into two types: humus and sapropelic caustobioliths.

Table 16.1 Comparison of chemistry and structure of peat, oil shale, and lignite

	Peat	Oil shale	Lignite
Fixed carbon, % (daf basis)	Up to 58	60–65	64–77
Ash, %	5–10	50–60	15–25
Moisture, %	40–50	15–20	20–35
Volatile matter, %	Up to 70	Up to 90	Up to 40
LHV, MJ/kg	8.38–10.47	5.87–10	10.6–15.9

The solid fossil fuels originating from land plants are referred to as humite (the Latin word "humus" denotes the vegetable mold, the earth formed by plant decomposition). The water-soluble components of humite were likely washed out into the sea and eventually laid down as sediment.

In standing water, sediment layers were deposited containing the product of biochemical conversion of microalgae and animal species, that is, plankton. The remains of these led to the deposition of the solid fossil fuel called sapropelite.

Quite frequently, the kerogen content of the oil shale (pure, ash-free organic matter content) comprises a mixture of different ratios of sapropelite components. Based on compositional variation, the following major types of oil shales are distinguished (Arens, 2001):

- Peat, lignite, and bituminous.
- Sapropelic, sapropelite, boghead coal, torbanite, asphalt, and oil.
- Mixed types—peat-sapropel, lignite-sapropel, and bituminous-boghead.

A high carbon (carbonate) content is mainly a characteristic of oil shale found in the Baltic Basin. The carbonate content of shale from other deposits is below 2%–12%.

Oil shale seams in the same deposit have variations in the kerogen content. Carbon content increases from shallow to deeper seams. Nitrogen in kerogen is a normally present constituent in oil shale. Its content may in some cases reach as much as 5%. Sulfur ($\sim$1%) is virtually always present as a component of oil shale.

The Estonian oil shale (kukersite) deposit occurs in the Baltic Basin, which is located in Estonia as well as in the Leningradskaya, Pskovskaya, and Novgorodskaya regions of the Russian Federation. The basin covers $\sim$60,000 km^2; however, only 10,000 km^2 of the basin contains commercially recoverable oil shale. The Estonian and Tapa deposits occur in the western part of the basin (Fig. 16.1).

Kukersites occur in the Middle Ordovician sediments. The thickest, closely spaced oil shale seams, most persistent areally and along strike, occur in the lower part of the Kukruse stage where they form a commercially mined seam.

The operating mines at the Estonian deposit are mining run-of-mine ore with a specific calorific value of 7.2–9.7 MJ/kg.

Fig. 16.2 is a cross section of the commercially mined multilayer unit at the Estonian oil shale (kukersite) deposit, as developed from data provided by V.V. Levikin; Tables 16.2–16.4 summarize their qualitative characteristics, the composition of the organic matter, and the results of semicoking.
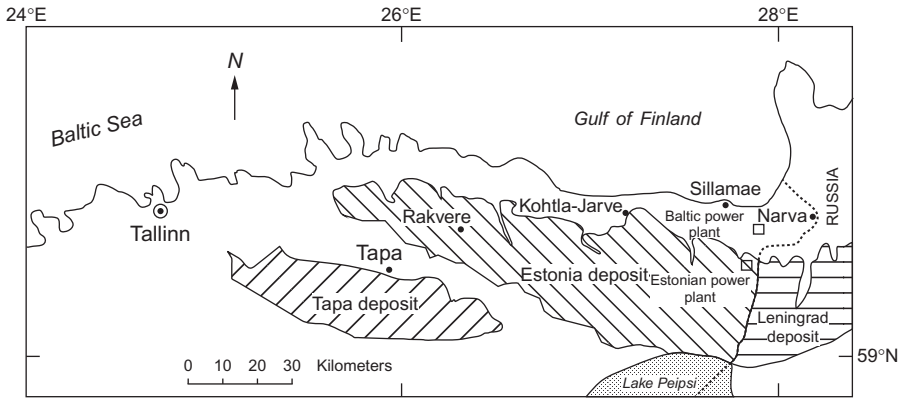
Fig. 16.1 Estonian oil shale (kukersite) deposit (Dyni, 2006).
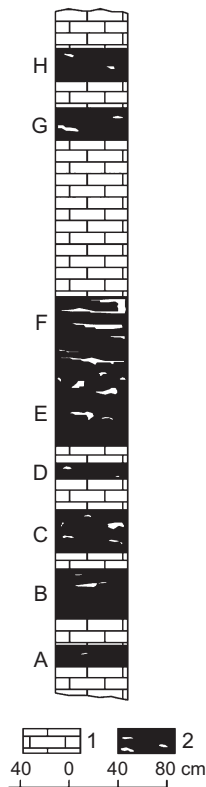
Fig. 16.2 The cross section of the commercially mined multilayer unit of the Estonian deposit. 1, limestone and 2, oil shale with limestone concretions. The oil shale seams are lettered A–H.

Table 16.2 **Oil shale quality (Estonian oil shale deposit)**

Seam	Density, t/m^3	Mineral ash, %	CO_2, %	S, %	Oil content (Fischer assay), %
A	1.53	40.7	10.6	0.7	55
B	1.5	37.9	13.4	1.5	69
C	1.5	44.9	10.4	0.6	66
D	1.66	54.0	12.8	0.4	56
E	1.34	30.4	8.4	0.8	66
F	1.5	37.9	11.7	0.5	66

Table 16.3 **Ultimate composition of organic matter in oil shale, %**

Oil shale seam	$C°$	$H°$	$(N+O)°$
A	74–75	9.5	15
B	74	9.3–9.4	15–16
C	74–75	9.4–9.6	14–15
D	74	9.5–9.7	15–16
E	75	9.7–9.9	14–15
F	74	9.6–9.8	15–16
G	75–76	9.7	13–15
H	76–77	9.8–9.9	14–15

Table 16.4 **Results of semicoking of oil shale**

Oil shale seam	Moisture	Tar	Semicoke	Gas and losses
A	1.52	24.29	69.6	5.59
B	2.04	33.0	57.0	7.92
C	1.24	20.2	73.9	4.69
D	1.32	17.36	75	6.32
E	1.43	20.67	70.5	7.5
F	1.21	17.47	76.8	4.52
G	1.44	24.86	68.0	5.73
H	1.26	20.55	74.5	3.69
Commercial unit	1.39	21.63	71.39	5.29

The cross section illustrates the seams starting from the bottom:

1. Oil shale (seam A), highly clayey in places, and containing some bituminous limestone concretions.
2. Bluish gray limestone at the base with a thin parting of clay (4–5 cm).
3. Oil shale (seam B) has a lighter color than seam A, with fairly large-sized bituminous limestone concretions and quite thin (5–10 mm) interbeds of bluish semicrystalline limestone. At the base, it contains a large amount of organic residue. Numerous pyritized zones are present in oil shale.
4. Bituminous limestone.
5. Oil shale (seam C) has a large number of white limestone wormlike trails in the upper part; a significant amount of bituminous limestone concretions is present in the oil shale.

Table 16.5 Ultimate composition of kerogen in some shale deposits, % (Pitin, 1957)

Oil shale deposit	C	H	N	S	O
Pushtos	56.7	5.8	0.9	–	36.4
Baltic	59.2	6.5	2.8	–	31.5
Kenderlik	66.5	7.8	1.8	–	24.6
Tereglitau	66.0	7.8	–	2.4	23.1
Baysunsky	68.0	7.7	–	2.3	21.0
Pulkovo	68.2	6.6	2.2	2.4	20.5
Dergunovsky	70.4	8.4	–	7.4	13.8
Torbanit	75.3	10.5	–	–	14.2
Gdovsky	75.5	8.5	0.9	1.8	13.2
Weimar	75.8	9.1	–	1.5	13.6
Green River (the United States)	80.5	10.3	2.4	1.0	5.8

6. Limestone has a bluish gray color, in two layers, dense.
7. Oil shale (seam D) has a yellowish green color, with very thin veins of limestone; the specific gravity of this oil shale (1.7) is greater than the specific gravity of oil shales in other seams (1.5).
8. Bituminous limestone.
9. Oil shale (seam E) has a high organic matter content, very lightweight, and contains few fossils. The shale has a lighter color in comparison with shales in other seams, mostly reddish.
10. Oil shale (seam F) contains a very a large amount of concretions (up to 40%) in the lower part, while within the upper part, interbeds of bituminous limestone are present.
11. Limestone, bituminous in places.
12. Oil shale (seam G).
13. This dense limestone has a bluish gray color.
14. Oil shale (seam H) with limestone concretions.

The commercially mined unit is made up of seams A, B, C, D, E, and F. Seam A is not mined in the vicinity of the Kiviyli mine due to a high clay content (Table 16.5).

16.2 International classification of oil shale

Oil shales are classified into three main types based on their geologic properties: oil shale with a high content of carbonate minerals and siliceous and carbonaceous shales, commonly referred to as cannel oil shale.

16.2.1 Carbonate-rich shale

Some of the higher-grade oil shales contain substantial amounts of carbonate minerals. Fine-grained calcite and dolomite can be the predominant mineral components that likely precipitated when oil shale was formed; however, some of them could have formed following changes in organic remains. Milton described more than 20 such carbonate-rich minerals in oil shale and marlstone of the Eocene Green River seam in Wyoming and Utah.

Of particular value are lacustrine deposits of oil shale. Seams containing large amounts of organic material are interbedded with partings of mostly carbonates.

As a general rule, these oil shale deposits are quite strong and resistant to atmospheric and mechanical exposure, which complicates the crushing and preparation of these solid fuels for commercial uses.

16.2.2   Siliceous shale

Oil shale that does not contain a significant amount of carbonate minerals can contain clastic minerals (quartz, feldspar, and clay) as its major organic components, but siliceous limestone or opal is not uncommon, some as diatom fossils and other fossils. Siliceous oil shale has generally dark brown or black color and is less resistant to atmospheric stress than carbonate-rich oil shale. Some Mesozoic and Tertiary sediments contain a large amount of shale oil, while the latter sediments yield small amounts of oil. The processes of compaction and deformations likely led to the migration of liquid components and devolatilization of the siliceous shales.

16.2.3   Cannel shale

Carbonaceous shale burns with a bright flame and consists of organic material that completely envelops the grains of mineral matter. Such rocks are often classified as semicarbonaceous shales, torbanite, and coal that formed at the bottom of an ancient sea. These shales consist mainly of the remains of seaweed and generally contain a large amount of mineral constituents, hence its exclusion from the category of commercial coals. The color of the carbonaceous shales is generally dark brown or black. A considerable proportion of organic matter is converted to shale oil during normal coking conditions, with the oil shale semicoke remaining in the rock matrix (Lee, 1991, p. 10).

Another classification of oil shales was developed by A.C. Hutton. Hutton developed a classification of oil shales primarily based on the origin of organic matter. This classification was useful in comparing different types of organic material in oil shale with the chemical composition of hydrocarbons derived from oil shale. Hutton (1991) singled out shale as one of the three broad types of organically rich sedimentary rocks: (1) humic coal, (2) bitumen-containing rock, and (3) oil shale. He further subdivided oil shale into three categories based on depositional setting, that is, terrestrial, lacustrine, and marine. Further, Hutton identifies six specific types of oil shale: cannel coal, lamosite, marinite, torbanite, tasmanite, and kukersite (Fig. 16.3).

For UCG purposes, the classification of coals developed in the Soviet Union is generally used. When discussing oil shales, the distribution of oil shales based on the kerogen content is used, which is cited in the works of Arens.

The Dobryansky classification of oil shales is based on the elemental composition (carbon, hydrogen, oxygen, nitrogen, and sulfur), whereby all shales are divided into several groups with the following properties:

1. *Class 1*: Shales with a carbon content of up to 60%; hydrogen content of up to 7.3%; and tar yield of up to 25% during coking, from 18% to 40% of the pyroligenous liquor and from 28% to 40% of char. Oil shale in this class has a high nitrogen content. The calorific value is 24–26 MJ/kg.
2. *Class 2*: Shales with a carbon content of 60%–65%, hydrogen content of 7.3%–7.8%, and also containing nitrogenous compounds. Tar yield 25%–35%, pyrogenic water 15%–18%, and char 22%–28%. The calorific value is 26–28.5 MJ/kg.
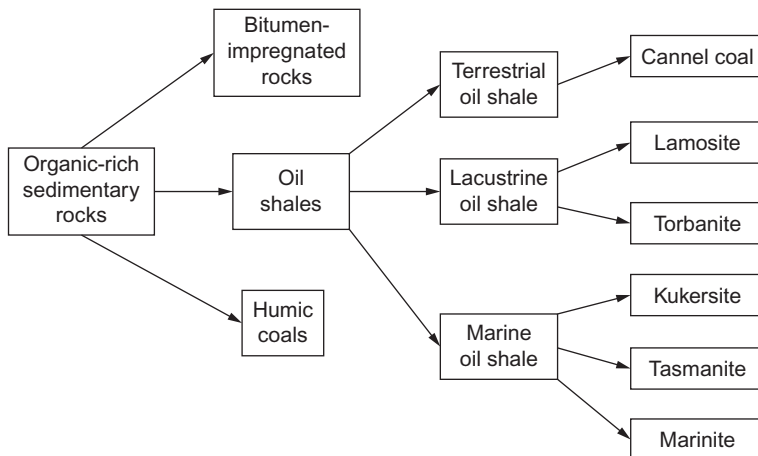
Fig. 16.3 Classification of oil shales (Dyni, 2006).
Based on A.C. Hutton.

3. *Class 3*: Carbon content 65%–75%, hydrogen content 7.0%–8.3%. Tar yield 35%–45%, pyrogenic water 10%–15%, char 18%–22%.
4. *Class 4*: Highly carbonized oil shale. Carbon content 70%–75%, hydrogen content 8.3%–8.9%. Tar yield 45%–47%, pyrogenic water 7%–10%. The calorific value is 31.5–35.5 MJ/kg.
5. *Class 5*: Carbon content 75%–80%, hydrogen content 9%–9.3%. Tar yield increased to 67%, sometimes higher; pyrogenic water is below 7%, with a shale char yield of 8%–13%. The calorific value is 35.5–38.5 MJ/kg.

The above properties of the five classes of oil shales are summarized in Table 16.6.

The above classification of oil shales developed by A.F. Dobryansky is based on the elemental composition of the kerogen of oil shales. However, of important note is that the elemental composition does not fully reflect the chemical and process-related properties of oil shales. Moreover, the direct correlation between carbon content and hydrogen does not always exist. An additional parameter is the tar yield.

I.M. Ozerov and associates developed the most universal commercial classification of oil shales (Table 16.7).

Table 16.6 Classification of oil shales

Oil shale class	C, %	H, %	Tars, %	Pyroligenous liquor, %	Char, %	Q, MJ/kg
First	<60	<7.3	<25	18–40	28–40	24–26
Second	60–65	7.3–7.8	25–35	15–18	22–28	28.5
Third	65–75	7.0–8.3	35–45	10–15	18–22	N/A
Fourth	70–75	8.3–8.9	45–47	7–10	N/A	31.5–35.5
Fifth	75–80	9–9.3	67	< 7	8–13	35.5–38.5

Based on Dobryansky.

Genetic type	Class, Q_O^C, kJ/kg	Subclass	Group $\frac{T}{Q_6^C}$	Subgroup	Type	Variety	Associated components	Principal commercial applications
Sapropelic	High CV values 12,500	High tar content Tar yield as related to kerogen > 50% As related to oil shale > 30% Low ash (up to 6%)	1.42	Thallus alginite Thallus colloalginite	Carbonate (CaO+ MgO 20%) aluminum silicate carbonate (CaO+ MgO 10%–20%)	Low-sulfur $S_t^d =$ 2% or less	Elevated concentrations of rare earth and trace elements, commercial compounds of Al, K, Na, Ca, P, etc.	Chemical (gas, chemical products), fuel (heating and electricity, liquid fuels)
Sapropel-humus	Medium calorific value, 8400–12,500	Medium tar; tar yield as related to kerogen 40%–50% As related to oil shale >10% Ash (61%–70%)	1.2–4.2	Thallus alginite saprohumosor-bomixstinitic Pseudovitrinite colloalginite	Aluminosilicate (CaO+MgO > 10%)	Medium-sulfur $S_t^d =$ 2%–4%		Production of building and cementing materials
Humus-sapropel	Lower calorific value, 6300–8400	Low tar Tar yield as related to kerogen 30%–40% As related to oil shale > 30% High ash content (> 70%)	1.2	Vitrinite-sapropel-humus-sorbo-mixtinite, colloalginite	Silicate ($SiO_2 + Al_2O_3 > 70\%$)	Sulfur $S_t^d > 4\%$		Chemical (gas, chemical products) Fuel (liquid fuel)

Table 16.7 **In situ shale oil resources of some oil shale deposits**

Country, region, and deposit[a]	Age[b]	In-place shale oil resources[c] (10^6 bbl)	In-place shale oil resources[c] (10^6 tons)	Date of estimation[d]	Source of information
Argentina		400	57	1962	
Armenia					
Aramus	T	305	44	1994	Pierce et al. (1994)[e]
Australia					
New South Wales	P	40	6	1987	Crisp et al. (1987)
Queensland	P	80	1	1987	Matheson (1987)[f]
Alpha	T	249	36	1999	Wright (1999, written commun.)[f]
Byfield	T	9700	1388	1999	Wright (1999, written commun.)[f]
Condor	T	4100	587	1999	Wright (1999, written commun.)[f]
Duaringa (upper unit)	T	1530	219	1999	Wright (1999, written commun.)[f]
Herbert Creek Basin	K	1700	243	1999	Wright (1999, written commun.)[f]
Julia Creek	T	740	106	1999	Wright (1999, written commun.)[f]
Lowmead	T	72	10	1999	Wright (1999, written commun.)[f]
Mt. Coolon	T	3170	154	1999	Wright (1999, written commun.)[f]
Nagoorin Basin	T	2600	372	1999	Wright (1999, written commun.)[f]
Rundle	T	3000	429	1999	Wright (1999, written commun.)[f]
Stuart	T	4100	587	1999	Wright (1999, written commun.)[g]
Yaamba	T_R	600	86	1999	Wright (1999, written commun.)[f]
South Australia	P	48	7	1987	Crisp et al. (1987)
Leigh Creek					
Tasmania					
Mersey River					
Austria		8	1	1974	
Belarus					
Pripyat Basin	D	6988	1000		

Continued

Table 16.7 **Continued**

Country, region, and deposit[a]	Age[b]	In-place shale oil resources[c] (10^6 bbl)	In-place shale oil resources[c] (10^6 tons)	Date of estimation[d]	Source of information
Brazil					
Iratí Formation	P	80,000	11,448	1994	Afonso et al. (1994)
Paraíba Valley	T	2000	286	1969	Padula (1969)
Bulgaria		125	18	1962	
Canada					
Manitoba-Saskatchewan	K	1250	191	1981	Macauley (1981, 1984a,b, 1986)[h]
Favel-Boyne Formations	P-IP	1174	168	1989	Smith et al. (1989)[h]
Nova Scotia	M	531	76	1990	Smith and Naylor (1990)
Stellarton Basin	M	269	38	1988	Ball and Macauley (1988)
Antigonish Basin	M	14	2	1988	Ball and Macauley (1988)
New Brunswick	M	3	0.4	1988	Ball and Macauley (1988)
Albert Mines	M	?	?	1984	Hyde (1984)[i]
Dover	O	?	?	1988	Davies and Nassichuk (1988)[j]
Rosevale	D	12,000	1717	1986	Macauley (1986)
Newfoundland		?	?	1986	Macauley (1986)
Deer Lake Basin					
Nunavut					
Sverdrup Basin					
Ontario					
Collingwood Shale					
Kettle Point Fm					
Chile		21	3	1936	
China		16,000	(2290)	1985	Du and Nuttall (1985)[k]
Maoming	T	(2271)	(325)	1988	Guo-Quan (1988)
Fushun	T	(127)	(18)	1990	Johnson (1990)

Congo, Republic of		100,000	14,310	1958	
Egypt					
Safaga-Quseir area	K	4500	644	1984	Troger (1984)
Abu Tartur area	K	1200	172	1984	Troger (1984)
Estonia					
Estonia deposit	O	3900	594	1998	Kattai and Lokk (1998)[l]
Dictyonema shale	O	12,386	1900		
France		7000	1002	1978	
Germany		2000	286	1965	
Hungary		56	8	1995	Pápay (1998)[m]
Iraq					May be very large
Yarmouk	K	?	?	1999	See Jordan
Israel		4000	550	1982	Minster and Shirav (1982)[n]
Italy		10,000	1431	1979	
Sicily		63,000	9015	1978	
Jordan					
Attarat Umm Ghudran	K	8103	1243	1997	Jaber et al. (1997)[o]
El Lajjun	K	821	126	1997	Jaber et al. (1997)[o]
Juref ed Darawish	K	3325	510	1997	Jaber et al. (1997)[o]
Sultani	K	482	74	1997	Jaber et al. (1997)[o]
Wadi Maghar	K	14,009	2149	1997	Jaber et al. (1997)[o]
Wadi Thamad	K	7432	1140	1997	Jaber et al. (1997)[o]
Yarmouk	K		(Large)	1999	Minster (1999)[p]
Kazakhstan					
Kenderlyk field		2837	400	1996	Yefimov (1996)[q]
Luxembourg	J	675	97	1993	Robl et al. (1993)
Madagascar		32	5	1974	
Mongolia					
Khoot	J	294	42	2001	Avid and Purevsuren (2001)

Continued

Table 16.7 **Continued**

Country, region, and deposit[a]	Age[b]	In-place shale oil resources[c] (10⁶ bbl)	In-place shale oil resources[c] (10⁶ tons)	Date of estimation[d]	Source of information
Morocco					
Timahdit	K	11,236	1719	1984	Bouchta (1984)[r]
Tarfaya Zone R	K	42,145	6448	1984	Bouchta (1984)[r]
Myanmar (Burma)		2000	286	1924	
New Zealand		19	3	1976	
Poland		48	7	1974	
Russia					
St. Petersburg kukersite	O	25,157	3600		
Timano-Petchorsk Basin	J	3494	500		
Vychegodsk Basin	J	19,580	2800		
Central Basin	?	70	10		
Volga Basin	?	31,447	4500		
Turgai and Nizheiljisk deposit	?	210	30		
Olenyok Basin	€	167,715	24,000		
Other deposits	–	210	30		
South Africa		130	19	1937	
Spain		280	40	1958	
Sweden					
Narke	€	594	85	1985	Andersson et al. (1985)
Ostergotland	€	2795	400	1985	Andersson et al. (1985)
Vastergotland	€	1537	220	1985	Andersson et al. (1985)
Oland	€	1188	170	1985	Andersson et al. (1985)
Thailand					
Deposit and (province)	T	6400	916	1988	Vanichseni et al. (1988)
Mae Sot (Tak)	T	1		1988	Vanichseni et al. (1988)
Li (Lampoon)					
Turkmenistan and Uzbekistan					
Amudarja basin[s]	P	7687	1100		

Turkey					
Deposit and (province)	T	35	5	1993	Güleç and Önen (1993)[t]
Bahcecik (Izmit)	T	398	57	1995	Sener et al. (1995)
Beypazari (Ankara)	T	28	4	1993	Güleç and Önen (1993)
Burhaniye (Bahkesir)	T	126	18	1993	Güleç and Önen (1993)
Gölpazari (Bilecik)	T	804	115	1995	Sener et al. (1995)
Göynük (Bolu)	T	203	29	1995	Sener et al. (1995)
Hatildag (Bolu)	T	349	50	1995	Sener et al. (1995)
Seyitömer (Kütahya)	T	42	6	1993	Güleç and Önen (1993)
Ulukisla (Nigde)					
Ukraine					
Boltysh deposit		4193	600	1988	Tsherepovski
The United States					
Eastern Devonian shale	D	189,000	27,000	1980	Matthews et al. (1980)[u]
Green River Fm	T	1,466,000	213,000	1999	This report
Phosphoria Fm	P	250,000	35,775	1980	Smith (1980)
Heath Fm	M	180,000	25,758	1980	Smith (1980)
Elko Fm	T	228	33	1983	Moore et al. (1983)
Uzbekistan					
Kyzylkum Basin		8386	1200		
Total (rounded)		2,826,000	409,000		

[a]The resources in the above table are listed by country in alphabetic order. For some countries, the deposits are listed under state or province.

[b]The age of the deposit, when known, is indicated by the following symbols: Є, Cambrian; O, Ordovician; D, Devonian; M, Mississippian (Early Carboniferous); IP, Pennsylvanian (Late Carboniferous); P, Permian; T_R, Triassic; J, Jurassic; K, Cretaceous; and T, Tertiary.

[c]The resources of shale oil are given in US barrels and metric tons. Resource numbers in boldface type are from the references cited; the associated number in nonboldface type was calculated for this table. In several cases, resource numbers in parentheses are included in the total resource number for the country. To determine tons of resources from volumetric data, it is necessary to know the specific gravity of the shale oil. In some cases, this value was given in the source reference; if not, a specific gravity of 0.910 was assumed.

[d]The "date of estimation" is the publication date of the source reference. If a reference is not listed for a deposit, the resource data are from Russell (1990). A few deposits for which no resource numbers are given are still listed in the table because they are believed to be of significant size.

[e]The resource was estimated by assuming seven beds of oil shale totaling 14 m in thickness, which underlie 22 km^2 and have an average oil shale bulk density of 2.364 gm/cc.

[f]Shale oil specific gravity (SG) of 0.910 was assumed. Resource data from Matheson (1987) augmented by a personal communication from Dr. Bruce Wright to Professor J.L. Qian dated 29 March 1999.

[g]McFarlane (1984) gives the Yaamba deposit as 2.92 billion in situ barrels of shale oil.

[h]Shale oil SG of 0.910 was assumed.

[i]The west side of the basin is largely unexplored and may contain oil shale deposits.

[j]Alginite-rich oil shale is found in the Lower Carboniferous Emma Fiord Formation at several localities in the Sverdrup Basin. On Ellesmere Island, the shale is geothermally overmature, but on Devon Island, the oil shale is immature to marginally mature.

[k]China's total oil shale resources are given by Du and Nuttall (1985, p. 211).

[l]A shale oil yield of 10 wt% and a shale oil SG of 0.968 were used to calculate barrels of resources (Yefimov et al., 1997, p. 600). Kogerman (1997, p. 629) gives the range of oil yields of Estonian kukersite as 12–18 wt%.

[m]Assumed a shale oil yield of 8 wt% and a shale oil SG of 0.910.

[n]Fainberg and Hetsroni (1996) estimate Israel's oil shale reserves at 12 billion tons, which equates to 600 million tons of shale oil.

[o]Shale oil SG of 0.968 was assumed.

[p]The oil shale deposit underlies several hundred square kilometers and reaches 400 m in thickness (Minster, 1999, written commun.).

[q]Shale oil SG of 0.900 was assumed.

[r]Shale oil SG of 0.970 was assumed. Occidental Oil Company made the estimate of the Timahdit resource, and Bouchta estimated the Tarfaya resource; details of both estimates are in Bouchta (1984).

[s]Amudarja Basin extends across border between Turkmenistan and Uzbekistan.

[t]Güleç and Önen (1993) reported 5196 million tons of oil shale in seven deposits but no shale oil numbers. Graham et al. (1993) estimate the Göynük resource at 9 billion tons of oil shale. Sener et al. (1995) reported 1865 million tons of oil shale in four Turkish deposits.

[u]The Devonian oil shale resource estimated by Matthews et al. (1980) is based on hydroretorting analyses. To make these results compatible with the rest of the resource data in this table, which are based mostly on Fischer assay analyses, the resource numbers given by Matthews et al. (1980) were reduced by 64%.

Classification parameters are as follows:

- Type of oil shale is determined by its genesis, by subclass, and by the semicoking tar yield. It determines the commercial application of oil shale.
- Group is determined based on the ratio of semicoking tar yield to calorific value $\frac{T}{Q^C}$, the subgroup by the petrographic composition of the organic material in oil shale. It is determined by the origin of the original component and affects the degree of conversion of its trace element content and chemical properties of kerogen.
- Type of the shale is determined based on the ash content, specifically by the carbonate content of alkaline earth metals (CaO + MgO), which are formed during combustion and thermal processing of shales. This parameter will determine the type of application the ash is suited for.

The following types of oil shales are differentiated:

- (CaO + MgO).%
- Carbonate (c) > 20.
- Carbonate-aluminosilicate (b) 19–10.
- Aluminosilicate (a) < 10.

The variety of oil shale is determined by the mass fraction of sulfur.

The properties of oil shale are represented as class number, group, and type. To this end, a classification diagram is used in which all the oil shales are subdivided into classes and six groups.

For example (Glushchenko, 1990),

Baltic shale with the following properties: $Q^C = 12,600$ kJ/kg, $T = 22\%$, $\frac{T}{Q^C} = 1.75$, and content of (CaO + MgO) in ash 25%. This oil shale is indexed 3.5b.

16.3 Oil shale resources

Oil shale deposits occur in many parts of the world (Dyni, 2006). The age of these deposits varies from Cambrian to Tertiary. They formed in various marine, continental, and lacustrine sedimentary environments. The largest known deposit of oil shale is the Green River seam in the western United States; the total shale oil resources of the Green River seam are estimated at 213 billion tons (~1.5 trillion US barrels).

The total aggregate deposits of oil shale in 33 countries (listed in Table 16.7) are estimated to be about 409 billion tons, which is equivalent to 2.8 trillion US barrels of shale oil. These amounts are very approximate, as several deposits have not been extensively studied which precludes an accurate estimate, while some deposits were not included in this overview.

The oil shale deposits in the CIS countries and the Baltic states number ~50 deposits with commercially exploitable oil shale reserves of at least 195 billion tons (of which 58.5 billion tons are conditioned). Prognostic (inferred) oil shale resources exceed 3000 billion tons. The oil shale resources found across the world have the highest tar content (from 13% to 25%), while their sulfur content is likewise

the highest. The highest tar contents are characteristic of the Volga deposits, such as the Kashpirskoye deposit (5.3% sulfur content).

The largest oil shale deposits are found in Siberia (the Olenek River basin), in Kazakhstan (Obshesyrtovskoye), in Middle Volga (Kashpirskoye), in Ukraine (Boltyshskoye and menilite oil shales in Zakarpattya), and in Belarus (Lubanskoye, Turovskoye).

The highest quality and economically recoverable are the oil shales (kukersites) found in the Baltic states (Fig. 16.4).

Most of the oil shale basins and deposits are yet to be extensively studied, which is why the data on the world oil shale resources are very contradictory. Approximately half of the potential shale oil resources (20%) belongs to the United States, while the rest is distributed between Brazil (20%), the CIS and Baltic countries (10%), China and Australia (5% each), Morocco (2.5%), Canada (2%), etc. The largest deposits are located in the western hemisphere, with the largest of the explored deposits being the Green River seam (the United States) and Irati seam (Brazil). The distribution of the world potential resources of shale oil is presented in Table 16.7.

Oil shales as a solid fuel should also be considered as deposits of gas, the so-called shale gas. The development of shale gas has a long and storied history. The first known shale gas production took place in the United States all the way back in 1821. Tom Ward and George Mitchell were among the first US innovators to scale up the development of shale gas. Shale gas is extracted from shale rock. Shale gas is mostly composed of methane. The total gas resources trapped within sedimentary rocks are not large. The main challenge is in accessing the in situ shale gas resources. Hydraulic fracturing (fracking) is the technology that is involved in shale gas development. The essence of hydraulic fracturing is in drilling a vertical well with a subsequent planned transition to a horizontal section of the well. The next stage is realized by
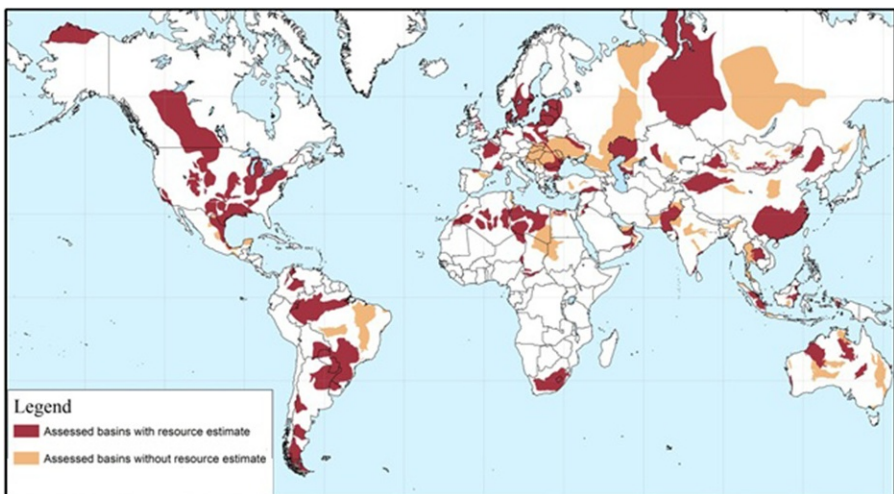
Fig. 16.4 Map showing distribution of oil shale deposits as of September 2015 (EIA, 2015).

employing an aqueous solution that is injected into shale rock under pressure of up to 1500 bar. This process fractures the rock formation, thereby releasing the natural gas. After hydraulic fracturing, operations are completed; a sand proppant is injected to prop open the fractures from which natural gas is harvested. In addition to shale gas, there is also shale oil to consider. However, shale gas can in fact become a force to be reckoned with in terms of tipping the energy balance of the world.

16.4   Methods of oil shale utilization

The following are the methods of development of oil shale deposits as a solid fuel. The choice of mining method is determined by the depth of the oil shale seam below the surface.

Opencast mining is a cost-effective and productive solution. It poses little or no hazard to miners. But opencast mining is environmentally destructive, leaving an indelible mark on the landscape.

Underground mining is more capital-intensive and poses a greater threat to personnel safety. Also, it is less disruptive to the environment. This mining method preserves the overburden in place. Nevertheless, hard-rock mine waste spoils accumulate on the ground surface during underground extraction, which are subject to wind and rain erosion.

Both the opencast and underground methods require massive amounts of capital and labor.

In situ development of most deposits is economically unviable, hence a greater focus of interest on geotechnological in situ processing using UCG or coking.

In utilizing existing mining methods, it is difficult to achieve increased productivity and lower the costs without damage to the environment.

Geotechnological mining techniques are commanding greater interest, as they do not involve bringing waste rock to the surface. Geotechnology is understood as a set of chemical, physicochemical, biochemical, and microbiological methods of in situ mining. Geotechnological methods have a number of advantages as compared with conventional mining methods, such as the following: Mining operations are conducted through wells; the working agent (heating agent and solvent) serves as the main means of mining; heavy work in a punishing environment is eliminated (process control is conducted from the ground); the processing of the natural resource is generally carried out in situ.

Geotechnological methods include borehole hydraulic mining, underground smelting, underground coal gasification, and distillation/sublimation, to name a few.

The use of oil shales mined in both opencast and underground operations envisions three major applications:

1. Electricity generation (combustion at thermal power plants).
2. Energy and processing (retorting to produce liquid and gaseous fuels for thermal power plants).
3. Thermal energy and chemical products (retorting with partial processing to produce chemical products and power plant feedstock).

In the 1970s and 1980s, 60% of oil shale was used as feedstock in power generation; however, oil shale as fuel has inherent disadvantages of low heating value and high ash content.

The processing of oil shale is based on its property to release when heated more high-grade liquid and gaseous products than any other fuel. Tar and gas are not only high calorific value fuels but also chemical feedstock for the manufacture of chemical products (ethyl alcohol, ammonia, chloroform, fuel oil, gasoline, kerosene, phenols, etc.).

Thermochemical reactions, which occur during heating of oil shale, have generally positive heat balance (starting with a certain initial heating temperature); as a result, increasing amounts of the initial product are involved in the reaction until it is consumed by it. The ratio of products of the reaction and their quality is determined not only by the composition of the original component but also by the conditions in which it underwent conversion. Thus, it is possible by changing the parameters of external influence to obtain final products that are different in proportion and quality.

Two basic types of oil shale processing technologies are distinguished: *gasification* (conversion of the organic constituents of solid or liquid fuel to liquid and gaseous hydrocarbons under high temperature and with an oxidizing agent (oxygen, air, water vapor, CO_2, or more often a mixture thereof)) and *retorting* (involves heating of solid particles of the fossil fuel without access to oxygen) using various methods (gasifiers, chamber and tunnel furnaces, and furnaces using a solid heat-transfer agent). For example, aboveground air-blown gasification of oil shales was carried out in Kohtla-Järve, Estonia, since 1948, producing domestic shale gas with a calorific value of 16,750 J/Nm3. Production of 1000 m^3 of gas required 3.29 tons of oil shale (Arens, 2001).

Along with household gas, oil shale processing plants in Estonia and the Leningrad Region produce liquid fuel, oil for coating wooden railroad ties, electrode coke, shale varnish, phenols, and other products. Mineral residue is utilized as an additive to agricultural fertilizers.

Gas desulfurization is performed using arsenic compounds. In employing this method, elemental sulfur and sodium thiosulfate are produced.

Along with implementation of opencast development methods, mastering in situ processing techniques of oil shale seams, fuel gas, and possibly liquid products may be of great practical importance.

Oil shale retorting is a thermochemical process of in situ conversion of oil shale to gaseous and liquid products.

Underground oil shale gasification relies on a number of processes that occur when an oxygen-containing injection agent is injected, with a high-temperature environment in the seam being maintained predominantly by exothermic reactions. The products of gasification are obtained thanks to the chemical reactions of oxygen in the injected air with the organic material in the oil shales.

In situ *retorting* involves a number of technological processes occurring within the deposit without access to air and with a chemically inert, hot heat-transfer agent injected into the seam ensuring that the temperature profile remains high; the hydrocarbons are primarily the products of pyrolysis and not of the chemical reaction of the organic material in the oil shale with oxygen.

In situ retorting is in essence quite similar to underground coal gasification.

However, significant dissimilarities exist between the two processes, which is a function of difference in chemical composition of coal and shale.

The geologic setting in the United States favors in situ thermal processing of oil shale (Rudina and Serebryakov, 1988). For example, the maximum thickness of the oil shale seam at the Piceance Creek basin in Colorado is 600 m, while in the Uinta Basin in Utah, the oil shale totals 300 m in thickness. The thickness of the most areally extensive and high-quality seams (with a laboratory measured tar yield of up to 11.4%) is greater than 60 m.

One of the most promising methods of in situ thermal processing of oil shale is the modified method. The essence of the modified in situ approach is using a combination of underground mining (20%–40% of the oil shale is processed using this ex situ technique) and explosive fracturing to effectively rubblize the remaining oil shale seam, thus forming an in situ retort for thermal processing of oil shale.

Occidental Petroleum Corporation made a major contribution to the development of in situ oil shale processing, conducting field trials in the Piceance Creek basin since 1972. Following these trials, industrial-grade technology for in situ oil shale processing technology was developed; however, the technology has not yet been applied at a commercial scale.

In situ oil shale retorts with a $60 \times 60 \times 10$ m cavity size were created at a depth of about 450 m. The thickness of the natural walls between adjacent retorts was 9–15 m. Processing was conducted successively in different retort groups. The in situ oil shale processing site is schematically presented in Fig. 16.5.
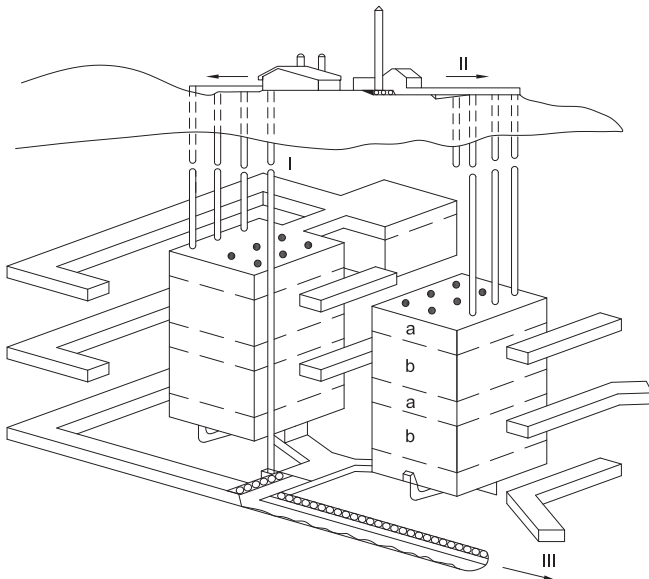
Fig. 16.5 Schematic representation of an in situ retorting site: I, gasifier gas; II, water vapor/air mixture; and III, tar/water condensate.

The initial stage of processing involves ignition of oil shale by injecting oil shale tar as fuel. After the temperature ramp-up to 480°C and with the start of thermal decomposition of kerogen, the injection of fuel from outside is stopped, and a mixture of air and water vapor is fed into the retort. The preponderance of heat required for thermal decomposition of oil shale derived from combustion of the residual carbon of the processed oil shale, while the rest from recirculation of the gas produced in the process. The advancement rate of the combustion front along the vertical direction is determined by the amount of air injected, averaging 0.3 m/day. The tar vapor migrates through the rubblized oil shale mass and condenses, with the condensate flowing down to the bottom part of the retort and is pumped to the surface. The gas rises to the surface via a separate pipe.

The oil shale that is brought to the surface is processed in aboveground processing facility. In addition to technological considerations, the ratio of oil shale processed in situ to aboveground is also determined by the quality of the oil shale: in A sections, the oil shale has a higher tar yield (up to 12.7%) than in B sections, where processing is planned to be conducted by the in situ method (tar yield below 10%).

In contrast with coal, oil shale has a higher ash content and the ashless organic part, while the ash-free components (kerogen) are two-thirds volatile hydrocarbons, so during gasification of oil shale, as it is heated, a very low proportion of the oil shale material participates in combustion proper (as coke-like residue), with the volatile matter being carried out with the gas. Moreover, oil shale contains a lot of bound (pyrogenic) moisture, which further reduces the combustion temperature.

16.5   Underground gasification of oil shale

Underground oil shale gasification is somewhere between underground coal gasification and the implementation of various enhanced oil recovery techniques during in situ burning of oil reservoirs.

The process flow of in situ oil shale gasification consists of the following stages:

- Precommissioning site activities (seam preparation work).
- Ignition of the oil shale seam.
- Gasification of the oil shale seam.
- Capture product gas and vaporous condensate.
- Treat products of gasification to the required levels.

First trials of in situ oil shale gasification and retorting were conducted as early as 1910 in the United States. In 1958–59, semicommercial trials of in situ gasification of Württemberg oil shale were conducted in Germany, similar to the experiments conducted by the Institute of Fossil Fuels of the Academy of Sciences of the USSR in the Baltic region. Due to the low oil shale quality containing a mere 3.5%–4.5% tar, a gas with a calorific value below 1930 kJ/Nm^3 was produced.

The energy crisis played a key role in spurring further development in this field in the United States since 1974. The scale of the activities does not go beyond semicommercial, since the cost of liquid fuel processed from oil shale still exceeds by far the cost of conventional crude oil. Since that time, an increase in the number of

applications (mainly in the United States) for various modifications of underground technology gasification has been recorded.

Royal Dutch Shell occupies a special place in the history of in situ oil shale development. Shell holds about 200 patents in the field of oil shale. However, information on experimental or commercial deployment of these patents on a wide scale is currently unavailable.

The development of in situ processing techniques for solid fuels amplifies the need for investigation of their properties that play a key role in the process of in situ processing, such as the following:

- Thickness of the seam
- Depth of the seam from the surface
- Ash content
- Sulfur content
- The presence and thickness of partings in the oil shale sequence

The movement of liquids and gases within the deposit has a significant impact on the management and control of in situ processing of solid fuels and its outcomes.

The study of solid fossil fuels intended for in situ processing should include the determination of their properties as a medium in which gases and liquids move. One of the most important properties of the medium through which gas or fluid flow is permeability, that is, the ability of a porous medium to transmit fluid and gas.

In the 1950s, studies of the in situ oil shale processing were conducted at the Kiviyli plant in Estonia by the Institute of Fossil Fuels of the Academy of Sciences (IFFAS) of the USSR. Experiments designed to investigate heating of a solid block of oil shale in conditions closely approximating nature preceded the industrial experiments in in situ oil shale processing conducted at the Kiviyli oil shale processing plant.

The first experimental study of oil shale permeability, which is a most important property characterizing the suitability of the resource for in situ processing, was the study that demonstrated that on heating oil shale to 200–400°C, a dramatic increase was noted in the permeability of kukersite shale samples.

Once the temperature of 500°C is reached, the permeability of the oil shale samples in the direction parallel to the bedding plane increases by thousands of times.

One distinctive feature of the in situ processing of solid fuels is their nonstationary nature. Over time, the temperature at a given point within the deposit is subject to change, and with it, changes in the composition will occur as well: both the structure of the material and its permeability.

Experimental studies are needed to obtain data on the changes in permeability of the deposit material relative to its temperature. Pursuant to that objective, the Institute of Fossil Fuels of the Academy of Sciences of the USSR carried out research on the permeability of the kukersite shales.

Proceeding from the Leybenzon equation, for the weight flow rate of gas in a steady-state one-dimensional gas flow and under isothermal conditions, the following expression is obtained for determining the permeability coefficient of the sample:

$$K = \frac{\mu Q L}{F(P_1 - P_2)}$$

where μ is the viscosity coefficient of gas (centipoise); Q is volumetric flow rate of gas (cm^3/s), corrected to the average pressure $\overline{P} = \frac{P_1 + P_2}{2}$; L is the length of the sample (cm); F is the area of its cross section (cm^2); absolute pressure P_1 at the inlet and P_2 outlet end faces of the sample (bar); and K is the permeability coefficient (darcy).

The above formula is valid only in cases when the conditions for the existence of a linear filtration law are met.

For purposes of experimental determination of the permeability of oil shale samples, nitrogen was used. Knowing the temperature at which the experiment was conducted, the dynamic viscosity of nitrogen is easily obtained from the corresponding reference tables.

Oil shale samples of cylindrical shape were used; the length of the sample (L) and the area of the cross section (F) were determined by measuring the dimensions of the sample.

The oil shale sample was prepared and secured in a cylindrical cartridge with an internal diameter slightly larger than the diameter of the sample. The annular gap between the lateral surface of the sample and the inner walls of the cartridge was filled with Wood's alloy, as shown in Fig. 16.6.

To determine the permeability of the sample, it was necessary to measure the gas flow during the experiment at a given pressure drop.

The schematic representation of the gas permeability testing apparatus is shown in Fig. 16.7. Nitrogen was passed from the cylinder to the buffer tank through a pressure reducer. The cartridge with the sample was clamped onto the frame of the permeability testing apparatus, and nitrogen was passed through the sample from the buffer tank. Nitrogen was then collected in a vessel, displacing water into a graduated cylinder. Atmospheric pressure was maintained inside the vessel throughout. The pressure in front of the sample was measured with a test gauge. At each pressure drop, the flow rate of the passing nitrogen was measured again. In order to gain an understanding of the gas flow patterns within the sample and its consistency with the linear law of filtration, the nitrogen flow was measured at different values of the pressure differential. The barometric pressure was measured by a mercury barometer.
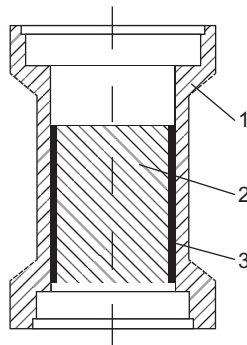
Fig. 16.6 Schematic diagram of the sample setup in the cartridge: 1, cartridge; 2, sample; and 3, Wood's alloy.
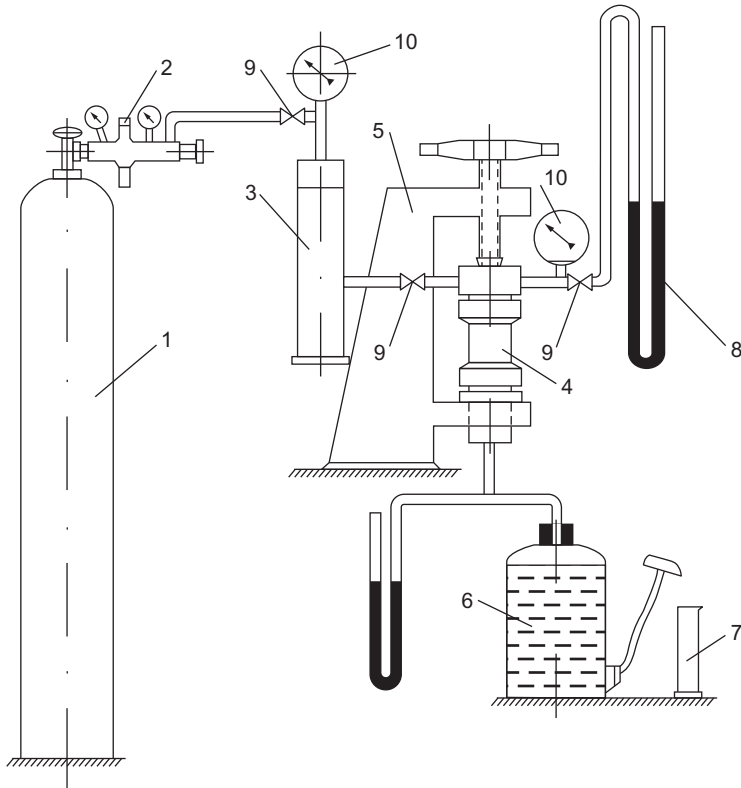
Fig. 16.7 Schematic diagram of the gas permeability rig for oil shale samples. 1, compressed gas cylinder; 2, pressure reducer; 3, buffer tank; 4, cartridge; 5, rig frame; 6, vessel filled with water; 7, graduated cylinder; 8, gauges; 9, needle valves; and 10, spring pressure gauges.

Based on the actual data obtained in the experiment, cross correlation diagrams were generated to evaluate the relationships between the pressure gradients (bar/cm) and filtration rates (cm^3/s cm^2), with average permeability values of the samples calculated $\frac{P_1+P_2}{L}\overline{q}$. The kukersite shales from the Estonian deposit were used for the study.

Table 16.8 summarizes oil shale quality data adapted from V.V. Levykin (air-dried basis).

The specific gravity of kukersite oil shale ranges from 1.30 to 1.80, while the specific gravity of the kerogen of oil shale is a little over 1.0 (1.08) (Table 16.9).

The data on Estonian kukersite oil shales discussed above support the conclusion that the deposits are nonuniform, which is manifested in fluctuations in the organic matter content in different seams, which is also manifested in fluctuations in their specific gravity values. Fig. 16.8 shows the correlation between the total ash content of oil shales and their specific gravity (data sourced from Table 16.8).

Table 16.8 **Oil shale quality data adapted from V.V. Levykin**

Seam	Specific gravity	Mineral ash, %	CO_2, %	Sulfur, %	Fischer assay oil yield from organic matter
A	1.53	40.7	10.6	0.7	55
B	1.5	37.9	13.4	1.5	69
C	1.5	44.9	10.4	0.6	66
D	1.66	54.0	12.8	0.4	56
E	1.34	30.4	8.4	0.8	66
F	1.5	37.9	11.7	0.5	66

Table 16.9 **Average composition of kukersite shale adapted from data provided by P. Kogerman**

Kukersite shale	Water, %	Ash, %	CO_2, %	Ash+ CO_2, %	Organic matter, %	Calorific value, kcal/kg
Freshly mined	18.2	30.0	7.9	37.9	49.9	3000–3500
Air-dried	1.5	36.1	9.5	45.6	52.9	4200–4500

Fig. 16.8 Density of kukersite oil shale relative to their total ash content. *A* is total sulfur content; γ is density, g/cm^3.
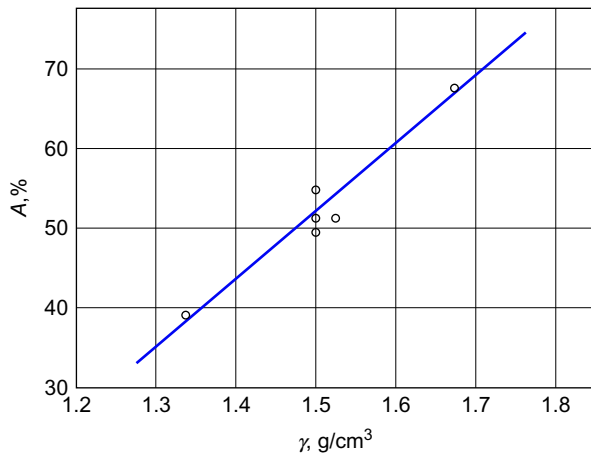
The presence of concretions and partings of bituminized limestone has a considerable impact on the total ash content of each specific oil shale sample.

Therefore, the ash content of oil shale and its specific gravity in some samples may exceed the values indicated in Table 16.8.

Oil shale samples for testing were selected at the mine by the staff of the Kiviyli oil shale processing plant, crated and shipped to Moscow. A few samples at a time were molded into a cylindrical shape, 35–46 mm in diameter and 15–47 mm long.

In one sample, the axis of the cylinder was parallel, in the other, perpendicular to the bedding plane.

Given the complexity and heterogeneity of oil shale, even from the same piece, samples may turn out different in terms of inclusions and partings of limestone.

Comparing permeability values of each seam in different directions can clearly be done using samples that are similar in limestone content, which can be indirectly inferred from their bulk density values.

Table 16.10 contains the results of permeability testing of two oil shale samples from seam F.

The data obtained from the permeability testing sequence of the samples are presented in Figs. 16.9–16.12.

The diagrams show that within the limits of the pressure gradients, the flow of nitrogen through the oil shale samples obeys the linear law of filtration.

The deviation from the average value of the permeability coefficient in parallel testing is ~4%.

The values obtained are consistent with to the lower limit of permeability of the oil shale material in the deposit.

The results of permeability testing of oil shale samples from different seams in the direction parallel to the bedding plane are summarized in Table 16.11.

Table 16.12 contains the results of permeability testing of oil shale samples from the same seam but in the direction perpendicular to the bedding plane.

The permeability values of the samples vary between different seams. This is likely attributable to the heterogeneity of specific oil shale seams both in organic matter content and in the degree of dilution by concretions and partings of limestone, which also affects the fluctuations of density.

The data contained in Tables 16.4 and 16.5 show that the permeability of dried samples is higher than the permeability of air-dried samples. It should also be noted that the permeability of oil shale samples with a higher bulk density, that is, with a higher limestone content, has lower values, while the permeability values are higher in samples with a lower bulk density.

For in situ processing, ascertaining the changes in the permeability of oil shale is of importance relative to the degree of thermal stress.

On heating oil shale, the volatiles are released, which is associated with changes in its physical state. During retorting, the pore size increases, with fractures likely developing in the oil shale formation.

These factors should lead to increased permeability as the temperature of oil shale processing rises.

To determine the correlation between variations in permeability of oil shale relative to the degree of thermal stress, a series of tests on various oil shale samples were undertaken using the following procedure. After determining the permeability of the oil shale sample that was dried at 100°C, the latter was removed from the cartridge and placed in a crucible furnace capped with a lid.

Table 16.10 Results of permeability measurements on oil shale samples from seam F

Test no.	Date	No.	Oil shale sample		Weight, g	Direction of the cylindrical sample axis relative to bedding orientation	Permeability, millidarcy	
			Dimensions, mm				Test results	Mean values
			Diameter	Length				
9	16.03.1948	1	40	24	49.35	Perpendicular	0.0571	0.0594
10	16.03.1948	1	40	24	49.35		0.0616	
7	16.03.1948	2	35	43	79.1	Parallel	0.148	0.142
8	16.03.1948	2	35	43	79.1		0.137	
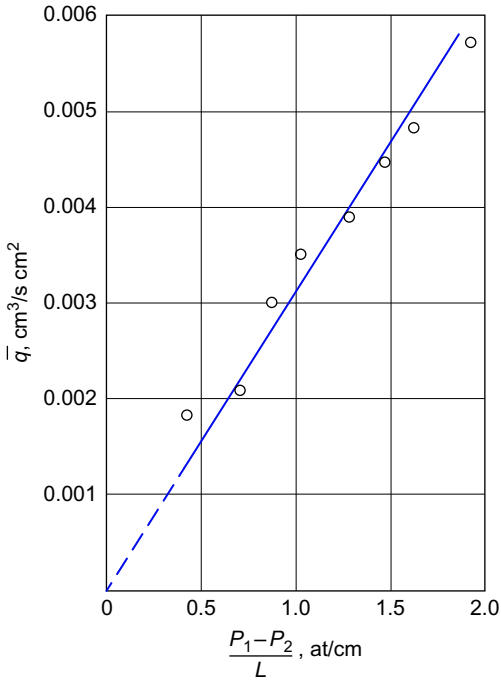
Fig. 16.9 Correlation between the filtration rate and pressure gradient in oil shale seam F (perpendicular to the bedding plane). Trial 9.
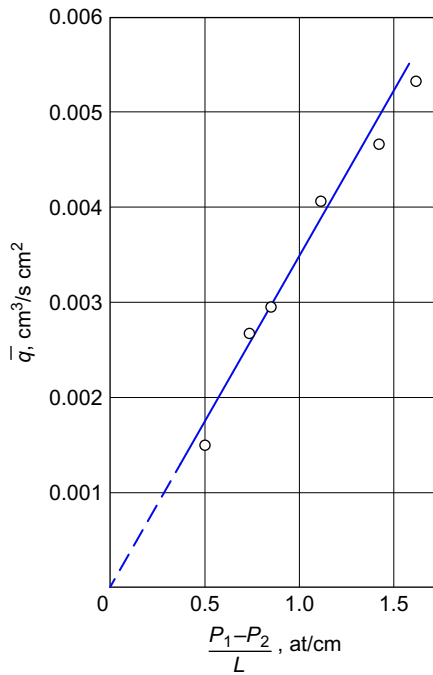
Fig. 16.10 Correlation between the filtration rate and pressure gradient in oil shale seam F (perpendicular to the bedding plane). Trial 10.

Fig. 16.11 Correlation between the filtration rate and pressure gradient in oil shale seam F (parallel to the bedding plane). Trial 7.
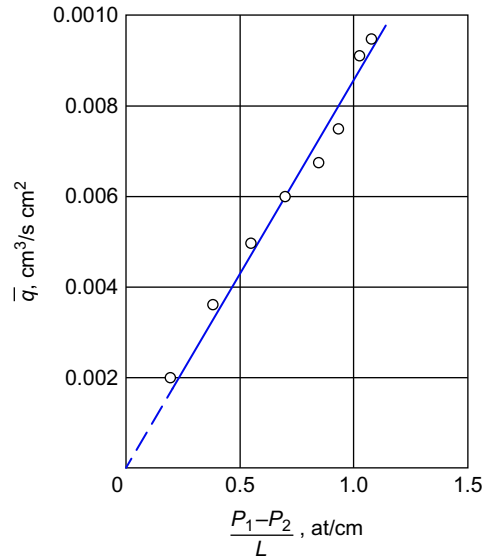
Fig. 16.12 Correlation between the filtration rate and pressure gradient in oil shale seam F (parallel to the bedding plane). Trial 8.
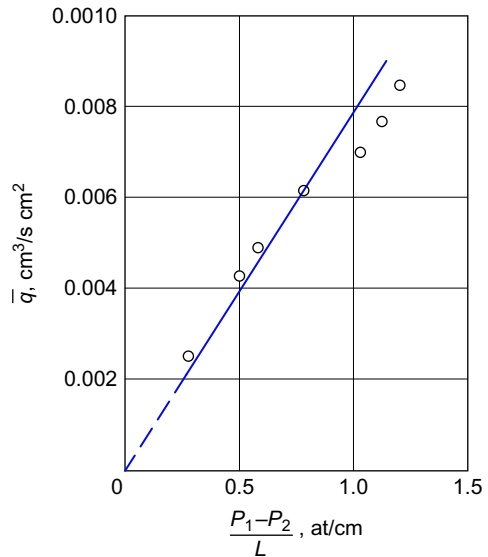
The temperature ramp-up rate in the furnace was constant during all the tests at 5 degrees/min. The samples were left at the same temperature for 4 h. Initially, the samples were heated and kept at a temperature of 200°C. The cooled sample was then sealed inside the cartridge, and its permeability was measured. The sample was placed in the furnace a second time, heated, and kept at a temperature of 300°C; the

Table 16.11 **The results of permeability testing of oil shale samples from different seams in the direction parallel to the bedding plane**

| Seam | Permeability, millidarcy | | Density, g/см^3 |
	Air-dried	After being dried in a dessicator	
B	–	2.99	1.36
C	0.055	0.187	2.19
D	0.0228	–	1.70
E	–	0.337	1.26
F	0.00707	0.0125	2.26
G	0.109	0.152	1.96

Table 16.12 **The results of permeability testing of oil shale samples from the same seam but in the direction perpendicular to the bedding plane**

| Seam | Permeability, millidarcy | | Density, g/см^3 |
	Air-dried	After being dried in a dessicator	
B	0.0269	0.0395	1.24
C	0.0103	0.0111	2.32
D	0.0113	–	1.65
E	–	0.0498	1.23
F	0.0035	0.00533	2.32
G	0.0397	–	1.84

permeability of the cooled sample was again measured. Thus, the permeability was determined of a sample successively heated to temperatures of 100, 200, 300, 400, 500, and 600°C.

The results of permeability testing of oil shale samples from different seams are shown in Figs. 16.13–16.17.

These graphs show the variations in permeability of the oil shale samples on increasing their preheating temperature.

In those cases where a change in permeability occurred within a significant range, the graphs show a change in the logarithm of the coefficient of permeability of the oil shale samples.

For better clarity, in Table 16.13 the changes in permeability of oil shale with temperature of processing are presented relative to the permeability of the dried samples. The data contained in Table 16.13 show that the permeability of air-dried oil shale samples is, on average, two times less than the permeability in the dried samples.

Heating the shale to 200°C generally leads to an increase in permeability by multiples of times. Further heating is accompanied by an even greater increase in
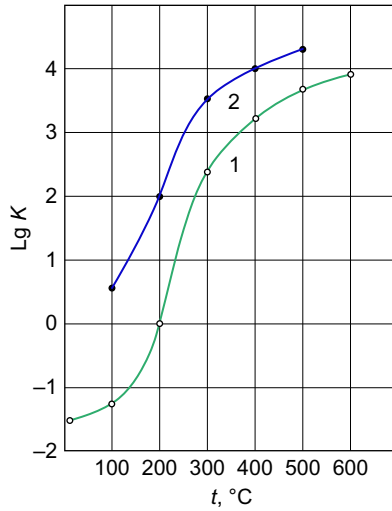
Fig. 16.13 Seam B. *K*, permeability, millidarcy; 1, perpendicular to the bedding plane; 2, parallel to the bedding plane.
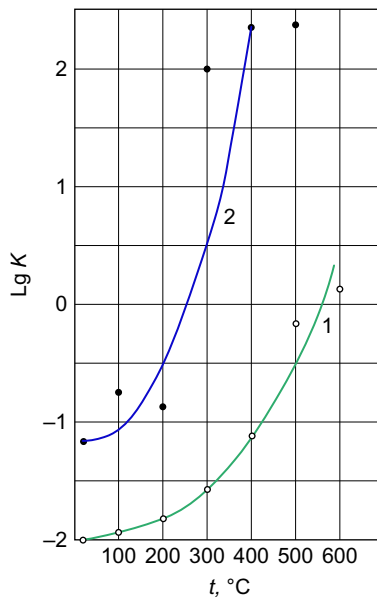
Fig. 16.14 Seam C. *K*, permeability, millidarcy; 1, perpendicular to the bedding plane; 2, parallel to the bedding plane.
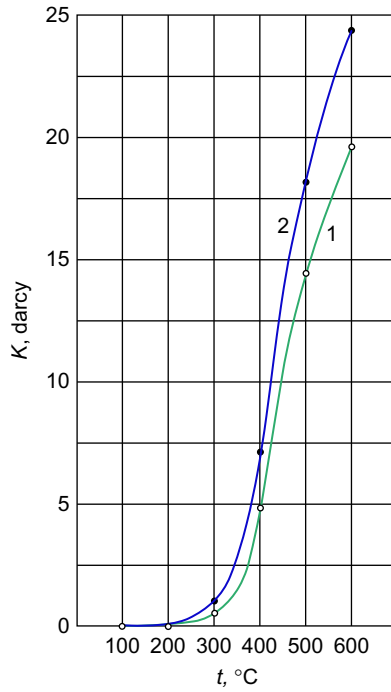
Fig. 16.15 Seam E. *K*, permeability, millidarcy; 1, perpendicular to the bedding plane; 2, parallel to the bedding plane.
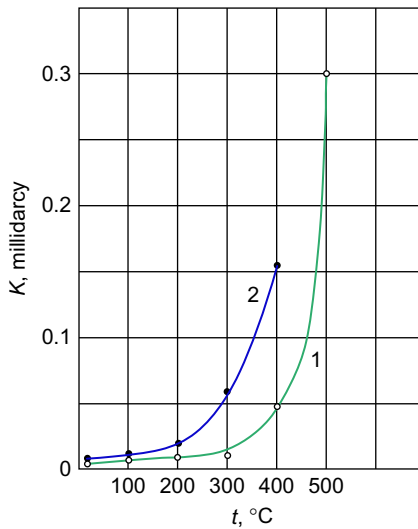
Fig. 16.16 Seam F. *K*, permeability, millidarcy; 1, perpendicular to the bedding plane; 2, parallel to the bedding plane.
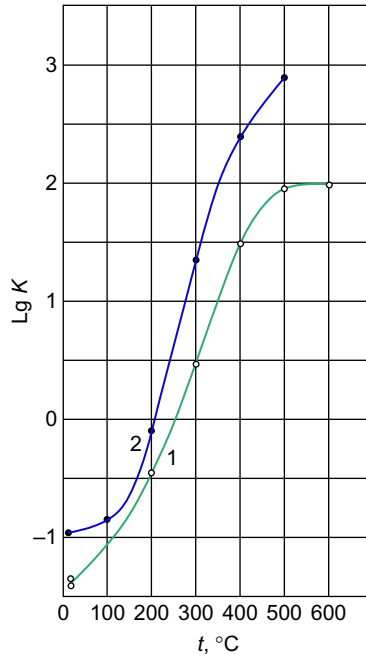
Fig. 16.17 Seam G. *K*, permeability, millidarcy; 1, perpendicular to the bedding plane; 2, parallel to the bedding plane.

permeability. Heating oil shale samples to higher temperatures caused fractures to occur, which greatly increased their permeability. Fractures formed both along and perpendicular to the bedding planes, frequently along the boundaries separating the veins of limestone concretions from the oil shale.

The absolute permeability value of samples of dried shale is quite small at a mere few hundredths or a few tenths of a millidarcy.

However, on heating, the permeability of the samples increases by hundreds and thousands of times, which is explained by fracturing.

Table 16.14 presents data on the correlation of permeability coefficients measured in directions parallel and perpendicular to the bedding planes in oil shale samples from different seams that were subjected to preheating.

As can be seen from the table, that permeability of oil shale samples in the direction of the bedding plane is much higher than in the direction perpendicular to the bedding plane.

When oil shale samples are heated, the correlation of these two types of permeability tends to increase initially, which indicates that when the samples are heated, fractures form primarily along the bedding.

With a further increase in the heating temperature of the oil shale samples, this cross correlation decreases. The development of fracturing at high temperatures appears to occur intensively in the direction perpendicular to the bedding plane.

Table 16.13 **Permeability of samples**

| Preheating temperature, °C | Permeability of different shale seams | | | | | | | | | |
| | B | | C | | E | | F | | G | |
	Perpendicular to the bedding plane	Parallel to the bedding plane	Perpendicular to the bedding plane	Parallel to the bedding plane	Perpendicular to the bedding plane	Parallel to the bedding plane	Perpendicular to the bedding plane	Parallel to the bedding plane	Perpendicular to the bedding plane	Parallel to the bedding plane
Air-dried	0.7	–	0.9	0.3	–	–	0.6	0.5	0.2	0.7
100	1.0	1.0	1.0	1.0	1.0	1.0	1.0	1.0	1.0	1.0
200	24.8	32.2	1.3	0.7	4.2	119	2.2	1.6	1.8	4.4
300	6200	1350	2.2	506	11,200	2830	1.7	3.9	14.5	140
400	44,000	3790	5.5	1240	95,000	19,800	7.6	10.8	153	1375
500	122,000	7860	68.8	1350	277,000	54,000	48.7	–	449	4460
600	20,800	–	111.0	–	393,000	72,000	–	–	472	–
Density, g/см^3	1.3	1.4	2.3	2.2	1.2	1.3	2.3	2.3	1.8	2.0

Table 16.14 Permeability of samples that were subjected to preheating

Preheating temperature, °C	Correlation of permeability coefficients measured in directions parallel and perpendicular to the bedding plane				
	B	**C**	**E**	**F**	**G**
Air-dried	–	5.3	–	2.0	2.5
100	75.0	16.8	6.8	2.3	–
200	98.3	10.0	190	1.7	2.0
300	16.6	3830	1.7	5.3	7.6
400	6.5	3820	1.4	3.3	7.1
500	4.8	3310	1.3	–	7.8
600	–	–	1.2	–	–

The information presented above supports the following conclusions (Pitin, 1957):

1. Experimental permeability testing of oil shale samples from different seams in air-dried and dried conditions showed that permeability values vary within 0.0035–3.0 md, depending mainly on the correlation of the oil shale and limestone components in the samples. The permeability of the dried samples was approximately twice the permeability of the air-dried samples.

   The correlation between the experimentally measured permeability of a number of oil shale samples and the temperature of their preheating shows that heating the oil shale samples to 200°C leads to an increase in their permeability by multiples of times in comparison with the permeability of the same samples when dried.

2. Further heating of the oil shale leads to a much sharper increase in permeability, which is due to fractures forming in the samples.

3. Comparison of the permeability of oil shale samples, measured both parallel and perpendicular to the bedding plane, shows that permeability is several times greater in the direction along the bedding plane. When the oil shale samples are heated, the correlation of their permeability parallel and perpendicular to the bedding plane initially increases; with further increase in temperature, this correlation decreases.

Laboratory modeling studies have demonstrated the feasibility of operating in situ processing of oil shale, specifically using modes of operation with and without air injection. This made it possible to conduct an experimental study of the process of in situ gasification of oil shale using an experimental installation. Theoretical investigations and experimental studies of in situ gasification of oil shale made it possible to establish in principle the feasibility of organizing an in-situ process of oil shale processing.

Subsequently, the Institute of Fossil Fuels of the Academy of Sciences of the USSR along with the Research Institute of the Ministry of Oil Shale Industry of the Estonian Republic designed a pilot plant (panel) to study in situ processing of oil shale. The construction and installation of this pilot plant were carried out by the Kiviyli oil shale processing plant.

16.5.1 Pilot panel BSH-1. (Pitin et al., 1957)

The oil shale-bearing sequence of the Kiviyli mine, where the pilot plant was located, is divided into two units of oil shale consisting of eight closely spaced oil shale seams interbedded with partings of limestone. The lower commercial unit consists of oil shale seams (counting from the bottom up) A, B, C, D, E, and F, with partings of limestone. The upper unit consists of oil shale seams G and H and is separated from the lower unit by a layer of limestone.

The section of the pilot panel was intersected by 56 vertical wells, of which 19 were process wells (injection and production), 16 ventilation wells ("ventilation ring"), and 21 natural ventilation wells.

Process wells, 270 mm in diameter, were drilled from the ground surface to the floor of the lower oil shale seam (seam A). The wells were cased with 150 mm pipe down to the roof of seam F, that is, to the top of the commercial oil shale unit. At the lower ends of the casing pipes were welded flanges (shells), which prevented the cement slurry from swamping into the well.

Cementing was initially done with a thin layer of clay, which prevented the cement slurry from leaking, and then with a special mixture of cement slurry and fireclay powder (Fig. 16.18). A flange was welded on top of the casing to accommodate a four-way fitting that connected the casing pipe with the injection and suction manifolds.

The process well design ensured sufficient integrity during subsequent cold testing and "hot" dry runs.

Fig. 16.18 shows cross sections of the ventilation wells.

The 19 process wells were distributed on a triangular grid. The wells were drilled as shown in Fig. 16.19.

The distance between the wells in each row and between the rows of wells was 2 m. This relatively short distance was due to the fact that the tests were the first of their kind in an oil shale block while there were not yet enough data available on its properties.

The wells were drilled on an area of $\sim$50 m^2 with a total oil shale resource in a commercial unit of about 200 tons. The well design of each of the 19 process wells permitted alternating pressurization or venting at the wellhead, the amount of which was determined by the parameters of the injection and suction machines and the hydrodynamic properties of the pilot site.

Air was injected into the wells using a compressor with a maximum CFM of 600 nm^3/h at a pressure of 6 bar.

An RMK-4 vacuum pump was used to draw off at the rate of up to 1200 nm^3/h. The RMK-4 pump was installed so that it can operate as a vacuum pump and a blower with a pressure of up to 250 mm Hg.

Two pipelines connected the panel with the blowers that injected air and drew off gas or air. The surface pipework is permitted injecting air into or drawing off gas from each of the wells. Each well was isolated from the manifolds by two valves. Both pipelines terminated in flares equipped with valves. The ends of the panel manifolds were fitted with special explosive valves. Isolation valves were installed on the main pipelines for general regulation of the air injection or gas production. A receiver was
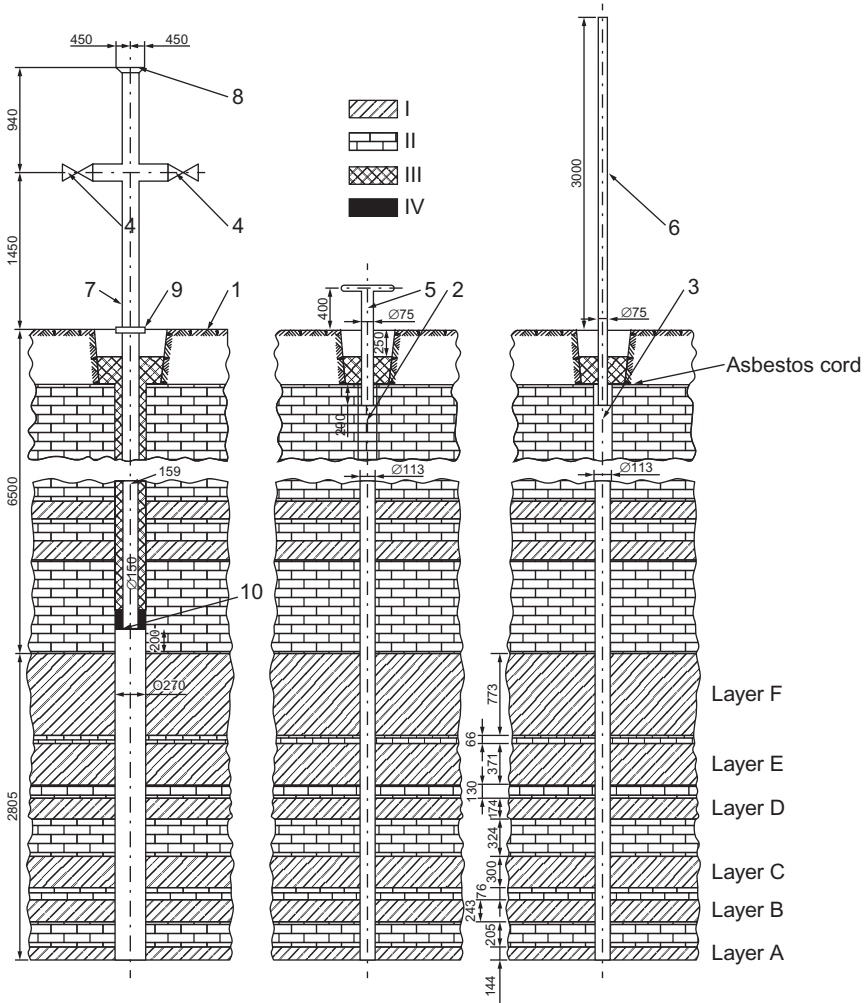
Fig. 16.18 Cross section (by process wells) of the Kiviyli oil shale formation: I, shale; II, limestone; III, cementing; and IV, clay. 1, process well; 2, "ventilation ring" well; 3, natural ventilation well; 4, process well valve; 5, "ventilation ring" pipeline; 6, natural ventilation well pipeline; 7, casing; 8, top flange of casing; 9, membrane; and 10, flange (shell ring).

installed on the process air pipe. A dilator filter was installed on the main gas pipeline to remove dust and tars. Two refrigeration units were set up on the production line to condense the tar.

The pilot panel was constructed 85 m from the operating Kiviyli mine and only 35 m from Gangway 13 of site V.

Concern was raised over the possibility of gas penetrating into the active parts of the mine. Preventive measures were put in place, including installing two rows of
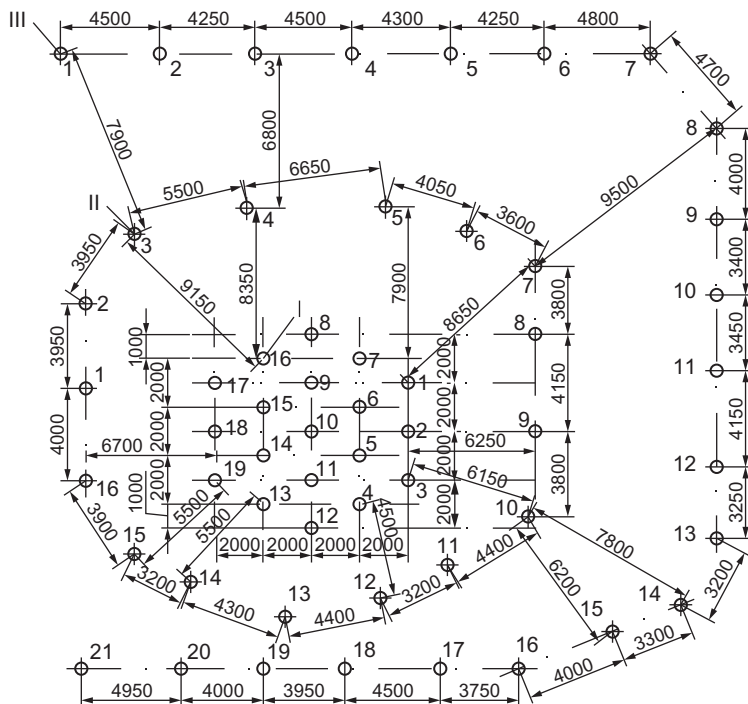
Fig. 16.19 Plan of pilot panel BSH-1: I, process wells (1–19); II, "ventilation ring" wells; and III, natural ventilation wells.

wells to separate the panel from the mine. Of these, 16 wells, 113 mm in diameter, circled the panel casings of these wells that were connected by a common pipeline equipped with a suction exhaust fan, resulting in a suction "ventilation ring" (Figs. 16.20–16.23).

Each well was fitted with a throttle valve. Adjustment of vacuum on the "ventricle" could be carried out by a latch installed on the bypass of the fan exhauster.

Another group of 21 wells, 113 mm in diameter, were drilled around the "ventilation ring," spaced 3.5–4.0 m, with pipes inserted into the wells and protruding 3 m above the ground surface. These wells were also designed to prevent the penetration of gas into the nearby mine and were serving as natural ventilation of the oil shale block.

In order to ensure site safety, an automatic shutoff switch was installed, which was designed to switch off the compressor motor and cut the air to the panel in the event of the exhaust fan or the RMK-4 stopped for any reason.

To measure the total amount of air/gas injected and drawn off, disk diaphragms were installed on the main pipelines, one after the receiver on the process air line and one before the PMK-4 pump on the production line. Pressure and pressure differentials, as well as temperature, were measured with the help of U-shaped water and mercury gauges.
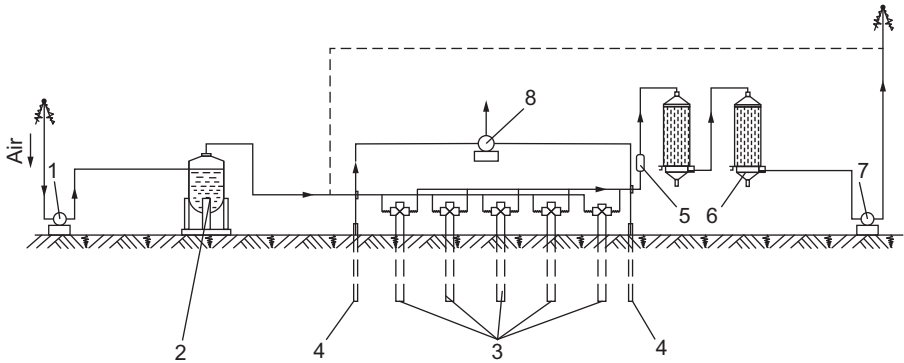
Fig. 16.20 Process scheme of underground gasification pilot panel of Estonian shales: 1, air compressor; 2, air receiver; 3, process wells; 4, "ventilation ring" wells; 5, filter; 6, refrigeration units; 7, RMK-4 vacuum pump; and 8, fan exhauster.
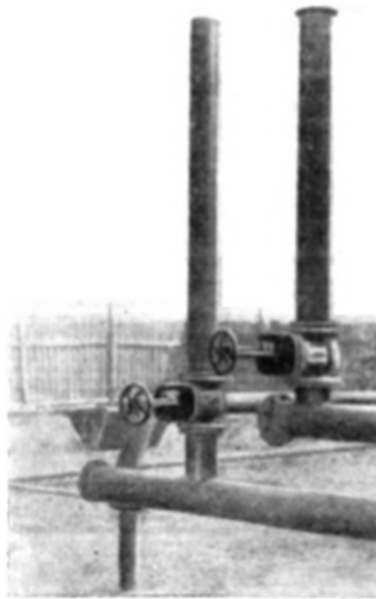
Fig. 16.21 Blowdown pipe.

During cold testing, the air flow (injected or drawn off) was measured on each well. Diaphragms were installed on the vertical section between the casing and the four-way fitting. At the wellhead of each well, the pressure (depressurization) was measured by U-shaped gauges.

Temperature in the wells was measured using alumel-chromel thermocouples, 1.5 m long, which were lowered into the wells through the top cover on the
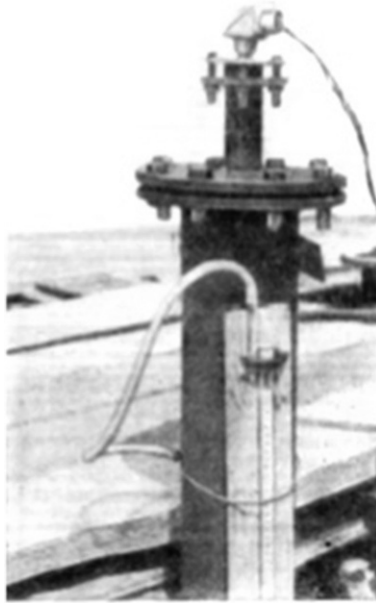
Fig. 16.22 Wellhead.
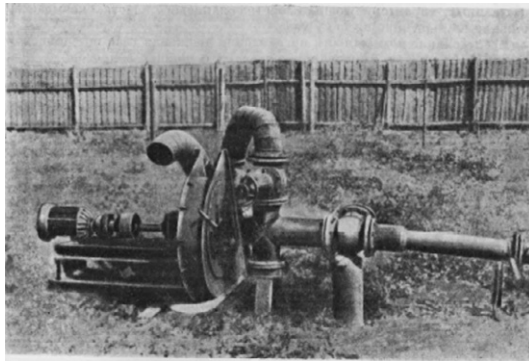
Fig. 16.23 Fan exhauster.

four-way fitting. Using 9-m-long alumel-chromel thermocouples, periodic temperature measurements were made at the bottom of some wells.

Adjacent to the panel in a special booth, 45 mW galvanometers with switches were installed.

At each well of the ventilation ring, U-shaped gauges were installed to measure depressurization.

16.5.2 Cold testing

Cold testing involved obtaining experimental data to characterize the properties of the oil shale seam, which affect the movement of gas within the seam.

The investigation of the feasibility of gas movement through the oil shale seam was aimed at elucidating the following main issues:

1. Determine effective permeability of the oil shale-bearing sequence intersected by experimental wells.
2. Develop and test measures of hydrodynamic fencing off of the pilot site to prevent penetration of gases beyond the pilot site.

The cold testing undertaken was designed to answer these fundamental questions:

1. *Determine effective permeability of the oil shale-bearing sequence (commercial multilayer units) of the pilot site.*

Effective permeability of the commercial unit had to be determined based on test results in order to be able to assess the productivity of air injection, the energy costs to create gas flow streams within the oil shale formation, and the direction of their propagation.

16.5.2.1 Methodology

The general procedure to determine the average effective permeability coefficients of the oil shale seam entails the following. Two wells are prepared which intersect the seam by b cm.

Let us assume that r_1 and r_2 are the radii of the first and second well and S is the distance between the wells.

Gas is injected into the first well and it is produced from the second well, with the weight flow rates of the first and second well per 1 cm of oil shale seam thickness equal to Q_1 and Q_2 kg/s, respectively.

The absolute pressures at the bottom of the first and second well are P_1 and P_2 kg/cm^2.

The boundary of the oil shale seam is located at a distance of R cm; the pressure at the boundary contour is constant and equal to $P_K = 1$ bar.

Supposing that $P_1 > P_2$ and $P_1 > P_K$, then $Q_1 < 0$, that is, the first well, is the source through which gas is injected into the seam.

The ratio of flow rate Q_2 to the absolute value of injection rate Q_1 characterizes the gas leakage into the seam:

$$\varphi = \frac{Q_2}{|Q_1|} = \left| \frac{\left(P_1^2 - 1\right) \ln \dfrac{R}{S} - \left(P_2^2 - 1\right) \ln \dfrac{R}{r_1}}{\left(P_1^2 - 1\right) \ln \dfrac{R}{r_2} - \left(P_2^2 - 1\right) \ln \dfrac{R}{S}} \right| \tag{16.1}$$

From this expression, we define the radius of boundary contour R:

$$\lg R = \frac{\varphi\left(P_1^2 - 1\right) \lg r_2 - \left(P_1^2 - 1\right) \lg S - \varphi\left(P_2^2 - 1\right) \lg S + \left(P_2^2 - 1\right) \lg r_1}{(1 - \varphi)\left(P_2^2 - P_1^2\right)} \tag{16.2}$$

Having defined the value of the radius of the boundary contour of the seam, the permeability value can be determined, for which we will use the expression for the well yield:

$$Q_1 = -\pi \frac{K\gamma_0}{\mu P_0} \frac{(P_1^2 - 1) \ln \frac{R}{r_2} - (P_2^2 - 1) \ln \frac{R}{S}}{\ln \frac{R}{r_1} \ln \frac{R}{r_2} - \ln^2 \frac{R}{S}} \tag{16.3}$$

$$Q_2 = \pi \frac{K\gamma_0}{\mu P_0} \frac{(P_1^2 - 1) \ln \frac{R}{S} - (P_2^2 - 1) \ln \frac{R}{r_1}}{\ln \frac{R}{r_1} \ln \frac{R}{r_2} - \ln^2 \frac{R}{S}} \tag{16.4}$$

where K is permeability coefficient (darcy); Y_0 is the weight of 1 cm^3 of gas (kg) at a pressure of P_0, 1 bar; and μ is the viscosity of gas (centipoise).

If we denote

$$\frac{Q_1}{\gamma_0} = q_1; \quad \frac{Q_2}{\gamma_0} = q_2 \tag{16.5}$$

where q is the volumetric flow rate of gas (cm^3/s) corrected to atmospheric pressure, per 1 cm of seam thickness, and using the absolute value of the flow rate (yield) in the first well

$$\frac{|Q_1|}{\gamma_0} = |q_1| \tag{16.6}$$

then from Eqs. (16.3), (16.4), we obtain expressions for determining the average effective permeability coefficient:

$$K = \frac{|q_1|\mu}{\pi} \frac{\ln \frac{R}{r_1} \ln \frac{R}{r_2} - \ln^2 \frac{R}{S}}{(P_1^2 - 1) \ln \frac{R}{S} - (P_2^2 - 1) \ln \frac{R}{r_1}} \tag{16.7}$$

$$K = \frac{q_2\mu}{\pi} \frac{\ln \frac{R}{r_1} \ln \frac{R}{r_2} - \ln^2 \frac{R}{S}}{(P_1^2 - 1) \ln \frac{R}{S} - (P_2^2 - 1) \ln \frac{R}{r_1}} \tag{16.8}$$

The value of the permeability coefficient obtained from formulas (16.7) and (16.8) characterizes the average effective permeability of the seam in the section between the two wells under consideration.

16.5.2.2   Testing results

During cold testing, air was injected into one well and produced from another. Once steady-state gas flow through the oil shale was reached, the flow rate of air passing through the first and second wells was measured as well as the pressure at the well-heads of these wells. This testing was conducted using 18 pairs of wells. The results of the testing are shown in Table 16.15.

The average value of the radius of the boundary contour of the seam was shown to be very small, which is fully consistent with the high average value of the effective permeability of the commercial unit of the oil shale-bearing sequence. The values of the calculated average effective permeability values turned out to be of the same order of magnitude.

Experimental data on flow rate and pressure measurements support the claim that creating a gas flow through an oil shale seam does not require the application of excessively large pressure gradients and that the steady-state gas flow through the seam occurs quite soon after the beginning of the test.

Comparison of the average coefficients of effective permeability of the commercial unit with the data on the permeability of oil shale in a single sample shows that the average effective permeability of the seam is many times greater than the permeability of a single piece (compared with the above results of oil shale testing for gas permeability after exposure to high temperature).

This can be explained by the presence of fracturing in an oil shale seam, which cannot be detected by examining a single piece of oil shale. The conclusion as to the presence of fractures in the commercial unit of the oil shale sequence, which can be drawn from comparison of the average effective permeability values of the oil shale seam and the permeability of a single piece of oil shale, is supported by the data of a geologic survey of the Kiviyli mine field conducted previously.

Comparison was attempted of the effective permeability values with the direction of the strike of the oil shale-bearing sequence.

Fig. 16.24 shows the calculated average effective permeability coefficients, plotted to scale, each according to its direction, based on tests nos. 4, 6, 10, 14, 16, and 18.

The diagram in Fig. 16.24 provides a visual representation of the principal directions of dispersal of the injected air in the commercial unit, which will clearly correspond to the directions that showed a high value of the average effective permeability during testing. It should be noted that the two predominant pathways of air migration were within the limits of the prevailing two main directions of vertical fracturing: northeasterly (40°–80°) and northwesterly (300°–350°) strikes. Data from other experiments in this series are also consistent with the claim stated above.

16.5.3   Develop and test measures for hydraulic fencing off of the pilot site

The results of determining the average effective permeability coefficient show that the commercial oil shale unit does not have a high gas flow resistance.

Table 16.15 **Results of testing**

Test	Mode of operation		Distance between wells, S, m	Wellhead pressure		Flow rate		Casing radius t, m	Radius of the boundary contour of the seam	K, darcy
	Injection	Production		Injection P_1, mm of mercury	Production P_2, mm of mercury	Injection Q_1, m³/h	Production Q_2, m³/h			
1	12	11	2.0	276	55.0	732	101.0	0.135	3.2	12.9
2	12	10	4.0	240	77.0	782	117.0	0.135	8.0	20.6
3	12	9	6.0	228	13.0	791	48.7	0.135	8.05	22.6
4	12	8	8.0	223	16.0	788	55.0	0.135	11.4	25.4
5	18	10	4.0	208	27.0	795	70.0	0.135	5.7	22.9
6	18	2	8.0	206	10.5	796	44.0	0.135	9.9	26.9
7	3	5	2.23	295	14.0	824	161.0	0.135	5.0	14.9
8	3	10	4.47	306.7	90.0	814.5	129.0	0.135	9.6	16.9
9	3	15	6.7	317.5	10.0	821.6	43.0	0.135	8.25	16.2
10	3	17	8.94	326	12.4	831	48.0	0.135	11.6	17.6
11	1	6	2.23	252	27.4	962.7	71.3	0.135	3.3	19.0
12	1	10	4.47	260	29.3	946	74.0	0.135	10.2	23.9
13	1	14	6.7	262	3.0	934	23.6	0.135	10.2	24.0
14	1	19	8.94	271	12.0	948	47.0	0.135	11.05	24.0
15	7	10	3.6	443	39.7	767	86.0	0.135	5.56	9.0
16	7	13	7.21	400	12.0	799	47.4	0.135	9.6	12.3
17	16	10	3.6	246	24.0	804	67.0	0.135	5.2	19.7
18	16	4	7.21	230.5	14.0	813	51.0	0.135	9.0	25.6
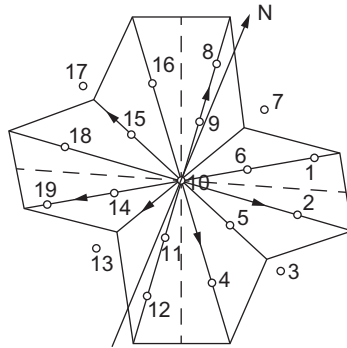
Fig. 16.24 One to nineteen numbers of production wells.

This finding supports the hypothesis that the dispersal of gases beyond the pilot site and penetration into adjacent mine workings is within the realm of possibility.

Considering that the distance between the pilot site and the adjacent mine workings is relatively small, it was necessary to develop measures that would make it impossible for gas to reach the mine workings.

One of the significant measures in this regard was the development of an appropriate hydrodynamic mode of operation of the pilot site.

16.5.3.1 Methodology

The general mode of operation at the pilot site is characterized hydraulically by air injection into some wells at a certain pressure and gas production through other wells at a known gas pressure.

If the denoted total air flow rate through the wells into which the air is injected, as ΣQ_1, then $\Sigma Q_1 = Q_1' Q_1'' \; Q_1''' + \ldots$, where Q_1', $Q_1''\ldots$ are flow rates of some specific wells through which the air is injected.

Similarly, if ΣQ_2 is the total gas flow rate through the wells from which the gas is produced, then $\Sigma Q_2 = Q_2' Q_2'' \; Q_2''' + \ldots$, where Q_2', $Q_2''\ldots$ are flow rates of some specific wells from which gas is produced.

The ratio of the total flow rate of gas produced from the pilot site during cold testing to the total air flow rate injected into the pilot site will characterize the degree of gas production:

$$\frac{\sum Q_2}{\sum |Q_1|} = \varphi_1$$

where $|Q_1|$ is the absolute value of the injected air flow rate into the injection wells.

The amount of the gas leakage will be characterized by the value of $(1 - \varphi)$.

It is evident that if $\varphi = 1$, there will be no gas leakage. If $\varphi < 1$, then there is a risk of gas dispersal beyond the pilot site boundaries. If $\varphi > 1$, then gas will be drawn from the surrounding rock into the experimental site.

16.5.3.2 Testing results

The greatest effect on the value of φ is exerted by the layout of injection and production wells and the value of the pressure applied to them.

Testing was conducted using four different layouts of interrelated injection and production wells (Fig. 16.25):

1. Injecting air into the central well, gas production from all the wells of the inner ring.
2. Injecting air into all the inner-ring wells, gas production from the central well.
3. Injecting air into the central well, gas production from all the outer-ring wells.
4. Injecting air into all the outer-ring wells, gas production from the central well.

During the testing, the flow rates in the injection wells $Q_1', Q_1'' \ldots$ and the flow rates of production wells $Q_2', Q_2''\ldots$

In addition, the overpressure or depressurization at the wellhead was measured at each well. When working using modes 2 and 4, leakage is greater than when working using modes 1 and 3, respectively. Consequently, from the point of view of leakage reduction, the central location of the injection wells is more advantageous than the peripheral one.

This is especially noticeable when the distance between the injection and production wells is increased (from comparison of the test results during experiments using modes 2 and 4).
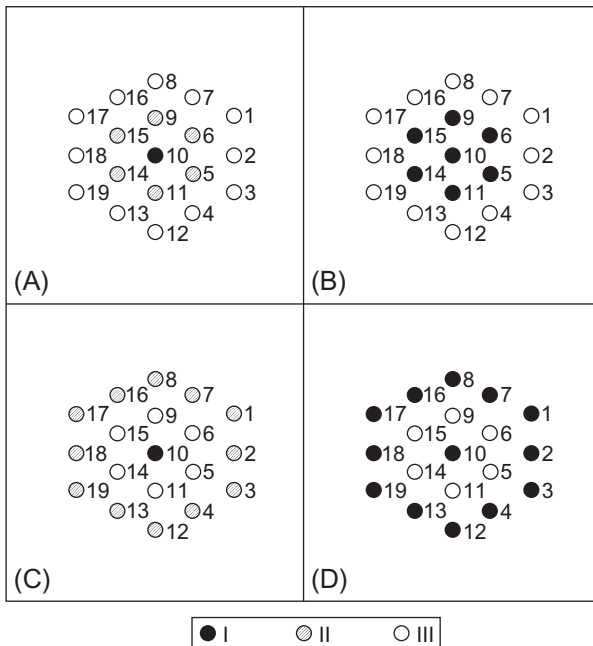
Fig. 16.25 Layout showing injection and production well locations during cold testing on the pilot site. Wells: I, injection; II, production; and III, closed. Layouts: A, no. 1; B, no. 2; C, no. 3; and D, no. 4.

Table 16.16 Test results

Layout of injection and production well locations	Test no.	Pressure, P_2, ata	φ
1	5	0.9452	2.770
	6	0.853	1.585
2	10	0.750	1.970
	9	0.745	2.145
3	16	0.9874	6.95
4	17	0.873	1.718

Table 16.16 summarizes the test results in which a negative pressure was created in the pilot site, while the pressure at the wellheads of the injection wells was equal to or near atmospheric pressure.

From the data contained in Table 16.16, in all the experiments $\varphi > 1$, that is, the creation of an underpressure in the pilot site not only eliminated leakage but also led to a drawing gas toward the pilot site from the zones adjacent to the seam.

Thus, the issue of mitigating gas leakage can be resolved by creating an underpressure in the pilot site.

Process-wise, drawing in air has an undesirable impact on gasification products. Hence, achieving a value of φ that is much greater than unity does not make sense. The results of activities using mode 2 show that the greater the underpressure, the greater the value of φ.

Creating a small underpressure in the peripheral wells is sufficient to bring the value of φ above unity.

However, when operating with an underpressure at the pilot site, drawing in gas could not be prevented. To create optimal operating conditions, that is, $\varphi = 1$, it was clearly necessary to establish a mode of operation that would combine an overpressure in the central wells and an underpressure in the peripheral wells. Table 16.17 contains a comparison of the results during testing using the above mode of operation.

Table 16.17 Comparison of the results during testing

Layout of injection and production well locations	Test no.	Pressure, P_1, ata	Pressure, P_2, ata	φ
1	8	1.3808	0.9530	0.923
	3	1.2108	0.9825	0.975
	7	1.1714	0.9272	1.236
3	13	1.272	0.9973	0.624
	14a	1.1990	0.9976	0.866
	15	1.1890	0.9966	0.904
	14b	1.1756	0.9962	1.010

The data contained in Table 16.17 show that by combining different values of over-pressure in the injection wellheads and underpressure on the production wellheads, values of φ greater and less than unity can be achieved.

Thus, it was proved empirically that it is feasible to minimize or eliminate gas leak-age while avoiding dilution of the gasification products with gas drawn in from the surrounding zones of the oil shale seam.

Overpressure and underpressure values in the process wells have a significant impact on the production rates of the pilot site.

The principle behind the hydrodynamic regime of the pilot site can meet or exceed the safety requirements, which are basically $\varphi \geq 1$.

However, in order to ensure the consistency of compliance with these require-ments, in the course hot testing, additional measures were taken with respect to the hydrodynamic regime of the pilot site, by defining the following:

- Maximum critical value of overpressure used in injection wells.
- Minimum critical value of $\varphi > 1$.
- Minimum critical value of underpressure in the "ventilation ring" wells.

Although these measures precluded dispersal of gas into the adjacent mine workings, they nevertheless created adverse conditions for the planned program of hot dry runs.

16.5.4   Hot testing

Hot testing entailed collecting experimental data characterizing the processes of igni-tion of the oil shale seam, maintaining the fire source and combustion linking of the wells, and was mostly qualitative in nature.

16.5.4.1   Methodology

Ignition was performed by adding hot coke into the well in addition to the main coke charge and 5–10 kg logs (Fig. 16.26). Air injection was ramped up immediately to the maximum possible flow rates.
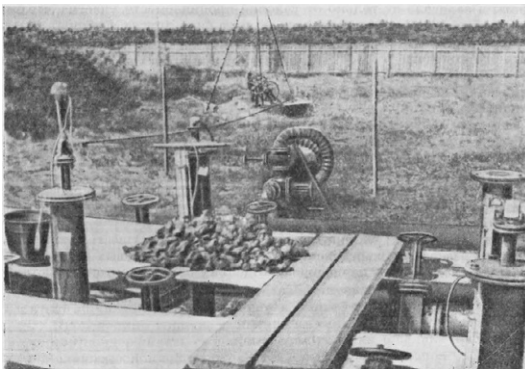
Fig. 16.26 Wellheads.

Combustion linking of the wells was conducted using the "unlimited" ignition approach, whereby the initial fire source was created at the bottom of the injection well.

Air was injected into the ignition well; air was drawn off from the production well; combustion linking proceeded along the direction of the injected air flow.

Combustion linking using the "limited ignition" mode was attempted, that is, injecting air into the well being linked to while drawing off air from the ignition well, but without success. Owing to the relatively slow rate of the ignition process in the solid oil shale block, the preponderance of heat generated by the hot coke was carried away by the flow of the gases being drawn off. A combination of rapid heating and vacuum caused the casing pipes to collapse.

The mode of ignition at the bottom of the production well, which had been proved in the Podmoskovny basin lignite, cannot be deemed sufficiently tested and requires further testing under natural conditions.

The combustion linking method used was marked by the following distinctive feature: as air was injected into a hot well, the pressure in the well began to increase at a certain negligible decrease in the air flow rate. The increase in pressure was due to the phenomenon of bituminization of the exposed surface of the oil shale seam and given a partial blockage of fractures. During this period, it would have been advisable to increase the pressure of the injected air, so as to break through the bituminous plug and expand the size of the initial fire source, which relies on the heat of burning coke.

However, it was necessary artificially to restrain pressure at a level not exceeding 350 mm Hg, which was set out by the health and safety manual.

Despite these unfavorable conditions, combustion linking was performed. A successful linking was marked by a drop in injection pressure and an increase in its flow. In most cases, increasing the flow that a given well takes occurs as a short-lived sharp spike. In the well being linked to, the temperature of the air (gas) likewise generally increases very abruptly. This is accompanied by a rapid gas production.

The need for continuous operation of the exhaust fan on the "ventilation ring" (for safety reasons) led to the drawing off of part of the gas, which were vented to atmosphere. There were instances of gas release in the natural ventilation wells.

All of the above findings made it necessary to reduce the intensity of the process due to concerns that gas penetrates the nearby mine workings, instead of increasing the air flow, as the process required.

16.5.4.2   Testing results

The data presented below indicate that despite rather challenging conditions, the first experiments of in situ gasification of oil shale produced very promising results.

Of the 19 process wells drilled in the pilot site, 14 were successfully linked (wells 1, 2, 7, 9, and 14 were not linked).

A 15-m combustion front was formed between the wells.

The duration of well linking varied in different modes of operation and was determined not only by the permeability of the site, which was revealed by cold testing, but also by a number of other factors (intensity of the initial fire source; air flow; the consistent, uninterrupted air flow, etc.)

The wells were linked over distances of 2–5 m. No repeating patterns or correlations were identified between the duration of the linking and the distance between the wells.

The rate of linking (or, more accurately, the velocity of propagation of the fire source from the injection well to the production well) ranged from 0.3 to 1.0 m/h, averaging about 0.7 m/h.

The distinctive feature of a successful linking was a sharp increase in temperature in the production well. This was accompanied by rapid gas production, with an underpressure in the well changing to overpressure. The CO_2 content in the gas increased abruptly.

Once the linking was complete, gasification was conducted using the reverse mode and alternating periods with and without air injection. The gas composition during no-injection periods for specific components is shown in Table 16.18.

16.6   Conclusions

1. Cold testing carried out at the pilot site showed that the gas flow resistance of the commercial multilayer unit in the oil shale-bearing sequence was insignificant. The average effective permeability value of the commercial unit was within 9.0–26.9 darcy for the pilot site. Therefore, ensuring the necessary gas flow through the commercial oil shale unit does not require significant pressure gradients.
2. Comparison of data on the permeability of specific oil shale samples with the results of average effective permeability of the commercial unit indicates the presence of fracturing within the oil shale-bearing sequence.

Table 16.18 Subsequent verification core drilling in the pilot site with vertical wells permitted verification of combustion of oil shale seams (A–G)

Test no.	Gas content							Calorific value of gas, kcal/m$_3$
	CO$_2$	C$_m$H$_n$	O$_2$	CO	H$_2$	CH$_4$	N$_2$	
6	3.6	6.7	9.8	2.1	29.9	14.6	33.3	3040
6	8.0	5.4	7.3	11.7	26.9	14.1	26.6	3030
7a	5.2	6.4	8.7	5.1	26.0	18.4	30.2	3320
9	8.1	3.1	9.8	9.6	26.6	5.6	37.2	1900
9a	6.0	13.6	0.4	5.8	43.0	19.5	11.7	4900
9a	1.8	6.5	11.1	2.7	15.7	11.6	50.6	2410
9b	12.5	6.1	6.8	13.1	19.4	7.0	35.1	2370
9c	10.3	7.2	0.5	15.3	52.9	9.4	4.4	3670
10	12.6	6.0	0.2	19.4	49.0	11.3	1.5	3680
10	6.2	12.7	0.7	5.6	43.6	15.6	15.6	4450
9c	9.7	5.0	5.9	11.6	25.9	22.8	19.1	3690

The testing results also showed that the directions of increased permeability of the commercial unit are within the prevailing two main directions of vertical fracturing, the northeasterly and northwesterly strikes, which had been noted in prior geologic investigations.

3. The results of the experiments demonstrated in principle the feasibility of using a new method of mitigating leakage by combining an overpressure in injection wells and underpressure in production wells.

4. The trialing of various layouts of interrelated injection and production wells showed that using the centrally located wells as injection wells and peripheral wells as production wells presents an advantage.

5. As a result of the experiments during cold testing at the pilot site, achieving a hydrodynamic regime that meets the safety requirements was proved feasible, with the fundamental requirement stating that the gas leakage be less than zero.

6. The feasibility and relatively simple methodology of creating the initial fire source in a solid oil shale block were proved.

7. Hot testing at the pilot site showed the feasibility of maintaining the fire source within the solid oil shale seam of the commercial multilayer unit over a relatively extended period of time; a number of tests lasted uninterrupted for about 4 days.

8. Advancing the fire source along the oil shale seam using the combustion linking method was proved to be practically feasible.

9. Hot testing made it possible to identify important qualitative characteristics for the process of in situ processing of oil shale in a solid block:

    a. Sufficiently high-temperature potential of the fire source (examining the temperature profile in the wells showed an achievable temperature of more than 1000°C).

    b. Despite the fact that the process operated at values of φ significantly greater than unity, the composition of the combustion products was characterized by a relatively small oxygen content.

    c. It was shown that when the air injection is stopped (no air injection periods), an intense high calorific value gas production ensues.

    d. Significant amounts of tar were produced along with the gas.

    e. In the course of hot testing at a given rate of the process, dust entrainment occurred, which led to dust buildup on the pipelines.

10. The testing established in principle the feasibility of in situ processing of the kukersite oil shale.

11. Analysis of the testing results indicates the need for further studies of in situ processing of the kukersite oil shale to experiment with and perfect this new method, to develop a reasonable technology, and to define the main process parameters. Further work may be conducted on a new, larger pilot site.

At the end of the 1950s, a combined method for the development of oil shale deposits was tested at the Kiviyli plant. Oil shale seams with a higher content of organic material are mined using conventional shaft mining methods; the resulting rooms are filled with pieces of oil shale and are isolated by means of barrier pillars. Wells are drilled above the rooms, from which magazined oil shale is ignited. The process is maintained by injecting air through neighboring wells.

Using the combined method, four panels were gasified, with 12,500 tons of oil shale processed in situ. During in situ oil shale gasification in the fourth panel, 3 million m³ of fuel gas was produced, along with 140 tons of tar.

Despite a number of advantages of the combined method, it has significant drawbacks. These include the need for people to conduct mining activities underground, with the risk of gas penetrating the workings from the active gasification panel. This places limitations on the application of the combined method during the development of oil shale deposits.

The main challenges of in situ gasification of oil shale are as follows:

1. Linking production wells in low-permeability oil shale strata in the presence of plastic surrounding rock.
2. Creating a stable fire source in oil shale with high moisture content.
3. Preventing the pore spaces in the oil shale formation from being clogged by condensation of volatile elements as solids.
4. Protecting equipment from the corrosive effect of wet sulfur-containing shale gas.

The technology of underground gasification of oil shale can be applied in new virgin oil shale deposits. This will require detailed studies of the oil shale deposit geology and oil shale properties. Based on the results, Ergo Exergy Technologies can propose a UCG-based mining method, complete with the underground gasifier design, and assess the feasibility and economic viability of in situ gasification of oil shales under given specific conditions.

Acknowledgments

References

Afonso, J.C., et al., 1994. Hydrocarbon distribution in the Iratí shale oil. Fuel 73, 363–366.

Andersson, A., Dahlman, B., Gee, D.G., Snäll, S., 1985. The Scandinavian Alum Shales: Sveriges Geologiska Undersoekning, Serie Ca. Avhandlingar och Uppsatser I A4, NR 56, 50 p.

Arens, V.J., 2001. Physical and Chemical Geotechnology. Publishing House of Moscow State Mining University, Moscow p. 656.

Avid, B., Purevsuren, B., 2001. Chemical composition of organic matter of the Mongolian Khoot oil shale. Oil Shale 18, 15–23.

Ball, F.D., Macauley, G., 1988. The geology of New Brunswick oil shales, eastern Canada. In: Proceedings International Conference on Oil Shale and Shale Oil. Chemical Industry Press, Beijing, pp. 34–41.

Bouchta, R., 1984. Valorization studies of the Moroccon [sic] oil shales. Office Nationale de Researches et Exploitations Petrolieres B.P. 774, Agdal, Rabat, Maroc, 28 p.

Crisp, P.T., Ellis, J., Hutton, A.C., Korth, J., Martin, F.A., Saxby, J.D., 1987. Australian Oil Shales—A Compendium of Geological and Chemical Data. CSIRO Inst. Energy and Earth Sciences, Div. of Fossil Fuels, North Ryde, NSW, p. 109.

Davies, G.R., Nassichuk, W.W., 1988. An Early Carboniferous (Viséan) lacustrine oil shale in Canadian Arctic Archipelago. Bull. Am. Assoc. Petrol. Geol. 72, 8–20.

Du, C., Nuttall, H.E., 1985. The history and future of China's oil shale industry. In: Eighteenth Oil Shale Symposium Proceedings. Colorado School of Mines Press, Golden, pp. 210–215.

Dyni, J.R., 2006. Geology and resources of some world oil-shale deposits: US Geological Survey Scientific Investigations Report 2005, p. 42.

Fainberg, V., Hetsroni, G., 1996. Research and development in oil shale combustion and processing in Israel. Oil Shale 13, 87–99.

Glushchenko, I.M., 1990. Theoretical foundations of solid fuel technology. Manual for High School. Metallurgiya, Moscow. p. 296.

Graham, U.M., Ekinci, E., Hutton, A., Derbyshire, F., Robl, T., Steward, M.L., et al., 1993. Derivation of Adsorbent Carbons From Oil Shale Residues, ACS Div. of Fuel Chemistry 206th Meeting Preprints, Chicago, USA. 38 (3), 914–919.

Güleç, K., Önen, A., 1993. Turkish oil shales—reserves, characterization and utilization. In: Proceedings, 1992 Eastern Oil Shale Symposium, November 17–20. University of Kentucky Institute for Mining and Minerals Research, Lexington, pp. 12–24.

Hutton, A.C., 1991. Classification, organic petrography and geochemistry of oil shale. In: Proceedings 1990 Eastern Oil Shale Symposium. University of Kentucky Institute for Mining and Minerals Research, Lexington, pp. 163–172.

Hyde, R.S., 1984. Oil shales near Deer Lake, Newfoundland. Newfoundland. Geological Survey of Canada Open-File Report OF 1114, 10 p.

Jaber, J.O., Probert, S.D., Badr, O., 1997. Prospects for the exploitation of Jordanian oil shale. Oil Shale 14, 565–578.

Kattai, V., Lokk, U., 1998. Historical review of the kukersite oil shale exploration in Estonia. Oil Shale 15 (2), 102–110.

Kogerman, A., 1997. Archaic manner of low-temperature carbonization of oil shale in wartime Germany. Oil Shale 14, 625–629.

Lee, S., 1991. Oil Shale Technology. CRC Press, Boca Raton, FL, p. 257.

Macauley, G., 1981. Geology of the oil shale deposits of Canada. Geological Survey of Canada Open-File Report, OF 754, 155 p.

Macauley, G., 1984a. Cretaceous oil shale potential of the Prairie Provinces, Canada. Geological Survey of Canada Open-File Report, OF 977, 61 p.

Macauley, G., 1984b. Cretaceous oil shale potential in Saskatchewan. Saskatchewan Geological Society Special Publication 7, pp. 255–269.

Macauley, G., 1986. Recovery and economics of oil shale development, Canada [preprint]. Canadian Society of Petroleum Geologists, Calgary, June 1986 Convention, 7 p.

McFarlane, D.B., 1984. Why the United States needs synfuels. In: Proceedings: 1984 Eastern Oil Shale Symposium, November 26–28. University of Kentucky Institute for Mining and Minerals Research, Lexington, pp. 1–8.

Matthews, R.D., Janka, J.C., Dennison, J.M., 1980. Devonian oil shale of the eastern United States: a major American energy resource [preprint]. Evansville, Ind., American Association of Petroleum Geologists Meeting, October 1–3, 43 p.

Moore, S.W., Madrid, H.B., Server, Jr., G.T., 1983. Results of oil-shale investigations on northeastern Nevada. U.S. Geological Survey Open-File Report 83-586, 56 p., 3 app.

Padula, V.T., 1969. Oil shale of Permian Iratí Formation, Brazil. Bull. Am. Assoc. Petrol. Geol. 53, 591–602.

Pápay, L., 1998. Varieties of sulphur in the alginite sequence of Kössen facies from the borehole Rezi Rzt-1 W-Hungary. Oil Shale 15, 221–223.

Pierce, B.S., Warwick, P.D., Landis, E.R., 1994. Assessment of the solid fuel resource potential of Armenia. U.S. Geological Survey Open-File Report 94-179, 59 p.

Pitin, R.N., 1957. About permeability of oil shales (kukersites). Proc. Inst. Fossil Fuel Acad. Sci. USSR VII, 30–41.

Pitin, R.N., Sporius, A.E., Farberov, I.L., 1957. First trials of underground processing of oil shale. Proc. Inst. Fossil Fuel Acad. Sci. USSR VII, 44–61.

Robl, T.L., Hutton, A.C., Dixon, D., 1993. The organic petrology and geochemistry of the Toarcian oil shale of Luxembourg. In: Proceedings 1992 Eastern Oil Shale Symposium. University of Kentucky Institute for Mining and Minerals Research, Lexington, pp. 300–312.

Rudina, M.G., Serebryakov, V.A., 1988. Handbook of Oil-Shale Processing. Himiya, Leningrad. p. 256.

Russell, P.L., 1990. Oil shales of the world, their origin, occurrence and exploitation. Pergamon Press, New York, 753 p.

Sener, M., Senguler, I., Kok, M.V., 1995. Geological considerations for the economic evaluation of oil shale deposits in Turkey. Fuel 74, 999–1003.

Smith, J.W., 1980. Oil shale resources of the United States. Colorado School of Mines, Mineral and Energy Resources, Golden, vol. 23(6), 30 p.

Smith, W.D., Naylor, R.D., 1990. Oil shale resources of Nova Scotia. Nova Scotia Department of Mines and Energy Economic Geology Series 90-3, 274 p.

Smith, W.D., Naylor, R.D., Kalkreuth, W.D., 1989. Oil shales of the Stellarton Basin, Nova Scotia, Canada—stratigraphy, depositional environment, composition and potential uses. In: Twenty-second Oil Shale Symposium Proceedings. Colorado School of Mines Press, Golden, pp. 20–30.

Troger, U., 1984. The oil shale potential of Egypt. Berliner Geowiss, Abh 50, 375–380.

Vanichseni, S., Silapabunleng, K., Chongvisal, V., Prasertdham, P., 1988. Fluidized bed combustion of Thai oil shale. In: Proceedings International Conference on Oil Shale and Shale Oil. Chemical Industry Press, Beijing, pp. 514–526.

World Shale Resource Assessments, 2015. Retrieved from: https://www.eia.gov/analysis/studies/worldshalegas/, September 24, EIA.

Yefimov, V., 1996. Creation of an oil shale industry in Kazakhstan may become a reality. Oil Shale 13, 247–248.

Further reading

Dobryansky, A.F., 1947. Oil Shale of USSR. Leningrad and Moscow: State Science Technical Publishing of Oil and Mining Literature, p. 232.

Glushchenko, I.M., 1980. Theoretical foundations of solid fuel technology. Manual for High School. Vishcha Shkola, Kiyv. p. 256.

Glushchenko, I.M., 1985. Chemical Technology of Fossil Fuels. Vishcha Shkola, Kiyv. p. 447.

Kamneva, A.I., 1974. Chemistry of Fossil Fuels. Himiya, Moscow. p. 272.

Zelenin, N.I., Ozerov, I.M., 1983. Handbook of Oil Shale. Leningrad, Nedra. p. 248.

This page intentionally left blank

Part Four

Fire underground: Prospective technologies

This page intentionally left blank

Underground fire prospective technologies

17

D. Saulov, A.Y. Klimenko, J.L. Torero
The University of Queensland, Brisbane, QLD, Australia

17.1 Introduction

Previous and current exploration of coal resources and natural events give rise to several underground fires around the world as presented in Fig. 17.1. These fires are known to result in significant environmental and socioeconomic problems (Stracher and Taylor, 2004; Michalski, 2011) while significantly undermining safety of local population and, potentially, destroying local infrastructure due to surface subsidence (Nolter and Vice, 2004). According to Page et al. (2002), such fires produce large amount of toxic gases and particulates and significantly contribute to the global emission of CO_2 into the atmosphere. Rein (2009) pointed out that underground fires consume a considerable amount of valuable, nonrenewable energy resources. Such fires also result in groundwater contamination (Finkelman, 2004; Finkelman and Stracher, 2011). While there is a significant burden of evidence that underground smoldering fires have adverse environmental and socioeconomic impact, this evidence has to be formulated in such terms that encourage intervention.

Underground fires can be ignited by human activities or by natural causes, such as lightning, or spontaneously. The fires are generally characterized by slow combustion (or smoldering) of porous combustible materials (Rein, 2009). Examples of such materials are coal, coal wash dump, or peat. Smoldering involves filtration of gases through a cascade of pores (usually of different sizes and complex structure) and the transport of heat through both gas phase and solid matrix. Heterogeneous oxidation reactions and heat release occur on pore walls.

Several publications have been devoted to smoldering over the years. It is important to note, however, that the number of publications on smoldering combustion constitutes only a very small fraction of the overall combustion research. The number of publications that specifically related to underground fires is even smaller. The smoldering research done prior to 1985 is reviewed by Ohlemiller (1985). Later, forward smoldering, where the combustion front propagates in the direction of the oxidant flow, has been studied, for example, by Schult et al. (1996), Aldushin et al. (1997), and Lu and Yortsos (2005a). The studies devoted to reverse smoldering, where the reaction front moves upstream of the flow of oxidant, include Britten and Krantz (1986), Schult et al. (1995), Liu et al. (2005), and Lu and Yortsos (2005b).
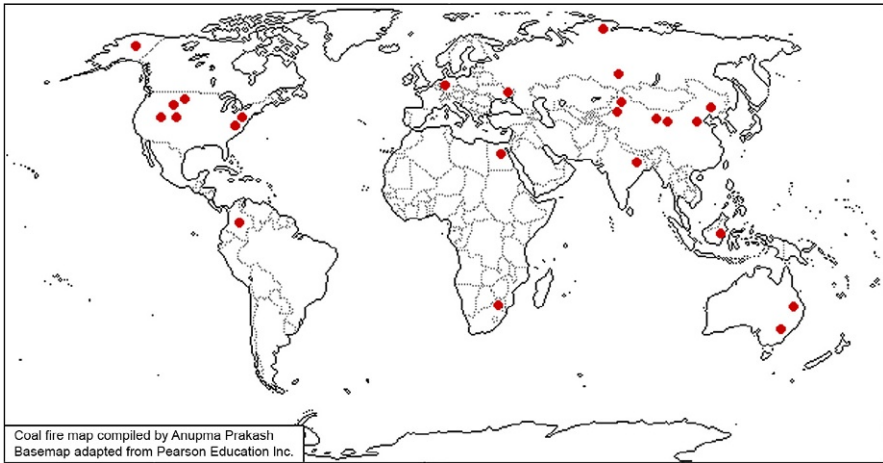
Fig. 17.1 Places of major underground fires around the world (Prakash, 2007). Each dot represents an underground fire (or a series of fires) that results in significant adverse environmental and socioeconomic impact.
Used with permission from Anupma Prakash.

Ohlemiller (2002) pointed out that, in contrast to flaming combustion, where the flame temperatures are within the range of 1200–1800°C, a typical smoldering process is characterized by relatively low combustion temperatures (500–700°C) and heat release rates (6–12 kJ/g). Propagation velocities are also very small (within 10–30 mm/h (Ohlemiller, 2002)). Due to the relatively low combustion temperatures, underground fires are difficult to detect, especially in their initial stages. Being undetected, an underground fire can spread over a large area. Even when detected, it is problematic to accurately estimate the current extent of an underground fire and predict its further propagation. This information is necessary for assessing the safety threat, for estimating the potential economic and environmental consequences, and for developing the optimal measures to control and extinguish the fire.

Since underground fires occur at different depths, a uniform approach to detecting, estimating the extent, and predicting further development of the fire is practically impossible. Indeed, the porosity and permeability, which control the flow through a porous medium, change with depth and soil type. Moreover, a directional preference in the flow field, like a fault at deeper depths, can significantly affect the heat and fluid flow to or from the source of fire. Clearly, this will have a significant impact on heat and fire propagation and on the strategy to extinguish and mitigate the fire.

Thermophysical properties of the porous medium will also affect the development of fire and reactions through the medium. These properties change with temperature and, in some cases, with time. As one would expect, the thermophysical properties of a wet medium are different from those of a dry one. For example, replacing water in porous medium by gas, which exhibits higher thermal resistance due to its lower thermal conductivity, will reduce the overall thermal conductivity. The presence of water and other volatiles will not only affect the thermohydraulic properties

but also play a key role on the chemistry and kinetics of reactions. Similar phenomena govern self-heating of coal stockpiles stored aboveground (Ejlali and Hooman, 2011).

In this work, we discuss harmful environmental and socioeconomic consequences of underground fires and review the existing methods of detecting and measuring the fires. We also analyze the currently used techniques to control and extinguish underground fires. Then, we discuss how the burden of knowledge and technologies developed over the years in underground coal gasification (UCG) can be applied to control and, possibly, extinguish an underground fire. Mainly, we concentrate on relatively deep underground fires, since the UCG technologies discussed below are more applicable to such fires. However, adverse environmental and socioeconomic impacts of peat fires are also discussed.

17.2   Adverse impacts of underground fires

17.2.1   Air and water pollution

In contrast to flaming fires, where the oxidation of combustible materials is almost complete, the smoldering underground fires are characterized by incomplete oxidation reactions. As a result, such fires yield significantly more toxic and asphyxiating carbon monoxide compared with flaming fires (Purser, 2002; Bertschi et al., 2003; Rein et al., 2009).

Due to the low reaction temperature compared with flaming fires (Ohlemiller, 2002) and incomplete oxidation, underground fires are also characterized by higher concentrations of toxic organic compound in the product gas. These compounds can severely affect the health of local population. As pointed out by Mumford et al. (1995), polycyclic aromatic hydrocarbons, for example, have been related to the higher lung cancer rate. The higher lung cancer rate, in its turn, gives rise to the overall mortality rate.

In addition, Bertschi et al. (2003) indicate that underground smoldering fires emit a significant amount of the particulate matter. While posing an increased risk for respiratory illness (Finkelman and Stracher, 2011), these particulate matters are usually loaded with dangerous inorganic substances, such as arsenic, mercury, lead, sulfur, and fluorine (Finkelman, 2004). Clearly, the composition of hazardous inorganic substances in the particulate matter depends on the mineral composition of the burning fuel.

As discussed by Finkelman (2004) and Finkelman and Stracher (2011), toxic organic and inorganic compounds released into the atmosphere and then condensed can result in local aquifer contamination. The inorganic matter and tar left underground also pose the higher risk of groundwater contamination due to the increased permeability of the media. In contrast to unburned fuel, toxic substances in the burned media can be easily leached into the local aquifer (Finkelman, 2004; Finkelman and Stracher, 2011).

Mumford et al. (1995) and Stracher and Taylor (2004) discussed the adverse effect of the air and water pollution due to underground fires on the health of local population. The Jharia coalfield fires, for example, result in the increase rates of asthma, chronic bronchitis, and skin and lung diseases. In addition, the confirmed illnesses

from the fires include stroke, pulmonary heart disease, and chronic obstructive pulmonary disease. This adverse impact forced the Indian Government to run a large-scale relocation of local population.

17.2.2   Economic impact and CO_2 emission

Apart from air and water pollution, underground coal fires consume a significant amount of valuable energy resources while substantially contributing to the global emission of greenhouse gas. According to Stracher and Taylor (2004), underground coal fires in northern China (see Fig. 17.2) result in the loss of up to 200 million tons of coal per year. Given the coal price of around US$50/t, the dollar value of the losses due to underground fires in northern China alone is 10 billion per year. Taking into account that these fires are burning for at least 20 years, the total economic impact of the fires is tremendous. Stracher and Taylor (2011) reported that the cost of the necessary firefighting measures is estimated to be US$2.5 million per year. This estimation, however, appears to be very conservative. According to US estimates, for example, more than US$651 million is required to control underground fires in abandoned mines in the United States (Stracher and Taylor, 2011). In addition to adverse economic impact, these fires contribute up to 3% to the annual global CO_2 emission to the atmosphere from fossil fuels (Stracher and Taylor, 2011).

Underground fires that are burning throughout the Jharia coalfield in India also adversely affect Indian economy (see Fig. 17.3). According to Stracher and Taylor (2011), the fires have been burning there since 1916. At present, around 70 fires are permanently burning in the area. These fires consume approximately 37 million tons of coal per year while blocking access to significant coal reserves. It is estimated

Fig. 17.2 The glow of an underground coal fire is visible through surface rocks at Ruqigou, China (Johnson, 2008). Significant amounts of valuable coal resources are lost annually. Even more coal resources are inaccessible due to underground fires.
Taken from https://en.wikipedia.org/wiki/Coal_seam_fire#/media/File:Kohlebrand_Detail.jpg.

Fig. 17.3 In Jharia, several houses have collapsed due to the fires (Schiller, 2015) (photo, Johnny Haglund). Toxic gases adversely affect the health of local population.

that approximately 1.5 billion tons of coal reserves are locked up under the fires (Stracher and Taylor, 2004). In addition, the relocation of local population program requires substantial funding.

An illustrative example of an underground fire that has detrimental safety, environmental, and economic consequences is the Centralia fire (Pennsylvania, the United States) (Nolter and Vice, 2004). This fire was ignited in 1962 in the abandoned coal mine and propagated through the coal seam. Commercial unviability to mine (at least at the present stage of mining technologies) of the coal consumed in this fire makes it difficult to estimate the economic impact of this fire due to the loss of resources. However, socioeconomic impact of this fire is devastating (see Fig. 17.4). Between 1985 and 1991, the

Fig. 17.4 Smoke emanating from a fissure in the road on the abandoned section of highway 61 near Centralia, PA. An underground mine fire has been burning there since 1962 (Matić, 2015). Taken from https://www.flickr.com/photos/citnaj/981132198. Image under Creative Commons license.

US government spent US$42 million for relocating 1100 residents form Centralia. According to Michalski (2011), the estimated price tag for complete extinguishing the Centralia fire is US$663 million. It is also important to note the losses in infrastructure, including road damaging due to surface subsidence.

During the El Niño dry season of 1997, the largest recorded peat fires started in Kalimantan, Indonesia. The fires continued for several months and affected millions of people not only in Indonesia but also in neighboring Malaysia and Singapore. According to Whitehouse and Mulyana (2004), it is estimated that these fires destroy more than 5 million hectares of forest while substantially reducing the habitant of already endangered species. Although peat is not considered as a valuable energy resource, the Indonesian peat fires ignited at least 76 coal fires (Whitehouse and Mulyana, 2004) and left a massive number of potential ignition points. Page et al. (2002) reported that the fires resulted in the emission of up to 2.6 GT of CO_2 into the atmosphere, which constitutes up to 40% of the global emission that year.

Several fire control measures have been implemented in many of the fires described above. However, no literature that provides quantification of the economic or environmental impact of any of these intervention activities has been found.

17.3   Current technologies in detection and measurement of underground fires

17.3.1   Detection

To be able to effectively control and even possibly extinguish an underground fire, it should be detected in its initial stage. Such a detection and measurement of the spread of the fire are extremely challenging problems. As discussed above, smoldering is the major combustion mechanism of underground fires, which is characterized by relatively low, compared with flame fires, combustion temperatures. As a result, the surface temperatures above an underground fire are usually not very high, until the fire has spread over a large area and move very closely to the surface. Furthermore, the exact physical, chemical, and thermal properties of the porous media (coal and soil) are often unknown, which makes it difficult to produce accurate computational models that can quantify fire spread and pollutants emitted. The local subsidence of the surface can lead to the exposure of the burning area underground. This, however, is relatively rare in the initial stages. In general, the exact area that is currently burning underground is difficult to quantify.

There are several techniques used to detect and quantify the extent of an underground fire. These techniques are based on surface measurements using satellite or aircraft imaging and quantifying the properties of the porous media in order to use these parameters for modeling (Wuttke et al., 2012). The techniques employed include geographic information system (GIS) imaging, thermal infrared (TIR) imaging (Prakash et al., 1999; Prakash and Vekerdy, 2004), and trace element/gas detection (Xue et al., 2010; Wu et al., 2012).

While the surface above underground fires are only a few degrees hotter than the surrounding areas, nighttime, satellite, TIR imaging in the 8–12 μm range has proved to be useful for detection (Prakash et al., 1999; Prakash and Vekerdy, 2004). However, the TIR images have a poor spatial resolution (Prakash and Vekerdy, 2004).

Recently, the technique involving the detection of radon (α-cup method) has been shown to be useful in underground fire detection (Xue et al., 2010; Wu et al., 2012). It has been demonstrated that this method is able to detect the location and range of the fire and to predict the changes in the trend of the fire.

Clearly, there is a need to develop diagnostic techniques for making subsurface measurements that can serve as validation data for predictive models. According to Torero et al. (1993) and Tse et al. (1999), past work using ultrasound detection in porous media can be explored as a useful tool. In this method, the decreased attenuation of acoustic waves in porous media with burnt char is used to detect and quantify the size of the smoldering zone (Torero et al., 1993). Similarly, X-ray tomographic methods (Naveed et al., 2013) that are being currently developed could also be used to make quantitative measurements of pore-size distribution and combustion reaction zones. The penetration depth and resolution potential of these techniques are still not sufficient for the purpose of detection or extinction of these fires.

17.3.2   Controlling and extinguishing

As pointed out, for example, by Colaizzi (2004), the fire control and extinguishing techniques are based on eliminating fire propagation factors such as oxidizer, fuel, and energy (heat). Traditional methods used to control and extinguish underground fires include complete excavation, trench excavation with subsequent soil backfilling, surface sealing, and inundation (Colaizzi, 2004).

Complete excavation involves the removal of overburden and then the burning fuel with subsequent cooling it with water. This method can possibly result in complete extinguishment of the fire. However, this technique is dangerous and requires a significant amount of heavy machinery (see Fig. 17.5). The economic and technical viability of complete excavation critically depends on the amount of overburden and fuel to be removed (Kim, 2011). Clearly, this method is not viable for deep underground fires or those in thick coal seams.

Less costly alternative to complete excavation is trench excavation and soil backfill. This method involves the excavation of a trench with subsequent backfilling with inert material (Colaizzi, 2004). It is assumed that the fire will stop at the created barrier. It is important to note that this fire control method does not ensure complete extinguishment. In some cases, the fire can propagate below or through the barrier (Kim, 2011). Again, the viability of this method depends on the depth of the fire and the coal seam thickness.

Another traditional method of controlling underground fires is surface sealing. In this method, the surface over the fire is sealed either with soil or with the special material to prevent the supply of oxygen to the fire (Colaizzi, 2004). It is important to note that the significant area of surface should be sealed in order to ensure that all the surface openings, which can potentially supply air to the fire, are closed. The surface

Fig. 17.5 Bulldozers remove burning coal from the coal fires at Jharia (Stracher, 2010). Credit Anupma Prakash.
Used with permission from Anupma Prakash.

seal has to be maintained for a long period of time (up to 20 years) to ensure that the fuel underground is cooled down below the reignition temperature (Kim, 2004). Thus, a surface seal requires proper construction and careful maintenance. Otherwise, it generally fails within 3 years (Kim, 2004).

In the case of availability of substantial water resources, inundation can be used to control underground fires. This technique, however, has not been routinely successful (Kim, 2004) due to mainly unpredicted distribution of water in underground mine or coal seam. Water has a tendency to create and flow through relatively large channels while avoiding hot spots of low permeability. It is also important to ensure that all the water will be contained in the fire area (Colaizzi, 2004), in order to prevent contamination of the aquifer.

Cryogenic injection has been recently tested to extinguish an underground coal fire (Kim, 2004). In this method, a slurry composed of CO_2 particles dissolved in liquid nitrogen is injected into the heated zone. Conversion of the slurry to a gas creates a cold front. The cold front propagation forces the high-temperature combustion gases out of the heated zone while cooling it down. It is important to ensure that the combustion gases are cooled down substantially. Otherwise, these gases will heat up the surrounding fuel making the fuel prone to ignition. Clearly, this approach will fail to completely extinguish the fire when the amount of cryogenic slurry is insufficient. However, the evaluation of the temperature profiles before and after the injections demonstrates effectiveness of this method in cooling localized hot spots (Kim, 2004).

In summary, all the above discussed techniques of controlling underground fires show some capacity to affect the fires in a desirable way. However, no evidence has been found that any of these techniques has being successful in a systematic way. In contrast, their implementation always introduces different forms of negative impact. The lack of adequate diagnostics, the drastic differences in the soil and different size, and the nature of the combustion reaction for every reported

example do not allow to generalize punctual successes to other scenarios. Therefore, currently, there is no conclusive methodology that can be used to address this problem.

17.4   Potential usage of UCG technologies in controlling underground fires

Here, we are not aiming at providing yet another review of UCG while referring a reader to such works as Klimenko (2009), Shafirovich and Varma (2009), and Bhutto et al. (2013). Neither we are able to present the results of a comprehensive research program. This research is yet to be done. Instead, we discuss the option of establishing control by, effectively, creating a UCG reactor inside an underground fire. This option provides the possibilities of utilizing UCG technologies, which have been developed over the many years, for controlling underground fires. To start with, the much broader and deeper burden of knowledge obtained in UCG research over the years can be applied (with some modifications) to underground fires. Secondly, a UCG reactor in an underground fire site can allow us to reduce the fire propagation and the unwanted environmental impact from the fire.

According to Imran et al. (2014), for example, UCG is the most environmentally friendly technology use of coal. Still, there are some environmental concerns associated with UCS operations. These concerns are mainly regard to groundwater contamination, when UCG operations are conducted at shallow depth (Yang and Zhang, 2008; Kapusta et al., 2013; Soukup et al., 2015). These concerns, however, are irrelevant when UCG operations are conducted on the site of an underground fire. Indeed, the fire is already burning, and some environmental damage is already done. If the fire left untouched, additional adverse environmental impact is inevitable. In what follows, we will show that further environmental damage can be reduced by using the UCG technologies.

17.4.1   Advances in modelling

An underground fire is a complex phenomenon, which involves thermal, hydraulic, chemical, and mechanical processes. Due to substantial difficulties in obtaining the real field data, comprehensive modeling is essential to improve our understanding of the involved processes and their interrelations (Wessling et al., 2008a). The comprehensive modeling of underground fires will allow improving our understanding of the phenomena underlying such fires and assist in estimating the temporal and local extent of a fire. In addition, such a model will allow predicting further propagation of the fire based on the key parameters. This information is of paramount importance for developing of the optimal strategies to control and extinguish underground fires in order to reduce their unwanted environmental and economic impacts although developing such a model is a challenging problem.

Despite some recent advances in underground fire modeling (Huang et al., 2001; Wolf and Bruining, 2007; Wessling et al., 2008a,b), accurate and comprehensive

modeling of the processes still remains as a gap in the literature. No comprehensive model, which is based on rigorous treatment of the physical phenomena involved and is able to accurately predict extension and propagation of underground fires, has been found.

In contrast to underground fires, the processes involved in UCG operations are much better understood and far much better described in the literature, where one can find both theoretical studies (mathematical modeling) and numerical simulation (computational modeling). To name a few, Yang and Liu (2003), Perkins and Sahajwalla (2006), and Seifi et al. (2011) were concerned with numerical simulation of the UCG reactor and the cavity growth, while Saulov et al. (2010) suggested the mathematical model describing the propagation of the combustion front in a gasification channel. Yang et al. (2014) and Najafi et al. (2014) devoted their studies to numerical analysis of stress distribution around a UCG reactor, while Blinderman and Klimenko (2007) developed the theory of the reverse combustion linking (RCL), which is the critical step in constructing a UCG reactor.

In addition to mathematical and computational modeling, the extensive "hands-on" experience obtained in numerous UCG trials and operations around the world is also described in the literature. Burton et al. (2006) summarized this experience while providing an interested reader with a good source of references.

17.4.2   Constructing a UCG reactor

When considering an option of creating a UCG reactor inside an underground fire, one should first ask the question if it is possible at all. Here, we can safely assume that two vertical wells can be drilled from the surface into the burning coal seam. At least, such wells can be drilled into unburned part of the seam in the vicinity of the burning part. Now, to construct the UCG reactor, one should link these two wells within the coal seam. As pointed out, for example, by Khadse et al. (2007), the selection of an appropriate linking technique is important.

Several linking techniques are now used in UCG technologies, while the main techniques are directional drilling and, predominantly, the RCL. Note, however, that forward combustion linking can be used in some circumstances. The differences between forward and RCL are analyzed by Blinderman et al. (2008a).

However, if the UCG reactor has to be created in the volume of an underground fire, the usage of directional drilling in this harsh, high-temperature environment seems to be problematic. In contrast, the selection of RCL as the linking technique appears to be a natural choice. RCL is a mature technology, which has been extensively used not only in the broad and long-lasting Soviet UCG program but also in US UCG trials in the 1970s and 1980s. The results of RCL usage in the Soviet operations have been summarized by Skafa (1960) and Kreinin et al. (1982), where an interested reader can find the essence of the entire Soviet USG program.

It is important to note that RCL usage was empirical, since no comprehensive theory of RCL exists at that time. The first attempt to suggest such a theory has been done by Britten and Krantz (1985). The comprehensive theory of RCL has been recently

developed by Blinderman and Klimenko (2007) and Blinderman et al. (2008b). The above said demonstrates that one can safely assume that UCG reactor can be created inside an underground coal fire.

17.4.3   Controlling an underground fire

The product gas for an underground fire is evacuated to the surface mainly through a path of relatively high hydraulic resistance (see Fig. 17.6). This resistance forces the part of the product gases to filtrate into unburned fuel surrounding the fire. The hot gas spreading into unburned fuel heats it up and subsequently ignites it. In this way, the volume of the fire underground potentially enlarges.

Due to that hydraulic resistance, part of the product gas can propagate through cracks in the coal seam to a significant distance apart from the main fire site. This process can result in the formation of new fire sites in a long distance from the main site. This makes the spread of the fire unpredictable.

The UCG reactor constructed on the fire site provides a pass of low hydraulic resistance to the product gas from the fire. In this way, almost all product gas will be evacuated to the surface and appropriately treated using the conventional UCG processes. The almost complete evacuation of the hot product gas from the burning fuel will reduce the local spread of the fire and prevent it from propagating through the cracks in the coal seam. The key element of UCG technology and the first stage in treating the underground fire is establishing control over air supply combined with evacuation and processing of the product gas. This evacuation can be conducted at slightly below atmospheric pressures to minimize fire spread and ecological damage. The second stage is the gradual localization of the process as the fire tends to move toward the
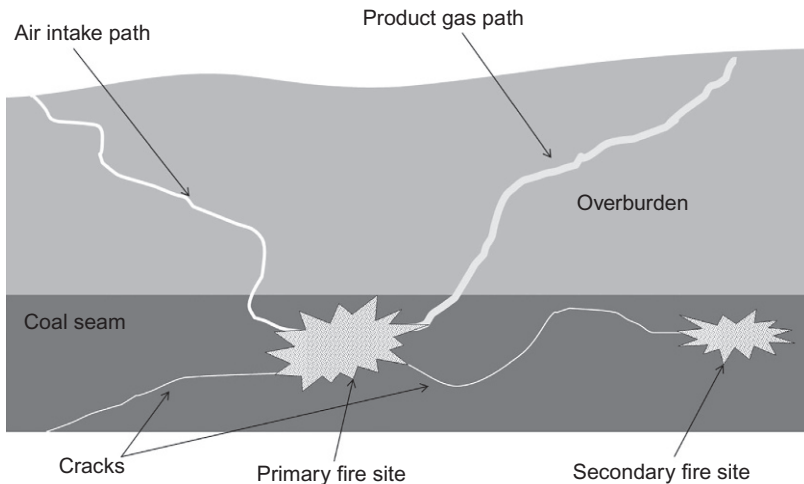
Fig. 17.6 Schematic view of an underground coal fire. The oxidant is supplied through the cracks, while the product gas is released into the atmosphere through the low-permeability (yet relatively high hydraulic resistance) path.

source of oxygen. The surrounding water table can be increased by injecting water at the peripheral regions, gradually propagating the water interface toward the reaction region. This results in a gradual and controlled extinction of the fire. Another possibility is operating the UCG reactor for a substantial amount of time to burn out almost all the fuel underground, in a manner that is safe, localized, and environmentally friendly in comparison with the uncontrolled fire. After that, the UCG reactor can be safely decommissioned in accordance with the best UCG practice (Burton et al., 2006).

Note that the suggested approach, based on UCG experience, is almost directly opposite to conventional injection of water directly into the fire region. The latter typically causes only temporal decrease of fire temperature and often results in subsequent spreading and multiplication of the fire regions due to the effective injection of large quantities of hot steam and product gas into the rest of the coal seam.

17.4.4   Reducing the aquifer contamination

As we pointed out before, one should take into account the initial environmental conditions while considering environmental concerns regarding to groundwater contamination from the UCG operations conducted at shallow depth. One should consider that the underground fire, if left untreated, will produce a significant amount of toxic inorganic matter and tar. These can be easily leached into the local aquifer due to increased permeability. In the UCG operations, significant part of these substances will be converted into gaseous phase and evacuated with the subsequent appropriate treatment on the surface. Therefore, the risk of the aquifer contamination will be decreased.

17.4.5   Reducing the emission of toxic gases

As discussed above, smoldering underground fires emit into the atmosphere extensive amount of toxic organic compounds and dangerous particulate matter that severely affect the health of local population. If UCG technologies are applied to control the underground fire, these gases and particulates will be captured and treated in the conventional UCG processes. Thus, the atmospheric pollution from the fire will be substantially reduced.

17.4.6   Potential for extracting revenue from underground fires

Until this point, we discuss the controlling underground fires with the help of the UCG technologies. However, one can consider this issue from the different perspective. Let's assume that the underground fire is in a thick (say more than 3 m) and deep (say 150 m and below the local water table) coal seam. Let's also assume that the seam is large. That is, substantial coal reserves are available. In this case, the project of controlling the fire can be turned to be a normal UCG project with the possibility of commercial production since, in these conditions, the gasification can be conducted at relatively high pressure (yet below the hydrostatic one), and good-quality syngas

can be produced in a continuous process. Such a UCG project would have additional advantages compared with other UCG operations. Namely, in addition to extracting revenue, this project will control the underground fire, which otherwise is difficult to control, and reduce adverse environmental consequences, which otherwise unavoidable. Furthermore, no other company would compete for these coal resources, since conventional mining techniques do not allow to mine a coal from the seam with a fire.

In most cases, however, underground fires occur in shallow, fragmented, and often thin seams above water table, where commercial production of syngas is hardly possible. At small depths, gasification has to be conducted at lower pressure in order to avoid potential breakthrough of gas to surface and possible contamination of groundwater with considerable heat losses. Irregular geometries and fractured overburdens would complicate operations, resulting in relatively low thermal efficiency and relatively lower syngas quality in a continuous process. However, using alternating injection of air, which can be enriched by oxygen, and steam (Yang et al., 2008; Eftekhari et al., 2015), higher-quality syngas can be produced. Detail economic analysis of such a UCG project is, clearly, beyond the scope of this work. However, the produced revenue can be used to partially (or fully) pay off the expenses of controlling the underground fire, even if the UCG project is not commercially successful.

17.5   Conclusions

Currently, underground fires have a major detrimental environmental and socioeconomic impact. Such fires consume valuable energy resources while polluting air and contaminating local aquifer. These fires also significantly contribute to the global greenhouse gas emission and pose substantial safety and health threads to local population.

Detection of underground fires, especially in their initial stages, using the conventional satellite or aircraft imaging is problematic due to relatively small increase in surface temperatures over the burning area. New approaches to address this problem have been recently suggested; nevertheless, none has proved viable so far at the scales and potential depths relevant to underground fires.

Traditional methods of controlling and extinguishing underground fires are mostly unproved and site-specific. Complete excavation is prohibitively costly for widely spread fires or those burned deep underground. Other traditional methods do not guarantee extinction or effective control of the fire due to a large number of uncertainties.

Our understanding of such a complex phenomenon as an underground fire remains limited. Difficulties in obtaining experimental data from underground fires are exacerbated by a relatively low number of studies devoted to comprehensive modeling such fires. In contrast, a significantly larger number of studies dedicated to UCG technologies are available in the literature. These include theoretical studies, computational modeling, and descriptions of "hands-on" experience.

RCL, which is the well-developed UCG technology, provides an option to construct a UCG reactor at the location of an underground fire. This option opens the

possibilities to apply other UCG technologies in order to effectively control and, possibly, extinguish the fire while substantially reducing local aquifer contamination and emission of toxic gases and particulates into the atmosphere.

In principle, application of UCG technologies for controlling an underground coal fire can be conducted as a commercial UCG operation under ideal conditions. Practically, the UCG-based method for controlling underground fires may need to be operated at a loss for some time to reduce the adverse environmental impact of the fire and gradually extinguish it.

References

Aldushin, A.P., Matkowsky, B.J., Schult, D.A., 1997. Upward buoyant filtration combustion. J. Eng. Math. 31 (2–3), 205–234.

Bertschi, I., Yokelson, R.J., Ward, D.E., Babbitt, R.E., Susott, R.A., Goode, J.G., Hao, W.M., 2003. Trace gas and particle emissions from fires in large diameter and belowground biomass fuels. J. Geophys. Res.: Atmos. 108 (D13) (1984–2012).

Bhutto, A.W., Bazmi, A.A., Zahedi, G., 2013. Underground coal gasification: from fundamentals to applications. Prog. Energy Combust. Sci. 39 (1), 189–214.

Blinderman, M.S., Klimenko, A.Y., 2007. Theory of reverse combustion linking. Combust. Flame 150 (3), 232–245.

Blinderman, M.S., Saulov, D.N., Klimenko, A.Y., 2008a. Forward and reverse combustion linking in underground coal gasification. Energy 33 (3), 446–454.

Blinderman, M.S., Saulov, D.N., Klimenko, A.Y., 2008b. Exergy optimisation of reverse combustion linking in underground coal gasification. J. Energy Inst. 81 (1), 7–13.

Britten, J.A., Krantz, W.B., 1985. Linear stability of planar reverse combustion in porous media. Combust. Flame 60 (2), 125–140.

Britten, J.A., Krantz, W.B., 1986. Asymptotic structure of planar nonadiabatic reverse combustion fronts in porous media. Combust. Flame 65 (2), 151–161.

Burton, E., Friedmann, J., Upadhye, R., 2006. Best Practices in Underground Coal Gasification. Lawrence Livermore National Laboratory. p. 119.

Colaizzi, G.J., 2004. Prevention, control and/or extinguishment of coal seam fires using cellular grout. Int. J. Coal Geol. 59 (1), 75–81.

Eftekhari, A.A., Wolf, K.H., Rogut, J., Bruining, H., 2015. Mathematical modeling of alternating injection of oxygen and steam in underground coal gasification. Int. J. Coal Geol. 150, 154–165.

Ejlali, A., Hooman, K., 2011. Buoyancy effects on cooling a heat generating porous medium: coal stockpile. Transp. Porous Media 88 (2), 235–248.

Finkelman, R.B., Stracher, G.B., 2011. Environmental and health impacts of coal fires. In: Stracher, G.B., Prakash, A., Sokol, E.V. (Eds.), Coal and Peat Fires: A Global Perspective. Elsevier, Amsterdam, pp. 116–125.

Finkelman, R.B., 2004. Potential health impacts of burning coal beds and waste banks. Int. J. Coal Geol. 59 (1), 19–24. http://www.australian-shares.com/forums/discussion/6330/hunter-valley-coal-mine-fire-still-burning.

Huang, J., Bruining, J., Wolf, K.H., 2001. Modeling of gas flow and temperature fields in underground coal fires. Fire Saf. J. 36 (5), 477–489.

Imran, M., Kumar, D., Kumar, N., Qayyum, A., Saeed, A., Bhatti, M.S., 2014. Environmental concerns of underground coal gasification. Renew. Sust. Energ. Rev. 31, 600–610.

Johnson, T., 2008. China's coal fires belch fumes, worsening global warming, 17 November, McClatchy Newspapers. http://www.mcclatchydc.com/news/nation-world/world/article24510001.html Accessed on June 27, 2017.

Kapusta, K., Stańczyk, K., Wiatowski, M., Chećko, J., 2013. Environmental aspects of a field-scale underground coal gasification trial in a shallow coal seam at the Experimental Mine Barbara in Poland. Fuel 113, 196–208.

Khadse, A., Qayyumi, M., Mahajani, S., Aghalayam, P., 2007. Underground coal gasification: a new clean coal utilization technique for India. Energy 32 (11), 2061–2071.

Kim, A.G., 2004. Cryogenic injection to control a coal waste bank fire. Int. J. Coal Geol. 59 (1), 63–73.

Kim, A.G., 2011. United States Bureau of Mines—study and control of fires in abandoned mines and waste banks. In: Stracher, G.B., Prakash, A., Sokol, E.V. (Eds.), Coal and Peat Fires: A Global Perspective. Elsevier, Amsterdam, pp. 268–304.

Klimenko, A.Y., 2009. Early ideas in underground coal gasification and their evolution. Energies 2 (2), 456–476.

Kreinin, E.V., Fedorov, N.A., Zvyagintsev, K.N., Pyankova, T.M., 1982. Underground Gasification of Coal Seams. Nedra, Moscow (in Russian).

Liu, Y., Chen, M., Buckmaster, J., Jackson, T.L., 2005. Smolder waves, smolder spots, and the genesis of tribrachial structures in smolder combustion. Proc. Combust. Inst. 30 (1), 323–329.

Lu, C., Yortsos, Y.C., 2005a. Dynamics of forward filtration combustion at the pore-network level. AICHE J. 51 (4), 1279–1296.

Lu, C., Yortsos, Y.C., 2005b. Pattern formation in reverse filtration combustion. Phys. Rev. E. 72(3). 036201.

Matić, L., 2015. Tura za pustolove: Napušteni gradovi sveta, 11 January, Ekonomske Vesti. http://ekonomskevesti.com/turizam/tura-za-pustolove-napusteni-gradovi-sveta Accessed on June 27, 2017.

Michalski, S.R., 2011. Brief history of coal mining. In: Stracher, G.B., Prakash, A., Sokol, E.V. (Eds.), Coal and Peat Fires: A Global Perspective. Elsevier, Amsterdam, pp. 30–46.

Mumford, J.L., Li, X., Hu, F., Lu, X.B., Chuang, J.C., 1995. Human exposure and dosimetry of polycyclic aromatic hydrocarbons in urine from Xuan Wei, China with high lung cancer mortality associated with exposure to unvented coal smoke. Carcinogenesis 16 (12), 3031–3036.

Najafi, M., Jalali, S.M.E., KhaloKakaie, R., 2014. Thermal-mechanical-numerical analysis of stress distribution in the vicinity of underground coal gasification (UCG) panels. Int. J. Coal Geol. 134, 1–16.

Naveed, M., Hamamoto, S., Kawamoto, K., Sakaki, T., Takahashi, M., Komatsu, T., de Jonge, L.W., 2013. Correlating gas transport parameters and X-ray computed tomography measurements in porous media. Soil Sci. 178 (2), 60–68.

Nolter, M.A., Vice, D.H., 2004. Looking back at the Centralia coal fire: a synopsis of its present status. Int. J. Coal Geol. 59 (1), 99–106.

Ohlemiller, T.J., 1985. Modeling of smoldering combustion propagation. Prog. Energy Combust. Sci. 11 (4), 277–310.

Ohlemiller, T.J., 2002. Smouldering combustion. In: DiNenno, P.J., Drysdale, D., Beyler, C.L., Walton, W.D. (Eds.), SFPE Handbook of Fire Protection Engineering, third ed, National Fire Protection Association, Inc., Massachusetts, pp. 2.200–2.210.

Page, S.E., Siegert, F., Rieley, J.O., Boehm, H.D.V., Jaya, A., Limin, S., 2002. The amount of carbon released from peat and forest fires in Indonesia during 1997. Nature 420 (6911), 61–65.

Perkins, G., Sahajwalla, V., 2006. A numerical study of the effects of operating conditions and coal properties on cavity growth in underground coal gasification. Energy Fuel 20 (2), 596–608.

Prakash, A., 2007. About coal fires: global distribution. http://www2.gi.alaska.edu/~prakash/coalfires/global_distribution.html Accessed on June 27, 2017.

Prakash, A., Vekerdy, Z., 2004. Design and implementation of a dedicated prototype GIS for coal fire investigations in North China. Int. J. Coal Geol. 59 (1), 107–119.

Prakash, A., Gens, R., Vekerdy, Z., 1999. Monitoring coal fires using multi-temporal night-time thermal images in a coalfield in north-west China. Int. J. Remote Sens. 20 (14), 2883–2888.

Purser, D.A., 2002. Toxicity assessment of combustion products. In: DiNenno, P.J., Drysdale, D., Beyler, C.L., Walton, W.D. (Eds.), SFPE Handbook of Fire Protection Engineering, third ed, National Fire Protection Association, Inc., Massachusetts, pp. 2.83–2.171.

Rein, G., 2009. Smouldering combustion phenomena in science and technology. Int. Rev. Chem. Eng. 1, 3–18.

Rein, G., Cohen, S., Simeoni, A., 2009. Carbon emissions from smouldering peat in shallow and strong fronts. Proc. Combust. Inst. 32 (2), 2489–2496.

Saulov, D.N., Plumb, O.A., Klimenko, A.Y., 2010. Flame propagation in a gasification channel. Energy 35 (3), 1264–1273.

Schiller, J., 2015. This Hellish underground fire has burned for 100 years. http://www.wired.com/2015/03/johnny-haglund-the-earth-is-on-fire/#slide-5 Accessed on June 27, 2017.

Schult, D.A., Matkowsky, B.J., Volpert, V.A., Fernandez-Pello, A.C., 1996. Forced forward smolder combustion. Combust. Flame 104 (1), 1–26.

Schult, D.A., Matkowsky, B.J., Volpert, V.A., Fernandez-Pello, A.C., 1995. Propagation and extinction of forced opposed flow smolder waves. Combust. Flame 101 (4), 471–490.

Seifi, M., Chen, Z., Abedi, J., 2011. Numerical simulation of underground coal gasification using the CRIP method. Can. J. Chem. Eng. 89 (6), 1528–1535.

Shafirovich, E., Varma, A., 2009. Underground coal gasification: a brief review of current status. Ind. Eng. Chem. Res. 48 (17), 7865–7875.

Skafa, P.V., 1960. Underground Coal Gasification. Gosgortechizdat, Moscow (in Russian).

Soukup, K., Hejtmánek, V., Čapek, P., Stanczyk, K., Šolcová, O., 2015. Modeling of contaminant migration through porous media after underground coal gasification in shallow coal seam. Fuel Process. Technol. 140, 188–197.

Stracher, G.B., 2010. The rising global interest in coal fires, 1 September, Earth The Science Behind the Headliness. http://www.earthmagazine.org/article/rising-global-interest-coal-fires Accessed on June 27, 2017.

Stracher, G.B., Taylor, T.P., 2011. The effects of global coal fires. In: Stracher, G.B., Prakash, A., Sokol, E.V. (Eds.), Coal and Peat Fires: A Global Perspective. Elsevier, Amsterdam, pp. 102–113.

Stracher, G.B., Taylor, T.P., 2004. Coal fires burning out of control around the world: thermodynamic recipe for environmental catastrophe. Int. J. Coal Geol. 59 (1), 7–17.

Torero, J.L., Fernandez-Pello, A.C., Kitano, M., 1993. Opposed forced flow smoldering of polyurethane foam. Combust. Sci. Technol. 91 (1–3), 95–117.

Tse, S.D., Anthenien, R.A., Fernandez-Pello, A.C., Miyasaka, K., 1999. An application of ultrasonic tomographic imaging to study smoldering combustion. Combust. Flame 116 (1), 120–135.

Wessling, S., Kessels, W., Schmidt, M., Krause, U., 2008a. Investigating dynamic underground coal fires by means of numerical simulation. Geophys. J. Int. 172 (1), 439–454.

Wessling, S., Kuenzer, C., Kessels, W., Wuttke, M.W., 2008b. Numerical modeling for analyzing thermal surface anomalies induced by underground coal fires. Int. J. Coal Geol. 74 (3), 175–184.

Whitehouse, A.E., Mulyana, A.A., 2004. Coal fires in Indonesia. Int. J. Coal Geol. 59 (1), 91–97.

Wolf, K.H., Bruining, H., 2007. Modelling the interaction between underground coal fires and their roof rocks. Fuel 86 (17), 2761–2777.

Wu, J., Wu, Y., Wang, J., Zhou, C., 2012. Radon measuring to detect coal spontaneous combustion fire source at Bulianta mine, Shendong. In: 12th Coal Operators Conference. University of Wollongong & The Australasian Institute of Mining and Metallurgy, Wollongong, NSW, Australia, pp. 300–304.

Wuttke, M.W., Halisch, M., Tanner, D.C., Cai, Z.Y., Zeng, Q., Wang, C., 2012. April. Underground coal-fires in Xinjiang, China: a continued effort in applying geophysics to solve a localproblem and to mitigate a global hazard. In: EGU General Assembly Conference Abstracts.Vol. 14. p. 7815.

Xue, S., Wang, J., Xie, J., Wu, J., 2010. A laboratory study on the temperature dependence of the radon concentration in coal. Int. J. Coal Geol. 83 (1), 82–84.

Yang, D., Sarhosis, V., Sheng, Y., 2014. Thermal-mechanical modelling around the cavities of underground coal gasification. J. Energy Inst. 87 (4), 321–329.

Yang, L., Liu, S., 2003. Numerical simulation on heat and mass transfer in the process of underground coal gasification. Numer. Heat Transfer A: Appl. 44 (5), 537–557.

Yang, L., Zhang, X., 2008. Modeling of contaminant transport in underground coal gasification. Energy Fuel 23 (1), 193–201.

Yang, L., Zhang, X., Liu, S., Yu, L., Zhang, W., 2008. Field test of large-scale hydrogen manufacturing from underground coal gasification (UCG). Int. J. Hydrog. Energy 33 (4), 1275–1285.

This page intentionally left blank

Using fire to remediate contaminated soils

J.L. Torero*, J.I. Gerhard[†], L.L. Kinsman[†], L. Yermán*
*The University of Queensland, Brisbane, QLD, Australia, [†]University of Western Ontario, London, ON, Canada

18.1   Introduction

Tens of thousands of sites worldwide exhibit contamination of groundwater and surface water by historical and continuing accidental releases of hazardous nonaqueous-phase liquids (NAPLs). Common NAPLs include petroleum hydrocarbons (oils and fuels), polychlorinated biphenyls (electric transformer oils), chlorinated ethenes (solvents and degreasers), creosote (wood treaters), and coal tar (manufactured gas plants). Complex and/or long-chain compounds, such as heavy oils, PCB oils and coal tar, are particularly recalcitrant, resisting degradation via physical (e.g., volatilization), biological (e.g., dehalogenation), and chemical (e.g., oxidation) treatments that are becoming accepted remedies for more amenable contaminants. Dealing with such wastes typically involves excavation and either disposal to a hazardous waste landfill or incineration at substantial cost. As an alternative, this research paper proposes a new approach—NAPL smoldering—as a potential remediation process.

The combustibility of NAPLs is a characteristic that has been successfully exploited through the ex situ incineration of NAPLs and contaminated soil (e.g., Howell et al., 1996). Incineration is primarily achieved via flaming combustion. Flaming combustion involves the gasification of a fuel and its exothermic oxidation in the gas phase. Incineration of NAPLs by flaming combustion is energy inefficient (i.e., high heat losses); as a result, incineration requires the continuous addition of energy.

Smoldering combustion, in contrast, is the gasification and exothermic oxidation of a condensed phase (i.e., solid or liquid) occurring on the fuel surface (Ohlemiller, 1985). Smoldering is limited by the rate of oxygen transport to the fuel's surface, resulting in a slower and lower temperature reaction than flaming. Importantly, smoldering can be self-sustaining (i.e., no energy input required after ignition) when the fuel is (or is embedded in) a porous medium. Self-sustaining smoldering occurs because the solid acts as an energy sink and then feeds that energy back into the unburnt fuel, creating a very energy-efficient reaction (Howell et al., 1996). Solid porous fuels such as polyurethane foam (Torero and Fernandez-Pello, 1996), cellulose (Ohlemiller, 1985), and charcoal are typical media that exhibit self-sustained smoldering. These studies have demonstrated that the rate of combustion front propagation, limits of self-sustained propagation, and net heat generation by the reaction are affected by the velocity (magnitude and direction) of air, pore diameter of the medium, and the fraction of porosity occupied by fuel, air, and nonreacting materials (DeSoete, 1966).

Smoldering reactions can leave a carbonaceous residue behind the reaction front (oxygen-limited reactions), or in some instances, they can result in complete combustion of the fuel (fuel limited) (Schult et al., 1995). The former is very common in reacting porous media (e.g., foam) where the insulating char minimizes heat losses and enables the reaction to propagate. The latter is common when the fuel is combined with an inert porous media (e.g., oil in silica sand) that provides the require insulation even in the absence of the fuel.

While smoldering of solid fuels has been the focus of most research, there are several examples of combustion where smoldering of a liquid fuel embedded in an inert or reacting porous matrix may be observed. Lagging fires occur inside porous insulating materials soaked in oils and other self-igniting liquids (Drysdale, 2011). To enhance oil recovery, combustion fronts are initiated in petroleum reservoirs purposely to drive oil toward an extraction point, a technique known for high energy efficiency (Greaves et al., 1993). The reactions involved in enhanced oil recovery through in situ combustion are described as heterogeneous gas-solid and gas-liquid between oxygen and the heavy oil residue (Sarathi, 1999).

NAPL smoldering would be different from existing thermal remediation techniques. In situ thermal treatment requires the continuous input of energy in order to primarily volatilize and, in some cases, thermally degrade (pyrolyze) and mobilize (via viscosity reductions) the organic phase. All of these processes are endothermic, and thus, remediation only continues as long as externally supplied energy input is sustained throughout the NAPL-occupied porous medium. In contrast, NAPL smoldering has the potential to create a combustion front that (i) initiates at a single location with the NAPL-occupied porous medium; (ii) initiates with a one-time, short-duration energy input; (iii) propagates through the NAPL-occupied medium in a self-sustained manner; and (iv) destroys the NAPL at a location as the front passes. NAPL smoldering would be different from in situ combustion for enhanced oil recovery in that the latter is designed so as to generate heat and gas pressure that will mobilize the entrapped oil toward recovery wells. NAPL smoldering, in contrast, may benefit from avoiding the recovery (and thus treatment) of NAPL and/or water.

18.2   Principles of smoldering

Smoldering is normally studied as a common fire initiation source. It appears in the form of cigarettes interacting with upholstered furniture, overheated wire insulation, spontaneous ignition of hay stacks or embers, etc. Smoldering is characterized by a slow exothermic reaction (propagation velocities are of the order of 0.1 mm/s) occurring at low temperatures (characteristic smolder temperatures are of the order of 400–800°C) and with almost unnoticeable smoke release.

Smoldering may occur in a variety of processes that range from smolder of porous insulating materials to underground coal combustion. Many materials can sustain smoldering, including wood, cloth, foams, tobacco and other dry organic materials, and charcoal. The ignition, propagation, transition to flaming, and extinction of the

smolder reaction are controlled by complex, thermochemical mechanisms that are not well understood.

Smoldering combustion of porous materials has been studied both experimentally and theoretically. From a fundamental point of view, smoldering is a basic combustion problem that encompasses a number of processes, including heat and mass transfer in a porous media, endothermic pyrolysis of the fuel, ignition, propagation and extinction of heterogeneous exothermic reactions at the solid/gas pore interface, and onset of gas-phase reactions (flaming) from the existing surface reactions (Ohlemiller, 1985).

From a practical point of view, smoldering has been discussed as a risk because the combustion can propagate slowly in the material interior and go undetected for long periods of time. It typically yields a substantially higher conversion of fuel to toxic compounds than does flaming (though more slowly) and may undergo a sudden transition to flaming (Interagency, 1987; Ortiz Molina et al., 1979; Williams, 1976). Flaming accelerates the process but is not a necessary event (Babrauskas, 1996).

Smoldering is characterized by an exothermic heterogeneous combustion reaction that occurs in the interior of porous combustible materials. The heat released during the heterogeneous oxidation of the solid is transferred toward the unreacted material by conduction, convection, and radiation, supporting the propagation of the smolder reaction. The oxidizer, in turn, is transported to the reaction zone by diffusion and convection. These transport mechanisms influence not only the rate at which the smolder reaction propagates but also the limiting factors of the smolder process, that is, ignition and extinction (lower bounds) and transition to flaming (upper bound). The propagation of the smolder reaction is, therefore, a complexly coupled phenomenon involving processes related to the transport of heat and mass in a porous media, together with surface pyrolysis and combustion reactions.

The main difference between smolder and any of the other combustion processes is that oxidation does not occur in the gas but rather in the condensed (e.g., solid) phase. Solid fuels that sustain smoldering are porous in nature; therefore, inside the porous matrix, the volume-to-surface-area ratio for the fuel is very small (Fig. 18.1). The oxidizer therefore has a large reaction surface with which to interact, and diffusion of oxygen to the fuel surface is faster than fuel evaporation. The result is a reaction that will propagate as the conduction heat transfer wave heats the porous solid.

As the reaction propagates, the oxygen inside the porous matrix is completely consumed leaving residual fuel, generally referred to as "char." Fig. 18.2 shows a picture

200 μm
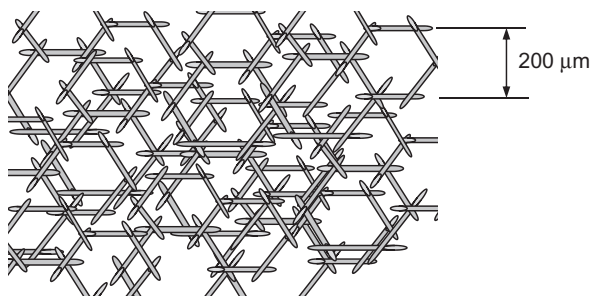
Fig. 18.1 Schematic of a typical, combustible, solid porous matrix; in gray are the fuel fibers.
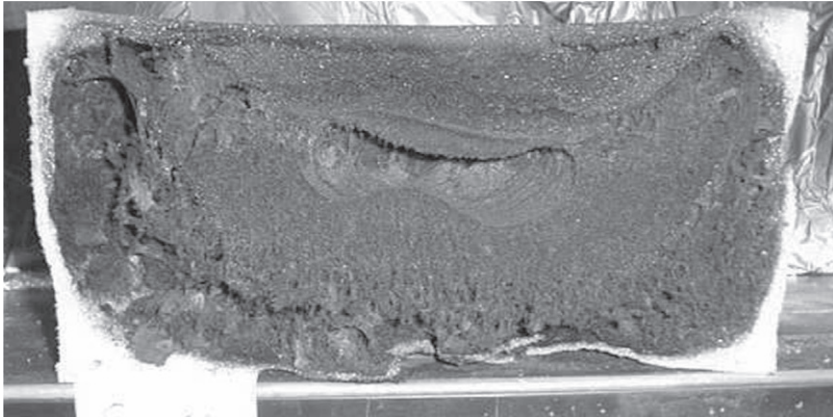
Fig. 18.2 Photograph of a polyurethane foam sample through which a smolder reaction has propagated.
From Anderson, M., Sleight, R., Torero, J.L., 2000. Downward smolder of polyurethane foam: ignition signatures. Fire Saf. J. 35, 131–148.
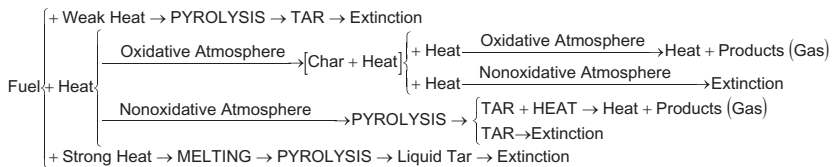
Fig. 18.3 Possible reaction pathways for a smolder reaction.

of smoldered polyurethane foam. The foam was ignited at the top of the sample, and the reaction was allowed to propagate downward leaving a black char behind.

A smoldering reaction is not always established when heat is applied to a porous fuel susceptible to smolder. Actually, the conditions for the onset of smoldering are in some cases very restrictive. Fig. 18.3 presents the possible pathways established as viable when heating a solid, porous fuel susceptible to smoldering.

The first step of the degradation process, as shown in Fig. 18.3, corresponds to the different magnitudes of the net heat flux imposed to the material. If the net heat flux is weak (i.e., for polyurethane foam $<6\ kW/m^2$), Fig. 18.3 shows that the fuel is degraded via pyrolysis. Nonetheless, a degraded material is formed. This material is generally of liquid form and is commonly referred as tar. If the net heat flux is very strong (i.e., for polyurethane foam $>7\ kW/m^2$), a similar process is observed where a liquid tar remains as the product of the degradation. Both degradation branches are endothermic, and once the external heat source is withdrawn, extinction follows. The main difference between the two branches seems to be that the amount of heat determines the fraction of tar that will be evaporated, thus the production of airborne aerosols. A typical ignition plot is presented in Fig. 18.4 for polyurethane foam.
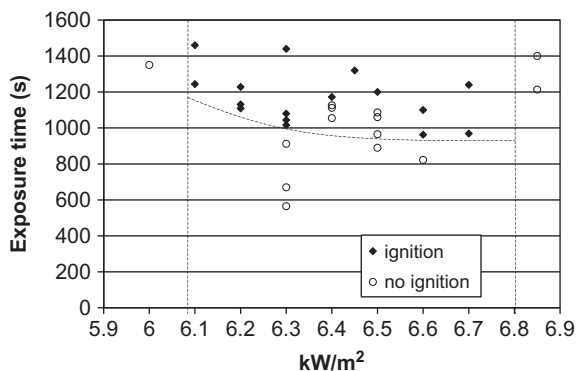
Fig. 18.4 Ignition characteristics of polyurethane foam as a function of an external heat flux (Anderson et al., 2000).

Smoldering of the material occurs only when the heat flux imposed on the material is in between the two limits described above. In the presence of an oxidative atmosphere, an exothermic surface reaction (smolder) will lead to the release of heat and gaseous products and the formation of a residual char. Char is a solid matrix that generally conserves the structure of the original fuel. The char has higher carbon content than the original solid and is more combustible. The char can further react in the presence of oxygen if its temperature is high enough. Reaction temperatures of char have been observed to be higher than the temperatures observed during direct smolder of the fuel. The final products are in most cases in gaseous form and particulate (smoke), but some fuels lead to a residual, noncombustible ash. If all the oxygen is consumed by the smolder reaction, the char will not react, and cooling will follow.

Even under the appropriate heating conditions, if not enough oxygen is available; the decomposition chemistry will privilege the endothermic pyrolysis of the fuel. This will again lead to the formation of tar and consequent extinction. Attempts to identify the exothermic and endothermic degradation processes have been made by means of thermogravimetric analysis (TGA) and differential scanning calorimetry (DSC) (Bilbao et al., 1996). These methods can provide important and insightful information about the smolder mechanisms; unfortunately, the results must be analyzed in a somewhat circular and iterative manner, where one must propose a model and see how TGA/DSC corresponds to it, and back and forth.

Once the smolder reaction has been initiated, the reaction front propagates across the porous matrix. The chemical processes occurring in the reaction front can be described in different ways, with the simplest being a one-step reaction. The determination of the number of steps required to model the reaction front depends on many variables. A brief summary of the different models available is presented by Rein et al. (2006). The fine balance between the energy generated, oxygen flow/consumption, and heat transfer/loss that will direct decomposition of the fuel to one of the specific branches is controlled by many factors such as buoyancy, geometry, oxygen concentration, external heat supply, relative location of the reaction front, and fuel.

This discussion of fundamentals has primarily focused on porous solid fuels because these have underpinned the majority of research on smoldering to date.

Smoldering of NAPLs shares many similar characteristics, and while much less work is available because of its novelty, the majority of the fundamentals described above are expected to hold. For example, a similarly fine mass and energy balance is required for self-sustained conditions; however, the fuel is a typically a long-chain hydrocarbon or a mix of hundreds of hydrocarbons (e.g., crude oil and coal tar), so its pyrolysis and oxidation chemistry will be complex and unique. The main differences from smoldering of solids that do exist result from the fact that the fuel is distributed as a liquid occupying some or all of the porosity within an inert matrix (e.g., sand and soil). So, for example, the porosity of the systems are typically different, with porous solids like Figs. 18.1 and 18.2 at greater than 90% compared with sands typically around 35%. Also, the volume-to-surface-area ratio of the fuel is expected to be greater than the very small values for foam. Moreover, the effective permeability to air, which dictates the mass flux of oxygen through the reaction for a given pressure gradient, will be significantly less in the NAPL/soil system. Also the effective heat capacity of the sand, which dominates the sand/NAPL system, greatly exceeds that of highly porous solid fuels. All of these will have an effect on heat and mass transfer characteristics and the extinction limits of the process. Also, it affects the reaction kinetics and completeness, so, for example, it is typical that with a high heat capacity and forced airflow in NAPL/sand systems, no char will remain after the reaction passes. As with solid fuels, for the case of NAPL/soil systems, detailed understanding of these processes and process limits and the practical implications for soil remediation can only be achieved via studies at different scales.

18.3   Small scale

To systematically study the different mechanisms controlling smoldering of NAPLs, it is necessary to conduct a multiplicity of experiments using a small-scale setup. Pironi et al. (2009) used a cylinder of 100 mm in diameter and a height of 175 mm to sustain smoldering of a liquid fuel for the first time. A schematic diagram of the experimental apparatus is shown in Fig. 18.5. Upward smoldering combustion tests were carried out with coal tar. Inert sand (Leighton Buzzard 8/16 sand, WBB Minerals) of bulk density of 1.7 kg/m^3, porosity of 0.40, and diameter of the grains in the range of 1–2 mm was used as a porous medium. The fuel/sand mixture to be studied was prepared by mixing coal tar and coarse sand in a mass ratio corresponding to the desired saturation level of the sand pack. The saturation of the sand pack indicates the fraction of the pore volume filled with fuel; for the base case considered in this work (25% saturation), the corresponding amount of fuel per unit volume is 0.12 kg/m^3. The maximum power used for these experiments was of approximately 320 W, which corresponds to a heat flux of 41 kW/m^2 over the area of the horizontal section of the beaker.

The smoldering velocity is calculated from the time lapse of the front arrival at two consecutive thermocouples and the known distance between thermocouples. Images from the digital camera captured the propagation of the visible part of the smoldering front (Fig. 18.6). CO/CO$_2$ ratios proved to be a good indicator that an oxidative reaction was occurring. Fig. 18.6 shows the upward propagation of the front in the sand for a Darcy airflow velocity of 16.2 cm/s and a coal tar saturation of 25% as an illustration
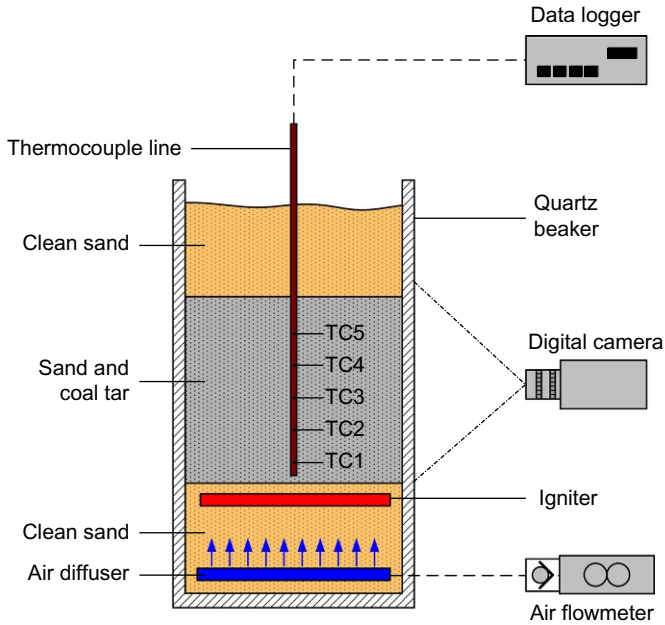
Fig. 18.5 Schematic of the experimental apparatus.
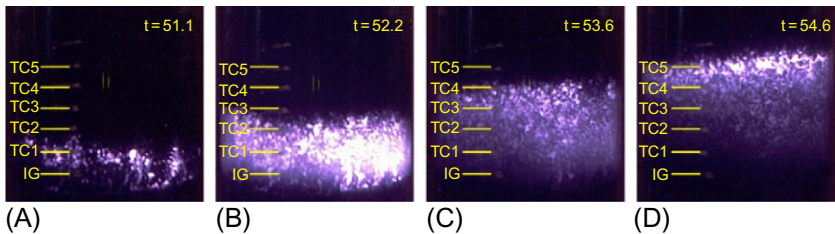
Fig. 18.6 Series images showing the ignition and propagation of the smoldering front for Darcy air velocity of 16.2 cm/s and a coal tar saturation of 25%. Numbers indicate the position of the thermocouples and the distance in cm from the igniter (IG). Times are in minutes and the sequence follows images from (A) (earliest) to (D) (latest).
From Pironi, P., Switzer, C., Rein, G., Gerhard, J.I., Torero, J.L., 2009. Small-scale forward smouldering experiments for remediation of coal tar. Proc. Combust. Inst. 32 (2), 1957–1964.

example. Similar observations could be made for other conditions. Although visible images are not a direct indication of the location and intensity of the reaction, they provide a qualitative description of the reaction front. The four images represent different moments in time. It can be seen that as the reaction front propagates through the contaminated porous media the reacting region increases in size. While propagation of the leading edge is controlled by heat transfer and the presence of oxygen, the trailing edge is controlled by total fuel consumption. It is important to note that all the oxygen is therefore not consumed at the reaction front, but it filtrates through the porous media

allowing for a thick reaction front. Fig. 18.2D shows that eventually, the fuel will be consumed and the region close to the igniter will cease to react. It is important to note that if the luminous intensity can be used as an indicator of the reaction rates, the intensity of the reaction initially increases (Fig. 18.2A and B), but once the ignition has been fully attained, a peak intensity is reached (Fig. 18.2B), and then, a dilution process follows (Fig. 18.2C and D). Oxygen will be consumed through the entire reaction region, and since the oxygen supply is fixed, the broader the reaction zone, the weaker the local smoldering. Image processing showed that the maximum luminous intensity was always at the leading edge of the reaction front.

Fig. 18.7A shows the temperature histories for the images presented in Fig. 18.6. The thermocouple traces confirm the progression established by the luminous intensity, where peak temperatures are attained by TC2 followed by a gradual decay. Furthermore, it can be seen that once the airflow is increase to the test value a sudden increase in temperature occurs showing the onset of a strong exothermic reaction. An important observation is that once the leading edge of the front has passed a thermocouple, the temperatures remain high for a short period of time and then decrease rapidly. Smoldering can occur through a wide range of temperatures; therefore, some oxidation seems to remain after the initial front has passed. The initial reduction of the fuel content might be the reason behind the reduction in temperature. This observation is important for remediation because it indicates that while most of the fuel is consumed with the initial front, continuation of the reaction is necessary for a complete cleanup of the soil.

Fig. 18.7B shows a particularity of self-sustained smoldering at a small scale; the leading and trailing edges of the reaction front progress at the same rate. After each experiment, the sand was excavated, and the degree of remaining contamination was visually estimated. In some cases, samples were analyzed by thermogravimetric
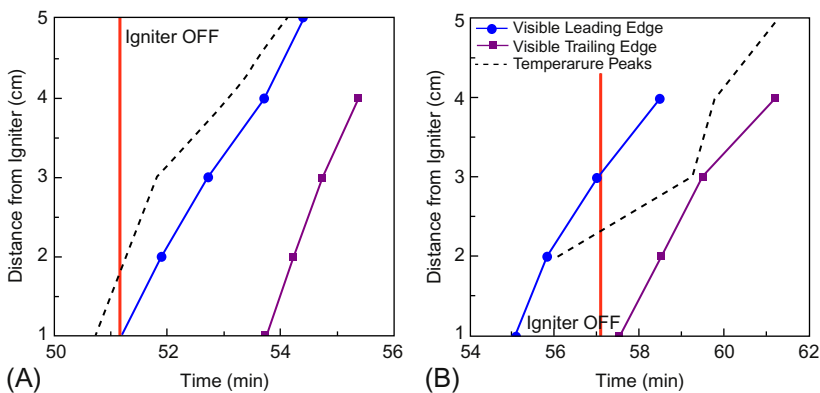
Fig. 18.7 Successive positions of the leading and trailing edges of the front in the visible range compared with the positions of the temperature peaks for (A) 16.2 cm/s and (B) 4.75 cm/s airflows.
From Pironi, P., Switzer, C., Rein, G., Gerhard, J.I., Torero, J.L., 2009. Small-scale forward smouldering experiments for remediation of coal tar. Proc. Combust. Inst. 32 (2), 1957–1964.

analysis and the gas products obtained by gas chromatography in order to assess the extent of fuel destruction and removal from the soil. No observable contamination was detected by visual inspection of sand coming from the central part of the beaker. A change of the sand color to red, attributable to iron oxidation, was indicative of exposure to high temperature (in excess of 600°C) for a long time. Samples taken from the sand in proximity of the beaker walls revealed the presence of visible residual contamination. While the images show a strong reaction through the extent of the sample, it is clear that in these zones, heat losses caused the extinction of the weaker residual smoldering reaction before complete conversion of the fuel. The mixture of sand and residual coal tar after cooling showed the presence of char not fully consumed. Gravimetric analysis following extraction by dichloromethane (DCM) revealed average rates of removal of 99.95% and 98%, respectively, for samples taken from the center of the beaker and in proximity of the walls. Volatile compounds (BTEX), determined by gas chromatography-mass spectrometry, were reduced down to not detectable levels in both the classes of sample.

Higher injected air velocities result always in faster propagation (Fig. 18.8) but not necessarily in higher temperatures (Fig. 18.9). This is typical of combustion in porous media and is mainly associated to the fine balance between oxygen consumption and heat transfer. The variation of the peak smoldering temperature along the sample is presented in Fig. 18.10 for the different airflow velocities. Peak temperatures at each location ranging from 789 to 1073°C were observed, with the highest values attained for the 4.25 cm/s airflow velocity. As mentioned before, it can be seen that peak temperatures are higher in the middle of the sample and decay toward the top end of it. As shown in Fig. 18.6, the reactive region width is increasing; therefore, the oxygen concentration is expected to decrease as the reaction propagates
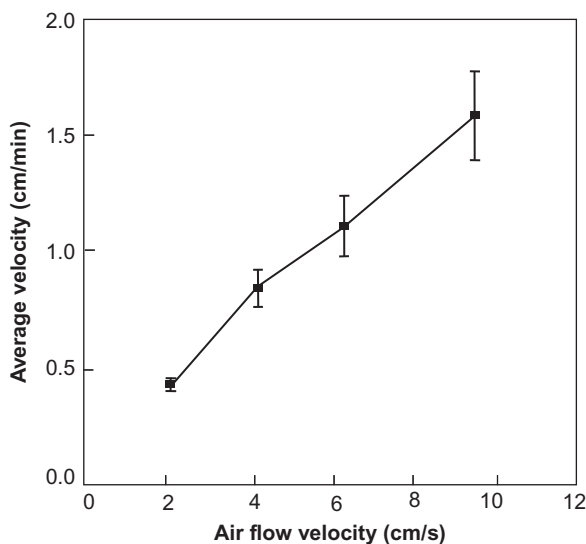
Fig. 18.8 Average smoldering velocity as a function of the airflow rate.
From Pironi, P., Switzer, C., Rein, G., Gerhard, J.I., Torero, J.L., 2009. Small-scale forward smouldering experiments for remediation of coal tar. Proc. Combust. Inst. 32 (2), 1957–1964

Fig. 18.9 Variation of the smoldering reaction maximum temperature along the sample for several airflow velocities.
From Pironi, P., Switzer, C., Rein, G., Gerhard, J.I., Torero, J.L., 2009. Small-scale forward smouldering experiments for remediation of coal tar. Proc. Combust. Inst. 32 (2), 1957–1964.
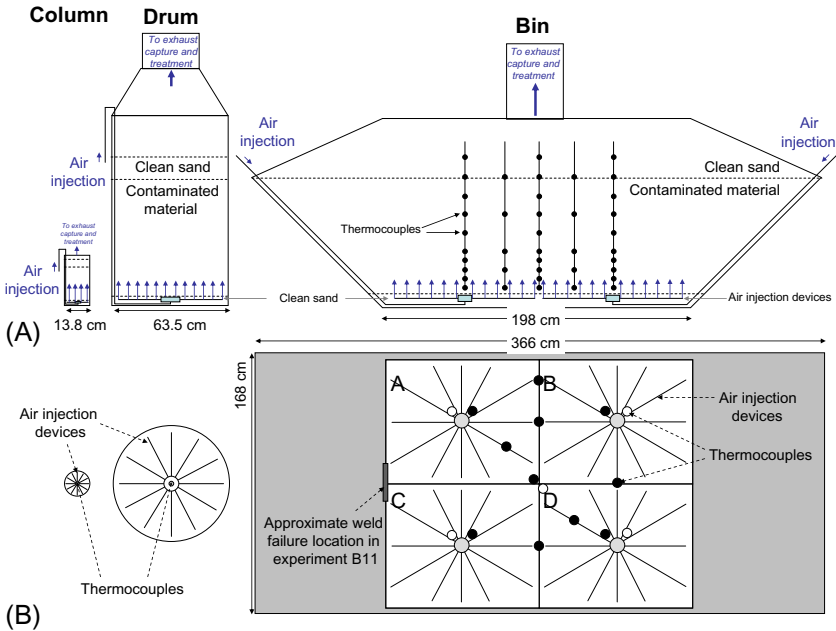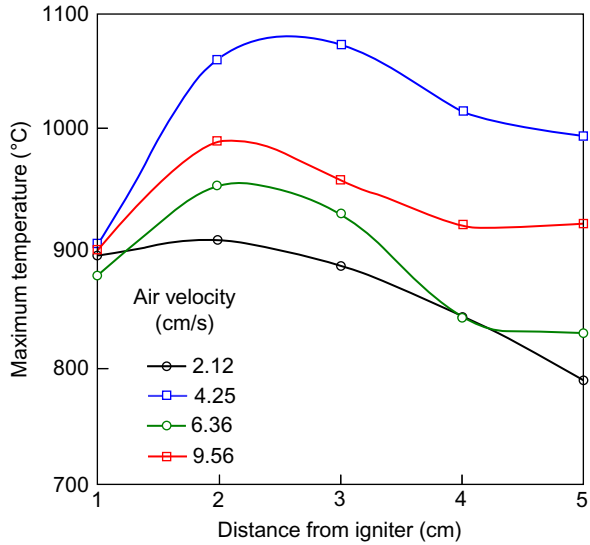
Fig. 18.10 Schematic diagrams detailing the setup of column, drum, and bin experiments with (A) side views showing geometry and layers of material and (B) top views showing air injection patterns and thermocouple locations (●○).
From Switzer, C., Pironi, P., Gerhard, J.I., Rein, G., Torero, J.L., 2014. Volumetric scale-up of smoldering remediation of contaminated materials. J. Hazard. Mater. 268, 51–60.

Table 18.1 **Variation of the average smolder velocity and the average peak temperature across the sample for different fuel saturation**

Saturation	10%	25%	50%
Average smolder velocity (cm/min)	0.94	0.84	0.61
Average peak temperature (°C)	784	1010	1045

leading to lower peak temperatures. Furthermore, for the lower air velocities, the reaction temperatures decrease below extinction values before the front reaches the end of the sample. The observed decay and extinction of the process in these experiments is indicative of weak propagation away from the igniter region. When propagation is weak, heat losses play a significant role. The effect of the heat losses to the external environment is to hamper smoldering propagation. In simple terms, the propagation velocity is proportional to the difference between the heat generated by the combustion and the heat lost to the exterior. A more detailed analysis is presented in (Bar-Ilan et al., 2004). It is important to note that the importance of the heat losses decrease as the area of the cross section of the reactor increases, due to a reduced surface-area-to-volume ratio, for the sample; therefore, a stronger smoldering process is expected at larger scales.

A set of tests were run varying the fuel saturation of the sample. The amounts of coal tar contained in the soil for each case were approximately of 0.048 kg/m^3 (10% saturation), 0.12 kg/m^3 (25%), and 0.24 kg/m^3 (50%). The inlet airflow was kept at a Darcy velocity of 4.25 cm/s. The results for the propagation velocity and peak temperature of these experiments are shown in Table 18.1. These results indicate that as the saturation increases the smolder velocity decreases approximately linearly, which confirms that for this range of saturation, the reaction is oxygen controlled. The results also indicate that the peak temperature increases with the fuel saturation.

18.4 Intermediate scale

A series of intermediate-scale experiments were conducted to extrapolate the small column results presented above (Switzer et al., 2014). Drum (intermediate-scale) experiments were carried out in a 0.3 m^3 oversize chemical drum (63.5 cm outer diameter and 104.1 cm height) designed almost identically to the column described above, representing a 100-fold volumetric scale-up. An air diffuser was embedded at the base of the drum and covered with a thin layer of sand. Three-coiled 3.8 m Inconel-sheathed heaters (240 V and 2000 W, Watlow Ltd, the United Kingdom) were emplaced above the air diffuser. The drum was packed with contaminated material to a depth of 40 cm and covered with 75 kg of clean sand, a depth of approximately

10 cm (Fig. 18.10A). The top of the drum was open to the atmosphere and operated under a purpose-built exhaust hood.

Bin (large-scale) experiments utilized a 3 m^3 chain-lift style dumpster as the experimental vessel, representing a scale-up of 10-fold from the drum and 1000-fold from the column. The base was 168×198 cm and the horizontal cross section increased to 168×366 cm at a height of 85 cm (Fig. 18.10A). Four air diffusers, similar in design to the drum experiments, were employed (Fig. 18.10B), effectively establishing the vessel as a four-quadrant simultaneous experiment for hardware installation and monitoring purposes; no physical divisions were embedded. The air diffusers were buried in a thin layer of clean sand layer. Twenty 3.8 m Inconel sheath cable heaters were laid across the clean sand lengthwise across the base. Contaminated material was loaded to a height of 80 cm. A clean sand layer of 5–15 cm was placed on top and heaped toward the center. The top boundary was open to the atmosphere and operated under a purpose-built exhaust canopy.

Surrogate contaminated soil was created by mixing coal tar with coarse sand in batches and loading them into them into the drum and bin, achieving starting concentrations of 46,400 and 31,000 mg/kg, respectively. In the bin experiments, approximately 80 thermocouples were divided into 16 vertical arrays of 5 sensors to avoid clusters of thermocouple rods forming large voids and preferential pathways that would disrupt the smoldering process (Fig. 18.10). The first two thermocouples were spaced 10 cm apart, and the remaining thermocouples were spaced 20 cm apart. Two arrays of thermocouples were placed at the center of each quadrant and the overall center of the bin, staggered to ensure thermocouples were present at 10 cm intervals to a depth of 80 cm; further, single arrays were deployed at interfaces between each of the quadrants (Fig. 18.10B).

The characteristic temperature evolution was observed at all thermocouple locations throughout the vessel (Fig. 18.11). While temperature evolutions reflected heterogeneities in packing and airflow delivery, the characteristic values were consistent with small-scale experiments. Imbalances generated by heterogeneities were overcome as the smoldering front moved upward through the porous material, consistent with a previous experiment (Pironi et al., 2009). Peak temperatures ranged from 800 to 1000°C as self-sustaining smoldering propagated through the vessel for approximately 6 h for the drum and 20 h for the bin before the reaction self-terminated when insufficient fuel remained. Complete smoldering was observed at all locations, indicating robustness of the process in the presence of sufficient fuel and oxygen.

Excavation of the experiments showed visibly clean material throughout the vessel (Fig. 18.12 for the bin). Postremediation contamination levels were an average of 17 ± 3 mg/kg (30 samples) throughout the bin and 10 ± 1 mg/kg (20 samples) in the area that was initially contaminated. This reduction in concentration represents 99.95% remediation across the 3 m^3 vessel. Slightly elevated contamination levels were observed on the surface, but these were all below 100 mg/kg and likely related to condensation of volatiles in the clean sand cover.
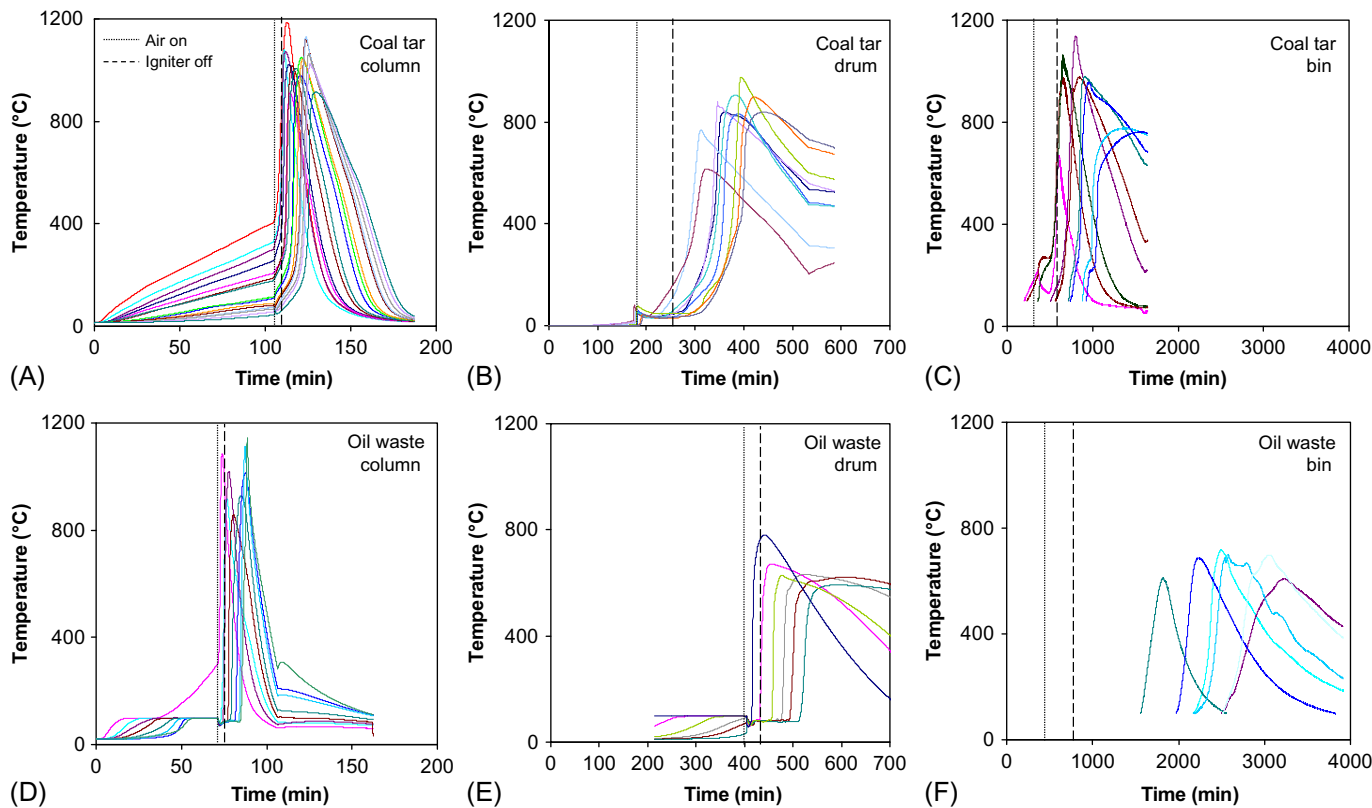
Fig. 18.11 Smoldering remediation experiments for (A) coal tar in sand (0.003 m^3), (B) coal tar in sand (0.3 m^3), (C) coal tar in sand (3 m^3), (D) mixed oil waste (0.003 m^3), (E) mixed oil waste (0.3 m^3), and (F) mixed oil waste (3 m^3).
From Switzer, C., Pironi, P., Gerhard, J.I., Rein, G., Torero, J.L., 2014. Volumetric scale-up of smouldering remediation of contaminated materials. J. Hazard. Mater. 268, 51–60.
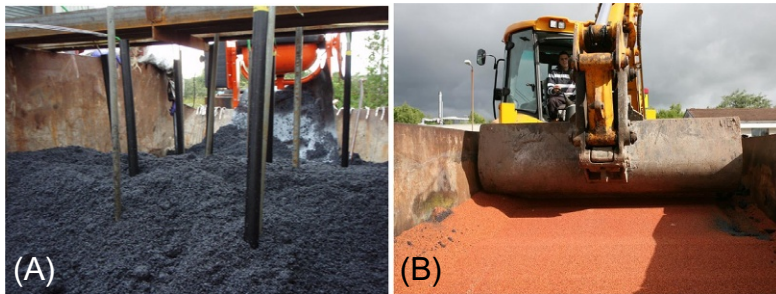
Fig. 18.12 Experiment B10 (3 m³). (A) Coal tar mixed with coarse sand before remediation, with thermocouple insertion sleeves visible. (B) Clean sand after remediation (99.95+% concentration reduction).
From Switzer, C., Pironi, P., Gerhard, J.I., Rein, G., Torero, J.L., 2014. Volumetric scale-up of smouldering remediation of contaminated materials. J. Hazard. Mater. 268, 51–60.

18.5 NAPL mobility

Potential mobilization of the fuel within the porous matrix is a unique issue for liquid fuels relative to solid porous fuels in the context of smoldering. Moreover, increases in scale enhance the importance of NAPL mobility. Considering NAPL mobility in the context of smoldering requires a new conceptual model. Fig. 18.13 illustrates
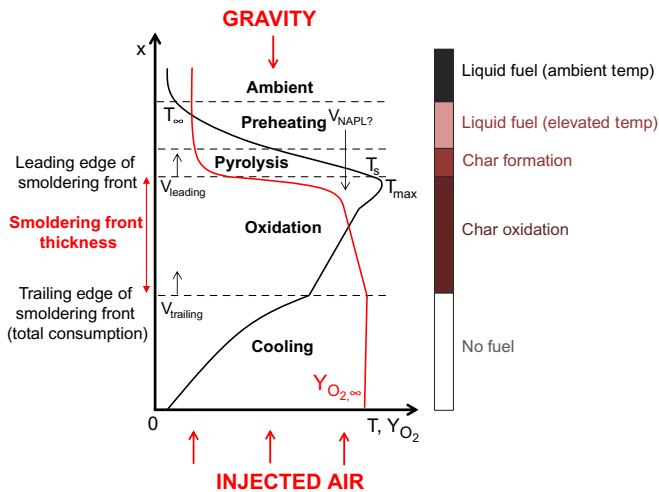
Fig. 18.13 Conceptual model of the distribution of temperature and oxygen concentrations in a column experiencing upward, forward propagation of a smoldering reaction. The key force vectors *(red arrows)* are labeled. The key regions in the system are named, and the associated form of the NAPL (fuel) is identified on the right-hand side.
From Kinsman, L., Gerhard, J.I., Torero, J.L., 2017. Smoldering remediation and non-aqueous phase liquid mobility. J. Hazard. Mater. 325, 101–112.

a snapshot of the vertical distribution of temperature and oxygen concentration for a smoldering reaction traveling upward in a one-dimensional column (Kinsman et al., 2017). The column contains a high viscosity NAPL (e.g., coal tar) embedded in an inert matrix (e.g., quartz sand) at a given saturation with the remaining porosity occupied by air. In the ambient region ahead of the front, NAPL and soil are at ambient temperatures (T_∞), and the NAPL is therefore unchanged physically or chemically. In the preheating region (e.g., 50–200°C), soil and NAPL are absorbing energy transmitted via conduction (through soil/NAPL) and convection (of heated air) from the smoldering front below. In the presence of the higher temperatures (e.g., 200–350°C) and lower oxygen concentrations of the pyrolysis region, the NAPL undergoes endothermic, nonoxidative decomposition of the fuel (Torero and Fernandez-Pello, 1996). These pyrolysis reactions are expected to convert the NAPL into a char, which is immobile. The top of the oxidation region, demarking the leading edge of the smoldering front, exists where the NAPL smoldering ignition temperature (T_s) is exceeded (e.g., >350°C) and oxygen concentrations are high, and therefore, exothermic oxidation reactions occur. In this region, oxygen is consumed, NAPL (now char) is consumed, and energy is generated leading to a characteristic peak temperature observed for the given contaminant (T_{max}).

The trailing edge of the smoldering front occurs at the point of total fuel consumption, below which no NAPL remains. Since they are governed by different processes, the velocities of the leading and trailing edges of the smoldering fronts ($V_{leading}$ and $V_{trailing}$) are not necessarily equal. $V_{leading}$ will generally be controlled by the rate that heat is transferred forward, while $V_{trailing}$ is determined by the rate of mass destruction, which is dictated primarily by combustion chemistry and oxygen mass flux. When $V_{trailing} < V_{leading}$, the smoldering front thickness will expand with time.

Just above the trailing edge in the oxidation region, temperatures are relatively low, so chemical reactions are relatively slow, and oxygen is slowly consumed. Oxygen consumption will result from a complex function of the relative speed of the oxidation with respect to residence times (i.e., Damköhler number). Closer to the leading edge the temperatures will be higher, the reaction rates faster and therefore oxygen consumption will be more significant. In the cooling region, all NAPLs have been consumed, and the inert porous matrix experiences decreasing temperatures due to heat loss, primarily via convection from the ambient temperature air injected below.

There is the potential for NAPL mobilization in the preheating region. NAPL may migrate at a certain velocity (V_{NAPL}) depending on the NAPL viscosity and the NAPL hydraulic gradient. The direction and magnitude of the gradient depend primarily on the relative influence of gravity and the forces induced by upward flowing air. At ambient temperatures, the high viscosity of long-chain hydrocarbons means migration is slow even in the presence of significant hydraulic gradients (Gerhard et al., 2007). However, liquid viscosity decreases rapidly with increasing temperatures (Potter and Wiggert, 2002), and therefore, V_{NAPL} may increase in the elevated temperatures of the preheating region. NAPL viscosity may decrease by a factor of 10–1,000,000 over this temperature range, and the sensitivity to temperature is highly dependent on NAPL chemistry.

Reduction of NAPL viscosity ahead of a heating front is known to result in mobilization in numerous applications. In situ combustion for enhanced oil recovery (Thomas, 2008) and steam injection for remediation (Kaslusky and Udell, 2005) take advantage of heat-induced viscosity reductions to mobilize residual NAPL. NAPL is intentionally mobilized for its recovery in those cases, and it is therefore applied in a horizontal sweep configuration in the subsurface; of course, NAPL loss via downward remobilization can also occur (Kaslusky and Udell, 2005). In the context of smoldering treatment of NAPL-contaminated soil in a vertical column (or applied as an ex situ vertical reactor), the reaction is traveling upward, and NAPL has the potential to migrate downward into the smoldering front (Fig. 18.14). NAPL migration could conceivably affect smoldering in numerous ways including changing the spatial distribution of the fuel (reduced NAPL saturations ahead of the front and increased saturation closer to the front), addition of extra fuel (i.e., energy) to the smoldering reaction, addition of a heat sink (i.e., colder fuel from above) to the reaction, or even penetration of the fuel through the reaction contaminating the cleaned soil below.

Fig. 18.14 shows the temperature history for the 90 cm column with a forced Darcy air flux of 2.5 cm/s. This experiment displayed typical smoldering behavior from approximately TC1 to TC12, including constant velocity of the leading edge (0.41 ± 0.07 cm/min) and trailing edge of the smoldering front (0.32 ± 0.07 cm/min) and consistent peak temperatures ($564 \pm 17°C$). However, atypical behavior is observed beginning at nondimensionalized time (NDT) $= 0.6$. Kinsman et al. (2017) choose to nondimensionalize the time by the time required to reach the end
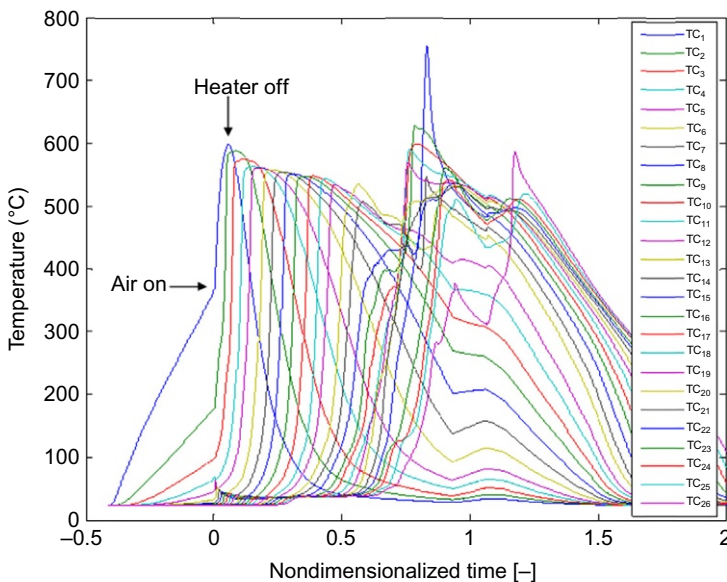
Fig. 18.14 Temperature history for 90 cm column with forced Darcy air flux of 2.5 cm/s. From Kinsman, L., Gerhard, J.I., Torero, J.L., 2017. Smoldering remediation and non-aqueous phase liquid mobility. J. Hazard. Mater. 325, 101–112.

of the contaminated soil sample. The steady progression of the front is interrupted and both dips and spikes in temperature are observed beyond this time. Understanding what at first appears to be chaotic behavior is assisted by examining individual thermocouples. As described previously, TC4 displays typical smoldering behavior. At TC14, ignition of smoldering is similar; however, it is interrupted before reaching standard peak temperature. The interruption consists of a cooling period followed by a second ignition event that results in a peak in temperature. Only after this peak is achieved is typical cooling behavior observed. This pattern is repeated for all TCs after NDT = 0.6, and the temperatures of these second peaks continue to increase, as shown in Fig. 18.14. As a result, the upper half of the column sees peak temperatures as high as 750°C, far beyond the typical peak smoldering temperature in the lower half (564 ± 17°C).

The most likely explanation for this is that very unusual smoldering behavior is downward NAPL migration. Consider TC14; (i) NAPL in the preheating zone, exhibiting reduced viscosity due to elevated temperature, migrates downward at a high enough rate or in a sufficient quantity that it impinges this location when the NAPL smoldering front is just arriving; (ii) this migrating NAPL is cooler than the combustion temperatures at TC14, acting as a heat sink; (iii) energy at TC14 is consumed in preheating and pyrolysis of this new fuel, adding to the temperature decline; (iv) the mobilized NAPL, now pyrolyzed, provides additional fuel that ignites, causing reignition and renewed smoldering; and (v) as the leading edge of the smoldering front continues to advance upward, this process is also shifted upward, and the TC14 location is able to smolder to completion and cool. The fact that higher/later thermocouples exhibit more substantial temperature dips and higher peaks suggest the process becomes more significant with the larger preheating zone thicknesses that evolve in taller systems. This is the reason that these NAPL migration effects should be observed after NDT = 0.6 and not before in this experiment and are observed only in columns 90 cm and not 30 cm columns.

It is noted that, despite the observed effects of NAPL mobility on the reaction characteristics, NAPL was never found to have penetrated or bypassed the smoldering front. Rather, in all cases, the reaction accommodated the incoming NAPL by increasing the thickness of the reaction zone and all cases resulted in completely clean material at the end of the test. This indicates the robust nature of smoldering, its energy efficiency enabling it to consume all fuel even when the fuel is distributed heterogeneously and in a manner that varies with time.

18.6   Large scale

Two large-scale pilot tests were conducted in the area of a backfilled lagoon at a contaminated site that was operated from the early 1900s until 1983 (Geosyntec, 2012) and are described by Scholes et al. (2015). The lagoon was 2.5–3.5 m deep and was used to dispose of coal tar and its by-products. Beneath this unit is a 0.3–0.6 m thick confining clay "meadow mat" layer composed of clay, silt, and peat. It is underlain by an alluvium unit, composed of medium to coarse sands up to 6 m thick (herein referred

to as the "deep sand unit"). The water table at the site is approximately 1 m below ground surface. Coal tar DNAPL (denser-than-water NAPL) exists as a potentially mobile, highly saturated pool up to 1.3 m thick within the shallow fill unit upon the meadow mat. Coal tar is also present in the upper 4–5 m of the deep sand unit in locations where the original lagoon excavation activities appear to have removed the meadow mat, thereby providing pathways for DNAPL migration into this deeper unit. The two pilot tests consisted of one in the shallow fill unit, referred to as the "shallow test," and a "deep test" conducted in the deep sand unit below the same lagoon and adjacent to the shallow test cell (Fig. 18.15). Each test area had a centrally installed 5 cm diameter stainless steel well with a 30 cm long wire-wrapped (10 slot) screen that served as the ignition well and for delivering heat and air. In both cases, the screen was located near the base of a significant coal-tar-contaminated interval as detected by investigational borings. Custom-built, removable, down-well electric heaters were used to ignite NAPL adjacent to the ignition wells via convective heat transfer. The heaters were turned off following ignition (confirmed by the detection of combustion gases in collected vapors), and air injection flow rates were manipulated manually at the well to maintain and propagate the combustion front in a self-sustaining manner. A vapor cap was installed to control and monitor combustion gases and vapors for both tests. Within each vapor cap, vertical or horizontal extraction conduits were emplaced to collect vapors for the shallow and deep tests, respectively. Direct-push coring methods were used to collect pre- and posttest soil samples.

A self-sustained smoldering reaction was maintained below the water table in both pilot tests, for 12 days and 11 days in the shallow and deep tests, respectively. The mass of coal tar destroyed in the shallow and deep tests were estimated to be 3700 and 860 kg, respectively. Mass destruction rates ranged from 1 to 43 kg/h in the shallow test and 1–7 kg/h in the deep test. Changes in combustion gas (CO and CO_2)
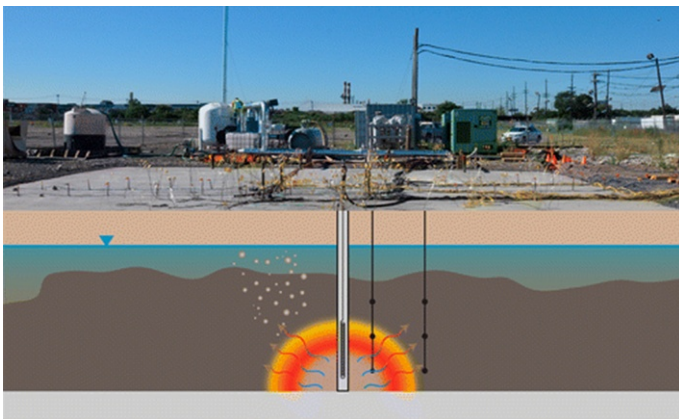
Fig. 18.15 Schematic of the large-scale tests.
From Scholes, G.C., Gerhard, J., Grant, G., Major, D., Vidumsky, J., Switzer, C., Torero, J., 2015. Smoldering remediation of coal-tar-contaminated soil: pilot field tests of STAR. Environ. Sci. Technol. 49 (24), 14334–14342.

concentrations versus time in extracted vapors from the shallow and deep tests reveal the strength of the reaction, thus indicating where intervention is necessary (either reignition or a new well for airflow).

Soil contaminant concentration was reduced in the shallow test cell from a mean pretest concentration of 37,900 mg/kg ($n=15$ and standard deviation$=50,800$ mg/kg) to a mean posttest concentration of 258 mg/kg ($n=8$ and standard deviation$=185$ mg/kg) equating to an average remediation efficiency of 99.3%. In the deep test, it was reduced from a mean pretest concentration of 18,400 mg/kg ($n=8$ and standard deviation$=13,400$ mg/kg) to a mean posttest concentration of 450 mg/kg ($n=14$ and standard deviation$=1100$ mg/kg) for an average remediation efficiency of 97.6%. Fig. 18.16 presents the concentrations of all pre- and post-field test soil samples collected from within the treatment areas for the shallow and deep field tests as a function of depth of sample. Posttest soil cores from both pilot tests (eight from the shallow test and nine from the deep test) from within the combustion zones indicated no NAPL and visibly reduced moisture levels. Gas analysis on the recovered emissions revealed that less than 2% of the coal tar was volatilized, indicating that in situ destruction by combustion (rather than mobilization or mass/phase transfer) was responsible for this extensive remediation.
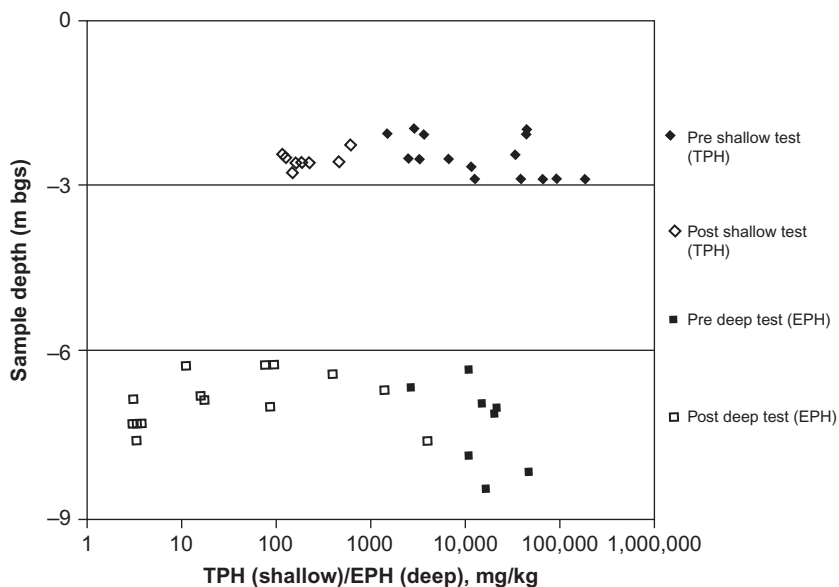
Fig. 18.16 Pre- and post-TPH (shallow fill) and EPH (deep sand) soil concentrations by sample depth. All posttest samples are collected from within inferred combustion zones. Note that the depth (vertical) axis is linear scale, and the soil concentration (horizontal) axis is logarithmic. From Scholes, G.C., Gerhard, J., Grant, G., Major, D., Vidumsky, J., Switzer, C., Torero, J., 2015. Smoldering remediation of coal-tar-contaminated soil: pilot field tests of STAR. Environ. Sci. Technol. 49 (24), 14334–14342.
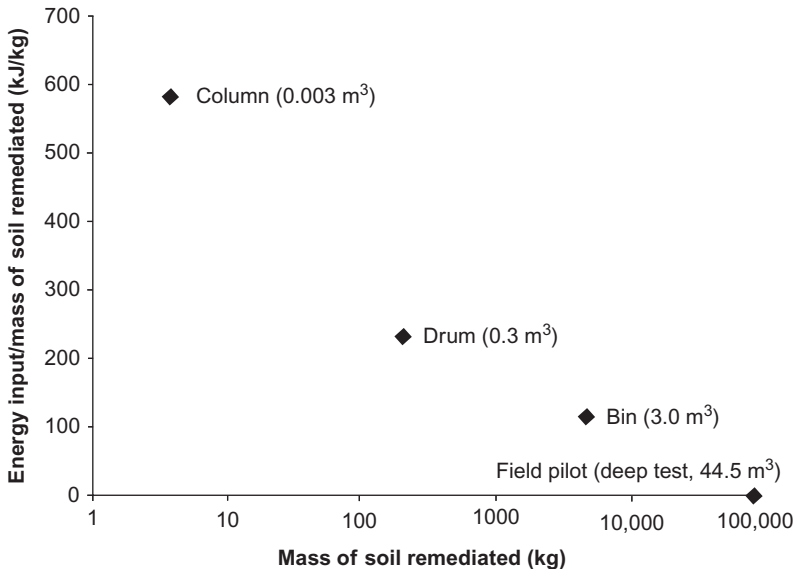
Fig. 18.17 Energy for ignition for increasing scales of coal tar smoldering experiments demonstrating the increasing energy efficiency of the smoldering process with scale of application. Data from column, drum, and bin scale ex situ experiments taken from Switzer et al. (2014) and Scholes et al. (2015).

The energy for ignition in the deep test was estimated to be 1.1 kJ/kg of soil remediated based on achieving self-sustained smoldering following approximately 3 h of heater operation and resulting, after 10 days, in 44.5 m^3 of soil remediated. Fig. 18.17 presents energy for ignition values as a function of scale and includes this calculated value for the deep test and the results of ex situ coal tar smoldering experiments conducted at a variety of scales by Scholes et al. (2015) and Switzer et al. (2014). This plot reveals that the self-sustained smoldering reaction becomes increasingly efficient (less heat energy input per mass of soil remediated) with increasing scale of application (note the logarithmic scale on the independent axis). This behavior is expected because heat losses to the external environment are reduced with increasing scale and the available radius of influence for a single ignition event increases substantially. This reveals a benefit of self-sustained smoldering, since all other thermal treatment methods utilize endothermic processes and require approximately constant and continuous energy input per mass of soil treated; for example, in situ thermal desorption typically requires between 300 and 700 kJ/kg at the field scale (Triplett Kingston et al., 2014). The short energy input required by self-sustaining smoldering relative to the potential treatment mass illustrates a clear benefit of smoldering, its energy efficiency.

The shallow and deep tests demonstrated ignition and propagation of a self-sustaining smoldering reaction in coal-tar-contaminated soils in situ and below the water table. In situ destruction of coal tar was observed at rates up to 43 kg/h resulting

from a single ignition well, and smoldering fronts were found to propagate greater than 4 m from an ignition well at rates up to 1 m/day. In situ heterogeneity was observed to play a role in the rate and uniformity of smoldering front spread because it strongly influences the distribution of air. Although not determined in these tests, it is expected that the radius of influence of a single well will be determined by the distance where the local air velocity falls below a threshold (oxygen mass flux) required to sustain the reaction. Petroleum hydrocarbon concentrations in treated soils (i.e., from combustion zones) were reduced on average by 98.5%.

18.7   Other applications

Due to the high energy efficiency, smoldering combustion is an attractive alternative for the treatment of organic waste with high moisture content. High moisture content results in a low effective calorific value, necessitating substantial predrying or the use of supplemental fuel to avoid quenching of the combustion reaction. Smoldering combustion overcomes these limitations by efficiently transferring reaction heat to unburned fuel, enabling comparable timescales of combustion and heat transfer (Howell et al., 1996).

Smoldering combustion of feces was studied by Yermán et al. as part of a new integrated, low-cost, on-site sanitation system aiming to rapidly disinfect human waste using minimal resources (Yermán et al., 2015). This application shows the potential of smoldering for other forms of in situ management of waste (e.g., waste landfills). The reactor configuration was similar to that showed in Fig. 18.5. Experiments of feces mixed with sand were carried out in a stainless-steel column (16 cm inner diameter and 100 cm height). A porous matrix is created with the necessary heat retention and air permeability properties for smoldering combustion by mixing the feces with sand. Sand is used because it is a low cost and because it has been identified as an effective agent for increasing the porosity of fuels for the NAPL destruction (Pironi et al., 2009). To manage the regulatory challenges of working with real feces and to control the experimental variables, surrogate feces were used. Additional experiments with dog feces were also conducted to confirm consistent results. Dog feces were selected because it contains minimal human pathogens. Overall, this work serves as an initial investigation into the feasibility of applying this approach in a waste treatment system.

A parameter space has been mapped for conditions yielding self-sustaining smoldering of surrogate feces mixed with sand by varying moisture content, mixture pack height, airflow rate, and sand-to-fuel ratio (S/F). Results showed that the ranges of self-sustainability for each parameter are not independent; rather, they are interdependent in a complex manner. The parameter space in which a robust self-sustaining process operates was identified. Fig. 18.18 shows the interdependency of some of these parameters for the smoldering of surrogate feces mixed with sand. For example, if the moisture content of the waste is increased, then the pack height of mixture in the reactor must be shortened and the sand concentration increased. A similar situation occurs with the relationship between airflow rate and sand concentration, where higher sand concentrations allow lower airflow rates.
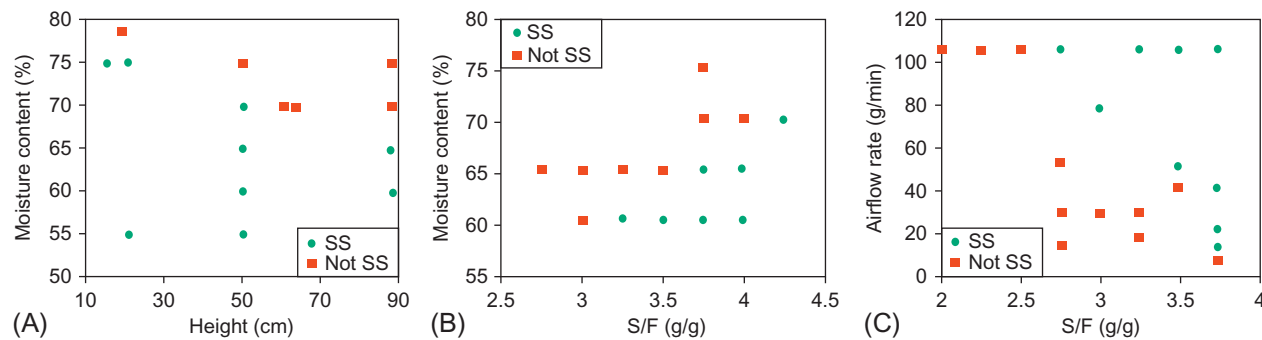
Fig. 18.18 Parameter space outlining the range of conditions yielding self-sustaining (SS) and not self-sustaining (not SS) smoldering: (A) moisture content versus height of sand-fuel mixture, (B) moisture content versus sand-to-fuel mass ratio (S/F), and (C) airflow rate versus sand-to-fuel mass ratio.

From Yermán, L., Hadden, R.M., Pironi, P., Torero, J.L., Gerhard, J.I., Carrascal, J., et al., 2015. Smouldering combustion as a treatment technology for faeces: exploring the parameter space. Fuel 147, 108–16.

The smoldering performance is usually assessed in terms of smoldering propagation velocity and average temperatures. The control of the smoldering velocity is useful to determine the reactor scale and other operative conditions, while the estimation of the temperature can shade light on the potential energy recovery of the overall process. Yermán et al. studied the influence of key operational parameters on the smoldering performance (Yermán et al., 2016). A set of experiments of smoldering combustion of feces mixed with sand under a range of experimental conditions were carried out under robust and self-sustaining conditions. The parameters studied were moisture content, sand-to-feces mass ratio, sand particle size, airflow, and ignition temperature. Ignition temperature was defined as the temperature at 2 cm from the heater when the airflow is initiated.

Results reveal that the airflow rate is by far the most crucial parameter affecting the smoldering velocity. Fig. 18.19A shows that there is a linear relationship between the air Darcy flux and the velocity of propagation. Therefore, the airflow can be easily utilized to modulate the smoldering velocity during the treatment process. This observation is consistent with other applications and therefore reaffirms that independent of the fuel and porous medium, airflow seems to be always the controlling parameter.

In contrast, in what regards smoldering temperatures, the relative amount of sand used appears to have the greatest impact. It was observed that by changing
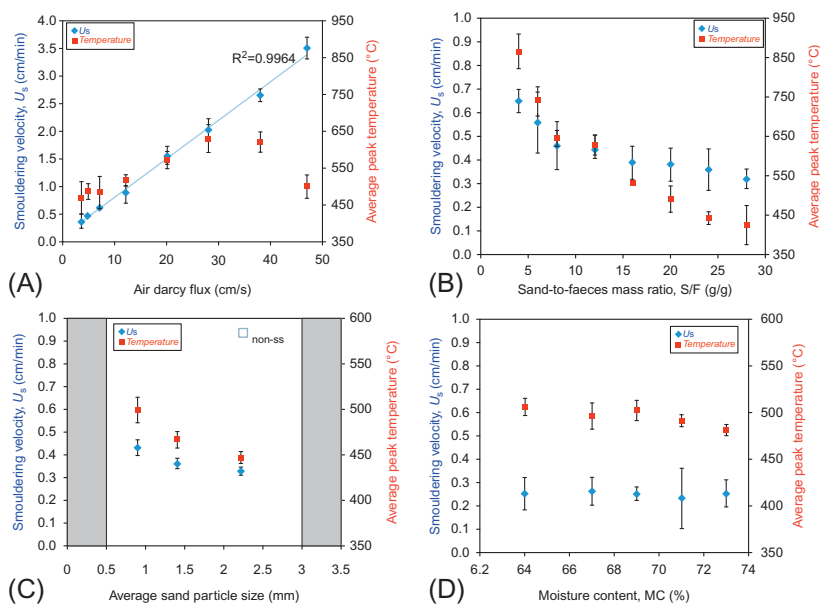
Fig. 18.19 Average peak temperature and smoldering velocity as a function of moisture content of feces (A), sand-to-feces mass ratio (B), air Darcy flux (C), and average sand particle (D). Adapted from Yermán, L., Wall, H., Torero, J.L., Gerhard, J.I., Cheng, Y.-L., 2016. Smoldering combustion as a treatment technology for faeces: sensitivity to key parameters. Combust. Sci. Technol. 188, 968–981.

the sand-to-feces mass ratio, the temperatures can be modulated within a range of almost 500°C. On the other hand, the impact of this ratio on the smoldering velocity is not as great as the influence of the airflow, showing differences below 0.4 cm/s for the same range studied (Fig. 18.19B).

The sand grain size shows to have a minor effect on the smoldering temperatures and velocities (Fig. 18.19C). Nevertheless, it does have an important impact in maintaining self-sustaining smoldering. Self-sustaining smoldering was not observed for sand particle sizes below 0.5 mm or above 3.0 mm.

The moisture content in the feces acts as an energy sink and is the most crucial parameter to determine the self-sustainability of the process. Higher velocities and temperatures were registered for dried feces compared with wet (67%) feces (not shown in figure). Nevertheless, results showed that within the applicability range of moisture content for feces (65%–73%), this seems to have a minimal impact on the smoldering velocity and temperature (Fig. 18.19D). This is of fundamental importance because it confirms the observation by Kinsman et al. (2017) that smoldering will be self-sustaining if the water front is displaced ahead of the smoldering front.

18.8   Summary

The viability of using smoldering combustion as a mechanism of in situ treatment of contaminated soils has been presented. It has been shown that fuel/sand content, air-flow, and fuel concentrations determine the rates of destruction of the contaminant. The role of heat losses is weak and its importance decreases with scale. Larger-scale in situ soil remediation has been proved viable but requires consideration of hetero-geneities and NAPL migration. Under robust self-sustained smoldering destruction rates always exceed 98%. Self-sustained smoldering has been achieved in a robust and consistent manner at scales ranging from 0.003 to approximately 45 m^3 including below the water table.

References

Anderson, M., Sleight, R., Torero, J.L., 2000. Downward smolder of polyurethane foam: igni-tion signatures. Fire Saf. J. 35, 131–148.

Babrauskas, V., July–August 1996. NFPA Journal.

Bar-Ilan, A., Rein, G., Fernandez Pello, A.C., Torero, J.L., Urban, D.L., 2004. Effect of buoy-ancy on forced forward soldering. Exp. Thermal Fluid Sci. 28, 743–751.

Bilbao, R., Mastral, J.F., Ceamanos, J., Aldea, M.E., 1996. Kinetics of the thermal decompo-sition of polyurethane foams in nitrogen and air atmospheres. J. Anal. Appl. Pyrolysis 37 (1), 69–82.

DeSoete, G., 1966. In: Eleventh Symposium (Int) on Combustion. The Combustion Institute, Pittsburgh, PA, pp. 959–966.

Drysdale, D.D., 2011. Introduction to Fire Dynamics, third ed. John Wiley and Sons, Chichester, West Sussex, UK.

Geosyntec Consultants, 2012. Remedial Action Work Plan. Geosyntec Consultants, Inc., Guelph.

Gerhard, J.I., Pang, T., Kueper, B.H., 2007. Time scales of DNAPL migration in sandy aquifers examined via numerical simulation. Ground Water 45 (2), 147–157.

Greaves, M., Tuwil, A.A., Bagci, S., 1993. Horizontal producer wells in in situ combustion (ISC) processes. J. Can. Pet. Technol. 32, 58–67.

Howell, J.R., Hall, M.J., Ellzey, J.L., 1996. Combustion of hydrocarbon fuels within porous inert media. Prog. Energy Combust. Sci. 22, 121–145.

Interagency Committee on Cigarette and Little Cigar Fire Safety, 29 October 1987. Toward a Less Fire Prone Cigarette, Report Submitted to United States Congress.

Kaslusky, S.F., Udell, K.S., 2005. Co-injection of air and steam for the prevention of the downward migration of DNAPLs during steam enhanced extraction: an experimental evaluation of optimum injection ratio predictions. J. Contam. Hydrol. 77 (4), 325–347.

Kinsman, L., Gerhard, J.I., Torero, J.L., 2017. Smoldering remediation and non-aqueous phase liquid mobility. J. Hazard. Mater. 325, 101–112.

Ohlemiller, T., 1985. Modeling of smoldering combustion propagation. Prog. Energy Combust. Sci. 11, 277–310.

Ortiz Molina, M.G., Toong, T.Y., Moussa, N.A., Tesero, G.C., 1979. Smoldering combustion of flexible polyurethane foams and its transition to flaming or extinguishment. In: Seventeenth Symposium (International) on Combustion. The Combustion Institute, pp. 1191–1200.

Pironi, P., Switzer, C., Rein, G., Gerhard, J.I., Torero, J.L., 2009. Small-scale forward smouldering experiments for remediation of coal tar. Proc. Combust. Inst. 32 (2), 1957–1964.

Potter, M.C., Wiggert, D.C., 2002. Mechanics of Fluids, third ed. Brooks Cole/Thompson Learning, Pacific Grove, CA.

Rein, G., Lautenberger, C., Fernandez-Pello, A.C., Torero, J.L., Urban, D.L., 2006. Smoldering combustion of polyurethane foam: using genetic algorithms to derive its kinetics. Combust. Flame 146 (1–2), 95–108.

Sarathi, P.S., 1999. In Situ Combustion Handbook—Principles and Practices. U.S. Department of Energy, National Petroleum Technology Office, Tulsa, OK, USA.

Scholes, G.C., Gerhard, J., Grant, G., Major, D., Vidumsky, J., Switzer, C., Torero, J., 2015. Smoldering remediation of coal-tar-contaminated soil: pilot field tests of STAR. Environ. Sci. Technol. 49 (24), 14334–14342.

Schult, A., Matkowsky, B.J., Volpert, V.A., Fernandez-Pello, A.C., 1995. Propagation and extinction of forced opposed flow smolder waves. Combust. Flame 101 (4), 471–490.

Switzer, C., Pironi, P., Gerhard, J.I., Rein, G., Torero, J.L., 2014. Volumetric scale-up of smoldering remediation of contaminated materials. J. Hazard. Mater. 268, 51–60.

Thomas, S., 2008. Enhanced oil recovery—an overview. Oil Gas Sci. Technol. 63 (1), 9–19.

Torero, J.L., Fernandez-Pello, A.C., 1996. Forward smolder of polyurethane foam in a forced air flow. Combust. Flame 106, 89–109.

Triplett Kingston, J.L., Johnson, P.C., Kueper, B.H., Mumford, K.G., 2014. In situ thermal treatment of chlorinated solvent source zones. Chlorinated Solvent Source Zone Remediation. Springer, New York, p. 527 (Chapter 14).

Williams, F.A., 1976. Mechanisms of fire spread. In: Sixteenth Symposium (International) on Combustion. The Combustion Institute, pp. 1281–1293.

Yermán, L., Hadden, R.M., Pironi, P., Torero, J.L., Gerhard, J.I., Carrascal, J., et al., 2015. Smouldering combustion as a treatment technology for faeces: exploring the parameter space. Fuel 147, 108–116.

Yermán, L., Wall, H., Torero, J.L., Gerhard, J.I., Cheng, Y.-L., 2016. Smoldering combustion as a treatment technology for faeces: sensitivity to key parameters. Combust. Sci. Technol. 188 (6), 968–981. https://doi.org/10.1080/00102202.2015.1136299.

This page intentionally left blank

Advanced measurements and monitoring techniques

A. Veeraragavan
The University of Queensland, Brisbane, QLD, Australia

19.1 Introduction

Measurement and monitoring techniques for both underground coal gasification (UCG) and underground coal fires have several commonalities. In this chapter, we will present several of these techniques that were initially developed for UCG but have subsequently found applications also in the detection of underground combustion pertaining to coal fires. The presence of an underground coal fire is usually felt through changes in the ambient air quality (foul smells), smoke, or heat emanating from the ground. Typically, these symptoms only manifest themselves long after the fire has persisted and spread over a wide area. In extreme cases, the detection becomes a relatively moot point as smoke emanating from the ground or subsidence of the soil makes it evident that there is an underground coal fire. For example, the Centralia underground coal fire shown in Fig. 19.1 is an easy to witness/detect fire after it has spread extensively over a large enough area such that it can visibly affect the terrestrial domain. In this case, the fire has caused the highway to crack apart. In such cases, it is often even possible to view the coal seam burning through fissures and cracks if the fire is not very deep underground. However, the detection of such fires at early stages or when it is deep underground is rather challenging and requires tools and diagnostics beyond the human sensory perception.

The science of detection of underground coal fires has rapidly advanced in the last two to three decades with the advent of modern computers, spectroscopic, thermographic, sonar, and other gas detection methods. Many of these techniques are covered in great detail in comprehensive reviews in literature (Song and Kuenzer, 2014). In this chapter, we present an overview of the various technologies and methods employed to detect, monitor, and measure the extent of underground combustion, for both fires and gasification technologies.

19.2 Detection and monitoring

19.2.1 Typical evidence of underground combustion/gasification

As mentioned in "Introduction," there are many typical evidences for an underground combustion process. The main ones are subsidence, noxious gas emissions, cracks/fissures, hot surface temperatures, and smoke.

Fig. 19.1 Centralia underground coal fire.
Source: https://www.flickr.com/photos/jsjgeology/8280902685/in/photostream/, Title: Cracked-highway 4, posted by James St. John under license, https://creativecommons.org/licenses/by/2.0/legalcode.

Noxious gases such as sulfur oxides (SOx) and nitrogen oxides (NOx) are formed by the process of smoldering combustion underground and seep their way to the surface through cracks in the ground. In particular, SOx has a smell like freshly struck matches or a "burnt" smell. With no other above surface visible fires in sight, this is a good indicator of an underground coal seam fire. The next most visible evidence is the presence of smoke, particularly visible when dark, emanating from the ground. Usually, the vegetation around such sites also gets affected and is easy to spot. In some cases, local cracks form and widen over a period of time, which can eventually lead to subsidence of the ground. These telltale signs of an underground fire are hard to miss, especially if the fire is close to the surface.

The evidence of the existence of current or past underground combustion usually warrants continued monitoring. The typical monitoring methods employed are discussed next and are useful in the decision-making regarding any immediate threats to civilian population or protected areas.

19.2.2   Types of monitoring

Monitoring of underground combustion/gasification can be broadly categorized into two main types: (1) ground-/underground-based and (2) aerial-based. The type of diagnostic tool utilized for making measurements (such as thermography and spectroscopy) in either of these monitoring methods will be discussed in the next subsection and will vary based on the type of coal seam, depth of the underground fire, extent of the spread, and available monetary and physical resources.

19.2.2.1   Ground and subsurface based

(a) Underground Fires: This method involves monitoring of the affected area by sensors that are at the either surface or subsurface level of the affected area. For example, surface-based monitoring can involve fieldwork, wherein the affected area is regularly inspected for subsidence; temperature measurements taken using handheld or fixed sensors and changes in other physical attributes such as electric conductivity or magnetic responses of the ground are undertaken. While subsurface monitoring involves drilling holes in key locations and monitoring the temperature or gas emissions in these holes. Subsurface methods are costlier owing to the drilling costs, in particular, if the spread of the fire warrants new holes to be drilled on an ongoing basis. These methods (both above and below the surface) are often time-consuming, especially if the affected area is large. Additionally, the data collected by the sensors are over a few limited locations based on availability of personnel, number of sensors, and time. Hence, a full picture of the affected area is usually not obtainable. Surface monitoring however provides the highest spatial accuracy for making measurements as the sensor (once reliably calibrated) is placed at a precise location in the affected area. Therefore, these sensors can provide validation data for the more widespread aerial-based monitoring. Changes in the measured quantities over time can also give clues regarding the temporal changes in the fire and the directional movement, if any, of the subsurface fire.

Pollutant gas monitoring is another method utilized where cracks and fissures allow gaseous emissions to occur. This involves using techniques such as collecting the sample emission gases and analyzing them using gas chromatography to determine concentration of pollutants. This can be used to determine the temperature at which combustion is occurring if the type of coal in the seam is well characterized.

(b) Underground Coal Gasification: For UCG, product gas monitoring, subsidence monitoring, particle sampling, and hydrogeology are chief surface/subsurface measurement options.

The primary purpose of UCG is to produce a combustible gaseous product. Therefore, this can be easily monitored using gas chromatography techniques to monitor changes in the underground reaction zone or combustion regime.

Subsidence monitoring is primarily focused on maintaining structural integrity of the feed-in pipes and other installed structures while also ensuring that the subsidence occurs in a planned manner. This can be engineered a priori through careful consideration of the geometry, the gasification rate, and the other geologic factors at play (Imran et al., 2014). The particle sampling method involves a postevent analysis of recovered particles from a UCG process to reconstruct the sequence of conditions (pressure, temperature, etc.) that occurred during the gasification process (Hamburg et al., 1987). A useful method is one that aims to map the characteristic features found on the surface of rock samples exposed to a UCG event back to the pressures and temperatures that were present along with the water vapor concentration that must have been present that promotes surface reactions on the rocks or coal samples recovered (Aiman et al., 1980). The high-temperature environment also causes sintering and formation of glass-like substances, which serve as a geologic thermometer to help us understand what conditions were present during the gasification process. The analytic methods employed in examining the samples can also include techniques that examine sorption and diffusion of gases on porous surfaces on the coal seam (Ludwik-Pardała and Stańczyk, 2015).

Pollutant monitoring in underground water tables is also an essential management option for UCG (LIU et al., 2007). Inorganic compounds that can be monitored include free and bound cyanides, free metals (Cr, Zn, Fe, Cd, Mo, etc.), and sulfates (Kapusta and Stańczyk, 2011). Organic compounds typically monitored include benzene, phenolics, and other polycyclic aromatic hydrocarbons (PAHS). The measured concentrations of these compounds coupled with a knowledge of the starting composition (type of coal) of the fuel can be used to model reaction progress.

Water hydrogeology is another promising surface/subsurface method employed for UCG monitoring (Daly et al., 1989). This technique involves measuring changes in the pressure head of water and level at different locations surrounding the UCG location. By measuring the changes in the water pressure, it is possible to correlate it back to the extent of gasification and also to the temperatures and pressures within the gasifier. The outcome of this measurement is potentiometric surface maps of the hydraulic head that can be used to track the progress of the UCG process.

19.2.2.2   Aerial based

Aerial methods offer some natural advantages over the surface-based methods of monitoring. Notably, a wider area can be mapped more rapidly and repeatedly, including the spots that may be unsafe for ground-based monitoring. Aerial-based monitoring can be further subdivided into aero-vehicle-based and satellite-based. Unmanned aero vehicles (UAVs) mounted with telemetric devices (Wang et al., 2015; Vasterling and Meyer, 2013) and satellite-based measurement systems (Chatterjee, 2006; Voigt et al., 2004) are often used to aerially monitor an underground fire. Both of these aerial methods clearly involve some type of imaging from above the surface and deciphering this image using appropriate physics and algorithms to infer the extent of the underground fire. UAV imagery offers the better spatial resolution for mapping, as it is closer to the surface and can provide a resolution of around 0.2×0.2 m (Wang et al., 2015), while satellite imagery at very high resolutions provides around 30×30 m (Voigt et al., 2004). UAV imaging also has other advantages such as selectivity of time of imaging, ability to map all terrains (such as mountainous regions that satellites cannot cope very well with), and no interference from atmospheric conditions or clouds that satellites often suffer from. However, satellite imaging has a unique advantage in that it can provide a large field of view for those fires that are widespread and need regular monitoring. Additionally, UAVs are highly limited by weight requirements in terms of the sensor that can be used, and typically, lightweight IR cameras are preferred over other more sophisticated but heavier sensors that satellites can accommodate. Fig. 19.2 shows a subsurface coal fire in Jharkhand, India, using data from the Landsat-5 Thematic Mapper (TM) over more than 350 km^2.

19.3   Advanced measurement techniques

Measurement techniques for underground coal gasification/fires exploit various physical and chemical attributes associated with the existence/extent of these events in an attempt to characterize and quantify the extent and depth of the reaction zone. Some main methods are discussed below.
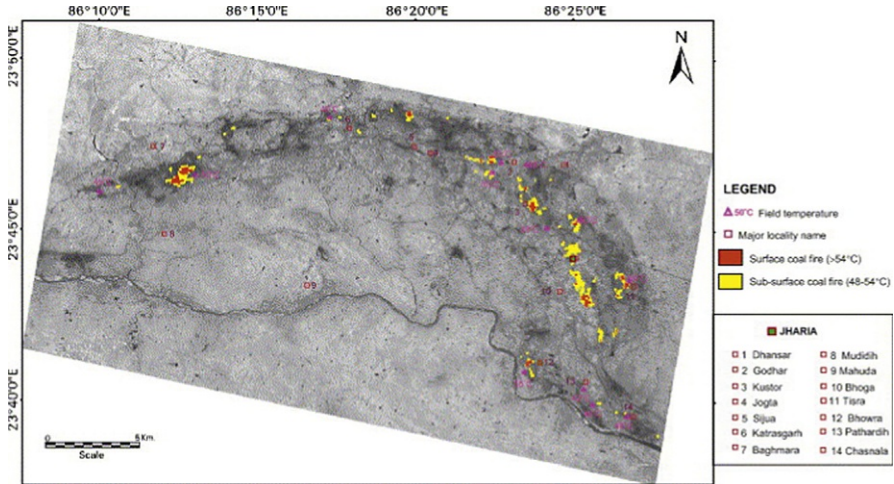
Fig. 19.2 Surface and subsurface coal fire areas of Jharia Coalfield, Jharkhand, India, using Landsat-5 TM band 6 data.
Reprinted from Chatterjee, R.S., 2006. Coal fire mapping from satellite thermal IR data—a case example in Jharia Coalfield, Jharkhand, India. ISPRS J. Photogramm. Remote Sens. 60, 113–128, with permission from Elsevier.

1. Electromagnetic properties based methods: These are usually surface-based monitoring methods and can be used to capture the depth of the reaction zone. The two main methods employed are 2-D electric imaging based on the resistivity variations in the ground owing to the presence of gaps or caves caused by underground combustion/gasification zones and transient electromagnetic method (TEM).

   Several devices have been developed to enable the 2-D electric imaging measurements such as the Wenner-Schlumberger array (Pazdirek and Blaha, 1996; Loke, 2001) with the electrodes arranged in a constant spacing. As discussed in the review by Song and Kuenzer (2014), this is a well-suited method for detecting combustion zones that have low resistivities (of the order of 9–70 Ω m) and has a high accuracy of predicting the depth of the reaction zone. The main drawback owing to the geometric design of the array is the requirement of a number of measured sites and a flat field. This might, however, be well suited for early-stage fires where the surface terrain has not been affected much by the sub-surface fire. This method can be used to measure fires up to the depth of 30 m quite accurately.

   TEM is a time-domain method in which an initial electromagnetic (EM) pulse is sent into the ground leading to an inductive eddy current being formed (Xin et al., 2015). The decay of the eddy current is affected by the presence of a coal fire and is used to detect its presence. This method can be used to detect much deeper reaction zones (over a 100 m) owing to its ability to cope with much larger ground resistivities (a few thousand Ω m) (Song and Kuenzer, 2014). TEM can also be used on an airborne mode and hence offers greater flexibility than the 2-D electric imaging methods.

2. Acoustics and Radar Based Methods: Acoustic method involves using sound waves to detect anomalies underground, which can then be used to local underground reaction zones. Ultra-sound detection in porous media has been experimentally demonstrated as a useful tool that can be exploited for this application (Torero et al., 1993; Tse et al., 1999). The changes in

attenuation of acoustic waves in porous media with burnt char (Tse et al., 1999) were used to detect and quantify the size of the smoldering zone using this technique in a tomographic sense to get a 2-D image of the reaction front. More recently, techniques based on sound generation from the reaction zone (known as acoustic emission or AE) are monitored to identify the reaction progress (Su et al., 2017). AE is indicative of crack formation in the seam and is used to study the growth rate of the reaction zone and resultant gas feeding rate. The AE can be closely correlated to the temperature in the reaction zone and the location/size of the reaction cavity.

Similarly, ground-penetrating radar (GPR) has also been employed by Cao et al. (2012) to characterize underground fires. Owing to the defects created by a smoldering combustion zone, sharp reflections of the radar signal occur, which can be used to map the location of the burning zone. Cao et al. (2012) suggest that owing to low interference capability of this technique, GPRs are particularly useful for mapping fires up to a depth of 50 m. They utilized a multilevel compound filtering-correction technique to process the radar section data.

3. Detection of Radioactive Gases: This is a chemical method wherein gases that are not commonly present in the atmosphere above trace quantities but are found above the surface of an underground coal fire are detected and measured. In particular, the detection of radon (^{222}Rn) has been employed for detection and monitoring of subsurface fires. This method of measurement has precedents of being used in volcanos, earthquakes, and other naturally occurring geologic phenomena (King, 1986). Laboratory-scale experiments conducted showed that the concentration of Rn could be used to assess the temperature of the coal from which it emanated (Xue et al., 2010). More recently, Wu et al. (2012) used the CD-1α cup radon measurement method in their experiments to detect underground fires at the Bulianta mine. The method involved burying the cups in preselected areas and taking samples that were later analyzed. This method has been shown to be useful to detect the location and range of the fire and to predict the changes in the trend of the fire.

4. Spectroscopic methods: Combustion studies often utilize spectroscopic techniques to monitor key combustion products such as carbon dioxide (Heatwole et al., 2009; Veeraragavan and Cadou, 2008). This usually involves monitoring a spectral region in which the species of interest has a rotational-vibrational (ro-vibrational) signature. In the context of underground fires, ground-based local monitoring is possible using either emission or absorption spectroscopy as a part of the field survey for index gases. Index gases consist of a range of gases expected to be emitted from a smoldering combustion zone involving some pyrolysis such as CO_2, CO, H_2, and trace hydrocarbons. However, this is an expensive exercise and would typically be used to validate bulk models that aim to estimate greenhouse gas (GHG) emissions based on the estimated amount of coal getting burned. Carbon monoxide is another noxious gas emitted by underground fires that can be monitored due to its strong signature in the mid-IR region when hot. Gas samples may be collected and analyzed *in situ* using an FTIR spectrometer (Tang et al., 2014). The method relies on *Beer's* law of absorption to accurately estimate the concentration (after calibration with well-characterized test gases) and the temperature of the gas by fitting against statistical temperature-dependent quantum mechanical models for the absorption bands once the concentration is known. Both information (species concentration and temperature) obtained using this technique can be utilized in subsurface fire modeling that is sometimes used in conjunction with satellite-based imaging. In practice, surface-based measurements such as these are required for validation and further development of aerial methods.

5. Thermography: Infrared thermography is a common method used to map the temperature of a suspected underground reaction zone. The physical premise for this method is the

well-known Planck's law of radiation, which can be inverted and expressed in terms of temperature as (Huo et al., 2014)

$$T = \frac{C_2}{\lambda \left(\ln \left(\varepsilon_\lambda C_1 \big/ \left(\pi L_\lambda \lambda^5 \right) \right) + 1 \right)} \tag{19.1}$$

where L_λ is the measured spectral radiance from the surface being imaged at a given wavelength λ, ε_λ is the emissivity of the surface being imaged at the given wavelength, C_1 and C_2 are known constants for Planck's law of radiation, and T is the temperature of the surface. The measured value is usually in terms of a digital signal that can be suitably processed to express it in terms of spectral radiance (Kang and Veeraragavan, 2015, 2017). This can then be inverted to obtain the temperature of the surface. The key unknown parameter in the above equation is the emissivity of the radiating surface at the given wavelength. This can be obtained via a calibration procedure using a few point measurements of the ground temperature using other sensors. Depending on the type of camera used, different parts of the IR spectrum can be captured, for example, thermal infrared (TIR) that ranges from 8 to 12 μm or shortwave infrared (SWIR) that ranges from 1.4 to 3 μm. SWIR offers better spatial resolution (around 30×30 m) than TIR (around 100×100 m) and does not get saturated at a low temperature like TIR does at around 70°C (Chatterjee, 2006). When TIR images are used, it is common to use some subpixel modeling techniques to better characterize the exact location of the hot spot within a pixel in order to build a high-resolution map of the underground fire (Prakash et al., 1999; Prakash and Vekerdy, 2004). The issues facing this technique include solar heating (if imaged during daytime), interference from other hot objects, the lack of a good measure of spectral emissivity or uneven spectral emissivity of the surface being imaged, and difficulties in differentiating between exposed and unexposed (subsurface) fires if they occur together in the area being imaged and low spatial resolution. However, once the underground fire is reasonably well characterized, this method of mapping becomes very valuable for continued monitoring to detect lateral spread of the fire with time.
6. Injection of tracers: This is a method particularly useful for monitoring UCG events. It involves injecting a tracer element (such as xenon or helium) alongside the oxidizer directly into the reaction zone (Pirard et al., 2000). By monitoring the tracers upon their passing through the reaction zone and emerging back out, useful information can be gathered to feed transfer functions that predict the progress of the gasification process. Helium and xenon are chosen as tracers as they have very few issues such as segregation and adsorption into the porous coal seam. Helium can be a tracer of choice for monitoring nitrogen filtration and detected via gas chromatography, while xenon is a more reliable tracer element for the combustion experiments. The issue with xenon, however, is its cost (rare element) and radioactivity.

19.4 Conclusion and future trends

Detection and monitoring of underground coal gasification/fires is a challenging task that requires an interdisciplinary approach. The range of technologies spans all areas of science such as electromagnetic fields, thermography, radar, chemical detection, spectroscopy, and acoustics. This invariably requires science and engineering to work cohesively together to develop more advanced measurement techniques that can

accurately quantify the size, depth, and speed of fire spread over areas as large as several hundreds of square kilometers. In this chapter, we reviewed several available technologies along with their advantages and disadvantages. Future methods could utilize other branches of physics such as X-ray tomography (Naveed et al., 2013) that are under development to measure pore-size distribution of the coal seams and the combustion reaction zones. A variety of improvements to the existing algorithms used in interpreting the raw data obtained via satellite imagery and improvement in quantum-based sensors can pave the way for better, faster, and more reliable characterization of the underground fires. With early detection and accurate characterization, it is often possible to progress and improve the outcomes of an underground coal gasifier or arrest and extinguish underground coal fires before they become an enormous problem as is the case with many of the existing underground fires that have spread across vast areas and have been burning for decades, some even for centuries. The availability of quantitative experimental data is particularly important for validation of simulation models that can then be employed as a powerful tool to predict the expansion of the reaction zone, along with what outcomes can be achieved by influencing the control parameters in play.

References

Aiman, W.R., Ganow, H.C., Thorsness, C.B., 1980. Hoe Creek II revisited: boundaries of the gasification zone. Combust. Sci. Technol. 23, 125–130.

Cao, K., Zhong, X., Wang, D., Shi, G., Wang, Y., Shao, Z., 2012. Prevention and control of coalfield fire technology: a case study in the Antaibao Open Pit Mine goaf burning area, China. Int. J. Min. Sci. Technol. 22, 657–663.

Chatterjee, R.S., 2006. Coal fire mapping from satellite thermal IR data—a case example in Jharia Coalfield, Jharkhand, India. ISPRS J. Photogramm. Remote Sens. 60, 113–128.

Daly, D.J., Schmit, C.R., Beaver, F.W., Evans, J.M., 1989. Role of hydrogeology in Rocky Mountain 1 underground coal gasification test, Hanna basin, Wyoming. In: AAPG Bulletin (American Association of Petroleum Geologists), USA.

Hamburg, G., Kühnel, R., Scarlett, B., Vleeskens, J., 1987. Potential of electron probe micro-analysis on ash particles for reconstruction of conditions in underground gasification chambers. Coal Sci. Technol. 11, 575–579.

Heatwole, S., Veeraragavan, A., Cadou, C.P., Buckley, S.G., 2009. In Situ species and temperature measurements in a millimeter-scale combustor. Nanoscale Microscale Thermophys. Eng. 13, 54–76.

Huo, H., Jiang, X., Song, X., Li, Z.-L., Ni, Z., Gao, C., 2014. Detection of coal fire dynamics and propagation direction from multi-temporal nighttime Landsat SWIR and TIR data: a case study on the Rujigou coalfield, Northwest (NW), China. Remote Sens. 6, 1234–1259.

Imran, M., Kumar, D., Kumar, N., Qayyum, A., Saeed, A., Bhatti, M.S., 2014. Environmental concerns of underground coal gasification. Renew. Sust. Energ. Rev. 31, 600–610.

Kang, X., Veeraragavan, A., 2015. Experimental investigation of flame stability limits of a mesoscale combustor with thermally orthotropic walls. Appl. Therm. Eng. 85, 234–242.

Kang, X., Veeraragavan, A., 2017. Experimental demonstration of a novel approach to increase power conversion potential of a hydrocarbon fuelled, portable, thermophotovoltaic system. Energy Convers. Manag. 133, 127–137.

Kapusta, K., Stańczyk, K., 2011. Pollution of water during underground coal gasification of hard coal and lignite. Fuel 90, 1927–1934.

King, C.-Y., 1986. Gas geochemistry applied to earthquake prediction: an overview. J. Geophys. Res. Solid Earth 91, 12269–12281.

Liu, S.-Q., Li, J.-G., Mei, M., Dong, D.-L., 2007. Groundwater pollution from underground coal gasification. J. China Univ. Min. Technol. 17, 467–472.

Loke, M., 2001. Electrical imaging surveys for environmental and engineering studies. A practical guide to 2-D and 3-D surveys: RES2DINV Manual, IRIS Instruments. www.iris-instruments.co m.

Ludwik-Pardała, M., Stańczyk, K., 2015. Underground coal gasification (UCG): an analysis of gas diffusion and sorption phenomena. Fuel 150, 48–54.

Naveed, M., Hamamoto, S., Kawamoto, K., Sakaki, T., Takahashi, M., Komatsu, T., Moldrup, P., Lamandé, M., Wildenschild, D., Prodanovic, M., 2013. Correlating gas transport parameters and X-ray computed tomography measurements in porous media. Soil Sci. 178, 60–68.

Pazdirek, O., Blaha, V., 1996. Examples of resistivity imaging using ME-100 resistivity field acquisition system. In: 58th EAEG Meeting.

Pirard, J.P., Brasseur, A., Coëme, A., Mostade, M., Pirlot, P., 2000. Results of the tracer tests during the El Tremedal underground coal gasification at great depth. Fuel 79, 471–478.

Prakash, A., Vekerdy, Z., 2004. Design and implementation of a dedicated prototype GIS for coal fire investigations in North China. Int. J. Coal Geol. 59, 107–119.

Prakash, A., Gens, R., Vekerdy, Z., 1999. Monitoring coal fires using multi-temporal night-time thermal images in a coalfield in north-west China. Int. J. Remote Sens. 20, 2883–2888.

Song, Z., Kuenzer, C., 2014. Coal fires in China over the last decade: a comprehensive review. Int. J. Coal Geol. 133, 72–99.

Su, F.-Q., Itakura, K.-I., Deguchi, G., Ohga, K., 2017. Monitoring of coal fracturing in underground coal gasification by acoustic emission techniques. Appl. Energy 189, 142–156.

Tang, X., Liang, Y., Dong, H., Sun, Y., Luo, H., 2014. Analysis of index gases of coal spontaneous combustion using Fourier transform infrared spectrometer. J. Spectrosc. 2014.

Torero, J.L., Fernandez-Pello, A.C., Kitano, M., 1993. Opposed forced flow smoldering of polyurethane foam. Combust. Sci. Technol. 91, 95–117.

Tse, S.D., Anthenien, R.A., Fernandez-Pello, A.C., Miyasaka, K., 1999. An application of ultrasonic tomographic imaging to study smoldering combustion. Combust. Flame 116, 120–135.

Vasterling, M., Meyer, U., 2013. Challenges and opportunities for UAV-borne thermal imaging. In: Kuenzer, C., Dech, S. (Eds.), Thermal Infrared Remote Sensing. Springer, Netherlands.

Veeraragavan, A., Cadou, C.P., 2008. Heat transfer in mini/microchannels with combustion: a simple analysis for application in nonintrusive IR diagnostics. J. Heat Transf. 130, 1–5.

Voigt, S., Tetzlaff, A., Zhang, J., Künzer, C., Zhukov, B., Strunz, G., Oertel, D., Roth, A., Van Dijk, P., Mehl, H., 2004. Integrating satellite remote sensing techniques for detection and analysis of uncontrolled coal seam fires in North China. Int. J. Coal Geol. 59, 121–136.

Wang, Y.-J., Tian, F., Huang, Y., Wang, J., Wei, C.-J., 2015. Monitoring coal fires in Datong coalfield using multi-source remote sensing data. Trans. Nonferrous Metals Soc. China 25, 3421–3428.

Wu, J., Wu, Y., Wang, J., Zhou, C., 2012. Radon measuring to detect coal spontaneous combustion fire source at Bulianta mine, Shendong. In: Coal Operators' Conference.

Xin, M., Zhu, H., Xiang, M., Zhang, Y., Liu, D., 2015. Application of transient electromagnetic method in coal mine fire detection. Metall. Mining Ind. 2015 (6), 321–326.

Xue, S., Wang, J., Xie, J., Wu, J., 2010. A laboratory study on the temperature dependence of the radon concentration in coal. Int. J. Coal Geol. 83, 82–84.

This page intentionally left blank

Index

Note: Page numbers followed by *f* indicate figures, and *t* indicate tables.

Underground coal gasification (UCG) processes convert solid coal resources which would otherwise not be mined into syngas. The resulting syngas can be used for power generation, fuel production or other petrochemical processes. In recent years there has been a resurgence of interest in UCG as it may offer financial, social and environmental benefits over the more conventional coal extraction methods. This book provides a comprehensive overview of the development of UCG, the current situation and likely future directions. After an introductory chapter reviewing the history of UCG, the following chapters focus on UCG technology, modern UCG projects, and prospective technologies.